Deciphering the Mechanism and Roles of Muscarinic and Purinergic Calcium Signals in the Human Colonic Epithelium

Alvin John Lee Kim Seong

Submitted for the degree of Doctor of Philosophy

University of East Anglia

School of Biological Sciences

Date of Submission: 31 March 2021

Abstract

The human large intestine is lined by a monolayer of polarized epithelial cells, which form invaginations known as 'Crypts of Lieberkühn' and serves as a barrier between the gut luminal contents and the systemic circulation. In order to maintain this barrier, the epithelium constantly renews and replenishes itself, a process known as tissue homeostasis. This process is driven by multipotent intestinal stem cells residing at the base of crypts which give rise to specialised epithelial cells. Loss of tissue homeostasis is associated with an increased risk of major intestinal diseases, such as colorectal cancer.

Stem cell-driven tissue renewal is regulated by luminal and systemic factors. Luminal-sensing of gut contents – nutrients, microbes, and their metabolites – triggers the release of hormones, cytokines and chemokines from the epithelium and gut immune cells. Higher levels of control that modulate the epithelium and integrate luminal inputs are exerted at the basal pole by neurotransmitters, such as acetylcholine and ATP. These neurotransmitters affect gut immunity and motility, mucus and fluid and electrolyte secretion, proliferation, and cancer development.

This thesis is interested in expanding our understanding of how the colonic epithelium integrates signalling inputs. Calcium is a signal integrator that regulates gut homeostasis. In drosophila, external signalling molecules causes calcium oscillations which influences intestinal stem cells. In mouse, carbachol – a non-hydrolysable analogue of acetylcholine – increases cytosolic calcium concentrations and modulates bicarbonate secretion. Calcium signalling also has a complex role on the development and progression of cancer. However, the spatial-temporal status of calcium signals in primary human intestinal epithelium remains unclear.

This thesis elucidates components of the calcium signalling toolkit and investigates the spatial-temporal status of calcium signals in cultured human intestinal crypts and organoids. It also explores the physiological roles of calcium signalling in maintaining gut tissue homeostasis and investigates the status of calcium signalling in colorectal cancer.

Declaration

I declare that this thesis represents my own work, except where due acknowledgement is made, and that it has not been previously included in a thesis, dissertation or report submitted to this University of to any other institution for a degree, diploma, or other qualifications.

_____

Alvin John Lee Kim Seong

PhD Candidate

Acknowledgements

This research would not have been possible without the support of many individuals.

I would first like to thank my primary supervisor, Dr Mark Williams. Five years ago, I entered your lab as a 3rd year undergraduate research project student. I now present this thesis, which would not be possible without your guidance and energy.

I also thank former (Dr Alyson Paris, Mr George Lines) and current (Dr Victoria Jones, Dr Nicholas Pelaez Llaneza, Mr Joseph Sandy, Mr Sean Tattan, Ms Jordan Champion, Ms Marietta Xagorari) members of the Williams group, my secondary supervisor Dr Michael Wormstone, and my tertiary supervisor Mr Jonathan Tang. For all their help throughout this research.

Next, I would like to thank my parents (Anthony & Alice Lee) and brothers (Andrew, Alex, Albert) for their unconditional support. Finally, I thank Beth, Atiff, Tarryn, Leda, Lloyd, Danial, and many others, for being a part of my journey.

Contents

List of Figures

List of Tables

Glossary

[Ca2+]:	Ca^{2+} concentration
2-APB:	2-Aminoethoxydiphenylborane
4-DAMP:	1,1-Dimethyl-4-diphenylacetoxypiperidinium iodide
5-HT:	Serotonin
ADPR:	ADP-ribose
ATP:	Adenosine triphosphate
Baf:	Bafilomycin A1
BCRE:	Bob Champion Research and Education
BF:	Brightfield
BMP:	Bone morphogenetic proteins
Ca^{2+}:	Calcium ions
cADPR:	cyclic ADP-ribose
CaM:	Calmodulin
CaMK:	CaM kinases
cAMP:	Cyclic AMP
CaN:	Calcineurin
CAX:	Ca^{2+}/H^+ exchanger
CBC:	Crypt base columnar
CCh:	Carbachol
CD38:	Cyclic ADP ribose
CFTR:	Cystic fibrosis transmembrane conductance regulator
ChAT:	Choline acetyltransferase
CHGA:	Chromogranin A
CICR:	Calcium-induced calcium-release
CLCA1:	Calcium-activated chloride channel regulator 1
CNS:	Central nervous system
COX:	Cyclooxygenase enzyme
CPA:	Cyclopiazonic acid

CRAC:	Ca^{2+} release-activated Ca^{2+}
CRC:	Colorectal cancer
CRTC:	CREB regulated transcription co-activator
DAG:	Diacyl glycerol
DCLK1:	Doublecortin-like kinase 1
DCS:	Deep crypt secretory
DZM:	Diltiazem
E-CAD:	Epithelial cadherin
EGF:	Epidermal growth factor
EGFR:	Epidermal growth factor receptor
EGTA:	Triethylene glycol diamine tetraacetic acid
ENS:	Enteric nervous system
FACS:	Fluorescence-activated cell sorting
GCG:	Proglucagon
GI:	Gastrointestinal
GLP1:	Glucagon-like peptide-1
HBS:	HEPES Buffered Saline
HILIC:	Hydrophilic interaction liquid chromatography
IBD:	Inflammatory bowel disease
IBS:	Irritable bowel syndrome
IP3:	Inositol trisphosphate
IP3R:	Inositol 1,4,5-trisphosphate receptors
iQC:	Internal quality control
IS:	Internal standard
ISC:	Intestinal stem cell
K^+:	Potassium ions
LGR5:	Leucine-rich repeat-containing G-protein coupled receptor 5
mAChR:	Muscarinic receptor
Mg^{2+}:	Magnesium ions

ML-SA1:	Mucolipin synthetic agonist 1
MRM:	Multiple reaction monitoring
MS/MS:	Tandem mass spectrometry
MS:	Mass spectrometry
MUC2:	Mucin-2
N.S:	Not (statistically) significant
NA:	Nicotinic acid
Na^+:	Sodium ions
NAADP:	Nicotinic acid adenine dinucleotide phosphate
NAD:	Nicotinamide adenine dinucleotide
NFAT:	Nuclear factor of activated T-cells
NGF:	Nerve growth factor
NKCC1:	Na^+-K^+-2Cl^- co-transporter
OLFM4:	Olfactomedin 4
Oxo:	Oxotremorine-M
P2Y2:	Metabotropic P2Y2
P2YR:	Metabotropic P2Y receptor
PCSK1:	Neuroendocrine convertase 1
PFA:	Paraformaldehyde
PI3K:	Phosphoinositide 3-kinase
PIP2:	Phosphatidylinositol 4,5-bisphosphate
PLC:	Phospholipase C
PMCA:	Plasma membrane Ca^{2+} ATPase
PTK7:	Protein tyrosine kinase 7
PYY:	Peptide YY
ROI:	Region of interest
ROS:	Reactive oxygen species
RPKM:	Reads per kilobase million
RT:	Room temperature

RYR: Ryanodine receptors

SCFA: Short-chain fatty acid

SERCA: Sarcoendoplasmic reticulum Ca^{2+}-ATPase

SLE: Supported liquid extraction

SOCE: Store-operated Ca^{2+} entry

SOICR: Store overload-induced Ca^{2+} release

SOP: Standard operating protocol

SPCA: Secretory pathway Ca^{2+} ATPase

SPE: Solid phase extraction

STIM: Stromal interaction molecule

TA: Transit-amplifying

TCA: Tricyclic anti-depressant

TMB: 3,4,5-Trimethoxy-benzoic acid, 8-(diethylamino)octyl ester

TPC: Two-pore channel

TRP: Transient receptor potential

TRPML: Mucolipin TRP

UTP: Uridine-5'-triphosphate

V-ATPase: Vacuolar ATPase

VGCC: Voltage-gated Ca^{2+} channels

VNUT: Vesicular nucleotide transporter

WCX: Weak-cation-exchanger

WFCD2:   WAP four-disulfide core domain 2

WREN: WNT3a, R-SPO, EGF, Noggin

Preface

The human large intestine is lined by a continuous monolayer of epithelial cells, which form invaginations known as 'Crypts of Lieberkühn'. These epithelial cells are polarized with the basal pole being supported by an extracellular basement membrane, its apical pole facing into the gut lumen, and lateral membranes connected to adjacent epithelial cells by tight junctions. In combination with the mucous layers secreted by goblet cells, the intact monolayer of epithelial cells forms a vital mucosal barrier between the luminal contents of the gut and the systemic circulation. The physiological role of the intestinal mucosal barrier is to preserve the epithelium's ability to absorb nutrients while preventing the translocation of harmful microorganisms and toxins from gut luminal contents on the apical pole to systemic circulation on the basal pole.

The lining of the gut is subject to constant mechanical, biochemical and microbiological insults. In order to maintain vital barrier function in such a hostile environment, the gut epithelium constantly renews and replenishes itself, a process known as tissue homeostasis. Intestinal stem cells play a crucial role in this process over the life course. Loss of tissue homeostasis is associated with an increased risk of major intestinal conditions such as colorectal cancer – of which there are more than 16,000 deaths per annum in the UK (Zitvogel, et al. 2015), inflammatory bowel disease – of which there are more than 400,000 sufferers in the UK (Antoni, et al. 2014); as well as many other health conditions such as food allergies (Samadi, Klems and Untersmayr 2018), irritable bowel syndrome (Barbara 2006), coeliac disease (Cardoso-Silva, et al. 2019), metabolic syndrome, diabetes, and obesity (Thaiss, et al. 2018). Thus, there is a critical need to study the cellular and molecular regulation of human gut homeostasis which will pave the way for better prevention and treatment strategies for intestinal disease, inflammatory bowel disease and colorectal cancer.

The intestinal epithelium has a rapid renewal time of 3-5 days (Barker 2014). This rapid renewal is driven by multipotent intestinal stem cells that reside at the base of intestinal crypts, a process that is tightly regulated by a high gradient of Wnt, Notch and EGF signalling that predominates at the crypt-base (Gehart and Clevers 2019). These stem cells divide asymmetrically, producing a daughter stem cell and a daughter transit amplifying cell, the latter of which undergoes multiple cell divisions and differentiate, giving rise to mature epithelial cells such as: nutrient-absorbing enterocytes, hormone-secreting enteroendocrine cells, mucous-secreting goblet cells, and immunosensing tuft cells (van der Flier and Clevers 2009). These terminally differentiated epithelial cell types gradually migrate up the crypt-axis and are ultimately shed into the intestinal lumen. Continuous tissue renewal is achieved by the replacement of shed cells with the progeny of stem cell division.

The processes of stem cell-driven tissue renewal are tightly regulated by luminal and systemic factors that converge on the epithelium to regulate tissue homeostasis and promote gut

health. Luminal-sensing of gut contents including nutrients, microbes and their metabolites triggers the transepithelial release of hormones, cytokines and chemokines from the epithelium and gut immune cells (Goto 2019), (Liang, et al. 2019), (McCauley, et al. 2020) which in health preserves of gut homeostasis. For example, epithelial tuft cells have been demonstrated to be capable of sensing parasitic helminths in the gut lumen and via TRPM5, mount an immune response by producing cytokines, which induces tuft cell expansion and promotes proliferation and activation of type-2 innate lymphoid cells (Howitt, et al. 2016).

Higher levels of control that modulate the mucosal response and integrate luminal input with the physiological status of the tissue, the organ system and the organism are exerted at the basal pole. The intestinal epithelium is innervated by neurotransmitters released by the enteric nervous system, such as cholinergic acetylcholine (Rao and Gershon 2016) and purinergic ATP (Burnstock 2014). The role of cholinergic signalling in the intestine is extensive, ranging from stimulation of ion transport (Hirota and McKay 2006) to modulating gut immunity (Dhawan, et al. 2012) to progressing the development of gastrointestinal cancers (Konishi, Hayakawa and Koike 2019). Similarly, purinergic signalling has a range of effects on the intestines, such as stimulating gut motility (Bornstein 2008), regulating fluid and electrolyte secretion (Roman and Fitz 1999), and modulating enterocyte and afferent neurons (Lu, et al. 2019). Thus, a multitude of signals from the gut lumen, the underlying mucosa and the epithelium itself converges to regulate the physiological processes that maintain gut epithelial tissue homeostasis to promote gut health. A focus of the current study is to increase our understanding of how the epithelium may integrate these signalling inputs at the level of intracellular signals. In this respect, a central role for calcium is emerging as an integrator of signals that regulate gut homeostasis (Yang, et al. 2018). This has been studied extensively in drosophila (Deng, Gerencser and Jasper 2016), but has not been investigated in humans.

Calcium signalling is an important second messenger in all cell types, including epithelial cells of the intestinal epithelium. Within each epithelial cell, certain organelles act as calcium-ion reservoirs which release calcium into the cytoplasm to regulate a range of processes including division, migration, death, and differentiation (Brodskiy and Zartman 2018). Calcium ions have recently been shown to function as a key signal integrator in drosophila intestinal stem cells (Deng, Gerencser and Jasper 2016), whereby distinct external signalling molecules causes specific patterns of calcium oscillations which influences the state of the intestinal stem cell. These findings compliment an earlier study, also in drosophila, which showed activation of host defence and intestinal stem cell proliferation in response to bacterial infection (Buchon, et al. 2009). In mouse models, activation of muscarinic receptors by carbachol – a non-hydrolysable pharmacological analogue of acetylcholine – causes a rapid increase in cytosolic calcium concentrations and modulate bicarbonate secretions (Yang, et al. 2018). A recent review (Wang, et al. 2019) also surmised several studies in normal and malignant human mucosa cell lines, which collectively demonstrate the complex role calcium signalling has on development and progression of colorectal cancer. As a result, studies have

targeted components of the calcium signalling pathway for potential therapeutic benefit, such as inflammatory bowel disease (Cunningham, et al. 2019) and intestinal inflammation (Murakami, et al. 2012).

While calcium has been demonstrated to be essential to regulating gut immunity and tissue homeostasis, the spatial-temporal status of calcium signals in primary human intestinal epithelium remains unclear. Seminal work in the Williams laboratory has developed 3D culture systems of native tissue to investigate the role of calcium signals in regulating gut epithelial physiology in health and disease (Lindqvist, et al. 1998), (Lindqvist, et al. 2002), (Reynolds, Parris, et al. 2007) and (Reynolds, et al. 2014).   This thesis is focused on investigating the spatial-temporal status of calcium signals in the human colonic epithelium and human colonic organoids using real-time fluorescence imaging. In addition, this thesis will elucidate components of the calcium signalling toolkit using transcriptomic sequencing, immunolabelling, and pharmacology. Finally, this thesis will explore the physiological role of calcium signalling in maintaining gut tissue homeostasis, and investigate the status of calcium signalling in colorectal cancer.

1 Chapter 1. General Introduction

1.1 The Gastrointestinal Tract

The primary purpose of the GI tract is to facilitate the ingestion, digestion and absorption of nutrients and water, and eliminate waste in the form of faeces. Movement of luminal content in the GI tract is achieved by the coordinated contractions of the *tunica muscularis*, the muscular layers of the alimentary canal – the muscular tube, which extends from the mouth to the anus (Sanders, Koh, Ro, & Ward, 2012). In humans, the gastrointestinal (GI) tract can be divided into the upper and lower GI tracts. The upper GI tract consist of the mouth, pharynx, oesophagus, stomach, and duodenum (US National Library of Medicine, 2003). The lower GI tract consist of the rest of the small intestine, large intestine, rectum, and anal canal (Figure 1).
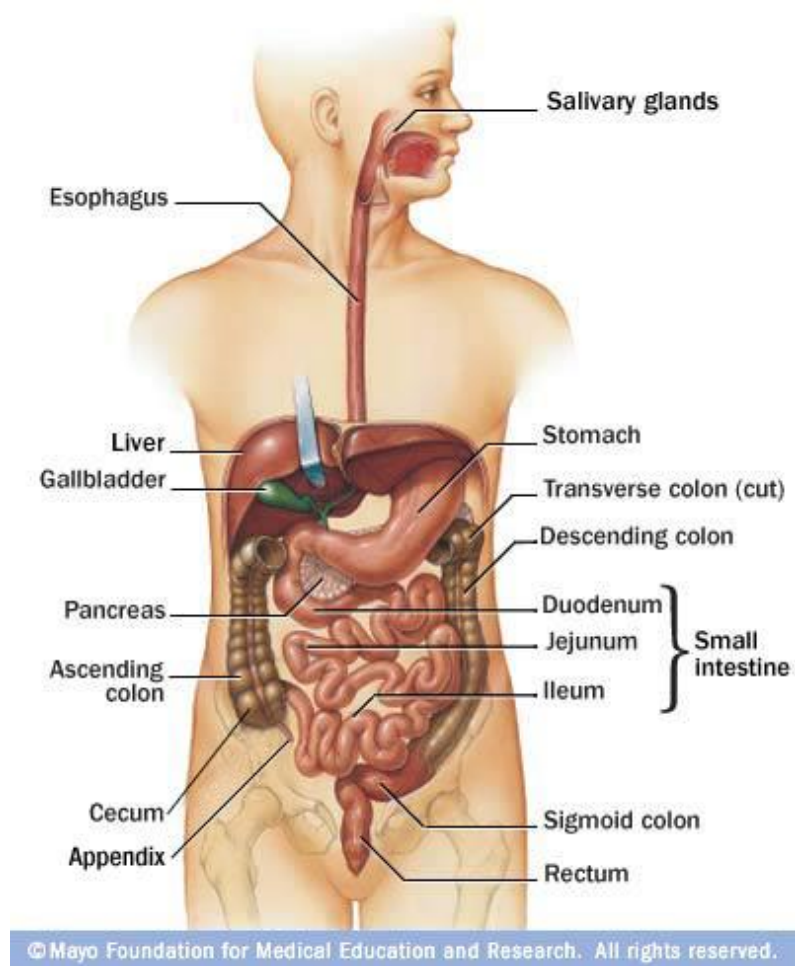
Figure 1 – Human Gastrointestinal Tract Anatomy.

Illustration and annotation of the upper and lower GI tract, along with organs of the digestive system. Adapted from Mayo Foundation for Medical Education and Research.

1.1.1 The Large Intestine

The large intestine consists of the cecum, colon, rectum, and anal canal. It is informally referred to as the colon, which makes up the largest portion of the large intestine. The primary functions of the large intestine are absorbing water and electrolytes, producing and absorbing vitamins, and forming and propelling faeces towards the rectum to be contained for eventual defecation (Azzouz and Sharma, Physiology, Large Intestine 2020). The average length of a human colon is 160 cm; ranging from 80-313 cm in men and 80-214 cm in women (Hounnou, et al. 2001). The colon can be divided into four regions: the cecum and ascending colon, the transverse colon, the descending colon, and the sigmoid colon (Figure 2A). Similar to all organs of the GI tract, the large intestine is comprised of four tissue layers: the mucosa, submucosa, muscularis propria, and serosa (Figure 2B). These layers are held together by connective tissue and are innervated by parasympathetic and sympathetic neurons (Browning & Travagli, 2014), lymphatic vessels (Alexander, Ganta, Jordan, & Wittec, 2010), and blood vessels.

The mucosa is the innermost layer of the GI tract. It consists of a monolayer of polarised epithelial columnar cells which separate the luminal contents of the GI tract from the body. In the large intestine, the epithelial monolayer is organized in tube-like glands termed "crypts of Lieberkühn", or simply crypts (Figure 2C). These epithelial cells are held together by tight junctions and their basal membranes are held by lamina propria, a basement membrane consisting of subepithelial connective tissue and lymph nodes. Underneath the lamina propria is a continuous sheet of smooth muscle cells, called the muscularis mucosae.

Below the mucosa is the submucosa, which contains a variety of inflammatory and ganglion cells, lymphatics, and autonomic nerve fibres. It is described as a branching and distribution zone for arteries and small venous channels (Rao & Wang, 2016). Recently, an update to the anatomy and histology of the submucosa was proposed (Benias, et al., 2018). Using confocal laser endomicroscopy, the presence of a previously unappreciated fluid-filled interstitial space that is drained by lymph nodes and supported by a complex network of thick collagen bundles was revealed. This submucosal space was also observed in the submucosa of GI tract and urinary bladder, the dermis, the peri-bronchial and peri-arterial soft tissues, and fascia.

Encasing the mucosa and submucosa are the muscularis propria, which consist of an inner layer of circular muscle and an outer layer of longitudinal muscle. These two smooth muscle layers serve the purpose of contraction in rhythmic waves to enable the movement of the luminal content through the GI tract. The final layer of GI tract, the serosa, is separated from the underlying longitudinal smooth muscle layer by a thin layer of loose connective tissue and consists of a continuous sheet of squamous epithelial cells – the mesothelium. The serosa forms a natural barrier against the spread of inflammatory and malignant processes (Rao & Wang, 2016).
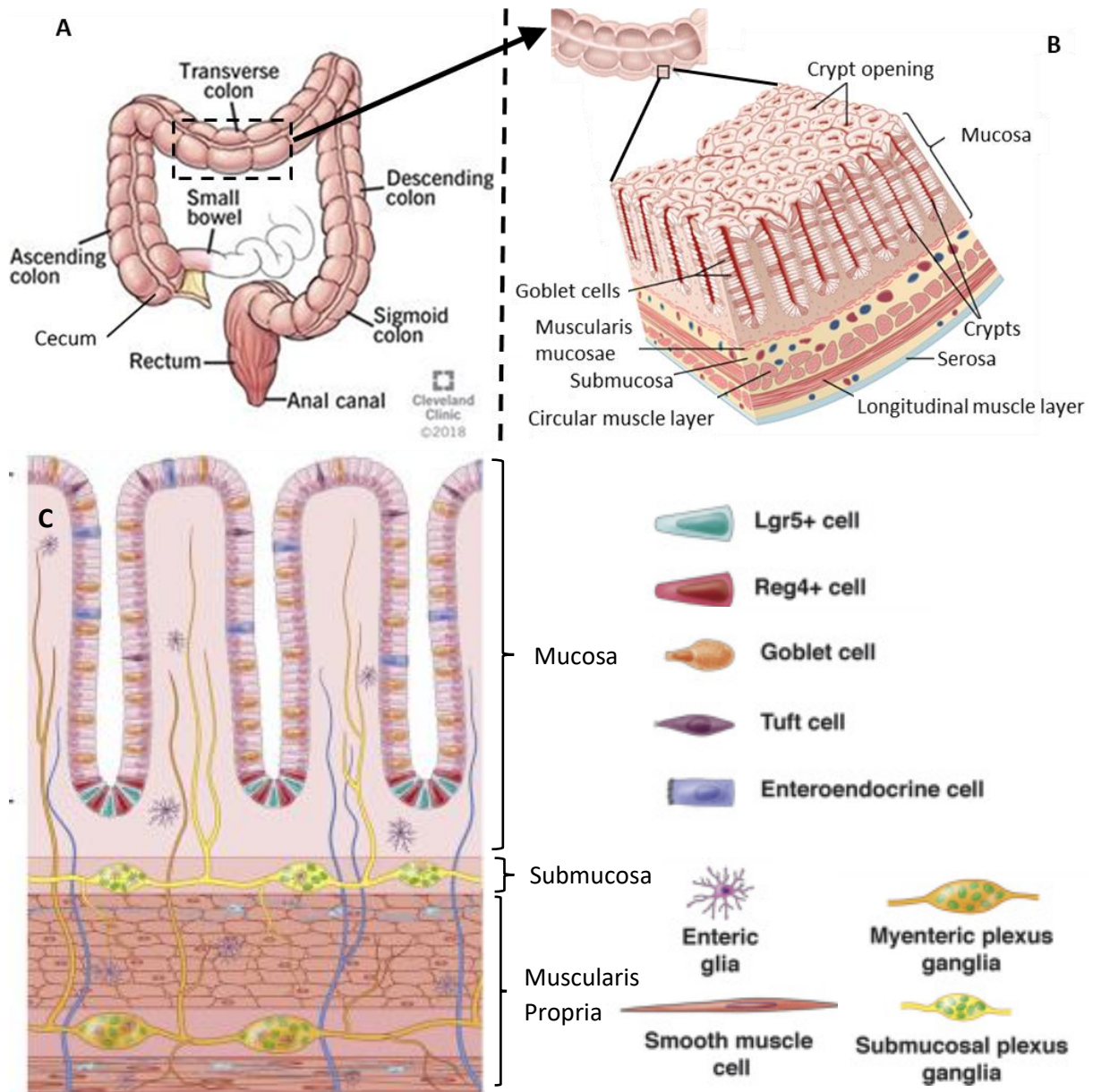
Figure 2 – Human Large Intestine Anatomy.

(A) Illustration and annotation of the large intestine. Adapted from Cleveland Clinic. (B) Illustration and annotation of the tissue layers comprising a segment of the colon. Adapted from Cleveland Clinic. (C) Cartoon depiction of a cross-section of the colonic epithelium depicting several differentiated epithelial cells in the mucosa, and composition of the submucosa and muscularis propria. The legend of cells depicted are on the right. Adapted from (Walsh & Zemper, 2019).

1.1.2 Diseases Affecting the Large Intestine

A wide range of diseases are known to affect the large intestine. These diseases can be categorised into three groups: dysmotility, colitis, and polyp (Azzouz and Sharma 2020), (Mayo Clinic, 2018). Dysmotility diseases of the large intestine include Irritable Bowel Syndrome (IBS), Hirschsprung disease, and diverticulosis. Colitis refers to inflammation of the colon and can be caused by numerous conditions, such as inflammatory bowel disease (IBD; further classified as Crohn's disease or ulcerative colitis), ischemic colitis, and infectious colitis. Polyp can be further classified as non-neoplastic (hyperplastic, inflammatory and hamartomatous polyps) and neoplastic (adenoma and serrated polyps). As implied by their name, non-neoplastic polyps typically do not develop into cancer. The risk of neoplastic polyps developing into colon cancer increases with polyp size, location, and the male gender (Qumseya, Coe, & Wallace, 2012), as well as the presence of other conditions such as IBD (Xie & Itzkowitz, 2008).

Diseases affecting the large intestine is a major global concern. In 2017, there were 6.8 million current global cases of IBD (GBD 2017 Inflammatory Bowel Disease Collaborators, 2019); compared to 1990 (79.5 per 100,000), the age-standardised prevalence rate of IBD had increased in 2017 (84.3 per 100,000). IBD prevalence rates were exponentially higher in high socio-demographic index (SDI) locations such as North America and the UK (464.5 and 449.6 per 100,000; respectively) compared to low SDI locations such as the Caribbean (6.7 per 100,000). Fortunately, the global age-standardised mortality rate associated with IBD had decreased in 2017 (0.51 per 100,000) compared to 1990 (0.61 per 100,000), with high SDI locations (e.g., Singapore; 0.08 per 100,000) having lower mortality rates compared to low SDI locations (e.g. Vanuatu; 1.8 per 100,000).

In the UK 2015-2017, over 40,000 new cases of CRC were diagnosed and 16,000 deaths were caused by CRC (Cancer Research UK, 2020). Colorectal cancer (CRC) is the fourth most-common cancer and the third most-common cause of cancer-related mortality in the world (Figure 3), with 1.8 million new cases and 880,000 deaths in 2018 (Rawla, Sunkara, & Barsouk, 2019). It is estimated that by 2030, there will be 2.2 million new cases of CRC and 1.1 million deaths caused by CRC (Arnold, et al., 2016). In a study which analysed the cancer registries of 51 countries between 1983-1987 to 1998-2002 (Center, Jemal, & Ward, 2009), the greatest contribution to global CRC incidence and mortality were found to be from developing countries (Eastern Europe, parts of Asia and South America), while CRC incidence and mortality have stabilised or declined in developed and long-standing economically developed countries (USA, Australia, New Zealand, parts of Western Europe). In addition to genetic predisposition and older age, lifestyle risk factors for CRC include insufficient dietary fibre, overconsumption of processed and red meat, being overweight or obese, alcohol, and tobacco (World Cancer Research Fund, 2020). The 5-year relative survival rates for patients with CRC is greater than 70% when localised (cancer contained in the colon or rectum) or regional (cancer present in nearby structures or lymph nodes), but drops to 15% when distant

(cancer present in distant lymph nodes or organs) (American Cancer Society, 2020). The overwhelming majority of CRC originate from a small percentage of adenomatous polyps (Mirzaie, Khakpour, Mireskandari, Shayanfar, & Fatahi, 2016) lining the colonic mucosa. If left untreated, these polyps may develop dysplasia and adenocarcinoma (Figure 4).
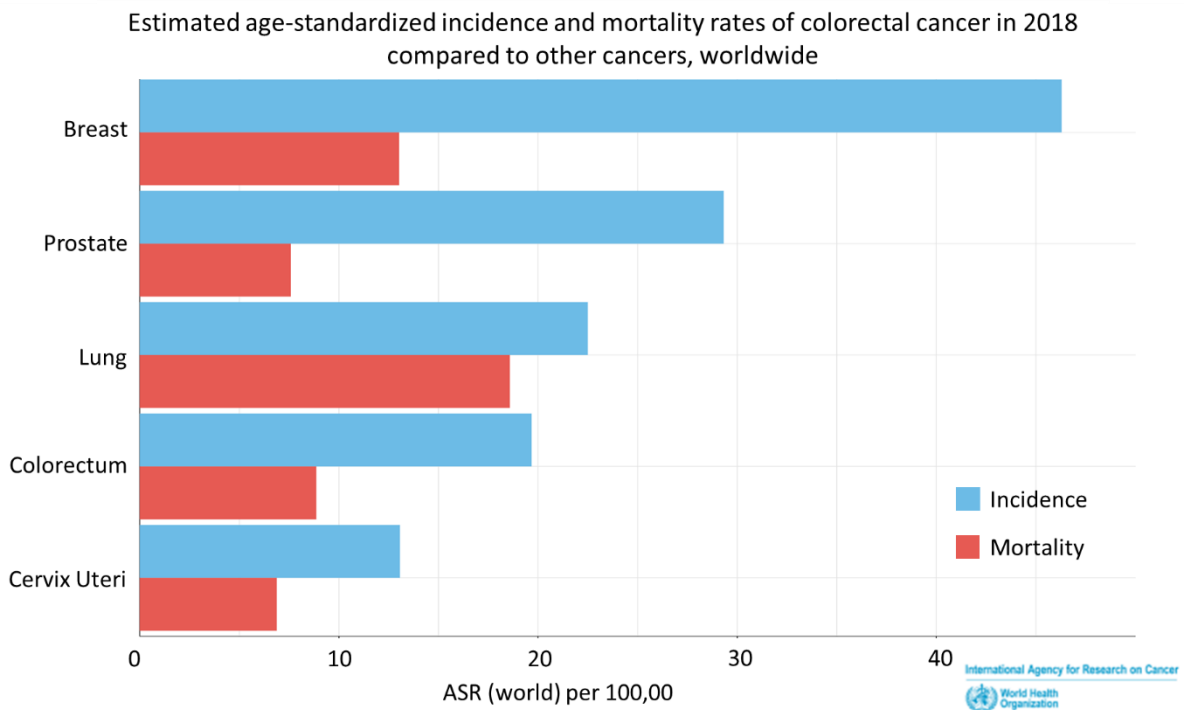
Figure 3 – Global Cancer Incidence and Mortality in 2018.

Bar chart illustration of the estimated age-standardized incidence and mortality rates of colorectal cancer globally in 2018, alongside other common cancers. Figure generated from (World Health Organization 2020)
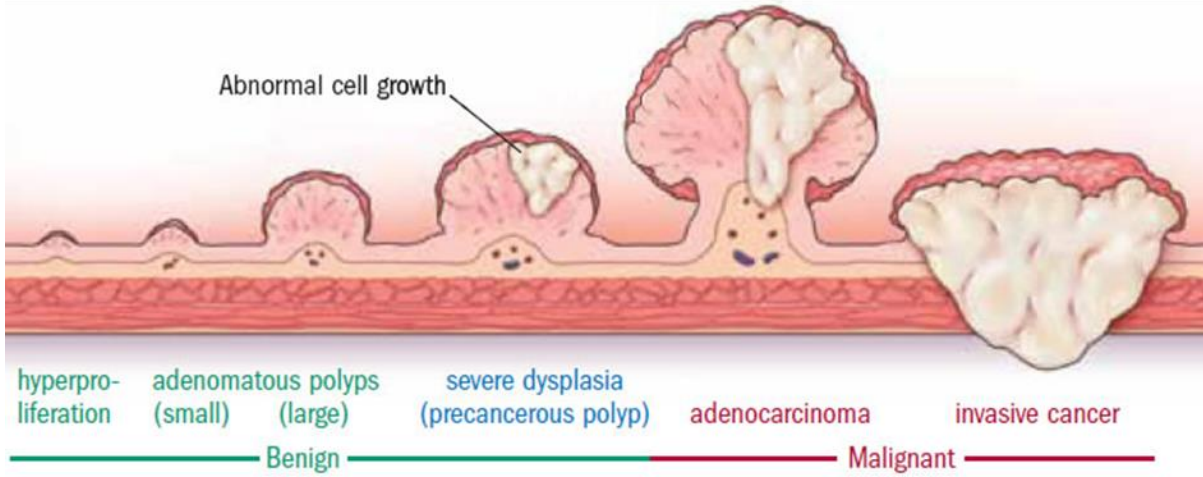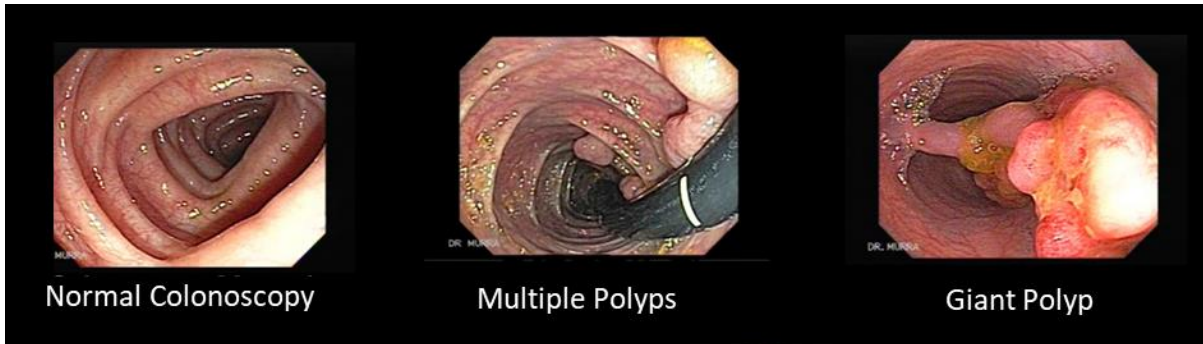
Figure 4 – Staged Development of Colorectal Cancer.

(Top) Comparison between normal colonoscopy (left), multiple small polyps that may develop dysplasia (middle), and a giant polyp that is at risk of developing into adenocarcinoma (right). (Bottom) Illustration of benign hyperproliferation of the mucosa (left)) to the development of adenocarcinoma and cancer (right). Adapted from Harvard Health Publishing.

1.1.3 Gut Microbiome

The human gastrointestinal tract is far from sterile. Between 300 and 1000 bacterial species reside in the human gastrointestinal system; there are 10 times more bacteria within the gut compared to the number of cells in the human body. Traditionally, it was assumed that microbial inoculation occurs after birth since the womb was thought to be sterile. However, increasing evidence show the presence of microbes in the placenta (Mueller, Bakacs, Combel, Grigoryan, & Dominguez-Bello, 2014), amniotic fluid (Collado, Rautava, Aakko, Isolauri, & Salminen, 2016) and meconium (Jiménez, et al., 2005), which indicate microbial development first occurs *in utero*. The next stage of flora development is during parturition – labour and delivery, when the baby descends through the birth canal and comes into contact with vaginal flora (Gabriel, Olejek, Stencel-Gabriel, & Miroslaw, 2018). Alternatively, babies delivered via Caesarean section experience less beneficial microbial inoculation and are at greater risk of developing asthma, celiac disease, type 1 diabetes, and gastroenteritis (Neu & Rushing, 2011). After this stage, the baby's gut microbiome is influenced by microbes in the environment. However, the biggest influencer to their gut microbiome comes from breast milk (Bode, 2012) which contains prebiotic oligosaccharides which provide a selective growth advantage for symbiotic bacteria over pathogens (Marcobal, et al., 2010), anti-adhesive antimicrobial agents which pathogens selectively binds to (Svanborg, Aniansson, Mestecky, & Sabharwal, 1991), antimicrobial and antibiofilm compounds (Ackerman, et al., 2018). For a full review on the development of the infant gut microbiome, see (Perez-Muñoz, Arrieta, Ramer-Tait, & Walter, 2017).

The gut microbiome has a diverse range of functions. In the colon, the microbiota secretes enzymes which break down host-indigestible carbohydrates (Tuddenham & Sears, 2016). Catabolism of these carbohydrates and resistant starches enable gut microbes to metabolise short-chain fatty acids (SCFAs) such as acetate, butyrate and propionate (Hollister, Gao, & Versalovic, 2015). Acetate provides protection from enteropathogenic infection (Fukuda, et al., 2011), butyrate regulates host immunity by inducing the differentiation of colonic regulatory T-cells (Furusawa, et al., 2013), and propionate – alongside acetate and butyrate – stimulates mucus secretion (Willemsen L. E., Koetsier, van Deventer, & van Tol, 2003) as well as regulate host immunity by binding to G protein-coupled receptors GPR41 and GRP43 (Brown, et al., 2003). In addition to SCFAs, the colon microbiota produces essential vitamins B and K (Hill, 1997), bactericides such as REG3γ (Vaishnava, et al., 2012), and numerous hormones (Table 1) which are targeted by epithelial and immune cells in the GI tract, or are transported across the epithelial barrier and delivered to effector organs via the bloodstream. These hormones have been shown to influence the development and function of the central nervous system, GI motility, wound healing, gut immunity, glucose metabolism, and more (Sommer & Bäckhed, 2013), (Quigley, 2013) and (Clarke, et al., 2014).

Table 1 – Hormones Produced or Regulated by the Gut Microbiota.

Class	Examples	Functions	Comment
SCFAs	Acetate	Energy source	Directly produced by bacteria; epigenetic and receptor-mediated effects; CNS effects linked to autism-like behaviours
	Butyrate	Host metabolism	
	Propionate	Signalling molecules	
Neuro-transmitters	Serotonin	Mood, emotion, cognition, reward (CNS)	Can be directly produced by bacteria or indirectly regulated
	Dopamine	Motility/secretion (ENS)	
	Noradrenaline		
Precursors to neuroactive compounds	Tryptophan	Precursor to 5-HT	Kynurenine is itself a metabolite of tryptophan, production subject to regulation by microbiota
	Kynurenine	, Kynurenic acid, quinolinic acid, Dopamine	
Bile acids	Secondary bile acids	Antimicrobial	Some effects mediated by bile acid receptors
Choline metabolites	Trimethylamine	Lipid metabolism (choline)	Metabolized in the liver to trimethylamine-N-oxide, linked to cardiovascular disease
HPA hormones	Cortisol	Stress response	Indirect regulation; HPA endocrine abnormalities prominent in stress-related psychiatric disorders
		Host metabolism	
		Anti-inflammatory	
		Wound healing	
GI hormones	Ghrelin	Host metabolism	Indirect regulation; possibly mediated by SCFAs via enteroendocrine cells
	Leptin	Appetite regulation	
	GLP1	GI motility/secretion	
	PYY		

Adapted from (Clarke, et al., 2014).

Due to the differences in the microenvironment (e.g., oxygen levels, pH, nutrient availability), the number and composition of the gut microbiota varies throughout the GI tract. For example, the highly acidic environment of the stomach result in it having the lowest number of microbes, ranging between 10^1 to 10^3. By comparison, the colon has the highest biodiversity of bacteria, ranging between 10^{10} to 10^{11} (Hillman, Lu, Yao, & Nakatsu, 2017). Over 400 bacterial phylotypes have been identified in the colon (Eckburg, et al., 2006), nearly all of which are anaerobic and few of which belong to known bacterial phyla – Firmicutes, Bacteriodetes, Proteobacteria, Verrumicrobia, Actinobacteria, Fusobacteria, and Cyanobacteria (Sommer & Bäckhed, 2013). Interestingly, there is a difference in the microbial populations found in the lumen versus in mucosal tissue samples (Eckburg, et al., 2006). A possible explanation for this difference is due to the presence of presence of two distinct mucus layers in the colon (Figure 5); the outer loosely adherent layer is colonized by bacteria while the inner strongly adherent layer is devoid of bacteria and acts as a physical barrier preventing direct contact between microbes and the underlying epithelium (Johansson, et al., 2008). In addition, the colonic mucosa secretes antimicrobial peptides to maintain the sterility of the inner mucus layer, and the monolayer of epithelial cells lining the colonic epithelium are connected by tight junctions to maintain the colonic mucosal barrier's integrity.
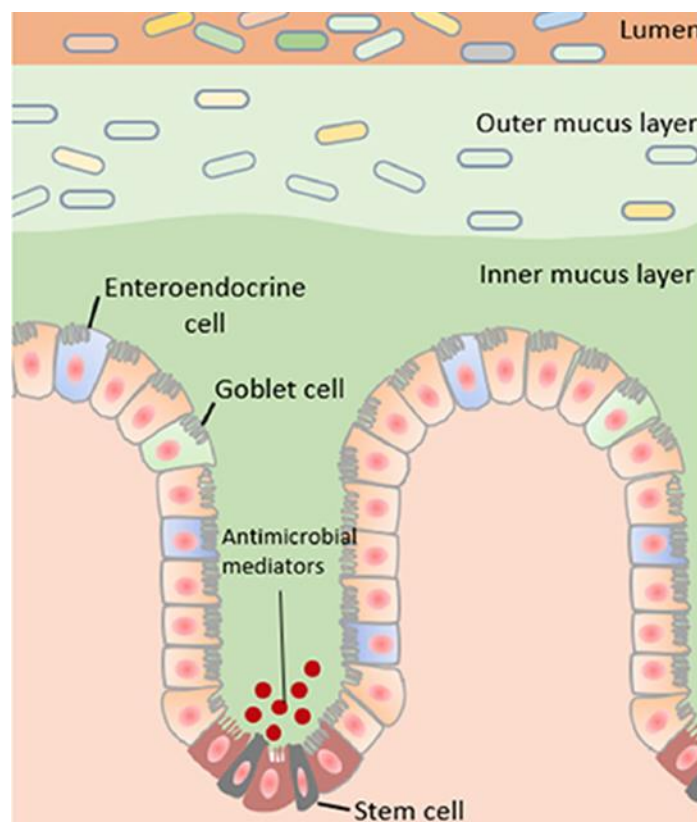
Figure 5 – Structure of the Mucus Layer in the Colonic Mucosa.

The colon contains two mucus layers: a stratified adherent inner mucus layer and loosely adhesive outer mucus layer. The inner mucus layer of the colon is essentially sterile and the outer mucus layer harbours the intestinal microbiota. Adapted from (Herath, et al. 2020).

1.2 The Intestinal Mucosa

The architecture of the intestinal mucosa consists of a monolayer of epithelial cells resting on a layer of connective tissue called the lamina propria, which contains myofibroblasts, blood vessels, nerves, and several different immune cells. The colonic mucosa and lamina propria are surrounded by the muscularis mucosae, a layer of smooth muscle. The architecture of the small intestinal mucosa is different from the colon (Figure 6). Both epitheliums form tube-like glands termed "crypts of Lieberkühn", or simply crypts. However, in the small intestines the epithelium project into the lumen termed villi.

The monolayer intestinal epithelium functions as a semipermeable barrier separating the luminal contents of the intestines from the internal milieu (Figure 7). Specifically, it allows the permeability of selective ions, nutrients, and water; physically and chemically inhibits the infiltration of pathogens and toxins; and coordinate gut immunity (Chelakkot, Ghim, & Ryu, 2018). The vanguard of this semipermeable barrier are the mucus layer(s). Next, the integrity of the colonic epithelium is maintained by numerous types of junctions along their lateral and basolateral membranes, with severe consequences when dysregulated. Lastly, the intestinal epithelium is supported by immune cells which coordinate gut immunity against pathogens, at the same time regulating tolerance against commensal microbes and dietary antigens.
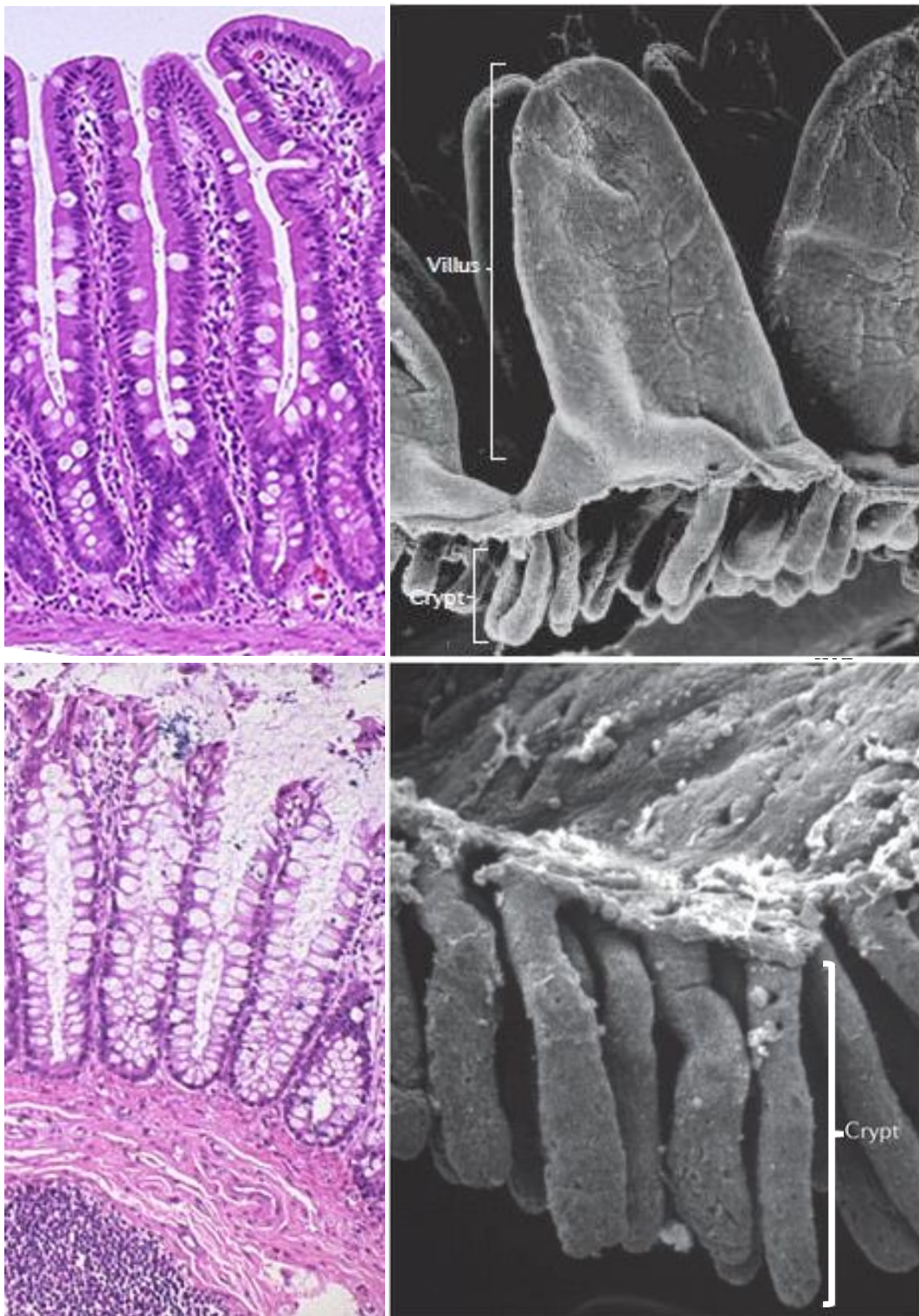
Figure 6 – Intestinal Mucosa Architecture.

(Left Column) Histological staining of human small-intestinal (top) versus colonic (bottom) mucosa, showcasing structural differences. Adapted from WebPath. (Right Column) Scanning electron micrographs of small-intestinal (top) versus colonic (bottom) epithelium from a mouse, illustrating crypts in both and villi in the small intestines. Adapted from (McCartney, Gleeson, & Brayden, 2016).
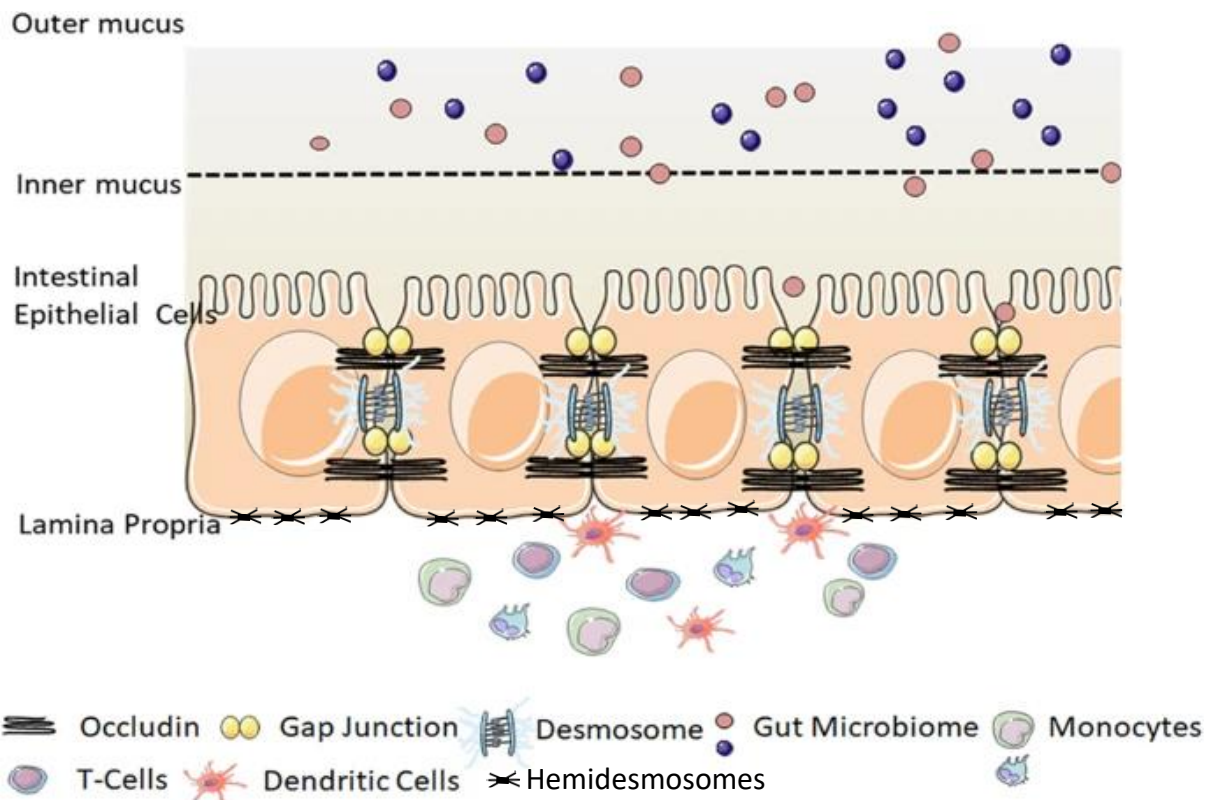
Figure 7 – The Colonic Epithelium's Semipermeable Barrier.

The monolayer colonic epithelium is a semipermeable barrier for selected nutrients and against the gut microbiome. It is anchored to the lamina propria by hemidesmosomes, and attached to neighbouring cells by desmosomes, adherens junctions, tight junctions (occludin) and gap junctions. In addition, it is supported by secreted mucus layers, immune cells (monocytes, T-cells, and dendritic cells) and specialized epithelial cells (not shown). Figure adapted from (Chelakkot, Ghim, & Ryu, 2018).

1.2.1 Mucus Layers

Throughout the GI tract, the mucosa's first level of protection is mucus secreted by epithelial goblet or mucus producing cells, which coat the entire gut lining and form a physical barrier against the luminal content (Johansson, Sjövall, & Hansson, 2013). The thickness of the mucus layer varies throughout the GI tract (Table 2). Compared to the stomach and large intestines, the small intestinal mucus layer possesses little to no firmly adherent layer, suggesting each mucus layer possessing distinct roles depending on their environment.

Table 2 – Mucus Thickness Comparison in the Gastrointestinal Tract.

Thickness (µm)	Stomach		Small Intestine			Large Intestine
	Corpus	Antrum	Duodenum	Jejunum	Ileum	Colon
Total	189 ± 11	274 ± 41	170 ± 38	123 ± 4	480 ± 47	830 ± 110
Firmly adherent	80 ± 5	154 ± 16	16 ± 3	15 ± 2	29 ± 8	116 ± 51
Loosely adherent	109 ± 12	120 ± 38	154 ± 39	108 ± 5	447 ± 47	714 ± 109

Adapted from (Atuma, Strugala, Allen, & Holm, 2001).

Mucus is an aqueous viscoelastic secretion composed of mainly water (95%), electrolytes (1%), free proteins (1%), glycoproteins (1%), lipids (1%), and other molecules (Creeth, 1978). However, their composition varies depending on their underlying secretory epithelium, which affects its physicochemical properties such as: pore size, viscoelasticity, pH, and ionic strength (Leal, Smyth, & Ghosh, 2018). Electrolytes are an important component of GI mucus since its composition is capable of affecting its hydration and rheology. Increased concentrations of divalent cations (Mg^{2+} or Ca^{2+}) causes the collapse of the mucus gel (Verdugo, Aitken, Langley, & Villalon, 1987), while increased concentrations of monovalent cations (Na^+ or K^+) reduces its viscosity (Snary, Allen, & Pain, 1971). Secretion of hydrochloric acid in the stomach increases the viscosity of gastric mucus due to it gelling below pH 4 (Celli, et al., 2007). Bicarbonate buffers the mucus layer adjacent to the epithelium to pH 7; particularly important in the stomach where it establishes a protective pH gradient through the mucus gel layer against hydrochloric acid secretion (Allen & Flemström, 2005). Most mucus secretions contain similar concentrations of electrolytes: sodium and potassium chloride, sodium bicarbonate, phosphate, magnesium, and calcium; approximately isotonic with serum at approximately 1% (w/v) total concentration (Bansil & Turner, 2018).

Free proteins which are present in GI mucus secretions mainly function to defend the mucus layer against pathogens. Defensive proteins which contribute to protecting the intestinal mucus against pathogens include: antimicrobial peptides alpha and beta defensins (Mahida

& Cunliffe, 2004), Gram-positive bacterial cell wall digestive enzyme lysozyme (Syngai & Ahmed, 2019), REG3A which is the human analogue of bacterial lectin REG3γ (Cash, Whitham, Behrendt, & Hooper, 2009), immunoglobin A which binds to and cause microbial aggregation (Slack, Balmer, & Macpherson, 2014), and antiprotease WFDC2 which prevents the premature conversion of inner mucus layer to the outer layer in health by inhibiting bacterial serine and cysteine proteases (Parikh, et al., 2019). Besides proteins, secreted reactive oxygen species such as hydrogen peroxide protects the mucus at low concentrations while damaging it at high concentrations (Brownlee, Knight, Dettmar, & Pearson, 2007). Lipids secreted in the GI mucus have been speculated to prevent microbial invasion of the epithelium (Carlson, Yildiz, Dar, Lock, & Carrier, 2018). Other molecules present in mucus are sugars and growth factors. Sugars such as fucose are induced by gut bacteria to serve as food source for beneficial gut symbionts, as well as suppress the virulence of pathogens and pathobionts (Pickard & Chervonsk, 2015).

Mucin glycoproteins are major structural component of mucus, consisting of a protein backbone of multiple tandem repeats of Serine and Threonine (ST repeats) where oligosaccharides are covalently O-linked (Perez-Vilar J. , 2007). The N- and C-terminals of this protein have little or no glycosylation, but are rich in cysteines, leading to dimerization and further multimerization via disulphide bonds (Bansil & Turner, 2018). Seventeen mucin genes have been identified in humans (NCBI, 2020), twelve of which are present in the human GI tract and can be classified as transmembrane or gel-forming (Table 3). In the mouth, salivary glands produce MUC5B and MUC7, which lubricate ingested food for passage through the oesophagus (Wickström, Davies, Eriksen, Veerman, & Carlstedt, 1998), (Bobek, Tsai, Biesbrock, & Levine, 1993). The stomach has two layers of mucus, built by the MUC5AC and MUC6 mucins secreted by distinct cell types (Ho, et al., 1995). The small intestine's one mucus layer is composed of MUC2, which is also the major component of both mucus layers in the colon; showcasing MUC2 possessing differential properties and functions in the small versus the large intestine.

Table 3 – Mucin Nomenclature in the Human GI Tract.

Mucin (type)	Number of amino acids	No. of mucin domains (and estimated length)	Cell type expression	Function
MUC1 (transmembrane)	~1,250	1 (~200 nm)	Epithelial cells	Signalling, protection
MUC2 (gel-forming)	~5,200	2 (~550 nm)	Goblet cells Paneth cells	Protection, lubrication, entrapment
MUC3 (transmembrane)	>2,550	1 (>350 nm)	Enterocytes	Apical surface, protection
MUC4 (transmembrane)	~5,300	1 (~800 nm)	Epithelial cells Goblet cells	Signalling, protection
MUC5AC (gel-forming)	>5,050	11 (>350 nm)	Mucous cells	Protection, lubrication, entrapment
MUC5B (gel-forming)	~5,700	7 (~550 nm)	Mucous cells Goblet cells	Protection, lubrication, entrapment
MUC6 (gel-forming)	~2,400	1 (~250 nm)	Mucous cells	Protection, lubrication, entrapment
MUC7 (gel-forming)	377	1 (~230 nm)	Mucous cells	Protection
MUC12 (transmembrane)	~5,500	1 (~1000 nm)	Enterocytes	Apical surface protection
MUC13 (transmembrane)	512	1 (~30 nm)	Enterocytes	Apical surface protection
MUC16 (transmembrane)	~22,000	1 (~2400 nm)	Epithelial cells	Apical surface protection
MUC17 (transmembrane)	~4,500	1 (~800 nm)	Enterocytes	Apical surface protection

Adapted from (Johansson, Sjövall, & Hansson, 2013).

Transmembrane mucins are found in the apical pole of the cells (Figure 7). As their name suggest, they possess a transmembrane domain that enables them to be anchored in the cell membrane. High levels of glycosylation shield the protein backbone of the extracellular domain from proteolytic attack by bacteria and host proteases. A wide range of oligosaccharides can be attached to mucins (Burdick, Harris, Reid, Iwamura, & Hollingsworth, 1997) and the structure of their glycans both within and between cell types (Hilkens, Buijs, & Ligtenberg, 1989). Under healthy conditions, the extended domains of transmembrane mucins form the dense enterocyte glycocalyx that is impermeable to virus- or bacteria-sized particles (Frey, et al., 1996). For example, MUC1 have been shown to protect against infection of bacterial pathogens *Helicobacter pylori* and *Campylobacter jejuni* in the stomach (Lindén, et al., 2009) and intestines (McAuley, et al., 2007), respectively.

The extracellular domains of transmembrane mucins either have a SEA-domain (MUC1, 3, 12, 13, 17) or NIDO-AMOP-vWD domains (MUC4) (Johansson, Sjövall, & Hansson, 2013). Though both these domains are cleaved during biosynthesis, they remain held together by strong non-covalent bonds. The SEA-domain is cleaved during folding in the endoplasmic reticulum by an autocatalytic mechanism (Levitin, et al., 2005) and (Macao, Johansson, Hansson, & Härd, 2006), yet are held together by four β-pleated sheets – two from the outer part of the mucin domain and two from the membrane anchored part. This led to the suggestion that SEA-domains evolved to protect epithelial cells from rupture by dissociating at the apical cell membrane because of mechanical stress (Macao, Johansson, Hansson, & Härd, 2006). That suggestion was later validated when they demonstrated the mechanical stress required to break the SEA-domain was smaller than the forces necessary for disrupting the membrane (Pelaseyed, et al., 2013). The same group also suggest epithelial cells can register mechanical shear at the mucosal surface if the dissociation is signalled via loss of the SEA-domain (Macao, Johansson, Hansson, & Härd, 2006). The breakage of the transmembrane mucins' extracellular domain can be detected in serum, the lumen of the intestinal tract, and culture supernatants of mucin-expressing cells. Excessive shedding of transmembrane mucin extracellular domains is often observed for metastatic carcinoma (Smorodinsky, et al., 1996), IBD (Shirazi, Longman, Corfield, & Probert, 2000), and cystic fibrosis (Khatri, Ho, Specian, & Forstner, 2001). For MUC4's NIDO-AMOP-vWD domains, it is cleaved in the vWD (von Willebrand D) domain by unclear mechanisms, though enzymatic and autocatalytic processes have been suggested (Soto, Zhang, & Carraway, 2006), (Lidell & Hansson, 2006). As for the remaining transmembrane MUC16, it is cleaved close to the transmembrane domain in an acidic compartment of the Golgi complex dependent on the acidic pH in the secretory pathway that is not yet elucidated (Das, et al., 2015). The normal functions of the transmembrane mucins are not fully understood, though high glycosylation of all transmembrane mucins likely contributes to maintaining a diffusion barrier in the gastrointestinal tract by inhibiting the passage of large molecules, thus ensuring a stable apical cell membrane milieu. The shed domains have been proposed to act as decoy receptors for pathogens, or can be sensed by the cell by activating signalling pathways through the intracellular cytoplasmic tail (van Putten & Strijbis, 2017).

The intracellular mucin domains of transmembrane mucins are linked to signalling pathways. All transmembrane mucin's intracellular tails contain putative phosphorylation sites, though they are dissimilar in sequence and length and do not contain any conserved domains, which suggest a high degree of functional divergence and likely signalling specificity between different transmembrane mucins (van Putten & Strijbis, 2017). In MUC3, MUC12 and MUC17, their cytoplasmic tails contain binding motifs that are instrumental in the trafficking and anchoring of receptor proteins and organize signalling complexes at the cell membrane (Lamprecht & Seidler, 2006). Through that binding motif, those mucins are functionally linked with the cystic fibrosis transmembrane conductance regulator (CFTR) chloride channel, which contains the same binding motif. MUC3 was shown to compete with CFTR for the same binding motif of a protein that targets them for lysosomal degradation, thus regulating the levels of both proteins (Pelaseyed & Hansson, 2011). In addition, stimulating enterocytes with carbachol – a cholinomimetic drug and structural analogue of the neurotransmitter acetylcholine – led to recruitment of CFTR to the plasma membrane and caused internalization of MUC17, but not MUC3 or MUC12 (Pelaseyed, Gustafsson, Gustafsson, Ermund, & Hansson, 2013). The reason why only MUC17 was internalized is not understood. The cytoplasmic tail of MUC1 can be phosphorylated at several conserved tyrosines, which mediates its interaction with other proteins (Wang, Lillehoj, & Kim, 2003). For example, phosphorylated MUC1 cytoplasmic tail promotes tumorigenicity by competing with E-cadherin for the binding of β-catenin, which destabilizes the β-catenin/E-cadherin complex and bind to the Wnt signalling transcription factors to promote anchorage-independent growth (Huang, et al., 2005).

The main functions of the gel-forming mucins are to protect and lubricate the gastrointestinal tract. All gel-forming mucins have central mucin domains flanked by an N-terminal part involved in oligomerisation and a C-terminal region involved in forming dimeric structures. Using their N-termini and C-termini these mucins form large polymers that, together with the mucin domains, form the protective gel lining the gastrointestinal tract (Kim & Ho, 2010). In the intestines, MUC2 is the prominent gel-forming mucin secreted by intestinal goblet cells. MUC2 consist of highly glycosylated tandem repeats of MUC2 mucins with cysteine-rich domains on both terminals. In addition, MUC2 is resistant to endogenous proteases due to glycans attached to the central mucin domains (Johansson, Sjövall, & Hansson, 2013). Human digestive enzymes are unable to digest glycans, suggesting a coincidental development during evolution to enable the intestines to digest amino acid bonds while maintaining the protective properties of MUC2 mucins.

MUC2 is synthesized in the endoplasmic reticulum and form disulfide-linked dimers, then transported to the *cis*-Golgi compartments where they are O-glycosylated, and finally reaches the *medial-* and *trans*-Golgi compartments where glycosyltransferases complete the biosynthesis of the O-linked oligosaccharides (Asker, Axelsson, Olofsson, & Hansson, 1998),

(Perez-Vilar & Hill, 1999). Before being released, MUC2 is packed in and stored in secretory granulae as five-, six-, and seven-sided ring structures. The synthesis, packaging, and release of MUC2 is pH and Ca^{2+}-dependent (Ambort, et al., 2012). The pH starts at 7.2 in the endoplasmic reticulum, drops to 6.0 in the trans-Golgi compartments, and is 5.2 in the secretory granulae. On the flipside, the concentration of intracellular calcium concentration is high during synthesis and packaging but is chelated during release. Upon release, the mucin unfolds and expands >1,000-fold in volume, forming nets that spontaneously organize into flat sheets with a tendency of stacking on top of one another in a lamellar structure (Round, et al., 2012). The secreted mucus layer remains anchored to the epithelial cells (Johansson, Sjövall, & Hansson, 2013); it cannot be aspirated off (thus its original name of firmly attached), is highly organized, is impenetrable to bacteria, and in the colon is renewed by surface goblet cells with a turnover time of an hour (Johansson M. E., 2012). By comparison, the outer mucus layer is loosely adherent and colonized by commensal bacteria. The conversion of the inner mucus layer to the outer mucus later occurs at a demarcation line that is much closer to the epithelium in the small intestines compared to the colon (Table 2). The exact mechanisms of conversion from inner to outer mucus layer remains a matter of contention. One suggestion is host-derived proteoses, which cleaves between MUC2 domains and allow the mucin to expand 3–4 times in volume without disrupting the polymeric network, as protease inhibitors partly inhibited the transition from firm to loose and is unaffected by germ-free mice (Johansson, et al., 2008). An alternative suggestion proposed the inner layer to be degraded by proteoses secreted by mucin-degrading species which use polysaccharides of MUC2 as an energy source (Okumura & Takeda, 2018) when deprived of dietary fibre, which degrades the colonic mucus barrier and enhance pathogen susceptibility (Desai, et al., 2016).

1.2.2 Lateral and Basolateral Membrane Junctions

The intestinal epithelium is anchored to the lamina propria along their basolateral membranes by multiprotein complexes called hemidesmosomes. One hemidesmosome protein which maintains epithelial basolateral membrane integrity is the α6β4 integrin receptor, which interconnects the BM laminin-332 to keratin filaments through the cytoplasmic-linker protein plectin (Nievers, Schaapveld, & Sonnenberg, 1999). In addition to adhering, hemidesmosomes can also act as signalling centres to regulate proliferation and differentiation (Borradori & Sonnenberg, 1999). One recent study has linked hemidesmosome dysfunction with colorectal diseases; mice with mutant α6 integrin spontaneously developed colitis which degenerated into infiltrating adenocarcinoma (De Arcangelis, et al., 2017).

The intestinal epithelium's lateral integrity is maintained by tight junctions (also known as occludin, the first tight junction protein identified), adherens junctions, and desmosomes, which connect and seal the paracellular space between neighbouring epithelial cells along their lateral membranes (France & Turner, 2017). Tight junctions are composed of numerous transmembrane and cytosolic proteins which interact with each other and with the cytoskeleton to form a complex architecture (Günzel & Yu, 2013). Dysregulation of tight

protein junctions have severe consequences for the intestinal epithelium. For example, downregulation of claudin-5 and claudin-8 has been shown to reduce epithelial barrier integrity (Zeissig, et al., 2007). In contrast, claudin-2 – which was found to be highly expressed in leaky epithelial tissues – was upregulated in IBD and promotes inflammation (Ahmad, et al., 2014).

Desmosomes are proteins which link to the intermediate filament cytoskeleton intracellularly, forming a hyper-adhesive network of bonds that result in the tissue resisting mechanical stress (Garrod & Chidgey, 2008). Specific genetic (ectodermal dysplasia, epidermolysis bullosa) and autoimmune (pemphigus vulgaris) diseases result in desmosomal adhesion failure, resulting in the tissues breaking due to mechanical stress. Desmosomal dysregulation have also been linked to colorectal cancer. One of the essential constituents of desmosomes are desmocollins, members of the desmosomal cadherin family of cell-cell adhesion molecules, of which 3 (Dsc1, Dsc2, Dsc3) has been described in humans. Dsc2 expression was found to be reduced in human adenocarcinoma, accompanied by increased expression of Dsc1 and Dsc3 (Khan, et al., 2006).

Adherens junctions initiates and maintains cell–cell adhesion, regulates the organization of the underlying actin and microtubule cytoskeleton, and establishes a hub for cell signalling and regulation of gene transcription (Takeichi, 2014). The main components of adherens junctions are members of the classical cadherin superfamily, such as epithelial cadherin (E-cadherin), neural cadherin (N-cadherin), placental cadherin (P-cadherin), as well as members of the catenin family of proteins, namely p120 catenin (p120), α-catenin, and β-catenin (Harris & Tepass, 2010). In the colonic epithelium, the main type of transmembrane protein comprising adherens junctions are E-cadherin, which has five extracellular cadherin repeat domains that engage in Ca^{2+}-dependent *trans* binding to a cadherin on the opposing cell surface (Shapiro & Weis, 2009). Disruption of adherens junctions can lead to numerous diseases, including inflammation and cancer (Daulagala, Bridges, & Kourtidis, 2019), (Bhat, et al., 2019). In particular, E-Cadherin has been shown to be a tumour-suppressor, by keeping β-catenin – a component of the pro-tumorigenic Wnt/B-catenin signalling pathway (Clevers H. , 2006) – at cell-cell contact areas, as opposed to the nucleus (Huels , et al., 2015).

In addition to tight junctions, adherens junctions and desmosomes, neighbouring intestinal epithelial cells are connected by gap junctions. Gap junctions consist of protein oligomers belonging to the connexin family. Six connexins oligomerize on the plasma membrane to form a connexon hemichannel, which align with a connexon hemichannel from a neighbouring cell to form a gap junction with a 2–4 nm gap connecting both cells (Meşe, Richard, & White, 2007). From this gap, they allow cell-cell exchange of cytoplasmic contents – ions, electrical signals, small molecules – and play a key regulatory role in cell differentiation and growth (El-Sabban, et al., 2003), (El-Sabban, Abi-Mosleh, & Talhouk , 2003). Gap junctions are voltage

gated (Bukauskas & Weingart, 1993), meaning they can be regulated rapidly (milliseconds) to coordinate intercellular communication. They are also regulated at a slower pace (hours) by the turnover rate of connexin, as well as regulating connexin biosynthesis and junctional plaque assembly (Goodenough & Paul, 2009). Gap junctions can promote and inhibit tumorigenesis in a complicated fashion; cell-surface expression of connexin-43 reduces tumour growth by increasing the expression of tumour suppressor gene coding p27 (Zhang, Morita, Ikeda, Ma, & Murota, 2001), yet the carboxyl-terminal tail of connexin-43 promotes cell-migration via p38 (Behrens, Kameritsch, & Wallne, 2010) and promotes tumour growth by interacting with β-catenin (Spagnol, et al., 2018). Cell-surface expression of Connexin-32 was also shown to inhibit tumorigenesis by enhancing cell-cell aggregation and thus prevent migration.

1.2.3 Immune Cells

Besides cell-cell adhesion, numerous types of immune cells function in close relation with intestinal epithelial cells to coordinate gut immunity and maintain tissue homeostasis. These include mononuclear phagocytes (dendritic cells and macrophages) and lymphocytes (T-cells and B-cells). They reside in gut-associated lymphoid tissue (GALT) distributed throughout the GI tract or in regional lymph nodes. In the small intestines, Peyer's patches have been well characterized as an important site for coordinating an immune response. In the large intestine, most lymphoid tissues are found on the serosal side of the muscularis mucosae, which protrude through the muscularis and form a narrow interface with the lumen (O'Leary & Sweeney, 1986). But besides that, the lamina propria of the large intestines is also home to isolated immune cells.

Intestinal dendritic cells are antigen presenting cells that reside in the lamina propria and act as sentinels. Without perturbing tight junctions and epithelial integrity, they acquire antigens either by sampling the luminal contents via the formation of transepithelial dendrites (Niess, et al., 2005) or accept antigens presented by epithelial cells. They then deliver it to lymphoid tissues to activate naïve T-cells (Stagg, Hart, Knight, & Kamm, 2003). Besides activating T-cells against pathogens, intestinal dendritic cells also mediate tolerance to dietary antigens, mediate immune tolerance against commensal bacteria, and are characterized in distinct subsets that have differential abilities in the colon versus the ileum (Esterházy, et al., 2016), (Stagg A. J., 2018), (Mann, et al., 2015). Also residing in the lamina propria are gut macrophages, which phagocytose bacteria that manages to cross the epithelial barrier and efferocytose apoptotic and senescent epithelial cells (Bain & Schridde, 2018). Monocytes perform similar functions to dendritic cells; they sample luminal bacteria (Kim , et al., 2011) and generating tolerance to dietary antigens (Mazzini, Massimiliano, Penna, & Rescigno, 2014). While intestinal monocytes have not been demonstrated to be effective at activating T-cells, they have been suggested to be involved in presenting antigens to locally activated T-cells (Schulz, et al., 2009). This is due to their high expression of MHCII, which when deleted in CX$_3$CR1+ monocytes decreased generation and/or maintenance of regulatory T-cells (Kim,

et al., 2019). Besides the mucosa, macrophages have also been identified in the submucosa and muscularis. In the submucosa they play a role in maintaining submucosal vasculature (De Schepper, et al., 2018), while in the muscularis they crosstalk with enteric neurons to regulate gastrointestinal motility (Muller, et al., 2014). Thus, similar to dendritic cells, macrophages fulfil niche-specific functions to meet the local demands of their microenvironment.

Lymphocytes (T-cells and B-cells) reside in lymph nodes and circulate through the lymphatic and blood circulatory system. However, lymphocytes are also present in nonlymphoid organs, especially in barrier tissues such as the intestines. Two types of T-cells have been characterized in the intestines: Conventional T-cells which reside close to the epithelium and in the lamina propria, and Nonconventional T-cells which mostly reside close to the epithelium (Table 2). T-cells mediate protective immune responses against viral infections by cytolysis of dysregulated intestinal epithelial cells and cytokine-mediated re-growth of healthy intestinal epithelial cells, and against bacterial infections by directly killing or producing cytokines (Ma, Tao, & Zhu, 2019). In addition, regulatory T-cells which are CD4$^+$ and express FOXP3 have been shown to mediate tolerance against dietary antigens and commensal microbes (Bilate & Lafaille, 2012). However, FOXP3-mediated tolerance seems to only apply in the colon (Atarashi, et al., 2014); while the numbers of FOXP3$^+$ regulatory T-cells in the colonic lamina propria is reduced in germ-free mice compared to normal mice, their numbers remain unchanged or is increased in various parts of the small intestinal lamina propria. This indicates a microbiota-independent induction of regulatory T-cells occurring in the small intestine that is yet to be elucidated. Furthermore, prominent commensal bacteria have been shown to induce and maintain FOXP3$^+$ regulatory T-cells in the colon via the immunomodulatory molecule, polysaccharide A (Round & Mazmanian, 2010). More interestingly, in that study polysaccharide A was shown to prevent and cure experimental colitis in animals, showcasing an example of the gut microbiome interacting with the host immune machinery in mutual symbiosis.

B-cells reside in small intestinal Peyer's patches or regional lymph nodes. Upon receiving the right signals from dendritic cells or helper T-cells, they undergo clonal expansion, hypermutation and selection into plasmablasts, which enter the bloodstream via the lymphatic system (Spencer & Sollid , 2016). These plasmablasts then home towards the lamina propria, where they differentiate into plasma cells and secrete IgA antibodies. These secreted antibodies are transported across the epithelium and bind to antigens to mediate immune exclusion and antigen clearance (Palm, et al., 2014). B-cells ensure persistent memory against gut pathogens and other antigens due to long-lived memory B-cells replenishing short-lived plasma cells. Although recent studies suggest some plasma cells may be long-lived (Nair, et al., 2016).

1.3 The Intestinal Epithelium

The intestinal epithelium consists of a continuous monolayer of epithelial cells. In the small intestines, the epithelium protrudes into the lumen as villi and forms invaginations called crypts (Figure 6), the which latter of which was discovered by Jonathan Lieberkühn in the 18th century. In the colon, the epithelium only form crypts. The intestinal epithelium renews itself within 5-7 days (Clevers H. , 2013), making it one of the fastest renewing tissues in the body. This renewal is driven by intestinal stem cells (ISCs) residing at the base of crypts. The current accepted model is that under homeostasis, ISCs proliferate once per day asymmetrically into a daughter stem cell and a daughter transit-amplifying cell (Barker, van de Wetering, & Clevers, 2008). However, ISCs may proliferate symmetrically into two daughter stem cells to maintain the ISC pool (Sei, Feng, Chow, & Wank, 2019). Transit-amplifying cells undergo up to six rounds of cell division within 2 to 3 days into specialized epithelial cells (Marshman, Booth, & Potten, 2002), which migrate up the crypt axis within a matter of days, detach from the basement membrane and are shed into the gut lumen where they undergo apoptosis. Besides maintaining a continuous intestinal epithelium to ensure mucosal barrier integrity, ISCs are responsible for tissue repair following stress and injury. The intestines are capable of surviving after losing their active ISCs by ionizing radiation (Kim, Yang, & Bialkowska, 2017), and stresses due to gastrointestinal infection (Hou, Ye, Huang, & Yu, 2017) or weaning (Chen, et al., 2019) elicits higher rates of ISC proliferation.

1.3.1 Intestinal Stem Cells

Multipotent ISCs reside at base of intestinal crypts, from the gut lumen. In the small intestines, stem cells are flanked by Paneth Cells which secrete antimicrobial peptides and proteins, as well as factors which help sustain and modulate stem and progenitor cells (Clevers & Bevins, 2013), (Figure 8). In contrast, stem cells of the colon are flanked by deep crypt secretory cells which are functionally equivalent to Paneth cells (Sasaki, et al., 2016), (Figure 2C). In addition, GL1-expressing subepithelial mesenchymal cells secrete Wnt signals to maintain the colonic stem cell niche (Degirmenci, Valenta, Dimitrieva, Hausmann, & Basler, 2018). Regulating proliferation and shedding is crucial to achieving crypt homeostasis. Numerous signals are capable of influencing ISCs, key ones being Wnt, Notch, BMP and TGF-β. Excessive shedding results in compromised mucosal barrier that is susceptive to infection (Okumura & Takeda, 2018), while insufficient cell death results in accumulation of genetic mutations that may led to tumorigenesis (Medema & Vermeulen, 2011).

Austrian physician Joseph Paneth (1857–1890) was the first person to propose stem cells to be the origin of epithelial cells lining the small-intestinal crypt and villi (Paneth, 1887). Several years later, intestinal mitosis was shown to only occur in crypts, thus daughter cells from crypts were concluded to extrude to the epithelium (Bizzozero, 1893). Half a century later, two significant studies by Charles Leblond demonstrated rat intestinal crypts producing large numbers of cells with life-spans lasting days, which the authors remarked "cells formed in the crypts of Lieberkühn move upward along the side of the villi to be ejected when they reach

the villi tips" (Stevens & Leblond, 1947), (Leblond & Stevens, 1948). Leblond published numerous papers for the next two decades, one which demonstrated the presence of 'column-like' cells wedged between Paneth cells at the base of small intestinal crypts, which they termed crypt-base-columnar (CBC) cells (Cheng & Leblond, 1974). Subsequent clonal labelling studies visualized the ribbon-like flow of cells from crypt-base to villus-tips (Winton, Blount, & Ponder, 1988), confirming Paneth's proposal a century prior. A latter clonal labelling study identified long-lived stem cells, which form a ribbon-like flow comprising most cell lineages from the crypt base to the villus; and short-lived cells restricted to the transit-amplifying compartment of the crypt (Bjerknes & Cheng, 1999).
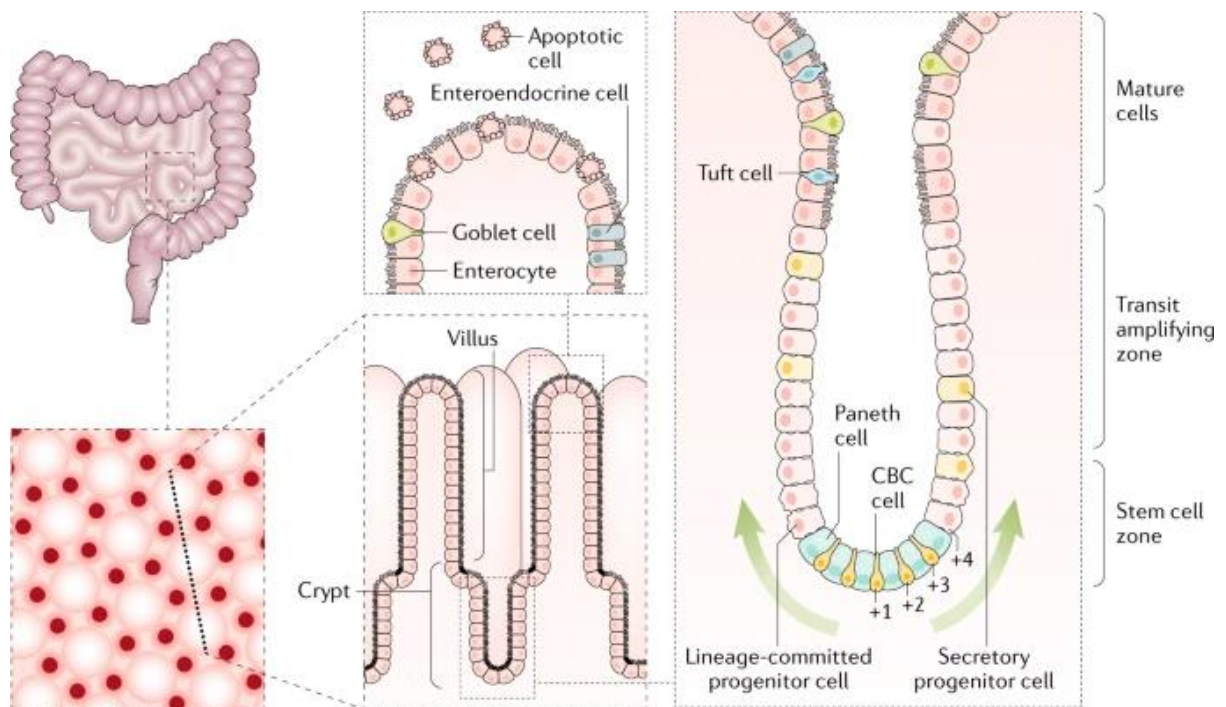
Figure 8 – Zones in the Small-Intestinal Epithelium.

The small-intestinal epithelium consists of villus protrusions and crypt invaginations. At the bottom of crypts and wedged between Paneth cells, crypt base columnar (CBC) cells proliferate continuously to generate new cells that differentiate and migrate towards the villus. Above the stem cell zone, lineage-committed progenitors divide rapidly in the transit-amplifying zone. Mature epithelial cells emerge from the transit-amplifying zone and move towards the villus tip where they undergo apoptosis. Adapted from (Gehart & Clevers, 2018)

The small-intestinal "stem cell zone" is defined as the region in which CBC cells and Paneth cells reside, encompassing the entire crypt base and up to five cells away from the uppermost Paneth cell (Bjerknes & Cheng, 1981). The colon "stem cell zone" is similar, except Paneth cells are replaced by Deep Crypt Secretory cells (Sasaki, et al., 2016). In the past two decades, dozens of markers have been proposed to be specific to ISCs. Key ones are listed in (Table 4). The first candidate marker for ISCs was a RNA-binding protein known to maintain neural stem cells, Musashi-1, (Kayahara, et al., 2003) and (Potten, et al., 2003). Kayahara and colleagues identified Musashi-1 in mice intestines, stomach, brain, and liver using RT-PCR; and using immunohistochemistry, showed Musashi-1 was expressed in small-intestinal CBC cells and a few cells just above Paneth cells, but importantly do not label Paneth cells. Potten and colleagues went further, using qRT-PCR and in situ hybridization they found higher expression of Musashi-1 mRNA in mice with small intestinal adenomas compared with adjacent normal tissue. However, in human samples they had weak antibody staining. Furthermore, they observed Musashi-1 staining more cells per crypt than the predicted number of actual stem cells per crypt. Collectively, this suggests Musashi-1 is not an exclusive marker of mice ISCs.

The most well-characterized marker for CBC cells of the small intestines and colon is the Leucine-rich repeat-containing G-protein coupled receptor 5 (Lgr5), identified by Hans Clevers' group (Barker, et al., 2007). In that study, they generated two sets of mice with knock-in alleles: one which causes the expression of the lacZ reporter at the amino-terminal of the Lgr5's first transmembrane domain, and one with EGFP-IRES-creERT2 at the first ATG codon of Lgr5. Lgr5^{lacZ} mice expressed lacZ-positive cells in the crypt base of the small intestine and colon, as well as the base of glands in the stomach. Similar to Lgr5^{lacZ} mice, Lgr5$^{EGFP-IRES-creERT2}$ mice expressed EGFP at the base of intestinal crypts. Next, they crossbred Lgr5$^{EGFP-IRES-creERT2}$ mice with Cre-activatable Rosa26-lacZ mice and performed histological analysis between 1-60 days post-tamoxifen induction (Figure 9A). While the progeny of Lgr5$^{EGFP-IRES-creERT2}$ cells will no longer express EGFP due to genetic recombination, they have an activated lacZ reporter to enable lineage tracing. After 1-day post-tamoxifen, lacZ cells were expressed exclusively at the bottom of intestinal crypts (Figure 9B-C), and after 60 days ribbons of lacZ cells were seen from the bottom of crypts to the tip of villus (Figure 9D-E). In addition, they showed co-expression of induced clones and other epithelial markers (Figure 9F-H). Thus, they confirmed Lgr5 to be a marker of multipotent stem cells of the small intestine and colon. However, Lgr5 is a challenging marker due to it being expressed in low levels, has low surface abundance, and lacks high-affinity anti-Lgr5 antibodies.

Besides Lgr5, two other candidate markers of intestinal CBC are OLFM4 and PTK7. Using in situ hybridisation, the Clevers group showed OLFM4 was highly expressed in CBC cells in human small intestines and colon, and in colon adenocarcinomas (van der Flier, Haegebarth, Stange, van de Wetering, & Clevers, 2009). A subsequent study by the group replicated the knock-in allele experiment they designed for Lgr5; OLFM4$^{EGFP-IRES-creERT2}$ mice were crossed with Cre-activatable Rosa26-lacZ mice to perform lineage tracing (Schuijers, van der Flier, van

Es, & Clevers, 2014). The lineage tracing results of OLFM4 in the small intestines were noted to be remarkably similar to Lgr5. However, LacZ-positive cells were not observed in the colon, stomach, bone marrow, or liver. They suggest this was due to OLFM4 having a more limited function in mice, as OLFM4 RNA was strongly expressed in the prostate, small intestine, and colon, moderately expressed in the bone marrow and stomach (Zhang, et al., 2002). Hence, they conclude OLFM4 to be an alternative tool to Lgr5 for characterizing ISCs.

As for PTK7, it was identified and quantified in cultured human colonic organoids (Jung, et al., 2015). Flow-cytometry analysis of these cultures revealed heterogeneous (i.e., diverse) surface expression of PTK7. They then performed quantitative mass spectrometry on organoids cultured with proliferation-promoting media (WNT3a, R-SPO, EGF, and Noggin; WREN) and organoids cultured treated with differentiation-promoting media (EGF and Noggin; EN). Organoids treated with WREN media had over 200 proteins that were enriched more than 2-fold, one of which was PTK7, and also markers of enteroendocrine lineage such as CHGA and CHGB. Organoids treated with EN media had over 100 proteins that were enriched, including mucus secreting MUC2, enterocyte FABP1, and enteroendocrine DPP4. Next, organoids were sorted using fluorescence-activated cell sorting (FACS) into PTK7-high and PTK7-low cells, and their ability to form organoids was compared. The organoid-forming capacity of PTK7-high cells were 16 times higher compared to PTK7-low cells. PTK7-high cells also had higher expression of stem cell marker Lgr5, and decreased expression of enterocyte marker FABP2. Thus, they concluded PTK7+ cells display features similar to Lgr5+ cells and include a fraction of cells that undergo differentiation into enteroendocrine cells.

Table 4 – List of Prominent Intestinal Stem Cell markers.

Marker (Year Discovered)	Function	Note
Musashi-1 (2003)	RNA-binding protein known to maintain neural stem cells	Not an exclusive marker of ISC
Lgr5 (2007)	Wnt target gene	Best characterized marker specific to ISCs
Bmi-1 (2008)	Essential in the self-renewal of hematopoietic and neural stem cells	Previously thought to mark +4 ISCs
TERT (2008)	Telomerase reverse transcriptase	Marks slow cycling stem cells distinct from Lgr5
ASCL2 (2009)	A Wnt target gene	Master regulator of ISC identity
DCAMKL-1 (2009)	Microtubule-associated kinase expressed in post-mitotic neurons,	Marker of quiescent ISCs and cancer stem cells
OLFM4 (2009)	Secreted protein that inhibits BMP and promotes proliferation	Alternative tool to characterize ISCs
Prominin-1 (2009)	Transmembrane glycoprotein commonly expressed by cancer stem cells	Marks small intestinal stem cells susceptible to tumorigenesis
SMOC2 (2012)	BMP signalling inhibitor	Marker of CBC cells
EPHB2 (2011)	A receptor tyrosine kinase required to position different cell types along the crypt axis	Surface marker for purifying colon stem cells
PTK7 (2015)	Regulator of Wnt signalling, heavily involved in embryogenesis	Labels Lgr5 cells, as well as LRCs

Adapted from (Umar, 2011).
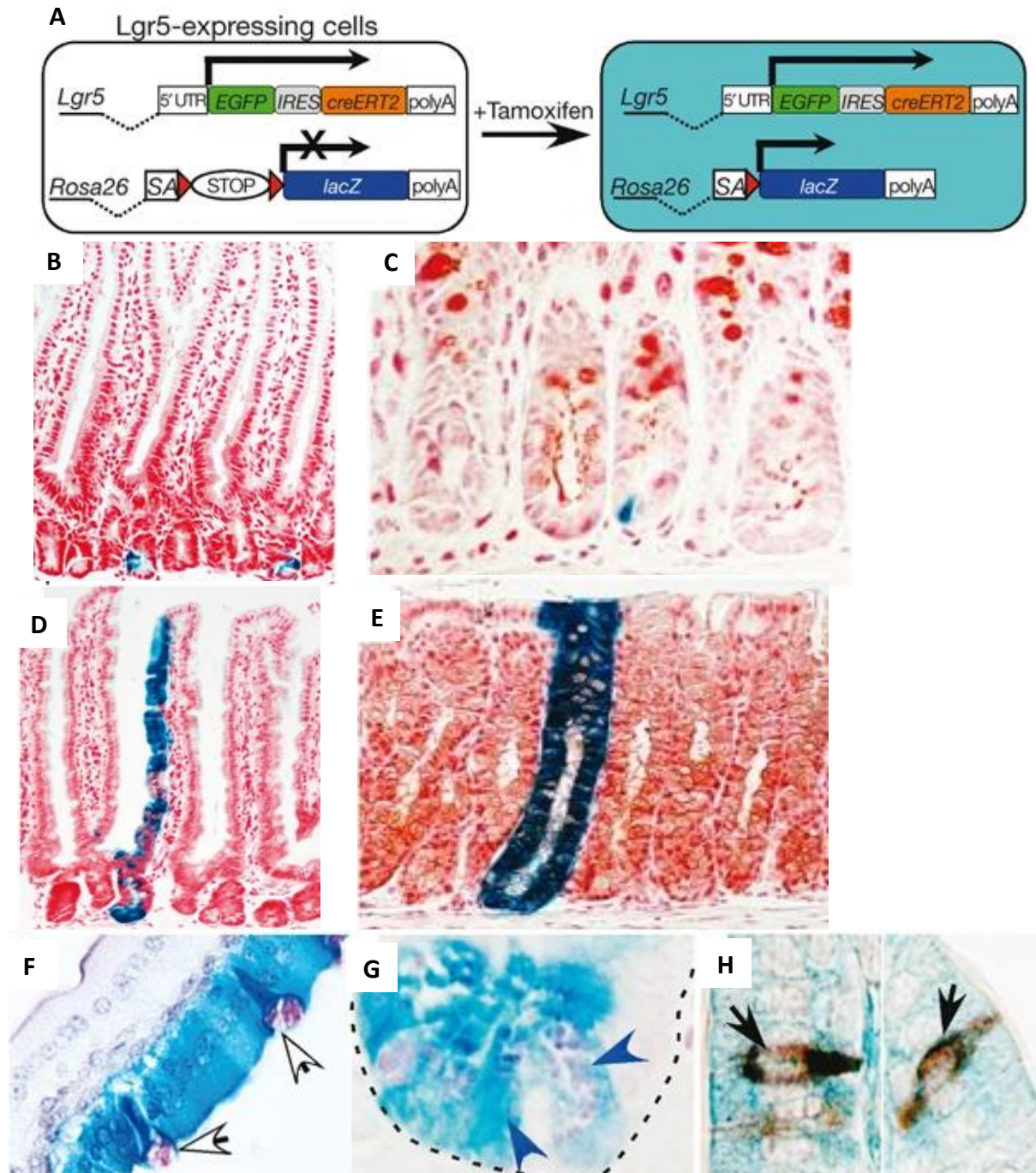
Figure 9 – Lineage Tracing of Lgr5+ Intestinal Cells.

(A) Generation of Lgr5[EGFP-IRES-creERT2] mice with Cre-activatable Rosa26-lacZ enables lineage tracing via selective activation of lacZ by tamoxifen. IRES prevents exocytosis of the Lgr5 protein. The creERT2 is activated by tamoxifen to code for an enzyme which cleaves the STOP sequence. SA, splice acceptor. UTR, untranslated region. (B-E) Vibratome sections showing red nuclei using DNA dye ToPro-3 and blue lacZ-cells using β-galactosidase after 1-day (B-C) and 60 days (D-E) tamoxifen induction in the small intestines (B & D) and colon (C & E). (F-H) Double-labelling of lacZ-positive cells in the small intestine using Periodic-Acid-Schiff (PAS) revealed goblet (F, white arrows) and Paneth cells (G, blue arrows); double-labelling with synaptophysin revealed enteroendocrine cells (H, black arrows). Figure from (Barker, et al., 2007).

1.3.2 Quiescence and/or Plasticity of Intestinal Stem Cells

Likely due to their high active metabolic and proliferative state, ISCs are sensitive to physiological and pathological injuries. For example, it is long known that CBCs are highly sensitive to ionizing radiation (Potten, 1977), during which they apoptose and cause the crypt to shrink (Merritt, et al., 1994) and (Maj, et al., 2003). However, the intestines are capable of recovering from catastrophic injuries. In the 70s, Potten's group proposed the existence of quiescent intestinal stem cells. They predicted these stem cells could be identified based on their slower rate of cell-cycling, which would lead to long-term retention of DNA labelling agents. These DNA label-retaining cells (LRCs) were initially identified using 3H-thymidine and BrdU (Potten, Gandara, Mahida, Loeffler, & Wright, 2009), and have also been identified in epidermal models (Braun & Watt, 2004). Currently, LRCs are characterized by the co-expression of ISC genes and markers of Paneth cells and enteroendocrine lineages (Buczacki, et al., 2013). The current view is that rapidly cycling Lgr5+ CBCs are highly sensitive to pathological injuries and whose function is to maintain tissue homeostasis of the intestinal epithelium, while quiescent stem cells assist the intestine in recovering from catastrophic injuries by replenishing Lgr5+ CBCs (Richmond, Shah, Carlone, & Breault, 2017). However, there is heavy debate whether a distinct population of quiescent stem cells exist in the intestines.

In the small intestines, small numbers of quiescent cells were reported to reside directly above the Paneth cell at the +4 position from the stem cell zone (Potten, Hume, Reid, & Cairns, 1978), (Umar, 2011). These quiescent stem cells were speculated to be distinct from Lgr5 stem cells which divide daily and were proposed to restore the CBC cell compartment following injury (Barker, 2013). Until recently, markers for these quiescent '+4' ISCs included Bmi1 (Sangiorgi & Capecchi, 2008), Tert (Montgomery, et al., 2011), Lrig1 (Powell, et al., 2012) and Hopx (Takeda, et al., 2011). However, these findings were challenged by Clevers' group using a combination of transcriptomics and proteomics (Muñoz, et al., 2012). They first identified over 500 stem cell-enrich genes in mice small intestines, of which half were expressed in a gradient with highest levels at the crypt base, while the other half was expressed uniquely in Lgr5 stem cells. Next, they separated GFP-positive cells derived from Lgr5[EGFP-ires-CreERT2] knock-in mice into five arbitrary fractions from Lgr5-highest to Lgr5-lowest, extracted their cDNA and performed qPCR for Bmi1, Tert, Lrig1 and Hopx. All four proposed quiescent ISC genes were expressed in each GFP fractions. To further validate those findings, they performed single molecule mRNA hybridizations on unmanipulated mouse crypts for Lgr5, OLFM4 and the four quiescent ISC genes. There was no specific enrichment of mRNA molecules of any markers at the +4 position. Thus, they confirmed the proposed quiescent ISC markers Bmi1, Tert, Hopx and Lrig1 are robustly expressed in CBC cells and not specific for supposedly quiescent cells at the +4 position. Another marker which was proposed to label quiescent intestinal stem cells is DCAMKL-1 (May, et al., 2009), due to their observations that DCAMKL-1+ cells isolated from adult mouse small intestine by FACs sorting are capable of forming spheroids in suspension culture. Yet mere months afterwards, DCAMKL-1 was convincingly argued to identify tuft cells rather than stem cells, as DCAMKL-1+ cells do not

express proliferation markers, were predominantly located on villi, were never found in a proliferative state, and do not co-stain with other known markers of mature epithelial cells, yet tellingly express cyclooxygenase enzymes 1 (COX1) and 2 (COX2) – markers of tuft cells (Gerbe, Brulin, Makrini, Legraverend, & Jay, 2009). In conclusion, a specific marker for quiescent stem cells at the +4 position has yet to be identified (Li & Clevers, 2014).

Even so, LRCs have been demonstrated to regenerate the intestinal epithelium in response to tissue injury. One such group of LRCs are Bmi1+ cells of the Prox1+ enteroendocrine lineage, shown to be capable of sustained clonogenic growth in vitro and generate long-lived clones during homeostasis and after radiation-induced injury in vivo (Yan, et al., 2017). Another study showed mice Bmi1+ preterminal enteroendocrine cells were capable of reverting into Lgr5+ cells, however they proposed chromatin accessibility to be the deciding factor in dedifferentiation of secretory precursors into Lgr5+ stem cells (Jadhav, et al., 2018). Another group of LRCs proposed to contribute to tissue regeneration are H2B+ cells expressing Paneth cell marker lysozyme (Roth, et al., 2012). However, these LRCs are not stem cells by definition. Coupled with the lack of markers for specific quiescent stem cells, it is debatable whether quiescent stem cells are truly quiescent and are in fact LRCs or slow cycling CBCs.

Clevers proposed stem and epithelial cell plasticity to be the answer to this dilemma, rather than a distinct population of quiescent stem cells (Clevers H. , 2013). Indeed, his group showcased secretory progenitor cells were capable of forming long-lived organoids upon brief Wnt exposure and developed stem cell tracing events in response to tissue damage (van Es, et al., 2012). When Lgr5 stem cells were specifically ablated by knocking in a human diphtheria toxin receptor into the Lgr5 locus, progeny production by Bmi1+ cells increased and gave rise to Lgr5+ cells, demonstrating plasticity of Bmi1+ cells (Tian, et al., 2011). Intermediate filament keratin-19 (Krt19) has been shown to mark long-lived, radiation resistant cells above the crypt base and are also capable of regenerating Lgr5+ stem cells that had been ablated using irradiation (Asfaha, et al., 2016). Highly proliferative yet short-lived Alpi+ enterocyte precursors are also capable of dedifferentiating into Lgr5+ stem cells, generating long-lived crypt-villus "ribbons" (Tetteh, et al., 2016). The same has been shown of Paneth cells, who acquire stem-like features through SCF/c-kit signalling in response to inflammatory stress (Schmitt, et al., 2018). Taken together, all these studies support the Clevers group's proposal that "stemness in the intestine should be regarded as a cellular 'state' determined by location, rather than a cellular 'fate' determined by history" (van Es, et al., 2012). As an aside, a study by Nusse in mice infected with parasitic helminths showed crypt cells which associated with granulomatous infiltrates forming fetal-like spheroids in culture in the absence of Lgr5+ stem cells, and hence speculate adult intestinal tissues are capable of activating transcriptional programs to acquire fetal-like development as a remodelling mechanism to maintain function after parasitic infection (Nusse, et al., 2018). Finally, plasticity has also been demonstrated in liver (Tarlow, et al., 2014), stomach (Stange, et al., 2013), and is of great interest in the brain and spinal cord (Johansson B. B., 2007).

1.3.3 Specialized Cells of the Intestinal Epithelium

While ISCs are essential to maintaining tissue homeostasis, they constitute a tiny proportion of the intestinal epithelium (Figure 10). Each crypt houses approximately 15 stem cells within the stem cell zone (Gehart & Clevers, 2018). In the small intestines, ISCs are intermingled with Paneth cells, whose functional analogue in the colon are Deep Crypt Secretory cells. Above the stem cell zone, the transit-amplifying region consist of precursors cells that belong to secretory or absorptive lineages. Secretory precursors will go on to become Paneth, Deep Crypt secretory, goblet, Enteroendocrine, and tuft cells. Enterocyte precursors will become enterocytes or Microfold cells which are only present in the small intestines.

A. Small Intestine
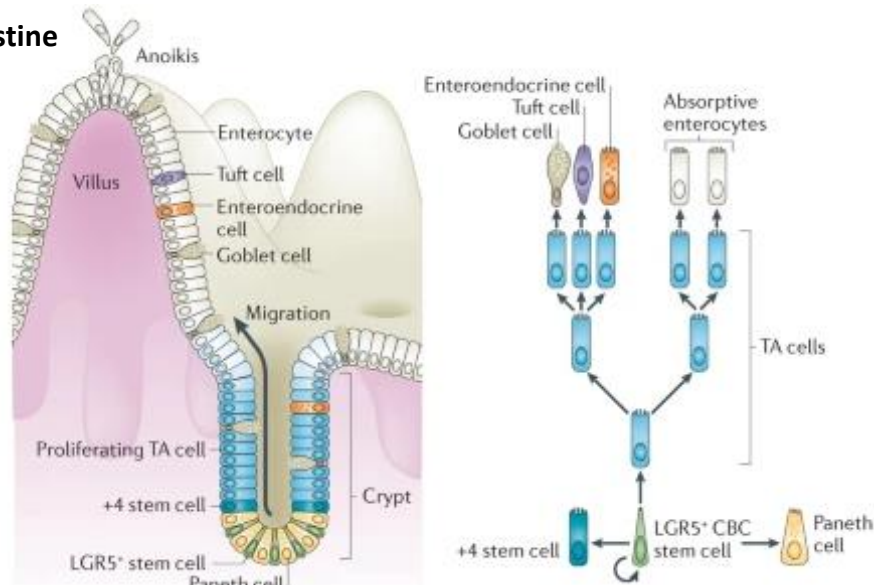
B. Colon
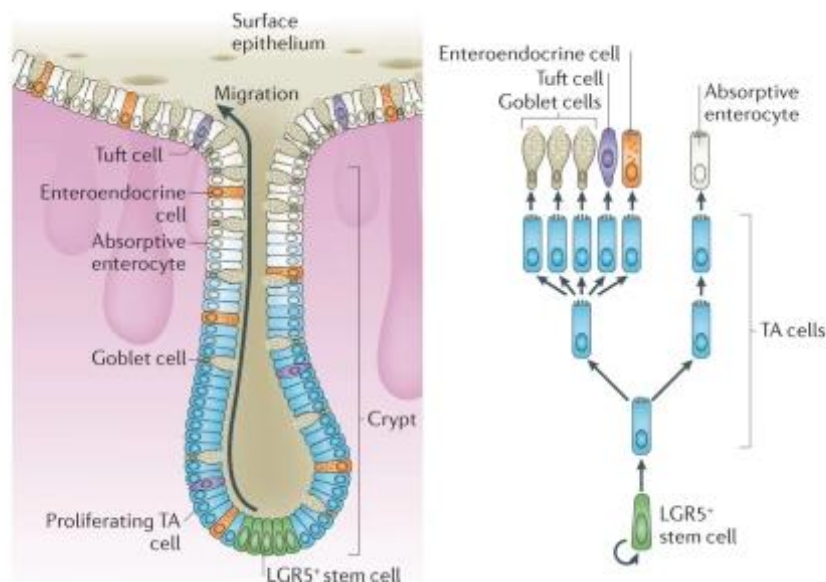
Figure 10 – Intestinal Epithelium Organization and Lineage Tree.

In both the small intestines (A) and colon (B), Lgr5+ stem cells situated at the bottom of crypts generate rapidly proliferating transit-amplifying cells, which differentiate and replace the various functional cells lost via anoikis on the villi (A) and shed at the crypt surface epithelium (B). Lineage tree depicted on the right. Adapted from (Barker, 2013).

Paneth cells

Around 5-12 (Elphick & Mahida, 2005) Paneth cells are intermingled with ISCs at the bottom of crypts and can be marked by lysozyme and DefensinA1 (Sato, et al., 2011). While other intestinal epithelial cells migrate upwards, they move downwards upon maturation. Proper cell migration is dependent on ephrins EphB2 and EphB3, as disruption of those genes result in proliferative and differentiated cell populations intermingling, and knocking-out the EphB3 gene specifically causes Paneth cells to scatter along the crypt and villus (Batlle, et al., 2002). Ephrin receptors can be mediated by phosphoinositide 3-kinase (PI3K) (Maekawa, et al., 2003); inhibiting PI3K using LY294002 resulted in increased displacement of Paneth cells (Genander, et al., 2010). Notably LY294002 treatment did not affect proliferation in colonic crypts, sensible given Paneth cells are non-existent in colonic crypts. However, inhibiting EphB signalling using ephrin-B2-Fc caused significant reduction in proliferation, which is telling since absorptive and secretory cells in the colonic crypt were recently shown to express ephrin genes Efnb1 and Efnb2 (Brügger, Valenta, Fazilaty, Hausmann, & Basler , 2020). Paneth cells produce a variety of antimicrobial products (lysozyme, α-defensins and phospholipase A2) (Gassler, 2017), which are constitutively secreted into the lumen and become a component of the mucus defensive layer. CBCs of the small intestines exist in close contact with at least one Paneth cell (Figure 8), a necessary organization since Paneth cells express epidermal growth factor (EGF), transforming growth factor alpha (TGF-α), Wnt3, and Notch ligand DLL4, all essential signals for stem cell maintenance (Sato, et al., 2011). In addition, Paneth cells provide lactate which are substrates for mitochondrial metabolism in CBC cells (Rodríguez-Colman, et al., 2017), and possibly a free-radical scavenger and antioxidant (Groussard, et al., 2000). Despite all this, they may not be critical for small intestinal CBCs. Two studies have shown small intestinal CBCs to be unaffected by the ablation of Paneth cells using Atoh1 (Kim, Escudero, & Shivdasani, 2012) and (Durand, et al., 2012). On the other hand, two other studies where Paneth cells were depleted via knockout of Sox9 (Bastide, et al., 2007) and Gfi1 (Shroyer, Wallis, Venken, Bellen, & Zoghbi, 2005) were revisited by Clevers' group and found reduction of OLFM4+ stem cells (Sato, et al., 2011). In addition, Paneth cells (Schmitt, et al., 2018) and their precursors (Roth, et al., 2012) are capable of the CBC population following injury, calling into question whether Paneth cells in the small intestine are strictly required or whether their function can be substituted by other cell populations.

Deep Crypt Secretory cells

Deep Crypt Secretory (DCS) cells are functional analogues of Paneth cells which intermingled with CBCs in the colon. DCS cells were first observed almost 40 years ago, who reported "mucous-type cells… with mucous vacuoles which stained differently from goblet cells" (Altmann, 1983). DCS cells can also be marked by numerous markers, key ones being MUC2, Reg4, cKit/CD117, DLL1, DLL4, EGF, and CD24, many of them notably also expressed in Paneth cells (Rothenberg, et al., 2012). However, MUC2 marks Mucin 2 and is a marker of goblet cells, while cKit was also noted to occur in mesenchymal cells (Hirota, et al., 1998) and circular muscle cells (Klein, et al., 2013), making them unsuitable markers. To confirm whether Reg4

were DCS cells and to study their function, Sasaki and colleagues inserted into mice a cassette consisting of a human diphtheria-toxin receptor (DTR) cDNA linked in frame to dsRed-Express2 fluorescent protein (Sasaki, et al., 2016). Reg4[DTR-Red/+] mice produced red-fluorescence in small-intestinal Paneth cells but not in pancreas, stomach, or liver. Reg4 also labelled subsets of entero-endocrine cells in the small intestines. However, in the colon, red fluorescence only occurred between Lgr5+ stem cells at the crypt base throughout the colon. They counted the numbers of Reg4+ cells: 2 in proximal, 8 in transverse, and 12-14 the distal colon in the cecum. They then performed RNA-sequencing of sorted Reg4-dsRed+ and Lgr5-GFP+ cells from colonic epithelium. Notably, Notch ligands (DLL1 and DLL4) and EGF were signature genes of Reg4+ cells, while Notch1 receptor and EGF receptor Erbb2 were signature genes of Lgr5+ cells; and both had high expression of Wnt receptor Fzd5. They determined Reg4+ cells were closer related to Paneth cells and less related to Goblet cells or enteroendocrine cells, and were enriched in genes required for membrane, signal, O-glycan biosynthesis, endoplasmic reticulum, calcium ion binding, and secretion. Administering diphtheria toxin to Reg4[DTR-Red/+] mice over six consecutive days eliminated DCS cells and caused most Lgr5+ stem cells to disappear, confirmed on the mRNA level using single-molecular fluorescent in-situ hybridisation. However, when Diphtheria Toxin treatment was stopped, Lgr5+ stem cells re-emerged after 7 days. Analysis of differentiation marker expression in Reg4[DTR-Red/+] mice crypts devoid of stem and DCS cells showed they did not contain entero/colonocytes, had sporadic enteroendocrine cells similar to control group, and increased numbers of Ki67+ cells which correlated with an enlarged proliferative compartment. In Reg4[DTR-Red/+] mice crypts devoid of stem and DCS cells, they found no cells with secretory phenotype and instead polarized cells with densely packed apical microvilli. The organoid forming capacity of Lgr5-Reg4-cells (8%) were highest compared to Lgr5-cells (>1%) and Reg4-cells (>1%) alone. Finally, Wnt signalling induced cell differentiation into DCS cells, while Notch signalling promoted differentiation into goblet cells. In conclusion, DCS differentiation is Notch dependent and controls apoptosis by tethering colonic ICSs to the stem cell zone and maintain stemness.

Goblet cells

Goblet cells are secretory cells responsible for lining the intestinal epithelium with mucus. They comprise approximately 9% of the intestinal epithelium (Umar, 2011) and up to 16% in the distal colon (Kim & Ho, 2010). As described by Sasaki (Sasaki, et al., 2016) and others (van Es, et al., 2010) and (Stanger, Datar, Murtaugh, & Melton, 2005), inhibition of Notch signalling induces differentiation of proliferative cells in the crypt into goblet cells. Other regulators of Goblet cell differentiation and maturation are Hath1 (Park, et al., 2006), and transcription factors Klf4 and Elf3 (van der Flier and Clevers 2009). Besides gel-forming and transmembrane mucins (see Chapter 1.2.1), goblet cells synthesize and secrete bioactive molecules such as trefoil peptides, resistin-like molecule β, Fc-γ binding protein, and WFDC2 (Dharmani, Srivastava, Kissoon-Singh, & Chadee, 2009), (Parikh, et al., 2019). These molecules may be secreted constitutively dependent on cytoskeletal movement of secretory granules, or secreted regulatorily via exocytosis of granules in response to external stimuli (Davis & Dickey,

2008). Normally, constitutive secretion of mucus maintains the integrity of mucus protective layer(s). However, during intestinal helminth infections, regulatory secretion of mucus by goblet cells mediated by Th2 immune response facilitates the expulsion of pathogens (Knight, Brown, & Pemberton, 2008) and (Hasnain, et al., 2010). The NLRP6 inflammasome is also capable of regulating goblet cell mucus secretion; NLRP6 deficiency leads to defective autophagy in goblet cells and abrogated mucus secretion into the large intestinal lumen in response to bacterial infection (Wlodarska, et al., 2014). In cystic fibrosis, impaired chloride anion transport by CFTR, coupled to persistent sodium absorption, reduces airway surface ion content and leads to increased mucus concentration with abnormal viscoelastic properties and osmotic pressures, resulting in impaired mucus clearance and increased susceptibility to inflammation, chronic infection (Hill, et al., 2018). Goblet cells are reduced in number and size during ulcerative colitis. Mice with deficient MUC2 have no identifiable goblet cells, resulting in compromised mucosal barrier (Johansson, et al., 2008) and develop spontaneous colitis (Van der Sluis, et al., 2006). A recent paper described WFDC2, an inhibitor of serine and cysteine prostates (Chhikara, et al., 2012), to be secreted by goblet cells on both apical and basal poles to prevent premature conversion of the inner mucus layer to the outer layer (Parikh, et al., 2019) and hence maintain sterility of the inner mucus layer (Figure 7), via inhibiting the proteolytic activity of matrix metalloproteinases MMP12 and MMP13. Pathological induction of those MMPs are known to cause tissue destruction in IBD (O'Sullivan, Gilmer, & Medina, 2015). They also potentiated WFDC2 to be a selective bactericide whose role is restricting epithelial–bacterial contact in vivo, due to marked dose-dependent reduction of viable bacteria against increasing concentrations of secreted WFDC2.

Enteroendocrine cells

Enteroendocrine cells are another type of secretory cells stimulated to release hormones and account for approximately 1% of the intestinal epithelium (Worthington, Reimann, & Gribble, 2017). The main driver of enteroendocrine fate is NEUROG3, a basic helix–loop–helix transcription factor activated downstream of Atoh1 in the common secretory progenitor cell (Gehart & Clevers, 2018). Markers for enteroendocrine cells include chromogranin A (CHGA), claudin-4, genes related to enteroendocrine cells (Ffar1, Ffar4, Gpr119), UEA-1 (Nagatake, Fujita, Minato, & Hamazaki , 2014), and hormonal peptides GLP1 (Lu, et al. 2019). Enteroendocrine cells are well known for having taste receptors for sweet, savoury and bitter (Rozengurt & Sternini, 2007) and (Chaudhari & Roper, 2010). Approximately 12 major enteroendocrine cell types have been identified, which collectively secrete more than 20 hormones which can act locally, on other cells (including immune cells), nerve endings, or organs at remote sites including pancreatic islets and the CNS (Furness, Rivera, Cho, Bravo, & Callaghan, 2013). The effects of these secreted hormones are diverse: appetite control, stimulate or inhibit gastric acid release, induction of nutrient transporters and digestive enzymes, stimulate or inhibit intestinal motility, triggering emesis and nausea, and release of other hormones (insulin, growth hormones). Enterochromaffin cells, L-cells and D-cells are the prominent enteroendocrine cells in the lower GI tract, each comprising roughly 70%, 15% and 5%, respectively (Gunawardene, Corfe, & Staton, 2011). Enterochromaffin cells are

triangular or pyramidal in shape, can be stained by CHGA and are known to secrete serotonin (5-HT). Hence, they can also be marked by antibodies against TPH, the initial enzyme in 5-HT biosynthesis (Modlin, Kidd, Pfragner, Eick, & Champaneria, 2006). 5-HT can act in an endocrine, autocrine, paracrine and neurocrine manner to fulfil numerous roles including: appetite, motility, fluid secretion, release of digestive enzymes and bone metabolism (Diwakarla, Fothergill, Fakhry, Callaghan, & Furness, 2018). L-cells are described as being bottle or flask shaped with an apical protrusion of cytoplasm extending to the luminal surface and basal processes that run along the basement membrane with secretory vesicles occurring adjacent to it (Buffa, Capella, Fontana, Usellini, & Solcia, 1978) and (Gunawardene, Corfe, & Staton, 2011). L-cells secrete peptide YY (PYY) into blood circulation to regulate appetite (Karra, Chandarana, & Batterham, 2009) and proglucagon-derived peptides (PGDPs) such as GLP1 and GLP2. GLP1 has a broad range of metabolic, cardio and neuroprotective effects: glucose-dependent stimulation of insulin secretion, decrease of gastric emptying, inhibition of food intake, increase of natriuresis and diuresis, amelioration of obesity, decrease inflammation and apoptosis, implicated for learning and memory, reward behaviour, and palatability (Kimura, et al. 2018), (Jones, et al. 2018), (Gribble and Reimann 2019), (Müller, et al., 2019). GLP2 regulates energy absorption, glucose metabolism, and maintains the mucosal morphology, function, and integrity of the intestine (Amato, Baldassano, & Mulè, 2016). D-cells are described as having one elongated apical extension and one shorter, wider basal extension (Hauso, Gustafsson, & Waldum, 2007). D-cells secrete somatostatin (SST), also known as the "growth hormone inhibiting hormone", which causes neuro-endocrine inhibitory effects in the GI, endocrine, exocrine, pancreatic, and pituitary secretions, modifies neurotransmission and memory formation in the CNS, prevents angiogenesis, and has anti-proliferative effects on healthy and cancerous cells (O'Toole & Sharma, 2020). As such, they can be identified by immunohistochemistry as somatostatin immunoreactive. Recently, a biobank for human ECCs was established (Beumer, et al. 2020) by inducing enteroendocrine cell formation in colonic organoids using NEUROG3, generating single-cell mRNA atlases for different enteroendocrine cell subtypes, and profiling their secreted products using mass-spectrometry.

Tuft cells

Tuft cells are very rare chemosensory epithelial cells comprising around 0.5% of the intestinal epithelium (Gerbe, Legraverend, & Jay, 2012). They are also known by other names, including brush cells due to having a "brush" of microvilli on their apical membrane (Nevo, Kadouri, & Abramson, 2019). However, some tuft cells also possess cytospinules, thin lateral microvilli which project from the tuft cell and penetrate neighbouring epithelial cells to wrap itself around their nuclear membrane (Hoover, et al., 2017). This unusual form of contact between cells was suggested to play a role in the transfer of cargo or even genetic material (Nevo, Kadouri, & Abramson, 2019). Tuft cells are differentiated from secretory progenitors of the DLL+ lineage and require the expression of the Pou domain, class 2, transcription factor 3 (POU2F3) (Gerbe, et al., 2016). Markers for tuft cells include doublecortin and calcium/calmodulin-dependent protein kinase-like-1 (DCAMKL-1), COX1 and COX2,

Doublecortin-like kinase 1 (Dclk1), and Trpm5. DCAMKL-1 is a microtubule-associated kinase which was previously considered a putative marker of intestinal stem cells (Gerbe, Brulin, Makrini, Legraverend, & Jay, 2009). COX1 and COX2 are involved in inflammation through generation of prostaglandin (Ricciotti & FitzGerald, 2012). Dclk1 was shown to co-localize with the microtubule acetylated-α-tubulin (Saqui-Salces, et al., 2013). And Trpm5 is a component of the taste reception signalling machinery (Kaske, et al., 2007). Two types of tuft cells have been recently proposed; tuft1 were enriched with signature genes related to neuronal development, while tuft2 were enrich with signature genes related to immunity (Haber, et al., 2018). While not fully understood, tuft cells are well known to be capable of sampling the luminal contents to trigger a variety of immune responses (Gerbe & Jay, 2016). For example, Sucnr2 receptors on tuft cells can be activated by the protozoa metabolite succinate to trigger Th2 immune responses (Nadjsombati, et al., 2018) and (Lei, et al., 2018), and remodel the intestinal epithelium (Schneider, et al., 2018). Intriguingly, tuft cells in the human GI tract were shown to contain choline acetyltransferase (ChAT), the enzyme responsible for the synthesis of the neurotransmitter acetylcholine (Pan, Zhang, Shao, & Huang, 2020). In neurons, extracellular choline is imported via CHT1, catalysed into acetylcholine with mitochondria-derived acetyl-CoA by ChAT in the cytoplasm, then packaged into vesicles and released via vAChT. However, vAChT and CHT1 are absent in tuft cells, hence their biosynthesis and release of acetylcholine remains unresolved (Schütz, et al., 2019) and (Yajima, Inoue, Matsumoto, & Yajima, 2011). Even so, various signals have been shown to trigger the release acetylcholine from tuft cells, including bitter (Deckmann, et al., 2014), bacterial metabolites (Saunders, Christensen, Finger, & Tizzano, 2014), and ATP (Ualiyeva, et al., 2020). In a study done in mice, ATP stimulation caused an increase of intracellular Ca^{2+} oscillations in Trpm5+ tuft cells and other cells in the olfactory epithelium, resulting in release of acetylcholine from Trpm5+ tuft cells (Fu, Ogura, Luo, & Lin, 2018). Other studies found bitter and other substances to trigger acetylcholine biosynthesis in tuft cells via canonical taste transduction cascade depended on gustducin and TRPM5 (Saunders, Christensen, Finger, & Tizzano, 2014), which also caused elevated Ca^{2+} levels (Hollenhorst, et al., 2020). Currently, it is unknown how tuft cells acquire choline due to their lack of CHT1. As for the release of acetylcholine in tuft cells despite their lack of VAChT, one proposed mechanism is that tuft cells might release acetylcholine directly from the cytoplasm rather than concentrate them in vesicles (Pan, Zhang, Shao, & Huang, 2020). An alternative mechanism is via organic cation transporters (OCT), which possess the ability to transport acetylcholine in airway epithelial cells (Kummer & Krasteva-Christ, 2014) and the placenta (Wessler, et al., 2001). However, it is unknown if they are expressed in tuft cells.

Enterocytes

Enterocytes make up 80% of cells in the intestinal epithelium. They are absorptive cells responsible for the uptake of ions, water, sugars, peptides, and lipids. Notch signals determine enterocyte fate; daughter stem cells leaving the stem cell zone loses Wnt signals but maintain Notch signals from neighbouring DLL+ cells become transit-amplifying cells of the absorptive lineage, leave the transit-amplifying zone after undergoing several cycles of cell division and

differentiating into mature enterocytes (Gehart & Clevers, 2018). Fatty acid binding proteins (FABP) are cytosolic proteins with high affinity binding for hydrophobic ligands like long chain fatty acids and are involved in uptake and trafficking of lipids in the intestines (Gajda & Storch, 2014). In intestinal enterocytes, two FABPs are present. FABP1 is largely present in absorptive intestinal villus cells but not crypt cells (Guilmeau, et al., 2007), but is also present in liver where it was first identified as well as in the kidneys (Storch & Corsico, 2008). FABP2 on the other hand is only present in intestinal enterocytes, making it a suitable specific marker for it. Besides uptake of nutrients, enterocytes are actively involved in shaping the intestinal immune environment. They possess MHC-II molecules and act as non-professional antigen-presenting cells (Hershberg & Mayer, 2000), presenting antigens to antigen-experienced T cells resident in LP as part of the protective immune response (Hershberg, et al., 1997). Recently, a novel colonocyte – colonic enterocyte – was discovered (Parikh, et al., 2019). These colonocytes distinctly expressed Bestrophin 4 (BEST4), a calcium-sensitive chloride channel, as well as the proton channel OTOP2, and hence were designated as "BEST4/OTOP2 cells". The numbers of BEST4/OTOP2 cells were fifty times less frequent compared to regular colonocytes, were capable of pH sensing, and proposed to maintain luminal homeostasis through regulation of the guanylate cyclase 2C (GC-C) signalling pathway.

Microfold cells

Microfold (M) cells are specialized absorptive cells that are only found in the small intestines. They are traditionally found in follicle-associated epithelium such as Peyer's patches, although inducible villous M cell have been observed in the small intestine (Jang, et al., 2004). Unlike other intestinal epithelial cells, M cell fate is not determined directly after exit from the stem cell zone. Instead, receptor activator of nuclear factor κ-B ligand (RANKL) is needed to induce functional M cell development in culture (de Lau, et al., 2012). M cells sample the intestinal lumen and transport antigens to lymphoid cells underneath Peyer's patches to generate mucosal-mediated immunity (Mabbott, Donaldson, Ohno, Williams, & Mahajan, 2013) and (Bennett, et al., 2016). Unlike enterocytes, they do not possess an apical microvilli brush border, which inversely correlates with their efficiency in luminal microparticle binding (Bennett, Walker, & Lo, 2014).

1.3.4 Essential Signals for Intestinal Epithelium Maintenance

The intestinal epithelium receives and produces a multitude of signals to maintain tissue homeostasis, carry out its functions and respond to infection. Signals which are vital for the intestinal epithelium include Wnt, Notch, EGF, BMP/TGF-β, YAP/TAZ and Hh signalling pathways. Many of these signals have a gradient expression throughout the crypt, and the spatio-temporal activities of these signals are vital for the cellular fates of the intestinal epithelium.

<u>Wnt signals</u>

The Wnt pathway is highly conserved across species and is broadly implicated in embryonic development, adult tissue homeostasis as well as disease pathophysiology (van Amerongen & Nusse, 2009) and (Clevers & Nusse, 2012). Mammals possess genes for 19 Wnt ligands and 10 Frizzled receptors, the latter being seven-pass transmembrane receptors that mediate downstream Wnt signalling (Mah, Yan, & Kuo, 2016). As described earlier, Wnt is essential for ISC maintenance and identity. In the intestinal epithelium, canonical Wnt signalling occurs to activate transcription of Wnt target genes (Figure 11) and is amplified by R-spondin (Figure 12). Wnt target genes include Lgr5 and Axin2, both known marker of intestinal CBCs (de Lau, Peng, Gros, & Clevers, 2014), Sox9 which is required for the differentiation of Paneth cells (Mori-Akiyama, et al., 2007), and c-Myc which is required for the formation of intestinal crypts (Bettess, et al., 2005) and regulating crypt size and proliferation (Muncan, et al., 2006). Wnt ligands are produced by Paneth cells (Sato, et al., 2011) and mesenchymal cells (Degirmenci, Valenta, Dimitrieva, Hausmann, & Basler, 2018). Increased Wnt signalling leads to excessive growth of the intestinal epithelium. Conditional deletion of APC, a component of the β-catenin destruction complex, leads to inappropriate stabilization of β-catenin (Rubinfeld, et al., 1996) and constitutive transcriptional activation due to constitutive complexes between β-catenin and TCF (Korinek, et al., 1997). In mice, conditional deletion of APC in ISCs caused the formation of large intestinal adenomas (Barker, et al., 2009). The loss of E3 ligases RNF43 and ZNRF3 also induced adenomatous expansion of crypts in mice (Koo, et al., 2012) and have been observed in a variety of human cancers (Nusse & Clevers, 2017), presumably by allowing malignant cells to depend on lower levels of Wnt. Even so, these cells are still dependent on exogenous Wnt signals and are implied to be treatable with inhibitors of Wnt secretion or inhibitors of Frizzled/LRP receptors (Vermeulen, et al., 2010) and (Tammela, et al., 2017).
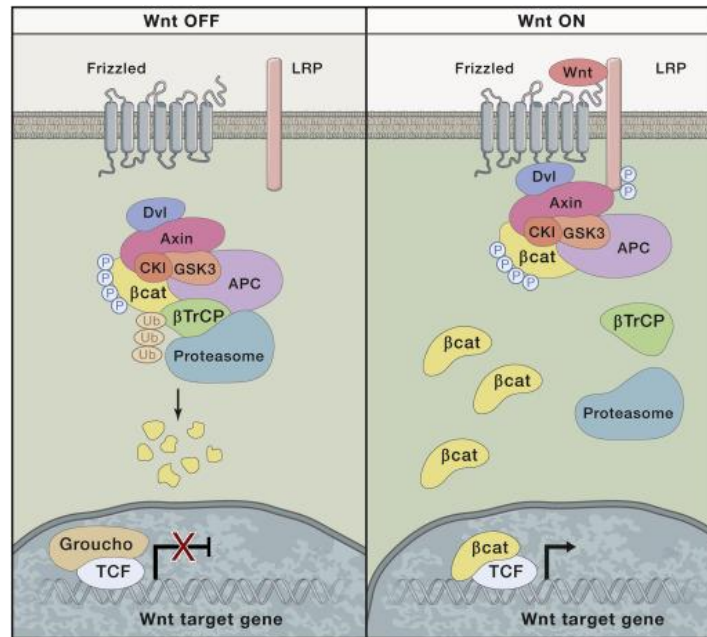
Figure 11 – Canonical Wnt Signalling.

(Left) In the absence of Wnt ligands, ubiquitinated β-catenin is marked for degradation by the APC destruction complex. (Right) Wnt ligands bind to Frizzled and activate co-receptors LRP, causing receptor dimerization and inducing a conformational change, allowing Dishevelled (Dvl) to bind with the intracellular domain of Frizzled and recruiting Axin to bind with the intracellular tail of LRP. β-catenin is de-ubiquitinated and de-phosphorylated, allowing it to accumulate and translocate to the nucleus where it displaces Groucho, binds to TCF, and activates Wnt target genes. Adapted from (Nusse & Clevers, 2017).
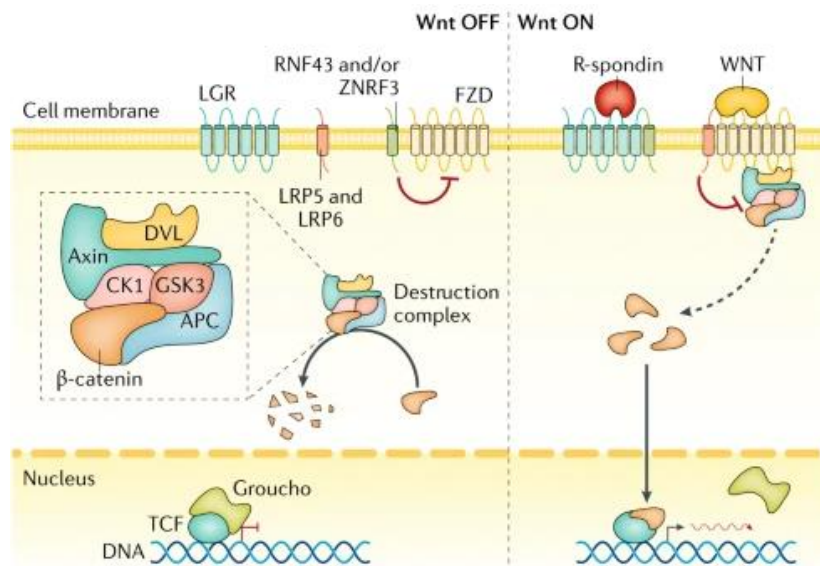
Figure 12 – R-spondin Amplifies Wnt Signalling.

(Left) In the absence of R-spondin, Frizzled (FZD) is ubiquitylated by E3 ligases RNF43 and/or ZNRF3, causing rapid endocytosis and lysosomal destruction. (Right) R-spondin binds to receptors of the LGR family, which sequesters RNF43 and/or ZNRF3 thus stabilizing FZD expression and sustaining Wnt signals. Adapted from (Gehart & Clevers, 2018).

Notch Signals

In the intestines, Notch signalling maintains crypt biology as it is essential for regulating cell fate. The canonical Notch signalling pathway requires membrane contact between two cells; one expressing Notch ligands and the other Notch receptors (Figure 13). This direct interaction results in opposite fate determinations known as lateral inhibition (Sancho, Cremona, & Behrens, 2015). Notch signalling in dependent on Wnt signals. Active Wnt signalling in the crypt bottom allows β-catenin to bind to Hes1 and stabilize Notch signals, promoting the initial absorptive or secretory cell differentiation decision by lateral inhibition (Kay, et al., 2017). However, the absence of nuclear β-catenin in cells higher up the crypt due to low Wnt causes oscillatory Notch activation and enables stochastic secondary fate decisions within a lineage, such as goblet cells versus enteroendocrine cells from secretory progenitors, and enterocyte from absorptive progenitors (Li, Kapoor, Giel-Moloney, Rindi, & Leiter, 2012). Inhibition of Notch signals promotes differentiation into goblet cells. In mice, Notch/γ-secretase causes intestinal proliferative cells and adenomas to differentiate into goblet cells (van Es, et al., 2010), and in another mouse study the loss of Math1 – the mouse homolog of human Atoh1 – caused loss of secretory cells (VanDussen & Samuelson, 2010).
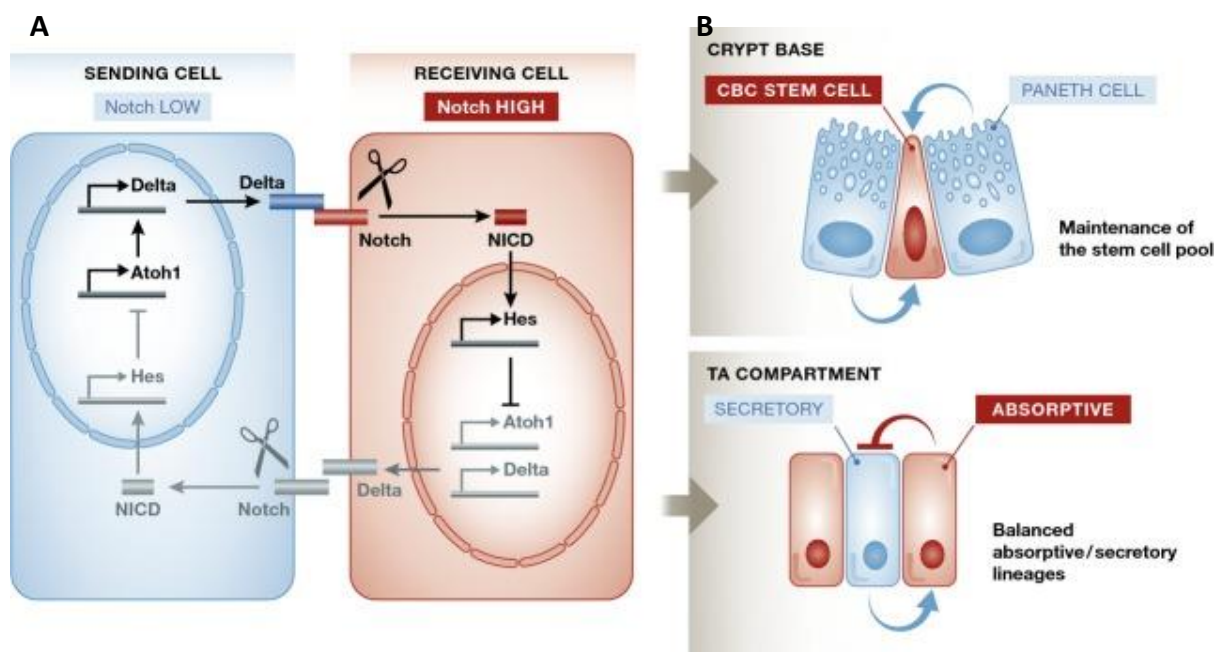
Figure 13 – Canonical Notch Signalling and Lateral Inhibition.

(A) Notch signals are initiated by the cell-surface expression of Delta ligand by sending cells. These ligands bind to Notch receptors expressed on the cell-surface of an adjacent receiving cell, upon which the receptor undergoes proteolytic cleavages by the metalloproteinase ADAM10 and γ-secretase complex, releasing the Notch intracellular domain (NICD) into the cytoplasm. NICD translocates to the nucleus and assembles into a transcriptional activation complex with several cofactors such as RBPJk to relieve repression of Notch target genes. Target genes which NCID relieves repression of includes the Hes family of transcriptional repressors which inhibits the expression of Atoh1, a direct activator of Delta transcription, as well as a variety of differentiation/proliferation genes. By doing so, the receiving cell becomes Notch-high and is prevented from producing and presenting Notch ligands to

the sending cell, which becomes Notch-low. This is known as lateral inhibition. This feedback loop amplifies and drives initial differences in Notch activity in neighbouring cells – due to stochastic or genetic reasons – into opposite spectrums of Notch-level status, and hence into different development pathways. (B) Paneth cells and DCS cells are examples of sending cells low in Notch activity. They constantly provide Notch ligands to ISCs to keep them in Notch-high. In the transit-amplifying (TA) compartment, the result of lateral inhibition drives Notch-high progenitors into absorptive lineages while driving their neighbouring Notch-low progenitors commit to secretory lineages. Adapted from (Sancho, Cremona, & Behrens, 2015).

EGF Signals

EGF is a core component of intestinal organoid culture medium (Sato, et al., 2011). Inhibiting EGF signals in intestinal organoids forces Lgr5+ stem cells into quiescence and stops organoid growth but is reversable when EGF signals are restored (Basak, et al., 2017). The receptor of EGF, EGFR/ErbB, is a receptor tyrosine kinase that is highly expressed in CBC cells (Gehart & Clevers, 2018). The ligands for this receptor are EGF and TGFα, which are produced by Paneth cells (Sato, et al., 2011), mesenchymal cells (Platt, Roman, Wells, Lauffenburger, & Griffith, 2011) and enteric glia cells (Van Landeghem, et al., 2011). The EGF signal transduction is highly complex (Figure 14) and when overactive, is a step towards neoplastic growth. This was observed in mice Lgr5+ stem cells with K-ras mutants, which caused increased activity of the EGF pathway, increased proliferation and gave those stem cells a selective advantage for dominance in their crypts (Snippert, Schepers, van Es, Simons, & Clevers, 2014). To prevent overactive EGF signalling, ISCs co-express ErbB receptors with their negative regulator, Lrig1. When Lrig1 was knocked out in mice, their intestines became enlarged due to crypt expansion (Wong, et al., 2012). The exact mechanism by which LRIG1 inhibits EGF signalling is not yet understood but is well characterised to regulate EGF signals by inhibiting ErbB in various stem and precursor cells (Wang, Poulin, & Coffey, 2013) and (Jeong, et al., 2020).
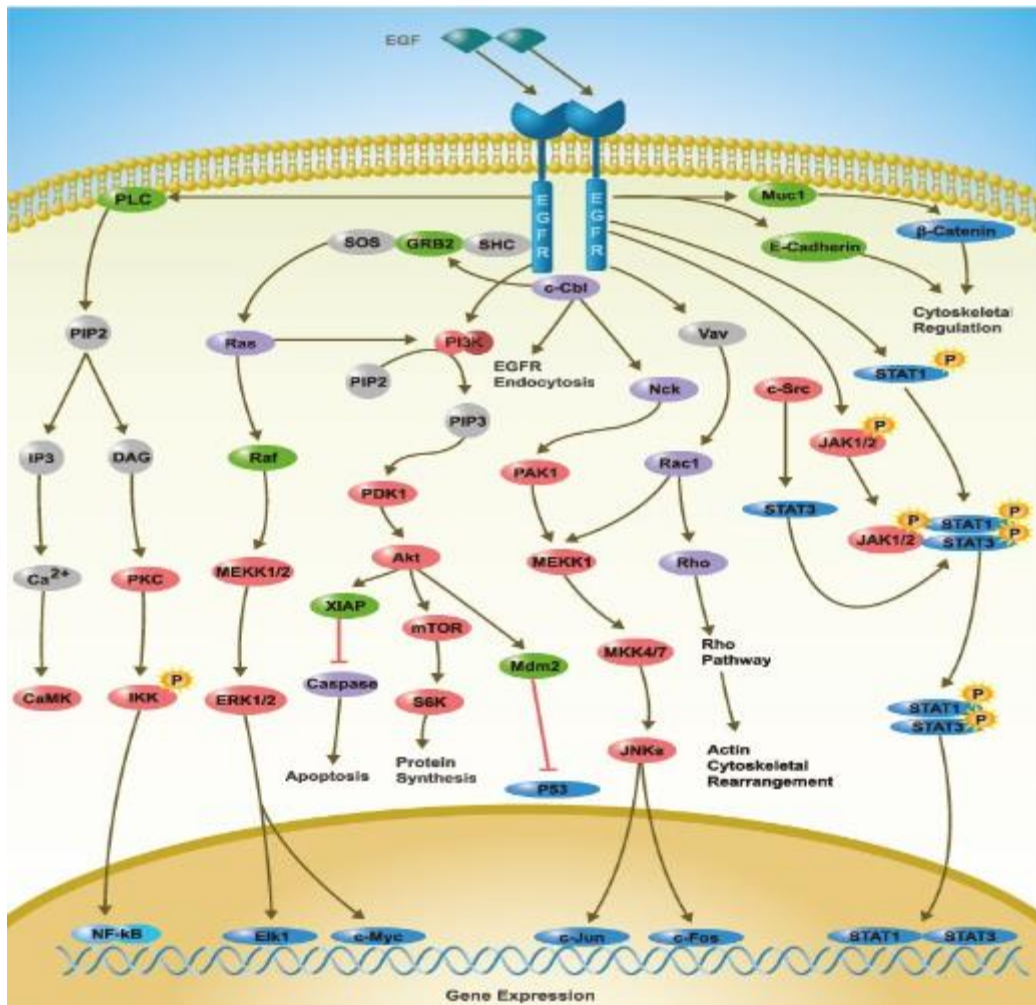
Figure 14 – EGF Signal Transduction.

Activated EGFR/ErbB recruits various cytoplasmic proteins (e.g., PLC, GRB2) which transduce and regulate the EGFR function. EGF signals are involved in various gene expression, apoptosis, protein synthesis, and cytoskeletal regulation/rearrangement. Adapted from (SinoBiological, 2020).

BMP Signals

Bone morphogenetic proteins (BMPs) are members of the transforming growth factor-β (TGF-β) superfamily of ligands. BMP signals regulate target gene expression through Smads and are regulated by co-receptors and inhibitors (Figure 15). In the intestines, BMP2 and BMP4 are the main ligands for BMP receptors, are secreted by mesenchymal cells surrounding crypts and villi, and are responsible for repressing stemness (Qi, et al., 2017). In that study, they showed BMP signalling led to Smad1/Smad4 heteromeric complexes recruiting histone deacetylase HDAC1 to repress transcription of stem cell genes such as Lgr5, which was absent in Smad4 knock-out mice. This was independent of Wnt/β-catenin signalling, as Wnt target genes were unaffected by BMP treatment. They concluded BMP signals played an indispensable role in restricting Lgr5+ stem cell expansion to maintain intestinal homeostasis and prevent premalignant hyperproliferation on damage. Another study showed that mutations in Bmpr1a, Smad4 and PTEN was responsible for various polyposis diseases (He, et

al., 2004). When the main receptor for BMPs in the intestinal epithelium, Bmpr1a, was conditionally deleted in the mouse, both stem cell and transit amplifying zones expanded and formed benign polyps. BMP signalling can be inhibited by Gremlin 1, Gremlin 2, Chordin-like 1 or Noggin, which are mainly secreted by myofibroblasts and smooth muscle cells underneath the crypt (Kosinski, et al., 2007) and (Stzepourginski, et al., 2017). In both these studies, they described a gradient of increasing BMP activity from the bottom to the top of crypts. And when these BMP inhibitors are present outside the stem cell zone, it resulted in the formation of numerous ectopic crypt units (Haramis, et al., 2004).
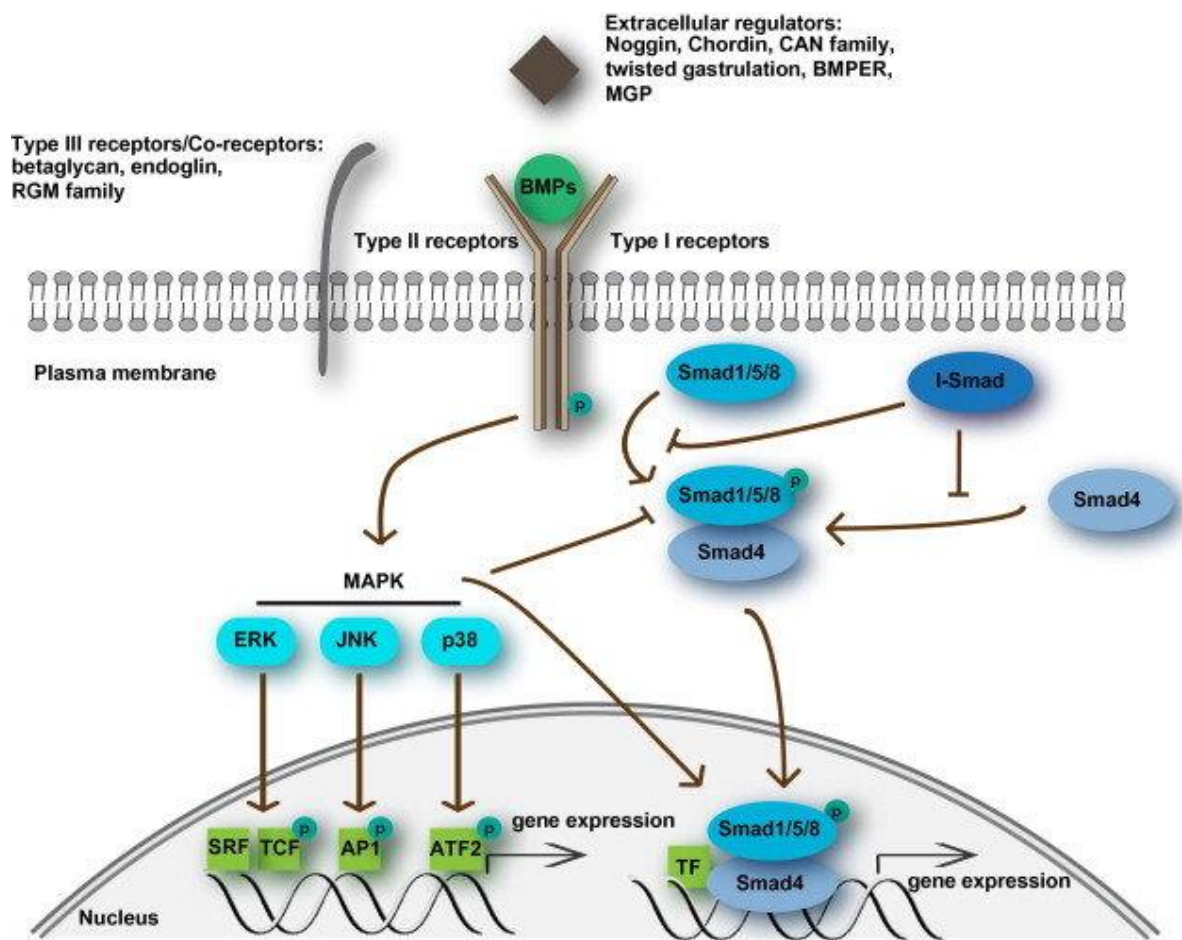
Figure 15 – BMP Signalling Pathway.

Binding of BMPs to their type II receptors leads to subsequent activation and phosphorylation of type I BMP receptors, which induces heteromeric complex formation between them. This activity is regulated by extracellular regulators type III receptors/co-receptors which promote BMP signals, and Noggin/Chordin/CAN family which inhibit BMP signals. After being activated by type II receptors, the type I receptor phosphorylates mothers against decapentaplegic homologue 1 (Smad1) or Smad5 or Smad8 (R-Smads). R-Smads form heteromeric complexes with Smad4 and translocate to the nucleus, where they interact with other transcription factors to regulate target gene expression. I-Smads (Smad6/7) inhibit receptor activation of R-Smads. BMP signalling can also activate non-Smad pathways. Activated MAPKs can regulate R-Smad activation by direct phosphorylation. Or, activated MAPKs can translocate to the nucleus to phosphorylate a number of transcription factors (TF), such

as serum response factor (SRF), ternary complex factor (TCF) family members, activator protein 1 (AP1) complexes and activating transcription factor 2 (ATF2), thereby changing target gene transcription. Adapted from (Cai, Pardali, Sánchez-Duffhues, & ten Dijke, 2012).

Hippo signalling

Hippo signalling is best known for controlling tissue size during embryogenesis and early development (Wu & Guan, 2021). However, in recent years it has been receiving increased attention due to its role in regenerating adult epithelial tissues and its influence in tumorigenesis (Gehart & Clevers, 2018). Hippo signals integrate numerous different inputs including mechanotransduction, GPCR signalling, metabolite sensing and receptor tyrosine kinase activation (Meng, Moroishi, & Guan, 2016), converging to the phosphorylation of YAP and TAZ, which are transcriptionally active when unphosphorylated (Figure 16). YAP expression is elevated during tissue injury (Cai, et al., 2010) and hyperactivation of YAP results in widespread early-onset polyposis. Another study found YAP to restrict Wnt signals during tissue regeneration (Barry, et al., 2013). Transgenic expression of YAP restricted Dishevelled, causing reduced Wnt target gene expression and resulting in the rapid loss of intestinal crypts. And, loss of YAP resulted in Wnt hypersensitivity during regeneration, leading to hyperplasia, expansion of ISCs and niche cells, and the formation of ectopic crypts and microadenomas. A later study also observed YAP to transiently inhibit Wnt signals and excessive Paneth cell differentiation during tissue injury, and also activate EGF signals to promote tissue regeneration (Gregorieff, Liu, Inanlou, Khomchuk, & Wrana, 2015). They further showed YAP inactivation abolished adenomas in Apc[min] mice models of colon cancer, and that the expansion of APC-knockout organoids requires YAP-driven EGF signals. It was subsequently shown that continuous activation of YAP and TAZ by deletion of MST1, MST2 or Salvador (a scaffold protein necessary for LATS phosphorylation) caused increased crypt proliferation and tumorigenicity (Zhou, et al., 2011). In summary, Hippo signals are responsible for maintaining WNT signals within the optimal range for regeneration, to prevent signal overshoot which leads to detrimental tumour formation.
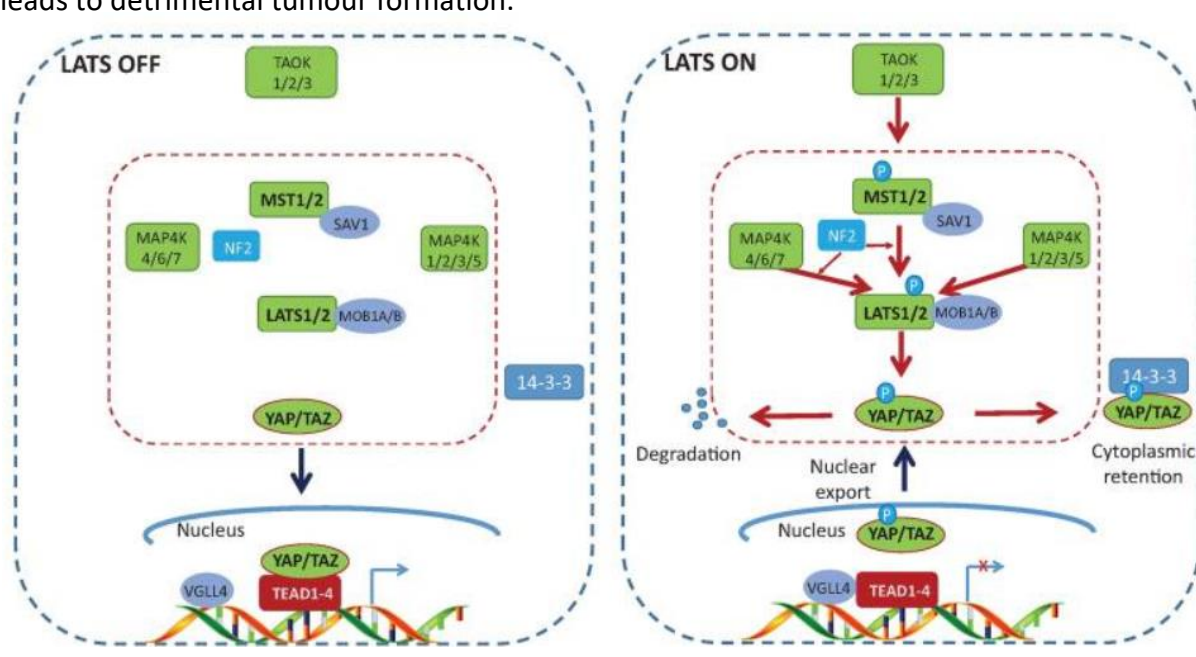
Figure 16 – Core Hippo Pathway in Mammals.

(Left) When the Hippo pathway is inactive, YAP and TAZ are unphosphorylated and localized in the nucleus to compete with VGLL4 for TEAD binding, thus activating gene transcription. (Right) The Hippo pathway can be activated by TAO kinases, which phosphorylate MST1/2 at its activation loop. MST1/2 in turn phosphorylate LATS1/2, facilitated by scaffold proteins SAV1, MOB1A/B, and NF2. MAP4K4/6/7 and MAP4K1/2/3/5 also phosphorylate and activate LATS1/2. Phosphorylation of LATS1/2 by MAP4K4/6/7 requires NF2. Activated LATS1/2 phosphorylates YAP and TAZ, leading cytoplasmic retention of YAP and TAZ by 14-3-3, or SCF-mediated YAP and TAZ degradation. The absence of nuclear YAP and TAZ allowed VGLL4 to bind with TEAD and repress gene transcription. Adapted from (Meng, Moroishi, & Guan, 2016).

Interleukin Signals

Interleukins are soluble cytokines protein mediators that are critical for intercellular communication and support intestinal mucosal homeostasis, but can also drive intestinal inflammation and inflammation-associated damage (Andrews, McLean, & Durum, 2018). For example, genetic deletion of IL-10 or IL-2 caused spontaneous colitis in mice, while IL-6 (also known as TNF), IL-18, IL-1β, and IL-17 are overexpressed in the inflamed intestine and are implicated to contribute to intestinal damage (Neurath, 2014). ILs may be derived from resident innate or adaptive immune cells, infiltrating inflammatory cells, or from intestinal epithelial cells. These interleukins have been shown to induce or restrict epithelial proliferation and cell death, support epithelial regeneration, increase ISC survival chances from irradiation, heal epithelial erosions and ulcerations or exacerbate them, affect progenitor cell lineage choice in response to parasitic infection, alter intestinal epithelial permeability via tight junctions, and recruit immune cells to sites of inflammation (Gehart & Clevers, 2018) and (Andrews, McLean, & Durum, 2018). However, due to failed clinical trials and conflicting literature evidence, there is the sentiment that "traditional labels of pro- and anti-inflammatory are too simplistic and perhaps even deceiving when used to describe cytokine actions in the intestine" (Andrews, McLean, & Durum, 2018).

Hedgehog Signals

Hedgehog signals are essential for the growth of the mesenchyme during development (Mao, Kim, Rajurkar, Shivdasani, & McMahon, 2010). As described earlier, mesenchymal provide essential support for crypt biology. The intestinal epithelium secretes the ligands Sonic Hedgehog (Shh) and Indian Hedgehog (Ihh) (Kolterud, et al., 2009) to activate target genes Pathed and Gli1 in the mesenchyme. Activated Hedgehog signals is an anti-inflammatory for the intestinal lamina propria (Zacharias, et al., 2010) and causes depletion of the colonic epithelial precursor cell compartment (van Dop, et al., 2009). One study showed intestinal epithelial Ihh signals to the mesenchymal compartment to regulate formation and proliferation of mesenchymal cells, which in turn regulated BMP signals, increased matrix metalloproteinase levels and disrupted extracellular matrix proteins, overall fostering a proliferative environment for ISCs and progenitor cells (Kosinski, et al., 2010). Diminished

stromal hedgehog signals was shown to enhance the development of CRC (Gerling, et al., 2016). Activation of stroma-specific Hedgehog signals reduced the expression of BMP inhibitors Noggin and Gremlin1, reduced the expression of stem cell genes Lgr5, and resulted in reduced tumour load as well as blocking progression of advanced neoplasms.

<u>Nutrition</u>

Rapid turnover in the intestinal epithelium is necessary, but energy intensive. Hence, it would be evolutionary beneficial for the existence of mechanisms to reduce proliferation rates during periods of low-calorie intake. Case in point, a study in long-term fasting rats described a 50% reduction in intestinal epithelial mass which was restored after 3 days of re-feeding (Dunel-Erb, et al., 2001). This was shown to be caused by increasing the numbers of stem cells and reducing proliferation of transit-amplifying cells. In one study, acute nutrient depravation increased the prevalence of slow-cycling Lgr5+ stem cells (Richmond, et al., 2015). Other studies showed calorie restriction increasing the numbers of Paneth cells and Lgr5+ stem cells (Tinkum, et al., 2015), at the same time reducing proliferation in the transit-amplifying region (Yilmaz, et al., 2012). In these papers, mTORC1 and PTEN were shown to be important. On the flipside, nutrient overabundance decreases Paneth cells numbers and increased CBC cells (Beyaz, et al., 2016). This observation appears contradictory since CBC cells require Notch signals from Paneth cells to maintain stemness, however the paper elucidated CBC cells became independent from Paneth cells by expressing their own JAG1 and JAG2 Notch ligands. In addition, they showed CBC cells were more sensitive to Wnt and were able to maintain stemness higher up the crypt. They found increased peroxisome proliferator-activated receptor delta (PPARδ) signalling to be responsible for both effects. They finally transplanted transit-amplifying cells of APC-null mice that had been treated with PPARδ into the colonic lamina propria of recipient mice and noted they had increased abilities of forming adenomas compared to vehicle-treated counterparts. Hence supporting the association between high fat diet and colorectal cancer likelihood, which had been observed since the early 90s (Vecchia, 1992).

1.4 Intracellular Calcium Signals

Calcium ions (Ca^{2+}) are used as second messengers to communicate and drive a vast number of intracellular processes through a complex network of signalling pathways. The intracellular Ca^{2+} concentration ($[Ca^{2+}]$) is typically much lower than the extracellular $[Ca^{2+}]$, which is maintained by buffers, as well as an assortment of channels, pumps, and transporters (Figure 17). The effects of Ca^{2+} signals are mediated either by direct binding to a target protein or stimulation of Ca^{2+} sensors (Berridge, 2004). Target proteins which Ca^{2+} binds to include Ca^{2+} channels on organelles, enzymes in the cytoplasm, and proteins which associate with other proteins. The spatio-temporal organization of Ca^{2+} signals allows the activation of different downstream effectors depending on the nature of the signal and their localisation (Berridge, 2004) and (Newton, Bootman, & Scott, 2016). In the intestinal epithelium, Ca^{2+} signals are a central regulator of ISC activity by dynamically adjusting proliferation and differentiation in response to stress and metabolic cues (Deng, Gerencser and Jasper 2016). Ca^{2+} signals are also indispensable for packing and releasing MUC2 (Ambort, et al., 2012), and modulating ion and fluid secretion (Yang, et al. 2018). Finally, Ca^{2+} signals play a critical role in inflammation (Murakami, et al. 2012), contributes to the pathogenesis of experimental colitis (Cunningham, et al. 2019), and has a complex role in the development and progression of colorectal cancer (Wang, et al. 2019).
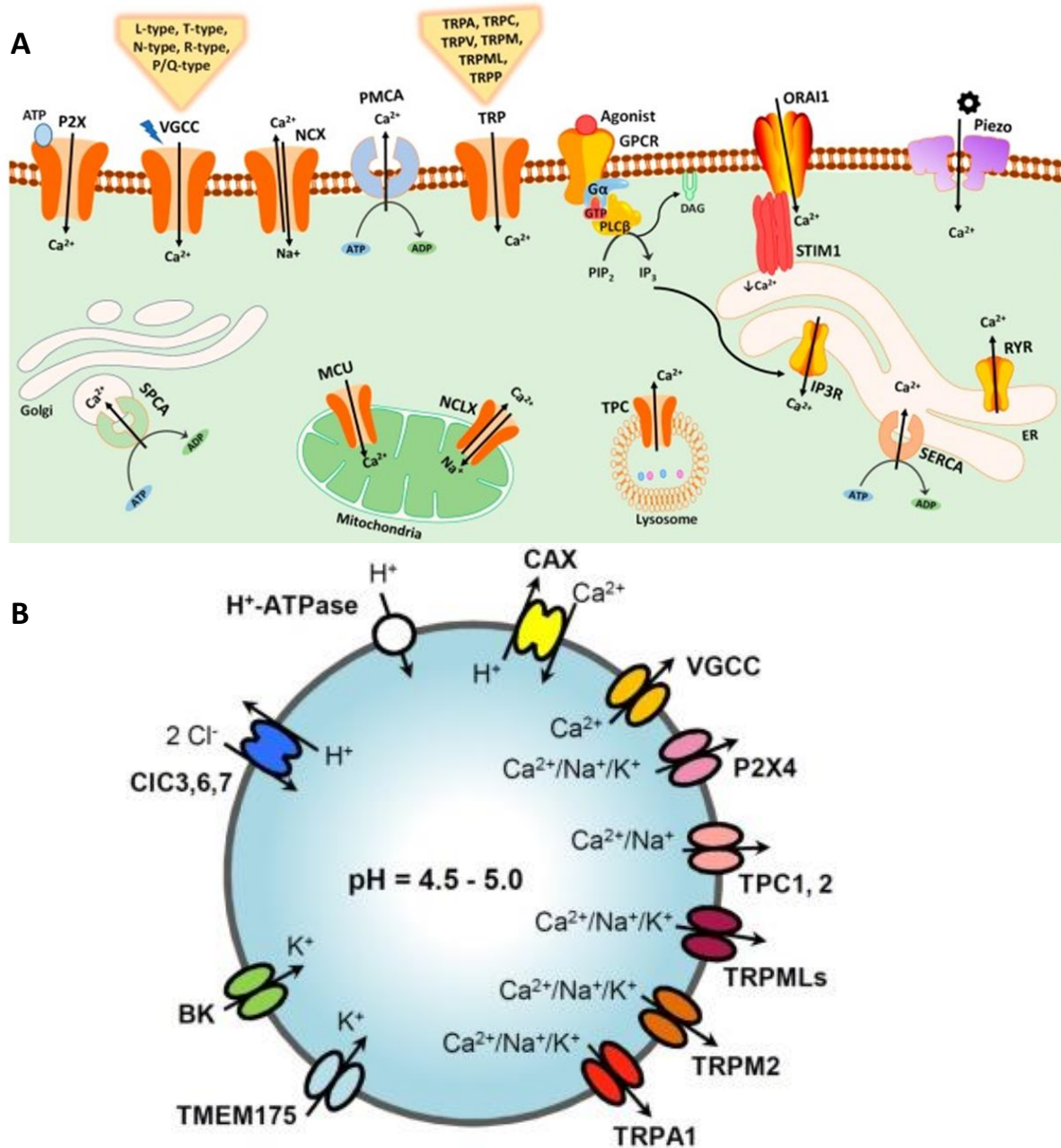
Figure 17 – Cellular and Lysosomal Ca^{2+} Channels, Pumps, Exchangers and Sensors.

A. Ca^{2+} influx is mediated by plasma membrane channels and receptors such as TRP, VGCC, P2X, and Piezo. Store operated Ca^{2+} entry is mediated by STIM1 sensor and ORAI1 channels. Distribution of Ca^{2+} across cell compartments is regulated by Ca^{2+} pumps including the PMCA, SERCA, and SPCA. Endoplasmic reticulum Ca^{2+} channels include RYR and IP3R; the latter activated by IP3 produced by GPCR via Gaq and PLCβ proteins. TPC regulate Ca^{2+} release from the endolysosomes. Mitochondrial Ca^{2+} levels are controlled by MCU and NCLX. Adapted from (Maklad, Sharma, & Azimi, 2019). **B**. H$^+$ transport and Ca^{2+} entry and release pathways in the lysosome. TRPMLs: Transient Receptor Potential Mucolipins. TRPM2: Transient Receptor Potential Melastatin 2. TRPA1: Transient Receptor Potential ankyrin 1. P2X4: Purinergic P2X receptor subtype 4. TPC1/2: Two pore channel 1/2. VGCC: voltage-gated Ca^{2+} channel. BK: big conductance Ca^{2+}-activated K$^+$ channel. TMEM175: endolysosomal K$^+$ channel. ClC: ClC family of chloride channels (Cl$^-$/H$^+$ exchangers). V-ATPase: vacuolar H$^+$-ATPase. CAX: Ca^{2+}-H$^+$ exchanger. Adapted from (Zhong, et al. 2017)

1.4.1 Components Affecting Intracellular Ca^{2+} Concentrations

Under resting conditions, the intracellular free [Ca^{2+}] is approximately 100 nM, 10^4 times lower than the 1 mM extracellular [Ca^{2+}] (Bagur & Hajnóczky, 2018). Inside the cell, the [Ca^{2+}] within the nuclear and mitochondrial matrixes are similar to the cytoplasm. However, other intracellular organelles accumulate Ca^{2+} at high concentrations; up to 500 µM in the endoplasmic reticulum (Vandecaetsbeek, Vangheluwe, Raeymaekers, Wuytack, & Vanoevelen, 2011), 1-2 mM in the Golgi apparatus (Van Baelen, et al., 2004), 500 µM in lysosomes (Christensen, Myers, & Swanson, 2002), and up to 2.5 µM in endosomes (Albrecht, Zhao, Nguyen, Campbell, & Johnson, 2015). The cell regulates organellar and cytoplasmic Ca^{2+} levels using various channels, pumps, and cytoplasmic and organellar buffers.

Plasma Membrane Ca^{2+} Efflux: PMCAs and NCX

Plasma membrane Ca^{2+} ATPase (PMCAs) help re-set and maintain cytoplasmic free Ca^{2+} levels in eukaryotic cells by expulsing Ca^{2+} through the hydrolysis of ATP (Strehler, et al., 2007), and also participate in dynamic and localized Ca^{2+} signalling in health and disease (Brini & Carafoli, 2009). Mammals express four different PMCA isoforms (PMCA1-4), but due to alternative splicing affecting two major sites located in the first intracellular loop (A site) and the C-terminal tail (C site) of the pump, the total number of PMCA variants is much larger (Strehler & Zacharias, 2001). PMCA1 and PMCA4 are expressed in colon epithelial cells (Aung, Roberts-Thomson, & Monteith, 2007), and in colon cancer cells PMCA1 expression is increased while PMCA4 is downregulated (Pérez-Riesgo, et al., 2017). PMCAs have high affinities for Ca^{2+} but low transport capacity – one Ca^{2+} per ATP hydrolysed (Albers & Siegel, 1999), meaning these pumps are unlikely to carry out bulk movements of Ca^{2+} but are most effective in maintaining very low concentrations of cytosolic Ca^{2+} in resting cells.

The sodium-calcium exchanger (Na$^+$/Ca^{2+} exchanger, or NCX) is an antiporter plasma membrane protein. NCX can exchange Na$^+$ and Ca^{2+} in either direction depending on the transmembrane electrochemical gradients and membrane potential (Khananshvili, 2014). Under physiological conditions, it uses the electrochemical gradient of Na$^+$ to flow down its gradient across the plasma membrane in exchange for the transport of Ca^{2+} against its electrochemical gradient; one Ca^{2+} is exported for every three Na$^+$ imported. However, reverse transport occurs under special conditions (such as cancer or inflammation), whereby three Na$^+$ are exported for one Ca^{2+} imported (Khananshvili, 2013). Three NCX genes (NCX1-3) and a number of alternative splicing products exist in mammals (Philipson & Nicoll, 2000). NCX1 and NCX2 are expressed in human colonic cells, and in colonic cancer cells NCX2 is dramatically enhanced (Pérez-Riesgo, et al., 2017).

<u>Plasma Membrane Ca^{2+} Influx: TRP Channels, Piezo, P2X Receptors, VGCCs</u>

Transient receptor potential (TRP) channels are responsible for the influx of extracellular Ca^{2+} across the plasma membrane into the cytoplasm. TRP a class of cationic channels that act as signal transducers by altering membrane potential or intracellular [Ca^{2+}] (Samanta, Hughes, & Moiseenkova-Bell, 2018). The mammalian TRP superfamily of ion channels consists of 28 cation permeable channels that are grouped into six subfamilies based on sequence homology: TRPC (Canonical), TRPV (Vanilloid), TRPM (Melastatin), TRPA (Ankyrin), TRPML (Mucolipin), and TRPP (Polycystic). Only TRPC1 is expressed in human colonic epithelial cells and is slightly higher in colonic tumour cells, but not significantly (Pérez-Riesgo, et al., 2017).

Piezo1 and Piezo2 are nonselective cationic ion channels which are activated by mechanical forces. Through mouse studies, they are known to be expressed in a diverse range of tissues (e.g., lymphatic, neurons, embryonic, epithelial) and are involved in a variety of physiological functions (Moroni, Servin-Vences, Fleischer, Sánchez-Carranza, & Lewin, 2018). In the GI tract, Piezo channels are expressed in the stomach, small bowel, and colon (Alcaino, Farrugia, & Beyder, 2017). Piezo2 has been shown to be expressed on a subset of mouse and human enterochromaffin cells which are mechanosensitive (Alcaino, et al., 2018). In response to mechanical stimulation, those enterochromaffin cells experienced a rapid inward ionic current caused by of Piezo2-dependent Ca^{2+} influx, leading to serotonin release to regulate intestinal fluid secretion. Another study showed Piezo1 having an inflammatory role in mice pancreatic acinar cells (Romac, Shahid, Swain, Vigna, & Liddle, 2018). Pharmacological activation of Piezo1 using Yoda1 stimulated Ca^{2+} influx and induced Ca^{2+}-dependent pancreatic injury, which was blocked using GsMTx4.

P2X are ion channel–forming receptors for ATP which form Ca^{2+}-permeable nonselective cation channels that allow Ca^{2+} influx. Seven subtypes of P2X receptors have been identified in mammals (P2X1-7), which form either homomeric or heteromeric channels (Li, Silberberg, & Swartz, 2013). All P2X receptors have been shown to be expressed in human epithelial cell lines (Coutinho-Silva, et al., 2005) and (Taylor, et al., 1999), the latter suggesting P2X receptor stimulation caused Cl$^-$ secretion across epithelial barriers. Outside the intestinal epithelium, P2X receptors are expressed in neurons within the enteric, myenteric and submucous plexus (Burnstock, 2011), and are heavily implicated in GI health and disease (Burnstock 2014).

Voltage-gated Ca^{2+} channels (VGCCs) are a group of Ca^{2+}-permeable voltage-gated ion channels, which include L- type and N-type Ca^{2+} channels. They initiate contraction in muscle cells, hormone secretion in endocrine cells, synaptic transmission in neurons, and regulate enzyme activity, gene expression, and other biochemical processes (Catterall, 2011). Certain VGCCs are expressed in colon smooth muscle cells and are implicated to cause pain during IBS (Choudhury, Shi, & Sarna, 2009), and whose mRNA and protein levels were elevated in colon cancer (Wang, et al. 2000).

Endoplasmic Reticular Ca^{2+} Influx: SERCA Pump and STIM-Orai Channels

The sarcoendoplasmic reticulum Ca^{2+}-ATPase (SERCA) pump maintains cytosolic $[Ca^{2+}]$ at low levels by translocating two Ca^{2+} for every ATP hydrolysed into the endo/sarcoplasmic reticulum. Vertebrates possess three SERCA genes (ATP2A1-3) which generate multiple SERCA isoforms (Brini & Carafoli, 2009). All three SERCAs are expressed in the colonic epithelium; in tumour cells, SERCA3 expression is unchanged, SERCA1 is significantly decreased while SERCA2 is significantly increased (Pérez-Riesgo, et al., 2017).

The stromal interaction molecule (STIM) and Orai proteins are components of the Ca^{2+} release-activated Ca^{2+} (CRAC) signalling cascade (Derler, Jardin, & Romanin, 2016). STIM and Orai are exemplar proteins for store-operated Ca^{2+} entry (SOCE), the process by which the emptying of endoplasmic reticular Ca^{2+} stores cause influx of Ca^{2+} across the plasma membrane. The STIM protein family includes two members, STIM1-2 (Soboloff, Rothberg, Madesh, & Gill, 2012), both of which are expressed on the endoplasmic reticulum. They are responsible for detecting decreasing $[Ca^{2+}]$ in the organelle (Liou, et al., 2005). Orai channels (historically known as CRAC channels) are 1,000 times more selective for Ca^{2+} than Na^+ (Hoth & Penner, 1993). The Orai protein family has three family members, Orai1-3 (Feske, et al., 2006). They form hexameric complexes in the plasma membrane with a ion-conducting pore in the centre that is highly selective for Ca^{2+} and whose purpose is to refill the endoplasmic reticulum (Hou, Pedi, Diver, & Long, 2012). STIM1-2 and Orai1-3 are expressed in colonic epithelial cells, however STIM1 and Orai2 were significantly higher in colonic tumour cells (Pérez-Riesgo, et al., 2017). STIM1 activates Orai in response to large drops in luminal $[Ca^{2+}]$ (Zhang, et al., 2005). STIM's Ca^{2+}-sensing domain is formed by the EF-hand and sterile-α-motif (SAM) domain, both located towards the NH_2 terminus which faces the lumen of the endoplasmic reticulum (Stathopulos, Zheng, Li, Plevin, & Ikura, 2008). In the resting state whereby endoplasmic reticular $[Ca^{2+}]$ is high, the EF-SAM domain is stable and compact, and STIM1 is homogenously distributed throughout the endoplasmic reticulum in structures organized by microtubules (Smyth, DeHaven, Bird, & Putney, Jr., 2008). Upon store depletion, the EF-hand alters its communication with the SAM domain and unfolds, exposing hydrophobic surfaces that allows aggregation of STIM proteins into dimers and oligomers (Zheng, et al., 2011). The signal is transmitted to the cytosolic portion and transforms STIM1 into its active conformation, leading to accumulation of STIM1 in punctae localized at the endoplasmic reticulum-plasma membrane junctions to interact with Orai1. While STIM1 is inactive in the cell resting state, STIM2 is partially active at smaller changes in luminal $[Ca^{2+}]$ (Brandman, Liou, Park, & Meyer, 2007). Their behavioural differences are reflected in the properties and structural stability of their EF-SAM domain (Derler, Jardin, & Romanin, 2016). The EF-hand of STIM1 has a higher Ca^{2+} affinity, meaning it is affected by larger drops in $[Ca^{2+}]$; the hydrophobic and electrostatic interactions of EF-hands and SAM is more stable in STIM2, resulting in slower Orai interactions.

<u>Endoplasmic Reticular Ca^{2+} Efflux: IP3 Receptors, RYR Receptors</u>

Inositol 1,4,5-trisphosphate receptors (IP3Rs) release Ca^{2+} from intracellular stores upon binding with its ligand, IP3. IP3Rs are primarily expressed on the endoplasmic reticulum (Berridge M. J., 1993) and Golgi apparatus (Wong, et al., 2013), but are also expressed in the nuclear envelope and nucleoplasmic reticulum (Echevarría, Leite, Guerra, Zipfel, & Nathanson, 2003). Vertebrate genomes encode three IP3Rs (IP3R1-3), which assemble into homo- and heterotetrameric channels which are regulated by many processes and can interact with an assortment of accessory proteins (Prole & Taylor, 2019). They capable of releasing large quantities (over 10^5/s) of Ca^{2+} (Vais, Foskett, & Mak, 2010) and are suggested to be mobile within the endoplasmic reticular membranes (Thillaiappan, Chavda, Tovey, Prole, & Taylor, 2017). The activation of IP3Rs requires binding of IP3 to all four subunits and binding of two Ca^{2+} onto each IP3R, although its exact mechanism and functions still remain unclear (Prole & Taylor, 2019). Many signalling pathways are coupled to IP3-induced IP3R Ca^{2+}-release, including: acetylcholine (Elsing, Hübner, Fitscher, Kassner, & Stremmel, 1997), ATP (Mori, Hosomi, Nishizaki, Kawahara, & Okada, 1997) and NADPH (Görlach, Bertram, Hudecova, & Krizanova, 2015). Interestingly, low concentrations of IP3 evoke openings of single IP3Rs leadings to Ca^{2+} "blips", while larger concentrations of IP3 evoke openings of a few IP3Rs within a small cluster leading to Ca^{2+} "puffs" (Prole & Taylor, 2019). Puffs are thought to arise when Ca^{2+} released by one IP3R ignite the activity of its IP3-bound neighbours through calcium-induced calcium-release (CICR), which induces "puffs" in other sites and generate Ca^{2+} waves that spreads across the cell; a phenomenon first described in hepatocytes (Rooney, Sass, & Thomas, 1990) and later in Xenopus oocytes (Marchant, Callamaras, & Parker, 1999). IP3R1 and IP3R2 were seen in both normal colorectal mucosa and colorectal cancer, while IP3R3 was only observed in colorectal cancer and was associated with decreased 5-year survival, suggesting a role for Ca^{2+} signalling via IP3R3 in colon cancer (Shibao, et al., 2010). This was supported by a recent transcriptomic analysis study using normal and cancerous human colonic cells; genes for IP3R1 and IP3R3 were upregulated in cancer cells while IP3R2 was downregulated, and IP3R3 was absent from normal cells but expressed in cancer cells (Pérez-Riesgo, et al., 2017).

Ryanodine receptors (RYRs) are also responsible for releasing Ca^{2+} from the endo/sarcoplasmic reticulum. It is named after the alkaloid ryanodine, an active compound from the South American plant *Ryania speciose* which binds to RYRs in an open state to release Ca^{2+}, but inhibits the receptor at concentrations >100 μM (Meissner, 1986). Three isoforms of RYRs (RYR1-3) have been identified in mammalian vertebrates which form homotetrameric assemblies (Van Petegem, 2012). RYR1 and RYR2 are expressed in human colonic epithelial cells, RYR2 being the most abundant isoform (Pérez-Riesgo, et al., 2017). The primary physiological ligand of RYRs is Ca^{2+}. In such circumstances, RYRs acts as a signal amplifier through CICR (Fabiato, 1983) like IP3Rs described earlier. However, high cytoplasmic [Ca^{2+}] can trigger closing of RYRs (Van Petegem, 2012) and RYRs can open spontaneously when the endoplasmic reticulum is overloaded with Ca^{2+} (Palade, Mitchell, & Fleischer, 1983), a process termed store overload-induced calcium release (SOICR) and is linked with sudden

death caused by ventricular tachycardia (Jiang, et al., 2004). Using RT-PCR, RYR2 and RYR3 have been identified from the microsomes – fragment of endoplasmic reticulum and attached ribosomes obtained by the centrifugation – of a human colon carcinoma cell line (Verma, Carter, Keable, Bennett, & Thorn, 1996). Stimulating those cells with acetylcholine (100 μM) caused increased levels of IP3 and induced sinusoidal Ca^{2+} oscillations, the latter of which can be inhibited by caffeine (5-50 mM) and Ryanodine (10 μM). However, in the continuous presence of Ryanodine, Ca^{2+} oscillations continued even when acetylcholine was removed, which was blocked by removing extracellular Ca^{2+} using EGTA or by higher concentrations of Ryanodine (100 μM). Thus, the authors conclude RYR2 and RYR2 to play a central role in Ca^{2+} oscillations in gut epithelial cells.

Acidic Stores: V-ATPase

The Vacuolar ATPase (V-ATPase) is a multi-subunit proton pump that is driven by ATP to pump protons into intracellular vesicles and extracellular milieu, thus acidifying them (Pamarthy, Kulshrestha, Katara, & Beaman, 2018). V-ATPase is a rotary nanomotor made up of fourteen subunits that can be categorized in two domains: the peripheral V_1 domain (subunits *A*, *B*, *C*, *D*, *E*, *F*, *G* and *H*) responsible for ATP hydrolysis and the integral membrane V_o domain (subunits *a*, *c*, *c'*, *c"*, *d*, and *e*) responsible for proton translocation (Wilkens, Zhang, & Zheng, 2005). Each subunit exists in different isoforms, hence V-ATPases are referred to as nature's most versatile proton pumps (Nishi & Forgac, 2002). V-ATPase are present on the membranes of endolysosomes, Golgi, and other specialized vesicles, as well as certain luminal compartments (Pamarthy, Kulshrestha, Katara, & Beaman, 2018). In each, V-ATPases are responsible for controlling their intracellular and extracellular pH to maintain a large number of biological functions (Forgac, 2007). In various cancers, plasma membrane V-ATPase expression has been shown to be increased in the leading edge of proliferating cancer cells to acidify the extracellular space (Cotter, Stransky, McGuire, & Forgac, 2015). The authors of a paper which observed that in breast cancer reasoned cancer cells expressed V-ATPase on the plasma membrane to create a hypoxic microenvironment with an acidic extracellular pH, since quantitative expression of V-ATPase correlated with invasiveness and metastatic potential (Sennoune, et al., 2004). In colon cancer cells, downregulation of V-ATPase activity using TM9SF4 was shown to inhibit tumour cell invasiveness and increased the cytotoxic effect of chemotherapeutic agent 5-FU (Lozupone, et al., 2015). Thus, while V-ATPases do not directly transport Ca^{2+}, acidic stores such as endolysosomes rely on them to maintain their organellar $[Ca^{2+}]$.

Acidic Store Ca^{2+} Influx: CAX and Beyond

Up until recently, it was unknown how Ca^{2+} is taken up by acidic organelles such as endosomes and lysosomes. However in lysosomes, the H$^+$ gradient was speculated to be essential for lysosomal Ca^{2+} store maintenance and refilling, as experimental dissipation of lysosomal acidity led to lysosomal Ca^{2+} release and is reversible by restoring the acidic luminal pH (Christensen, Myers, & Swanson, 2002). And then, Patel and colleagues published a paper identifying the Ca^{2+}/H$^+$ exchanger (CAX) family in non-placental mammals (Melchionda, Pittman, Mayor, & Patel, 2016). They identified widespread expression of CAX RNA in many nonplacental animal species, confirmed CAX localized to acidic organelles, showed CAX regulated cytosolic Ca^{2+} signalling, and demonstrated CAX enable acidic organelles to play important roles in Ca^{2+} signalling. Unfortunately, CAX homologues have not been identified in placental animals. One suggestion is that pH gradients may drive Ca^{2+} uptake through Na$^+$/H$^+$ exchangers and Na$^+$/Ca^{2+} exchangers, however Na$^+$/H$^+$ exchangers have so far been observed in endosomes but not lysosomes (Morgan, Platt, Lloyd-Evans, & Galione, 2011). An alternative suggestion is that the endoplasmic reticulum, and not the pH gradient, drives Ca^{2+} refilling of lysosomes (Garrity, et al., 2016). In that paper, they used Bafilomycin-A (5 µM) to Concanamycin-A (1 µM) to inhibit V-ATPase and found it did not inhibit Ca^{2+} refilling of lysosomal stores depleted using ML-SA1. However, depleting or chelating endoplasmic reticular Ca^{2+} did, and so did inhibiting IP3Rs using Xestospongin-C (10 µM). A review supported that suggestion by highlighting studies which showed membrane contact sites (MCSs) between the endoplasmic reticulum with mitochondria and lysosomes (Phillips & Voeltz, 2016). Notably, one study showed release of Ca^{2+} from acidic stores stimulated mobilisation of endoplasmic reticular Ca^{2+} (Kilpatrick, Eden, Schapira, Futter, & Patel, 2013), and another study showed the reverse (Morgan, et al., 2013); release of endoplasmic reticular Ca^{2+} using IP3 or cADPR caused Ca^{2+} release from acidic stores. The latter phenomenon was supported by a study showing endoplasmic reticular Ca^{2+}-release increasing fluorescence of Oregon Green BAPTA, an endocytosed dextran-conjugated indicator capable of quantifying lysosomal Ca^{2+} levels by its change in fluorescence (López-Sanjurjo, Tovey, Prole, & Taylor, 2013). In summary, the exact mechanisms for which acidic stores store Ca^{2+} remain elusive, however it is likely to involve crosstalk between the endoplasmic reticulum and may be regulated by changes in lysosomal [Ca^{2+}]; similar to STIM-Orai interactions between the endoplasmic reticulum and the plasma membrane.

Acidic Stores Ca^2 Efflux: TPC Receptors

Two-pore channels (TPCs) mediate Ca^{2+} release from acidic endolysosomal organelles. The animal TPC family contains three subtypes (TPC1-3) which homodimerize to form active channels. TPC1-3 have different distributions and properties. TPC1 is voltage-gated and found in a range of endolysosomal organelles (Ruas, et al., 2014). TPC2 is lipid gated and more commonly found in late endosomes and lysosomes (Kintzer & Stroud, 2018). TPC3 is also voltage-gated and found on endolysosomes as well as plasma membranes, but it is not present in primates (Ogunbayo, et al., 2015).

Despite extensive studies, much remain uncertain about TPCs. NAADP is the first ligand proven to mobilize Ca^{2+} from acidic organelles via TPC2 and possibly TPC1 to cause an increase in cytosolic $[Ca^{2+}]$ (Calcraft, et al., 2009). However, photoaffinity labelling experiments in sea urchin eggs, human cell lines and mouse models showed NAADP does not directly bind TPCs (Walseth, et al., 2012) and (Lin-Moshier, et al., 2012), suggesting an unidentified binding protein is required for TPC activation. While it is still unclear how NAADP causes Ca^{2+} release from TPCs, subsequent studies have identified a range of regulators for TPC2 such as PI(3,5)P2, Mg^{2+}, JNK, P38, and m-TORC1 (Jha, Ahuja, Patel, Brailoiu, & Muallem, 2014) and (Ogunbayo, et al., 2018). The voltage-gated TPC1 has also been shown to be activated by NAADP, and it is regulated by luminal pH, cytosolic and luminal Ca^{2+} (Rybalchenko, et al., 2012) and (Lagostena, Festa, Pusch, & Carpaneto, 2017). On the flipside, TPC1 and TPC2 have also be described to be selective for Na^+ rather than Ca^{2+} and are activated by PI(3,5)P2 rather than NAADP (Wang, et al., 2012). Indeed, a latter study describe TPC1 and TPC2 as voltage-gated Na^+ channels which senses pH changes and confer electrical excitability to organelles (Cang, Bekele, & Ren, 2014).

In spite of this, TPCs are known to influence cell processes in health and disease (Jin, et al., 2020). For example, Ca^{2+} signalling mediated by TPCs are involved in acrosome reaction and embryo development, osteoclastogenesis is mediated by TPC2 through Mg^{2+}-signalling, and NAADP induced Ca^{2+} signals through TPC2 modulates neural and skeletal muscle differentiation (Arndt, et al., 2014), (Ramos, Reich, & Wessel, 2014), (Notomi, et al., 2017), (Zhang, Lu, & Yue, 2013) and (Aley, et al., 2010). Pharmacological inhibition and knockdown of TPCs reduced virus trafficking and infection of Ebola virus (Sakurai, et al., 2016), suppressed the fusion of Middle East Respiratory Syndrome Coronavirus (MERS-CoV) with host cell membranes (Gunaratne, Yang, Li, Walseth, & Marchant, 2018), suppressed the efficiency of HIV replication in host cells (Khan, et al., 2020), and has been speculated to block SARS-CoV2 infectivity (Filippini, D'Amore, Palombi, & Carpaneto, 2020). TPCs have also been studied extensively in the context of development and differentiation (Webb, Kelu, & Miller, 2020), as well as tumorigenesis and metastasis (Alharbi & Parrington, 2019). In a study using human breast cancer cell lines, the expression of TPC1 transcripts is three to eight times higher than TPC2 transcripts (Brailoiu, et al., 2009). In another study using metastatic colorectal cancer cells, NAADP-mediated TPC1 lysosomal Ca^{2+} release triggered ERK and the PI3K/AKT signalling pathways to promote proliferation, which can be inhibited pharmacologically using Ned-19 (Faris, et al., 2019). Similar to TPC1, amplification of TPC2 genes also correlated with cancer (Wilkerson & Reis-Filho, 2013), which was observed in oral squamous cell carcinoma cell lines (Huang, Godfrey, Gooding, McCarty, & Gollin, 2006). A recent study using mouse and human cancer cell lines found TPC2 overexpression to inhibit autophagy and vesicle trafficking but increase proliferation (Sun & Yue, 2018). NAADP-mediated Ca^{2+} signalling via TPC2 has also been shown to promote VEGF-induced angiogenesis in two studies (Favia, et al., 2014) and (Pafumi, et al., 2017), which was abolished by TPC antagonists Ned-19 and naringenin. Thus, NAADP-mediated Ca^{2+} release via TPC1 and TPC2 are very likely to be connected to tumorigenesis and may be a viable target for pharmacological intervention.

Acidic Store Ca2+ Efflux: TRPMLs, P2X4 receptors

TRPMLs are mucolipin members of the TRP channels, of which there are members (TRPML1-3), and are activated by PI(3,5)P2 (Santoni, Santoni, Maggi, Marinelli, & Morelli, 2020). Localized in late endosomes and lysosomes, TRPML1 mediate the release of Ca^{2+} and possibly heavy metal ions (Fe^{2+}/Zn^{2+}) into the cytoplasm to regulate membrane trafficking, signal transduction, and ionic homeostasis (Wang W. , Zhang, Gao, & Xu, 2014). TRPML2 and TRPML3 are expressed in early and late endosomes as well as lysosomes. TRPML2 modulates the inflammatory response through its role in chemokine secretion (Plesch, et al., 2018), while Ca^{2+} signals via TRPML3 has been suggested to be required for autophagy (Kim, Soyombo, Tjon-Kon-Sang, So, & Muallem, 2009). TRPML1 and TRPML2 have been shown to be expressed in healthy and cancerous human colon cells, while TRPML3 is totally absent (Pérez-Riesgo, et al., 2017). A number of studies found TRPML1 to be pro-tumoral. Increased TRPML1 expression has also been positively correlated in human cancers with HRAS mutations, and inversely correlated with patient prognosis (Jung, et al., 2019). In patients with pancreatic ductal adenocarcinoma (PDAC), high TRPML1 was associated with worse survival chances, and knockdown of TRPML1 blocked PDAC cell proliferation *in vitro* and reduced the formation and growth of tumours in *in vivo* mouse models (Hu, et al., 2019). TRPML1 is upregulated in triple-negative breast cancer (TNBC), which when genetically downregulated and pharmacologically inhibited, suppressed the growth of TNBC (Xu, et al., 2019). On the other hand, a study using human non-small-cell lung carcinoma (NSCLC) found the gene for TRPML1 (MCOLN1) to be significantly decreased in stage I-II TNBC compared to normal lung tissues, but increased in stage III-IV. Finally, a transcriptomic analysis found TRLMP1 and TRPML2 to be decreased in colon cancer cells compared to healthy colon cells (Pérez-Riesgo, et al., 2017). Taken together, these studies suggest TRPMLs may confer a survival advantage in certain advanced tumours, or TRPMLs may be deleted to increase oxidative stress and genetic instability and thus support tumorigenesis.

P2X4 is unique within the P2X family due to it being located predominantly within endolysosomes, and is activated by intra-lysosomal ATP at pH 7.4 to cause Ca^{2+} influx (Suurväli, Boudinot, Kanellopoulos, & Boudinot, 2017). Very few studies have investigated the role of endolysosomal P2X4 in epithelial cells. Those that do involve lysosome-related organelles in alveolar epithelial cells, where P2X4 has been described to play a critical role in the secretion and activation of pulmonary surfactant (Murrell-Lagnado, 2018).

<u>Golgi Ca^{2+} influx: SPCA</u>

In addition to SERCA pumps, the secretory pathway ATPase (SPCA) pump is responsible for loading the Golgi complex with Ca^{2+} and Mn^{2+} (Vandecaetsbeek, Vangheluwe, Raeymaekers, Wuytack, & Vanoevelen, 2011). Two SPCA (SPCA1 and SPCA2) proteins exist. SPCA1 is the housekeeping Ca^{2+} and Mn^{2+} pump of the secretory pathway expressed in the Golgi apparatus. High [Ca^{2+}] within the Golgi is indispensable for proper protein transcription, translation, translocation, folding, and processing; Mn^{2+} is a necessary cofactor for several enzymes within the Golgi. SPCA2 mRNA expression is more restricted – abundant throughout the gastrointestinal tract, in trachea, thyroid, salivary gland, mammary gland and in prostate (Vanoevelen, et al., 2005). The majority of cells which express SPCA2 are notable for being secretory. For example, in human goblet cells, SPCA2 colocalize with SPCA1 near the apical pole of the nucleus, suggesting an important role for SPCA2 in protein secretion.

<u>Mitochondria Ca^{2+} Influx: MCU and Others</u>

The mitochondrial Ca^{2+} uniporter (MCU) complex is one of several proteins responsible for Ca^{2+} influx into the mitochondria. It exists on the inner mitochondrial membrane as a multi-protein complex consisting of transmembrane subunits (MCU, MCUb and EMRE) and membrane-associated regulatory subunits (MICU1-3), which are capable of changing MCU activity (Mishra, et al., 2017). The MCU complex has a low Ca^{2+} affinity, relies on the inner mitochondrial membrane's membrane potential to drive Ca^{2+} uptake, and is in close contact with the endoplasmic reticulum to ensure a prompt accumulation of Ca^{2+} into the mitochondria when Ca^{2+} is effluxed from the latter (Marchi & Pinton, 2014). In colon tumour cells, MCU and its positive modulator MICU1 is overexpressed while negative modulator MICU2 is under expressed (Pérez-Riesgo, et al., 2017), and upregulation of MCU was associated with poor prognosis in patients with CRC (Liu, et al., 2020). Liu and colleagues also showed that upregulation of MCU enhanced mitochondrial Ca^{2+} uptake to promote mitochondrial biogenesis, which in turn facilitated CRC cell growth in vitro and in vivo. Besides MCU, other mitochondrial Ca^{2+} channel/transporters include voltage dependent anion channel (VDAC), mitochondrial ryanodine receptor 1 (mRyR1), rapid mode of uptake (RaM), mCa1 & 2, Coenzyme Q 10 (CoQ10), the transient receptor potential channel 3 (TRPC3), and the Leucine zipper-EF-hand containing transmembrane protein 1 (LETM1) (Mishra, et al., 2017). The Na$^+$/Ca^{2+} exchanger, which also mediates Li$^+$/Ca^{2+} exchange hence its abbreviation (NCLX), is responsible for the efflux of Ca^{2+} in exchange for Na$^+$.

<u>Ca^{2+} Buffers</u>

Besides the channels, transporters and pumps mentioned earlier, cytoplasmic Ca^{2+} signals are also shaped by a range of cytoplasmic buffers (Schwaller, Cytosolic Ca2+ Buffers, 2010). Ca^{2+} buffers also exist within the endoplasmic and sarcoplasmic reticulum, Golgi, and mitochondria (Prins & Michalak, 2011).

1.4.2 Intracellular Ca^{2+} Signalling Proteins

Ca^{2+} is a versatile and fast intracellular messenger which controls a wide range of cellular functions through regulation of a wide range of target proteins. Various stimuli can cause an increase in cytoplasmic [Ca^{2+}], due to influx of Ca^{2+} from the plasma membrane or efflux of Ca^{2+} from organellar stores. As described earlier, Ca^{2+} can bind to other Ca^{2+} channels such as IP3Rs or RYRs. Besides that, Ca^{2+} can bind to Ca^{2+}-sensitive proteins such as Calmodulin, which reacts with Calmodulin kinases and Calcineurin to activate downstream responses.

Calmodulin (CaM) is a Ca^{2+} sensing protein widely expressed in all eukaryotic cells. CaM is a versatile Ca^{2+} sensor – capable of responding to micro to picomolar [Ca^{2+}] and is known to interact with a diverse array of target proteins such as CaM kinases and ion channels. It mediates a variety of cellular signalling processes including regulation of enzymatic activities, modulation of ion channel activities, synaptic transmission and plasticity, and regulation of gene expression (Zhang, et al., 2013). CaM has four EF-hands, two on the N-terminus and two on the C-terminus, which serve as high affinity Ca^{2+} binding motifs (Meador, Means, & Quiocho, 1992). Upon binding Ca^{2+}, CaM changes its conformation from the closed configuration to the open one, exposing hydrophobic surfaces within the N- and C-terminus for Ca^{2+}-dependent interactions with target proteins.

CaM kinases (CaMK) is a target protein of CaM. CaMK can be divided based on their substrate specificity: restricted or multifunctional (Skelding & Rostas, 2012) and (Skelding & Rostas, 2019). Restricted CaMK have three families: phosphorylase kinase (PhK), elongation factor 2 kinase (eEF2K), and myosin light chain kinase (MLCK). Multifunctional CaMK have four families: CaMKI, CaMKIV, CaMKK, and CaMKII. Though all of them are activated by Ca^{2+}-bound CaM, each CaMK has distinct activation mechanisms and subcellular localization (Takemoto-Kimura, et al., 2017). CaMKII in particular has been shown to be overexpressed in human CRC and was associated with cancer differentiation and migration via the ERK1/2 and p38 pathways (Chen, et al., 2017).

Calcineurin (CaN) is a serine/threonine phosphatase which is activated by increased intracellular [Ca^{2+}] and forms a crucial connection between intracellular Ca^{2+} signalling the phosphorylation states of numerous substrates (Creamer, 2020). Along with CaMK, CaN directly links Ca^{2+} signalling to protein phosphorylation states and plays an essential role in numerous signalling processes. One such signalling process is calcineurin-mediated dephosphorylation of the nuclear factor of an activated T cell (NFAT) (Park, Yoo, Kim, & Kim, 2020), which is associated with metastatic capacity in colon cancer (Tripathi, et al., 2015).

1.4.3 Spatio-Temporal Properties of Ca^{2+} Signalling

The spatiotemporal variability of intracellular Ca^{2+} signals is extreme. In single neurons, action potential influx of Ca^{2+} followed by neurotransmitter release occurs within milliseconds (Südhof, 2012). On the other hand, Ca^{2+} signalling during fertilization, embryogenesis and organogenesis occurs over days and affects neighbouring cells several millimetres away via gap junctions (Paudel, Sindelar, & Saha, 2018). Within the intestinal epithelium, the spatiotemporal characteristics of Ca^{2+} signalling is essential for ISC activity, packing and releasing MUC2, and ion and fluid secretion.

Ca^{2+} Signals are Critical for Intestinal Stem Cell Activity

In 2016, Deng and colleagues identified Ca^{2+} signals as a central regulator of ISC activity in *Drosophila* (Deng, Gerencser and Jasper 2016). They first identified dietary L-Glu as a stimulus which binds to mGluR – a GPCR which recruits Gaq, caused a reduction in frequency but increase the intensity of ISC cytosolic Ca^{2+} oscillations, and increased ISC proliferation. When they knocked down STIM/SERCA/PMCA, or over-expressed STIM-Orai/IP3R, they observed sustained elevation of cytosolic [Ca^{2+}] and increased ISC proliferation rates. They then showed that CaN promoted the nuclear translocation of CREB regulated transcription co-activator (CRTC) to induce ISC proliferation; silencing a regulatory subunit of CaN significantly abrogated ISC proliferation, while constitutive activation of CRTC was sufficient to induce ISC proliferation independently of mGluR, Gaq and IPR3. Besides dietary L-Glu, they monitored Ca^{2+} oscillations within ISCs under mitogenic conditions, during *Erwinia carotovora carotovora 15* (Ecc15) infection, during Notch knockdown, and during Bleomycin treatment - which causes DNA damage and results in compensatory proliferation of ISCs. Mitogenic conditions included the over-expression of Insulin Receptor, Ras^{V12} – a constitutively active allele of Ras, or Upd2 – a ligand of the JAK/Stat pathway which stimulates ISC proliferation after tissue damage. In all cases, oscillation frequency decreased while average signal intensity increased. They also showed that Ca^{2+} oscillations induced by Ecc15 infection was reversible; returning to basal states after 24 hours when ISC proliferation subsided. To confirm that Ca^{2+} signalling is key in the integration of different stimuli to control ISC proliferation, loss of function of STIM/Orai/IP3R/CaN/CRTC resulted in significant reduction of ISC activity induced by over-expression of Insulin Receptor or Ras^{V12}, Ecc15 infection, or Bleomycin treatment. And accordingly, IP3R or Orai loss of function prevent the increase in cytosolic [Ca^{2+}]. Finally, they identified an additional ISC state besides the two under homeostatic conditions: quiescent ISCs which show frequent and robust Ca^{2+} oscillations with a low level of cytosolic Ca^{2+}, and highly proliferative ISCs which show reduced Ca^{2+} oscillations with high levels of cytosolic Ca^{2+}. ISCs with impaired Ca^{2+} signalling had reduced oscillation frequency, low cytosolic [Ca^{2+}] and are proliferation deficient. Thus, cytoplasmic Ca^{2+} signalling is critical for the ability of ISCs to undergo rapid and reversible activation, and dynamically controls ISC's proliferative activity in response to a wide range of signals.

Mucin Synthesis, Packing and Secretion is Dependent on Ca^{2+} Signals

The packing and release of gel-forming MUC2 is dependent on Ca^{2+} (Ambort, et al., 2012), which has been elaborated earlier (in Chapter 1.2.1). Calcium-activated chloride channel regulator 1 (CLCA1) has recently been highlighted to play an essential role in goblet cell mucus production and processing in the epithelium of the respiratory tract (Liu & Shi, 2019) and the colon (Nyström, Arike, Ehrencrona, Hansson, & Johansson, 2019). Four CLCA members have been identified in humans (hCLCA1-4). In humans, CLCA1 is expressed in the intestinal epithelia and is activated by Ca^{2+} to conduct Cl^- across the epithelial plasma membrane (Gruber, et al., 1998). However, CLCA1 can also be secreted from cells and function as a metalloprotease. Nyström and colleagues previously showed CLCA1 controlled colonic mucus expansion by proteolytically cleaving MUC2 (Nyström, et al., 2018), and thereby contribute to mucus homeostasis by converting the firm inner mucus layer to the loose outer mucus layer. They also CLCA1 proteolysis was Ca^{2+}-dependent, as removing Ca^{2+} from the proteolysis assay buffer blocked the reaction. CLCA1 has also been associated with cancer. In colorectal cancer, reduced CLCA1 expression correlates with disease relapse and poor survival (Yang, et al., 2015), and a genetic study using fixed human colorectal carcinoma samples indicated a negative association between CLCA1 levels and cancer stage (Ostasiewicz, Ostasiewicz, Duś-Szachniewicz, Ostasiewicz, & Ziółkowski, 2016). However, the reverse is true with ovarian cancer. RT-PCR and immunoblot analyses showed CLCA1 was overexpressed during ovarian cancer progression, and silencing CLCA using siRNA prevented ovarian cancer cells from forming multicellular aggregates (Musrap, et al., 2015). Thus, CLCA1 may have different roles depending on the tumour type.

During mucus exocytosis, the membranes of mucus granules fuses with the plasma membrane. This membrane-to-membrane fusion is tightly regulated SNARE proteins – syntaxin (Syt), SNAP25 and VAMP – which are located on both membranes and form SNARE complexes to regulate fusion and exocytosis (Südhof & Rothman, 2009). SNARE complexes are also involved in another exocytic process involving vesicle-to-vesicle fusion, which is called compound exocytosis (Pickett & Edwardson, 2006), and is thought to be a way of enhancing secretory output. Syt2 has been shown to be Ca^{2+}-dependent and serves as a critical sensor of stimulated mucin secretion (Pang, et al., 2006) and (Adler, Tuvim, & Dickey, 2013). A wide variety of stimuli can induce goblet cell compound exocytosis. Two stimuli which will be discussed later are acetylcholine (Birchenough, Johansson, Gustafsson, Bergström, & Hansson, 2015) and ATP (Kreda, et al., 2010).

Generation of Reactive oxygen species (ROS) can lead to elevated cytosolic $[Ca^{2+}]$, possibly via RYR1 (Hidalgo, Sánchez, Barrientos, & Aracena-Parks, 2006). Notably, ROS have also been shown to be involved in some cases of mucus secretion in colonic goblet cells in a Ca^{2+}-dependent manner (Patel, et al., 2013). They found the autophagy protein LC3 to localize to intracellular multi-vesicular vacuoles, which are fusions of autophagosomes and endosomes. Both LC3 and endosome formation were required for maximal production of ROS derived

from NADPH oxidases, which also localized to and enhanced the formation of LC3-positive vacuoles. The generation of ROS promoted mucus secretion and thus prevent accumulation of mucin granules. They confirmed that ROS-induced mucus secretion is Ca^{2+}-dependent by showing the addition of BAPTA-AM inhibited mucin release induced by ROS. Furthermore, they released stored intracellular Ca^{2+} using ionomycin and found diminished intracellular mucin as a result.

Fluid Secretion is Dependent on Ca^{2+} Signals

Besides mucus, the intestinal epithelium also secretes ions and fluid into the lumen. Briefly, regulated secretion of Cl^-, HCO_3^- and smaller amounts of other anions into the lumen establishes a negative electrical driving force for trans-epithelial Na^+ secretion via the paracellular pathways, together generating the osmotic driving force for water flow (Frizzell & Hanrahan, 2012). In the intestinal epithelium, the secretion of Cl^- and HCO_3^- provides the driving force for water absorption or secretion to maintain the liquid homeostasis in the human body (Yang, et al. 2018). This process is activated via muscarinic receptors and mediated Ca^{2+} release via IP3R. The dependence of Ca^{2+} in epithelial Cl^- secretion was observed in rat intestines over thirty years ago and shown to be induced by acetylcholine, which was inhibited by removing extracellular Ca^{2+} using EGTA and using intracellular Ca^{2+} antagonist TMB8 and verapamil (Hardcastle, Hardcastle, & Noble, 1984). Carbachol – a muscarinic receptor agonist and pharmacological analogue of acetylcholine, was shown to mobilize intracellular Ca^{2+}, which was blocked by muscarinic receptor antagonist atropine and IP3R antagonist 2-APB. Muscarinic receptor activation induced SOCE on the basal side of the intestinal epithelium, which was blocked by TRPC3/7 antagonist Flufenamic acid and STIM1 antagonist SKF-96365. This supported an older study which showed the intestines' ability to secrete fluid was Ca^{2+}-dependent (Reynolds, Parris, et al. 2007).

1.4.4 Influence of Acetylcholine-Induced Ca^{2+} Signals on the GI Track

In the GI tract, acetylcholine has been shown to regulate peristalsis by inducing muscle contraction (Nezami & Srinivasan, 2013), stimulate fluid and ion transport across the epithelium (Keely, 2011), regulate gut immunity (Pan, Zhang, Shao, & Huang, 2020), stimulate mucus secretion (Specian & Neutra, 1980), and promote ISC proliferation (Takahashi, Shiraishi, & Murata, 2018). In the case of gut peristalsis, enteric neurons were the source of ACh. However, non-neuronal acetylcholine is implicated in fluid and ion transport, gut immunity, and ISC proliferation. The synthesis of neuronal and non-neuronal acetylcholine has been discussed earlier in the context of tuft cells (Chapter 1.3.3). Acetylcholine binds to two families of receptors: metabotropic muscarinic receptors and the ionotropic nicotinic receptors. As the research conducted in this thesis only covers muscarinic receptors, the role of nicotinic receptors in GI health and disease is deliberately being omitted.

Metabotropic receptors are defined as membrane receptors which do not form an ion channel pore but use signal transduction mechanisms, such as G-proteins, to activate a series of intracellular events using second messenger chemicals. Muscarinic receptors (mAChRs) are named as such due to being discovered to be activated by muscarine, a toxin from the mushroom *Amanita muscaria*, and inhibited by atropine, a toxin from *Atropa belladonna*. Five subtypes of mAChRs exist (M1-5) and all of them are expressed in the human GI tract. Three mAChRs subtypes (M1, M3 and M5) couple to G$_q$/$_{11}$ while two subtypes (2 and 4) couple to G$_{i/o}$ (Kruse, et al., 2014). G$_i$ is known to inhibit the cAMP-dependent protein kinase, resulting in decreased production of cAMP. G$_q$ is known to activate beta-type phospholipase C (PLC-β) enzymes, which hydrolyses phosphatidylinositol 4,5-bisphosphate (PIP2) to diacyl glycerol (DAG) and inositol trisphosphate (IP3). IP3 is a ligand for IP3Rs which induces release of stored endoplasmic reticular Ca^{2+} (Figure 17) and is also a component of the EGF signal transduction (Figure 14). Thus, cholinergic stimulation of mAChRs using acetylcholine or its pharmacological analogues such as Carbachol (CCh) is expected to influence GI function during homeostasis and disease, and those involving M1, M3 and/or M5 are expected to occur in a Ca^{2+}-dependent manner.

In two studies which used mice to investigate GI contractibility, M2 and M3 were found to be preferentially expressed throughout the intestinal smooth muscle layer (Gao, et al., 2016) and are sensitive to acetylcholine stimulation (Joo, et al., 2011). Interestingly, Joo and colleagues found M3 to stimulate contraction while M2 inhibited contraction; inhibiting M3 using 4-DAMP resulted in reduced contractility after acetylcholine treatment, inhibiting M2 using AQ-RA741 resulted in increased contractility after acetylcholine treatment. Unfortunately, neither studies investigated the status of Ca^{2+} signals in their systems. Cholinergic-stimulated mAChR activation has also been studied in the GI with regards to modulating gut immunity. Two knockout mice studies have shown cholinergic-activation of gut lymphoid cells which express M3 to be essential for mounting an effective immune response against helminth and bacterial infection (McLean, et al., 2016) and (Darby, et al., 2015). Darby and colleagues

confirmed this process was dependent on release of endoplasmic reticular Ca^{2+}-stores, as M3 knockout mice had impaired cytosolic Ca^{2+} elevation induced by ionophore ionomycin.

Many studies have investigated mAChRs in the context of GI secretion. Using mAChR knock-out mice, cholinergically stimulated gastric acid secretion was shown to be mediated by M3 and M5 but not M1 (Aihara, Nakamura, Taketo, Matsui, & Okabe, 2005). A later study which also used knock-out mice confirmed CCh caused increased acid secretion which could be inhibited by mAChR antagonist atropine (Takeuchi, Endoh, Hayashi, & Aihara, 2016). They also found M4 to inhibit release of somatostatin from D-cells, resulting in enhanced acid secretion mediated by M3 on parietal cells. But again, neither studies investigated the status of Ca^{2+} signals. Cholinergic stimulation is a known regulator of ion and fluid transport in the intestinal epithelium (Hirota and McKay 2006) and is Ca^{2+}-dependent, the latter of which was briefly described in (Chapter 1.4.3). Several studies highlight basolateral activation of M3 by cholinergic stimulants raised intracellular $[Ca^{2+}]$ (Haberberger, Schultheiss, & Diener, 2006) and (Hirota and McKay 2006), resulting in Ca^{2+}-dependent basolateral K^+ efflux (Bajnath, Dekker, Vaandrager, de Jonge, & Groot, 1992) which creates the driving force for Cl^- secretion into the gut lumen (Kachintorn, Vajanaphanich, Traynor-Kaplan, Dharmsathaphorn, & Barrett, 1993).

Finally, cholinergic activation of mAChRs have been heavily studied in the context of regulating ISC proliferation. A recent paper suggested M1 to mediate intestinal mucosal growth, as it was highly expressed throughout the mouse intestines (Greig, Armenia, & Cowles, 2020). And when they continuously stimulated M1 *in vivo* using a specific agonist, McN-A-343, it resulted in increased villus height, crypt depth, and crypt-cell proliferation. This is in contrast of an older study which proposed M3 and M5 to regulate stem/progenitor cells and thus maintain the intestinal epithelial barrier (Lundgren, Jodal, Jansson, Ryberg, & Svensson, 2011). However, the evidence in that study are not definitive, as they showed M3/5 expression using only immunolabelling and used a non-selective mAChR antagonist, atropine, in their BrdU assay. In contrast to these two, another study found M2 to be expressed at the stem cell zone and in fact co-localize with Paneth cells (Muise, Gandotra, Tackett, Bamdad, & Cowles, 2017). Besides acting directly on ISCs, a recent study identified M3 to be expressed in mouse Prox1+ endocrine cells and provide negative feedback (Middelhoff, et al., 2020). During homeostasis, Prox1+ endocrine cells inhibited the expansion of tuft cells – which can synthesize and secrete non-neuronal acetylcholine (Chapter 1.3.3). However, when muscarinic signals were disrupted, they promote tuft cell expansion who adopt an enteroendocrine phenotype and contribute to acetylcholine synthesis and induce proliferation. A few years ago, a study confirmed non-neuronal acetylcholine to be an endogenous regulator of proliferation and differentiation of Lgr5+ ISCs in mice by activating mAChRs, however they observed reduced organoid growth due to cholinergic stimulation, while antagonising mAChRs pharmacologically enhanced organoid growth and differentiation (Takahashi, et al., 2014).

1.4.5 Influence of ATP-Induced Ca²⁺ Signals on the GI

Adenosine triphosphate (ATP) is an intracellular energy source in all known forms of life. The hydrolysis of ATP to ADP and further to AMP provides energy to a broad range of cellular functions such as ion transport, muscle contraction, nerve impulse propagation, substrate phosphorylation, and chemical synthesis (Dunn & Grider, 2020). For example, ATP's direct involvement in PMCA, SERCA, V-ATPase and SPCA (Chapter 1.4.1) is crucial for the maintenance of cytosolic Ca^{2+} homeostasis. That said, ATP is also an important extracellular signalling molecule through its activation of purinergic P2 receptors (Burnstock 2014). P2 receptors can be further divided into metabotropic P2Y receptors and ionotropic P2X receptors. As the research conducted in this thesis only covers P2Y receptors, the role of P2X receptors in GI health and disease is likewise deliberately being omitted.

As defined earlier, metabotropic receptors use signal transduction mechanisms, such as G-proteins, to activate intracellular events using second messengers. P2Y receptors are no different. Eight P2Y receptor subtypes are known to exist, each unique in their ligands and G-protein binding properties (Puchałowicz, Tarnowski, Baranowska-Bosiacka, Chlubek, & Dziedziejko, 2014), summarized in (Table 5). Notably, P2Y2 receptors is activated by ATP and UTP, and couples to G_q. Thus, similar to cholinergic stimulation of mAChRs, purinergic stimulation of P2Y receptors via ATP/ADP/UTP/UDP is expected to influence GI function during homeostasis and disease, and those involving P2Y1, P2Y2, P2Y4, P2Y6 and P2Y11 are expected to occur in a Ca^{2+}-dependent manner.

Table 5 – P2Y Receptor Ligand and G-protein Binding Characteristics.

Receptor	P2Y1	P2Y2	P2Y4	P2Y6	P2Y11	P2Y12	P2Y13	P2Y14
ATP-binding	Yes	Yes	No	No	Yes	No	Yes	No
ADP-binding	Yes	Yes	No	No	No	Yes	Yes	No
UTP-binding	No	Yes	Yes	No	No	No	No	No
UDP-binding	No	Yes	No	Yes	No	No	No	Yes
G-protein coupled	G_q	G_q	G_q	G_q	G_q	G_i	G_i	G_i

P2Y receptors are heavily involved in modulating gut immunity. Activation of P2Y1 and/or P2Y11 receptors by low doses of ATP is suspected to suppress immune responses and generate tolerance, however high doses of ATP triggers pro-inflammation (Di Virgilio, Boeynaems, & Robson, 2009). P2Y receptors are also heavily involved in modulating GI motility. Studies in mice indicate P2Y1 receptor to be the main receptor subtype in mediating inhibitory and excitatory NANC (non-adrenergic, non-cholinergic) responses, by directly acting on smooth muscle and by activating enteric neurons to release ATP and other neurotransmitters (Giaroni, et al., 2002). P2Y2 and P2Y4 have also been shown to induce

smooth muscle contractions in the small intestines, albeit in lower vertebrates, while in P2X receptors have been shown to mediate the same effect in mammals (Burnstock 2014).

Activation of P2Y receptors by ATP also modulates GI secretions. Early studies showed ATP inhibiting gastric acid secretion (Kidder, 1973), which a later study elaborated on by showing ATP acting directly on parietal cells to selectively inhibit histamine-stimulated gastric acid (Percy, Warren, & Brunz, 1999). On the flipside, ATP has been shown to increase cytosolic $[Ca^{2+}]$ and stimulate mucous secretion in cultured rabbit gastric mucous cells (Ota, et al., 1994). While P2Y receptors are expected to be directly involved, no receptor subtype has been identified yet (Burnstock 2014). Furthermore, ATP/UTP activation of P2Y1/2/4 have been shown to stimulate intestinal ionic, fluid and/or mucin secretions (Christofi, et al., 2004), (Merlin, et al., 1994), (Ghanem, et al., 2005), (Matos, Robaye, Boeynaems, Beauwens, & Leipziger, 2005) and (Kreda, et al., 2010), which one study found to be mediated by increased cytosolic $[Ca^{2+}]$ and could be blocked by 2-APB (Dong, et al., 2009).

While P2Y receptors have not been studied in the context of ISCs, their expressions and functions have been studied in colon cancer cell lines and other epithelial cancers. A study using two human epithelial carcinoma cell lines found P2Y1 to be highly expressed (Coutinho-Silva, et al., 2005). They also found high concentrations of ATP to be pro-apoptotic and caused an increase in cytoplasmic $[Ca^{2+}]$, while lower concentrations of ATP stimulated proliferation instead. P2Y2 and P2Y4 receptors have also been shown to be overexpressed in human colon cancer cell lines (Nylund, Hultman, Nordgren, & Delbro, 2007) and were proposed to regulate cell growth in non-neoplastic as well as neoplastic tissues through binding with ATP and subsequent downstream signalling. A latter study, also on human cancer cell lines, elaborated on how activation of P2Y receptors by ATP promoted cancer cell proliferation by showing it activated the phosphorylation of ERK1/2, p46 JNK and p38 MAP kinases (Buzzi, Boland, & de Boland, 2010), all components of the EGF signal transduction pathway (Figure 14). A recent study implicated P2Y2 receptor to promote growth and invasion of breast cancer via endogenous release of ATP (Kim, et al. 2020). They showed P2Y2 receptor expression was higher in breast cancer tissues compared to normal, and when they compared breast cancer cells, found highly metastatic cells releasing more ATP and exhibiting greater P2Y2 receptor activity compared to lowly metastatic cells.

1.4.6 Aberrant Ca^{2+} Signals and Colorectal Cancer

Under resting conditions, intracellular $[Ca^{2+}]$ remain low compared to the extracellular $[Ca^{2+}]$. This is achieved by cytosolic buffers and a vast array of pumps, enzymes, exchangers and channels on the plasma membrane and organelles. The increase in cytoplasmic $[Ca^{2+}]$ via influx through the plasma membrane or release of organellar Ca^{2+} stores allows Ca^{2+} to modulate a wide range of cellular functions through regulation of numerous target proteins. The spatiotemporal nature of Ca^{2+} signalling varies between and within cells, influencing

physiological processes such as adaptive immunity and tolerance, GI motility, mucus and ion secretion, and proliferation. Thus, when Ca^{2+} signals become dysregulated, especially within cells in the intestinal stem cell zone, it predisposes the tissue to tumorigenesis.

The role of Ca^{2+} in CRC has long been controversial (Wang, et al. 2019). There are studies which suggest upregulation of Ca^{2+} promoted tumorigenesis (Lipkin & Newmark, 1985), and studies which suggest the opposite (Garland, et al., 1985). The latest World Cancer Research Fund recommend Ca^{2+} supplements as a preventive measure against CRC and other cancers (World Cancer Research Fund, 2018), yet a conflicting study found Ca^{2+} supplements to have no significant association with CRC (Kahwati, et al., 2018). While some studies found Ca^{2+} signals playing anti-tumour roles (Wang, et al. 2019), the expression of various components involved in regulating cellular Ca^{2+} is known to be altered during CRC (Pérez-Riesgo, et al., 2017), many of which were mentioned earlier (Chapter 1.4.1). This indicates that the spatio-temporal characteristics of Ca^{2+} signals are altered in CRC, thereby changing its function from anti-tumorigenic to pro-tumorigenesis.

Aberrant autologous secretion of non-neuronal acetylcholine acts as an autocrine growth factor to promote CRC, likely through stimulation of mAChRs and causing aberrant Ca^{2+} signals which favour tumorigenesis. This was first reported over ten years ago (Cheng, et al., 2008), and since then a lot more is known about the mechanism by which it occurs (Konishi, Hayakawa and Koike 2019). As tuft cells are capable of synthesizing and secreting acetylcholine (Pan, Zhang, Shao, & Huang, 2020), they are the likely source of non-neuronal acetylcholine. Indeed, non-neuronal acetylcholine has been shown to be released by Dclk1+ tuft cells and act on M3 on the GI epithelium, causing clonal expansion of ISCs which induced overexpression of nerve growth factor (NGF) to facilitate innervation of enteric nerves and promote carcinogenesis (Hayakawa, et al., 2017). They showed that activation of M3 led to activation of YAP/TAZ by phosphorylation, leading to increased activation of Wnt target genes. The regulatory mechanism of Wnt activation by cholinergic M3 activation has been explored in another study (Raufman, et al., 2011), in which they found β-catenin nuclear staining to be attenuated in M3 knockout mice.

ATP has also been shown to cause Ca^{2+} signals in olfactory Trpm5+ tuft cells, which also resulted in non-neuronal acetylcholine release (Fu, Ogura, Luo, & Lin, 2018). ATP activation of G_q coupled P2Y receptors are also implicated in CRC (Coutinho-Silva, et al., 2005) and (Nylund, Hultman, Nordgren, & Delbro, 2007), by causing increased cytoplasmic $[Ca^{2+}]$ which may activate the EGF signalling cascade (Buzzi, Boland, & de Boland, 2010). However, the role of purinergic receptor signalling in CRC is less well characterized (del Rocío Campos-Contreras, Díaz-Muñoz, & Vázquez-Cuevas, 2020).

Amplification of TPC genes are correlated with cancer (Wilkerson & Reis-Filho, 2013). In recent years, TPCs have been studied extensively in the context of development and differentiation (Webb, Kelu, & Miller, 2020), as well as tumorigenesis and metastasis (Alharbi & Parrington, 2019). Release of lysosomal Ca^{2+} stores via TPCs have been shown to induce proliferation (Faris, et al., 2019) and angiogenesis (Pafumi, et al., 2017), both of which can be inhibited. Thus, Ca^{2+} release via TPCs is very likely to be connected to tumorigenesis and may be a viable target for pharmacological intervention.

1.5 Hypothesis

From the above general introduction, it is clear that the gut epithelium is a dynamic tissue. It fulfils vital physiological functions such as forming a selective barrier between the luminal contents of the gut and the systemic circulation, whilst facilitating the digestion of food and absorption of nutrients and water. These physiological functions are under the control of extracellular signals that converge on the gut epithelium bilaterally – from the gut lumen and from the submucosa. Acetylcholine and ATP are exemplar extracellular neuronal ligands which influence gut epithelial biology via cholinergic/muscarinic and purinergic signalling, respectively. These extracellular signals are transduced into an extensive range of intracellular signals that regulate tissue homeostasis and physiological function. More importantly, studies have shown that these ligands can be synthesized non-neuronally – within colonic epithelial cells – and are secreted to induce autocrine/paracrine signalling. Recent observations of oscillating and propagating Ca^{2+} signals originating from within the intestinal stem cell zone of flies (Deng, Gerencser and Jasper 2016), rodents and human (Satoh and Sperelakis 1995), (Lindqvist, et al. 1998) and (Reynolds, Parris, et al. 2007) indicate a central role for Ca^{2+} signals in coordinating the physiological processes that underpin intestinal tissue homeostasis.

The focus of this thesis is to investigate the molecular nature of human colonic crypt Ca^{2+} signals, explore how they might regulate key physiological functions to maintain tissue homeostasis, and how they might be undermined in conditions such as colorectal cancer. In conjunction with profiling the status of Ca^{2+} signalling toolkit expression in health and cancer, this thesis describes the molecular basis of prototypical muscarinic and purinergic-coupled Ca^{2+} signals and investigates their spatio-temporal characteristics. Utilisation of mucosal tissue samples, isolated and cultured colonic crypts, and intestinal organoids; in combination with transcriptomic analysis, fluorescence immunolabelling, Fura-2 Ca^{2+} imaging, quantitative tandem mass spectrometry, biochemistry, and physiological and pharmacological assays; addresses the hypothesis that human colonic crypt Ca^{2+} signatures and their molecular basis are ligand-dependent and are perturbed in colorectal cancer (Figure 18). This hypothesis is discussed in the context of the following aims:
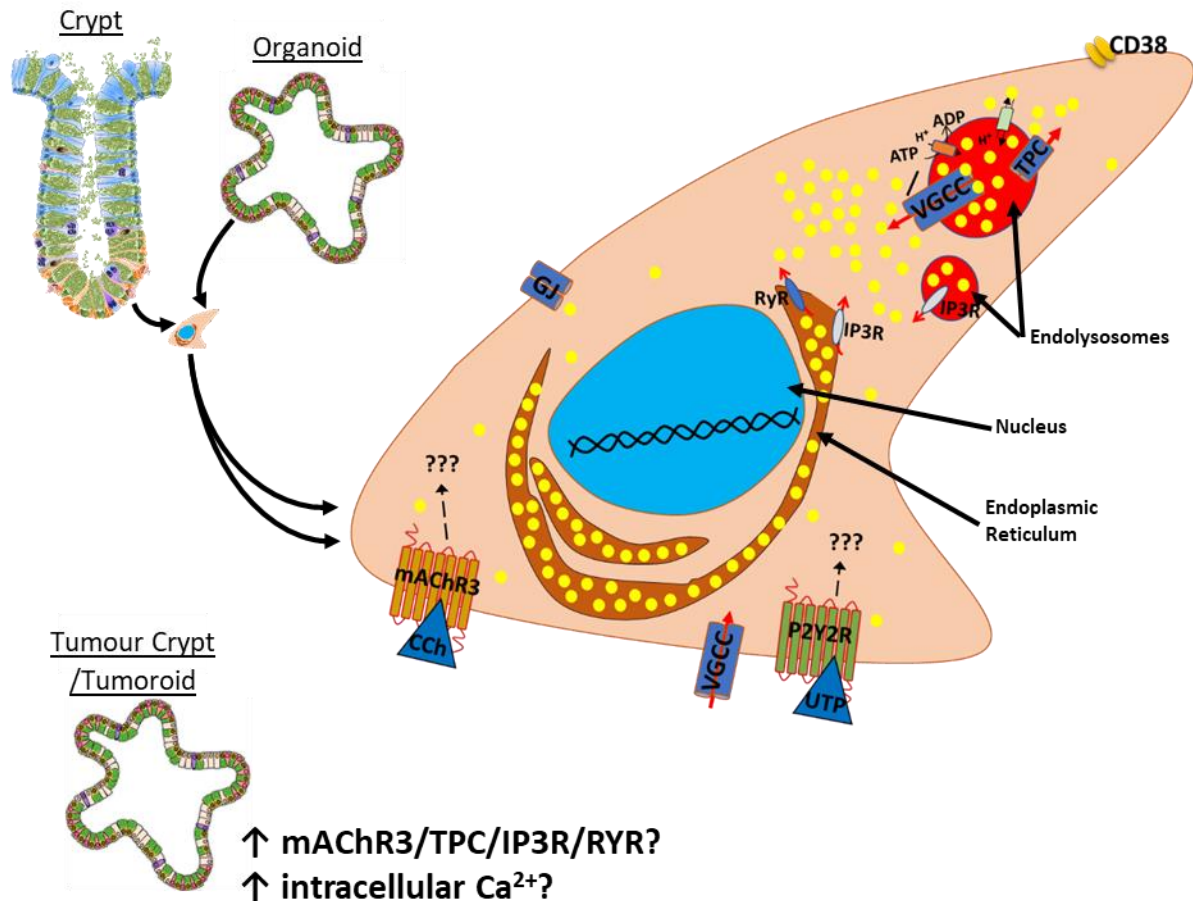
Figure 18 – Deciphering Muscarinic and Purinergic Ca^{2+} Signals.

Human colonic crypts and organoids will be used to test the hypothesis whether muscarinic and purinergic reception activation generates different spatio-temporal characteristics of Ca^{2+} signals. This will be compared against the Ca^{2+} signals generated by tumour crypts and tumoroids.

1.6 Aims

1. Identify and visualize the gene and protein expression of muscarinic and purinergic Ca^{2+}-signalling toolkit components in human colonic tissue using RNAseq and immunolabelling.
2. Elucidate the spatio-temporal characteristics of muscarinic and purinergic-induced Ca^{2+} signals using Fura-2 Ca^{2+} imaging, and the consequences of muscarinic and purinergic-induced Ca^{2+}-signals in the presence of pharmacological antagonists/inhibitors.
3. Develop a method of quantifying non-neuronal acetylcholine in media cultured in human colonic epithelium using HILIC-MS/MS.
4. Investigate the relevance of muscarinic and purinergic induced Ca^{2+} signals in modulating colonic epithelial mucus and fluid secretion, and proliferation.
5. Compare the gene and protein expression of muscarinic and purinergic Ca^{2+}-signalling toolkit components in tumour versus normal human colonic tissue, followed by evaluating their muscarinic and purinergic-induced Ca^{2+}-signals in the presence of pharmacological antagonists/inhibitors.

2   Chapter 2. Materials and Methods

2.1 Reagents and Buffers

2.1.1 Chemicals and Reagents

Table 6 – Chemicals and Reagents.

Chemical or Reagent	Supplier
Acetic Acid	Sigma
Acetonitrile	Sigma
Acetylcholine	Sigma
Advanced/DMEM	Invitrogen
Agarose	Sigma
Ammonium Chloride (NH_4Cl_2)	Fisher Scientific
Ammonium formate	Sigma
B27	Fisher Scientific
Bovine Serum Albumin (BSA)	Sigma
Calcium Chloride ($CaCl_2$)	VWR International
Click-IT EdU Reaction Kit	Fisher Scientific
D4-Acetylcholine	MERCK
D-Glucose	Fisher Scientific
Dimethyl Sulfoxide (DMSO)	Sigma
Disodium Hydrogen Phosphate (Na_2HPO_4)	Fisons Scientific Apparatus
Donkey Serum	Sigma
DTT	Fisher Scientific
Ethanol	Sigma
Fluo-4-AM	Invitrogen
FM 1-43	Fisher Scientific
FM 1-43X	Fisher Scientific
Formic Acid	Fisher Scientific
Fura-2-AM	Invitrogen
Glacial Acetic Acid	Fisher Scientific
Goat Serum	Abcam
Hepes	Fisher Scientific
Hoechst	Life Technologies
IGF-1	Sigma
Isopentane	Sigma
L-Glutamine	Gibco
Magnesium Chloride ($MgCl_2$)	Fluka (Sigma)
MEM Non-essential amino acid (MEM NEAA)	Fisher Scientific
Methanol	Sigma

N-acetylcysteine	Sigma
Nicotinic Acid	Sigma
Noggin	Sigma
Paraformaldehyde (PFA)	Sigma
Penicillin / Streptomycin (P/S)	Gibco
Phosphate buffered saline (PBS)	OXOID
Potassium Chloride (KCl)	Fisher Scientific
Propionate	Sigma
Rivastigmine Tartrate	Sigma
RSPO-1	Sigma
Sodium Bicarbonate (NaHCO$_3$)	Fisher Scientific
Sodium Chloride (NaCl)	Fisher Scientific
Sodium Dodecyl Sulphate (SDS)	Melford
Sodium Hydroxide	Fisher Scientific
SYTOX Blue	Invitrogen
Triton-X-100	Roche
Vectashield	Vector laboratories
Water, UHPLC Grade	Fisher Scientific
Wnt3A	Sigma

2.1.2 Buffers
Table 7 – Buffers.

Buffer	Composition
HEPES Buffered Saline (HBS), pH 7.4	NaCl (140 nM), KCl (5 mM), HEPES (10 mM), D-Glucose (17.5 mM), Na$_2$HPO$_4$ (1 mM), NaHCO$_3$ (10 mM), MgCl2 (1 mM), CaCl$_2$ (1 mM), MEM NEAA (10 µL/ml),P/S (50 U/ml, 50 µg/ml), L-Glutamine (3 mM)
HBS with Nicotinic Acid (HBS+NA), pH 7.4	HBS + Nicotinic Acid (1 µL/mL)
HBS+NA with Fura-2-AM (HBS+NA+F2), pH 7.4	HBS + NA (1 µL/mL) + Fura-2-AM (5 µM)

2.1.3 Primary and Secondary Antibodies

Table 8 – Primary and Secondary Antibodies.

Primary Antibody	Species	Clonality	Supplier
Advillin	Rabbit	Polyclonal	Cell Signalling Technology
β-catenin	Rabbit	Polyclonal	BD Transduction Lab
CD38	Rabbit	Monoclonal	Abcam
Choline acetyltransferase (ChAT)	Goat	Polyclonal	Abcam
Chromogranin A (CHGA)	Mouse	Monoclonal	Abcam
COX1	Goat	Polyclonal	Santa Cruz
COX2	Goat	Polyclonal	Santa Cruz
E-Cadherin	Goat	Polyclonal	BD Transduction Lab
E-Cadherin	Mouse	Monoclonal	R&D Systems
Glucagon-like peptide-1 (GLP1)	Rabbit	Monoclonal	Abcam
Inositol trisphosphate receptor 1 (IP3R1)	Rabbit	Polyclonal	Abcam
Inositol trisphosphate receptor 2 (IP3R2)	Goat	Polyclonal	Santa Cruz Biotechnology
Inositol trisphosphate receptor 3 (IP3R3)	Mouse	Monoclonal	Abcam
LGR5	Mouse	Monoclonal	Origene Technologies
Mucin 2 (MUC2)	Mouse	Monoclonal	Santa Cruz Biotechnology
Muscarinic acetylcholine receptor 1 (M1)	Rabbit	Polyclonal	Research & Diagnostic Antibodies
Muscarinic acetylcholine receptor 3 (M3)	Rabbit	Polyclonal	Research & Diagnostic Antibodies
Muscarinic acetylcholine receptor 5 (M5)	Rabbit	Polyclonal	Research & Diagnostic Antibodies
Olfactomedin 4 (OLFM4)	Rabbit	Monoclonal	Cell Signalling Technology
P2Y2 receptor	Rabbit	Monoclonal	Abcam
Ryanodine receptor 1 (RYR1)	Rabbit	Polyclonal	Millipore
Ryanodine receptor 2 (RYR2)	Rabbit	Polyclonal	Alomone Labs
Ryanodine receptor 3 (RYR3)	Rabbit	Polyclonal	Alomone Labs
PTK7	Mouse	Monoclonal	Miltenyi Biotec
Two-pore channel 1 (TPC1)	Rabbit	Polyclonal	Alomone Labs
Two-pore channel 2 (TPC2)	Rabbit	Polyclonal	Alomone Labs
WFDC2	Rabbit	Monoclonal	Abcam
Secondary Antibody	**Species**		**Supplier**
anti-mouse Alexa Fluor 488	Donkey		Invitrogen
anti-mouse Alexa Fluor 568	Donkey		Invitrogen
anti-mouse Alexa Fluor 647	Donkey		Invitrogen

anti-rabbit Alexa Fluor 488	Donkey	Invitrogen
anti-rabbit Alexa Fluor 568	Donkey	Invitrogen
anti-rabbit Alexa Fluor 647	Donkey	Invitrogen
anti-goat Alexa Fluor 488	Donkey	Invitrogen
anti-goat Alexa Fluor 568	Donkey	Invitrogen
anti-goat Alexa Fluor 647	Donkey	Invitrogen

2.2 Experimental Approaches

Every experiment described in this thesis relies on the acquisition of human colonic tissue from patients undergoing colon surgery. From the acquired tissue, colonic crypts were isolated and cultured in a 3D culture system, which in the short-term maintains the topological hierarchy of crypts observed *in-vivo* (Parris and Williams 2015), (Reynolds, Wharton, et al. 2014). Alternatively, colonic tissue was fixed in PFA, embedded using liquid nitrogen and sectioned using a cryostat. In addition, colonic organoids and tumoroids were generated from normal and tumour colonic crypts, respectively. Organoids were used to validate experiments performed on cultured crypts and tumoroids were used as a disease model system in contrast to organoids.

Several techniques and methods were utilised in this research project. Immunolabelling and RNAseq were used to characterise the muscarinic and purinergic Ca^{2+} signalling components. Extensive pharmacological studies were done on both cultured crypts and organoids to elucidate the muscarinic and purinergic pathway, and on tumoroids to compare the effects in contrast to organoids. In order to quantify nanomolar concentrations of non-neuronal acetylcholine present in crypt-cultured media, a liquid-chromatography and mass spectrometry method was developed. The method was validated for specificity, linearity, accuracy, precision, recovery, and stability according to the FDA guidelines on bio-analytical validation.

2.3 Human Colonic Tissue Samples

2.3.1 Human Colorectal Tissue Samples

This study has been approved by the East of England National Research Ethics Committee (2013/2014 – 62 HT (ongoing approval)). Human colorectal tissue samples were obtained with informed consent from patients undergoing sigmoid endoscopy, right-hemicolectomy or anterior resection at the Norfolk and Norwich University Hospital. For crypts and organoids, samples consist of histologically normal mucosa obtained from at least 10 cm away from tumour sites, and only used if there was no apparent intestinal pathology. For tumoroids, samples consist of mucosa obtained from tumour sites.

2.3.2 Isolation and Culture of Human Colonic Crypts

Human colonic crypts were isolated by members of the Williams group using a previously described methodology (Reynolds, Parris, et al. 2007), (Reynolds, Wharton, et al. 2014), (Parris and Williams 2015). In summary, fresh intestinal tissue samples were collected in ice-cold PBS, transferred to the laboratory, and placed in HBS (supplemented with DTT (1 mM) and EDTA (1 mM), and devoid of Mg^{2+} and Ca^{2+}) for 1hr at room temperature. Crypts were liberated by vigorous shaking and left to sediment. Once settled, crypts were collected, embedded in growth-factor reduced Matrigel and seeded onto glass coverslips (20 μL Matrigel/coverslip) arranged in 12-well plates. The Matrigel was left to polymerise at 37°C for 10 minutes, then flooded with human colonic crypt culture medium (hCCCM) consisting of: advanced F12/DMEM containing B27, N2, N-acetylcysteine (1 mM), Hepes (10 mM), Pen/Strep (100 U/mL), L-Glutamine (2 mM), Wnt-3A (100 ng/mL), IGF-1 (50 ng/mL), Noggin (100 ng/mL), (RSPO-1 (500 ng/mL) and A83-01(0.5 μM). Colonic crypts were cultured at 37°C and 5% CO_2 for up to 4 days in hCCCM, which was further modified depending on the experimental conditions.

2.3.3 Fixing and Sectioning of the Human Colonic Epithelium

Fresh intestinal tissue samples were immediately fixed in 4% PFA for 2 hours at 4°C, washed twice in cold PBS and refrigerated overnight in PBS. The fixed tissue samples were then embedded in lamb liver and frozen using isopentane chilled in liquid nitrogen, before being stored at -20°C overnight. Using a cryostat microtome, the frozen block was sectioned into 10 μm slices onto microscope slides and stored at -20°C.

2.3.4 Long-term Culture of Human Colonic Crypts into Organoids and Tumoroids

Using the same protocol described in Method 2.3.2, Matrigel containing human colonic crypts were cultured directly onto 24-well plates. Each well was flooded with 150 μL of hCCCM, which was replaced every 3 days. Human colonic organoids were generated from these crypts after 7 days of culture. A pipette tip was used to scratch the Matrigel containing human colonic organoids off the bottom of the well and mechanically dissociate it into smaller fragments. The suspension containing organoid fragments was pelleted by centrifugation at

4°C. After aspirating the supernatant, fresh media was added to resuspend the organoid fragments. Resuspended organoid fragments were embedded in Matrigel, seeded into new 24-well plates or coverslips arranged in 12-well plates, and left to polymerise. Wells were flooded with hCCCM and cultured at 37°C and 5% CO_2. Organoids cultured in 24-well plates were destined for long-term culture; hCCCM was replaced every 3 days and passaged after 5-7 days in culture. Tumoroids were generated from crypts that were isolated and cultured from intestinal tissue samples from tumour sites using the same protocol described in Method 2.3.2, except Wnt and R-spondin being absent in the hCCCM throughout the whole process. Besides that, the methodology of generating tumoroids is identical to that of organoids.

2.4 RNA sequencing

At least four crypt/organoid/tumoroid subject lines (N≥4) were processed for RNAseq. First, RNA was isolated from primary colonic mucosa, isolated crypts, cultured organoids and tumoroids using the ReliaPrep™ RNA Miniprep System according to the manufacturer's instructions. Total RNA concentration and purity was then measured using a NanoDrop™ ND-1000 spectrophotometer. Next, a library was prepared for patient-matched primary colonic mucosa, isolated crypts, cultured organoids and tumoroids. Finally, Illumina RNAseq was performed at Earlham Institute Genome Centre. The data is expressed as reads per kilobase million (RPKM).

2.5 Immunolabelling

2.5.1 Immunolabelling of Cultured Human Colonic Crypts, Organoids and Tumoroids

Immunolabelling was done on crypts, organoids and tumoroids cultured on glass coverslips, and on microscope slides containing fixed human colonic tissue sections. For cultured samples, fixation was achieved using PFA or Methacarn. Negative controls were performed for antibodies not previously characterised in the lab using a blocking peptide to the primary antibody or by omitting the primary antibody during a control experiment.

Samples were fixed with 4% PFA on ice for 1hr, then rehydrated by washing with cold PBS. Samples were then treated with NH_4Cl_2 for 13 minutes to remove excess aldehyde bonds, after which the membrane was permeabilised using 1% SDS for 5 minutes followed by 1% Triton X-100 for 30 minutes. Non-specific binding of antibodies was prevented using 10% Donkey serum and 1% BSA for 2 hrs. Samples were then incubated overnight with the primary antibodies at 4°C (Table 8). The following day, specific Alexa Fluor-conjugated secondary antibodies were added to the samples for 2hrs. Samples were next embedded in Vectashield mounting solution containing cell nuclear stain Sytox Blue or Hoechst for 30 minutes. Finally, coverslips were mounted onto microscope slides and sealed using nail varnish.

Alternatively, colonic crypts were fixed with Methacarn (methanol-Carnoy; a 3:1 solution of methanol and acetic acid) for 5 minutes at -20°C and then washed 5 times with PBS. Samples were treated with NH_4Cl_2 for 13 minutes and permeabilised with 0.1% SDS for 2 minutes. From this point, crypts were processed following the same protocol as described above.

2.5.2 Immunolabelling of Fixed Human Colonic Epithelium

Microscope slides containing fixed human colonic tissue sections (Chapter 2.3.3) were rehydrated using cold PBS. At this point, the immunolabelling protocol is the same as detailed above, from the NH_4Cl_2 treatment.

2.5.3 Microscopy

Immunolabelled samples were visualised using epifluorescence (Nikon Ti) or confocal laser scanning microscopy (Zeiss LSM510-META or Zeiss LSM980-Airyscan). Objective lenses used on the epifluorescence microscope include the 40 x 1.1 NA oil immersion lens and the 4 x 0.20 NA dry objective. Objective lenses used on the confocal laser scanning microscopes included the 63 x 1.4 NA oil immersion objective lens, the 40 x 1.3 NA oil immersion objective lens, and the 4 x 0.20 NA dry objective lens. Where necessary, multiple images were taken along the z-axis at 3-4 μm intervals.

2.6 Real-time Live Intracellular Ca^{2+} Imaging

Ca^{2+} experiments were done on coverslips containing crypts, organoids or tumoroids that had been in culture for 1-3 days using the acetoxymethyl ester form of Fura-2 (Fura-2-AM), a well-characterised fluorescent dye used to monitor cytoplasmic Ca^{2+} levels (Roe, Lemasters and Herman 1990), (Gillis and Gailly 1994). The ester chain allows Fura-2-AM to permeate with the phospholipid bilayer and become internalized, upon which intracellular esterases hydrolyses the ester bond to liberate Fura-2 into the cell cytoplasm. Fura-2-AM has the excitation wavelengths of 340 nm (Ca^{2+}-bound Fura-2) and 380 nm (Ca^{2+}-free Fura-2) and emission wavelength of 510 nm. The ratiometric fluorescence (340 nm/380 nm) was recorded to monitor cytoplasmic [Ca^{2+}].

2.6.1 Fura-2-AM Loading & Imaging Protocol

Coverslips containing crypts/organoids/tumoroids were loaded with HBS containing Fura-2-AM (5 µM) for 2 hours in darkness. Samples were then washed with HBS and left for 20 minutes to allow de-esterification of the dye. In the meantime, experimental solutions (Table 9) were prepared in HBS. Coverslips were then mounted onto a fast exchange open diamond bath chamber and imaged on an inverted fluorescent microscope (Nikon TE200) using a 40 x 1.1 NA oil immersion objective lens. A UXL-75XE xenon short arc lamp (Ushio) was used to provide the excitation wavelengths and the emission wavelength was detected using a cooled CCD camera (Quantum, Roper Scientific). A minimum of three repeats (n≥3) was performed for every experimental condition. More than one pharmacological antagonist may be used during the day, however only one crypt/organoid subject line (N=1) was used per pharmacological antagonist per given day; additional crypt/organoid subject lines were repeated on different days.

Table 9 – Solutions Used for Ca^{2+} Imaging.

Name (Abbreviation); Literature Reference	Working Conc. (µM)	Incubation Condition	Supplier
Inhibitors/Antagonists			
2-Aminoethoxydiphenylborane (2-APB); (Meissner 1986)	50 & 100	30 min RT	Sigma
1,1-Dimethyl-4-diphenylacetoxypiperidinium iodide (4-DAMP); (Greenwood and Dragunow 2010)	0.1	10 min RT	Tocris
AR-C118925XX; (Muoboghare, Drummond and Kennedy 2019)	5	10 min RT	Tocris
Bafilomycin A1 (Baf); (Steen, Kirchberger and Guse 2007)	2.5	2hrs 37ºC, 2hrs RT	Tocris
Caffeine; (Ehrlich, et al. 1994), (Sei, Gallagher and Daly 2001)	10,000	30 min RT	Sigma

Carbenoxolone; (Manjarrez-Marmolejo and Franco-Pérez 2016)	125, 300, 600	2hrs 37°C, 2hrs RT	Tocris
Chloroquine hydrochloride; (Wu, et al. 2017)	10, 25, 50	30 min RT	Tocris
Dantrolene; (Zhao, et al. 2001)	50	2hrs 37°C, 2hrs RT	Tocris
Diltiazem hydrochloride (DZM); (He, et al. 2020)	250 & 500	30 min RT	Tocris
Triethylene glycol diamine tetraacetic acid (EGTA)	500, 1000	20 min RT	Sigma
Flecainide; (Hilliard, et al. 2010)	100	2hrs 37°C, 2hrs RT	Sigma
GsMTx4; (Bae, Sachs and Gottlieb 2011)	5	30 min RT	Tocris
Trans NED-19; (Rosen, et al. 2009), (Ruas, Rietdorf, et al. 2010)	125, 250, 500	2hrs 37°C, 2hrs RT	Tocris
Nifedipine; (Curtis and Scholfield 2001)	50	2hrs 37°C, 2hrs RT	Tocris
Procaine; (Charlesworth, et al. 1992), (Zahradníková and Palade 1993)	1,000 & 10,000	30 min RT	Tocris
Ryanodine; (Meissner, 1986)	50	30 min RT	Tocris
3,4,5-Trimethoxybenzoic Acid 8-(Diethylamino) octyl Ester, Hydrochloride (TMB-8); (Poutrain, et al. 2009), (Leipziger, et al. 1996)	50, 100	30 min RT	Tocris
Tetrandrine; (Sakurai, et al., 2016). (Patel and Kilpatrick 2018)	20	2hrs 37°C, 2hrs RT	Tocris
Verapamil hydrochloride; (He, et al. 2020)	50	30 min RT	Tocris
Xestospongin-C; (Oka, et al. 2004)	4	2hrs 37°C, 2hrs RT	Tocris
Agonists			
Adenosine triphosphate (ATP)	1, 10, 100	-	Sigma
Carbamoylcholine chloride (CCH)	10	-	Sigma
Cyclopiazonic acid (CPA); (Beck, et al. 2004)	20	-	Tocris
Chlorpromazine; (Zhang, et al. 2019)	100	-	Tocris
Nortriptyline; (Zhang, et al. 2019)	100	-	Tocris
Oxotremorine (Oxo)	1	-	Sigma
Mucolipin synthetic agonist 1 (ML-SA1); (Tedeschi, Petrozziello and Sisalli, et al. 2019)	100	-	Tocris
Tetracaine; (Xu, Jones and Meissner 1993)	1000	-	Sigma
Uridine-5'-triphosphate (UTP)	10, 50	-	Sigma
Yoda1; (Botello-Smith, et al. 2019)	100	-	Tocris

Room Temperature (RT). Micromolar (μM).

2.6.2 Imaging

Using PTI EasyRatioPro software (Horiba), region of interests (ROIs) were drawn along the crypt base and buds of organoids and tumoroids; the 340 nm, 380 nm and ratio were presented as pseudo-colour images (Figure 19). Experiments were conducted by aspirating and pipetting solutions onto the coverslips while the 340/380 nm ratio was recorded live over time. This ratiometric changes in fluorescence was plotted over time (Figure 20), from which the peak amplitude was measured by subtracting the resting ratio from the maximal ratio.
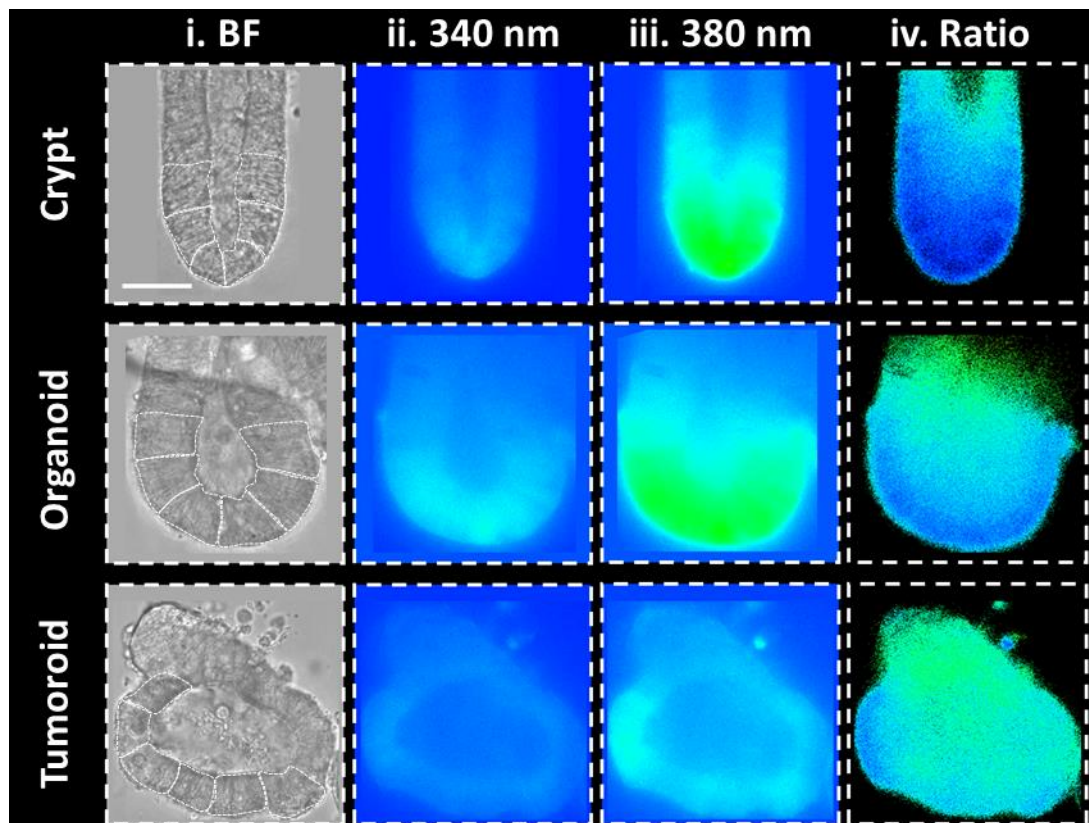
Figure 19 – Brightfield and Fluorescent Images of Coverslips Loaded with Fura-2.

Representative images of human isolated colonic crypts (top row), cultured organoids (middle row) and tumoroids (bottom row) loaded with Fura-2. (i) Brightfield image, (ii) Fura-2 fluorescence at 340 nm excitation, (iii) Fura-2 fluorescence at 380 nm excitation, (iv) Fura-2 fluorescence ratio (340/380 nm) with the background subtracted. ROI outlined in the BF column. Scale bar = 50 µm.
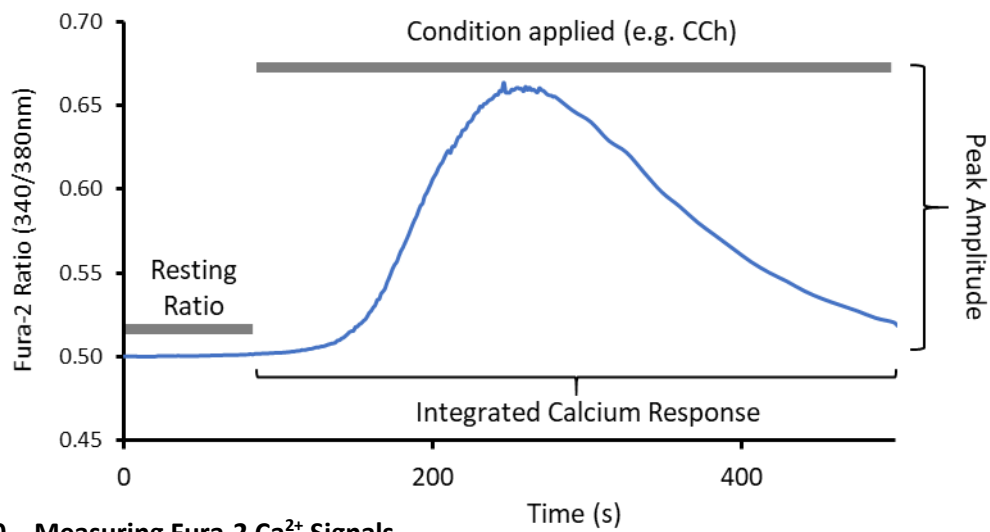
Figure 20 – Measuring Fura-2 Ca²⁺ Signals.

Representative trace of a Ca²⁺ signal induced by the muscarinic agonist CCh (10 µM).

2.6.3 Analysis

Bulk data analysis was done using Microsoft Excel. Results were expressed as mean peak amplitude response (peak amplitude – resting ratio) with SE bars. Comparison between two groups was evaluated by using F-tests and t-tests provided in Microsoft Excel's Analysis Toolpak. P-value of less than 0.05 was considered significant. Where specified otherwise, a minimum of two crypt subject lines (N≥2) were conducted per condition, with a minimum of three repeats (n≥3) conducted per crypt subject line.

2.7 Chromatography and Mass Spectrometry

2.7.1 Sample Collection and Preparation

Human colonic crypts were isolated and cultured using the methodology described earlier (Method 2.3.2). Rivastigmine (500 µM) was added to the culture media to inhibit the hydrolysis of acetylcholine by acetylcholinesterase (Willams, Nazarians and Gill 2003). Media from crypts and organoids were collected, first by scratching away the Matrigel, then collected by pipette aspiration. Additional Rivastigmine (final concentration of 1 mM) was added to the media. Samples were then centrifuged briefly to separate the culture media from the Matrigel and colonic tissue. The culture media was collected, kept chill in ice, and transported to the Bob Champion Research and Education (BCRE) building to undergo preparation and extraction, followed by hydrophilic interaction liquid chromatography tandem mass spectrometry (HILIC-MS/MS).

2.7.2 HILIC-MS/MS

Media that had been chilled in ice was put through a sample preparation and extraction protocol, which was developed at the BCRE. Briefly, samples were thawed and filtered using a 10 µm cell strainer. Then, 100 µL of sample was mixed with 100 µL of aqueous internal standard. At the same time, calibration standards and quality control samples were prepared. Sample, calibration standards and quality control samples were then loaded into a weak-cation-exchanger 96-well plate (Waters Corp Oasis), which bonds with weak-cationic compounds – such as acetylcholine – and retained them while remaining compounds were discarded. The extracted cationic compounds were reconstituted, then injected into a Shimadzu LC-20 HPLC system to undergo liquid chromatography with a wash gradient involving two mobile phases. Liquid chromatography was achieved using a hydrophilic interaction liquid chromatography (HILIC) column (YMC-Triart Diol-HILIC), which specializes in separating hydrophilic compounds by charge and size. Compounds which were expected to include acetylcholine were diverted to enter the API 4000 MS/MS System to undergo tandem mass spectrometry.

2.7.3 Analysis and Method Validation

Data analysis was done using Analyst Software 1.6. Comparison between two groups was evaluated by using F-tests and t-tests provided in Microsoft Excel's Analysis Toolpak. P-value of less than 0.05 was considered significant. The developed HILIC-MS/MS method was validated following guidelines from the FDA (FDA 2018) and elaborated further in (Chapter 5.3).

2.8 Mucous Secretion

2.8.1 Immunolabelling

Day one organoids and human colonic crypts cultured using Method 2.3.4 were used to investigate mucous secretion. Organoids and crypts were cultured in hCCCM containing pharmacological agents used to induce or inhibit mucous secretion. Immunolabelling was then done using methacarn fixation described in Method 2.5.1 and imaged using confocal microscopy described in Method 2.5.3. A minimum of three repeats (n≥3) was performed for every experimental condition. More than one pharmacological agent may be used during the day, however only one crypt/organoid subject line (N=1) was used per pharmacological agents per given day; additional crypt/organoid subject lines were repeated on different days.

2.8.2 FM 1-43, FM 1-43X, Cell Tracker^{TM} Deep Red

Cultured organoids and human colonic crypts were used to visualize mucous and fluid secretion in living cells in real-time under confocal microscopy. FM 1-43 (4 μM), a lipophilic fluorescent dye, was used to visualize the plasma membrane. Cell Tracker^{TM} Deep Red (1 μM) was used as an alternative fluorescent dye. Short term culture (2 hrs) of samples with these dyes allowed the labelling of the plasma membrane, while long term culture (1-3 days) allowed the labelling of intracellular granules. Following short or long-term culture, samples were mounted onto an incubation chamber supplied with 5% CO_2 and maintained at 37°C, and allowed to rest for 30 minutes. After this, plates were imaged and recorded in real-time under confocal microscopy following the addition of cholinergic agonist Carbachol (10 μM).

The fixable analogue of FM 1-43, FM 1-43X (4 μM), was also used. Besides using it similarly to FM 1-43, samples that were loaded with FM 1-43X in the short term were stimulated with Carbachol then fixed with PFA, following which they were imaged under confocal microscopy. A minimum of three repeats (n≥3) was performed for every experimental condition. More than one pharmacological agent may be used during the day, however only one crypt/organoid subject line (N=1) was used per pharmacological agents per given day; additional crypt/organoid subject lines were repeated on different days.

2.8.3 Quantifying Mucus Secretion

Mucous secretion was quantified by measuring the fluorescence intensity of immunolabelled Muc2 in red (Figure 21). Using ImageJ, regions of interests were drawn to encompass the cytoplasm of each Muc2 positive cells at the base of colonic crypts and organoids. The brightfield channel visualized the cut-off point between cytoplasm and lumen, while E-Cadherin was used to differentiate one cell from another. Notably, regions of interests do not include the bright-red region close to the nucleus, due to it being the Golgi apparatus where immature Muc2 is folded, and therefore not relevant for the analysis.

2.8.4 Analysis

Data analysis was done using Microsoft Excel. Results were expressed as Muc2 immunofluorescence with SE bars that has been normalised compared to control. Comparison between two groups was evaluated by using F-tests and t-tests provided in Microsoft Excel's Analysis Toolpak. P-value of less than 0.05 was considered significant. Where specified otherwise, a minimum of two crypt subject lines (N≥2) were conducted per condition, with a minimum of ten crypts (n≥10) measured per subject line.
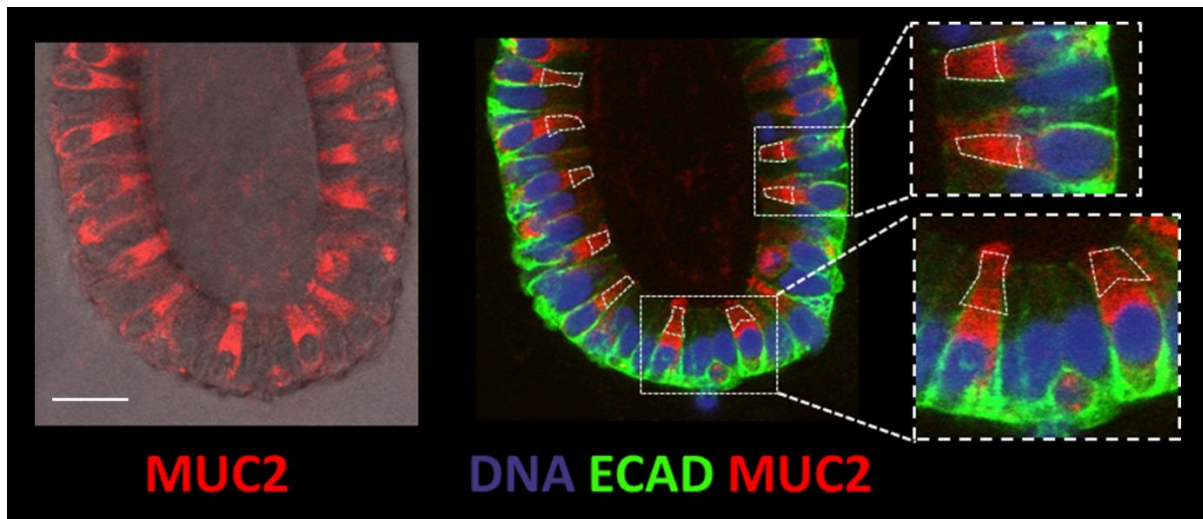
Figure 21 – Quantifying Mucus Secretion.

Brightfield channel (left) visualizes the cut-off point between plasma membrane and lumen. E-Cad and DNA (middle) were used as reference for drawing regions of interests. Regions of interests encompass the cytoplasm, from the apical pole of each cell to just beyond the bright regions close to the nucleus (right). Scale bar = 10 μm.

2.9 Organoid Swelling Assays

2.9.1 Imaging and Measurement

Day 1 cultured human colonic organoids were passaged and plated into 24-well plates with hCCCM; cultured with or without agonists carbachol (10 μM) for 2hrs; and cultured with or without and pharmacological antagonists (Table 9). Plates were imaged under the epi-fluorescence microscope (Nikon-Ti) on an incubation chamber supplied with 5% CO_2 and maintained at 37°C. A minimum of twenty organoids (n≥20) were measured for every experimental condition. Organoid swelling was measured by the change in luminal cross-sectional diameter at T=2hrs compared to T=0 using ImageJ.

2.9.2 Analysis

Data analysis was done using F-tests and t-tests provided in Microsoft Excel's Analysis Toolpak. Comparisons between two or more groups was assessed using one-way ANOVA with Tukey's post-hoc analysis. P-value of less than 0.05 was considered significant. Where specified otherwise, a minimum of two organoid lines (N≥2) were conducted per condition, with a minimum of twenty organoids (n≥20) measured per organoid lines.

2.10 EdU Labelling of Cultured Crypts

Edu (10 μM) was added to the crypt culture for 2-4 hours. During this period, crypt cultures were incubated with pharmacological antagonists at the appropriate concentration and duration (Table 9). Crypts were then fixed with 4% PFA at RT for 1hr, then rehydrated by washing with cold PBS. The Click-IT reaction was prepared following the manufacturer's instructions and crypts were incubated in the dark for 40 minutes at room temperature. The reaction was stopped with 3% BSA. Samples then undergo immunolabelling (Method 2.5.1), starting from washing with 10% donkey serum and 1% BSA for 2hrs, and imaged (Method 2.5.3) using epifluorescence (Nikon Ti) or laser confocal microscopy (Zeiss LSM). A minimum of three repeats (n≥3) was performed for every experimental condition. More than one pharmacological agent may be used during the day, however only one crypt subject line (N=1) was used per pharmacological agent per given day; additional subject lines were repeated on a different day.

The percentage of EdU positive cells were counted in the four regions of the crypt. The crypt-base was defined as the first twenty cells from the bottom of the crypt. The crypt-supra-base was defined as the next twenty cells above the crypt-base. The crypt-mid was defined as the next twenty cells above the crypt-supra-base. And the crypt-top was defined as the remaining cells above the crypt-mid region. Comparison between two groups was evaluated by using F-tests and t-tests provided in Microsoft Excel's Analysis Toolpak. P-value of less than 0.05 was considered significant. Where specified otherwise, a minimum of two crypt subject lines (N≥2) were conducted per condition, with a minimum of three repeats (n≥3) conducted per crypt subject line.

3 Chapter 3 – Results Part 1: Ca²⁺ Signalling Toolkit Expression in Human Colonic Native Mucosa, Cultured Crypts, and Organoids.

3.1 Introduction

Intracellular Ca²⁺ signals are thought to play a diverse role in maintaining the intestinal epithelium. These include regulating ISC activity (Deng, Gerencser and Jasper 2016), packing and releasing MUC2 (Ambort, et al., 2012), and stimulating secretion of ions and fluids (Yang, et al. 2018). Intracellular Ca²⁺ signals can be generated by the release of stored Ca²⁺ within organelles such as the endoplasmic reticulum and acidic vesicles such as endolysosomes (Figure 17). A range of extracellular ligands are capable of generating intracellular Ca²⁺ signals via activation of plasma membrane GPCRs, including acetylcholine-induced activation of muscarinic receptors and ATP-induced activation of purinergic receptors. In this chapter, the gene expression and localisation of Ca²⁺ signalling toolkit components will be characterised in the human colonic epithelium using transcriptomic analysis and immunolabelling, respectively.

Release of Ca²⁺ stored within the endoplasmic reticulum are mediated by inositol 1,4,5-trisphosphate receptors (IP3Rs) and ryanodine receptors (RYRs) (Berridge M. J., 1993) and (Meissner, 1986). Three subtypes exist for both receptors (IP3R1, IP3R2, IP3R3; RYR1, RYR2, RYR3). While IP3Rs are receptors for inositol trisphosphate (IP3), RYRs are sensitive to Ca²⁺. Both are capable of promoting the release of endoplasmic reticular Ca²⁺ through calcium-induced calcium-release (CICR). A transcriptomic analysis using Next Generation Sequencing (NGS) found mRNA expression of all IP3R subtypes and two RYR subtypes (RYR1-2) in human colonic cell lines (Pérez-Riesgo, et al., 2017).

Release of Ca²⁺ stored within acidic vesicles are mediated by a range of channels (Yang, et al. 2018) and (Tedeschi, Petrozziello and Secondo 2019). These include voltage-gated calcium channels, purinergic receptors, transient receptor potential channels, and two-pore channels (TPCs). This thesis focuses on TPCs, which are present on endolysosomes. Three subtypes of TPCs exist (TPC1, TPC2, TPC3), although the third subtype is not present in primates (Ogunbayo, et al., 2015). The function and mechanism of TPCs is a subject of debate. Ligands which activate TPCs include NAADP, PI(3,5)P2, Mg²⁺, JNK, P38, and m-TORC1 (Jha, Ahuja, Patel, Brailoiu, & Muallem, 2014) and (Ogunbayo, et al., 2018). NAADP synthesis is catalysed by CD38, which have been shown to be expressed on immune cells and promote intestinal inflammation (Figure 22) (Schneider, et al. 2015).

Secreted extracellular ligands such as acetylcholine and ATP are capable of generating intracellular Ca²⁺ signals within the GI tract. Acetylcholine is catalysed by choline acetyltransferase (ChAT), which has been shown to be expressed in tuft cells (Pan, Zhang, Shao, & Huang, 2020). In neurons, acetylcholine is loaded into secretory vesicles by vAChT,

which are absent in tuft cells (Schütz, et al., 2019). ATP is produced by virtually all metabolically active cells via various processes, such as glycolysis and the citric acid cycle. ATP can also be loaded into secretory vesicles via vesicular nucleotide transporter (VNUT) to initiate transmission of purinergic signals (Moriyama, et al. 2017). Interestingly, a recent study has shown intestinal L-type enteroendocrine cells to be capable of secreting ATP alongside gut peptide hormones such as GLP1 and LYY (Lu, et al. 2019). In that study, they showed GLP1-positive cells contained VNUT, demonstrated ATP was released from GLP1-positive cells, and showed it activated P2Y2 receptors in neighbouring enterocytes.

Plasma membrane receptors for acetylcholine include ionotropic nicotinic receptors and metabotropic muscarinic receptors. Plasma membrane receptors for ATP include ionotropic P2X receptors and metabotropic PY2 receptors. Muscarinic receptors (mAChRs) are GPCRs which use second messengers to activate intracellular events upon receptor activation. Five subtypes of mAChRs exist (M1, M2, M3, M4, M5), all of which are expressed in the human GI tract (Kruse, et al., 2014). Of those, M1, M3 and M5 couple to G_q, which activates beta-type phospholipase C (PLC-β) enzymes to hydrolyse phosphatidylinositol 4,5-bisphosphate (PIP2) to diacyl glycerol (DAG) and IP3, the latter being a ligand of IP3Rs. P2Y receptors are also GPCRs. Eight P2Y receptors exist (Table 5), of which three (P2Y1, P2Y2 and P2Y11) are receptors for ATP and couple to G_q, and of which only P2Y2 also binds to UTP.
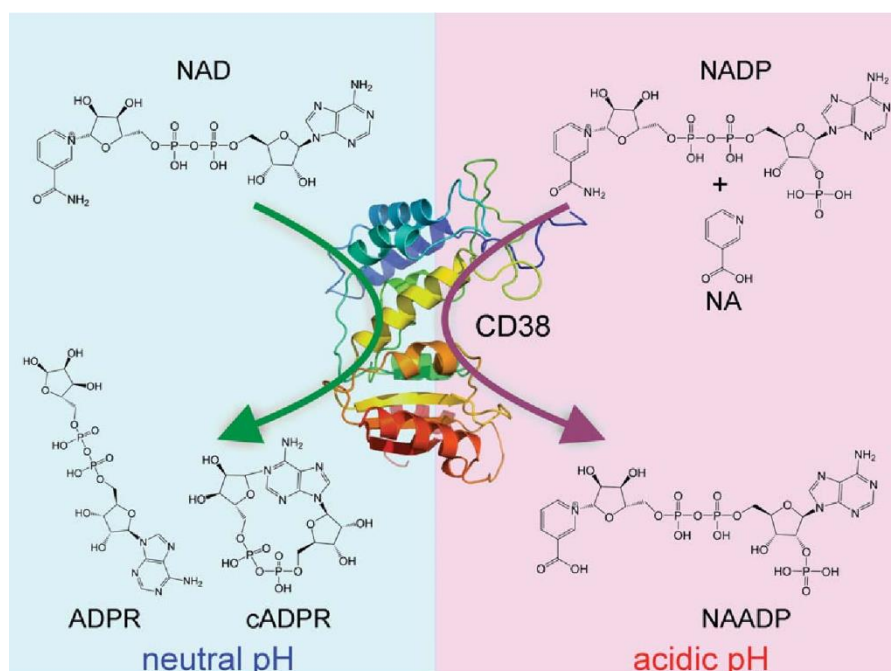
Figure 22 – Enzymatic Catalysation of NAADP by CD38.

(Right) Under acidic pH, CD38 catalyses the production of nicotinic acid adenine dinucleotide phosphate (NAADP) from nicotinamide adenine dinucleotide phosphate (NADP) and nicotinic acid (NA). (Left) Under neutral pH, CD38 catalyses the production of cyclic ADP-ribose (cADPR) and subsequently ADP-ribose (ADPR) from nicotinamide adenine dinucleotide (NAD). Adapted from (Zhao, Graeff and Lee 2012).

3.2 Results

Crypt isolation, cell culture and organoid growth conditions were carried out based on current literature and on methods developed by the Williams group. Firstly, transcriptomic analysis of Ca^{2+} signalling toolkit expression was performed on native human colon mucosa (mucosa), freshly isolated human colonic crypts (crypts), and cultured human colonic organoids (organoids). Next, Ca^{2+} signalling toolkit components were labelled in mucosa, crypts, and organoids using immunolabelling and their localisation visualized using confocal imaging.

3.2.1 Transcriptomic Analysis of Ca^{2+} Signalling Toolkit Expression

RNA sequencing (Chapter 2.4) was used to compare the gene expression of Ca^{2+} signalling toolkit components in native human colonic mucosa, isolated crypts, and cultured organoids. These components can be divided as intracellular Ca^{2+} release channels, muscarinic and purinergic GPCRs, and proteins related to production or packaging of endogenous ligands. Intracellular Ca^{2+} release channels refer to endoplasmic reticular IP3Rs and RYRs, and endolysosomal TPCs. In addition to those, CD38 which catalyses the synthesis of TPC ligand NAADP, was analysed. Purinergic GPCRs specifically refers to ATP-sensitive P2Y receptors. Endogenous ligands specifically refer to acetylcholine and ATP. Proteins related to the production acetylcholine are ChAT. Packaging of ATP is mediated by VNUT. In addition, proteins related to GLP1 production were also compared. These are proglucagon and neuroendocrine convertase 1; the latter processes the former to form GLP1.

Analysis of IP3R gene expression confirmed the presence of all three subtypes in every tissue sample (Figure 23). Notably, IP3R3 gene expression was approximately ten times higher than IP3R2 and over a hundred times higher than IP3R1. Gene expression of IP3R2 and IP3R3 were similar in mucosa, crypts, and organoids. In comparison, gene expression of IP3R1 was reduced in crypts and organoids compared to mucosa.
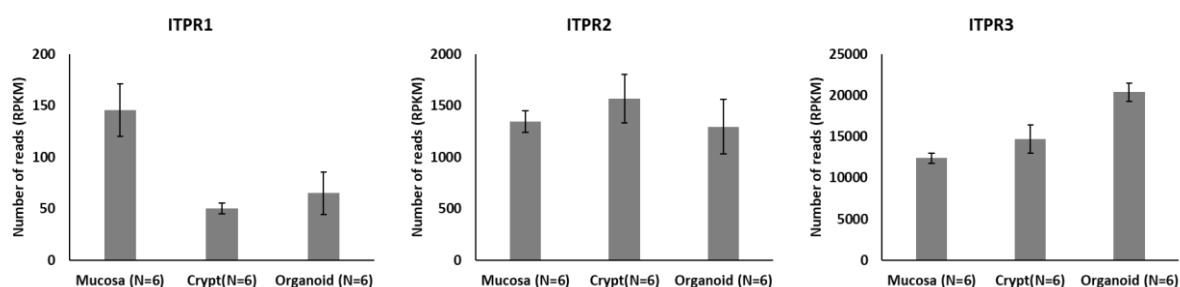
Figure 23 – Gene Expression of IP3Rs.

Bar chart representation of the gene expression for IP3R1 (ITPR1), IP3R2 (ITPR2) and IP3R3 (ITPR3) in native human colonic mucosa, isolated crypts, and cultured organoids. N=6 indicate six human samples. Data is expressed as number of reads per kilo base per million mapped reads (RPKM).

Analysis of the RYR gene expression also confirmed the presence of all three subtypes in every tissue sample (Figure 24). However, their expression was remarkably low; more so in crypts and organoids compared to mucosa.
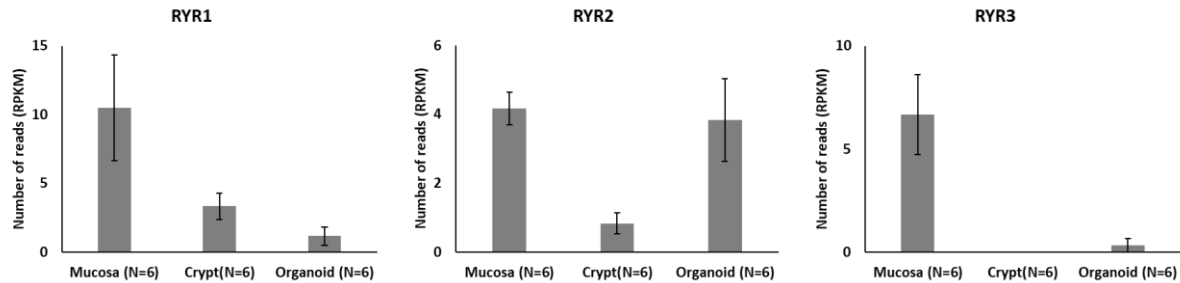
Figure 24 – Gene Expression of RYRs.

Bar chart representation of the gene expression for RYR1, RYR2 and RYR3 in native human colonic mucosa, isolated crypts, and cultured organoids. N=6 indicate six human samples. Data is expressed as number of reads per kilo base per million mapped reads (RPKM).

Analysis of TPC gene expression confirmed the presence of TPC1-2 subtypes in every tissue sample (Figure 25). TPC1 gene expression was approximately five times the levels of TPC2. Gene expression of TPC1 were similar in mucosa, crypts, and organoids. In comparison, gene expression of TPC2 was increased in crypts compared to mucosa and organoids.
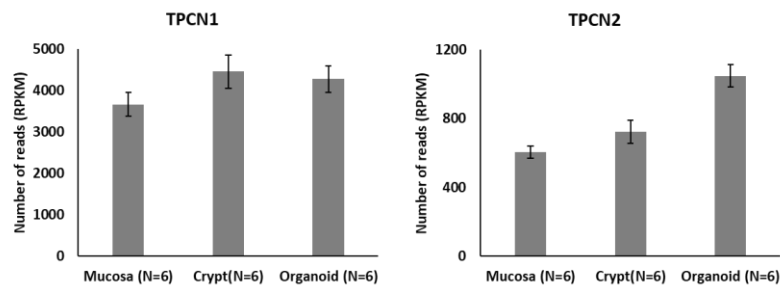
Figure 25 – Gene Expression of TPCs.

Bar chart representation of the gene expression for TPC1 (TPCN1) and TPC2 (TPCN2) in native human colonic mucosa, isolated crypts, and cultured organoids. N=6 indicate six human samples. Data is expressed as number of reads per kilo base per million mapped reads (RPKM)

Analysis of the gene expression for CD38 confirmed its presence in every tissue sample (Figure 26). The expression of CD38 was reduced in crypts compared to mucosa. Its expression in organoids varied tremendously, hence the large error bar.
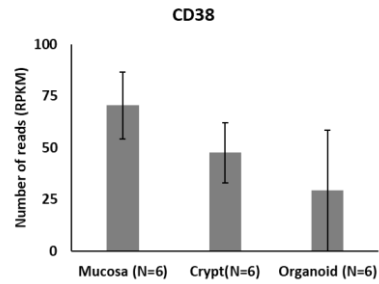
Figure 26 – Gene Expression of CD38.

Bar chart representation of the gene expression for CD38 in native human colonic mucosa, isolated crypts, and cultured organoids. N=6 indicate six human samples. Data is expressed as number of reads per kilo base per million mapped reads (RPKM).

Analysis of muscarinic receptor gene expression showed differential expression across tissue sample and between receptor subtypes (Figure 27). M1 and M3 expression were much higher than M2 and M4. Expression of M1, M3 and M4 were similar between mucosa, crypts, and organoids. For M2, no gene expression was detected in crypts and organoids. Unfortunately, the RNAseq for M5 was not done and thus cannot be analysed in this thesis.
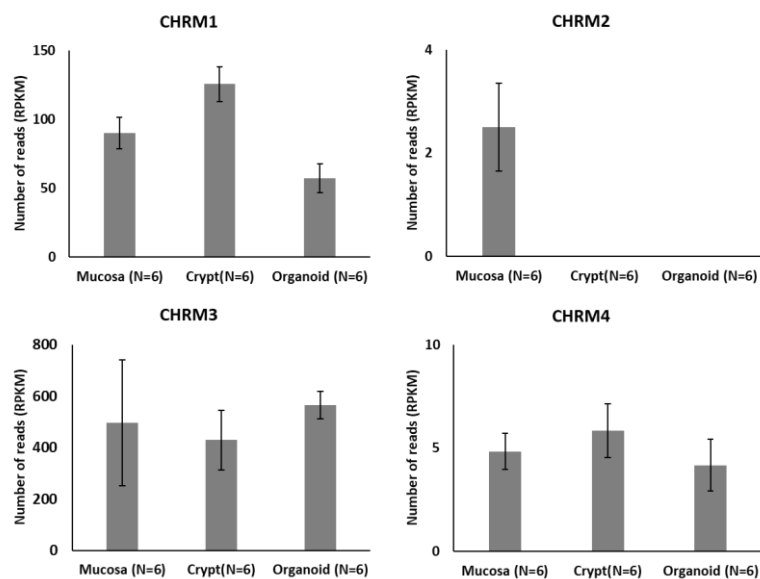
Figure 27 – Gene Expression of mAChRs.

Bar chart representation of the gene expression for M1 (CHRM1), M2 (CHRM2), M3 (CHRM3) and M4 (CHRM4) in native human colonic mucosa, isolated crypts, and cultured organoids. N=6 indicate six human samples. Data is expressed as number of reads per kilo base per million mapped reads (RPKM).

Analysis of ATP-sensitive purinergic P2Y receptor gene expression showed differential expression across tissue sample and between receptor subtypes (Figure 28). Expression of P2Y1 and P2Y2 were remarkably similar, and higher than P2Y11 expression. The expression of these three were similar between tissue types. Small amounts of P2Y13 were expressed in mucosa, which was much lower in crypts and non-existent in organoids.
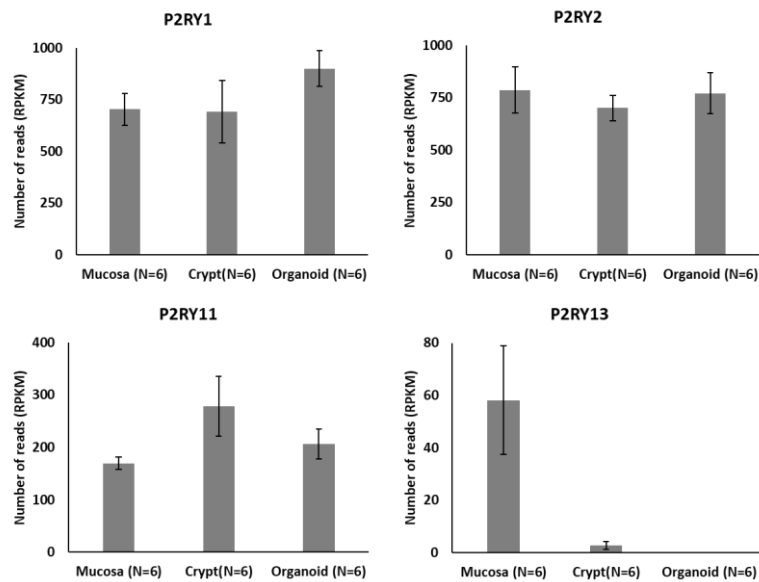
Figure 28 – Gene Expression of ATP-sensitive Purinergic P2Y receptors.

Bar chart representation of the gene expression for P2Y1 (P2RY1), P2Y2 (P2RY2), P2Y11 (P2RY11) and P2Y13 (P2RY13) in native human colonic mucosa, isolated crypts, and cultured organoids. N=6 indicate six human samples. Data is expressed as number of reads per kilo base per million mapped reads (RPKM).

Analysis of ChAT gene expression showed differential expression across tissue sample (Figure 29). Compared to mucosa, expression of ChAT was lower in crypts and nearly non-existent in organoids.
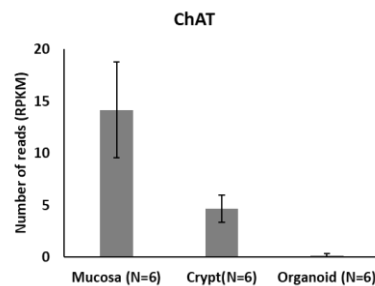
Figure 29 – Gene Expression of ChAT.

Bar chart representation of the gene expression for choline acetyltransferase (ChAT) in native human colonic mucosa, isolated crypts, and cultured organoids. N=6 indicate six human samples. Data is expressed as number of reads per kilo base per million mapped reads (RPKM).

Analysis of VNUT gene expression confirmed its presence in every tissue sample (Figure 30). Intriguingly, its expression is higher in crypts and more so in organoids. Lastly, analysis of the gene expression for proglucagon and neuroendocrine convertase 1 confirmed their presence in every tissue sample (Figure 31). Expression of proglucagon was similar in mucosa and crypts, and higher than in organoids. By contrast, expression of neuroendocrine convertase 1 was higher than organoids compared to mucosa and crypts.
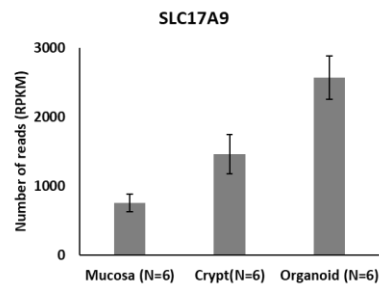
Figure 30 – Gene Expression of VNUT.

Bar chart representation of the gene expression for VNUT (SLC17A9) in native human colonic mucosa, isolated crypts, and cultured organoids. N=6 indicate six human samples. Data is expressed as number of reads per kilo base per million mapped reads (RPKM).
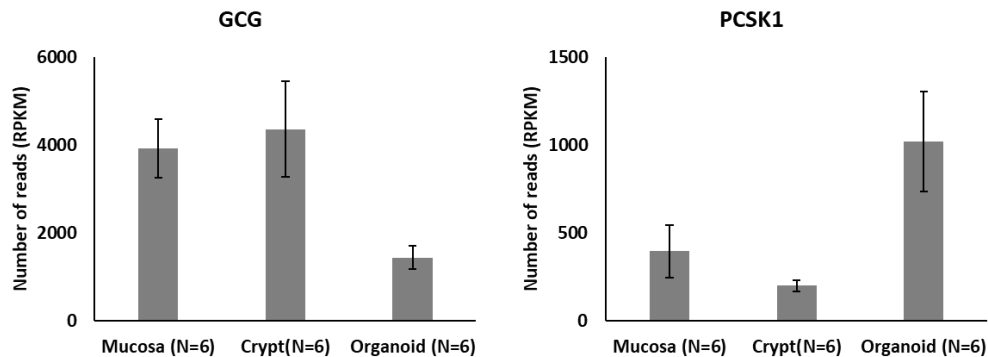
Figure 31 – Gene Expression of GCG and PCSK1.

Bar chart representation of the gene expression for proglucagon (GCG) and neuroendocrine convertase 1 (PCSK1) in native human colonic mucosa, isolated crypts, and cultured organoids. N=6 indicate six human samples. Data is expressed as number of reads per kilo base per million mapped reads (RPKM).

3.2.2 Immunofluorescent Localisation of Intracellular Ca²⁺ Release Channels

Transcriptomic analysis using RNA sequencing confirmed the presence of Ca²⁺ signalling toolkit RNA within mucosa, crypts, and organoids. Thus, the next question was whether protein expression of these Ca²⁺ signalling toolkit were present. Immunolabelling and confocal imaging (Chapter 2.5) were used to visualize and characterize the localisation of intracellular Ca²⁺ release channels at the base of mucosal crypts, cultured crypts, and organoids. Intracellular Ca²⁺ release channels refer specifically to endoplasmic reticular IP3R1-3 and RYR1-3, endolysosomal TPC1-2, with the complementary addition of CD38. Furthermore, cells which contained TPC1-2 and CD38 were identified by co-labelling them with markers for epithelial stem cells (LGR5 or PTK7), goblet cells (MUC2), enteroendocrine cells (CHGA), and tuft cells (COX2). Contributors to this data include Dr Victoria Jones, Dr Nicolas Pelaez Llaneza and Dr Kristy Kam.

IP3R1 and IP3R2 were shown to be present in crypts and organoids (Figure 32). In crypts, IP3R1 labelling was present within the cytoplasmic space, on some basal membranes, and possibly on the lateral membranes (Figure 32A). This IP3R1 labelling pattern was similar in organoids (Figure 32C). In crypts, IP3R2 labelling was more prominent at the base of the cell, including the nucleus (Figure 32B). By contrast, organoid IP3R2 labelling was strongly limited to the basal pole and the basal membrane.
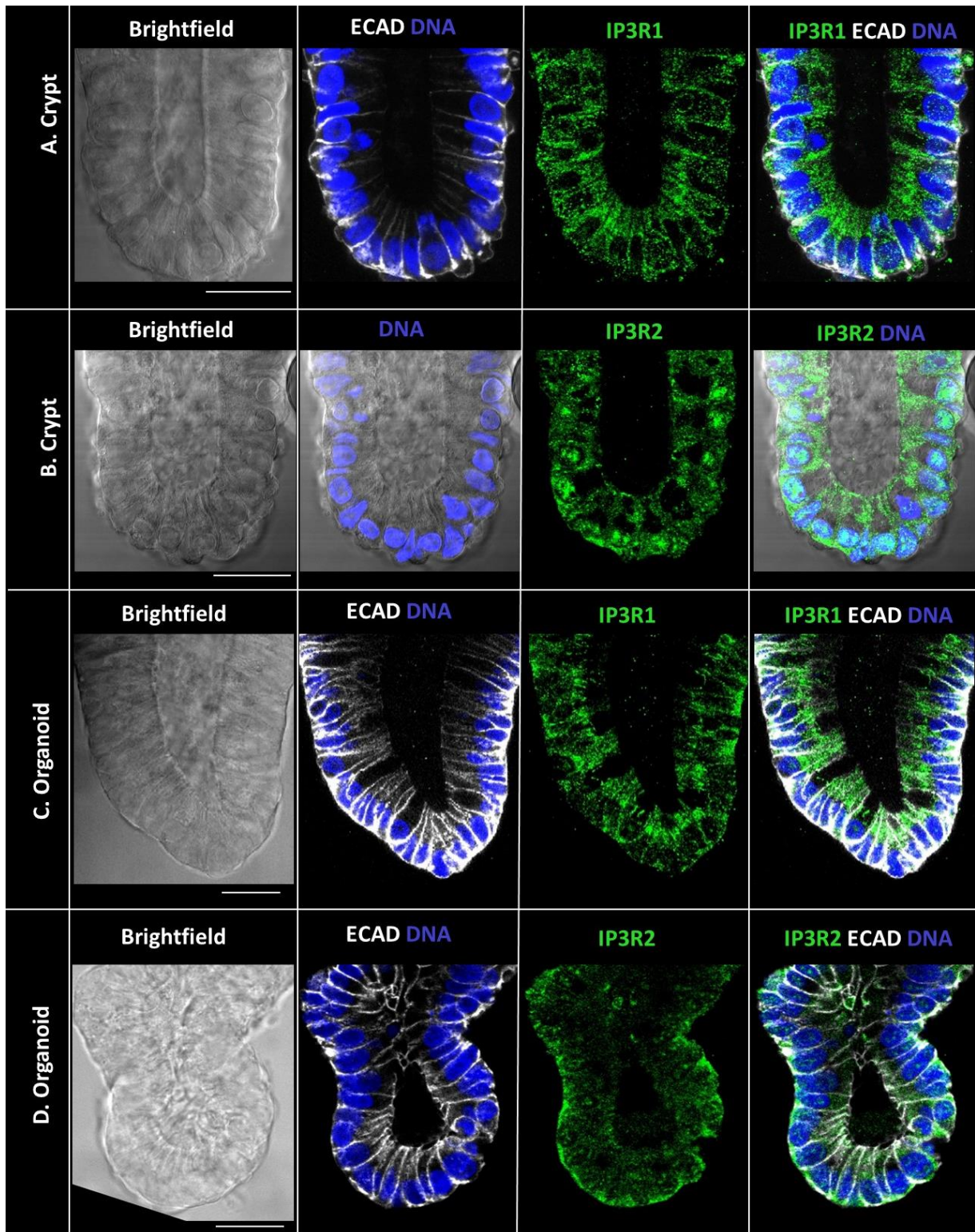
Figure 32 – Immunolabelling of IP3R1 and IP3R2 in Crypts and Organoids.

Representative confocal images of the base of crypts **(A & B)** and organoids **(C & D)** immunolabelled with E-Cadherin (ECAD) in white and IP3R1 **(A & C)** or IP3R2 **(B, D)** in green. Nuclei was stained with Sytox Blue (DNA). Brightfield depicted on the left. Scale bar = 25 μm.

IP3R3 was shown to be present in all three tissue samples (Figure 33). Mucosal IP3R3 labelling was mainly along the apical membrane and the apical pole, with some labelling outside the epithelium (Figure 33A). In crypts, IP3R3 labelling was predominantly along the apical membrane (Figure 33B). This was the same in organoids, although it also labelled the apical pole and basolateral membranes of some cells (Figure 33C).

Figure 33 – Immunolabelling of IP3R3 in Mucosa, Crypts, and Organoids.

Representative confocal images of the base of mucosa **(A)**, crypts **(B)**, and organoids **(C)** immunolabelled with E-Cadherin (ECAD) in white and IP3R3 in green. Nuclei was stained with Sytox Blue (DNA). Brightfield depicted on the left. Scale bar = 25 μm.

RYR1 was shown to be present in all three tissue samples (Figure 34). Mucosal RYR1 labelling seemed to be concentrated on the apical side of the nucleus within the epithelium, as well as some basolateral membrane labelling (Figure 34A). In crypts, cytoplasmic and apical membrane RYR1 labelling was present at the very bottom, while basal membrane labelling was prominent higher up the crypt base (Figure 34B). This was similar to RYR1 labelling in organoids (Figure 34C).

Figure 34 – Immunolabelling of RYR1 in Mucosa, Crypts, and Organoids.

Representative confocal images of the base of mucosa **(A)**, crypts **(B)**, and organoids **(C)** immunolabelled with E-Cadherin (ECAD) in white and RYR1 in green. Nuclei was stained with Sytox Blue (DNA). Brightfield depicted on the left. Scale bar = 25 µm.

RYR2 was also shown to be present in all three tissue samples (Figure 35). Mucosal RYR2 labelling appeared to be limited to the cytoplasmic space of slender cells scattered throughout the epithelium (Figure 35A). In crypts, RYR2 labelling was strong along the basal membrane, with some labelling within the cytoplasm and within the nucleus (Figure 35B). Similarly, in organoids RYR2 labelling was strong along their basal membrane and surrounding the nucleus of some cells, with weak apical labelling (Figure 35C).
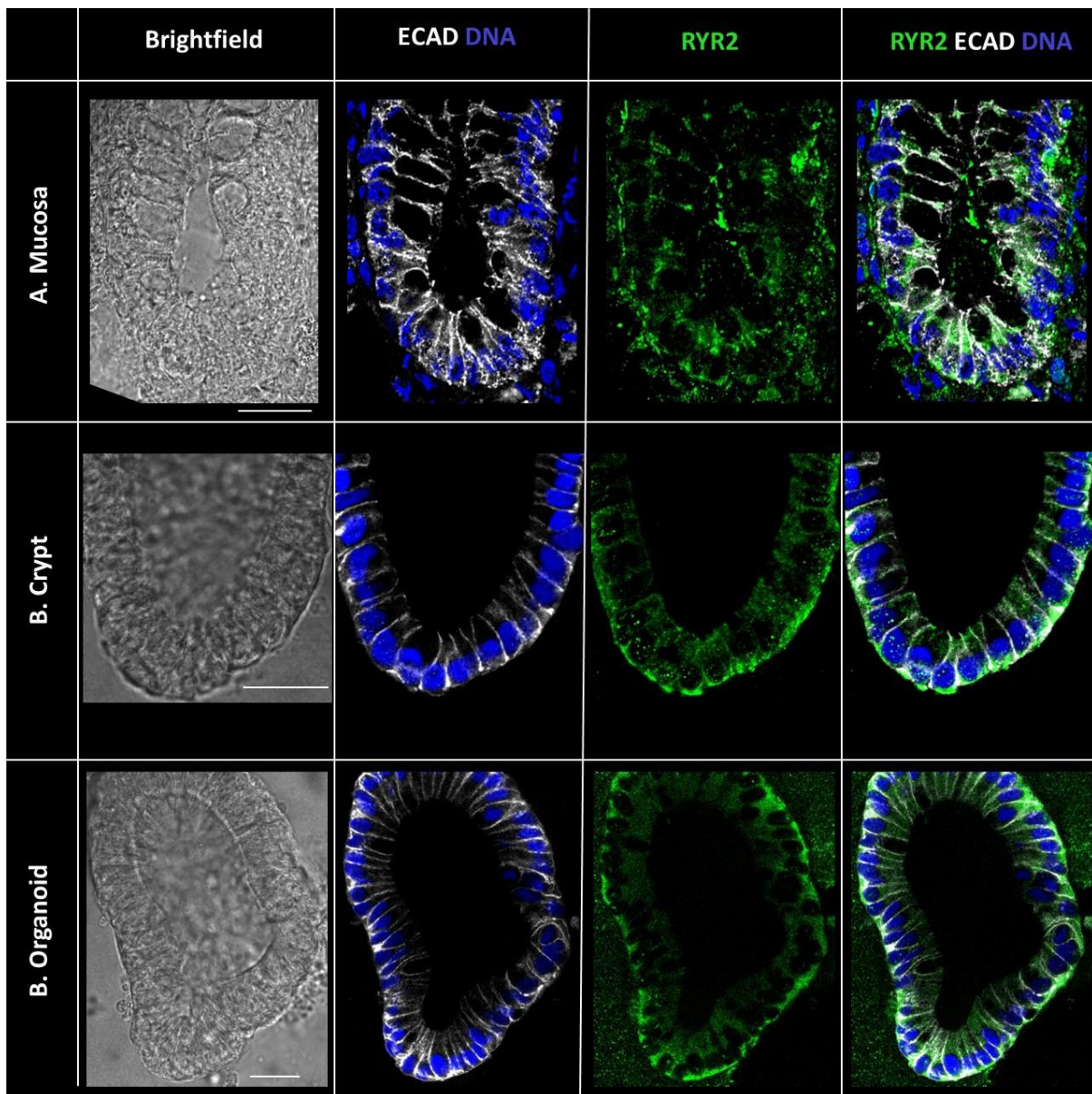
Figure 35 – Immunolabelling of RYR2 in Mucosa, Crypts, and Organoids.

Representative confocal images of the base of mucosa **(A)**, crypts **(B)**, and organoids **(C)** immunolabelled with E-Cadherin (ECAD) in white and RYR2 in green. Nuclei was stained with Sytox Blue (DNA). Brightfield depicted on the left. Scale bar = 25 μm.

The third RYR subtype was shown to be present in all three tissue samples (Figure 36). Mucosal RYR3 labelling also appeared to be limited to the cytoplasmic space of slender cells scattered throughout the epithelium, with some labelling outside and surrounding the epithelium (Figure 36A). In crypts, RYR3 labelling was present on the basal membrane of most cells (Figure 36B). In organoids, RYR3 labelling was strongly along the basal pole and basal membrane.

Figure 36 – Immunolabelling of RYR3 in Mucosa, Crypts, and Organoids.

Representative confocal images of the base of mucosa **(A)**, crypts **(B)**, and organoids **(C)** immunolabelled with E-Cadherin (ECAD) in white and RYR3 in green. Nuclei was stained with Sytox Blue (DNA). Brightfield depicted on the left. Scale bar = 25 μm.

Moving on to endolysosomal TPCs, TPC1 was shown to be present in all three tissue samples (Figure 37). Mucosal TPC1 labelling was prominent outside the epithelium; within the epithelium, labelling appeared to be concentrated along the basal membrane, as well as on the apical membrane of some cells (Figure 37A). In crypts, TPC1 labelling was prominent in the nuclear space and within the cytoplasm of most cells, as well as some apical membrane labelling (Figure 37B). Organoid labelling of TPC1 is similar to crypts, prominent in the nuclear space, cytoplasm, and some apical membrane (Figure 37C). Next, the intracellular localisation of TPC1 was evaluated within colonic stem cells and goblet cells (Figure 38). TPC1 labelling was present within the cytoplasmic and nuclear space of PTK7+ stem cells (Figure 38A). In MUC2+ cells at the base of crypts, TPC1 labelling was strong within the cytoplasmic space, alongside weaker labelling in the nucleus.

In addition to TPC1, TPC2 was also present in all three tissue samples (Figure 39). Mucosal TPC2 labelling appeared to be ubiquitous throughout the epithelium, except for the cytoplasmic space of wide cells which are indicative of goblet cells (Figure 39A). In crypts, TPC2 labelling was restricted to the basal pole and nuclear space, as well as weak labelling in the cytoplasm (Figure 39B), the labelling pattern of which was similar in organoids (Figure 39C). Next, the intracellular localisation of TPC2 was evaluated in colonic stem cells and goblet cells (Figure 40). TPC2 labelling was barely present within the cytoplasmic space of PTK7+ stem cells (Figure 40A). In MUC2+ cells at the base of crypts, TPC2 labelling was absent from the cytoplasmic but present in the nucleus.

Most recently, TPC1-2 immunolabelling was conducted on organoids and visualised on the LSM910 confocal microscope, which provided much clearer TPC labelling (Figure 161). During that experiment, TPC1-2 were co-immunolabelled with Rab (5 & 11), proteins Ras superfamily of small G proteins who are involved in endocytic trafficking (Wandinger-Ness and Zerial 2014). Once again, TPC1 labelling was concentrated on the apical membrane and co-labels with Rab11 (Figure 161A-B), while TPC2 labelling was prominent on the basal side and co-labels with Rab5 (Figure 161C-D).

Figure 37 – Immunolabelling of TPC1 in Mucosa, Crypts, and Organoids.

Representative confocal images of the base of mucosa **(A)**, crypts **(B)**, and organoids **(C)** immunolabelled with E-Cadherin (ECAD) in white and TPC1 in green. Nuclei was stained with Sytox Blue (DNA). Brightfield depicted on the left. Scale bar = 25 µm.

Figure 38 – Immunolabelling of TPC1 with Colonic Epithelial Cells.

Representative confocal images of TPC1 immunolabelled in crypts or organoids with E-Cadherin (ECAD) in white, TPC1 in green, and co-labelled with stem cell marker PTK7 **(A)** or goblet cell marker MUC2 **(B)** in red. Nuclei was stained with Sytox Blue (DNA). Brightfield depicted on the left. Scale bar = 25 µm.

Figure 39 – Immunolabelling of TPC2 in Mucosa, Crypts, and Organoids.

Representative confocal images of the base of mucosa **(A)**, crypts **(B)**, and organoids **(C)** immunolabelled with E-Cadherin (ECAD) in white and TPC2 in green. Nuclei was stained with Sytox Blue (DNA). Brightfield depicted on the left. Scale bar = 25 μm.

Figure 40 – Immunolabelling of TPC2 with Colonic Epithelial Cells.

Representative confocal images of TPC2 immunolabelled in crypts or organoids with E-Cadherin (ECAD) in white, TPC2 in green, and co-labelled with stem cell marker PTK7 **(A)** or goblet cell marker MUC2 **(B)** in red. Nuclei was stained with Sytox Blue (DNA). Brightfield depicted on the left. Scale bar = 25 μm.

Following the immunolabelling expression of endoplasmic reticular IP3Rs and RYRs, and endolysosomal TPCs, expression and localisation of CD38 was determined. CD38 was shown to be present in crypts and organoids (Figure 41). In both crypts and organoids, CD38 labelling was predominantly within the nuclear space, alongside slight labelling in the apical cytoplasmic space and apical membrane (Figure 41A-B). Finally, the intracellular localisation of CD38 was evaluated in colonic stem cells, goblet cells, enteroendocrine cells, and tuft cells (Figure 42). Similar to its immunolabelling pattern in crypts and organoids (Figure 41), CD38 labelling was present in the nucleus and apical membrane of LGR5+ stem cells (Figure 42A), and in the nucleus of MUC2+ goblet cells (Figure 42B), CHGA+ enteroendocrine cells (Figure 42C), and COX2+ tuft cells (Figure 42D).
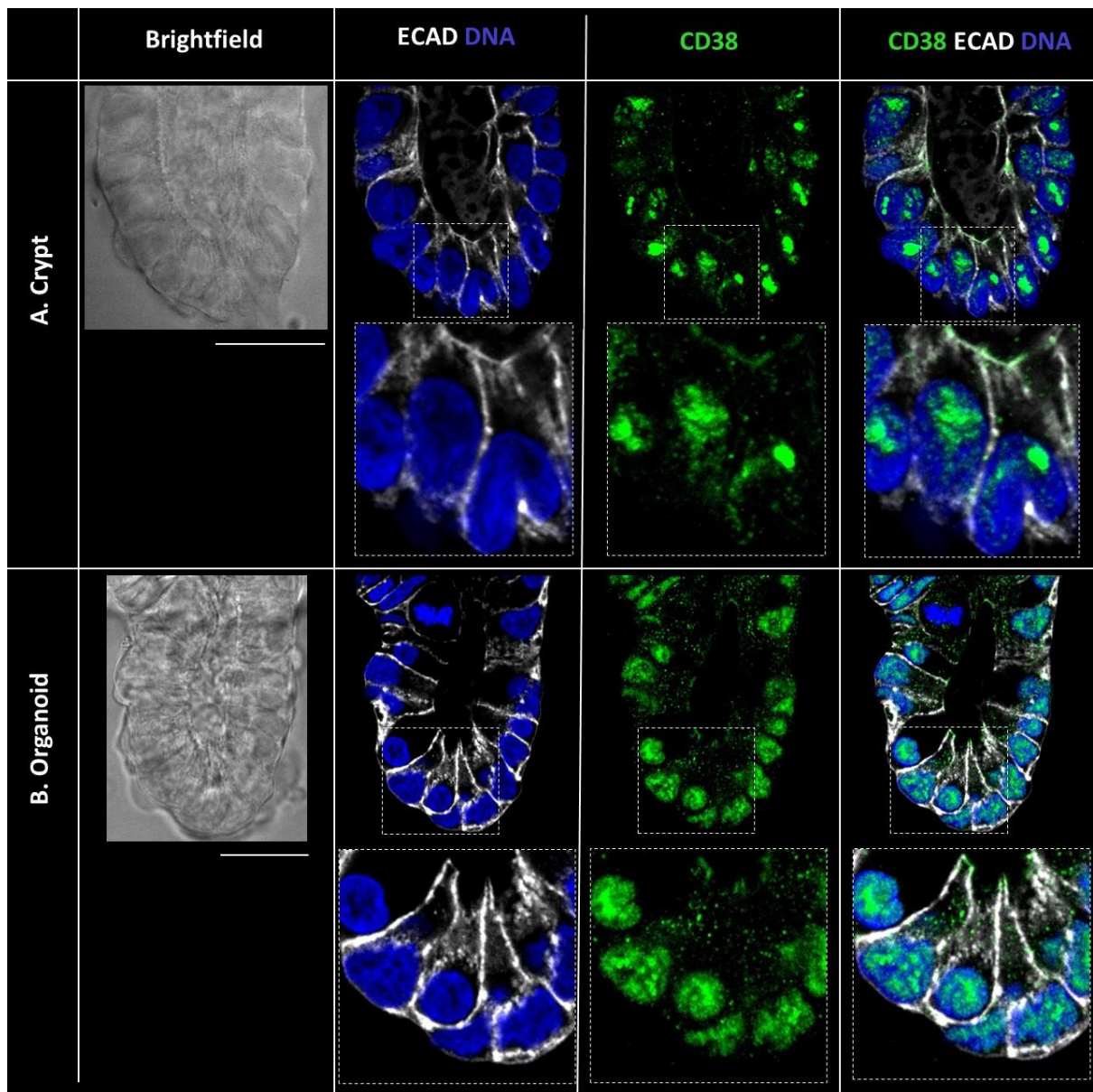
Figure 41 – Immunolabelling of CD38 in Crypts and Organoids.

Representative confocal images of the base of crypts **(A)** and organoids **(B)** immunolabelled with E-Cadherin (ECAD) in white and CD38 in green. Nuclei was stained with Sytox Blue (DNA). Brightfield depicted on the left. Scale bar = 25 µm.
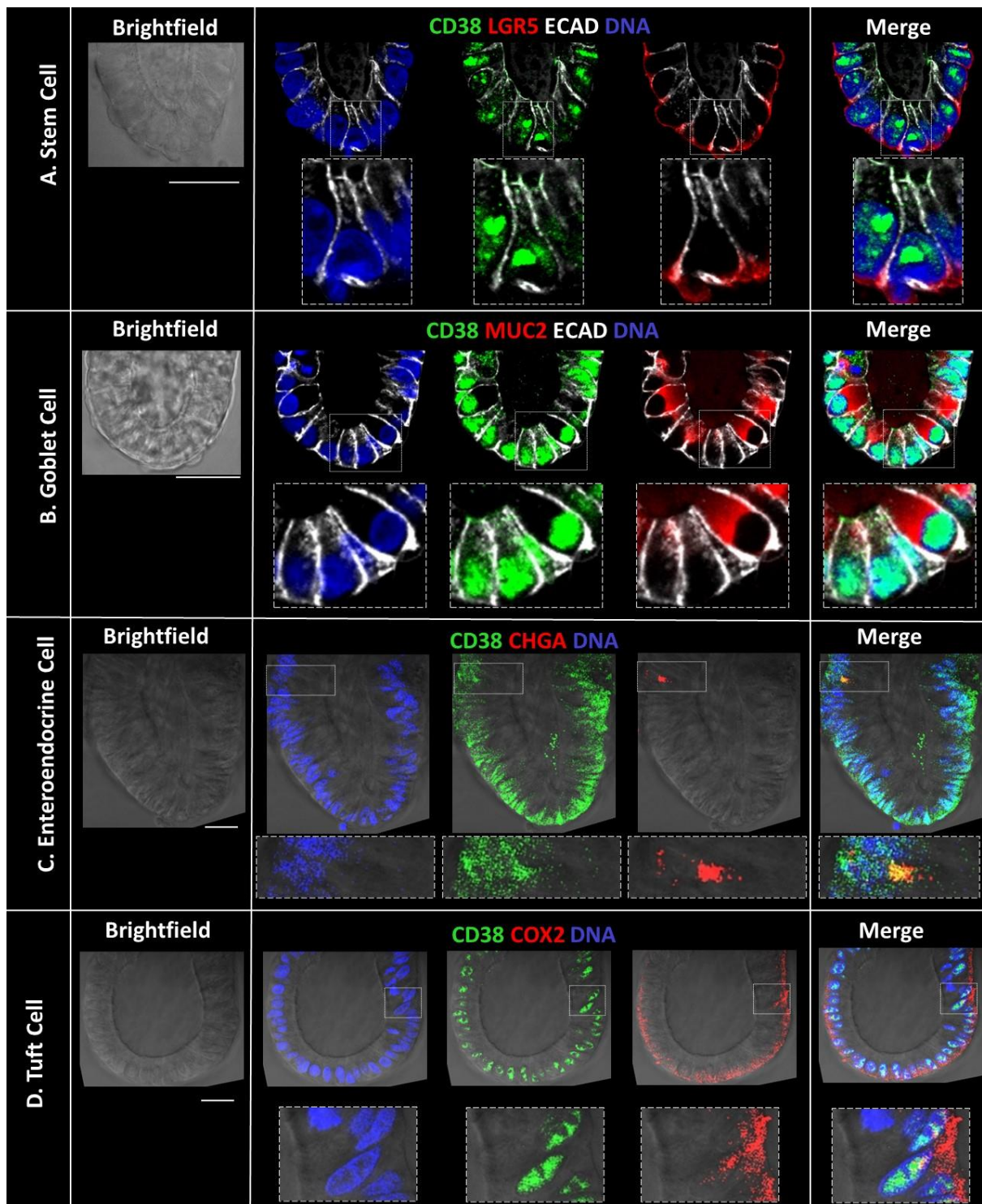
Figure 42 – Immunolabelling of CD38 with Colonic Epithelial Cells.

Representative confocal images of CD38 immunolabelled in crypts or organoids with E-Cadherin (ECAD) in white, CD38 in green, and co-labelled with stem cell marker LGR5 **(A)**, goblet cell marker MUC2 **(B)**, enteroendocrine cell marker CHGA **(C)**, or tuft cell marker COX2 **(D)** in red. Nuclei was stained with Sytox Blue (DNA). Brightfield depicted on the left. Scale bar = 25 µm.

3.2.3 Immunofluorescent Localisation of Ca^{2+} Coupled GPCRs

Immunolabelling and confocal imaging were next used to visualize and characterize the localisation of Ca^{2+} coupled muscarinic and purinergic GPCRs at the base of mucosal crypts, cultured crypts, and organoids. This referred specifically to G$_q$-coupled M1, M3, M5, as well as P2Y2. Furthermore, cells which contain these GPCRs were evaluated by co-labelling them with markers for epithelial stem cells (LGR5 or PTK7), goblet cells (MUC2), and enteroendocrine cells (CHGA). Contributors to this data include Dr Victoria Jones, Dr Nicolas Pelaez Llaneza and Dr Kristy Kam.

M1 was shown to be present in all three tissue samples (Figure 43). Mucosal M1 labelling showed high expression along the basolateral membrane of most cells (Figure 43A). In crypts, M1 labelling was exclusive to the basal membrane with some lateral membrane labelling (Figure 43B), which was similar to M1 labelling in organoids (Figure 43C). M3 was also shown to be present in all three tissue samples (Figure 44). Mucosal M3 labelling showed high expression within the basal pole of most cells (Figure 44A). In crypts, M3 labelling was exclusive to the basal membrane (Figure 44B), which was similarly observed in organoids (Figure 44C). M5 was also shown to be present in all three tissue samples (Figure 45). Mucosal M5 labelling showed high expression within the basal pole of most cells (Figure 45A). In crypts, M5 labelling appeared to also be prominent along the basal pole with strong nuclear labelling at the bottom, with some weak labelling on the apical pole and apical membrane (Figure 45B). However, in organoids M5 labelling was restricted to the basal membrane and even labelled outside the plasma membrane (Figure 45C).

Next, the intracellular localisation of M1, M3 and M5 was evaluated in colonic stem cells, goblet cells and enteroendocrine cells (Figure 46-48). With the exception of M5 labelling in stem cells (Figure 48A), expression of all three mAChRs were exclusive to the basal membrane. Stem cells, which were labelled with LGR5 along the basal membranes of cells at the base of crypts or organoids, co-labelled with M1 (Figure 46A) and M3 (Figure 47A). Goblet cells, which were packed with MUC2, expressed M1 (Figure 46B), M3 (Figure 47B) and M5 (Figure 48B) along their basal membranes. Sparse numbers of enteroendocrine cells, which were labelled with CHGA, also expressed M1 (Figure 46C), M3 (Figure 47C) and M5 (Figure 48C) along their basal membranes.
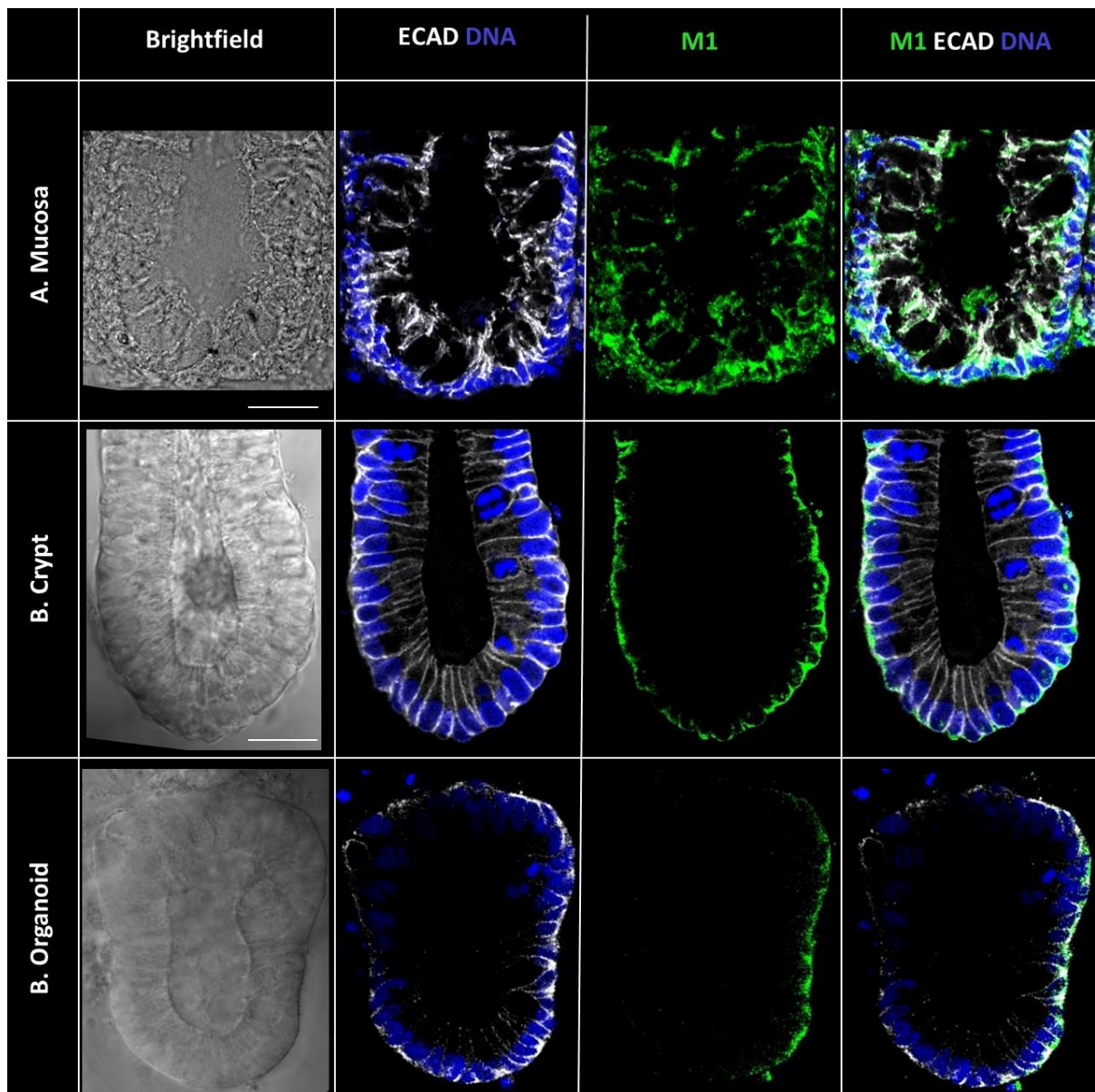
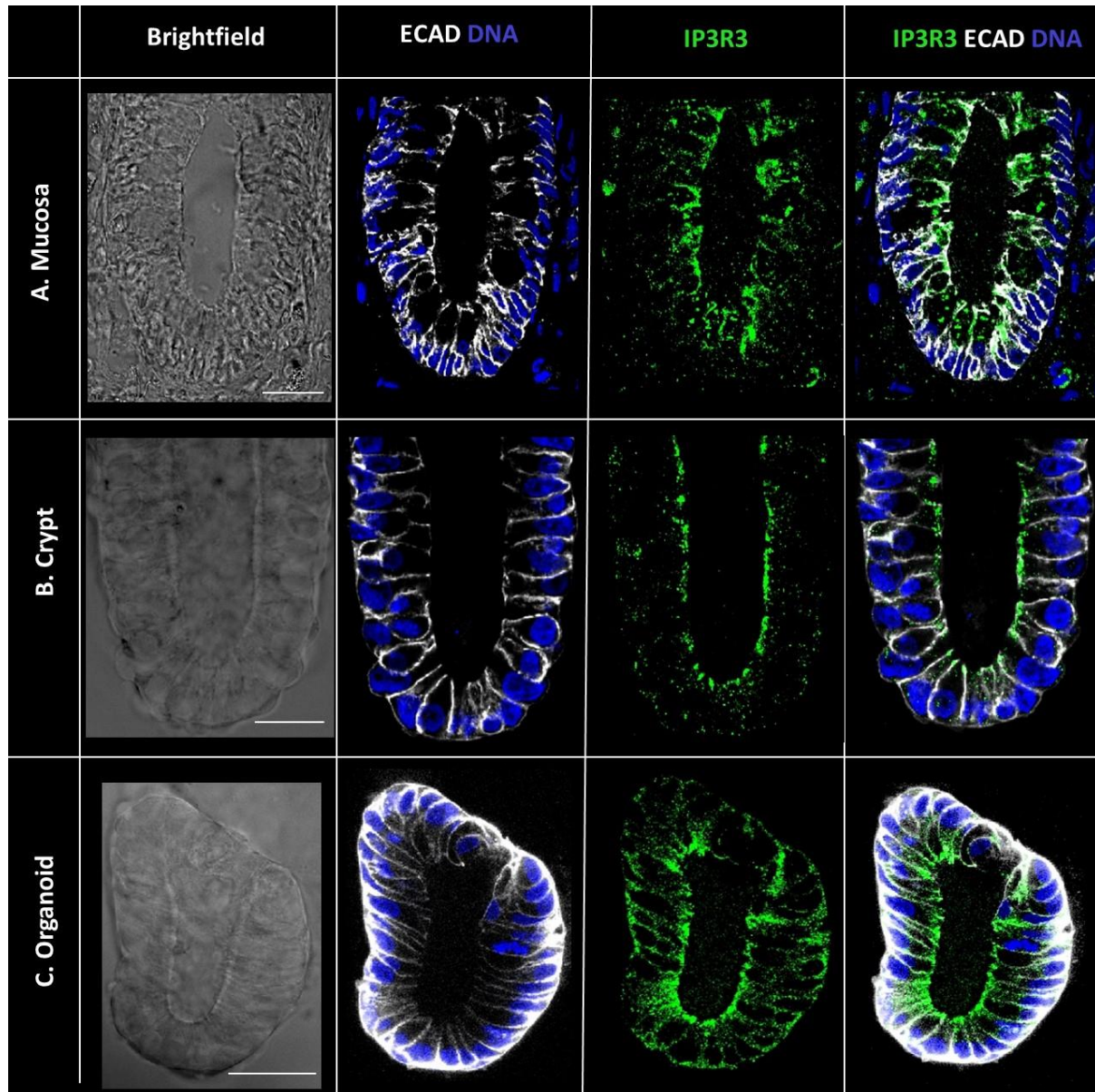**Figure 43 – Immunolabelling of M1 in Mucosa, Crypts, and Organoids.**

Representative confocal images of the base of mucosa **(A)**, crypts **(B)**, and organoids **(C)** immunolabelled with E-Cadherin (ECAD) in white and M1 in green. Nuclei was stained with Sytox Blue (DNA). Brightfield depicted on the left. Scale bar = 25 µm.
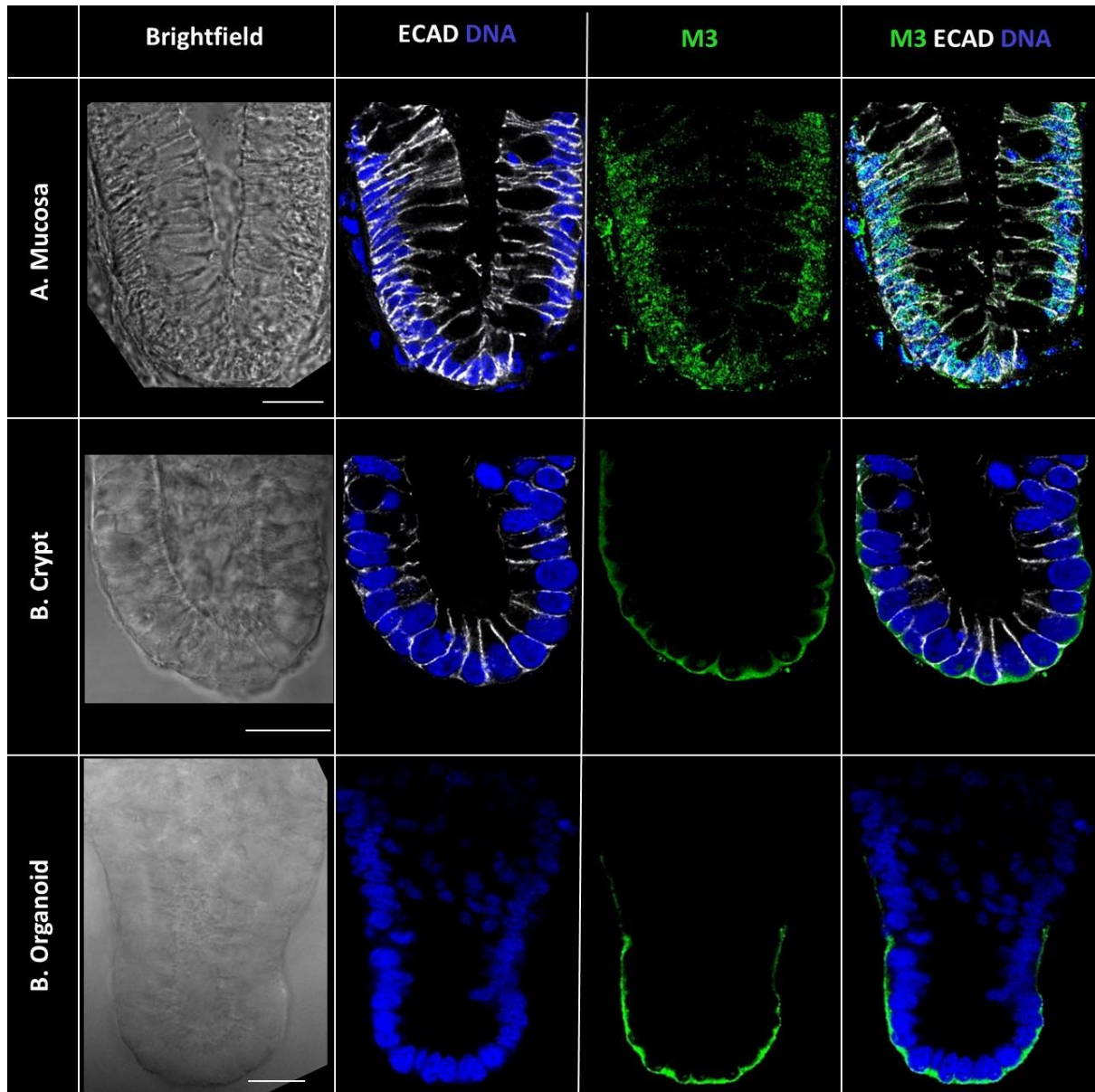
Figure 44 – Immunolabelling of M3 in Mucosa, Crypts, and Organoids.

Representative confocal images of the base of mucosa **(A)**, crypts **(B)**, and organoids **(C)** immunolabelled with E-Cadherin (ECAD) in white and M3 in green. Nuclei was stained with Sytox Blue (DNA). Brightfield depicted on the left. Scale bar = 25 μm.
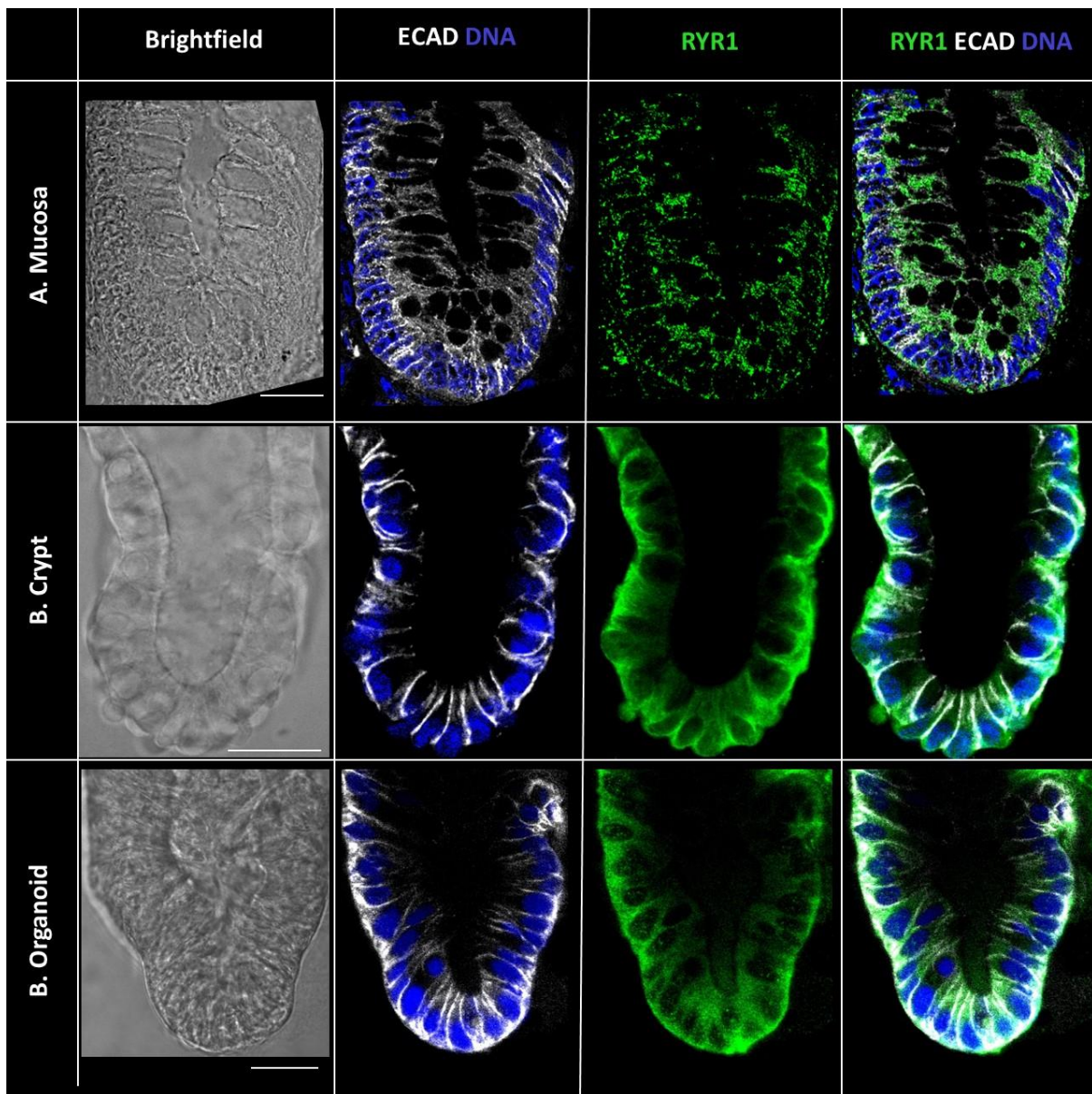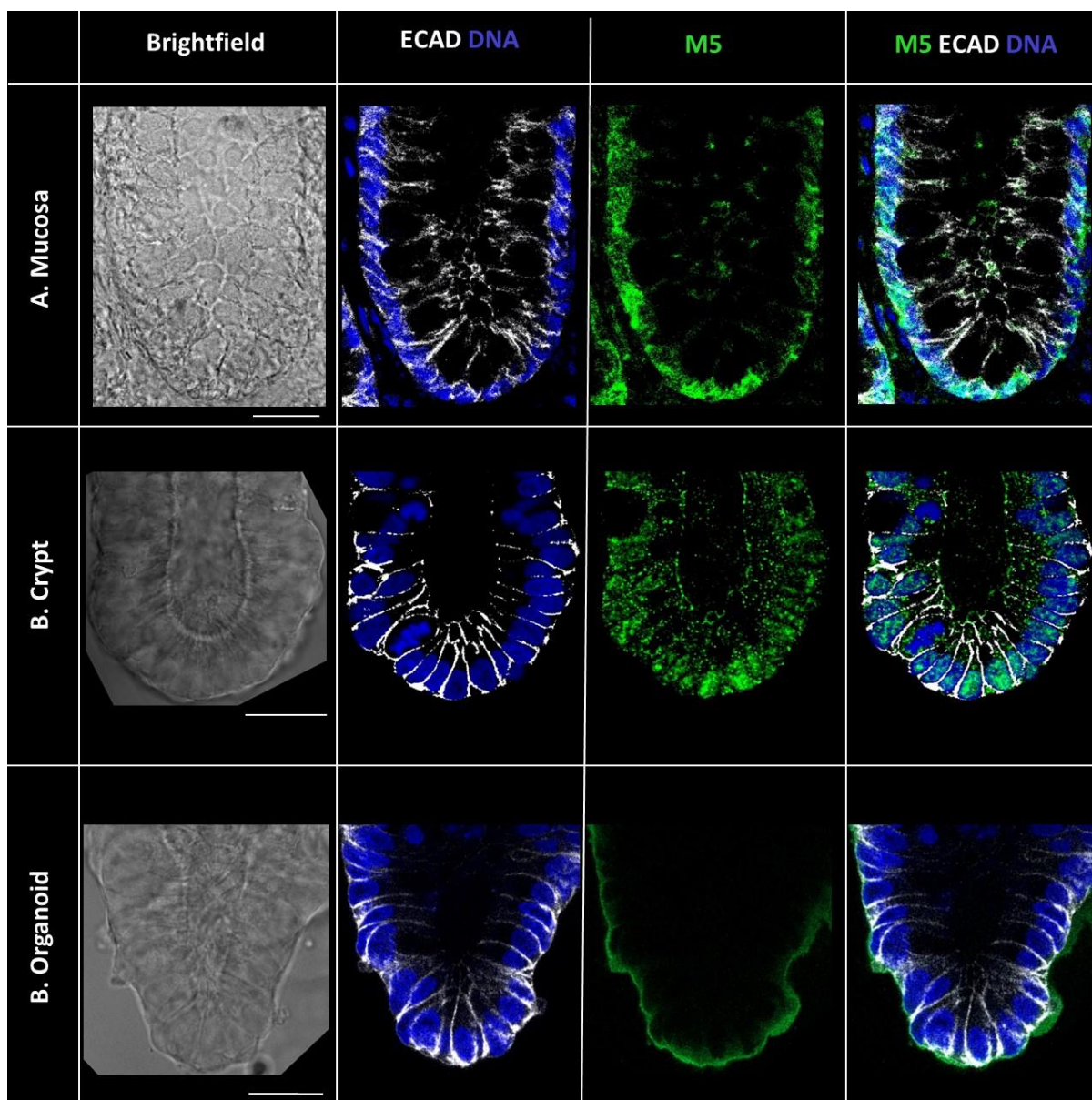
Figure 45 – Immunolabelling of M5 in Mucosa, Crypts, and Organoids.

Representative confocal images of the base of mucosa **(A)**, crypts **(B)**, and organoids **(C)** immunolabelled with E-Cadherin (ECAD) in white and M5 in green. Nuclei was stained with Sytox Blue (DNA). Brightfield depicted on the left. Scale bar = 25 μm.
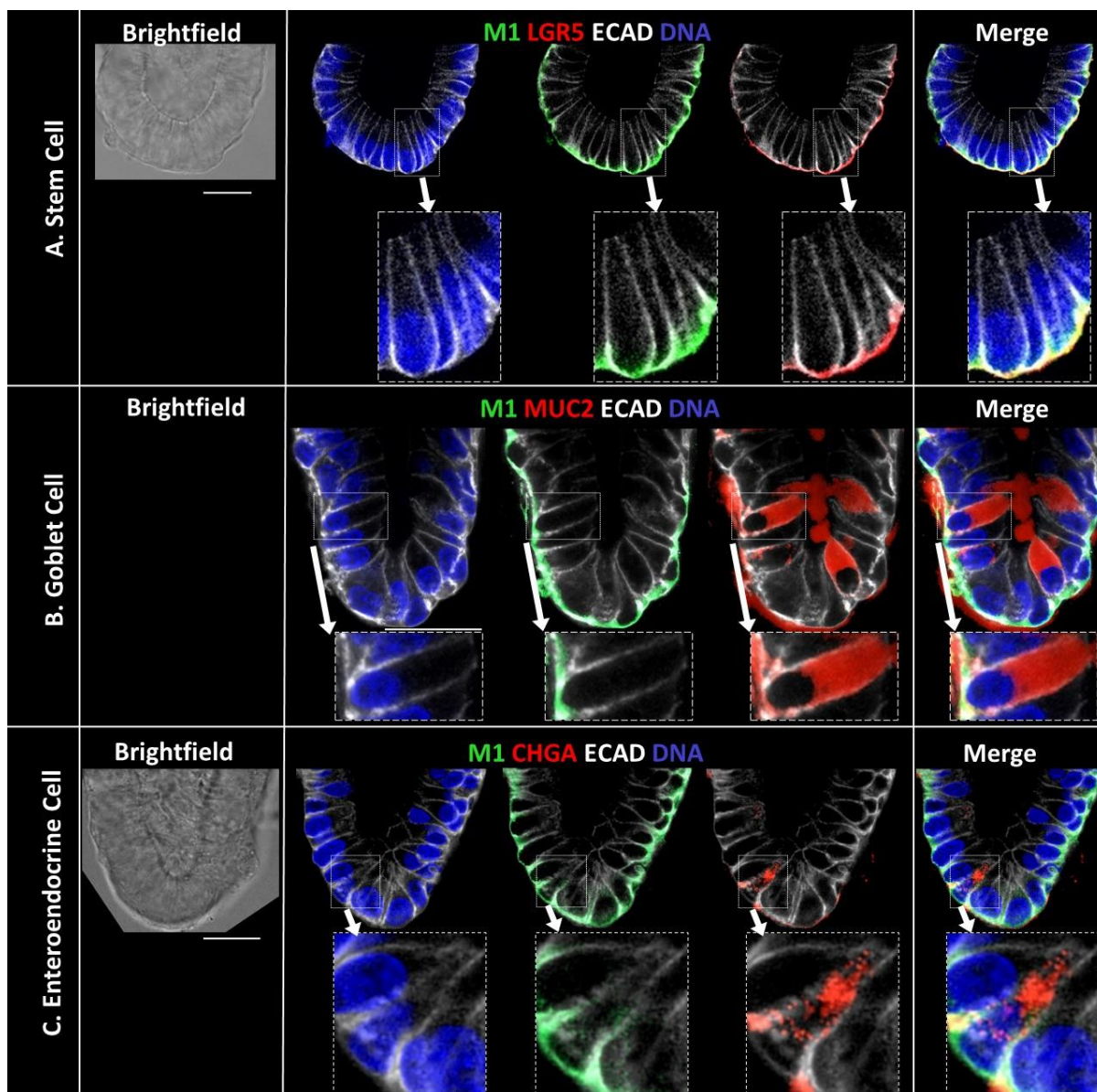
Figure 46 – Immunolabelling of M1 with Colonic Epithelial Cells.

Representative confocal images of M1 immunolabelled in crypts or organoids with E-Cadherin (ECAD) in white, M1 in green, and co-labelled with stem cell marker LGR5 **(A)**, goblet cell marker MUC2 **(B)**, and enteroendocrine cell marker CHGA **(C)** in red. Nuclei was stained with Sytox Blue (DNA). Brightfield depicted on the left. Scale bar = 25 μm.
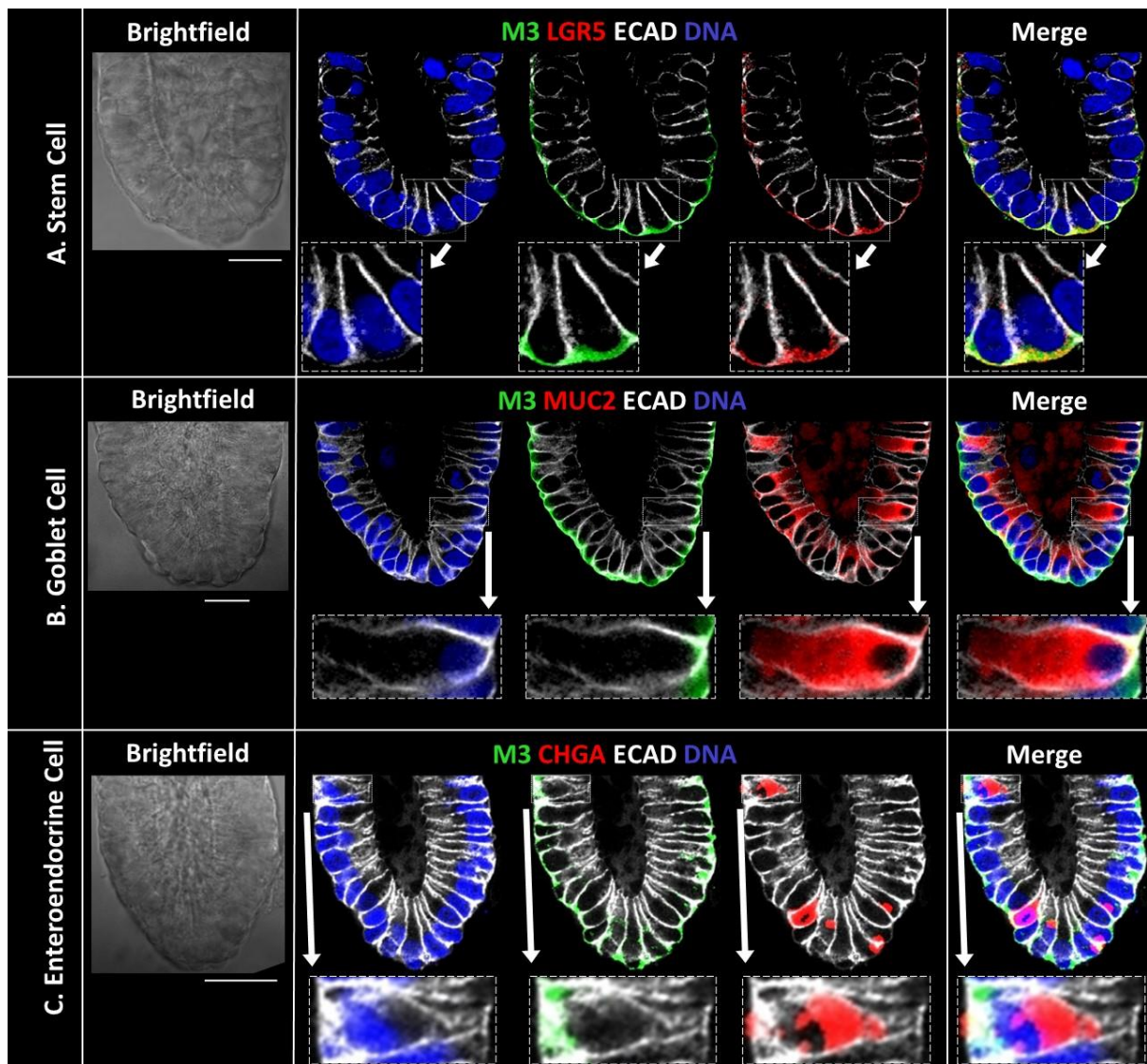
Figure 47 – Immunolabelling of M3 with Colonic Epithelial Cells.

Representative confocal images of M3 immunolabelled in crypts or organoids with E-Cadherin (ECAD) in white, M3 in green, and co-labelled with stem cell marker LGR5 **(A)**, goblet cell marker MUC2 **(B)**, and enteroendocrine cell marker CHGA **(C)** in red. Nuclei was stained with Sytox Blue (DNA). Brightfield depicted on the left. Scale bar = 25 μm.
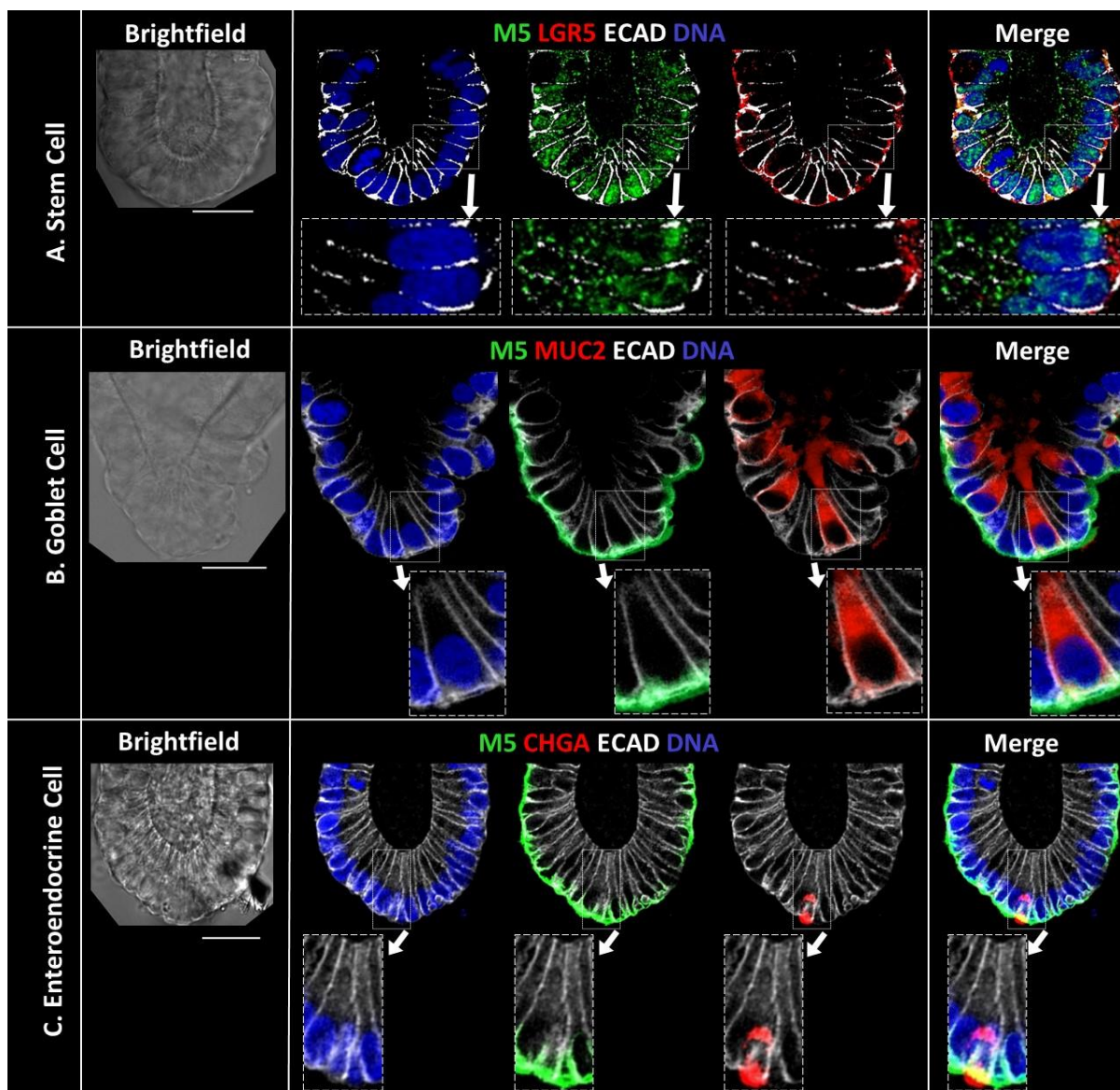
Figure 48 – Immunolabelling of M5 with Colonic Epithelial Cells.

Representative confocal images of M5 immunolabelled in crypts or organoids with E-Cadherin (ECAD) in white, M5 in green, and co-labelled with stem cell marker LGR5 **(A)**, goblet cell marker MUC2 **(B)**, and enteroendocrine cell marker CHGA **(C)** in red. Nuclei was stained with Sytox Blue (DNA). Brightfield depicted on the left. Scale bar = 25 μm.

Of the four ATP-sensitive P2Y receptors identified using RNA sequencing transcriptomic analysis (Figure 28), only P2Y2 coupled to G_q and was sensitive to both ATP and UTP (Table 5). Hence, this purinergic receptor was focused on in this thesis. P2Y2 was shown to be present at the base of all three tissues (Figure 49). Mucosal P2Y2 labelling showed uniform expression along the basal pole and on lateral membranes (Figure 49A). In crypts, P2Y2 labelling appear to also be prominent along the basal pole and basal membrane, as well as within the lumen (Figure 49B). In organoids, P2Y2 labelling was also prominent in the basal pole, with some cytoplasmic and lateral membrane labelling (Figure 49C).
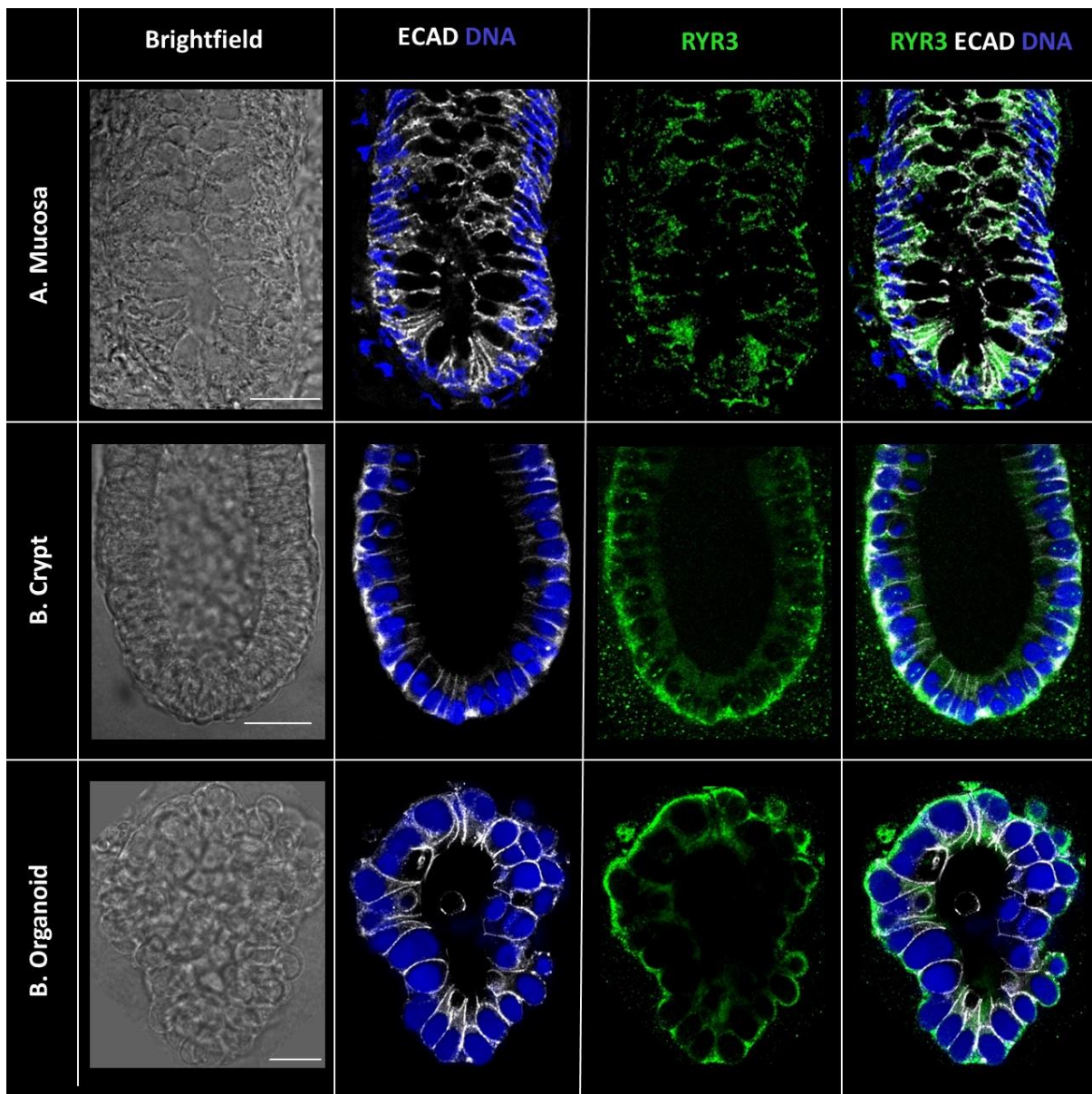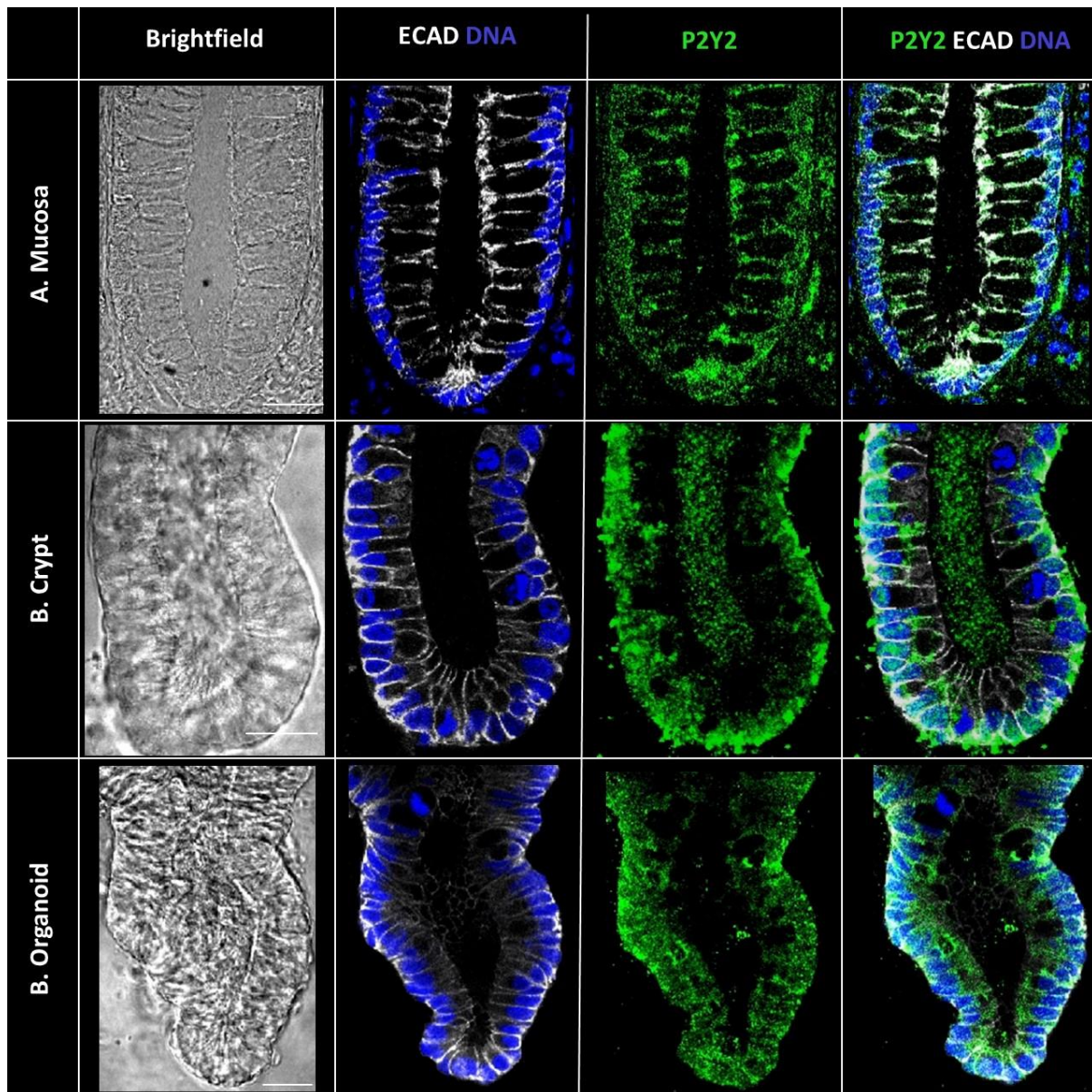

Figure 49 – Immunolabelling of P2Y2 in Mucosa, Crypts, and Organoids.

Representative confocal images of the base of mucosa **(A)**, crypts **(B)**, and organoids **(C)** immunolabelled with E-Cadherin (ECAD) in white and P2Y2 in green. Nuclei was stained with Sytox Blue (DNA). Brightfield depicted on the left. Scale bar = 25 μm.

Next, the intracellular localisation of P2Y2 was evaluated in colonic stem cells, goblet cells and enteroendocrine cells (Figure 50). P2Y2 co-labelled with LGR5+ stem cells along their basal membranes at the crypt base, in addition to labelling the lateral membrane on the basal pole of the cell (Figure 50A). In MUC+ goblet cells, P2Y2 labelling was present on their basal pole (Figure 50B). Sparse numbers of enteroendocrine cells, which were labelled with CHGA, also contain P2Y2 labelling on the basal pole (Figure 50C).
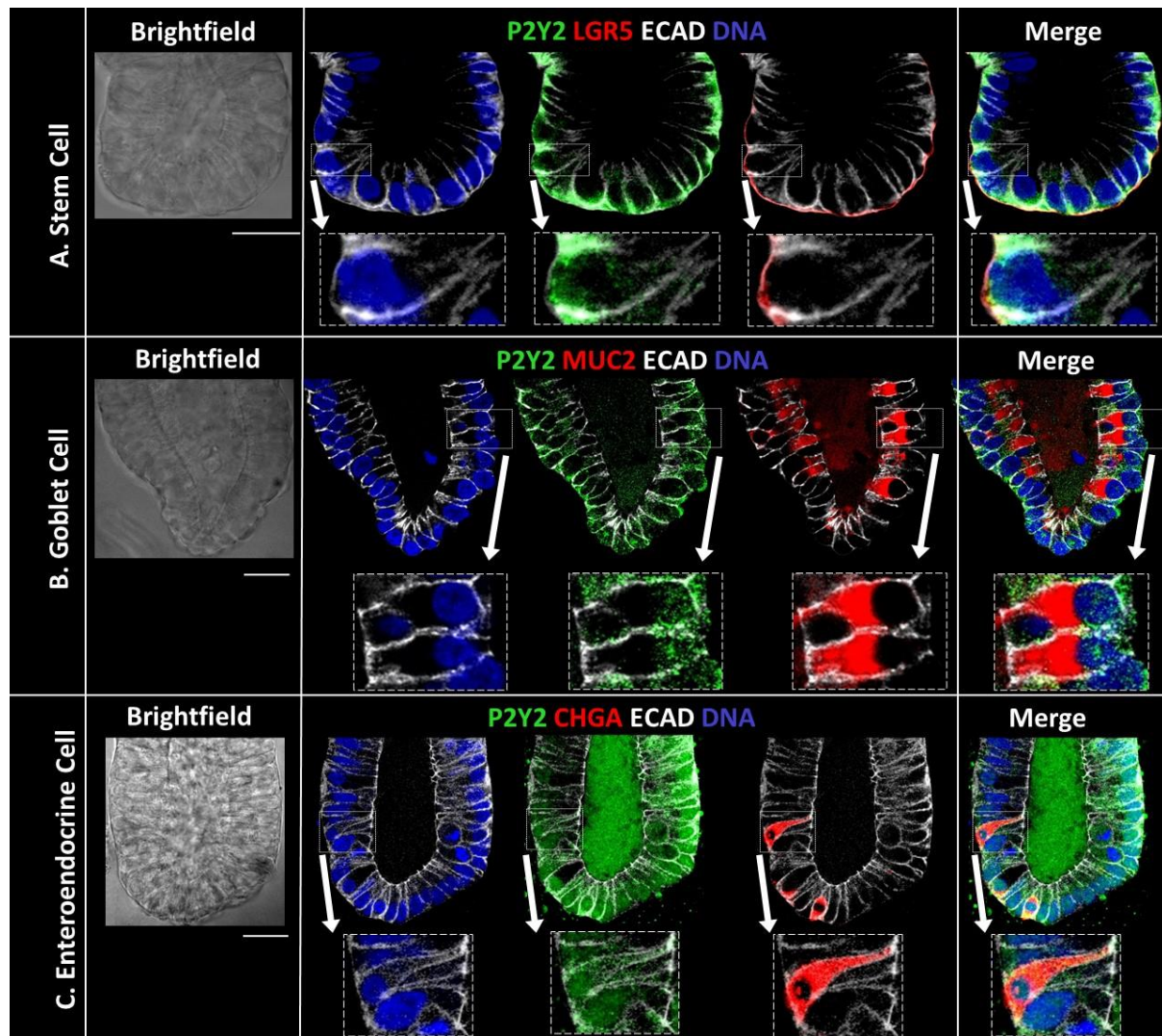
Figure 50 – Immunolabelling of P2Y2 with Colonic Epithelial Cells.

Representative confocal images of P2Y2 immunolabelled in crypts or organoids with E-Cadherin (ECAD) in white, P2Y2 in green, and co-labelled with stem cell marker LGR5 **(A)**, goblet cell marker MUC2 **(B)**, and enteroendocrine cell marker CHGA **(C)** in red. Nuclei was stained with Sytox Blue (DNA). Brightfield depicted on the left. Scale bar = 25 μm.

3.2.4 Immunofluorescent Localisation of ChAT

Finally, immunolabelling and confocal imaging were used to visualize and characterize the localisation of ChAT in the base of mucosal crypts, cultured crypts, and organoids. Furthermore, cells which contained ChAT were evaluated by co-labelling them with markers for goblet cells (MUC2 and WFDC2), enteroendocrine cells (CHGA and GLP1), and tuft cells (ADVILLIN, COX1 and COX2). Contributors to this data include Dr Victoria Jones and Dr Nicolas Pelaez Llaneza.

ChAT was shown to be present in mucosa and crypts, but not in organoids (Figure 51). In mucosa, ChAT labelling were either small punctate, parts of apical or lateral membrane, or the entire cytoplasmic space of a few slender cells (Figure 51A). In crypts, ChAT labelling were predominantly the cytoplasmic space of slender cells (Figure 51B). ChAT labelling was not present in organoids (Figure 51C), which reflected the absence of ChAT RNA in organoids during transcriptomic analysis (Figure 29).

Last of all, the intracellular localisation of ChAT was evaluated in colonic goblet cells, tuft cells and enteroendocrine cells. ChAT labelling were either absent or low in goblet cells (Figure 52). ChAT labelling was absent in WFDC2+ goblet cells, and the few cells containing ChAT labelling within their cytoplasmic space did not contain WFDC2 labelling (Figure 52A). Similarly, ChAT labelling was absent or low in MUC2+ goblet cells, and the few slender cells containing ChAT labelling within their cytoplasmic space did not contain MUC2 labelling (Figure 52B). ChAT labelling occurred in most tuft cells (Figure 53); ChAT co-labelled with most ADVILLIN+, COX1+ and COX2+ tuft cells (Figure 53A-C). ChAT labelling was also present on most enteroendocrine cells (Figure 54); ChAT co-labelled with CHROA+ and GLP1+ enteroendocrine cells (Figure 54A-B).
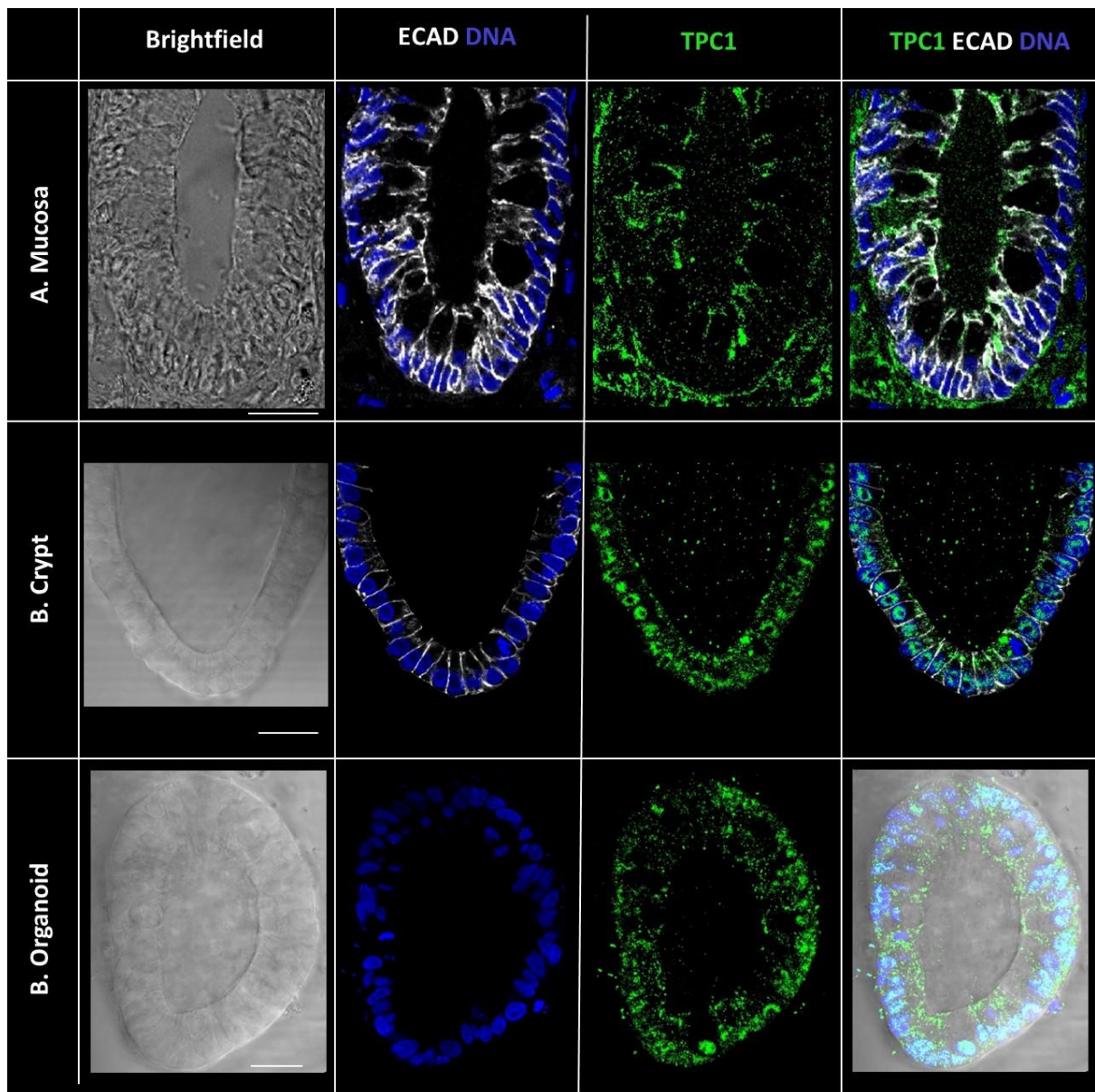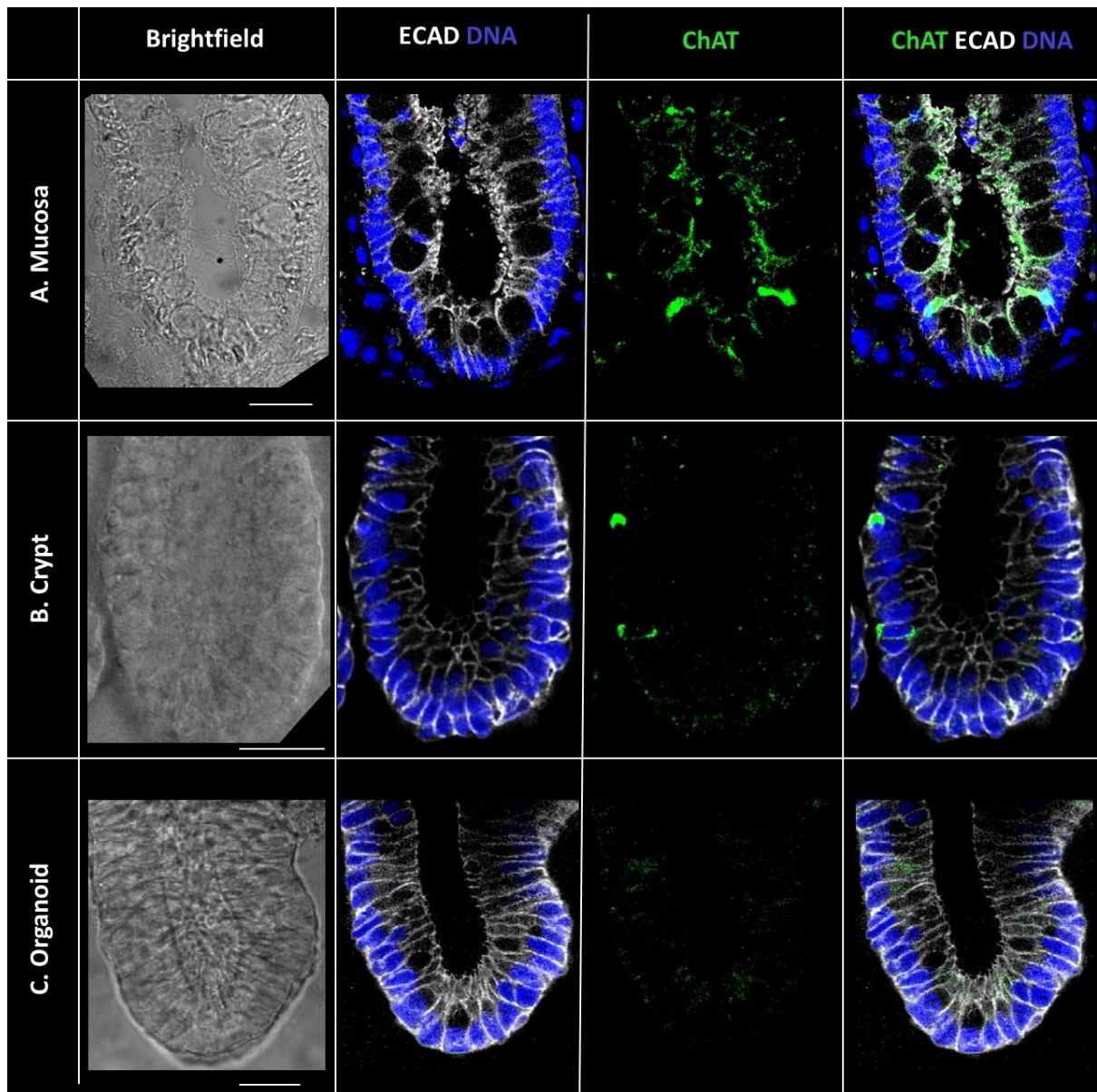
Figure 51 – Immunolabelling of ChAT in Mucosa, Crypts, and Organoids.

Representative confocal images of the base of mucosa **(A)**, crypts **(B)**, and organoids **(C)** immunolabelled with E-Cadherin (ECAD) in white and ChAT in green. Nuclei was stained with Sytox Blue (DNA). Brightfield depicted on the left. Scale bar = 25 μm.
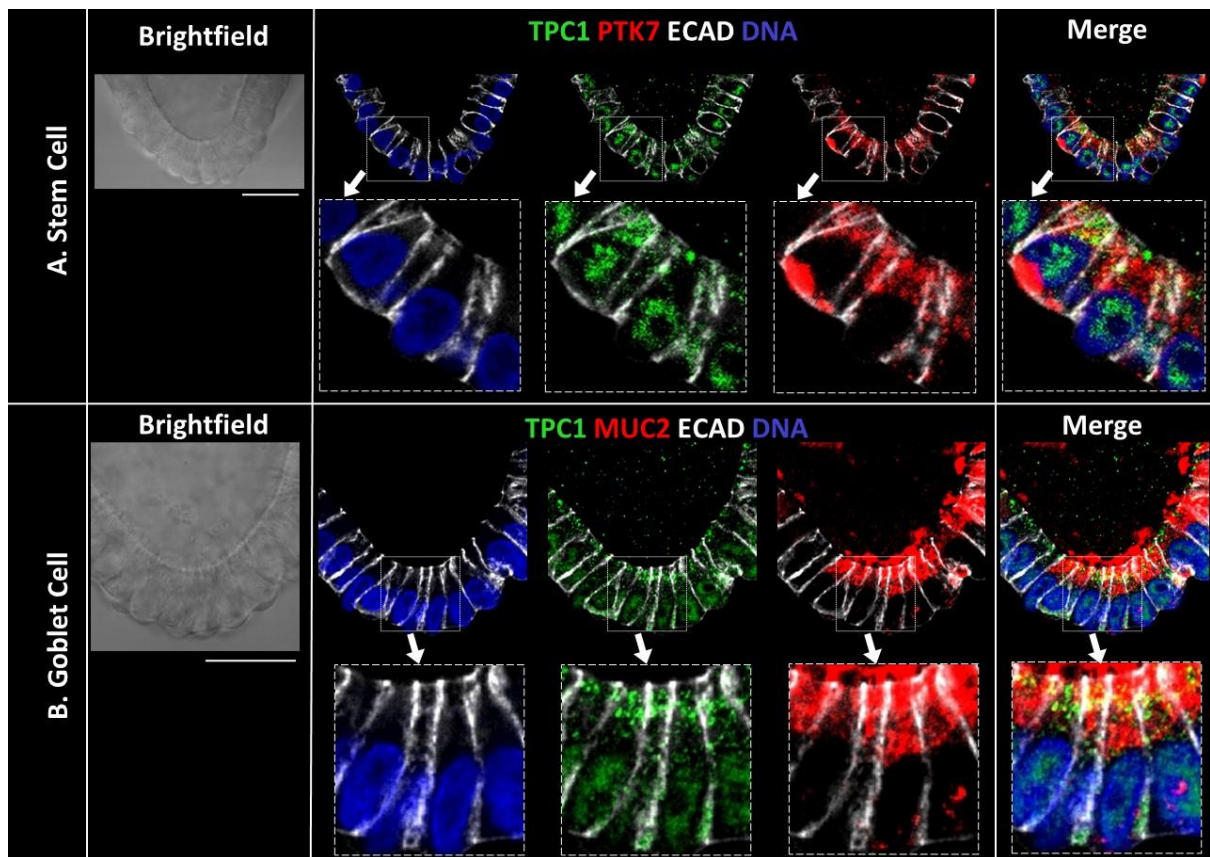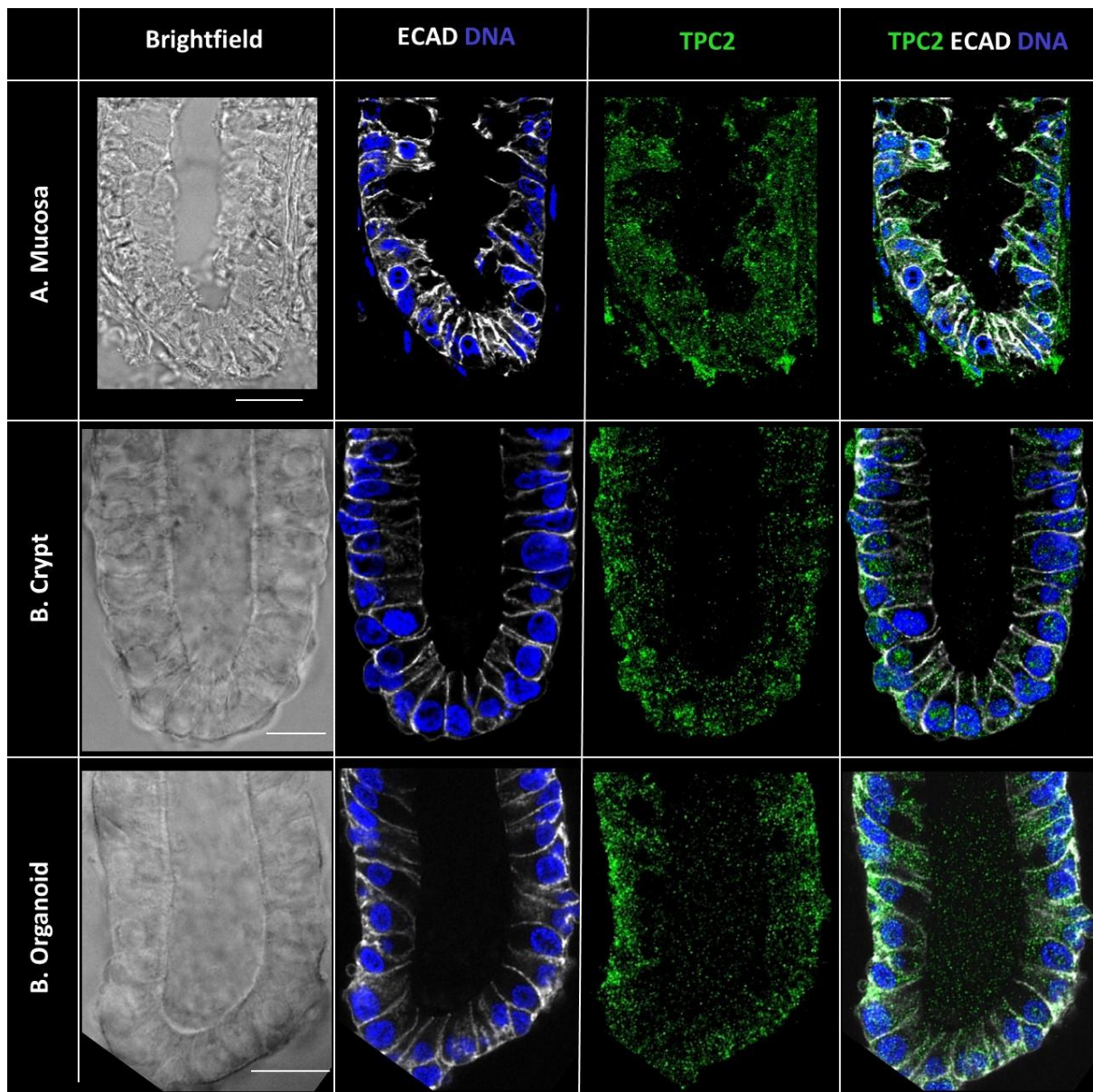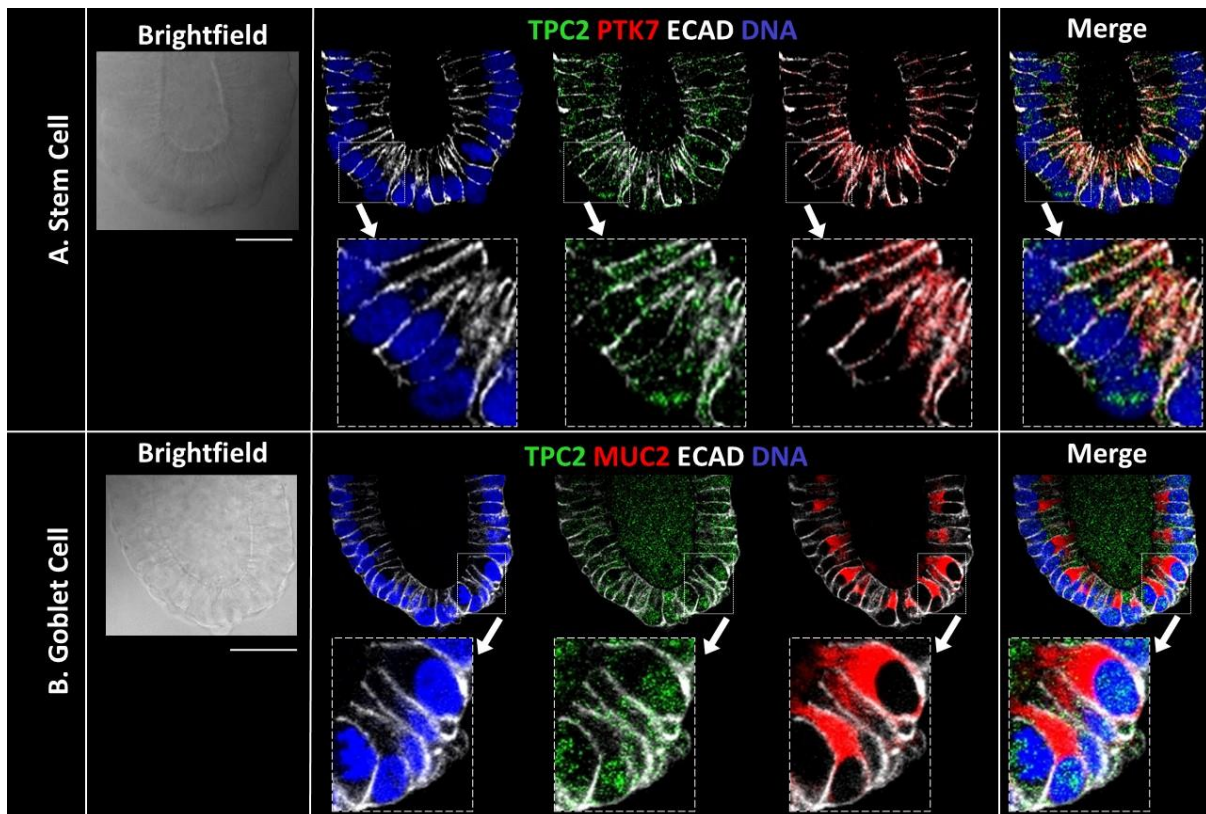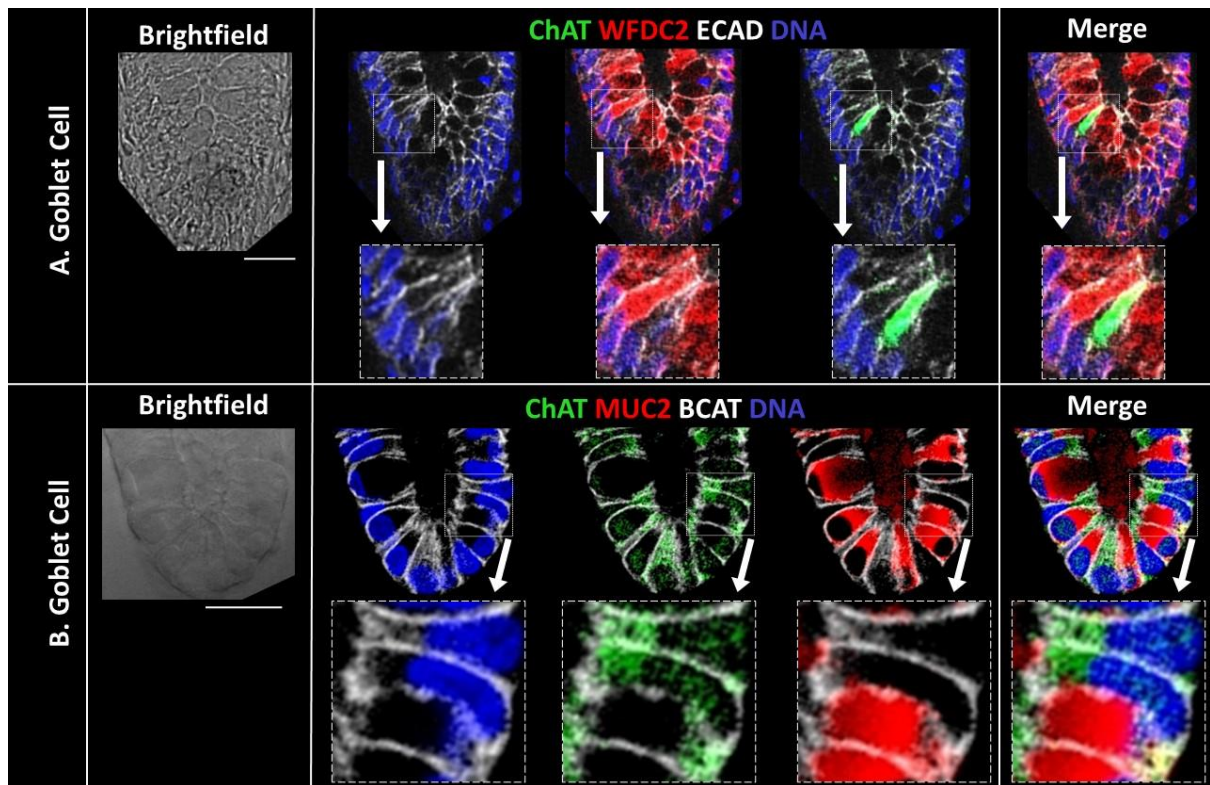
Figure 52 – Immunolabelling of ChAT with Colonic Goblet Cells.

Representative confocal images of ChAT immunolabelled in mucosa or crypts or organoids with E-Cadherin (ECAD) in white, ChAT in green, and co-labelled with goblet cell marker WFDC2 **(A)** or MUC2 **(B)** in red. Nuclei was stained with Sytox Blue (DNA). Brightfield depicted on the left. Scale bar = 25 μm.
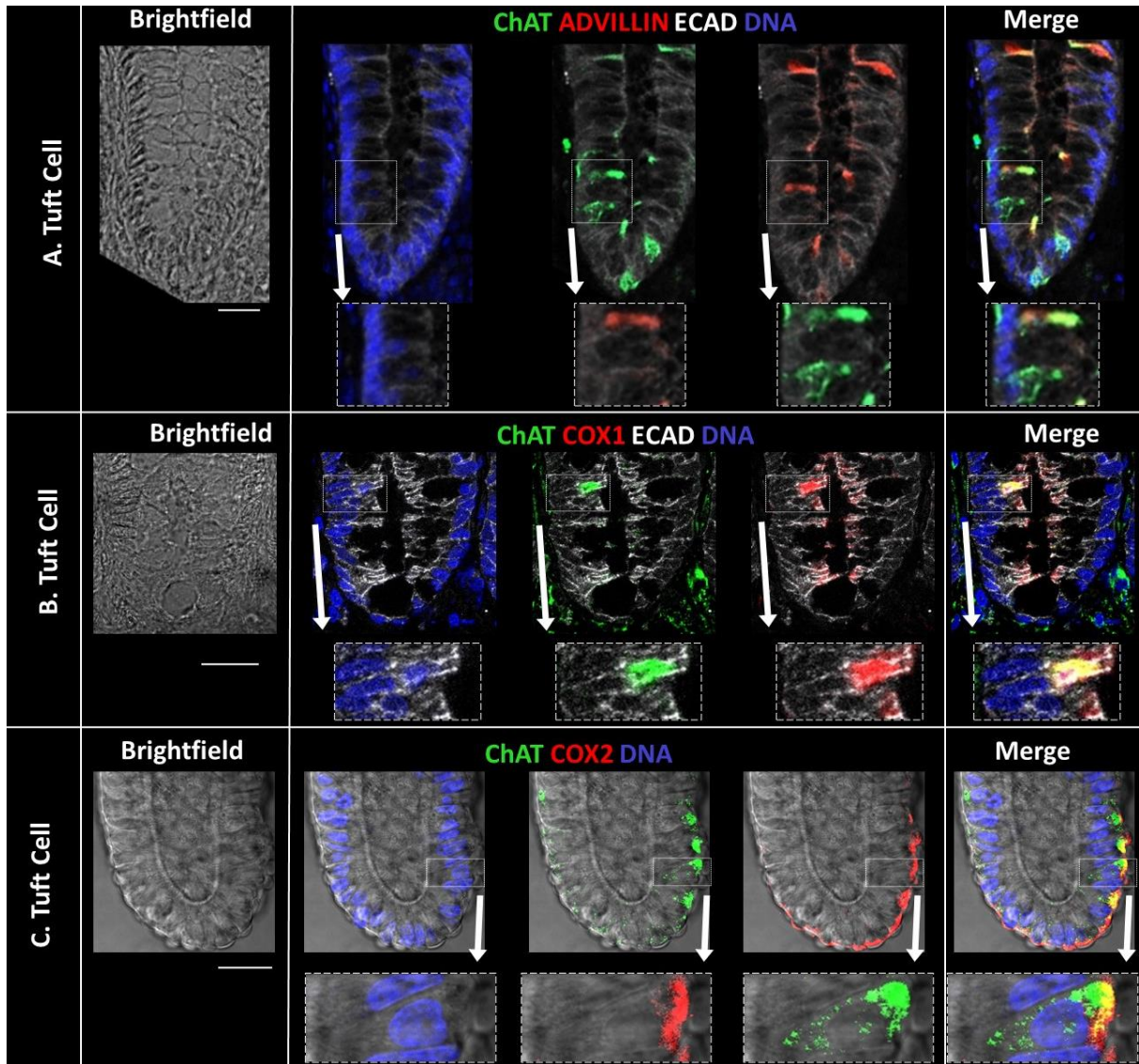
Figure 53 – Immunolabelling of ChAT with Colonic Tuft Cells.

Representative confocal images of ChAT immunolabelled in mucosa or crypts or organoids with E-Cadherin (ECAD) in white, ChAT in green, and co-labelled with tuft cell marker ADVILLIN **(A)**, COX1 **(B)** or COX2 **(C)** in red. Nuclei was stained with Sytox Blue (DNA). Brightfield depicted on the left. Scale bar = 25 µm.
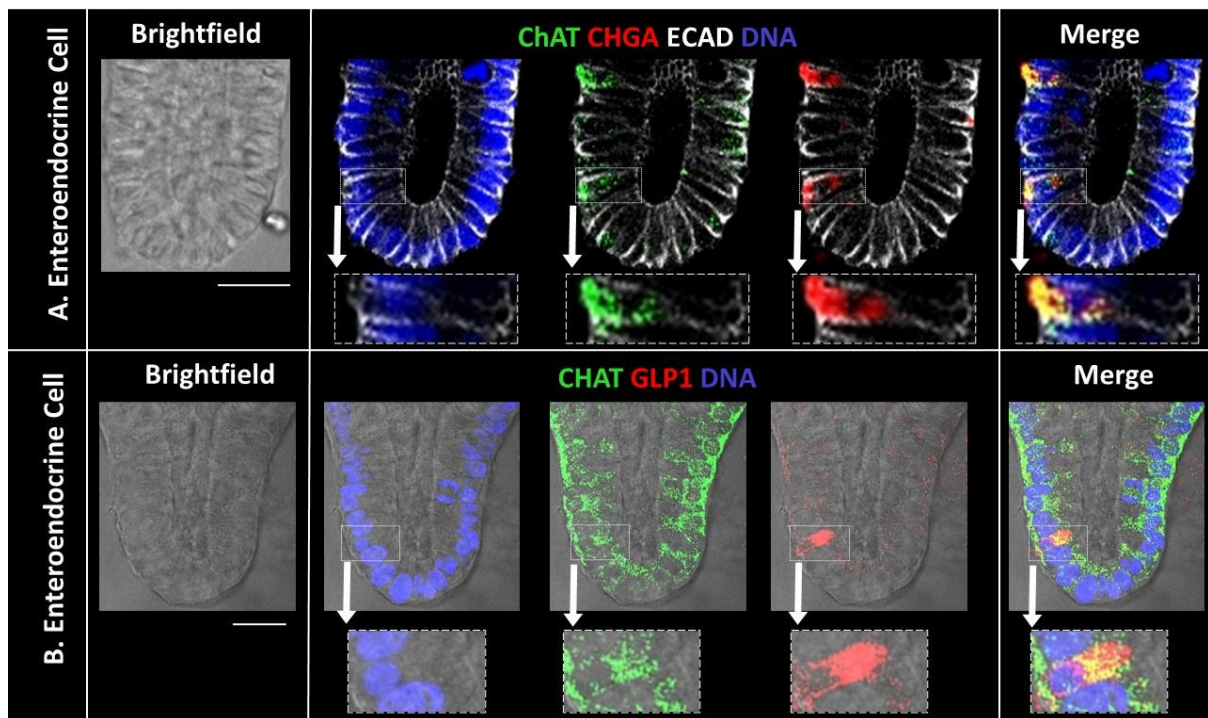
Figure 54 – Immunolabelling of ChAT with Colonic Enteroendocrine Cells.

Representative confocal images of ChAT immunolabelled in mucosa or crypts or organoids with E-Cadherin (ECAD) in white, ChAT in green, and co-labelled with enteroendocrine cell marker CHGA **(A)** or GLP1 **(B)** in red. Nuclei was stained with Sytox Blue (DNA). Brightfield depicted on the left. Scale bar = 25 μm.

3.3 Discussion

This chapter's results quantified the gene expression followed by visualisation of the protein expression of Ca^{2+} signalling toolkit components in human colonic native mucosa, cultured crypts, and organoids. Transcriptomic analysis using RNA sequencing demonstrated the gene expression of intracellular Ca^{2+} release channels, muscarinic and purinergic GPCRs, and proteins related to production or packaging of endogenous acetylcholine and ATP. Next, immunolabelling and confocal imaging were used to reveal the presence of these proteins and identify their cellular localisations within colonic epithelial cells at the base of mucosal crypts, cultured crypts, and organoids. These findings indicate the presence of Ca^{2+} signalling pathways that are mediated by muscarinic and purinergic receptor activation.

3.3.1 Differential RNA Expression in Mucosa, Crypts, and Organoids

Within the same family of receptors, the gene expression of certain receptor subtypes was higher compared than others. Among IP3Rs, IP3R3 gene expression was the highest while IP3R1 gene expression was the lowest (Figure 23). That study also showed the absence of RYR3 gene expression in colonic cell lines, which was identical to this thesis's findings in crypts and organoids (Figure 24). For TPCs, TPC1 was higher than TPC2 (Figure 25); TPC3 gene expression was not explored as they are known to not be expressed in primates (Ogunbayo, et al., 2015). M3 gene expression was highest of M1-4 (Figure 27). And, P2Y1 and P2Y2 genes were expressed higher than P2Y11 and P2Y13 (Figure 28).

On the other hand, the differential expression between human colonic native mucosa, cultured crypts, and organoids are an interesting subject to analyse. For example, expression of IP3R1 mRNA in crypts and organoids was less than half compared to mucosa (Figure 23). This can be explained by the nature of these samples. Mucosa, as the name implies, consists of the epithelium embedded to its lamina propria basement membrane, which contain subepithelial connective tissue and non-epithelial cells such as neurons and immune cells. By comparison, crypts consist solely of the isolated monolayer epithelium which were separated from the lamina propria using collagen degrading enzymes. And lastly, organoids consist of epithelial cells grown from single cells cultured in media within Matrigel to form 'mini-guts'. Thus, the RNA isolated and analysed from mucosa will originate from epithelial and non-epithelial cells, while the RNA isolated and analysed from crypts and mucosa should solely be from epithelial cells.

Since these crypts were isolated from mucosa and immediately put through RNA extraction, their transcriptomic analysis data reflects the *in-vivo* gene expression of the human colonic epithelium. On the other hand, organoids reflect the *ex-vivo* gene expression of the human colonic epithelium. Due to this, similarity in RPKM between crypts and organoids indicate the advantage of cultured organoids as a model of studying the human colonic epithelium. However, a drastically lower organoid RPKM (RYR1, M1) would indicate a paradigm of gene

upregulation in the colonic epithelium by the mucosa which was not replicated by the organoid culture conditions. And on the flipside, a drastically increased organoid RPKM (IP3R3, RYR2, TPC2) would indicate a paradigm of gene downregulation in the colonic epithelium by the mucosa which similarly was not replicated by the organoid culture conditions.

Even so, one should be cautious about using this data to infer whether the protein expression of one receptor subtype would be higher or lower in the human colonic epithelium. This is because gene and protein expression can be affected by the rate of protein synthesis and degradation. For example, the half-life of IP3R3 proteins may be short and thus require constant gene expression, while IP3R1 proteins may have a long half-life and thus gene expression is infrequent. By that extension, the low gene expression of RYRs (Figure 24) may indicate a slow rate of protein turnover rather than not being expressed. One way to evaluate whether the genes being expressed by mucosa crypts, isolated crypts and organoids are highly or lowly expressed, would be to measure housekeeping genes – essential genes which are required for the maintenance of basic cellular functions. Since housekeeping genes would be expected to be expressed at a constant level in every cell regardless of condition (Eisenberg and Levanon 2013), it would be a suitable internal control to compare relative gene expression. Future studies should also consider splice variants for the same protein subtype. For example, the M3 cDNA consists of over four thousand base pairs in eight exons, which can generate multiple splice variants (Forsythe, et al. 2002). It would be of interest to compare the expression of splice variants between different tissue models, as well as comparing their expression between normal and abnormal tissues, to determine whether splice variants contribute to the development of disease.

3.3.2 Differential Intracellular Ca^{2+} Release Channel Expression

To validate the transcriptomic analyses, immunolabelling was done to visualize the protein expression for these Ca^{2+} signalling toolkit components. In addition, the cellular localisation of these proteins was determined by labelling tissue samples with markers of colonic epithelial cells. Imaging was restricted to the base of crypts and organoids as stem cells reside within that region, and subsequent experiments were focused on the base of crypts and organoids. Due to disruptions caused by the coronavirus pandemic, some gaps are present in this body of data.

Endoplasmic reticular IP3Rs (Figure 32-33) and RYRs (Figure 34-36) were shown to be expressed by human colonic native mucosa, cultured crypts, and organoids. IP3R1 and IP3R2 in mucosa could not be achieved due to lack of access of human colonic tissue samples during the pandemic. However, the existing data sufficiently showed differential expression of receptor subtypes. Differences in IP3R subtype distribution suggests specialized functions for each receptor, which was explored by a study which characterized and identified differential

IP3R expression in rat colonic epithelium (Siefjediers, et al. 2007). In that study, IP3R1 was not present, IP3R2 labelled the nuclei, and IP3R3 stained the apical side of cells near the opening colonic crypts. By comparison, this thesis showed IP3R1 to be present in the human colonic epithelium (Figure 32). Irrespective of tissue type, IP3R1 and IP3R3 labelling were more prominent on the apical pole, while IP3R2 labelling was prominent on the basal pole. Notably, the expression of IP3R3 in organoids was more widespread than in crypt or mucosa, which correlated with the IP3R3 transcriptomic analysis (Figure 23). As for RYR1-3, in mucosa they seemed to favour the apical pole of cells, while in crypts and organoids their labelling was prominent on the basal membrane with some apical labelling. Non-specific labelling was ruled out using blocking peptides (data not shown). One possibility is the inability of RYR1-3 antibodies to permeate the Matrigel or plasma membrane of crypts and organoids, which might explain their high prevalence of basal labelling. On the other hand, mucosa samples consist of 10-micron sectioned slices, which poses no problem for antibody penetration.

Endolysosomal TPCs were next shown to be expressed on human colonic native mucosa, cultured crypts, and organoids. TPC1 labelling appear to be concentrated in the nuclear space and in the cytoplasm, as well as some apical membranes (Figure 37). This labelling pattern was observed in both stem cells and goblet cells, where TPC1 was present inside the nucleus and in the cytoplasmic space of PTK7+ cells (Figure 38) and on the apical side of MUC2+ cells. On the other hand, TPC2 labelling was prominent on the basal side in crypts and organoids, and prominent in the cytoplasm of some cells in mucosa (Figure 39). One complication regarding TPC2 was high background labelling in the lumen or outside the epithelium. This was observed in stem cells and goblet cells labelled with TPC2 (Figure 40) which complicates data interpretation. Even so, it is clear that TPCs are present in the colonic epithelium. Recent TPC immunolabelling with Rab5/11 on the LSM910 confocal microscope not only confirmed the apical labelling of TPC1 (Figure 161A-B) and basal labelling of TPC2 (Figure 161C-D), but it also highlighted the endosomes which TPCs were expressed on. Rab5 is involved in the maturation of early endosomes into late endosomes via the *trans*-Golgi (Nagano, et al. 2019), while Rab11 localised on early endosomes (Kobayashi and Fukuda 2013). The co-labelling of TPC1 with Rab5 (Figure 161B) indicate TPC1 are present on late endosomes, while the co-labelling of TPC2 with Rab11 (Figure 161C) indicate TPC2 are present on early endosomes.

To support the hypothesis that endolysosomal TPCs were involved in intracellular Ca^{2+} signalling in the colonic epithelium, CD38 gene expression confirmed (Figure 26). Next, CD38 protein was shown to be prominent in the nucleus, alongside some labelling on the apical membrane (Figure 41) and (Figure 42). This indicate CD38 playing a role in catalysing the formation of NAADP to act on endolysosomal TPCs to induce release of stored Ca^{2+}.

3.3.3 Differential Expression of Ca^{2+} Coupled GPCRs

Having characterized the protein expression of intracellular Ca^{2+} release channels and CD38, the expression and localisation of GPCRs which couple to those channels were determined. Transcriptomic analysis confirmed the gene expression of M1-4 (Figure 27) and P2Y1/2/11/13 (Figure 28). Of the five mAChRs, only M1/3/5 couple to G_q (Kruse, et al., 2014) to activate PLC to hydrolyse PIP2 to DAG and IP3; the latter being the ligand of IP3Rs. Thus, only those three were evaluated in this thesis. However, another member of the Williams group has characterized M1-5 using RT-PCR, RNA sequencing and immunolabeling during their PhD (Pelaez-Llaneza 2019). In this thesis, M1/3/5 were consistently shown to label the basal membrane of every cell marked within the base of crypts and organoids (Figure 43-48), which supports the hypothesis of them being basal plasma membrane receptors for acetylcholine in the colonic epithelium. Of the eight P2YRs, only P2Y2 couples to G_q and is sensitive to both ATP and UTP. As subsequent experiments focused on the consequence of P2Y2-induced purinergic signals, only P2Y2 protein expression was evaluated. P2Y2 labelling was shown to be prominent on the basal pole, however apical and luminal P2Y2 labelling was also characterized (Figure 49 & 50).

Due to the observation that M1, M3 and M5 immunolabelling appeared largely similar, one point of concern is that the suitability of muscarinic acetylcholine receptor antibodies – and others such as IP3Rs and RYRs – may not be optimal. For example, the amino acid sequences which these antibodies were raised against may be between two or more proteins, especially if these two proteins belong to the same family, are isoforms, or are splice variants. This point was echoed by another study (Jositsch, et al. 2009), which evaluated twenty-four muscarinic receptor antibodies using twenty-one different protocols in different tissue sections within gene-deficient mice. During this study, they found that the immunohistochemical localization of muscarinic receptors subtypes to be unreliable; it varied between tissue sections and protocols and resulted in some false positives.

3.3.4 ChAT Preferentially Labels Tuft Cells

Finally, this chapter evaluated the human colonic epithelium's potential of synthesizing acetylcholine, which other studies have shown tuft cells to be capable of (Pan, Zhang, Shao, & Huang, 2020). Transcriptomic analysis confirmed gene expression for ChAT in mucosa and crypts, but not in organoids (Figure 29). This was reflected by the absence of ChAT protein in organoids using immunolabelling (Figure 51). Labelling ChAT with epithelial cell markers showed ChAT labelling being absent/low in goblet cells (Figure 52), strong co-labelling with tuft cells (Figure 53), and some co-labelling with enteroendocrine cells (Figure 54). In the literature, ChAT labelling was shown to be expressed specifically in DCLK1 tuft cells (Schütz, Jurastow, et al. 2015). One study has shown tuft cells adopting an enteroendocrine phenotype as a result of disrupted muscarinic signals (Middelhoff, et al., 2020). Since the majority of human tissues samples obtained by the Williams group originate from patients undergoing colon surgery, it is possible that the same is occurring here (N>3), resulting in ChAT+

enteroendocrine cells which could be explored in future studies. The absence of ChAT+ cells in organoids will be discussed in a latter chapter.

The gene expression of vesicular nucleotide transporter (VNUT), SLC17A9, was shown to be present in mucosa, crypts, and organoids (Figure 30). This suggests that the colonic epithelium is capable of packing ATP into secretory vesicles. In addition, gene expression for proteins related to GLP1 production, GCG and PCSK1, were also shown to be present in all three tissue samples (Figure 31). However, immunolabelling for those proteins were not carried out due to time limitations and subject to further studies. A more in-depth discussion for these findings will be presented in the final conclusion (Chapter 8.4.4).

3.4 Conclusion

This chapter identified the gene and protein expression of Ca^{2+} signalling toolkit components in human colonic native mucosa, cultured crypts, and organoids. Gene expression was identified using RNA sequencing transcriptomic analysis, which was validated by protein localisation using immunolabelling. Immunolabelling identified specific labelling patterns for IP3 and RYR receptors, which suggest differential receptor function. In addition, the human colonic epithelium expresses muscarinic and purinergic receptors, CD38 which catalyses TPC-ligand NAADP, tuft cells that are capable of synthesizing and secreting acetylcholine, and TPC1 may be involved in mucus secretion from goblet cells. The next chapter of this thesis will elucidate the muscarinic and purinergic-induced pathway by selectively activating and/or inhibiting these Ca^{2+} signalling toolkit components.

4 Chapter 4 – Results Part 2: Spatio-Temporal Characteristics of Ca²⁺ Signals Induced by Muscarinic and Purinergic Receptors

4.1 Introduction

The previous chapter characterised the mRNA and protein expression for Ca^{2+} signalling toolkit components in human colonic mucosa, native isolated crypts, and cultured organoids. Specifically, the expression of muscarinic and purinergic receptor subtypes were studied using RNAseq and fluorescent immunolabelling techniques. Expression patterns in the stem cell zone suggested that these GPCRs can potentially to couple to numerous intracellular Ca^{2+} release channels to invoke colonic epithelial Ca^{2+} signals. This chapter describes a series of experiments that combine Ca^{2+} signalling with a pharmacological approach to identify specific receptor coupling to intracellular Ca^{2+} store mobilisation. These experiments were carried out using the ratiometric fluorescent dye that is specifically sensitive to Ca^{2+}, Fura-2 (Figure 55) and (Figure 56).
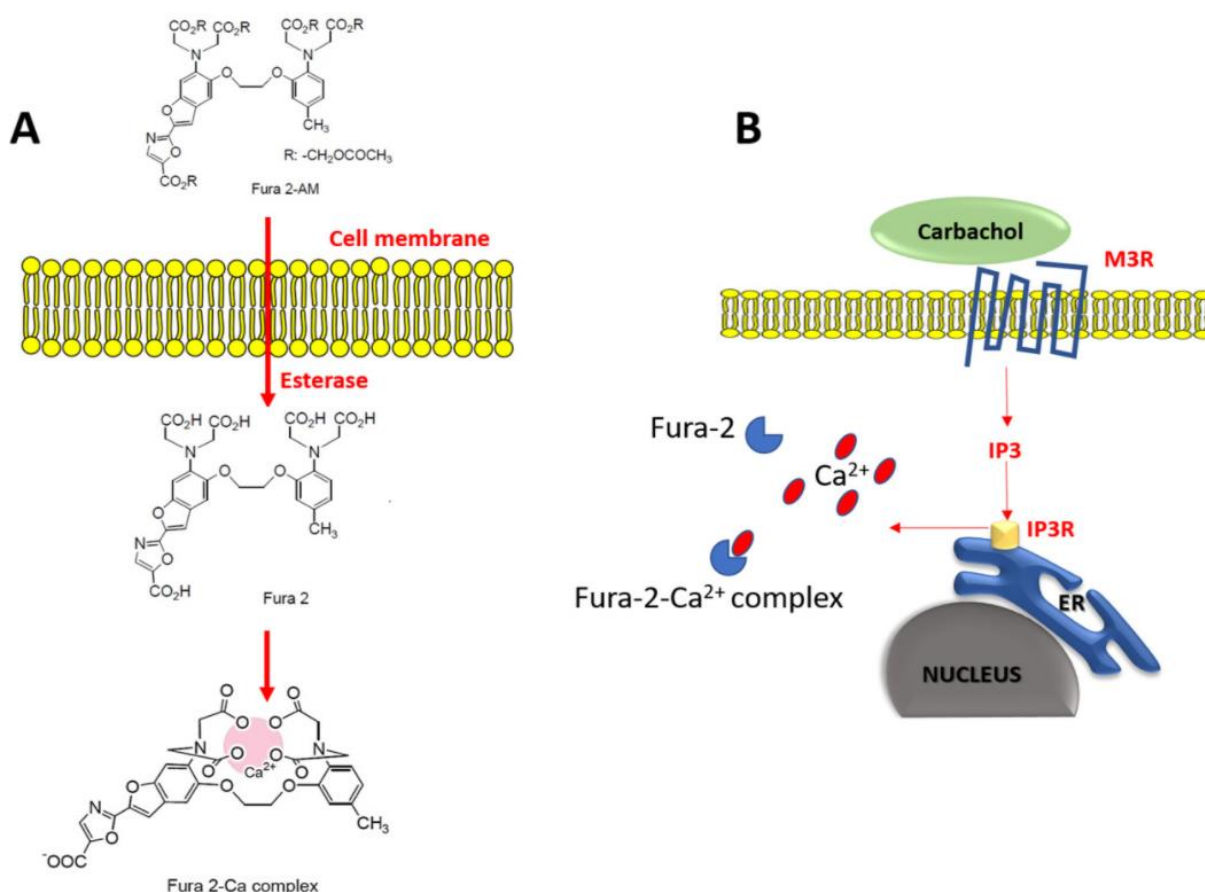
Figure 55 – Detection of Intracellular Ca^{2+} by Fura-2.

A. Outside the cell, the Fura-2-AM ester is Ca^{2+} insensitive and nonpolar. Upon interacting with the plasma membrane and becoming internalized, esterase enzymes cleave the AM groups, trapping Fura-2 inside the cell, where it is sensitive to Ca^{2+}. **B.** Upon release of organellar stored Ca^{2+}, such the ER via the muscarinic signalling pathway induced by Carbachol, Fura-2 exhibits a Ca^{2+} dependent excitation spectral shift. Adapted from (Shaalan, Carpenter and Proctor 2017).
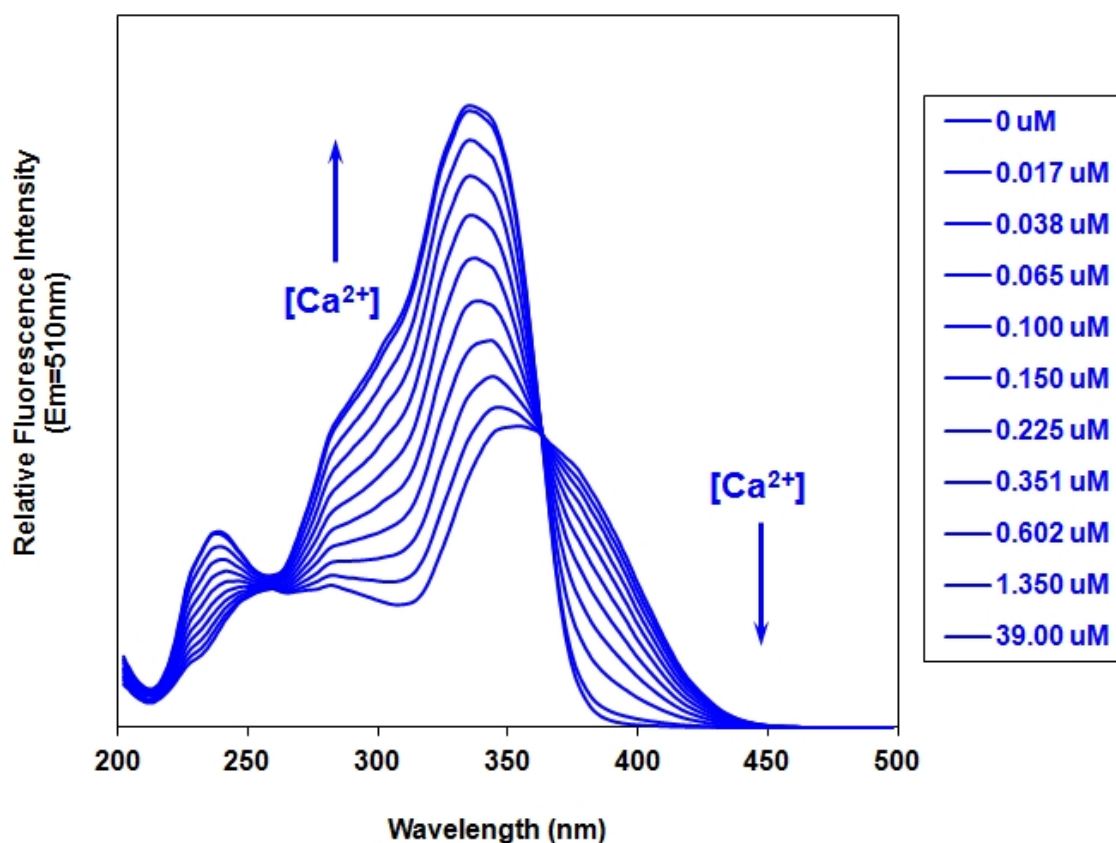
Figure 56 – Fluorescence Excitation Spectra of Fura-2.

Fura-2 has an emission peak of 505 nm and is excited by at 340 nm and 380 nm of light. The 340 nm emission corresponds to Fura-2 bound to Ca^{2+}, while the 380 nm emission corresponds to Fura-2 unbound to Ca^{2+}. The ratio of those wavelength emissions (340/380 nm) is directly related to changes in $[Ca^{2+}]$. Fura-2 operates well in solutions containing low concentrations of free Ca^{2+}.

Muscarinic and purinergic Ca^{2+} signals were generated in cultured crypts and organoids. First, the spatio-temporal characteristics of muscarinic and purinergic Ca^{2+} signals were determined. A range of pharmacological agents (Table 9) were then used to show that the muscarinic Ca^{2+} signalling pathway was mediated by Two-Pore Channels (TPCs) while the purinergic Ca^{2+} signalling pathway was mediated by IP3-Receptors (IP3Rs). Next, muscarinic and purinergic signals were shown to preferentially couple to distinct organellar Ca^{2+} stores but crosstalk with one another by converging on ryanodine receptors (RYRs). In addition to muscarinic and purinergic Ca^{2+} signalling, additional experiments were conducted to investigate other means of generating Ca^{2+} signals in crypts and organoids. These include a member of the TRP ion channels called Mucolipin-1 (TRPML1), and mechanosensitive Piezo channels.

4.2 Results

Cultured crypts and organoids which had been grown for 24-72 hours were loaded with Fura-2-AM (5 µM) for 2 hours in HBS at room temperature (Chapter 2.6). Certain antagonists which require incubation in culture media at 37°C (Table 9) were done prior to Fura-2 loading. "N" denotes the number of patients whose colonic crypts or organoids were used to generate data. Each patient sample would further be tested at least three times (n≥3). "N.S." denotes the data is not statistically significant (P>0.05). "*" denotes the data is statistically significant (P<0.05).

4.2.1 Spatio-Temporal Characteristics of Muscarinic and Purinergic Ca^{2+} Signals

The spatio-temporal characteristics of muscarinic Ca^{2+} signalling was investigated on crypts stimulated with carbachol (CCh; 10 µM), a pharmacological analogue of acetylcholine that is resistant to acetylcholinesterase hydrolysis (Streichert and Sargent 1992). The ratiometric fluorescence imaging (340/380 nm) showed CCh causing an increase in fluorescence initiating at the crypt base (Figure 57), which spreads to neighbouring cells before propagating up the crypt axis; all of which occurring within 1-3 minutes. The topology of CCh-induced Ca^{2+} signals were determined by drawing regions of interest (ROI) at three positions along the crypt axis (Figure 58A). Fluorometric measurements of those ROIs confirmed the Ca^{2+} signal originating at the crypt base and spreading up the crypt axis over time (Figure 58B). Next, the polarity of CCh-induced Ca^{2+} signals were determined by drawing two pairs of ROIs at two positions along the crypt axis (Figure 58C). Fluorometric measurements of those ROIs confirmed the Ca^{2+} signal originating at the apical pole and spreading to the basal pole at the crypt base, before the same occurs higher up the crypt axis (Figure 58D).
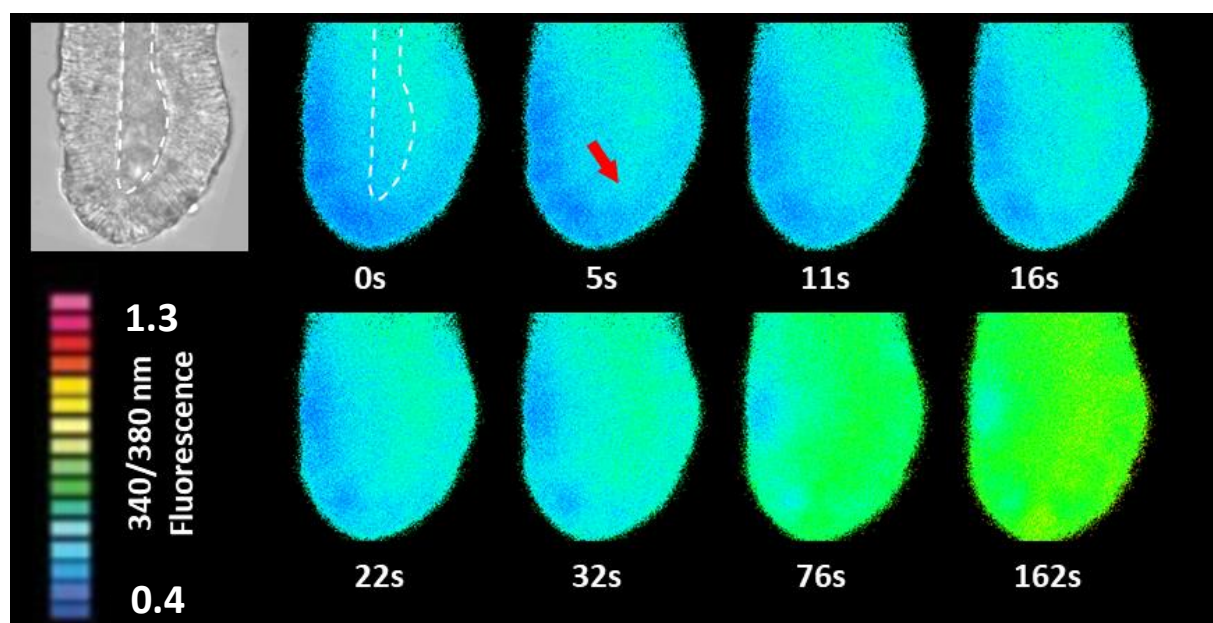
Figure 57 – CCh-induced Ca^{2+} Signals Originate at the Crypt Base.

Representative series of epi-fluorescent live images of a crypt loaded with Fura-2 (5 µM) being stimulated with CCh (10 µM) over time in seconds (s). Increase in Fura-2 ratio (340/380 nm) fluorescence is visualized by a colour map ranging from blue (0.4) to green then red (1.3).
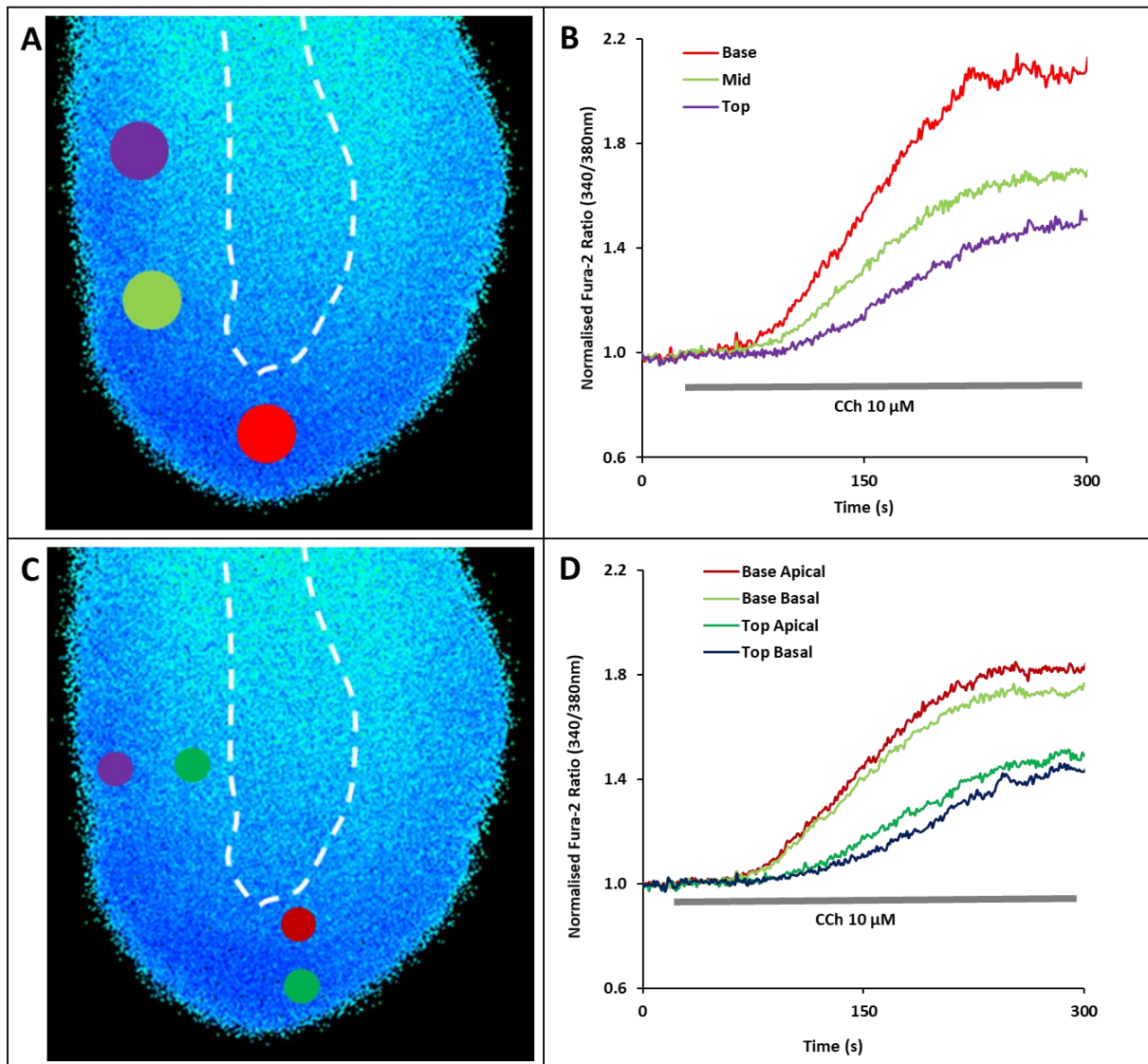
Figure 58 – Topology and Polarity of CCh-induced Ca2+ Signals.

Topology **(A-B)** and polarity **(C-D)** of Ca^{2+} signals induced by CCh (10 µM) over time. Left-side images depict crypts with drawn ROIs. Right-side line graphs represent the normalized Fura-2 ratio changes in each ROI.

CCh-induced Ca^{2+} release was not significantly affected by the absence of extracellular Ca^{2+} which was chelated by EGTA (1 mM), (Figure 59), indicating intracellular organelles were the source of Ca^{2+} release. CCh was confirmed to induce release of stored organellar Ca^{2+} via muscarinic receptors (Figure 60), as it was ablated by 4-DAMP, which inhibits M1 and M3 but prefers the latter (Greenwood and Dragunow 2010). In the absence of 4-DAMP, paired CCh responses with a 25-minute resting time between each (Figure 60A) demonstrated the crypt's ability to produce a second Ca^{2+} signal which was not statistically significant compared to the first (Figure 60B). However, addition of 4-DAMP (100 nM) after the first CCh response (Figure 60C) abolished the second CCh-induced Ca^{2+} signal (Figure 60D).
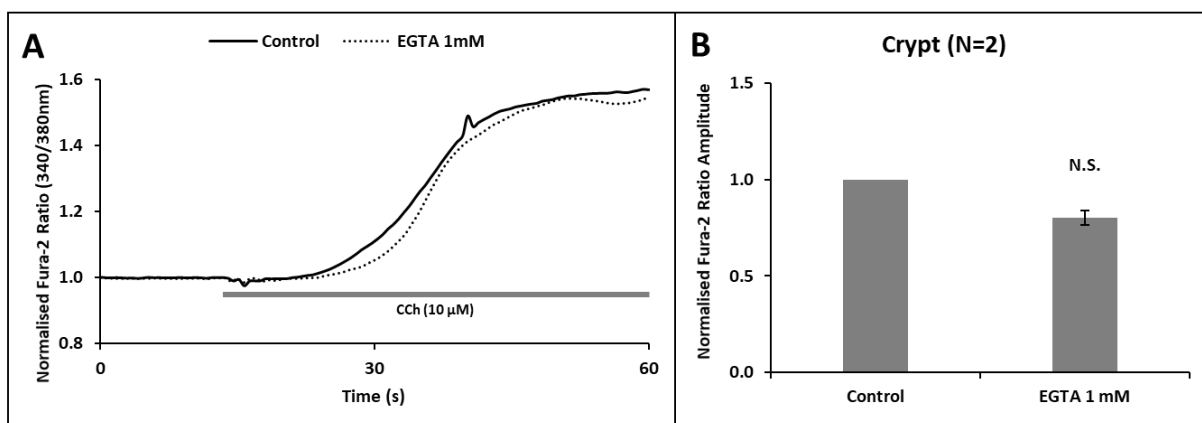
Figure 59 – CCh-induced Ca^{2+} Signals Originate from Intracellular Stores.

Example traces of crypts stimulated with CCh (10 µM) over time in the presence (control) or absence (EGTA 1 mM) of extracellular Ca^{2+} **(A)**. Bar chart summarising the normalized Fura-2 ratio amplitude comparing the CCh-induced Ca^{2+} signals with and without EGTA on crypts **(B)**. Data normalised to control and displayed as mean +/- SEM. Not significant (N.S). P>0.05 (*). N=2. For every "N", n≥3.
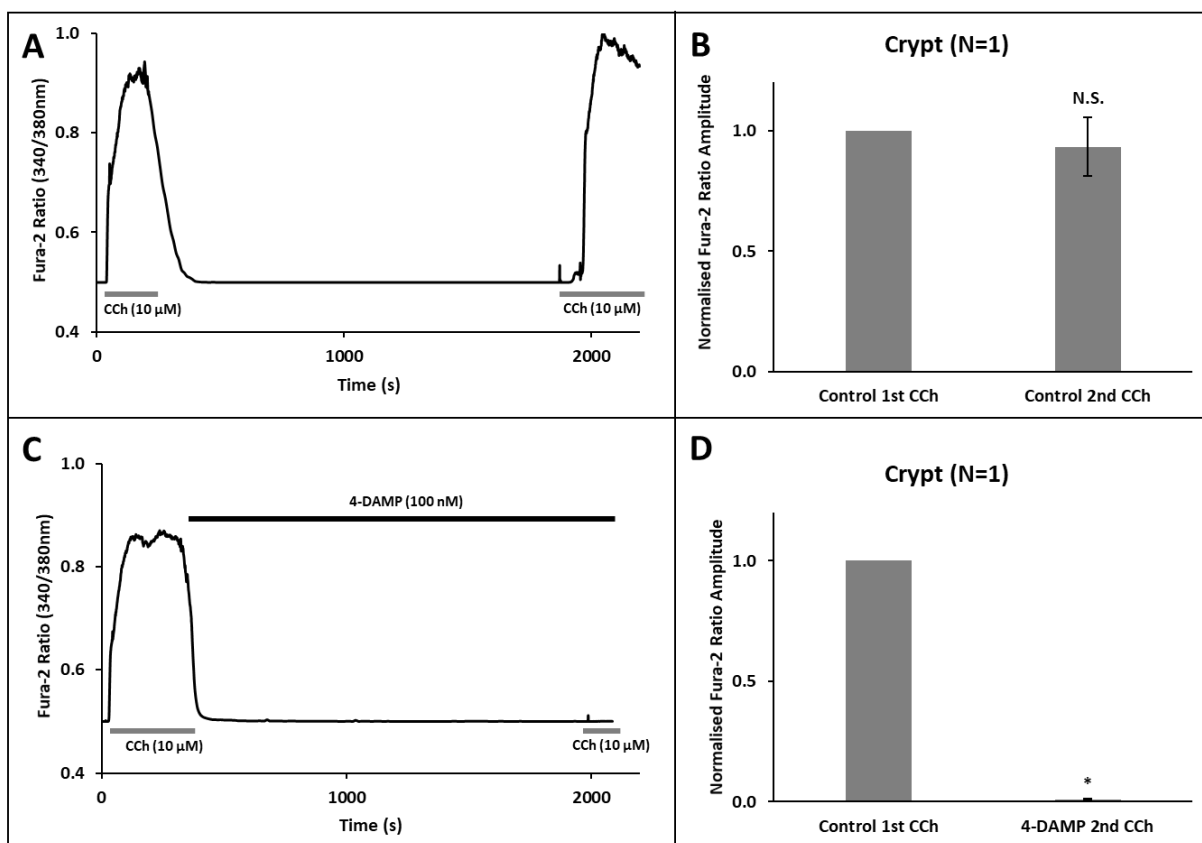
Figure 60 – Muscarinic Antagonist 4-DAMP Inhibits CCh-induced Ca^{2+} Signals.

Example traces of crypts stimulated with CCh (10 µM) once followed by another after 25 minutes rest, in the absence **(A)** or presence **(C)** of 4-DAMP (100 nM). Bar charts summarising the normalized Fura-2 ratio amplitude comparing the 1st and 2nd CCh stimulation in crypts, in the absence **(B)** or presence **(D)** of 4-DAMP. Data normalised to control and displayed as mean +/- SEM. Not significant (N.S). P>0.05 (*). N=1. For every "N", n≥3.

Next, the spatio-temporal characteristics of purinergic Ca^{2+} signalling was investigated on crypts. Initial experiments using ATP and UTP (Figure 61) determined both agonists were capable of causing Ca^{2+} signals. Since the Fura-2 ratio amplitude change induced by ATP (10 µM) and UTP (50 µM) were equivalent to CCh (10 µM), all subsequent experiments using those agonists were conducted using those concentrations. The ratiometric fluorescence imaging (340/380 nm) showed UTP causing an increase in fluorescence initiating higher up the crypt axis (Figure 62), which spreads to neighbouring cells before propagating down the crypt axis; all of which occurring within 1-3 minutes after the addition of UTP. The topology of UTP-induced Ca^{2+} signals were determined by drawing ROI at three positions along the crypt axis (Figure 63A). Fluorometric measurements of those ROIs confirmed the Ca^{2+} signal originating higher up crypt axis and spreading downwards over time (Figure 63B). Next, the polarity of UTP-induced Ca^{2+} signals were determined by drawing two pairs of ROIs at two positions along the crypt axis (Figure 63C). Fluorometric measurements of those ROIs showed the Ca^{2+} signal may originate from either the apical or basal pole (Figure 63D).
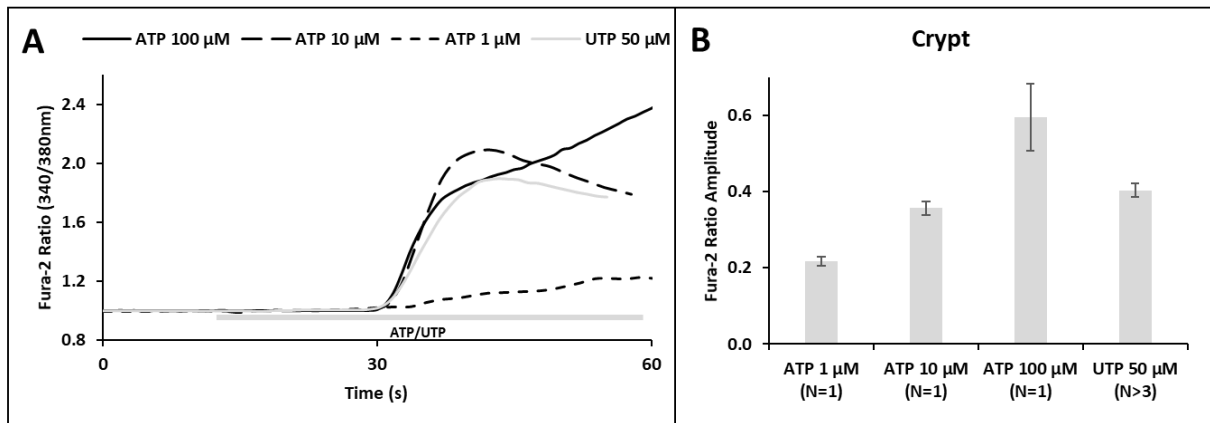
Figure 61 – Characterisation of Ca^{2+} Signals Induced by ATP/UTP.

Example normalized Fura-2 ratio traces in crypts stimulated by varying concentrations of ATP, as well as UTP, over time **(A)**. Bar chart summarising the normalized Fura-2 ratio amplitude comparing ATP/UTP-induced Ca^{2+} signals on crypts **(B)**. N≥1. For every "N", n≥3.
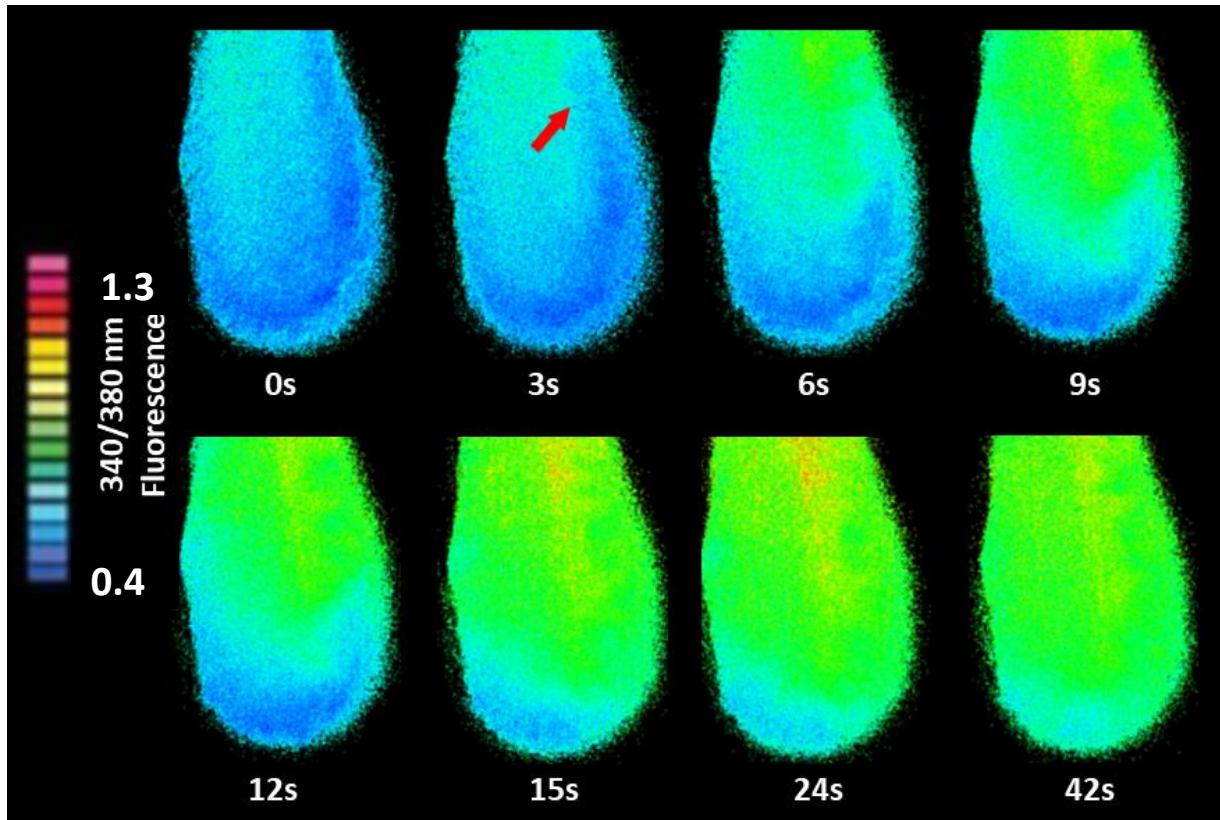
Figure 62 – UTP-induced Ca²⁺ Signals Originate Higher Up the Crypt Axis.

Representative series of epi-fluorescent live images of a crypt loaded with Fura-2 (5 µM) being stimulated with UTP (50 µM) over time in seconds (s). Increase in Fura-2 ratio (340/380 nm) fluorescence is visualized by a colour map ranging from blue (0.4) to green to red (1.3).
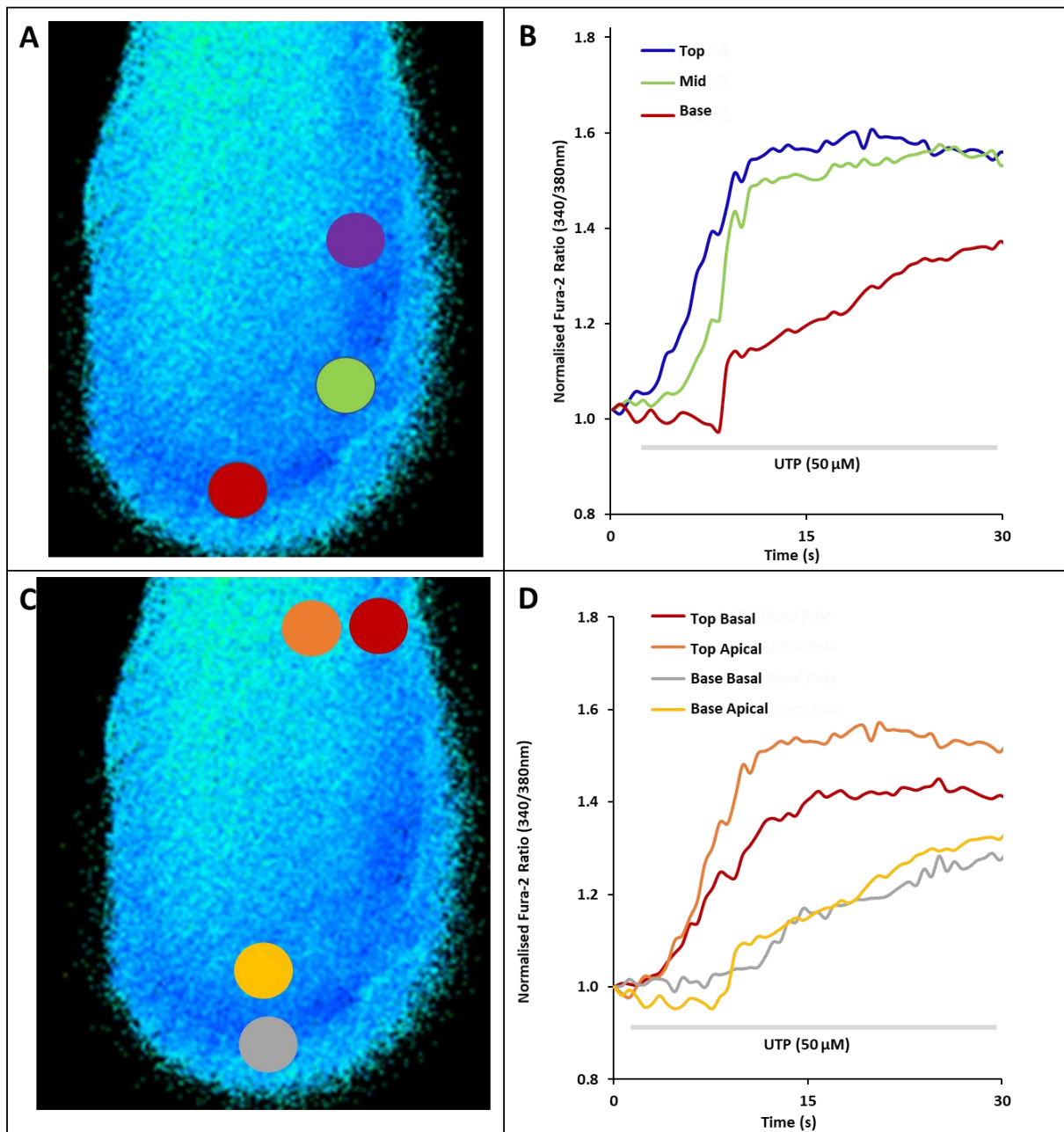
Figure 63 – Topology and Polarity of UTP-induced Ca^{2+} Signals.

Topology **(A-B)** and polarity **(C-D)** of Ca^{2+} signals induced by UTP (50 µM) over time. Left-side images depict crypts with drawn ROIs. Right-side line graphs represent the normalized Fura-2 ratio changes in each ROI.

Next, UTP was confirmed to induce release of stored organellar Ca^{2+} via P2Y2 receptors. UTP-induced Ca^{2+} signals were not significantly affected by the absence of extracellular Ca^{2+} (Figure 64) which was chelated by EGTA (1 mM), indicating intracellular organelles were the source of Ca^{2+} release. UTP was confirmed to induce Ca^{2+} release by via P2Y2 receptors (Figure 65) by designing an experiment using AR-C118925XX, which specifically inhibits P2Y2 receptors (Muoboghare, Drummond and Kennedy 2019). First, a control experiment was conducted (Figure 65A), whereby an initial UTP stimulation was followed by a secondary CCh stimulation with a 25-minute resting time between each. However, in the presence of AR-C118925XX (5 µM) the initial UTP stimulation was ablated (Figure 65B) while the secondary CCh stimulation produced a Ca^{2+} signal which was not statistically significant to the control. This was conducted in both crypts (Figure 65C) and organoids (Figure 65D), with similar trends observed in both. As an aside, P2Y2 receptors were shown to not be the only form of ATP-sensitive purinergic receptors present in colonic crypts (Figure 66), as the Ca^{2+} signals induced by ATP (10 µM) was not inhibited by AR-C118925XX (5 µM).
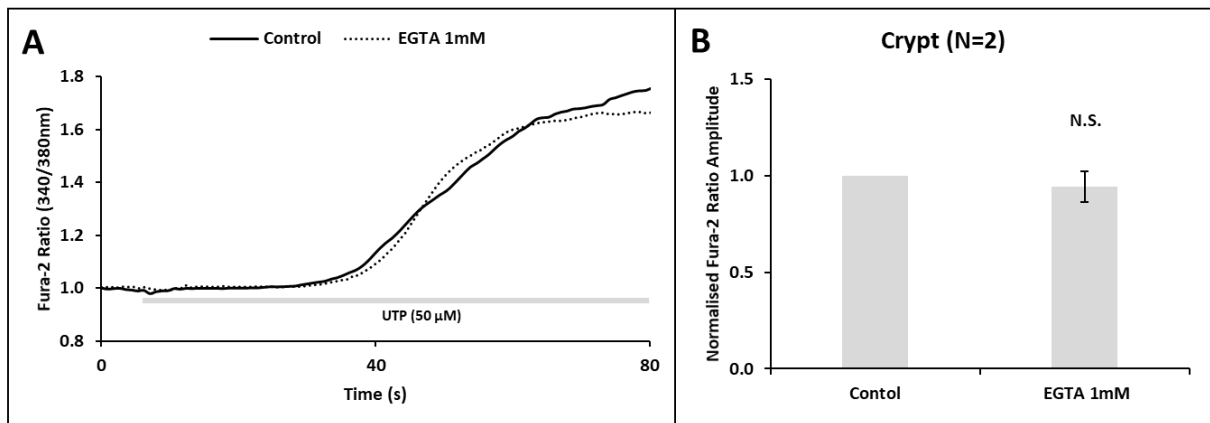
Figure 64 – UTP-induced Ca^{2+} Signals Originate from Intracellular Stores.

Example traces of crypts stimulated with UTP (50 µM) over time in the presence (control) or absence (EGTA 1 mM) of extracellular Ca^{2+} **(A)**. Bar chart summarising the normalized Fura-2 ratio amplitude comparing CCh-induced Ca^{2+} signals with and without EGTA performed on crypts **(B)**. Data normalised to control and displayed as mean +/- SEM. Not significant (N.S). N=2. For every "N", n≥3.
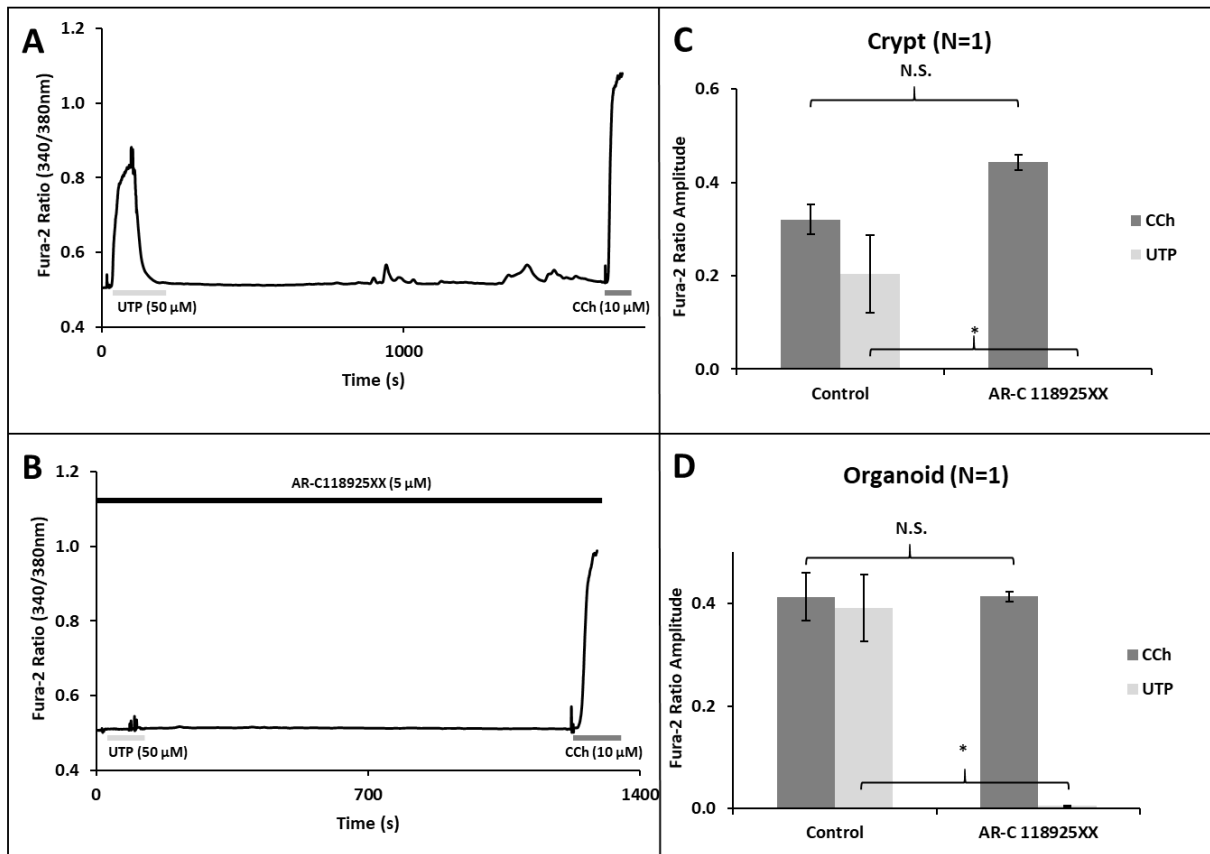
Figure 65 – P2Y2 Receptor Antagonist AR-C118925XX Inhibits UTP-induced Ca2+ Signals.

Example traces of crypts stimulated with UTP (50 µM) followed by CCh (10 µM) after 25 minutes rest, in the absence **(A)** or presence **(B)** of AR-C118925XX (5 µM). Bar charts summarising the normalized Fura-2 ratio amplitude comparing CCh and UTP-induced Ca^{2+} signals with and without AR-C118925XX in crypts **(C)** and organoids **(D)**. Not significant (N.S.). P>0.05 (*). N=1. For every "N", n≥3.
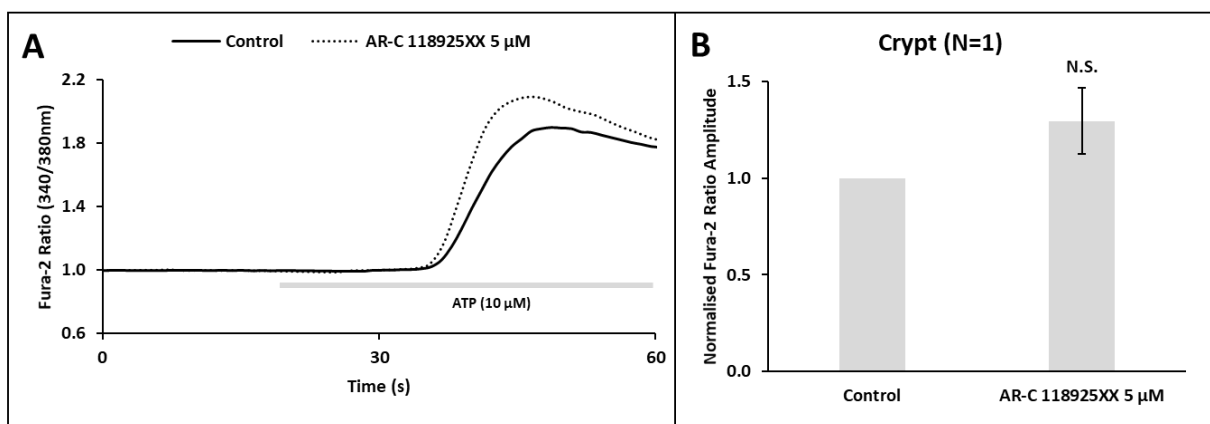
Figure 66 – Purinergic Antagonist AR-C118925XX Does Not Inhibit ATP-induced Ca2+ Signals.

Example traces of crypts stimulated with ATP (10 µM) over time in the absence (control) or presence of AR-C118925XX (5 µM) **(A)**. Bar chart summarising the normalized Fura-2 ratio amplitude comparing ATP-induced Ca^{2+} signals with and without AR-C118925XX performed on crypts **(B)**. Data normalised to control and displayed as mean +/- SEM. Not significant (N.S). N=1. For every "N", n≥3.

4.2.2 Effects of Intracellular Ca^{2+} Release Channel Antagonists on Muscarinergic and Purinergic Coupled Ca^{2+} Signals

Having confirmed the spatio-temporal characteristics of muscarinic and purinergic Ca^{2+} signals, their signalling pathway was investigated by targeting intracellular receptors (TPCs and IP3Rs) using pharmacological compounds. Besides those, the muscarinic and purinergic Ca^{2+} signal was evaluated against an array of non-specific pharmacological compounds which have been shown to affect Ca^{2+} signals in the literature.

Muscarinic and purinergic Ca^{2+} signals were first evaluated in the presence of TPC-inhibiting pharmacological compounds. The first TPC-inhibiting pharmacological compound used was *trans* Ned-19, which binds to TPCs to inhibit binding of NAADP to TPCs as well as inhibit NAADP-mediated Ca^{2+} release (Rosen, et al. 2009) and (Ruas, Rietdorf, et al. 2010). In crypts and organoids, high concentrations of Ned-19 (500 µM) were found to significantly inhibit CCh (Figure 67A-C) but not UTP (Figure 67D-F), while lower concentrations of Ned-19 (125 & 250 µM) increased the sensitivity of crypts and organoids to CCh and UTP. Another TPC-inhibiting pharmacological compound used was tetrandrine, a plant alkaloid used in traditional medicine, which was first shown to inhibit TPCs and thereby disrupt endosomal vesicle trafficking to impact the micropinocytosis of Ebolavirus (Sakurai, et al., 2016) and (Patel and Kilpatrick 2018). Similar to Ned-19, tetrandrine (20 µM) significantly inhibited CCh (Figure 68A-C) but not UTP (Figure 68D-F) in both crypts and organoids.

Next, muscarinic and purinergic Ca^{2+} signals were evaluated in the presence of IP3R-inhibiting pharmacological compounds. The first IP3R-inhibiting pharmacological compound used was 2-APB, which has a long history of being used as a membrane-permeable blocker of IP3Rs (Missiaen, et al. 2001). In crypts and organoids, 2-APB (50 µM) was consistently found to not inhibit CCh-induced Ca^{2+} signals (Figure 69A-C) but significantly inhibited UTP-induced Ca^{2+} signals (Figure 69D-F), while higher concentrations of 2-APB (100 µM) were capable of significantly reducing CCh-induced Ca^{2+} release in organoids (Figure 69C). Another IP3R-inhibiting pharmacological compound used was xestospongin-C, which also has a long history of being used as a blocker of IP3Rs (Oka, et al. 2004), although studies have also shown it being non-specific towards IP3Rs and instead inhibit Ca^{2+}-ATPase of the sarcoendoplasmic reticulum (Solovyova, et al. 2002). Interestingly, neither CCh nor UTP was affected by xestospongin-C (4 µM) in either crypts or organoids (Figure 70). Another IP3R antagonist used in this thesis is caffeine, which was first proposed to inhibit IP3Rs close to thirty years ago (Ehrlich, et al. 1994) and (Sei, Gallagher and Daly 2001). In this case, caffeine (10 mM) significantly inhibited CCh-induced Ca^{2+} signals (Figure 71A-C) in crypts and organoids, but did not inhibit UTP-induced Ca^{2+} signals in crypts (Figure 71D-E).
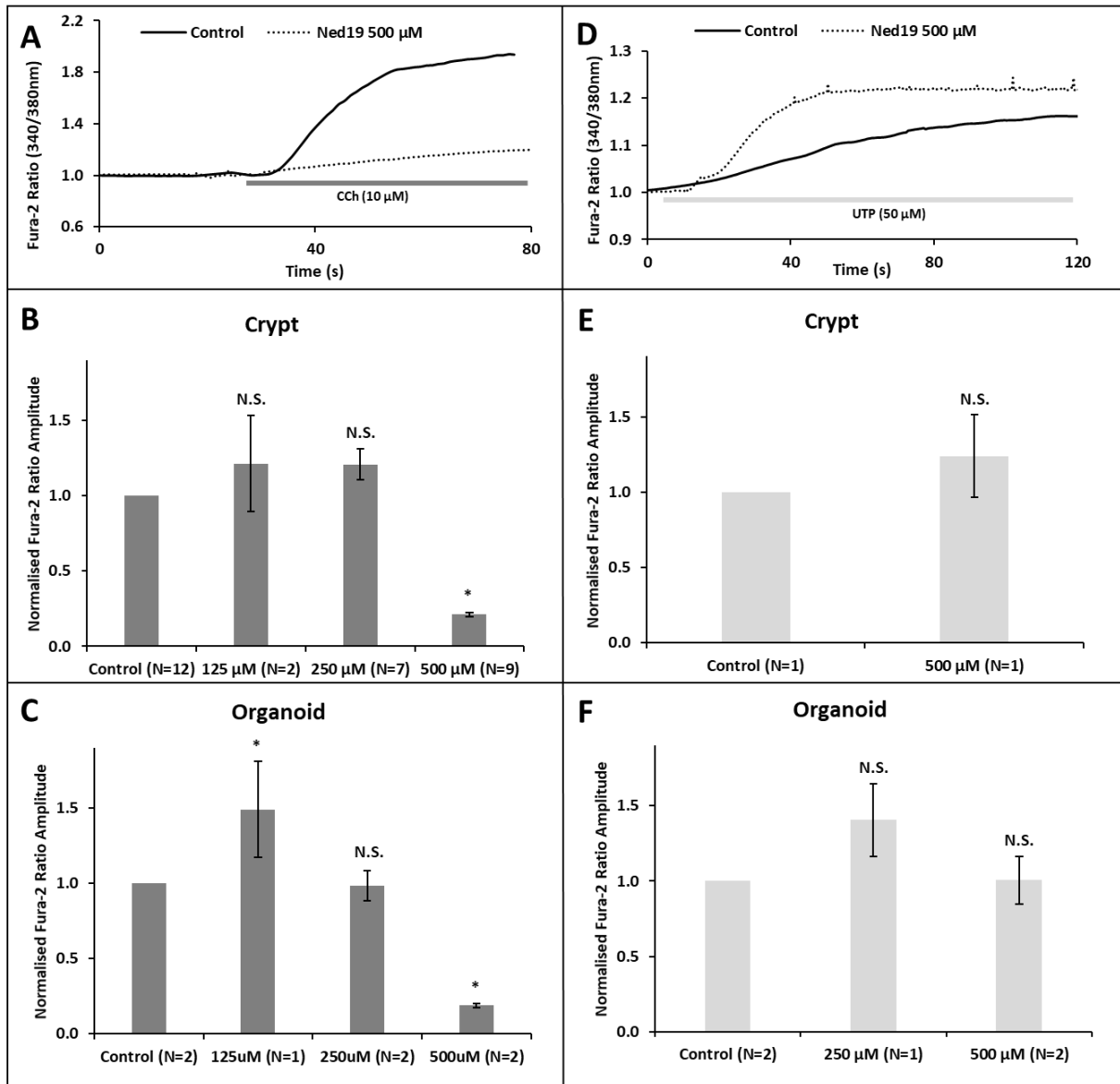
Figure 67 – High Concentrations of Ned-19 Inhibits CCh but not UTP-induced Ca^{2+} Signals.

Example traces of crypts stimulated with CCh **(A)** or UTP **(D)**, in the presence or absence of Ned-19 (500 μM). Bar charts summarising the normalized Fura-2 ratio amplitude comparing CCh-induced Ca^{2+} signals with various concentrations of Ned-19 in crypts **(B)** and organoids **(C)** against control, as well as comparing UTP-induced Ca^{2+} signals with various concentrations of Ned-19 in crypts **(E)** and organoids **(F)** against control. Data normalised to control and displayed as mean +/- SEM. Not significant (N.S). P>0.05 (*). N≥1. For every "N", n≥3.
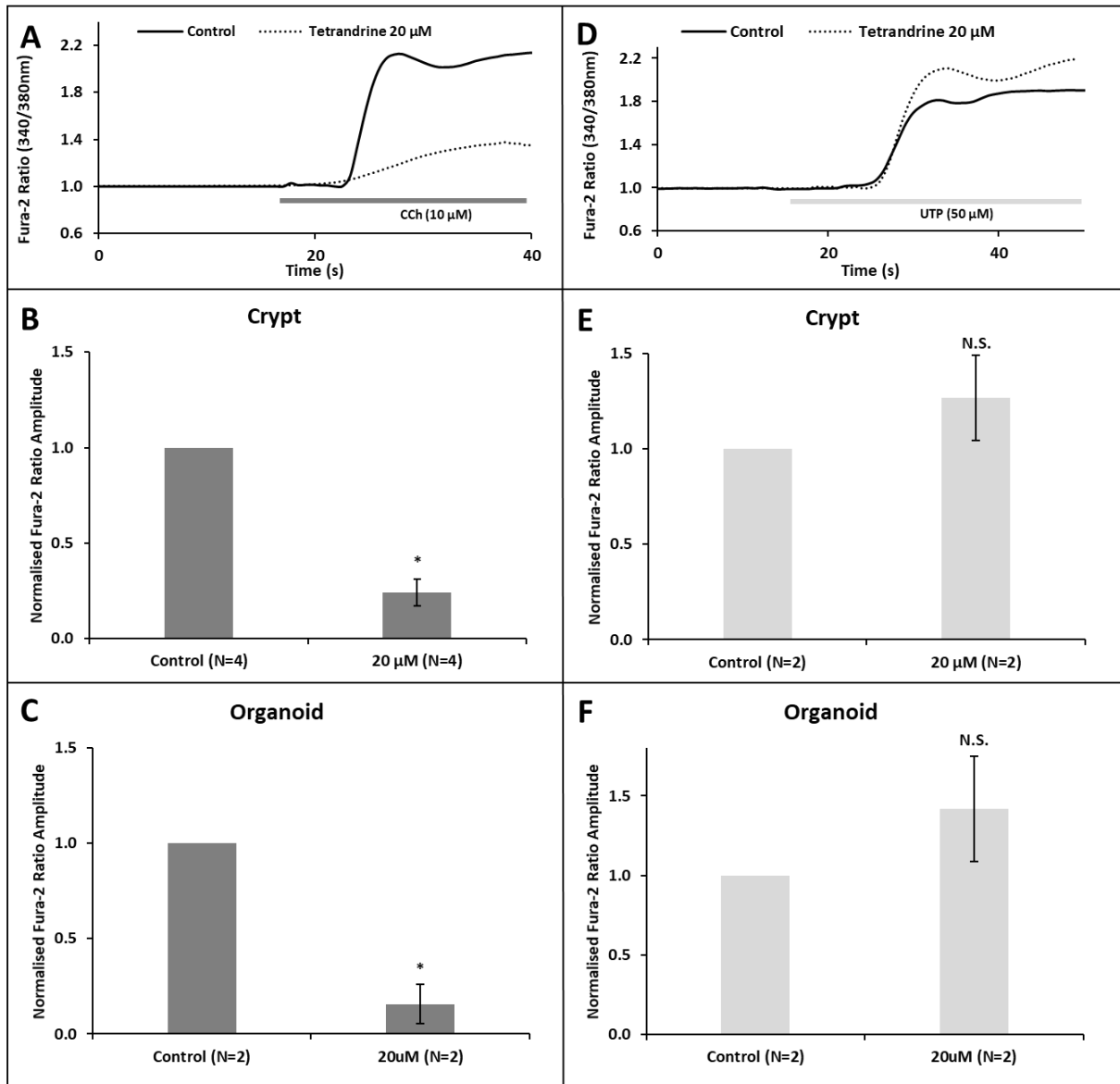
Figure 68 – Tetrandrine Inhibits CCh but not UTP-induced Ca^{2+} Signals.

Example traces of crypts stimulated with CCh **(A)** or UTP **(D)**, in the presence or absence of tetrandrine (20 µM). Bar charts summarising the normalized Fura-2 ratio amplitude comparing CCh-induced Ca^{2+} signals with and without tetrandrine in crypts **(B)** and organoids **(C)**, as well as comparing UTP-induced Ca^{2+} signals with and without tetrandrine in crypts **(E)** and organoids **(F)**. Data normalised to control and displayed as mean +/- SEM. Not significant (N.S). P>0.05 (*). N≥2. For every "N", n≥3.
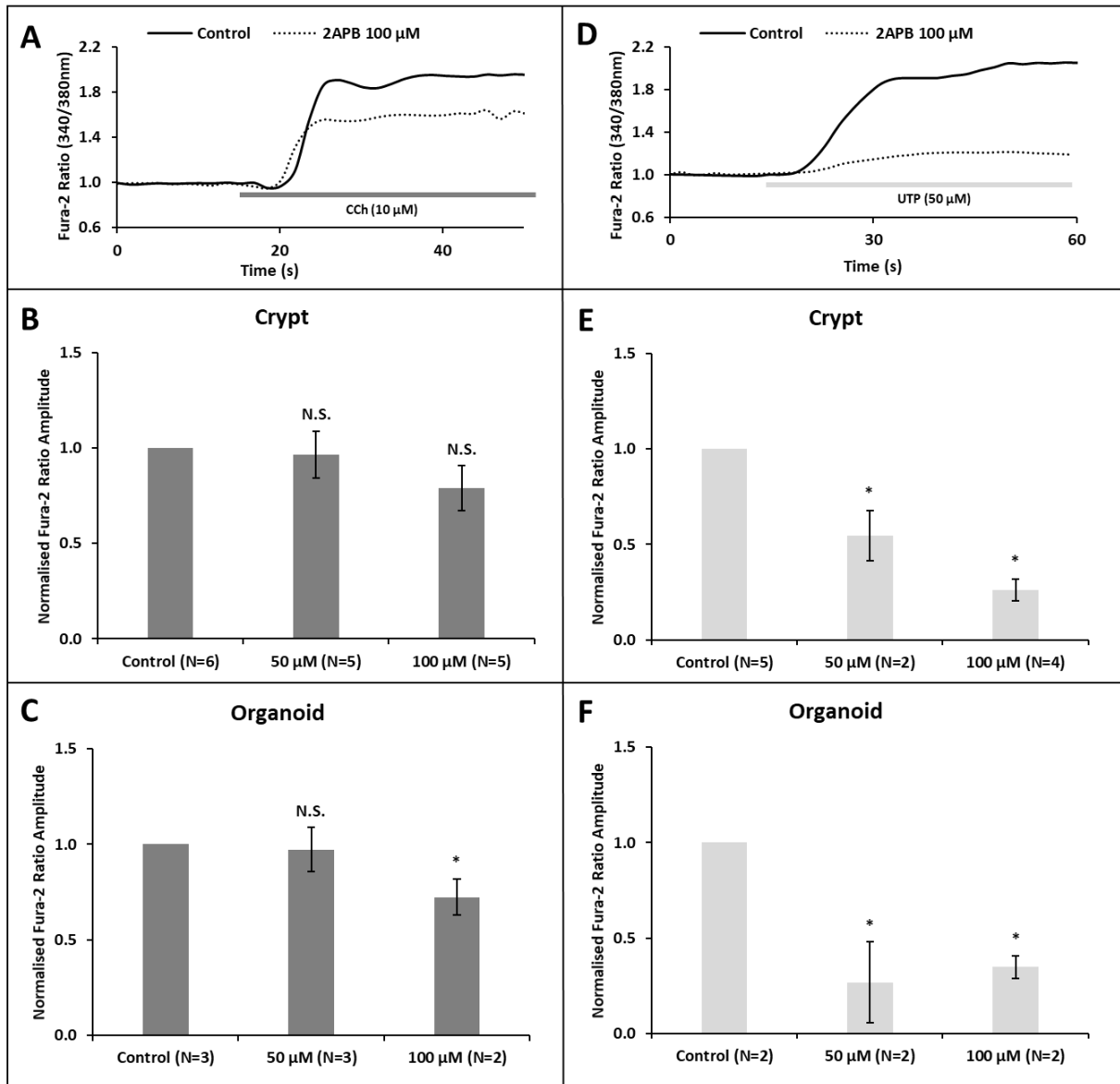
Figure 69 – 2-APB Inhibits UTP but not CCh-induced Ca^{2+} Signals.

Example traces of crypts stimulated with CCh **(A)** or UTP **(D)**, in the presence or absence of 2-APB (100 µM). Bar charts summarising the normalized Fura-2 ratio amplitude comparing CCh-induced Ca^{2+} signals with various concentrations of 2-APB in crypts **(B)** and organoids **(C)** against control, as well as comparing UTP-induced Ca^{2+} signals with various concentrations of 2-APB in crypts **(E)** and organoids **(F)** against control. Data normalised to control and displayed as mean +/- SEM. Not significant (N.S). P>0.05 (*). N≥2. For every "N", n≥3.
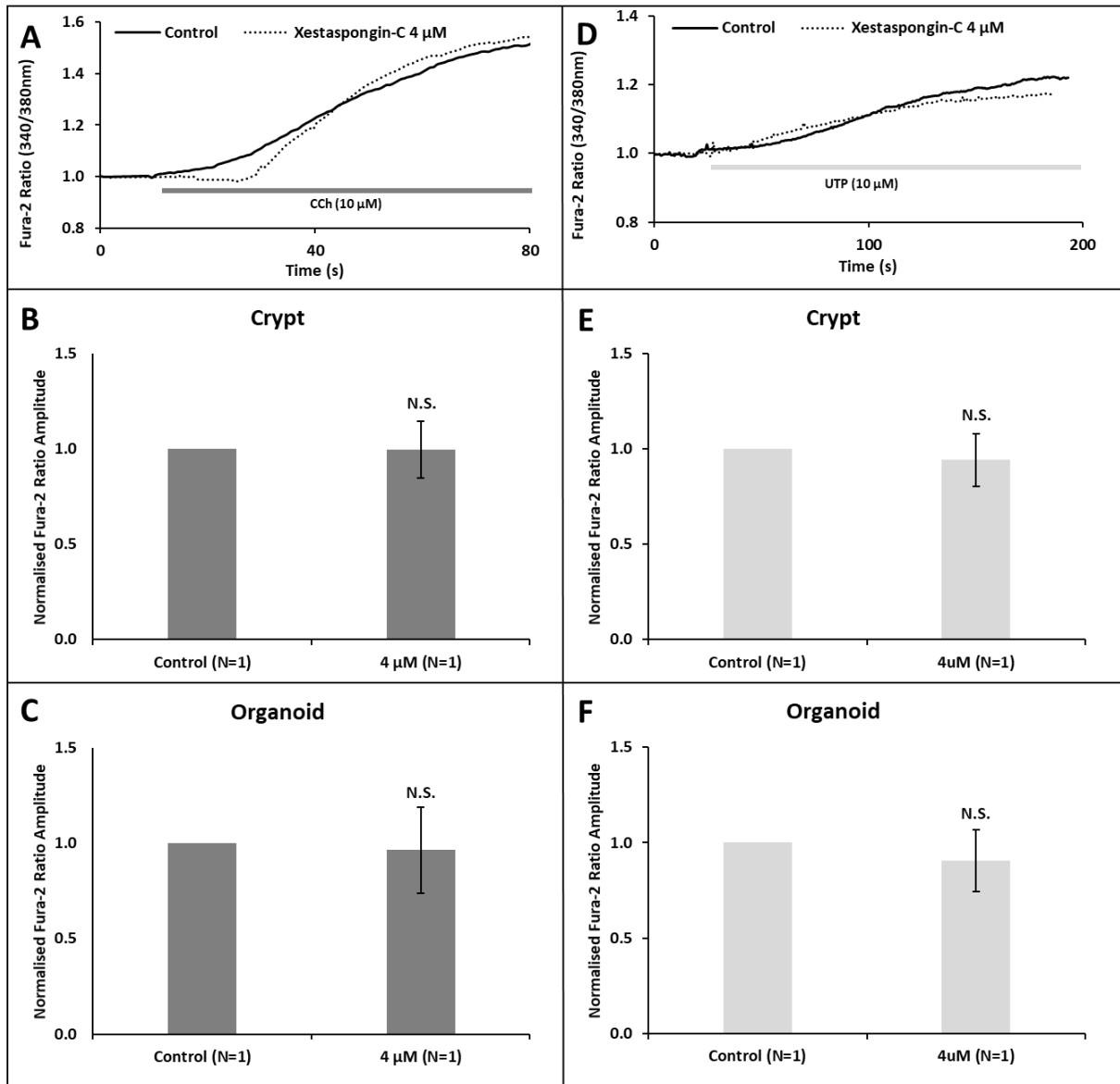
Figure 70 – Xestospongin-C Inhibits Neither UTP nor CCh-induced Ca²⁺ Signals.

Example traces of crypts stimulated with CCh **(A)** or UTP **(D)**, in the presence or absence of Xestospongin-C (4 μM). Bar charts summarising the normalized Fura-2 ratio amplitude comparing CCh-induced Ca²⁺ signals with and without Xestospongin-C in crypts **(B)** and organoids **(C)**, as well as comparing UTP-induced Ca²⁺ signals with and without Xestospongin-C in crypts **(E)** and organoids **(F)**. Data normalised to control and displayed as mean +/- SEM. Not significant (N.S). P>0.05 (*). N=1. For every "N", n≥3.
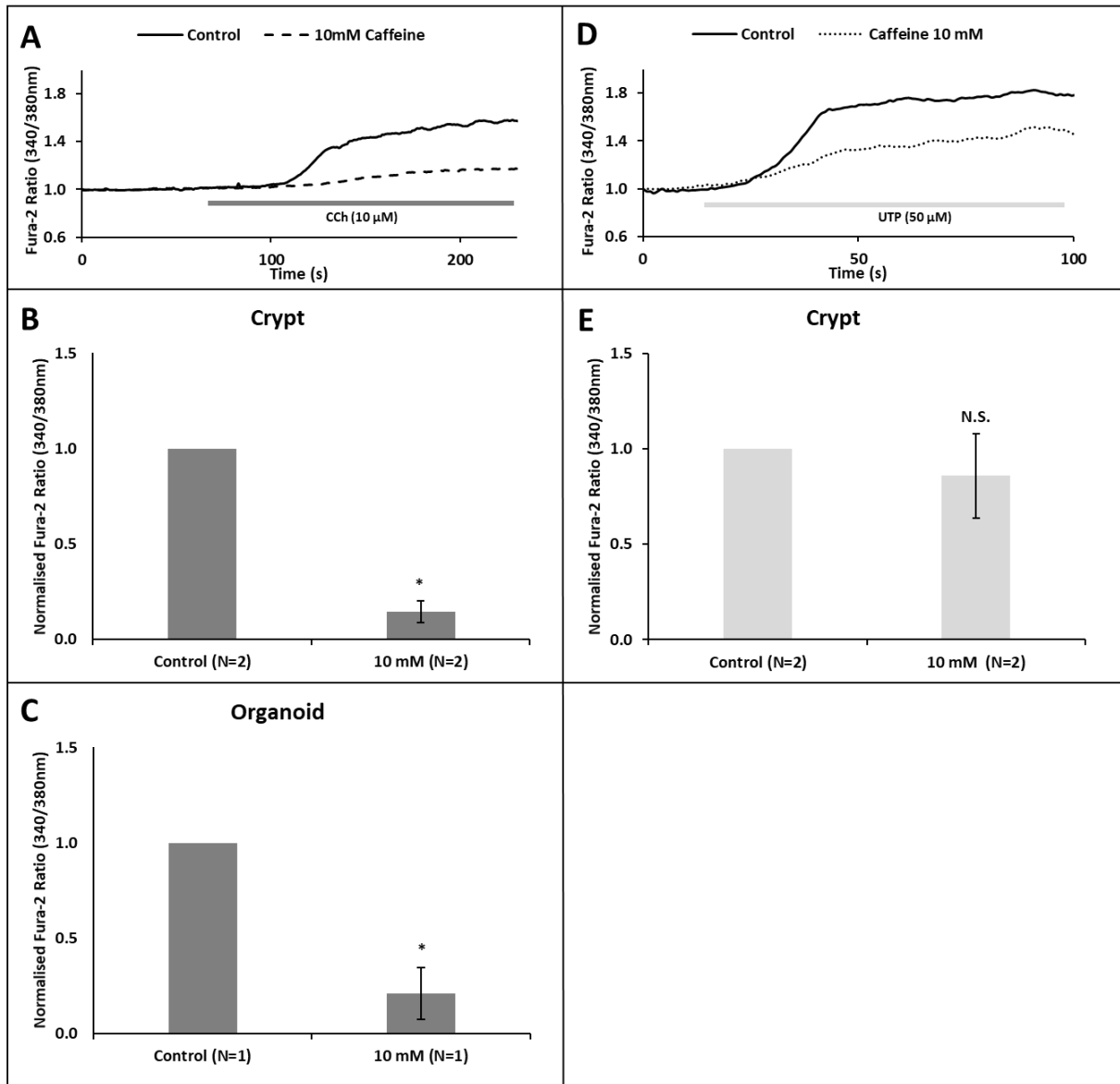
Figure 71 – Caffeine Inhibits CCh but not UTP-induced Ca²⁺ Signals.

Example traces of crypts stimulated with CCh **(A)** or UTP **(D)**, in the presence or absence of caffeine (10 mM). Bar charts summarising the normalized Fura-2 ratio amplitude comparing CCh-induced Ca^{2+} signals with and without caffeine in crypts **(B)** and organoids **(C)**, as well as comparing UTP-induced Ca^{2+} signals with and without caffeine in crypts **(E)**. Data normalised to control and displayed as mean +/- SEM. Not significant (N.S). P>0.05 (*). N≥1. For every "N", n≥3.

Bafilomycin A1 has been shown to inhibit lysosomal H^+-ATPase (Steen, Kirchberger and Guse 2007), including V-ATPases which resulted in disrupted acidification in lysosomes (Mauvezin and Neufeld 2015). As described earlier (Chapter 1.4.1), acidic stores such as endolysosomes rely on the proton gradient developed by V-ATPases to maintain their organellar $[Ca^{2+}]$. Incubation of organoids with bafilomycin A1 (2.5 µM) resulted in significantly diminished CCh-induced Ca^{2+} signals compared control (Figure 72A-B), while the UTP-induced Ca^{2+} signals remained unaffected.

Another pharmacological compound which was evaluated in this thesis was carbenoxolone. Carbenoxolone had been shown to inhibit gap junctions (Manjarrez-Marmolejo and Franco-Pérez 2016) as well as voltage-gated Ca^{2+} channels (Vessey, et al. 2004) which, alongside TRP Channels, Piezo, P2X Receptors, are responsible for influx of Ca^{2+} across the plasma membrane and lysosomal membranes (Chapter 1.4.1). Intriguingly, both CCh (Figure 73A-B) and UTP (Figure 73C-D) induced Ca^{2+} signals were increasingly reduced in crypts and organoids correlating with increasing dosage of carbenoxolone.
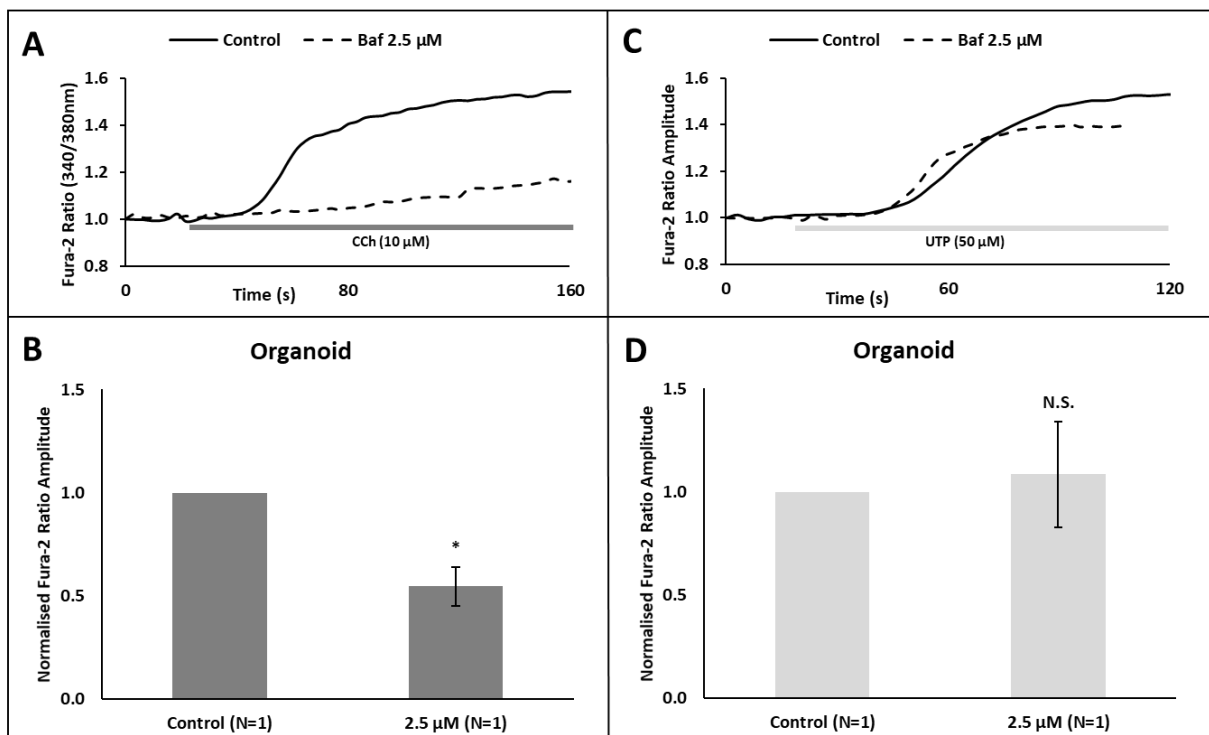
Figure 72 – Bafilomycin A1 Inhibits CCh-induced Ca^{2+} Signals.

Example traces of organoids stimulated with CCh **(A)** or UTP **(C)**, in the presence or absence of bafilomycin A1 (2.5 µM). Bar charts summarising the normalized Fura-2 ratio amplitude comparing CCh **(B)** and UTP **(D)** -induced Ca^{2+} signals with and without bafilomycin A1 in organoids. Data normalised to control and displayed as mean +/- SEM. Not significant (N.S). P>0.05 (*). N=1. For every "N", n≥3.
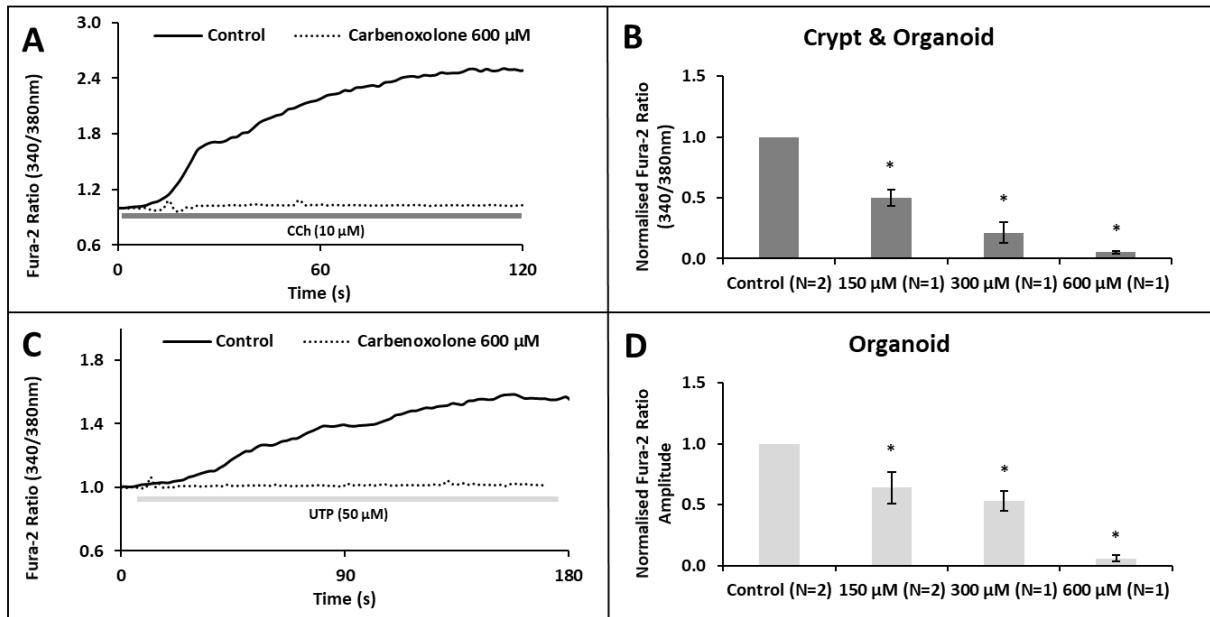
Figure 73 – Dose Inhibition of Carbenoxolone on CCh-induced Ca^{2+} Signals.

Example traces of crypts stimulated with CCh **(A)** and UTP **(C)** in the presence or absence of carbenoxolone (600 µM). Bar charts summarising the normalized Fura-2 ratio amplitude comparing CCh **(B)** and UTP **(D)** induced Ca^{2+} signals against increasing concentrations of carbenoxolone in crypts/organoids. Data normalised to control and displayed as mean +/- SEM. P>0.05 (*). N≥1. For every "N", n≥3.

In addition to carbenoxolone, muscarinic and purinergic Ca^{2+} signals were evaluated using nifedipine, verapamil and diltiazem, three 'slow channel blocking agents' (Henry 1980). Nifedipine is regarded as a blocker of L-type Ca^{2+} channels and other VGCCs (Curtis and Scholfield 2001), which have been shown to reduce caecum contractions induced by acetylcholine but not CCh (Mitchelson and Ziegler 1984), and also inhibit UTP-induced emptying of intracellular Ca^{2+} stores (Krutetskaia, et al. 1997). Indeed, in this thesis, crypts which were incubated with nifedipine (50 µM) did not result in diminished CCh-induced Ca^{2+} signals (Figure 74). Due to lack of time, UTP-induced Ca^{2+} signals were not evaluated in the presence of nifedipine. Verapamil is another blocker of L-type Ca^{2+} channel (Davis and Bauer 2012) which has been shown to inhibit the contraction of pulmonary tissues in-vitro induced by CCh (Deal, Cherniack and Eberlin 1984) and also inhibited UTP-induced emptying of intracellular Ca^{2+} stores (Krutetskaia, et al. 1997). Verapamil is also capable of inhibiting TPCs (He, et al. 2020). In this thesis, verapamil (50 µM) significantly inhibited CCh-induced Ca^{2+} signals in crypts and organoids (Figure 75A-C), while the UTP-induced Ca^{2+} signals were unaffected in crypts and organoids (Figure 75D-F). Diltiazem is yet another L-type Ca^{2+} channel antagonist (Chen, et al. 2013) which reduces airway reactivity to CCh in asthmatic subjects (Hartmann and Magnussen 1985) and also inhibits UTP-induced vasoconstriction in canine coronary artery (Matsumoto, Nakane and Chiba 1997). It has also been reported to inhibit TPCs (He, et al. 2020). Diltiazem (250 and 500 µM) consistently and significantly inhibited CCh-induced Ca^{2+} signals in crypts and organoids (Figure 76A-C), while the UTP-induced Ca^{2+} signals were unaffected in crypts and organoids (Figure 76D-F).
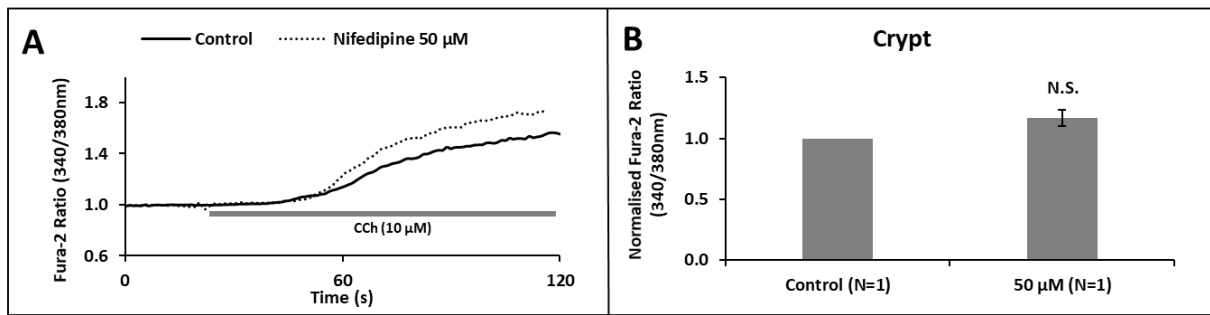
Figure 74 – Nifedipine Does not Inhibit CCh-induced Ca^{2+} Signals.

Example traces of crypts stimulated with CCh **(A)** in the presence or absence of nifedipine (50 µM). Bar charts summarising the normalized Fura-2 ratio amplitude comparing CCh-induced Ca^{2+} signals in the presence or absence nifedipine in crypts **(B)**. Data normalised to control and displayed as mean +/- SEM. Not significant (N.S). N=1. For every "N", n≥3.
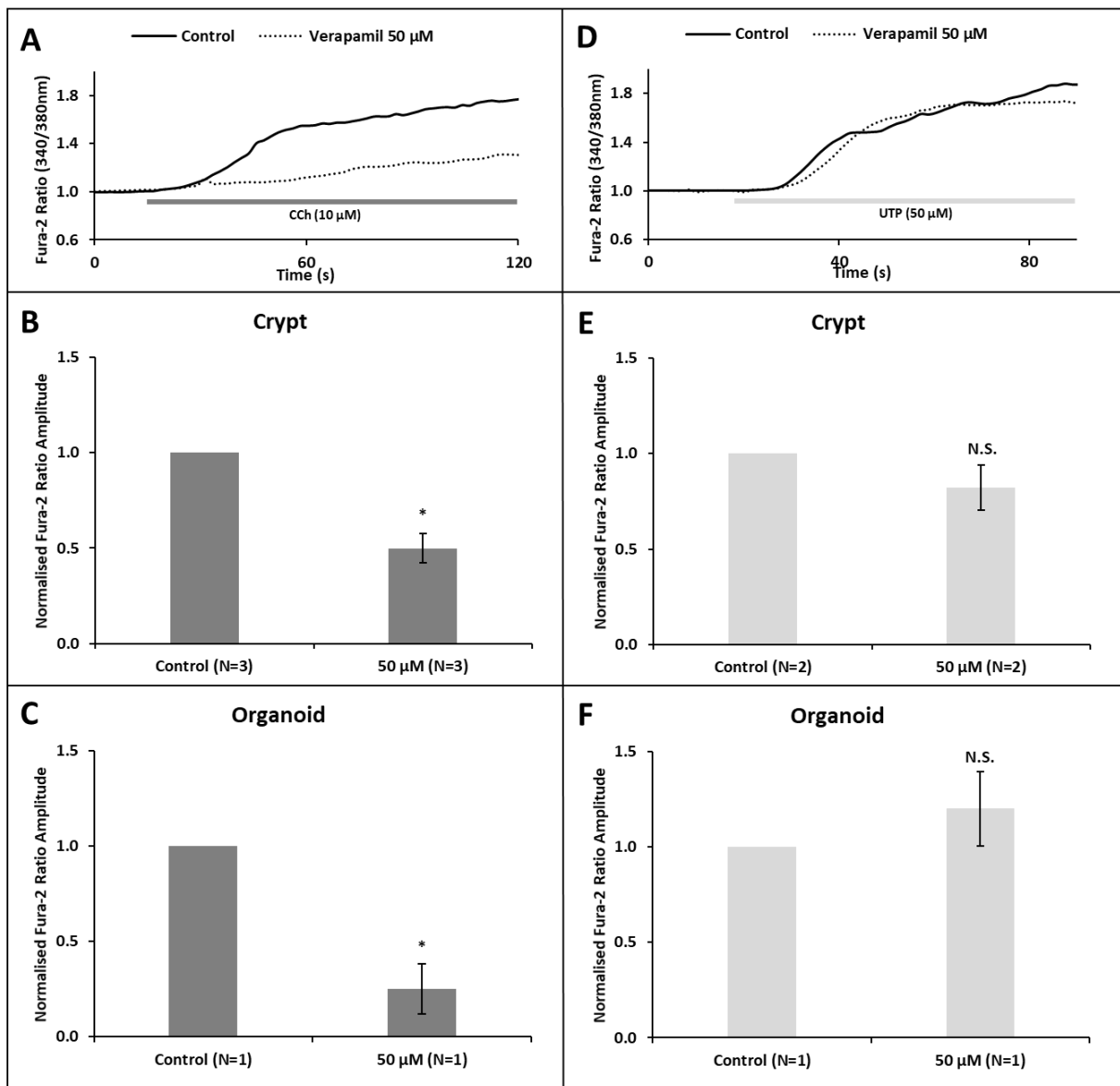
Figure 75 – Verapamil Inhibits CCh but not UTP-induced Ca²⁺ Signals.

Example traces of crypts stimulated with CCh **(A)** or UTP **(D)**, in the presence or absence of verapamil (50 µM). Bar charts summarising the normalized Fura-2 ratio amplitude comparing CCh-induced Ca²⁺ signals with various concentrations of verapamil in crypts **(B)** and organoids **(C)** against control, as well as comparing UTP-induced Ca²⁺ signals with various concentrations of verapamil in crypts **(E)** and organoids **(F)** against control. Data normalised to control and displayed as mean +/- SEM. Not significant (N.S). P>0.05 (*). N≥1. For every "N", n≥3.
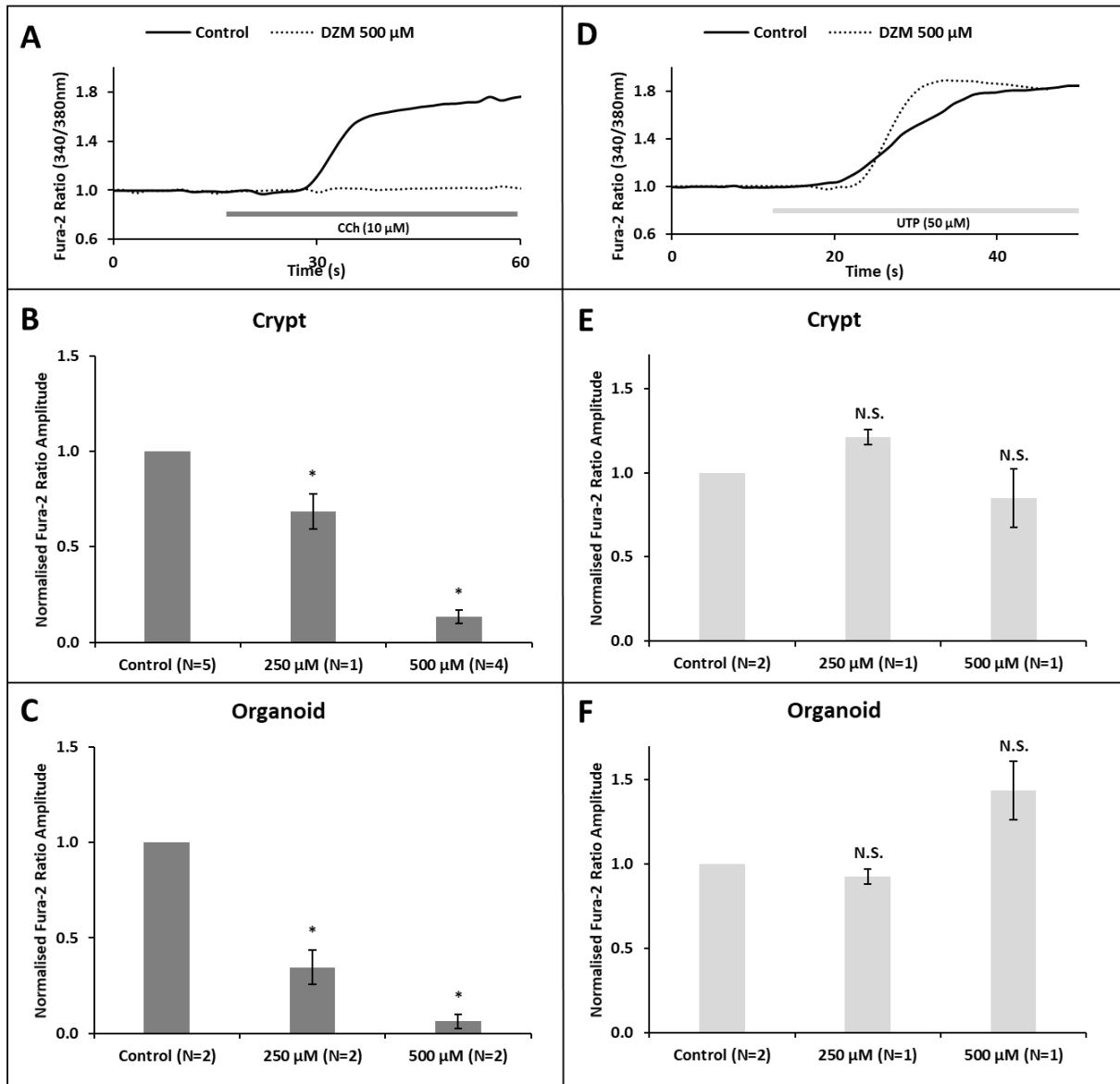
Figure 76 – Diltiazem Inhibits CCh but not UTP-induced Ca²⁺ Signals.

Example traces of crypts stimulated with CCh **(A)** or UTP **(D)**, in the presence or absence of diltiazem (500 µM). Bar charts summarising the normalized Fura-2 ratio amplitude comparing CCh-induced Ca²⁺ signals with various concentrations of diltiazem in crypts **(B)** and organoids **(C)** against control, as well as comparing UTP-induced Ca²⁺ signals with various concentrations of diltiazem in crypts **(E)** and organoids **(F)** against control. Data normalised to control and displayed as mean +/- SEM. Not significant (N.S). P>0.05 (*). N≥1. For every "N", n≥3.

Muscarinic and purinergic Ca^{2+} signals were next evaluated against three other non-specific Ca^{2+} antagonists – TMB8, procaine, and chloroquine. Unlike the previous antagonists, TMB8 is a nonspecific Ca^{2+} antagonist which have been shown to antagonize IP3Rs in plants (Poutrain, et al. 2009), as well as nicotinic (Bencherif, et al. 1995) and muscarinic receptors (Leipziger, et al. 1996). In this thesis, TMB8 (50 and 100 μM) abolished CCh-induced Ca^{2+} signals in crypts and organoids (Figure 77A-C), while sometimes increasing the sensitivity of the UTP-induced Ca^{2+} signals in crypts and organoids (Figure 77D-F).

Procaine is used a local dental anaesthetic and vasodilator; it is a non-specific antagonist whose targets includes muscarinic and nicotinic acetylcholine receptors (Drugbank 2005). Procaine has been shown to inhibit CCh-induced neurotransmitter secretion (Charlesworth, et al. 1992) and also been proposed to inhibit ryanodine receptors (Zahradníková and Palade 1993). Intriguingly, low concentrations of procaine (1 mM) was capable of significantly inhibiting CCh-induced Ca2+ signals in crypts and organoids (Figure 78A-C) but not UTP-induced Ca2+ signals in crypts and organoids (Figure 78D-F), however UTP-induced Ca^{2+} signals was inhibited by high concentrations of procaine (10 mM).

Chloroquine is an outdated medication for malaria since the 1940s; chloroquine and its derivative – hydroxychloroquine – are currently used to treat rheumatoid arthritis, lupus and HIV (Drugbank 2005). It has recently been touted as a 'cure' for SARS-COV-2 despite the lack of definitive studies proving its efficacy in preventing SARS-COV-2 infection or improving recovery (The BMJ 2020). It has a high affinity for the intracellular space of lysosomes (Derendorf 2020), resulting in increased pH within the intracellular vacuoles (Fox 1993). A recent review described chloroquine as a lysosomotropic agent (Tian, et al. 2021), meaning it penetrates cells/lysosomes due to its lipophilic nature, and are weak bases meaning they are protonated at low pH and become trapped in lysosomes. This gradually destabilises the lysosomal membranes and loss of lysosomal acidification, and eventually block lysosomal function. Chloroquine has also been proposed to inhibit Ca^{2+} signals by inhibiting IP3Rs, TRPs and/or STIM/Orai channels (Wu, et al. 2017), and also blocks ATP-sensitive potassium channels (Ponce-Balbuena, et al. 2012). In this thesis, chloroquine (10-50 μM) caused a significant reduction of Ca^{2+} signals induced by CCh (Figure 79A-B) and UTP (Figure 79C-D) in organoids; CCh was more susceptible than UTP towards lower concentrations (10 and 25 μM) of chloroquine.
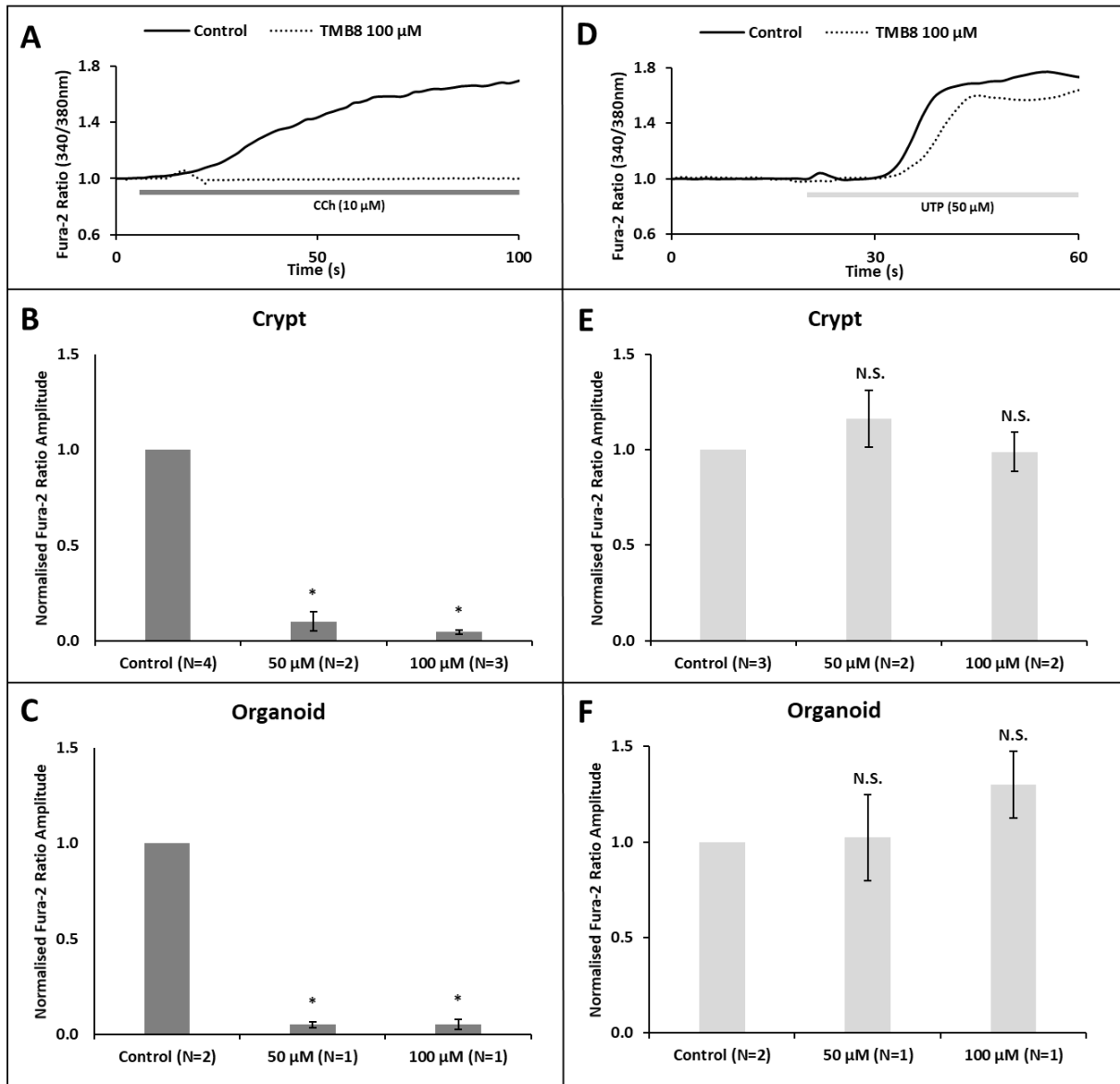
Figure 77 – TMB8 Inhibits CCh but not UTP-induced Ca²⁺ Signals.

Example traces of crypts stimulated with CCh **(A)** or UTP **(D)**, in the presence or absence of TMB8 (100 µM). Bar charts summarising the normalized Fura-2 ratio amplitude comparing CCh-induced Ca²⁺ signals with various concentrations of TMB8 in crypts **(B)** and organoids **(C)** against control, as well as comparing UTP-induced Ca²⁺ signals with various concentrations of TMB8 in crypts **(E)** and organoids **(F)** against control. Data normalised to control and displayed as mean +/- SEM. Not significant (N.S). P>0.05 (*). N≥1. For every "N", n≥3.
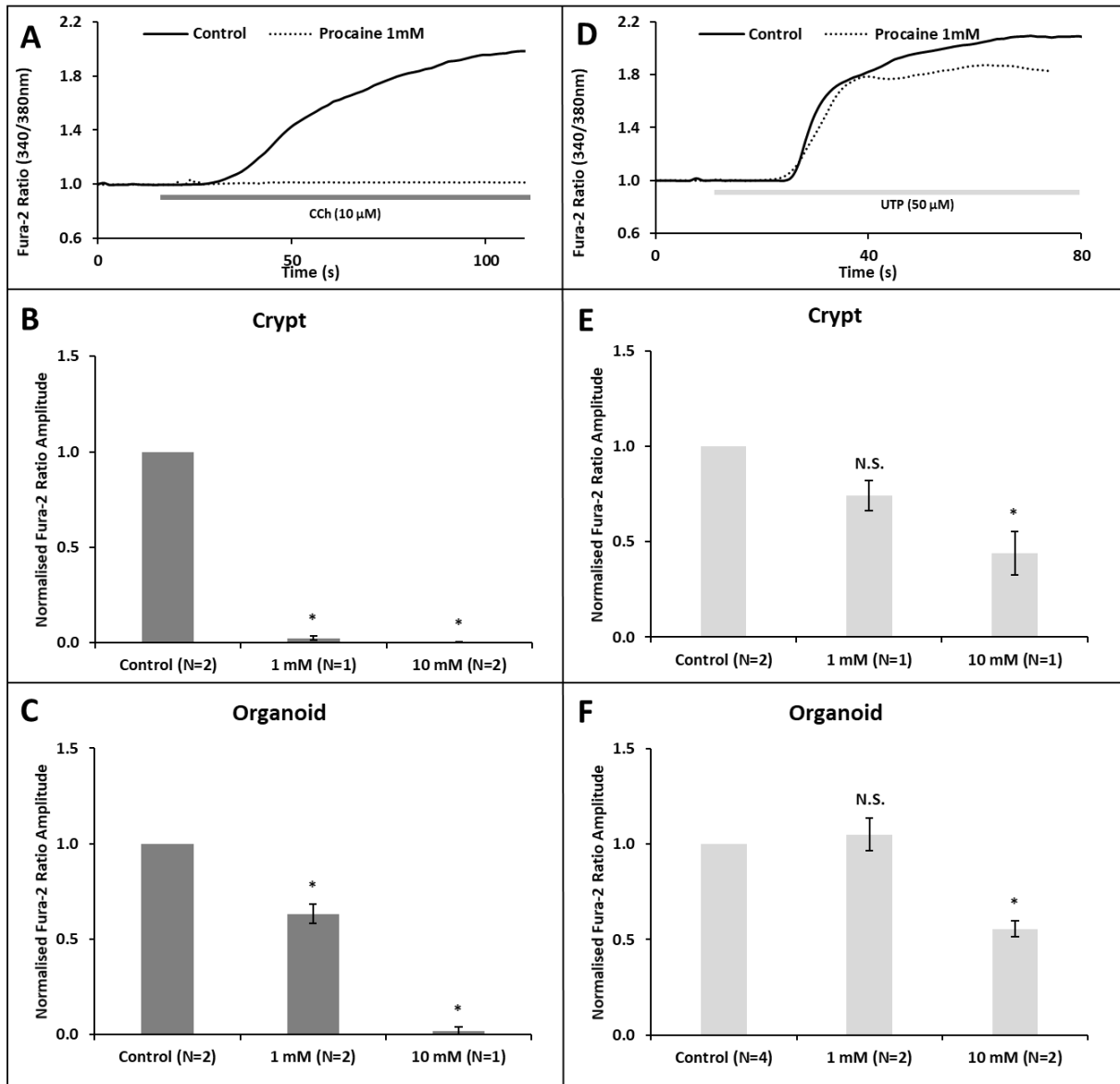
Figure 78 – Procaine Inhibits both CCh and UTP-induced Ca²⁺ Signals.

Example traces of crypts stimulated with CCh **(A)** or UTP **(D)**, in the presence or absence of low procaine dosage (1 mM). Bar charts summarising the normalized Fura-2 ratio amplitude comparing CCh-induced Ca²⁺ signals with various concentrations of procaine in crypts **(B)** and organoids **(C)** against control, as well as comparing UTP-induced Ca²⁺ signals with various concentrations of procaine in crypts **(E)** and organoids **(F)** against control. Data normalised to control and displayed as mean +/- SEM. Not significant (N.S). $P > 0.05$ (*). N≥1. For every "N", n≥3.
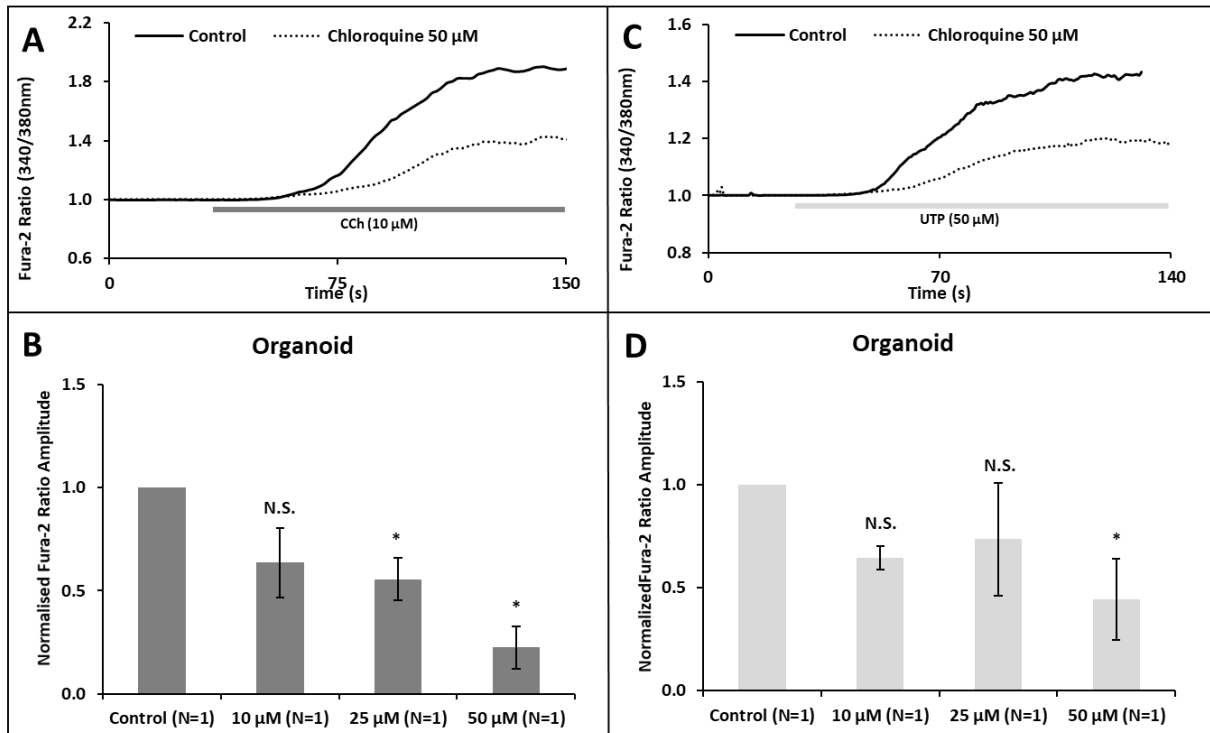
Figure 79 – High Doses of Chloroquine Inhibits Both CCh and UTP-induced Ca^{2+} Signals.

Example traces of organoids stimulated with CCh **(A)** or UTP **(C)**, in the presence or absence of chloroquine (50 µM). Bar charts summarising the normalized Fura-2 ratio amplitude comparing CCh **(B)** and UTP **(D)** responses in organoids with various concentrations of chloroquine against control. Not significant (N.S). P>0.05 (*). N≥1. For every "N", n≥3.

Two direct agonists of TPCs were evaluated against some of the pharmacological agents used so far. The two TPC agonists used in this thesis are chlorpromazine and nortriptyline, both tricyclic anti-depressants (TCAs) with an EC50 of 50-60 µM (Zhang, et al. 2019). Both chlorpromazine (100 µM) and nortriptyline (100 µM) caused a Ca^{2+} signal that is comparable to CCh (Figure 80A). Chlorpromazine (Figure 80B) and nortriptyline-induced (Figure 80C) Ca^{2+} signals were abolished by TPC-antagonist tetrandrine (20 µM) and inhibited by non-specific Ca^{2+} antagonists diltiazem (500 µM) and TMB8 (100 µM). High concentrations of 2-APB (100 µM) also significantly inhibited chlorpromazine-induced and nortriptyline-induced Ca^{2+} signals. High concentrations of caffeine (10 mM) reduced chlorpromazine-induced Ca^{2+} signals by half but was not statistically significant, but reduced nortriptyline-induced Ca^{2+} signals by 80% and was statistically significant.
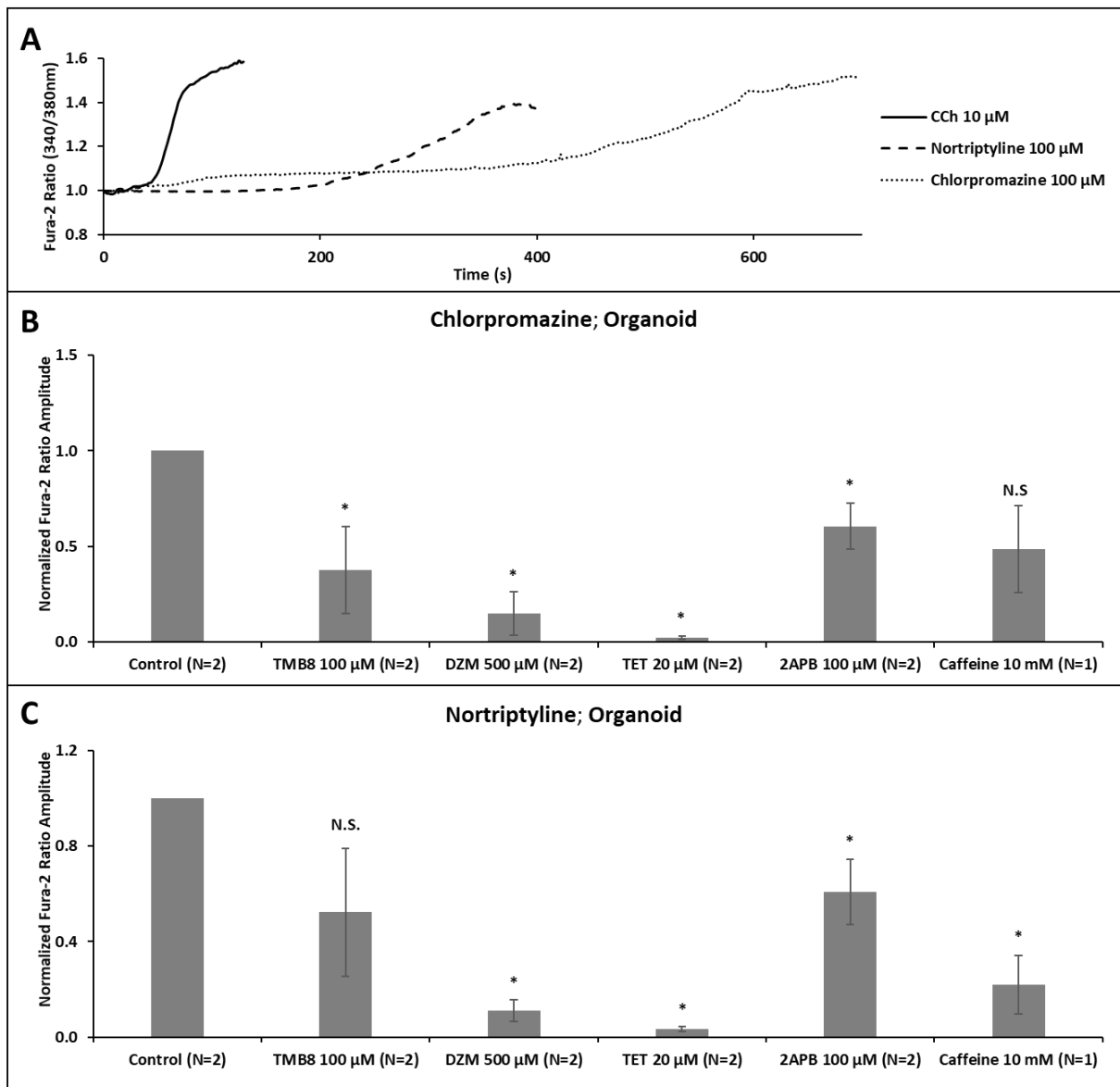
Figure 80 – Pharmacological Characteristics of TPC Agonists.

Example traces of organoids stimulated with CCh, nortriptyline and chlorpromazine **(A)**. Bar charts summarising the normalized Fura-2 ratio amplitude comparing the Ca^{2+} signals induced by chlorpromazine **(B)** and nortriptyline **(C)** in organoids with various pharmacological Ca^{2+} antagonists against control. Data normalised to control and displayed as mean +/- SEM. Not significant (N.S). $P > 0.05$ (*). $N \geq 1$. For every "N", $n \geq 3$.

4.2.3 Muscarinic and Purinergic Signals Couple to Distinct Stores but Converge on RYRs

In order to determine whether the Ca^{2+} signals elicited by activation of muscarinic and purinergic receptors originate from distinct intracellular stores, an experiment was designed to sequentially empty intracellular stores (Figure 81). First, a control experiment was conducted to demonstrate intracellular Ca^{2+} stores which were emptied by CCh or UTP were capable of refilling upon removal of agonist. Crypts which were stimulated by CCh were capable of eliciting a secondary response to CCh after the agonist was removed and the tissue sample was allowed to rest for 25 minutes (Figure 81A), and likewise with UTP (Figure 81B). The secondary Ca^{2+} signal induced by CCh and UTP were not statistically significant from the first (Figure 81C). Next, extracellular Ca^{2+} was removed by adding Ca^{2+}-chelator EGTA (1 mM) to the buffering solution. During this condition, crypts were unable to produce a secondary CCh response (Figure 81D) and likewise with UTP (Figure 81E). However, crypts which were stimulated first with CCh followed by UTP produced a secondary Ca^{2+} response (Figure 81F), and likewise when the order was reversed (Figure 81G). In the absence of extracellular Ca^{2+}, stimulating crypts with CCh then UTP (and vice versa) elicited a secondary response that was lower than the initial CCh/UTP (Figure 81H). This indicates a proportion of Ca^{2+} release induced by CCh and UTP originating from a common store/receptor, which this thesis proposes to be endoplasmic reticular RYRs.

The antagonist of RYRs, ryanodine, was used to test the proposal whether CCh and UTP-induced Ca^{2+} signals converge on RYRs. Peculiarly, ryanodine (50 µM) reduced but did not significantly inhibit CCh (Figure 82A-B) or UTP-induced (Figure 82D-E) Ca^{2+} signals in crypts. It in fact elicited a greater CCh and UTP-induced Ca^{2+} signal in organoids (Figure 82C&F). Undeterred by this, other RYR-antagonists were turned to. One of them was dantrolene, a skeletal muscle relaxant which is a selective antagonist of RYR1 and RYR3, but not RYR2 (Zhao, et al. 2001). Excitingly, dantrolene consistently and significantly reduced the CCh and UTP-induced Ca^{2+} signals by 70-90% in both crypts and organoids (Figure 83A-F). Another RYR-antagonist used in this thesis was flecainide, which specifically inhibits RYR2 (Hilliard, et al. 2010). Intriguingly, the CCh and UTP-induced Ca^{2+} signal response in flecainide (100 µM) was remarkably similar to ryanodine (Figure 84); it reduced but did not significantly inhibit CCh (Figure 84A-B) or UTP-induced (Figure 84D-E) Ca^{2+} signals in crypts and it in fact elicited a greater CCh and UTP-induced Ca^{2+} signal in organoids (Figure 84C&F). One other RYR-antagonist considered in this thesis was tetracaine, a local anaesthetic which has been shown to inhibit RYR1 (Xu, Jones and Meissner 1993), but also blocks glutamate and sodium channels (Gammaitoni, et al. 2013). Puzzlingly, tetracaine (1 mM) was capable of inducing a Ca^{2+} signal in crypts (Figure 85A) which was reduced but not significantly in the presence of EGTA (Figure 85B), indicating it mobilised an intracellular source of Ca^{2+}. Brief experiments using dantrolene (50 µM) and procaine (10 mM) showed a reduction of tetracaine-induced Ca^{2+} signals which were not significant due to huge variation (Figure 85C). Another non-specific RYR antagonist used in this thesis was procaine, which was described earlier (Figure 78).
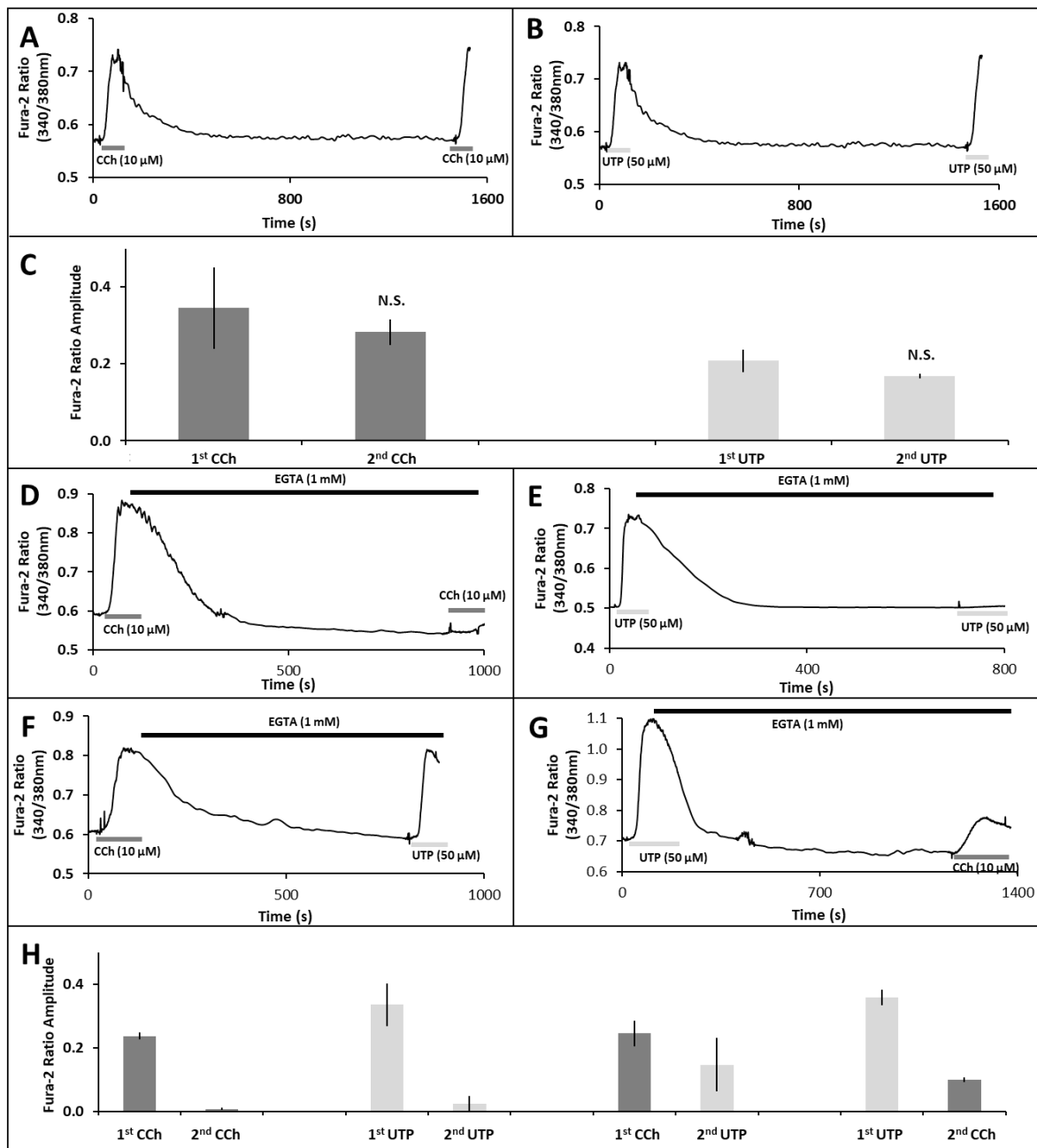
Figure 81 – Sequential Emptying of Ca²⁺ Stores in Crypts Using CCh and UTP.

Traces from control experiments demonstrate CCh **(A)** and UTP **(B)** are capable of eliciting a secondary Ca²⁺ signal after 25 minutes of rest following an initial stimulation. Bar chart summarising the Fura-2 ratio amplitude comparing the initial and secondary Ca²⁺ signals induced by CCh and UTP **(C)**. Traces demonstrating the secondary CCh **(D)** and UTP **(E)** Ca²⁺ signals are abolished in the absence of extracellular Ca²⁺ (EGTA 1 mM); however, an initial CCh stimulation followed by a secondary UTP stimulation **(F)** and vice versa **(G)** elicited a smaller yet pronounced Ca²⁺ signal. Bar chart summarising the Fura-2 ratio amplitude comparing the initial and secondary Ca²⁺ signals induced by CCh and UTP in the absence of extracellular Ca²⁺ **(H)**. N=1 for every experiment. Not significant (N.S). N=2 for every experiment. N=1. For every "N", n≥3.
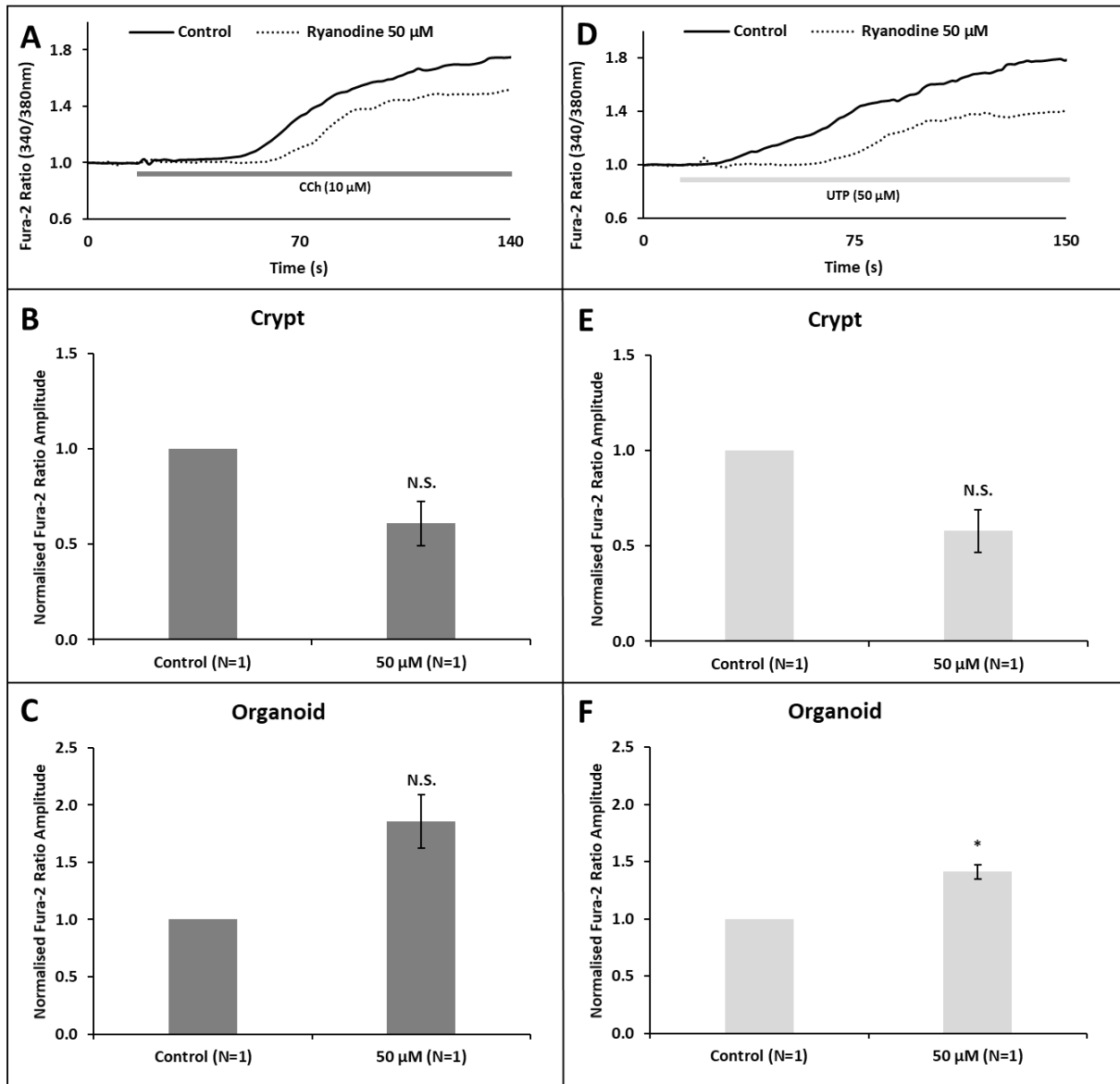
Figure 82 – Ryanodine Inhibits Neither UTP nor CCh-induced Ca²⁺ Signals.

Example traces of crypts stimulated with CCh **(A)** or UTP **(D)**, in the presence or absence of ryanodine (50 μM). Bar charts summarising the normalized Fura-2 ratio amplitude comparing CCh-induced Ca^{2+} signals with and without ryanodine in crypts **(B)** and organoids **(C)**, as well as comparing UTP-induced Ca^{2+} signals with and without ryanodine in crypts **(E)** and organoids **(F)**. Data normalised to control and displayed as mean +/- SEM. Not significant (N.S.). P>0.05 (*). N=1. For every "N", n≥3.
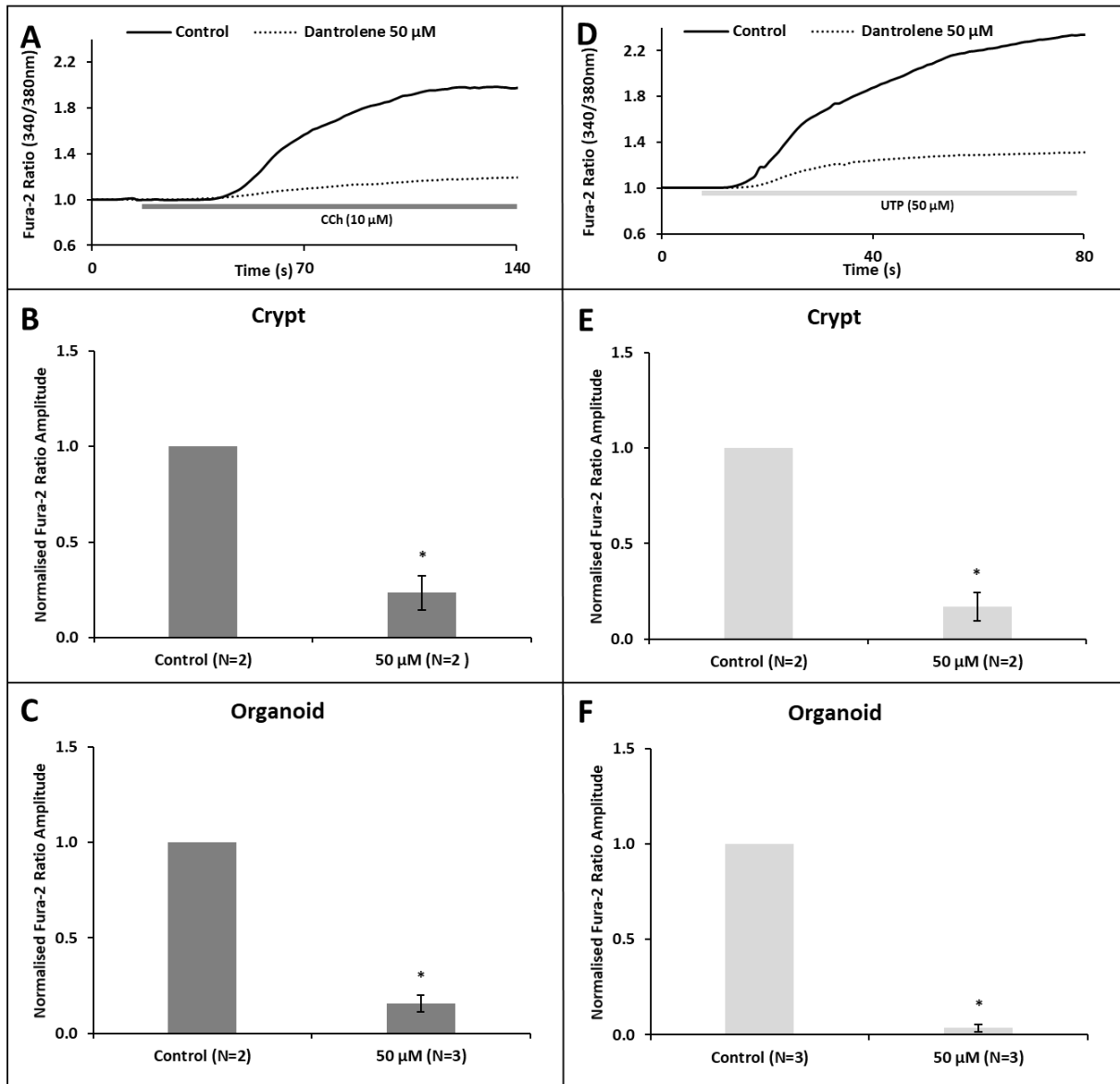
Figure 83 – Dantrolene Inhibits both CCh and UTP-induced Ca^{2+} Signals.

Example traces of crypts stimulated with CCh **(A)** or UTP **(D)**, in the presence or absence of dantrolene (50 µM). Bar charts summarising the normalized Fura-2 ratio amplitude comparing CCh-induced Ca^{2+} signals with or without dantrolene in crypts **(B)** and organoids **(C)** against control, as well as comparing UTP-induced Ca^{2+} signals with or without dantrolene in crypts **(E)** and organoids **(F)** against control. Data normalised to control and displayed as mean +/- SEM. P>0.05 (*). N≥2. For every "N", n≥3.
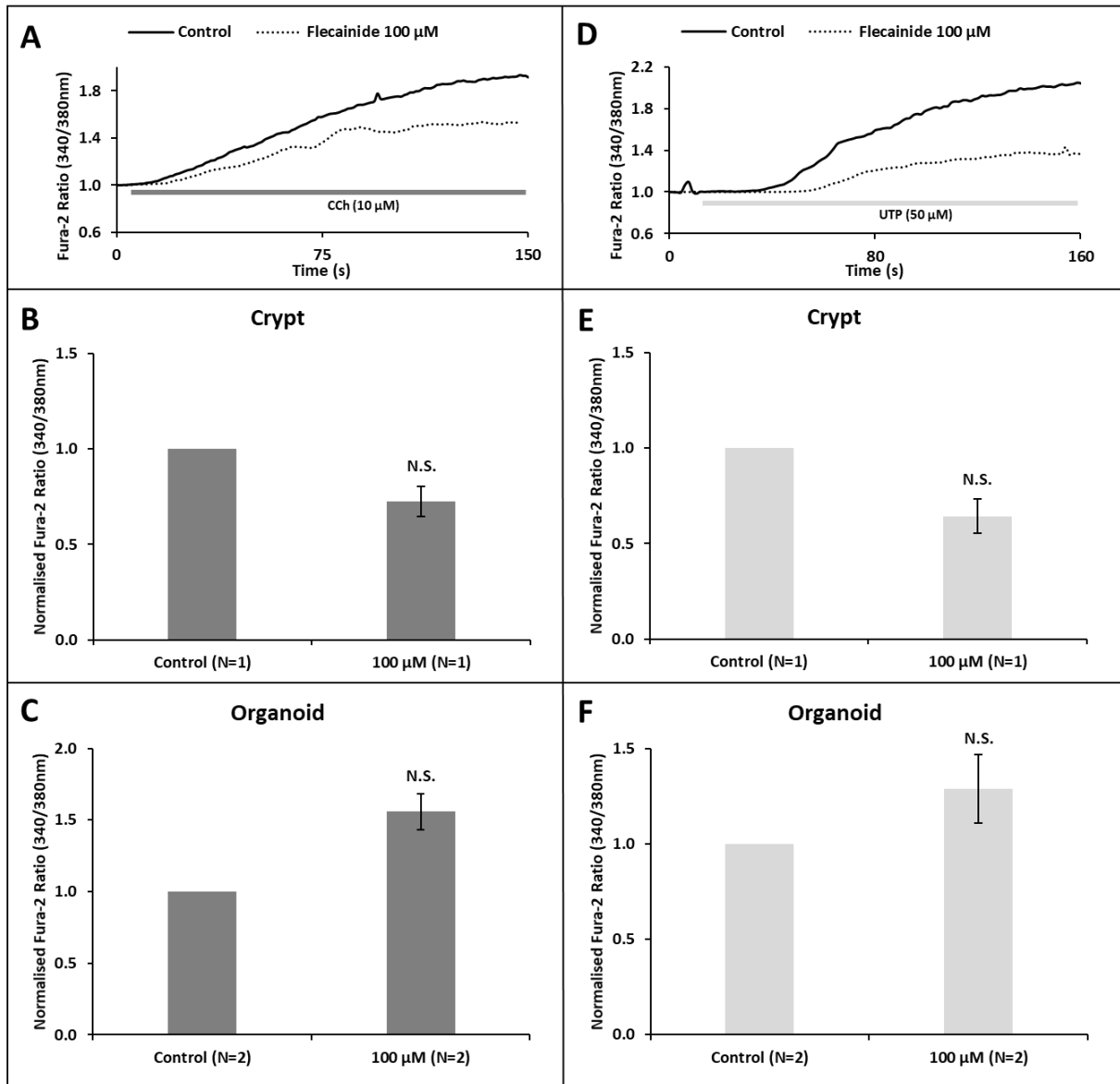
Figure 84 – Flecainide Inhibits Neither UTP nor CCh-induced Ca²⁺ Signals.

Example traces of crypts stimulated with CCh **(A)** or UTP **(D)**, in the presence or absence of flecainide (100 μM). Bar charts summarising the normalized Fura-2 ratio amplitude comparing CCh-induced Ca²⁺ signals with and without flecainide in crypts **(B)** and organoids **(C)**, as well as comparing UTP-induced Ca²⁺ signals with and without flecainide in crypts **(E)** and organoids **(F)**. Data normalised to control and displayed as mean +/- SEM. Not significant (N.S). N≥1. For every "N", n≥3.
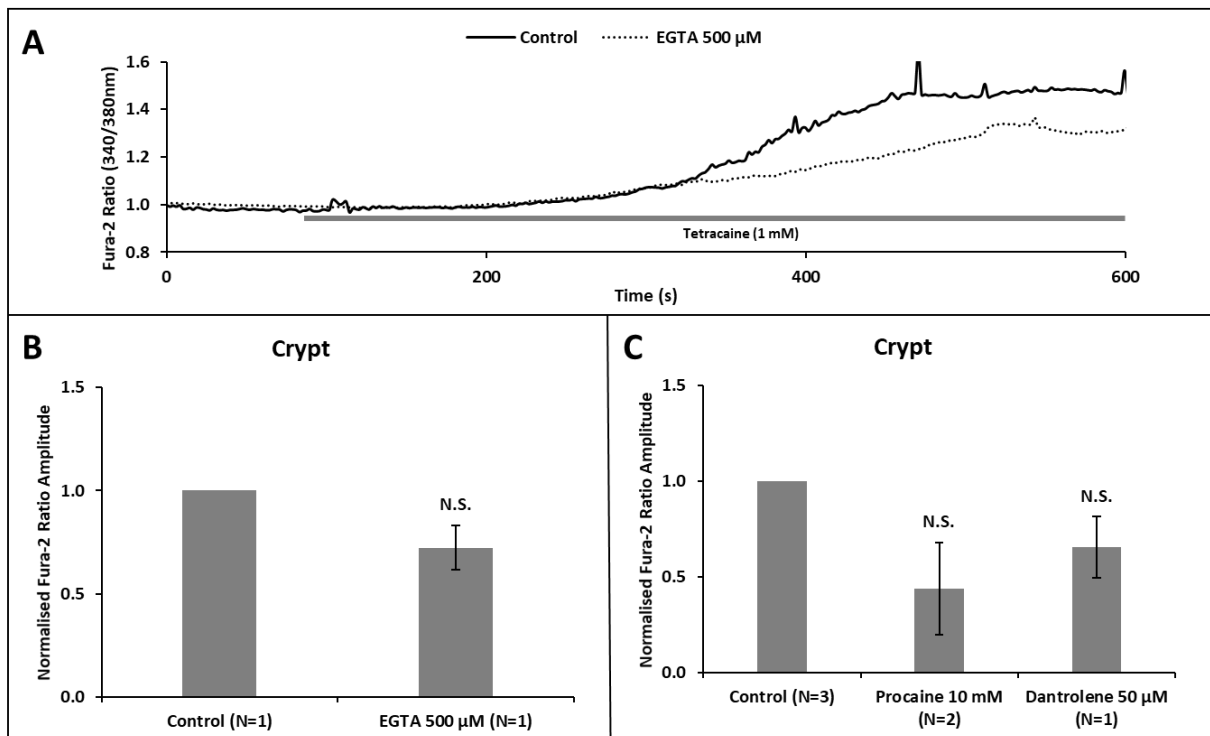
Figure 85 – Tetracaine Induces Ca²⁺ Signals in Crypts.

Example traces of crypts stimulated with tetracaine **(A)** in the presence or absence of EGTA (500 μM). Bar chart summarising the normalized data comparing tetracaine-induced Ca^{2+} signals with and without EGTA in crypts **(B)**. Bar chart summarising the normalized Fura-2 ratio amplitude comparing tetracaine-induced Ca^{2+} signals in the presence of dantrolene (50 μM) and procaine (1 mM) against control in crypts **(C)**. Data normalised to control and displayed as mean +/- SEM. Not significant (N.S). N≥1. For every "N", n≥3.

Sequential stimulation of crypts using CCH/UTP in the presence of EGTA demonstrate they couple to distinct intracellular stores to induce Ca^{2+} signals (Figure 81). To further validate that finding, another experiment was designed involving the use of cyclopiazonic acid (CPA). Cyclopiazonic acid is a fungal metabolite which inhibits the sarcoendoplasmic reticulum Ca^{2+}-ATPase (SERCA) pump (Soler, et al. 1998) and has been shown to evoke a transient 'leak' of sarcoendoplasmic reticular Ca^{2+} (Beck, et al. 2004). Interestingly, crypts which were stimulated with CPA (20 μM) in the absence of EGTA (1 mM) elicited a Ca^{2+} response that was considerably higher than crypts stimulated CPA with EGTA (Figure 86A-B). More importantly, crypt and organoids that were stimulated with CPA were capable of eliciting a small but noticeable Ca^{2+} signal in response to CCh, which was abolished when the experiment was repeated in the presence of TPC-antagonists tetrandrine (Figure 86C-D) and diltiazem (Figure 86E-G). This experiment was repeated but CCh was replaced by chlorpromazine, with similar results obtained (Figure 87A-B); the chlorpromazine response was abolished after the initial CPA-induced Ca^{2+} signal when tetrandrine or diltiazem was present.
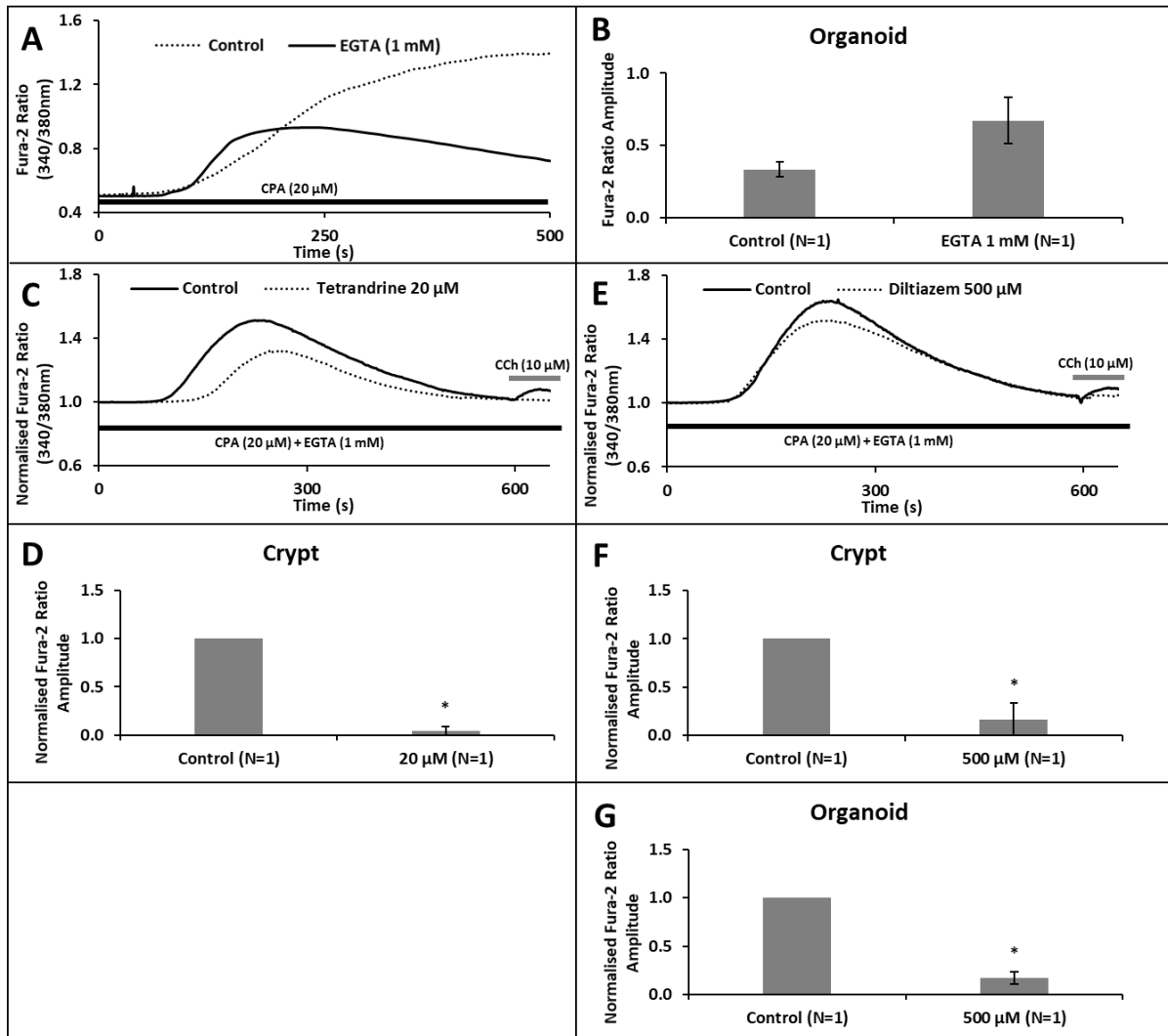
Figure 86 – CCh Induces Ca²⁺ Signals in Crypts Following Cyclopiazonic Acid Stimulation

Example traces of crypts stimulated with cyclopiazonic acid (CPA) in the presence and absence of EGTA **(A)**, and crypts with EGTA stimulated by CPA followed by CCh in the presence and absence of tetrandrine **(C)** or diltiazem **(E)**. Bar charts summarising the Fura-2 ratio amplitude of CPA-induced Ca²⁺ signals in crypts with and without EGTA **(B)**, and the normalized Fura-2 ratio amplitude of the CCh-induced Ca²⁺ signals crypts and/or organoids with EGTA and tetrandrine **(D)** or diltiazem **(E-G)**. Data normalised to control and displayed as mean +/- SEM. P>0.05 (*). N=1. For every "N", n≥3.
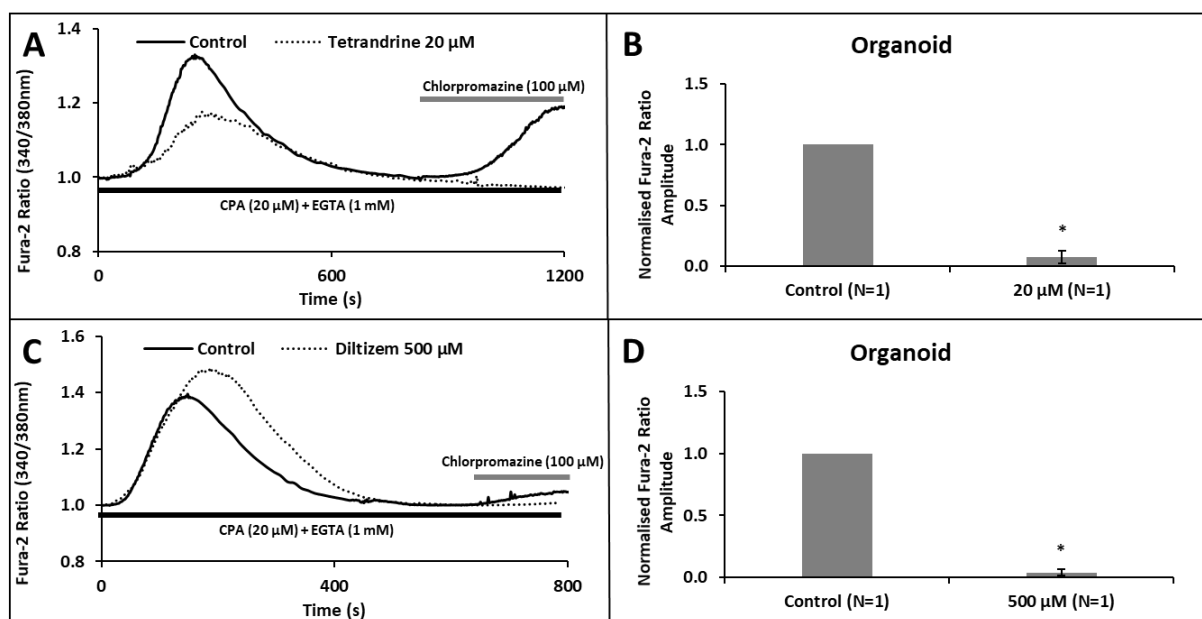
Figure 87 – Chlorpromazine Induces Ca²⁺ Signals in Crypts Following CPA Stimulation.

Example traces of crypts with EGTA (1 mM) stimulated with cyclopiazonic acid (CPA) followed by Chlorpromazine in the presence and absence of tetrandrine **(A)** or diltiazem **(C)**. Bar chart summarising the normalized Fura-2 ratio amplitude comparing CPA-induced Ca²⁺ signals with and without tetrandrine **(B)** or diltiazem **(D)** in crypts with EGTA. Data normalised to control and displayed as mean +/- SEM. P>0.05 (*). N=1. For every "N", n≥3.

Another Ca²⁺ channel which this thesis explored was Mucolipin-1 (TRPML1), a member of the TRP ion channels. TRPML1 is expressed on lysosomes (Wang W. , Zhang, Gao, & Xu, 2014) and is involved in autophagosome biogenesis (Rosato, et al. 2019). ML-SA1 is an agonist of TRPML1 which induces lysosomal Ca²⁺ release in motor neuronal cells (Tedeschi, Petrozziello and Sisalli, et al. 2019). Knowing this, a series of experiments were carried out to determine if Ca²⁺ signals induced by ML-SA1 was capable of emptying lysosomal stores and thus affect Ca²⁺ signals induced by CCh. ML-SA1 (100 µM) was shown to be capable of causing Ca²⁺ signals in crypts (Figure 88A) and organoids (Figure 88C) which rendered crypts and organoids to be unable respond to a second stimulation of ML-SA1. However, subsequent CCh stimulation was still capable of inducing Ca²⁺ signals both crypts (Figure 88B) and organoids (Figure 88D) of an amplitude which was comparable to control CCh responses (Figure 65C&D). Out of curiosity, we then evaluated the potential of non-specific Ca²⁺ antagonists – diltiazem (Figure 88E) and TMB8 (Figure 88G) – in inhibiting ML-SA1-induced Ca²⁺ signals in organoids. Interestingly, diltiazem (500 µM) utterly blocked ML-SA1 and subsequent CCh-induced Ca²⁺ signals (Figure 88F), while TMB8 (100 µM) did not affect ML-SA1 but blocked CCh-induced Ca²⁺ signals (Figure 88H).
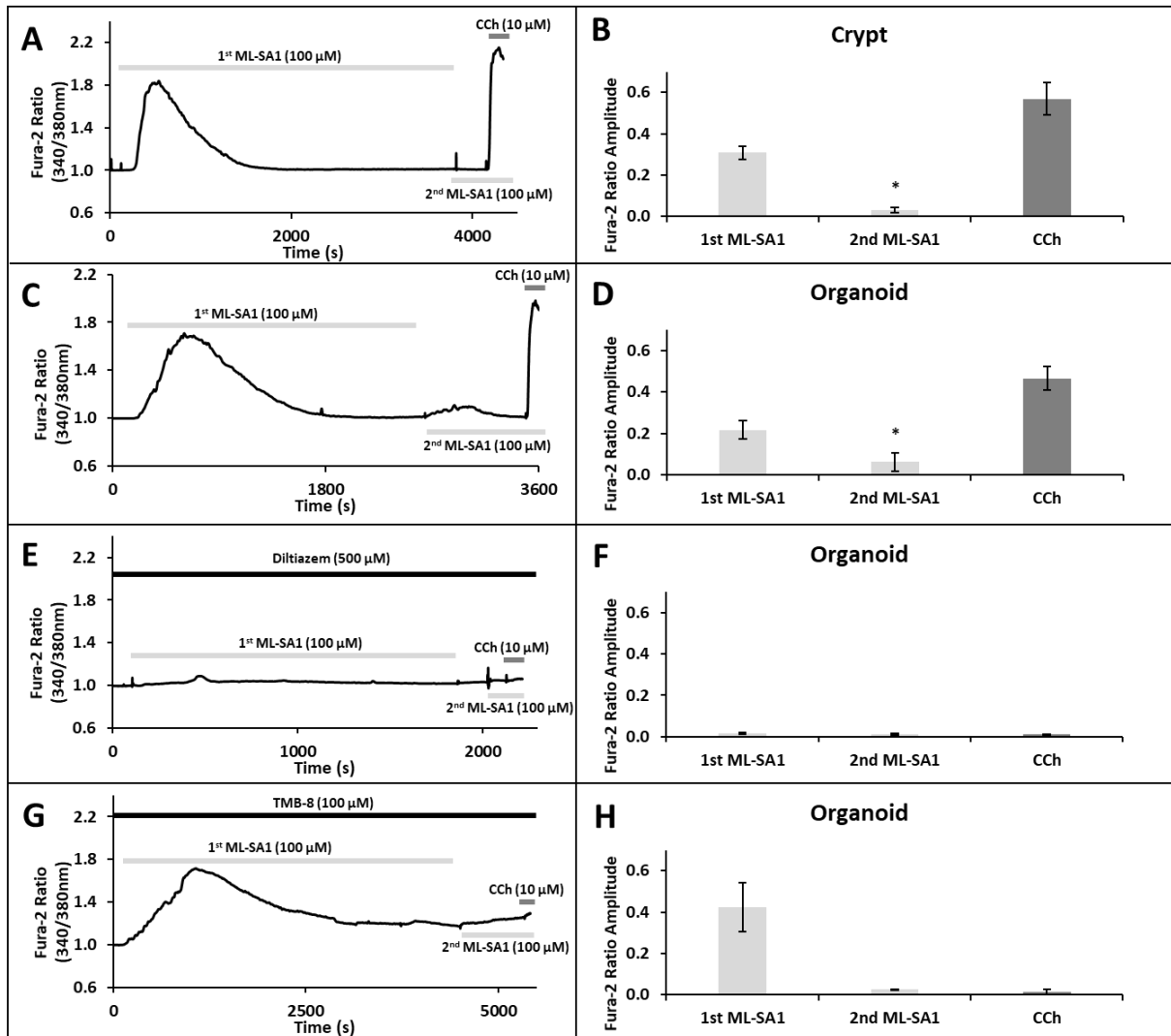
Figure 88 – ML-SA1 Induces Ca²⁺ Signals Via TRPML Receptors.

Example traces of crypts **(A)** and organoids **(C)** stimulated with ML-SA1 (100 µM) twice followed by CCh, and when in the presence of diltiazem **(E)** or TMB8 **(G)**. Bar charts summarising the Fura-2 ratio amplitude comparing the two ML-SA1 and subsequent CCh-induced Ca²⁺ signals in crypts **(B)** and organoids **(D)**, and when in the presence of diltiazem **(F)** or TMB8 **(H)**. N=1 for all conditions. P>0.05 (*). N=1. For every "N", n≥3.

This thesis also explored other means of generating Ca^{2+} signals in crypts and organoids. Mechanosensitive Piezo1 and Piezo2 ion channels convert mechanical stimuli into biological signals and are crucial for organ development and homeostasis, modulating a diverse range of cellular functions such as migration, proliferation, differentiation, and apoptosis (Volkers, Mechioukhi and Coste 2015). Both Piezo1 and Piezo2 are expressed throughout the GI tract (Coste, et al. 2010) on epithelial and non-epithelial cells, such as enterochromaffin cells, smooth muscle cells, interstitial cells of Cajal, and numerous types of neurons. A recent study showed the mechanical threshold for Piezo1 activation was reduced by Yoda1 (Botello-Smith, et al. 2019). And, GsMTx4 was shown to be capable of inhibiting Piezo1 (Bae, Sachs and Gottlieb 2011). With this is mind, an experiment was carried out using Yoda1 and GsMTx4 (Figure 89A). Yoda1 (100 µM) was capable of eliciting a Ca^{2+} signal which was reduced by GsMTx4 (5 µM), albeit not significantly due to wide variation (Figure 89B).
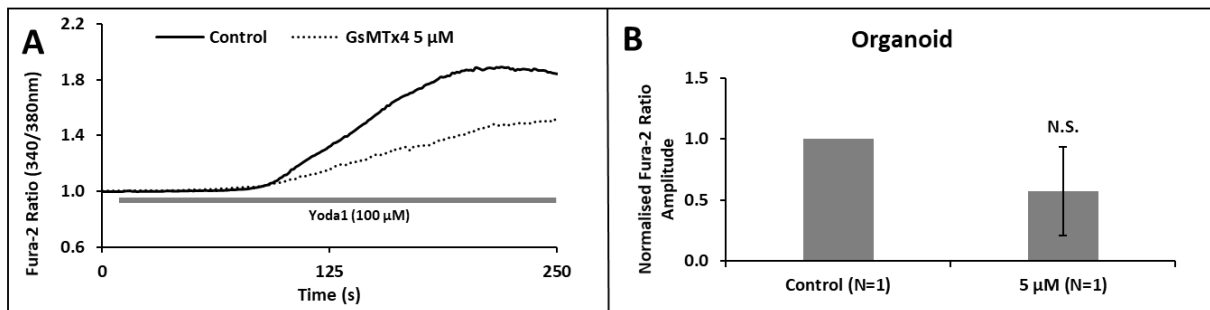
Figure 89 – Yoda1-Induced Ca^{2+} Signals is Partially Inhibited by GsMTx4.

Example traces of organoids stimulated with Yoda1 **(A)** in the presence or absence of GsMTx4 (5 µM). Bar charts summarising the normalized Fura-2 ratio amplitude comparing Yoda1-induced Ca^{2+} signals in the presence or absence GsMTx4 in organoids **(B)**. Data normalised to control and displayed as mean +/- SEM. Not significant (N.S). N=1. For every "N", n≥3.

4.3 Discussion

Early work by the Williams group showed that cultured human colonic crypts responded to acetylcholine stimulation by inducing an intracellular Ca^{2+} signal originating the base of colonic crypts (Reynolds, Parris, et al. 2007). Since then, the Williams group elucidated acetylcholine-induced Ca^{2+} signals to initiate from muscarinic receptors and be mediated by TPCs, which then induces CICR through IP3Rs and RYRs (Kam 2015) and (Pelaez-Llaneza 2019). This thesis further validated those findings using a range of pharmacological agents, as well as investigate the role of purinergic Ca^{2+} signals in colonic crypts and organoids. This chapter's results first determined the spatio-temporal characteristics of muscarinic and purinergic Ca^{2+} signals. Next, it demonstrated muscarinic-induced Ca^{2+} signals were mediated by TPCs while purinergic-induced Ca^{2+} signals were mediated by IP3Rs. Finally, it confirmed muscarinic and purinergic signals preferentially couples to distinct intracellular stores but converges on RYRs.

4.3.1 Spatio-Temporal Characteristics of Muscarinic & Purinergic Ca^{2+} Signalling

CCh (10 µM) was used in lieu of acetylcholine to activate muscarinic receptors and induce intracellular Ca^{2+} signals. Besides mimicking the effects of acetylcholine on both the muscarinic and nicotinic receptors (National Library of Medicine 2004), CCh is resistant to hydrolysis by acetylcholinesterase (Streichert and Sargent 1992). Previous work in the Williams group had characterized the EC_{50} of CCh to be 6.1 µM (Pelaez-Llaneza 2019). Topology-wise, CCh-induced Ca^{2+} signals consistently initiated at the crypt base, within the stem cell zone, and propagated up the crypt axis (Figure 57) and (Figure 58A). Polarity-wise, CCh-induced Ca^{2+} signals consistently initiated on the apical pole and spreads to the basal pole (Figure 58B). The apical initiation of CCh-induced Ca^{2+} signals corelated with the apical expression of TPC1 (Figure 37-8) and IP3R3 (Figure 33) and suggest these receptors are responsible for the origins of CCh-induced Ca^{2+} signals.

The use of 4-DAMP (100 nM), a specific antagonist of M3, confirmed CCh-induced Ca^{2+} signals were initiated by M3 (and possibly M1) but not M5 or nicotinic receptors (Figure 60C-D). The Ca^{2+} signals that were generated by CCh-induced M3 receptor activation was determined to originate from intracellular stores and was independent of influx of extracellular Ca^{2+}, as the Ca^{2+} signal was not significantly reduced by the presence of a Ca^{2+} chelator EGTA (1 mM) in the buffering solution (Figure 59). That said, the response was 20% reduced compared to control, which likely reflects the gradual leakage of Ca^{2+} from the cell. In addition, that experiment showed crypts were capable of being stimulated by CCh twice (following a period of rest) and elicited a secondary Ca^{2+} response that was not significantly different to the first (Figure 60A-B).

ATP and UTP were then shown to stimulate Ca^{2+} signals (Figure 61), during which the Fura-2 ratio amplitude for ATP (10 µM) and UTP (50 µM) were found to be similar to CCh (10 µM). This narrows the list of potential P2Y receptors down to P2Y2, as it is the only purinergic

receptor which couples to G_q and were sensitive to ATP and UTP (Table 5). Topology-wise, UTP-induced Ca^{2+} signals were inconsistent; signal initiation may occur at the crypt base or higher up the crypt axis before propagating to adjacent cells (Figure 62) and (Figure 62A-B). Polarity-wise, UTP-induced Ca^{2+} signals were also inconsistent; signal initiation may occur on the apical or basal pole (Figure 63C-D).

The use of AR-C118925XX (5 µM), a specific antagonist of P2Y2 receptors, confirmed UTP-induced Ca^{2+} signals were initiated by P2Y2 receptors (Figure 65). Due to the design of this experiment, UTP and CCh-induced Ca^{2+} signals were shown to be independent of one another in both crypts and organoids, as CCh-induced Ca^{2+} signals were unaffected by targeted inhibition of P2Y2 receptors (Figure 65B-D). The Ca^{2+} signals that were generated by UTP-induced P2Y2 receptor activation was also determined to be released by intracellular stores and was independent of influx of extracellular Ca^{2+}, as the Ca^{2+} signal was not significantly reduced by the presence of a Ca^{2+} chelator EGTA (1 mM) in the buffering solution (Figure 64). Interestingly, the response was only 6% reduced compared to control, which also reflects the gradual leakage of Ca^{2+} from the cell and more importantly, suggests that CCh-induced Ca^{2+} signals originate from different stores which were more sensitive to Ca^{2+} leakage. Notably, this thesis only considers the Ca^{2+} signals initiated by P2Y2 receptors. Since ATP-induced Ca^{2+} signals were not inhibited by AR-C118925XX (Figure 66), it implies the activation of other ATP-sensitive P2Y receptors which also couple with G_q – P2Y1/11 receptors – whose gene transcripts were present in comparable quantities (Figure 28) and should be explored in future work. Due to this caveat, UTP (50 µM) was used for all subsequent experiments to specifically evaluate purinergic Ca^{2+} signals initiated by P2Y2 receptor activation.

4.3.2 Muscarinic Ca^{2+} Signals via TPCs vs Purinergic Ca^{2+} Signals vis IP3Rs
TPC-antagonists *trans* Ned-19 (Figure 67A-C) and tetrandrine (Figure 68A-C) were shown to be capable of inhibiting CCh-induced Ca^{2+} signals in both crypts and organoids, but not UTP-induced Ca^{2+} signals (Figure 67D-F) and (Figure 68D-F). This strongly suggests that TPCs are responsible for CCh-induced Ca^{2+}-signals. While both Ned-19 (500 µM) and tetrandrine (20 µM) severely inhibited (70-80%) CCh-induced Ca^{2+} signals, it is highly unlikely that CCh only induces the release of Ca^{2+} stored within endolysosomes. Instead, this thesis proposed CCh induces local Ca^{2+} signals via endolysosomal TPCs on the cell's apical pole (Figure 58B) which couples with IP3Rs and/or RYRs to cause global Ca^{2+} signals. One point to note is that the concentration of Ned-19 (500 µM) found to be capable of inhibiting CCh was a magnitude higher compared to other studies; 65 µM (Rosen, et al. 2009) and 10 µM (Ruas, Rietdorf, et al. 2010). Likewise, the concentration of tetrandrine (20 µM) used in this thesis was far higher than in literature; 55 nM (Sakurai, et al., 2016). This could be due to pharmacokinetic differences in models used (sea urchin egg homogenate by Rosen; HeLa cells by Sakurai) or treatment conditions (12 hours by Ruas).

Next, IP3R-antagonists 2-APB (Figure 69), xestospongin-C (Figure 70) and caffeine (Figure 71) were evaluated against CCh and UTP-induced Ca^{2+} signals. Only 2-APB (50 µM) consistently inhibited UTP-induced Ca^{2+} signals in crypts (Figure 69E) and organoids (Figure 69F), and at high concentrations (100 µM) caused a small but noticeable reduction of CCh-induced Ca^{2+} signals (Figure 69B) which was significant in organoids (Figure 69C). These 2-APB concentrations were not too different from the EC50 of 36-91 µM seen in literature (Missiaen, et al. 2001). Since 2-APB is an antagonist of IP3R1 (Saleem, et al. 2014), it would imply endoplasmic reticular IP3R1 to be the intracellular channel origins of UTP-induced Ca^{2+} signals. On the other hand, xestospongin-C (4 µM) affected neither CCh nor UTP-induced Ca^{2+} signals, supporting studies which propose it being a non-specific antagonist of IP3Rs (Solovyova, et al. 2002). One suggestion is to use xestospongin-B in future work, due to it being touted to be a specific antagonist of IP3Rs (Jaimovich, et al. 2005). Lastly, caffeine (10 mM) inhibited CCh but not UTP-induced Ca^{2+} signals (Figure 71). This was rather interesting, as a study showed 2-APB and caffeine both inhibited IP3R1 (Saleem, et al. 2014). That said, caffeine has also been proposed to inhibit IP3R3 (Kang, et al. 2010). Thus, it is possible that UTP initiates local Ca^{2+} signals via IP3R1 which is inhibited by 2-APB, while CCh initiates local Ca^{2+} signals via TPCs and induces CICR via IP3R3, that latter of which is inhibited by caffeine.

One pharmacological compound which supported this thesis's hypothesis that CCh-induced Ca^{2+} signals initiate from endolysosomal TPCs was bafilomycin A1. Bafilomycin A1 inhibits lysosomal H^+-ATPase (Steen, Kirchberger and Guse 2007) including V-ATPases, resulting in disrupted acidification in lysosomes (Mauvezin and Neufeld 2015). The resulting lack of endolysosomal H^+ prevents the uptake of Ca^{2+} by voltage-gated Ca^{2+} channels (VGCCs) and encourages leakage of Ca^{2+} via Ca^{2+}-H^+ exchangers (CAXs), resulting in a net loss of lysosomal $[Ca^{2+}]$. Likewise, in this thesis, the incubation of organoids with bafilomycin A1 (2.5 µM) significantly diminished CCh-induced Ca^{2+} signals compared control (Figure 72A-B) and did not affect UTP-induced Ca^{2+} signals, which strongly implicate CCh-induced Ca^{2+} signals to initiate from endolysosomal stores. The response elicited by CCh in the presence of bafilomycin (54% of control) may imply a small release of local Ca^{2+} from endolysosomes, resulting in smaller global Ca^{2+} release via IP3Rs. Or, it may imply Ca^{2+} release independent of endolysosomal TPCs, possibly IP3Rs via IP3 through PLC (Figure 17), which should be considered in future studies.

Another pharmacological compound used to evaluate CCh and UTP-induced Ca^{2+} signals was the carbenoxolone, which inhibits gap junctions (Manjarrez-Marmolejo and Franco-Pérez 2016) as well as VGCCs (Vessey, et al. 2004). Experiments in crypts and/or organoids (Figure 73) showed both CCh and UTP-induced Ca^{2+} signals being inhibited by carbenoxolone (150-600 µM). Interestingly, the inhibition patterns for both agonists were similar across increasing concentrations of carbenoxolone. One explanation could be that increasing concentrations of carbenoxolone has a greater inhibitory effect on gap junctions. As the fluorescence measured in these experiments were recorded from drawn ROIs which do not separate one cell from

another or differentiate cells on different planes of focus, the resulting reduction in CCh and UTP-induced Ca^{2+}-signals may reflect the reduction in Ca^{2+} crossing to neighbouring cells via gap junctions to induce CICR. That said, it is also possible that carbenoxolone is inhibiting other intracellular Ca^{2+}-signalling components. One example would be plasma membrane VGCCs (Vessey, et al. 2004), resulting in reduced transport of Ca^{2+} into the cell which would reduce the overall $[Ca^{2+}]$ within intracellular stores. Another proposal is that high concentrations carbenoxolone may be inhibiting muscarinic and/or purinergic receptors, which have been implied in other studies (Boittin, et al. 2013) and (Sui, et al. 2014). Whether carbenoxolone is specific for gap junctions or not, will be a matter of interest for future studies. It would also be worth investigating gap junctions using other pharmacological antagonists, of which there are a huge number described in the literature such as quinine, mefloquine, quinidine, anandamide, oleamide, heptanol, octanol, meclofenamic acid, niflumic acid, flufenamic acid, glycyrrhetinic acid and retinoic acid (Manjarrez-Marmolejo and Franco-Pérez 2016).

The use of three 'slow channel blocking agents' – nifedipine (50 µM), verapamil (50 µM) and diltiazem (250-500 µM) – were done to evaluate whether they were capable of inhibiting CCh and not UTP-induced Ca^{2+} signals. Nifedipine has been shown to block VGCCs including L-type Ca^{2+} channels (Curtis and Scholfield 2001) and TPCs (Rahman, et al. 2015). However, in this thesis nifedipine did not inhibit CCh-induced Ca^{2+} signals (Figure 74). On the other hand, verapamil (Figure 75) and diltiazem (Figure 76) inhibited CCh but not UTP-induced Ca^{2+} signals. In addition to both being L-type Ca^{2+} channel blockers (Davis and Bauer 2012) and (Chen, et al. 2013), they are also blockers of TPCs (He, et al. 2020). Taken together, verapamil and diltiazem may be considered non-specific Ca^{2+} antagonists which, in the colonic epithelium, inhibits CCh-induced Ca^{2+} signals by possibly blocking TPCs.

Other nonspecific Ca^{2+} antagonists – TMB8 (50-100 µM), procaine (1-10 mM), chloroquine (10-50 µM) – were used to explore whether their physiological functions in the human colonic epithelium correlated with the findings of other research groups. TMB8 has been shown to inhibit IP3Rs in plants (Poutrain, et al. 2009) but has also been proposed to antagonize nicotinic receptors in human muscle cells (Bencherif, et al. 1995) and muscarinic receptors in human epithelial cell lines (Leipziger, et al. 1996). Hence it was used in this thesis as a non-selective antagonist (Figure 77). As it inhibited CCh but not UTP-induced Ca^{2+} signals, it may be acting as an antagonist of muscarinic receptors. In addition to also inhibiting nicotinic acetylcholine receptors (Drugbank 2005), procaine also inhibits RYRs (Zahradníková and Palade 1993). Low concentrations of procaine (1 mM) significantly inhibited CCh-induced Ca^{2+} signals in crypts and organoids (Figure 78A-C) but not UTP-induced Ca^{2+} signals in crypts and organoids (Figure 78D-F), while both CCh and UTP-induced Ca^{2+} signals were inhibited by high concentrations of procaine (10 mM), presumably through RYR inhibition. The last nonspecific Ca^{2+} antagonists, chloroquine, was used due it being a lysosomotropic agent which is able to become entrapped in lysosomes, gradually destabilise lysosomes membranes, and eventually

causing loss of lysosomal acidification and blockade of lysosomal function (Tian, et al. 2021). However, another study proposed it inhibited IP3Rs, TRPs and/or STIM/Orai channels (Wu, et al. 2017). In this thesis, both CCh and UTP-induced Ca^{2+} signals were shown to be inhibited by chloroquine (Figure 79A-D), with CCh-induced Ca^{2+} signals being more sensitive than UTP to the same concentrations of chloroquine. This would imply CCh mobilising Ca^{2+} from acidic stores which is reduced when in the presence of chloroquine, however chloroquine might also be blocking other receptors which affects the Ca^{2+} mobilisation induced by UTP.

Lastly, specific agonists of TPCs were used in conjunction with other pharmacological agents used thus far to support the hypothesis that CCh-induced Ca^{2+} signals initiate from TPCs. Chlorpromazine and nortriptyline were the two tricyclic anti-depressants (TCAs) used to stimulate Ca^{2+} release from TPCs (Zhang, et al. 2019). At 100 μM, both TCAs were capable of inducing a Ca^{2+} signal of an amplitude that was comparable to CCh (Figure 80A). Notably, the time which the TCA-induced Ca^{2+} signal takes to reach peak amplitude was much slower than CCh. This may reflect the difficulty of TCAs crossing the plasma membrane and binding to TPCs. It also reflects the significance of G-protein-coupled signal-transduction, whereby activation of plasma membrane GPCRs by extracellular ligands leads to downstream signal transduction within milliseconds. In this case, CCh activates M3 receptors which is proposed to activate CD38 to synthesize NAADP, the ligand of TPCs. To validate that these TCAs were TPC agonists, organoids were incubated with TPC-specific antagonist tetrandrine (20 μM), non-specific Ca^{2+} antagonist diltiazem (500 μM) and TMB8 (100 μM), and IP3R antagonists 2-APB (100 μM) and caffeine (10 mM). The pharmacological patterns for these two TCAs (Figure 80B-C) were largely similar to that observed in CCh. The only peculiar result was the 50-60% inhibition when in the presence of TMB8, which suggest TMB8 may also inhibit TPCs. Taken together, these findings strongly imply that TCAs are TPC agonists and that CCh-induced Ca^{2+} signals initiate from TPCs. However, future studies should conduct a thorough pharmacological profile of TCAs to match what has been done in CCh.

4.3.3 Muscarinic and Purinergic Signals Couple to Distinct Stores but Converge on RYRs

Direct and/or indirect pharmacological inhibition of TPCs and IP3Rs show CCh and UTP initiating Ca^{2+} signals via TPCs and IP3Rs, respectively. Furthermore, TCAs were validated to be TPC agonists and whose pharmacological profiles were comparable to CCh. Consequently, experiments were conducted to validate muscarinic and purinergic receptor activation by CCh and UTP preferentially couples to distinct stores (CCh via endolysosomes; UTP via endoplasmic reticulum) but converges on RYRs to induce CICR. Lastly, tentative experiments showed intracellular Ca^{2+} signals could be generated by other means.

An elaborate experiment was designed to sequentially empty intracellular stores using CCh and/or UTP in crypts (Figure 81). Crypts which were stimulated by CCh/UTP were capable of eliciting a secondary response to CCh/UTP after the agonist was removed and the tissue was

allowed to rest for 25 minutes (Figure 81A-B), which shows that upon agonist removal, the human colonic crypt is capable of refilling their intracellular Ca^{2+} stores and regain its sensitivity to subsequent agonist stimulation. The refilling of intracellular Ca^{2+} stores was shown to depend on influx of extracellular Ca^{2+}, as repeating those experiments in the absence of extracellular Ca^{2+} by the addition of Ca^{2+}-chelator EGTA (1 mM) resulted in the ablation of a secondary CCh/UTP response (Figure 81D-E & H). The means by which influx of extracellular Ca^{2+} into the colonic crypt was not explored, however it likely occurs via STIM-ORAI channels in conjunction with plasma membrane channels/receptors (Figure 17A) and would be worth investigating in future studies. Finally, the experiment was repeated but the second agonist was different to the first (Figure 81F-G). The small secondary CCh-induced Ca^{2+}-signal following UTP stimulation (Figure 81G) showed that after the endoplasmic reticulum is emptied with UTP, the remaining Ca^{2+} release by CCh – likely from endolysosomes – is quite small. The noticeably lower Fura-2 ratio amplitude of the secondary UTP/CCh in this experiment (Figure 81H) compared to the CCh-CCh/UTP-UTP control experimental group (Figure 81A-C) strongly implies that CCh and UTP-induced Ca^{2+} signals were not independent of one another. In other words, a proportion of the Ca^{2+} signal from CCh and UTP likely originate from a common Ca^{2+} store via a common receptor, which this thesis proposed to be endoplasmic reticular RYRs.

To test that proposal, ryanodine was used to block RYRs (Figure 82). Despite some variability, neither CCh nor UTP-induced Ca^{2+} signals were significantly affected by ryanodine. However, this may reflect the pharmacology of ryanodine; binding of ryanodine to RYRs has been described to 'reflect the open probability' of those Ca^{2+} channels (Sigalas, et al. 2009). Hence in crypts and organoids, RYRs may be closed and thus be unaffected. Or, it may indicate RYRs playing a non-essential role in releasing endoplasmic reticular Ca^{2+} which might explain its low gene transcription (Figure 24). Undeterred by this, other RYR antagonists such as dantrolene and flecainide were turned to. Dantrolene selectively inhibits of RYR1 and RYR3 but not RYR2 (Zhao, et al. 2001), while flecainide selectively inhibits RYR2 (Hilliard, et al. 2010). As dantrolene (50 μM) inhibited both CCh and UTP-induced Ca^{2+} signals (Figure 83) while flecainide (100 μM) did not (Figure 84), it would suggest CCh and UTP-induced Ca^{2+} signals converge on RYR1 and/or RYR3. In addition to these, non-specific RYR antagonists were considered. One of these was procaine which at high concentrations (10 mM) inhibited both CCh and UTP-induced Ca^{2+} signals (Figure 78). Another non-specific RYR antagonist used in this thesis was tetracaine which inhibits RYR1 (Xu, Jones and Meissner 1993) as well as glutamate and sodium channels (Gammaitoni, et al. 2013)Knowing this, tetracaine (1 mM) was expected to inhibit CCh and/or UTP-induced Ca^{2+} signals. Interestingly, rather than inhibit, tetracaine was shown to be capable of inducing a slow release intracellular Ca^{2+} signals (Figure 85A-B) and were reduced – albeit not significantly – by procaine and dantrolene (Figure 85C). A search in the literature found a study where this phenomenon was also observed in rat ventricular myocytes, whereby low concentrations of tetracaine (0.25-1.25 mM) caused a slow spontaneous Ca^{2+} release from the sarcoplasmic reticulum while at high concentrations (> 1.25 mM) it abolished all forms of spontaneous release (Györke,

Lukyanenko and Györke 1997). This could indicate that the off-target inhibitory effects of tetracaine may be causing Ca^{2+} release and should be explored in future studies.

While the sequential stimulation of crypts using CCh/UTP in the presence of EGTA demonstrate they coupled to distinct intracellular stores to induce Ca^{2+} signals (Figure 81), it could be argued that the results of CCh-CCh/UTP-UTP in EGTA may reflect receptor/channel desensitisation rather than reliance on endolysosomal/endoplasmic reticular Ca^{2+}. Thus, another experiment was designed to validate the theory of two-store preferential coupling. Cyclopiazonic acid (CPA, 20 µM) was used to inhibit the sarcoendoplasmic reticulum Ca^{2+}-ATPase (SERCA) pump, in order to evoke a transient 'leak' of sarcoendoplasmic reticular Ca^{2+} (Figure 86). Crypts without EGTA (1 mM) that were stimulated with CPA resulted in higher Ca^{2+} responses than crypts with EGTA (Figure 86A), which indicate that the transient 'leak' of sarcoendoplasmic reticular Ca^{2+} by CPA resulted in influx of extracellular Ca^{2+}, likely through STIM-ORAI which could be investigated in the future. Hence, subsequent CPA experiments were carried out with EGTA. As CPA was expected to empty sarcoendoplasmic reticular Ca^{2+}, a subsequent CCh stimulation was expected to induce a small Ca^{2+} signal via endolysosomal TPCs. Indeed, crypts and organoids which were stimulated CCh after a period of CPA exposure were capable of inducing a small Ca^{2+} signal (Figure 86C&E). And more importantly, this small Ca^{2+} signal induced by CCh could be inhibited by TPC-antagonist tetrandrine (Figure 86D) and non-specific antagonist diltiazem (Figure F-G). Hence, the small Ca^{2+} signal induced by CCh was highly likely to represent Ca^{2+} which had been released from endolysosomal stores. Lastly, chlorpromazine was used in lieu of CCh to validate chlorpromazine to be a TPC agonist. Though only conducted in organoids, chlorpromazine was capable of inducing a small Ca^{2+} signal which was also inhibited by Ned-19 antagonists tetrandrine and diltiazem (Figure 86A-D).

Mucolipin TRP channels (TRPMLs) as such TRPML1 have recently been highlighted to play an important role in cancer (Santoni, Santoni, Maggi, Marinelli, & Morelli, 2020). This was due to an earlier article which reviewed the roles of endolysosomal TRPML1-3 and TPC1-2 in vesicle trafficking, autophagy, membrane repair, and inducing local or global Ca^{2+} signals (Faris, Shekha, et al. 2019). In this thesis, TRPML1 was activated using ML-SA1 (100 µM) in crypts and organoids (Figure 88). Interestingly, crypts and organoids which were stimulated with ML-SA1 were unresponsive to a second stimulation of ML-SA1 but were sensitive to CCh (Figure 88A-D), implying TRPML1 and TPC released Ca^{2+} via independent mechanisms. Fascinatingly, diltiazem (500 µM) was capable of inhibiting ML-SA1 and CCh-induced Ca^{2+} signals (Figure 88E-F), indicating a broader function for diltiazem. By contrast, TMB8 (100 µM) did not inhibit the ML-SA1-induced Ca^{2+} signal (Future 89G-H), reflecting its function as a cholinergic receptor antagonist (Bencherif, et al. 1995) and (Leipziger, et al. 1996). Future studies should expand on elucidating the signalling pathway leading to endolysosomal Ca^{2+} signals released by TRPML1.

Finally, tentative experiments were carried out exploring other means of inducing Ca^{2+} signals in the colonic epithelium. Mechanosensitive Piezo ion channels were of interest, as sensation of mechanical forces is critical for normal GI function such as gastric motility and satiety (Alcaino, et al., 2018), and abnormalities in mechanosensation are linked to GI pathologies including obesity (Acosta, et al. 2014), constipation (Neshatian, et al. 2015), and colon cancer pathogenesis (Fernández-Sánchez, et al. 2015). In this thesis, Yoda1 (100 µM) was used to reduce the mechanical threshold for Piezo1 activation, while GsMTx4 (5 µM) was used to inhibit Piezo1 (Figure 89). While at first glance it appears as if Yoda1 induced a Ca^{2+} signal in organoids which was reduced by GsMTx4, it is more likely that the Yoda1-induced Ca^{2+} signal was due to the mechanical forces applied during pipetting and aspiration of solutions. Indirect evidence for that proposition is that crypts and organoids which were stimulated with blank HBS were incapable of inducing a Ca^{2+} signal (data not shown). Thus, future work should expand on elucidating the mechanism of Ca^{2+} signals induced by Piezo channel activation. One compound which should be explored in the future is Dooku1, a modified analogue of Yoda1 which reversibly antagonizes Yoda1 and thereby prevent the Yoda1 from reducing the sensitivity threshold of Piezo1 (Evans, et al. 2018).

4.4 Conclusion

This chapter's results elucidated the signalling transduction pathway for muscarinic and purinergic Ca^{2+} signals in cultured human colonic crypts and organoids, using the Ca^{2+}-sensitive ratiometric fluorescent dye – Fura-2. CCh activates M3 receptors and induces an intracellular Ca^{2+} signals that initiates on apical pole of cells at the base of crypts. Endolysosomal TPCs are the origin of M3-activated Ca^{2+}-signals, which is accompanied by CICR from endoplasmic reticular IP3Rs and RYRs. In parallel, UTP activates P2Y2 receptors and induces Ca^{2+} signals that initiates randomly. Endoplasmic reticular IP3Rs are the origin of P2Y2 receptor-activated Ca^{2+}-signals, which is also accompanied by CICR from adjacent RYRs. The propagation of CCh and UTP-induced Ca^{2+} waves from one cell to the next may occur via gap junctions. Lastly, mucolipin TRP and mechanosensory channels are also capable of evoking intracellular Ca^{2+}-signals from the human colonic epithelium. Having shown that tuft cells of the human colonic epithelium express ChAT in the previous chapter, this thesis goes on to describe the development and application of a HILIC-MS/MS method to quantify non-neuronal acetylcholine secreted from human colonic epithelium.

5 Chapter 5 – Results Part 3: Quantification of Non-Neuronal Acetylcholine in the Colonic Epithelium

5.1 Introduction

Colonic epithelial tuft cells are capable of synthesizing and secreting acetylcholine (Pan, Zhang, Shao, & Huang, 2020). While the functions of non-neuronal acetylcholine have been studied extensively in humans in both health and disease (Wessler, Kirkpatrick and Racké 1998) and (Beckmann and Lips 2013), none has yet to quantify it. This results chapter will outline the method developed and validated for quantifying low nanomolar (1-100 nM) concentrations of non-neuronal acetylcholine secreted by the human colonic epithelium. In addition, it will determine if the non-neuronal acetylcholine synthesized by crypts are capable of inducing a Ca^{2+} signal.

One of the earliest studies to quantify non-neuronal acetylcholine used gas chromatography and mass spectrometry (MS) in bull spermatozoa, reporting approximately 4.3 pmol/10^6-cells (Bishop, Sastry and Stavinoha 1977). Another study used radioimmunoassay on blood plasma and reported approximately 456.1 pg/ml (Kawashima, et al. 1987), or approximately 3.1 nM of acetylcholine in plasma. A later study developed a liquid chromatography–tandem mass spectrometry (LC-MS/MS) method of measuring acetylcholine in plasma which can quantify down to 0.005 ng/10^6-cells, however they failed to detect any acetylcholine in plasma (Zhang, et al. 2016). Another study used ultra-performance LC-MS/MS (UPLC-MS/MS) to quantify acetylcholine in peripheral blood mononuclear cells, reporting between 0.01-0.14 ng/10^6-cells (Han, et al. 2017). Two studies have quantified non-neuronal acetylcholine in animal models; one in rat colon (Yajima, et al. 2011) and one in mouse gut and organoid (Takahashi, Ohnishi, et al. 2014). Yajima and colleagues combined high-performance liquid chromatography with post-column enzyme reactors, reporting 2-12 nmol/g of wet weight tissue. Takahashi and colleagues used LC-MS/MS to quantify acetylcholine in cultured media, reporting 2.38 nmol/mg from gut tissue and 0.40 nmol/mg from organoid tissue.

Due to scent amount of literature for quantifying acetylcholine and variability between their methodology, a significant component of this thesis was devoted to developing an effective standard operating protocol (SOP) for quantifying acetylcholine (henceforth referred to as 'analyte of interest') in media cultured in human colonic tissue (henceforth referred to as 'sample') using chromatography combined with mass spectrometry (Chapter 2.7). This SOP was developed using the facilities available at the Bob Champion Research and Education centre, located at the Norwich Research Park, under the supervision of Mr Jonathan Tang, a Research Fellow at the Norwich Medical School.

5.2 Method Development

First, a sample preparation and extraction protocol was developed to remove compounds which may contaminate the equipment or interfere with the analysis, as well as extract analytes of interest for subsequent analysis. Next a hydrophilic interaction liquid chromatography protocol was developed using a gradient flow of two mobile phases to selectively isolate analytes of interest by molecular size and ionic charge. Finally, the mobile phase containing the analytes of interest was put through a tandem mass spectrometer and interpreted using Analyst Software 1.6.

5.2.1 Sample Preparation and Extraction

Human colonic crypts were isolated and cultured overnight using the methodology described earlier (Method 2.3.2). Rivastigmine (500 µM) was added to the culture media to inhibit the hydrolysis of acetylcholine by acetylcholinesterase (Willams, Nazarians and Gill 2003). Media from crypts and organoids were collected, first by scratching away the Matrigel, then collected by pipette aspiration. Additional Rivastigmine (final concentration of 1 mM) was added to the media. Samples were then centrifuged briefly to separate the culture media from the Matrigel and colonic tissue. The culture media was collected, kept chill in ice, and transported to the Bob Champion Research and Education (BCRE) building.

Within the BCRE building laboratory, samples were first thawed and filtered using a 10 µm cell strainer before being put through the sample preparation and extraction protocol (Figure 90), which was developed after sampling several weak-cation-exchanger (WCX) plates from Thermo Scientific, IST Evolute, Phenomenex, and Waters Corp Oasis. The Oasis WCX 96-well Plate (30 mg/ Well) and Strata-WCX microelution 96-well plate (2 mg/well) were found to be suitable, with the former being the most reliable and thus used to prepare the sample and extract the analytes of interest. WCX-plates serve as a Solid Phase Extraction (SPE) component of extracting analytes of interest by their physical and chemical properties. In the case of acetylcholine, it is a polar compound with a positively charged ammonium group.

The first step of the protocol (Figure 90.1) involved mixing 100 µL of sample with 100 µL of internal standard (D4-ACh, 100 nM, aqueous) in a glass test tube. D4-ACh (Acetylcholine-1,1,2,2-d4) is a pharmacologically synthesized analogue of acetylcholine which replaced four hydrogens with deuterium, thus having a molecular weight of 151 compared to 146. This stage also includes preparation of calibration standards and internal quality control standards in separate test tubes, following the same method. The second step (Figure 90.2) followed the manufacturer's recommendation of priming the WCX-plate's sorbent bed using UPLC grade methanol followed by water, then removing residual liquids with a short burst of high-pressure nitrogen gas. The purpose of this step was to remove possible contaminants in the wells acquired during the manufacturing process, as well as priming the sorbent bed for interacting with analytes of interest. In the case of Oasis WCX 96-well Plates, its sorbent bed

consists of weakly charged mixed-mode groups bound to copolymer resins which operate at pH 5-10. The third step (Figure 90.3) involves loading the samples, calibration standards and quality controls prepared in step one (Figure 90.1) into individual wells. Samples were allowed to interact with the sorbent bed for 15 minutes before low-pressure nitrogen gas was applied for 15 minutes. In this stage, positively charged analytes of interests such as acetylcholine and D4-ACh interact with the weakly negatively charged solvent bed and become chemically bound to it. In step four (Figure 90.4), residual contaminants were removed following manufacturer guidelines of washing the wells with UPLC grade water followed by methanol, then removing residual liquids with a short burst of high-pressure nitrogen gas. In step five (Figure 90.5), 105 µL of elution solution (80 µL acetonitrile, 20 µL water, 5 µL formic acid) was added to the wells under low-pressure nitrogen gas, and the eluent was collected in a 96-well collection plate. During this stage, the presence of formic acid causes the elution solution to a pH of lower than 5, which changes the properties of the sorbent bed to become positively charged, allowing formic acid to outcompete analytes of interests bound to the sorbent bed. This exchange frees positively charged analytes of interest from the sorbent bed and allows it to be eluted and collected. In the final sixth step (Figure 90.6), the collected eluent was inserted into the plate holder of the HPLC system for liquid chromatography.

Prior to the final version of this sample preparation and extraction protocol, an alternative elution procedure was trialled following guidelines issued by WCX-plate manufacturers (Figure 91). After step four (Figure 90.4), analytes of interest were eluted using two washes of 99% methanol and 1% formic acid, then dried using nitrogen gas at 40°C and reconstituted with the same elution used described earlier (Figure 90.5). However, this process proved to be time-consuming and liable to decrease subsequent analysis. Hence this method was modified to eliminate drying and reconstitution.
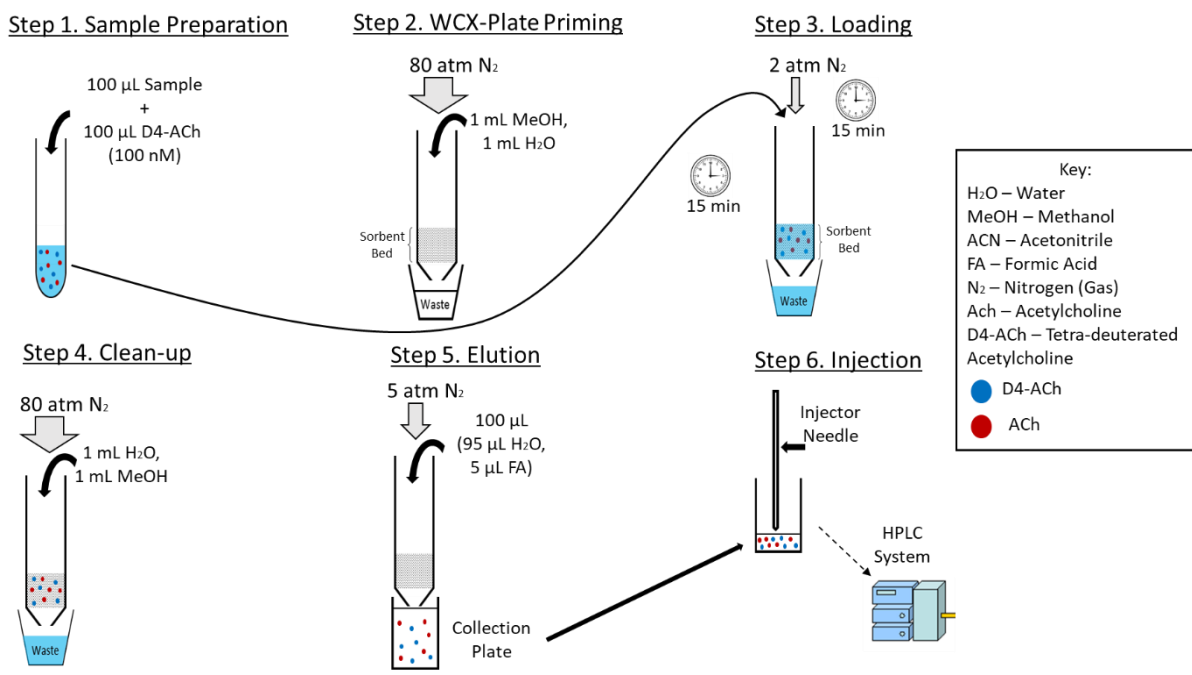
Figure 90 – Schematic Flow of the Sample Preparation and Extraction Protocol.

Step **(1)** involves mixing the sample with the internal standard. Step **(2)** involves priming the WCX-plate following manufacturer recommendation. In Step **(3)**, the solutions prepared in step **(1)** is loaded into individual WCX-plate wells and allowed to interact with the sorbent bed. In step **(4)**, residual contaminants were removed following manufacturer guidelines. Step **(5)** involves eluting analytes of interests from the WCX-plate, which is then injected into the HPLC system in step **(6)**. Key depicted on the right.
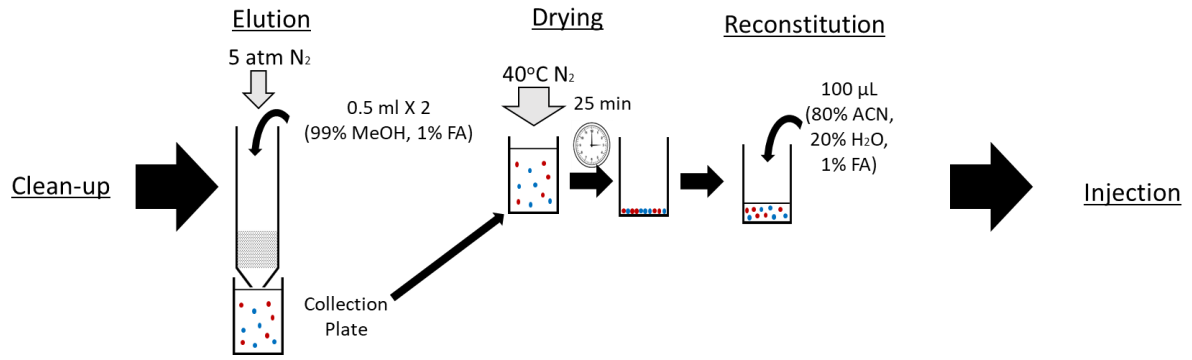
Figure 91 – Schematic Flow of Alternative Elution Procedure.

Elution was carried out using two washes, bringing the final elute volume to 1 ml. This elute was dried and reconstituted before being injected into the HPLC.

5.2.2 Hydrophilic Interaction Liquid Chromatography

A liquid chromatography protocol was developed using the Shimadzu LC-20 HPLC system. Specifically, it was used to separate compounds within the elution solution (Figure 90.6) and extract analytes of interest using hydrophilic interaction liquid chromatography (HILIC), which incorporates both SPE and supported liquid extraction (SLE). SPE consist of the HILIC column which separates compounds based on size and charge. SLE consist of extracting compounds from the SPE component using a gradient-flow of two mobile phases.

HILIC is a variant of HPLC. It operates by subjecting a hydrophilic stationary phase (a.k.a. column) at high pressure to interact with hydrophilic analytes of interest (Figure 92). Like other chromatography methods, HILIC relies on two different mobile phases, solvents which move through the column to interact and carry compounds through the stationary phase. The mobile phases developed in this thesis, henceforth referred to as Mobile Phase A (aqueous; 100% Water, 10 mM Ammonium Formate, 0.1% Formic Acid) and Mobile Phase B (organic; 90% Acetonitrile, 10% Water, 10 mM Ammonium Formate, 0.1% Formic Acid) were made using UPLC-grade solvents. Their composition was developed following guidelines issued by column manufacturers, as well as simulating mobile phases used in literature. Ammonium formate and formic acid are modifiers used to improve peak shape and increase sample load tolerance (Johnson, Boyes and Orlando 2013). While the composition mentioned above reflects the methodology used for quantifying acetylcholine in cultured media, during early method development the composition of Mobile Phase A and B were highly variable. For example, ammonium acetate was initially used but replaced with ammonium formate. Both ammonium formate acetate at 10 mM were liable to precipitate out of Mobile Phase B, a common point of concern in chromatography and colloquially referred to as 'crashing out'. To prevent precipitation, ammonium acetate or formate were first dissolved in water, then acetonitrile would be added in incremental quantities to reach the final concentration.

During sample injection (Figure 90.6), the HILIC column undergoes a gradient flow cycle delivered by pumps which had been programmed into the system. At this stage, the HILIC column's polar stationary phase interacts with compounds carried by the mobile phases. Analyte retention within the HILIC column is dependent on the analyte's physical and chemical properties, as well as the chemical properties of the Mobile Phases. Like other chromatography methods, large compounds travel slower in HILIC columns compared to smaller compounds, and specifically in HILIC columns, polar compounds are retained longer compared to non-polar compounds. Next, the aqueous Mobile Phase A interacts well with the HILIC column's polar stationary phase while mainly organic Mobile Phase B does not. Thus, polar analytes such as acetylcholine and D4-acetylcholine are retained by HILIC columns when in the presence of mainly organic Mobile Phase B. However, when the mobile phase becomes aqueous, acetylcholine and D4-acetylcholine are displaced.
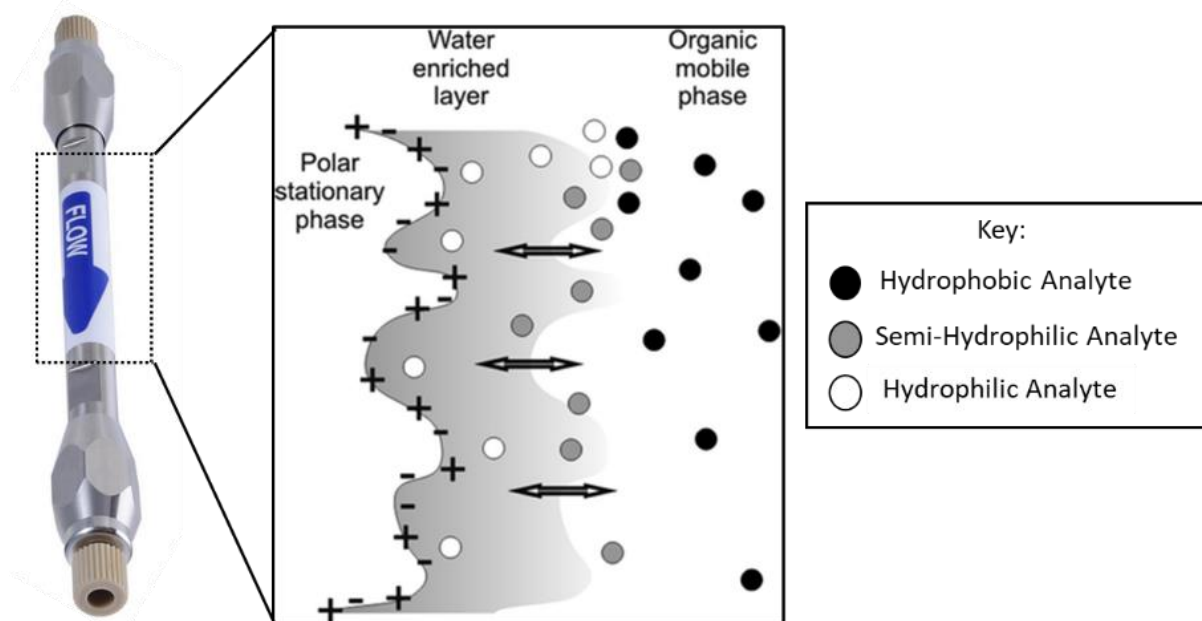
Figure 92 – HILIC Principle.

A HILIC column is depicted on the right. A representation of the principles of HILIC is depicted on the left. HILIC separation is based on passing a mostly organic mobile phase over a polar stationary phase. This forms a water enriched layer next to the stationary phase. The hydrophilic analytes partition into this layer and as the mobile phase becomes more hydrophilic, they are eluted in order of increasing hydrophilicity. Key depicted to the right. Figure adapted from (Jensen, et al. 2013).

Settings for the Shimadzu LC-20 HPLC system was configured by following the user manual and optimized by trial and error. These include Pumps, Autosampler, Oven, Time Program, Injection and Valco Valve. Pumps refer to the pumps and lines used to deliver Mobile Phase A and B. Settings include selecting binary flow (of Mobile Phase A and B), setting the total flow (volume of mobile phase per minute) to 0.4 mL/minute, setting pump B to deliver a linear concentration of 90% Mobile Phase B, and establishing the maximum pressure limits of 5999 PSI. When applied, this produced a system pressure ranging from 800 to 2000 psi, far under the maximum pressure limits. Autosampler refer to the compartment in which the collection plate was placed to be injected into the Shimadzu LC-20 HPLC system. The autosampler compartment temperature was set at 10°C and the injection needle was programmed to rinse before and after an injection with 200 µL of needle rinse solution, which consisted of isotone, acetonitrile, and water at a 3:3:1 ratio. Oven refers to the desired and maximum temperature of another compartment which held the HILIC column, which was set to 27°C and 85 °C, respectively. Time Program refers to the time and gradient flow cycle, which was developed and optimized (Figure 93). Injection refers to the volume of collected sample to be injected into the HPLC system, which was set to 20 µL. Valco Valve refers to the time during which the HPLC system injected mobile phase that had gone through the HILIC column following the gradient flow cycle (Figure 93) into the mass spectrometer. This time was set to 2.5 and 4.5 minutes. These configurations varied during the method development stage, however the settings listed above were used when measuring acetylcholine in cultured media.

Finally, two HILIC columns were trialled during the development of this liquid chromatography protocol (Table 10). Of the two, the Triart Diol-HILIC plus column was shown to be superior in many aspects. First, the analyte count upon injecting a known quantity of acetylcholine and D4-acetylcholine were 60% higher in the Triart Diol-HILIC plus column, indicating the column was more sensitive to acetylcholine. Second, the retention time of 2.3-2.5 min was somewhat more favourable than 1.2-1.6 min; the longer elution time provides flexibility should the gradient flow or other configurations require modification, and it had a narrower peak duration. Lastly, the signal noise generated from the Triart Diol-HILIC plus column was lower and thus preferable.
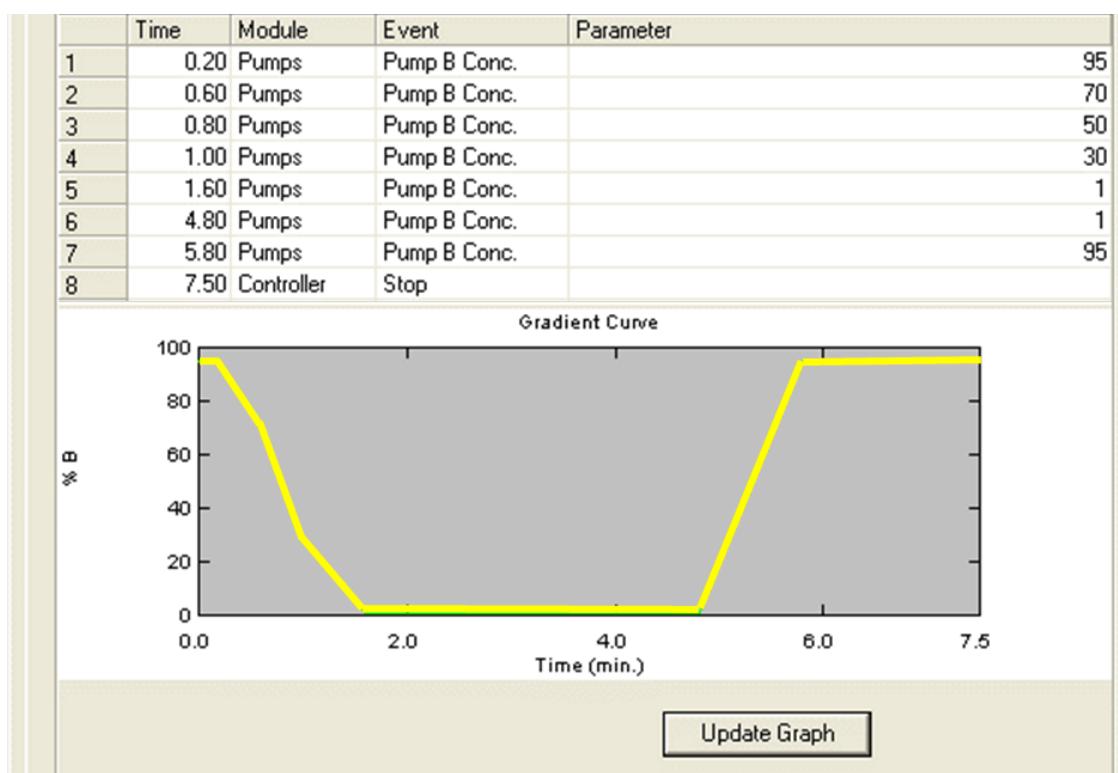
Figure 93 – Mobile Phase Gradient Curve for Each Sample Injection.

Between 0.0 to 1.6 minutes, the mobile phase steadily decreases from 95:5 (95% Mobile Phase B: 5% Mobile Phase A) to 1:99. After this point, the mobile phase returns to 95:5 and maintains there until the cycle ends at 7.5 minutes, after which the gradient curve repeats for subsequent sample injections.

Table 10 – Comparison Between Two HILIC Columns.

Column Brand	Triart Diol-HILIC plus	YMC-Triart Diol-HILIC
Column Size & Properties	100 mm x 3.00 mm; S-3um, 12 nm	100 mm x 2.1 mm; S-3um, 12 nm
Acetylcholine	100 ng/mL	
Analyte Peak Area (Counts)	**209027**	129414
D4-Acetylcholine	100 nm/mL	
Analyte Peak Area (Counts)	**563045**	342360
Analyte Retention Time (min)	2.3 – 2.5	1.2 – 1.6
Signal Noise (Counts)	<100	200-500

5.2.3 Tandem Mass Spectrometry

Having optimized the HILIC methodology, the API 4000 tandem mass spectrometer was configured following the user manual and optimized by trial and error. The following mass transitions for the analyte of interest (acetylcholine) and its internal standard (D4-acetylcholine) were determined:

Acetylcholine: 146.1 < 86.0

D4-Acetylcholine: 150.2 < 90.9

Next, the parameters for the Source/Gas and Compound were configured:
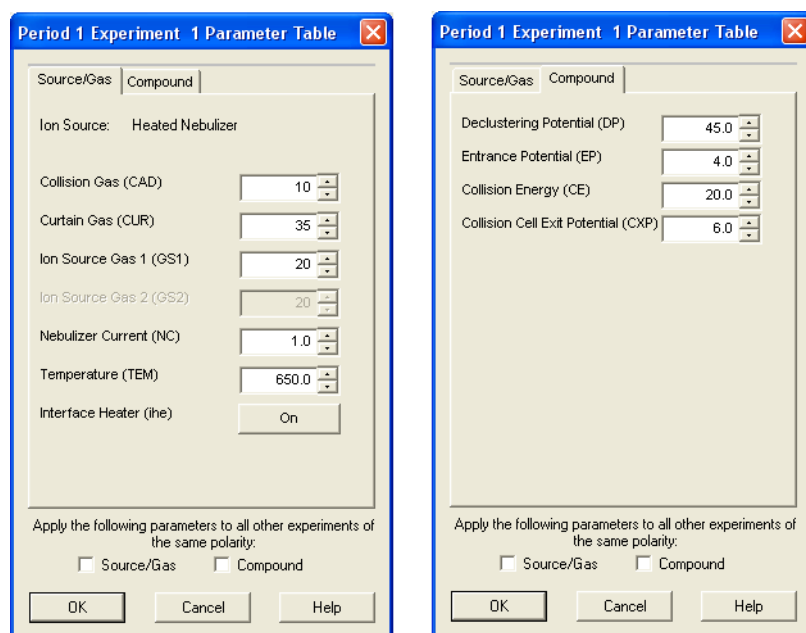
Tandem mass spectrometry (also known as Multiple-stage Mass Spectrometry) consists of an ionizing chamber connected to three quadrupoles (triple-quadrupole) and a detector (Figure 94). Following the HPLC system settings, the mobile phase that had gone through HILIC column following the gradient flow cycle is injected into the first component of the mass spectrometer – the ionizing chamber. The ionizing chamber (also known as the source chamber) is a vacuum chamber set to 650°C. In combination with the spray needle delivering the mobile phase, its purpose is to ionize and vaporize the mobile phase, subsequently directing the ionized gas through the curtain plate and the quadrupoles (Figure 95). The ionized gas then enters the first quadrupole (Q1), where precursor ions are selectively separated by its specific mass transition, which is measured by the mass divided by the ionic charge number (m/z). For acetylcholine and D4-acetylcholine, their precursor ion m/z values are 146.1 and 150.2, respectively. Precursor ions are then energized and collided with argon gas to generate product ions at the second quadrupole (Q2). Product ions are then selectively separated by its (m/z) at the third quadrupole (Q3). For acetylcholine and D4-acetylcholine, their product ion m/z values are 86.0 and 90.9, respectively. Product ions with those m/z values are detected and displayed as a chromatogram on the Analyst Software 1.6.
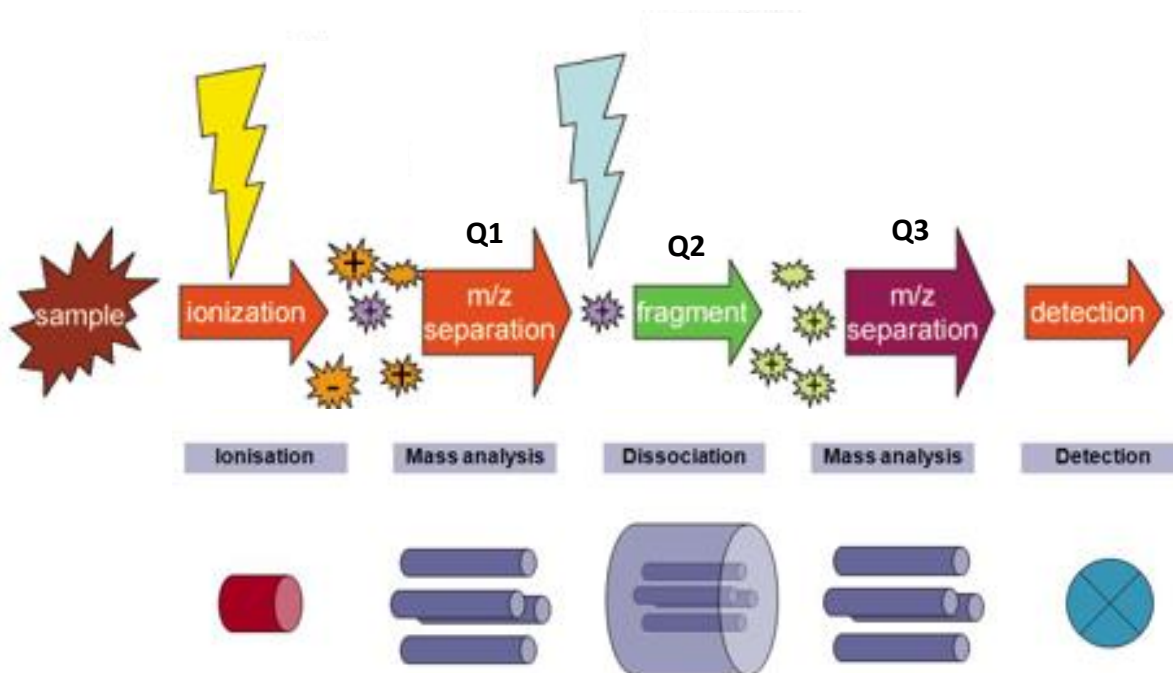
Figure 94 – Schematic Diagram of the Principles of Tandem Mass Spectrometry.

Tandem mass spectrometry involves ionizing the sample, followed by mass analysis (1st m/z separation) of the precursor ion at the first quadrupole (Q1), fragment dissociation at the second quadrupole (Q2) and mass analysis (1st m/z separation) of the daughter fragment ions at the third quadrupole (Q3), which then reaches the detector. Figure adapted from (National High Magnetic Field Laboratory 2015).
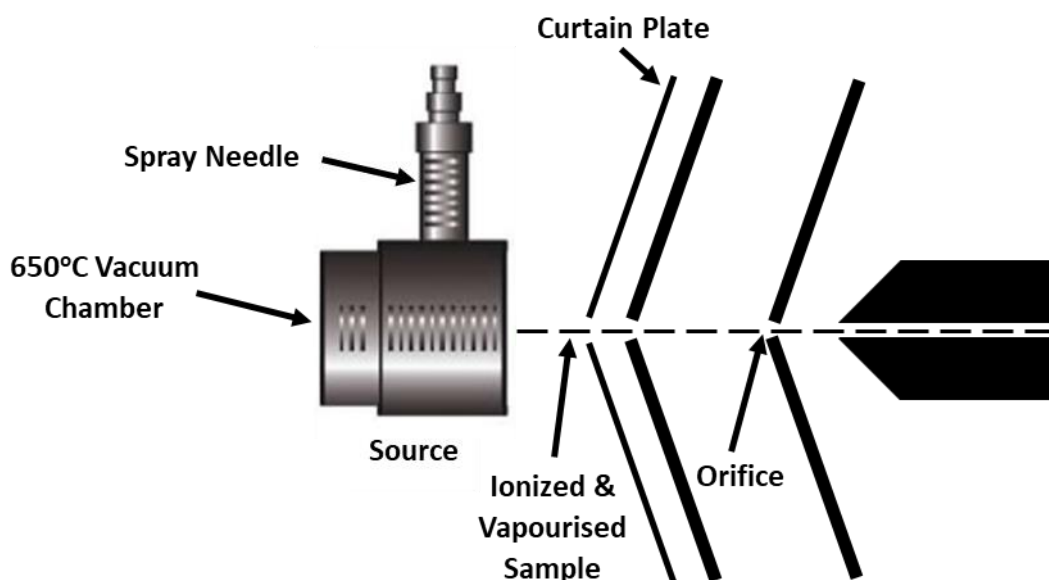
Figure 95 – Ionizing and Vaporising the Sample at the Source Chamber.

The source chamber is responsible for ionizing and vaporising the sample delivered by the spray needle and directing the ionized gas through the curtain plate and into the orifice.

5.2.4 Data Interpretation

Data quantitation and interpretation was carried out using the Quantitation Wizard feature built into Analyst Software 1.6. This included chromatograms of acetylcholine and D4-acetylcholine (Figure 96). Quantitation of that chromatogram was done automatically using a pre-set method (Table 11), although manual quantification was carried out where necessary.
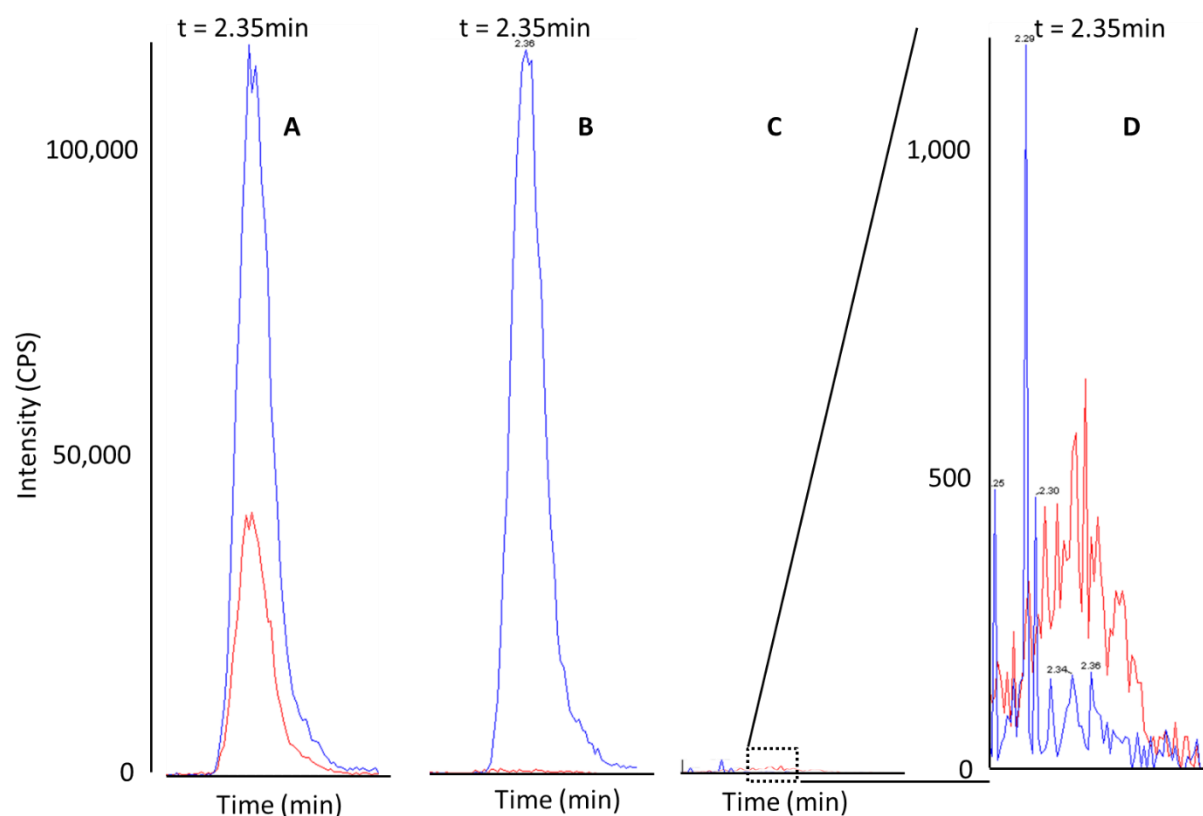
Figure 96 – HILIC-MS/MS Chromatogram of Acetylcholine and D4-Acetylcholine.

Chromatogram traces of intensity count per second (CPS) of an aqueous sample spiked with acetylcholine and D4-acetylcholine **(A)**, D4-acetylcholine alone **(B)**, double-blank which had neither **(C)**, and a zoom-in view illustrating the signal generated by the double blank **(D)**. Blue line represents D4-acetylcholine; red line represents acetylcholine.

Table 11 – Chromatogram Quantification.

Sample Type	Analyte Peak Area	IS Peak Area
Acetylcholine + D4-acetylcholine	177066	484255
D4-acetylcholine	3430	489418
Double Blank	1055	561

5.3 Method Validation

The developed HILIC-MS/MS method of quantifying acetylcholine in cultured media was validated using guidelines issued by the FDA (FDA 2018). These include determining the method's specificity and selectivity, its calibration curve linearity and signal-to-noise ratio, its accuracy and precision, its lower limits of detection and quantification, and analyte recovery.

5.3.1 Specificity and Selectivity

Specificity and selectivity were achieved by using multiple reaction monitoring (MRM) to determine the specific mass transition for the analytes of interest, which is measured by the mass divided by the ionic charge number (m/z). In other words, the specific mass transition of parent product ions (acetylcholine and D4-acetylcholine) and specific mass transition of their daughter fragment ions were determined to be selective for them and no other compound. The first mass transition occurs at the first quadrupole (Q1), where the detected 146.1 m/z and 150.2 m/z are specific for the parent product ion of acetylcholine and D4-acetylcholine, respectively. The second mass transition occurs at the third quadrupole (Q3), where the detected 86.0 m/z and 90.9 m/z are specific for the daughter fragment ions of acetylcholine and D4-acetylcholine, respectively. These values were determined by injecting 1 mg/ml of acetylcholine or D4-acetylcholine diluted in methanol into the mass spectrometer at a constant flow, then using the MRM scan function to identify the peak m/z values for the parent product ions at Q1 and daughter fragment ions at Q3.

5.3.2 Calibration Curve Linearity, Signal to Noise Ratio, and Lower Limits of Detection

A calibration curve had to be developed in order to quantify acetylcholine in culture media. A calibration curve to 100 nM was first developed in aqueous solution, which was quantified (Table 12) and determined to be linear ($R^2 > 0.95$), (Figure 97). This was then repeated in culture media (Figure 98). A batch of calibration curve standards was prepared in culture media, with one set extracted alongside each sample. The upper limit of linearity was done up to 1 mM (data not shown) but was not used since the working range found to be much lower. In order for a chromatogram peak to be accepted, the ratio of the peak signal to background noise (signal to noise ratio) must be greater than 10. This was also the lower limit of detection, which was less than 1 nM in both aqueous solution and culture media (data not shown).

Table 12 – Data Quantitation for Acetylcholine (0-100 nM) in Aqueous Solution.

Analyte Conc. (nM)	Analyte Peak Area	IS Peak Area	Area Ratio	Signal to Noise Ratio
100	818948	58165	14.08	2348.9
50	529455	68835	7.69	780.3
25	306816	62204	4.93	1427.1
12.5	204808	63916	3.2	941
6.3	160406	65937	2.43	512.1
3.1	84668	46685	1.81	235.5
1.6	129343	75512	1.71	167.6
0	17266	48610	0.36	27.9
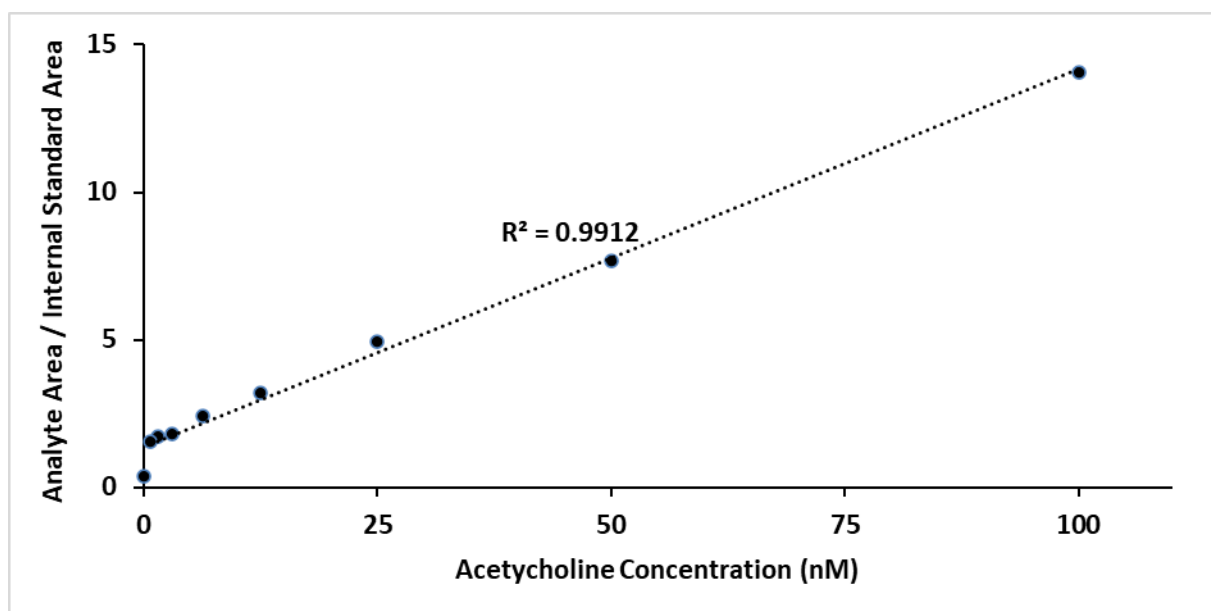
Figure 97 – Calibration Curve for Acetylcholine (0-100 nM) in Aqueous Solution.

Calibration curve of 0-100 nM acetylcholine spiked in UPLC-grade water. X-axis depicts concentration. Y-axis depicts area ratio (analyte area / internal standard area). R^2 value listed above.
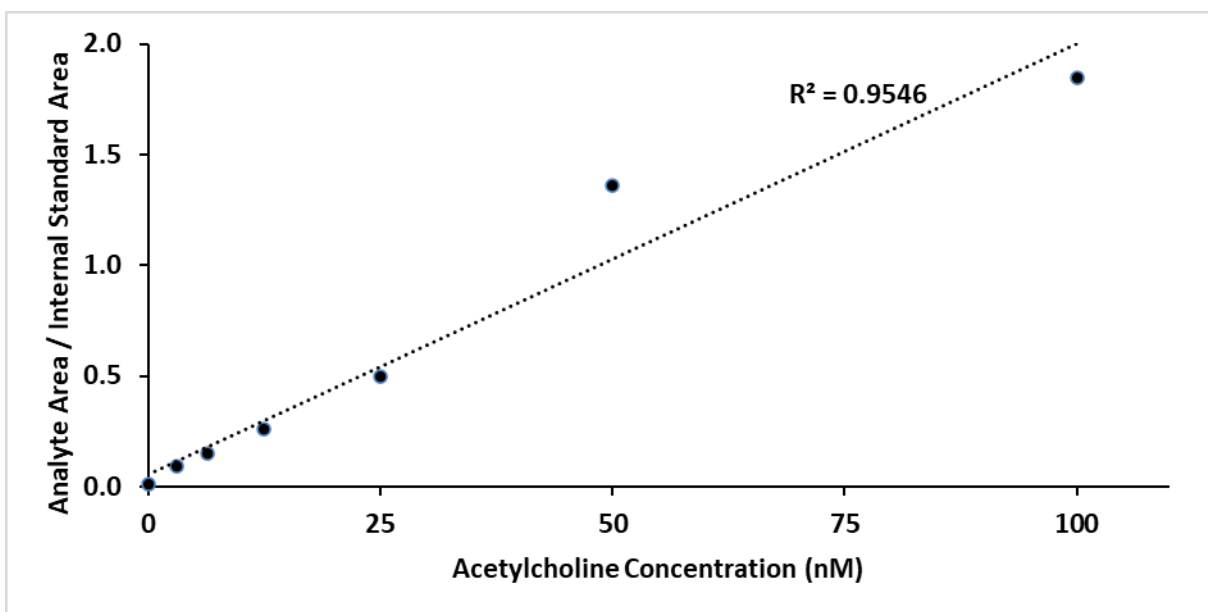
Figure 98 – Calibration Curve for Acetylcholine (0-100 nM) in Media.

Calibration curve of 0-100 nM acetylcholine spiked in blank culture media. X-axis depicts concentration. Y-axis depicts area ratio (analyte area / internal standard area). R^2 value listed above.

5.3.3 Accuracy, Precision, and Lower Limits of Quantification

In addition to the calibration curve, internal quality control (iQC) standards were made to assess the reliability and stability of the system for each sample analysed. To that end, a batch of low (6.3 nM) medium (25 nM) and high (100 nM) acetylcholine iQC standards were made in blank culture media. Ten sets of these iQCs were extracted and plotted on the calibration curve (Table 13) to determine the mean, standard deviation, coefficient of variation, and upper-lower limits. The upper-lower limits are defined to be +/- twice the standard deviations of the mean value. A set of iQCs were extracted alongside the calibration curve during each day of extraction to ensure the accuracy and precision of the HILIC-MS/MS protocol. Should more than one iQC fall outside the upper-lower limits and could not be resolved, the analysis was considered inaccurate.

With the calibration curve and iQCs established, the method was ready to quantify acetylcholine in media which had been cultured in crypts and organoids. During each day of extraction, the linearity ($R^2 > 0.95$) of the calibration curve must be confirmed (Table 14) and at least two of the iQCs must fall within the upper-lower limits (Table 15) to ensure intra-batch accuracy and precision. If necessary, up to three calibration curve standards were allowed to be ignored if it improved the linearity ($R^2 > 0.95$). The lower limit of quantification, which is defined as having the coefficient of variation of equal to or less than 15%, was calculated by plotting the coefficient of variation of the intra-batch calibration curve standards against the mean values. This value was determined to be around 11.5 nM. The lower limit of detection of the aqueous calibration curve (data not shown) was 3 nM.

Table 13 – Internal Quality Control Standards.

Set	Internal Quality Control Standards		
	Low (6.3 nM)	Medium (25 nM)	High (100 nM)
1	7.5	23.3	97.0
2	6.7	27.1	70.2*
3	6.3	31.1*	95.1
4	7.1	24.0	95.3
5	6.9	27.9	97.5
6	6.2	25.4	94.7
7	7.0	23.8	105.9
8	6.6	24.7	99.1
9	6.9	26.0	95.9
10	7.4	25.0	70.8*
Mean (nM)	**6.8**	**25.2**	**97.6**
Standard Deviation	**0.4**	**1.5**	**3.7**
Coefficient of Variation (%)	**6.0**	**6.1**	**3.8**
Upper-Lower Limits	**5.5-7.1**	**22.2-28.2.6**	**90.2-105.0**

* Values which fell outside the upper-lower limits were excluded from the analysis.

Table 14 – Intra-batch Calibration Curve Standards.

Date (yyyy-mm-dd)	Calibration Curve (nM)						
	100 nM	50 nM	25 nM	12.5 nM	6.3 nM	3.2 nM	0 nM
2018-10-10	91.9	*	20.3	10.9	*	*	<0
2018-10-16	96.3	43.8	24.6	10.7	*	3.7	<0
2018-11-1	95.4	42.3	25.8	11.1	*	2.5	<0
2018-11-20	97.7	47.9	22.6	*	4.6	*	<0
2018-11-28	94.0	43.7	21.5	*	*	2.4	<0
2018-14-04	87.1	*	24.8	*	5.2	2.1	<0
2019-01-18	*	52.1	23.7	*	6.7	4.4	<0
2019-02-26	*	41.7	26.2	*	6.4	*	<0
2019-03-05	86.1	58.2	28.4	*	*	*	<0
2019-03-12	86.0	55.6	23.3	14.4	5.6	*	<0
2019-03-22	91.3	*	31.7	*	*	2.3	<0
2019-05-03	*	44.4	23.1	10.8	6.3	2.2	<0
Mean (nM)	**91.7**	**47.8**	**24.7**	**11.6**	**5.8**	**2.8**	**0**
Standard Deviation	**4.5**	**6.1**	**3.1**	**1.6**	**0.8**	**0.9**	**0**
Coefficient of Variation (%)	**4.9**	**12.9**	**12.5**	**13.5**	**14.0**	**31.6**	**N/A**

* Value ignored to improve calibration curve linearity.

Table 15 – Intra-batch Internal Quality Control Standards.

Date (yyyy-mm-dd)	Internal Quality Control Standards		
	Low (6.3 nM)	Medium (25 nM)	High (100 nM)
2018-06-05	6.0	22.2	141.4*
2018-06-08	6.1	31.9*	101.9
2018-06-11	6.5	24.0	99.0
2018-06-12	6.3	25.7	87.7
2018-06-22	7.5*	25.2	95.3
2018-06-25	5.3	23.4	93.3
2018-06-26	5.3	24.5	91.5
2018-07-24	5.3	25.9	92.9
2018-07-31	6.9	22.7	96.6
2018-08-08	7.3*	27.3	98.0
2018-08-29	6.7	25.0	94.6
2018-10-10	8.2*	30.7*	94.7
Mean (nM)	**6.4**	**25.7**	**95.0**
Standard Deviation	**0.9**	**3.0**	**3.1**
Coefficient of Variation (%)	**14.5**	**11.6**	**4.1**

* Values which fell outside the upper-lower limits.
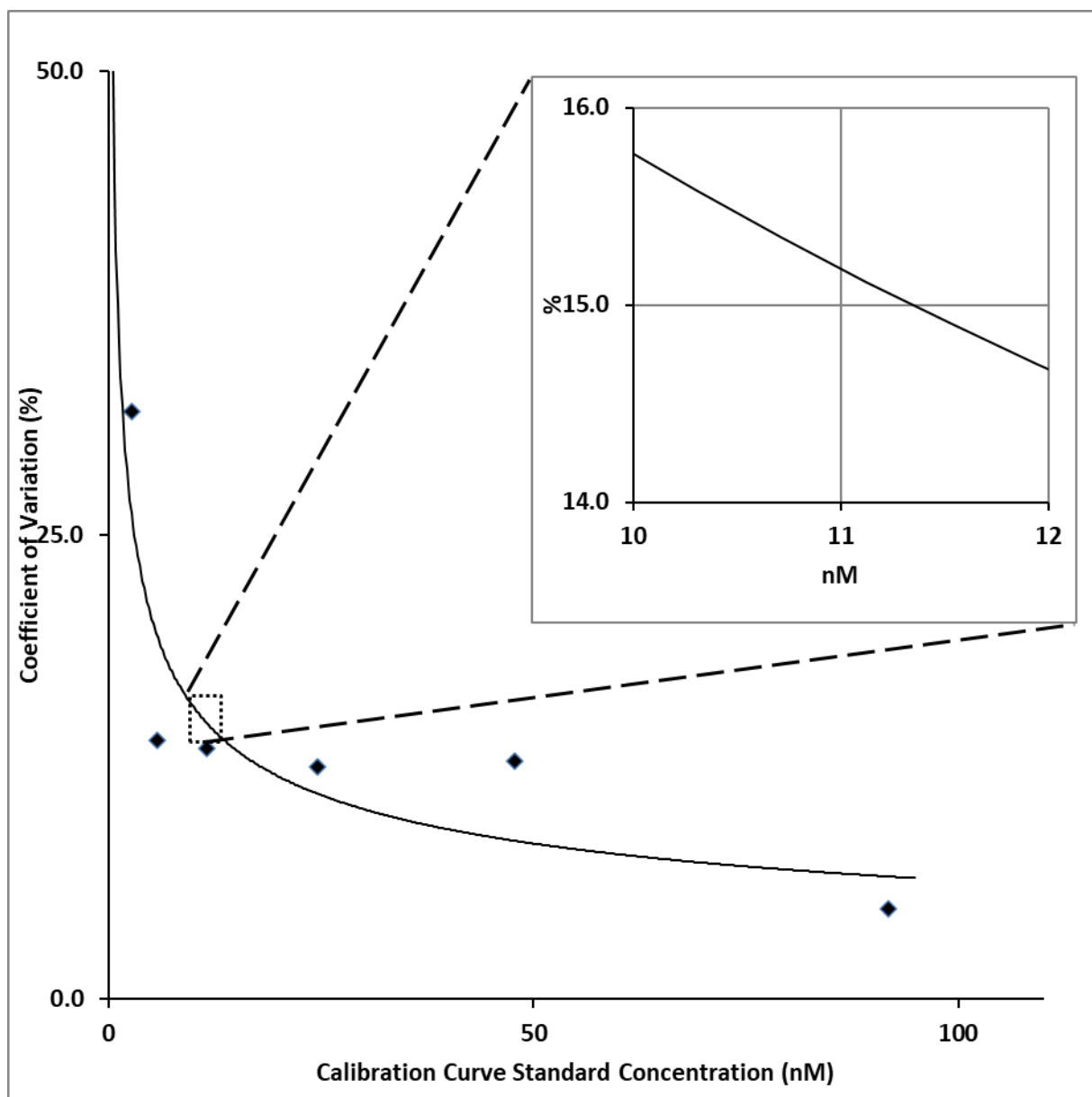
Figure 99 – HILIC-MS/MS Lower Limits of Quantification for Acetylcholine

Line graph of the mean calibration curve standard concentration (nM) plotted agaisnt the coffecient of variation (%), and the zoomed in view of the line graph showcasing the lower limit of detection (CV 15%).

5.3.4 Analyte Recovery

Lastly, the effect of Matrigel and the efficiency of the developed HILIC-MS/MS protocol was evaluated by calculating the recovery of a known quantity (100 nM) of analyte – acetylcholine – which had been spiked into sample media. The recovery of the spiked analyte ranged between 76.9-133.5%, averaging 104.7% with a standard error of 3.8%.

5.4 Results

First, choline acetyltransferase (ChAT) was shown to be expressed in the colonic epithelium using immunolabelling and its expression was shown to be higher towards the bottom half of the crypt. Next, HILIC-MS/MS was used to quantify the amount of non-neuronal acetylcholine present in media which had been cultured in crypts. Finally, Fura-2 experiments were carried out to show that culture media was capable of inducing Ca^{2+}-signals.

5.4.1 Differential ChAT Expression in the Colonic Epithelium

In an earlier chapter, ChAT was shown to be expressed within mucosa and crypts, but not in organoids (Figure 51). However, this was confined to the base of crypts. Thus, confocal images of whole human native colonic tissue (mucosa), cultured human colonic crypts (crypts), and cultured human colonic organoids (organoids) that were immunolabelled with ChAT were carried out. In mucosa, ChAT labelling was contained within slender cells, which were more prominent towards the lower half of crypts (Figure 100A). In crypts, ChAT labelling was prominent in the lower half of crypts and rare higher up the crypt (Figure 100B). In organoids, ChAT labelling was consistently absent (Figure 100C).

Next, the number of ChAT+ cells were counted in immunolabelled mucosa from six patients (N=6), during which at least three mucosal crypts (n=/>3) were counted for each patient. The average number of ChAT+ cells within the lower half of mucosal crypts was significantly higher (P<0.05) compared to the average number of ChAT+ cells within the upper half of mucosal crypts (Figure 101). Data contributed by Mr Luke Tye.

5.4.2 Quantification of Acetylcholine in Media Cultured in Colonic Tissue

Having confirmed the presence of ChAT in mucosal crypts, we set out to quantify the amount of acetylcholine synthesized by crypts which were isolated and cultured from the human colonic mucosa. Using the developed (Chapter 5.2) and validated (Chapter 5.3) HILIC-MS/MS method, non-neuronal acetylcholine was quantified in media that had been cultured overnight in crypts isolated from eight patients (Table 16). Media which had been cultured in crypts overnight contained non-neuronal acetylcholine ranging from 22.0 to 124.2 nM, with an average of 69.6 nM.
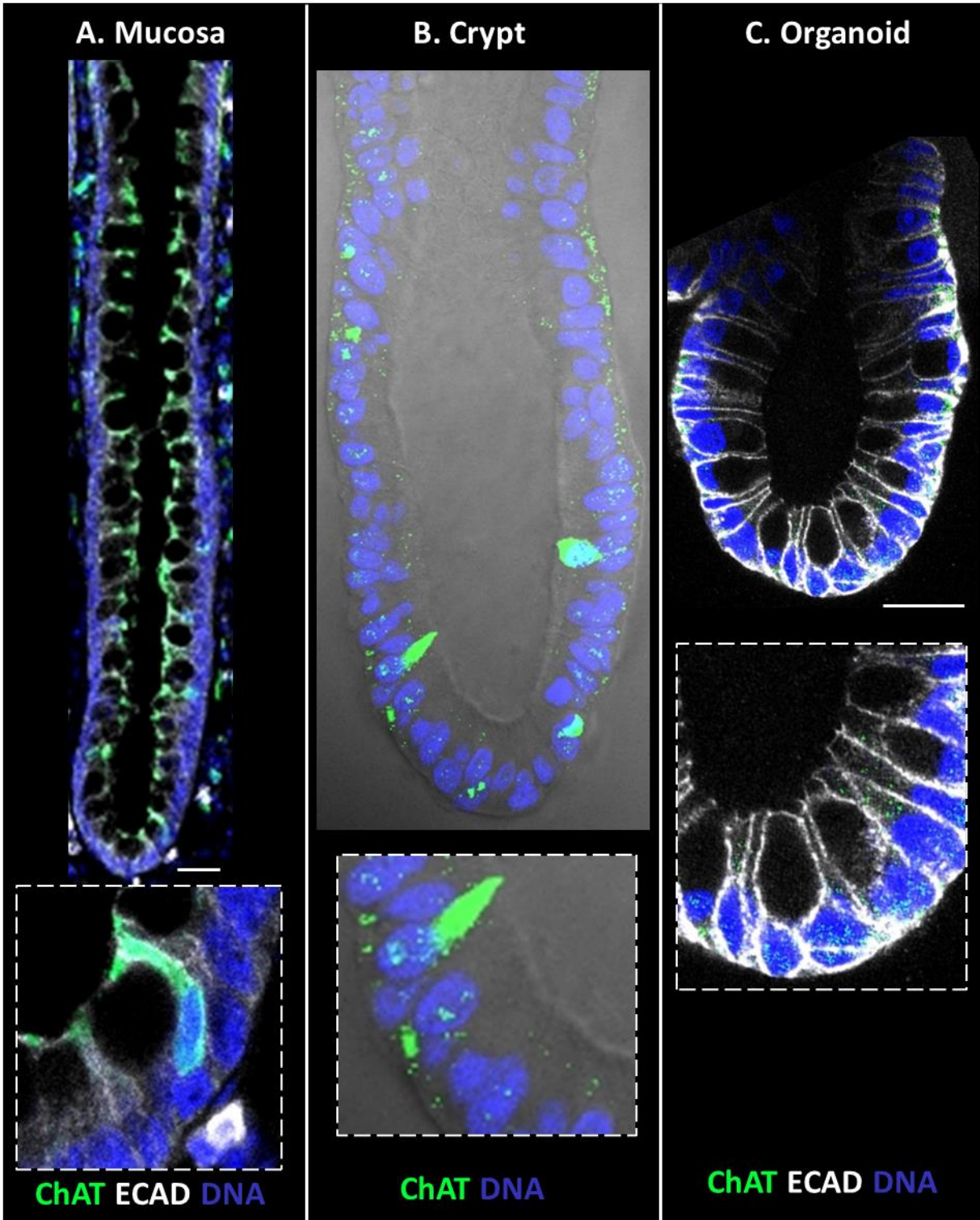
Figure 100 – Immunolabelling of ChAT in Mucosa, Crypts, and Organoids.

Representative confocal images of ChAT immunolabelled in mucosa **(A)**, crypts **(B)**, and organoids **(C)** with E-Cadherin (ECAD) in white and ChAT in green. Nuclei was stained with Sytox Blue (DNA). Brightfield depicted on the left. Scale bar = 25 µm.
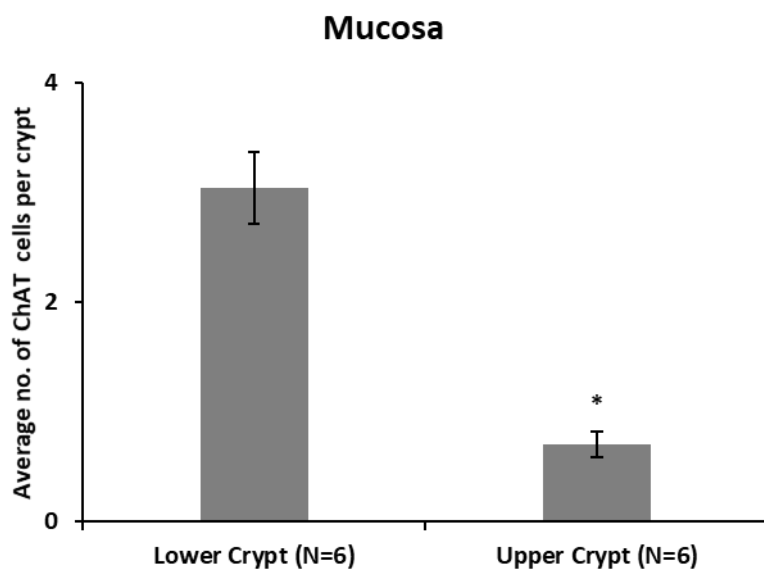
Mucosa

Figure 101 – Average Number of ChAT+ Cells in Mucosal Crypts.

ChAT+ cells were counted within the lower and upper half of immunolabelled mucosal crypts. P>0.05 (*).

Table 16 – Quantification of Non-neuronal Acetylcholine from Crypt-Cultured Media.

Patient ID (yyyy-mm-dd)	Quantified acetylcholine (nM)
2018-11-01	97.7
2018-11-06	124.2
2018-11-07	100.1
2018-11-20	68.2
2018-11-28	32.9
2018-12-04	110.8
2019-01-18	31.9
2019-01-22	22.0
2019-03-12	8.62*
2019-03-22	38.6
Average (nM)	**69.6**
Standard Error	**11.7**

* Value which fell outside the lower limit of quantification and thus not included.

Besides quantifying non-neuronal acetylcholine, this thesis attempted to increase the amount of acetylcholine synthesized/secreted by crypts. One means of achieving that was the addition of propionate (2 mM) into the culture media, which in Ussing chamber experiments was shown to induce release of acetylcholine across the basolateral membrane of rat colonic mucosa (Bader, Klein and Diener 2014). To that end, crypts which were isolated from three patients (N=3) were cultured overnight with media which did/did not contain propionate (2 mM). The non-neuronal acetylcholine from these crypt-cultured media was quantified and found to not be significantly different (Figure 102). In addition to the quantification provided by post-HILIC-MS/MS data analysis, the amount of acetylcholine secreted by each crypt was estimated. First, images of the cultured crypts were taken on the Nikon microscope and counted (Figure 103). Next, the amount of acetylcholine quantified was divided by the number of crypts (Figure 104), which was also shown to not be significantly different. Data contributed by Mr Luke Tye.
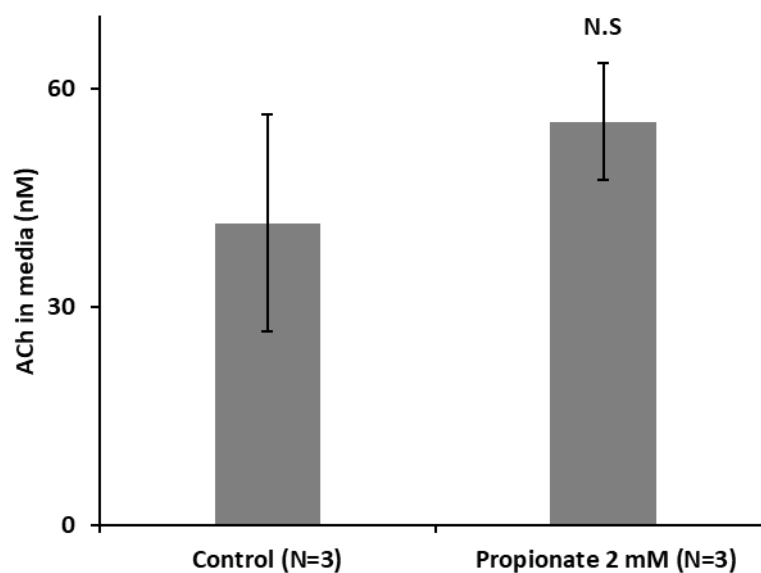
Figure 102 – Propionate Has No Effect on Acetylcholine Concentration in Crypt-Cultured Media.

HILIC-MS/MS quantification of non-neuronal acetylcholine from crypt-cultured media in the presence/absence of propionate (2 mM). Not significant (N.S). N=3.
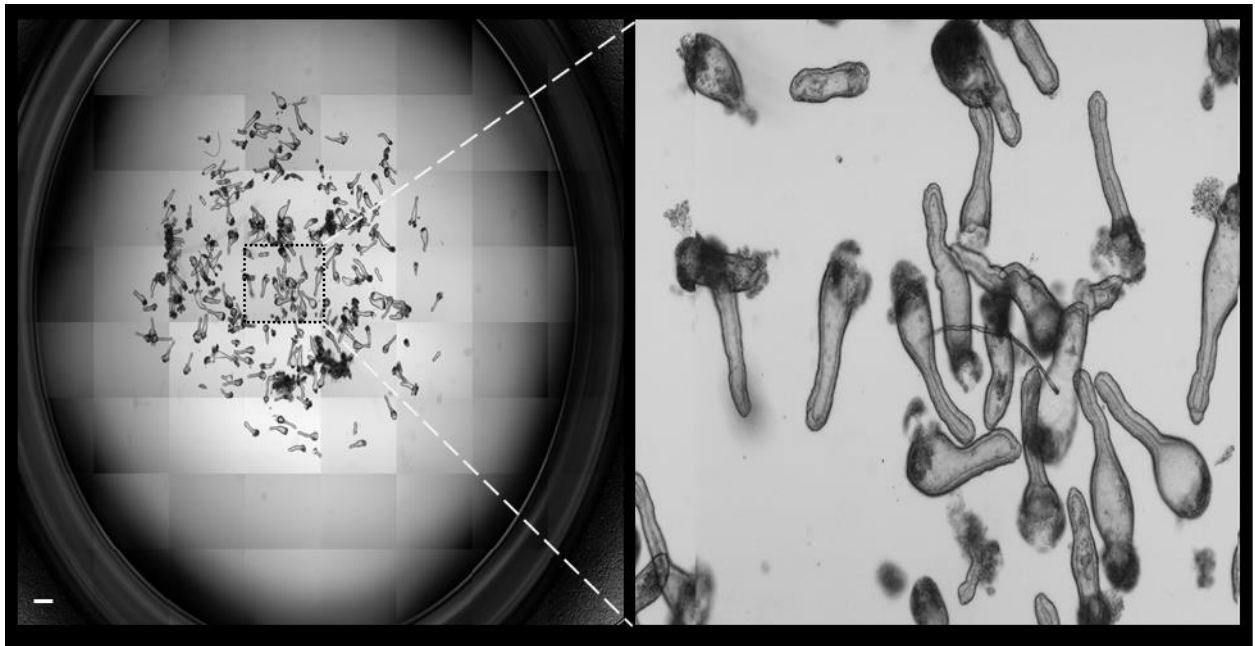
Figure 103 – Brightfield Images of Isolated Human Colonic Crypts.

Representative brightfield image of isolated human colonic crypts within a well of a 24-well plate.
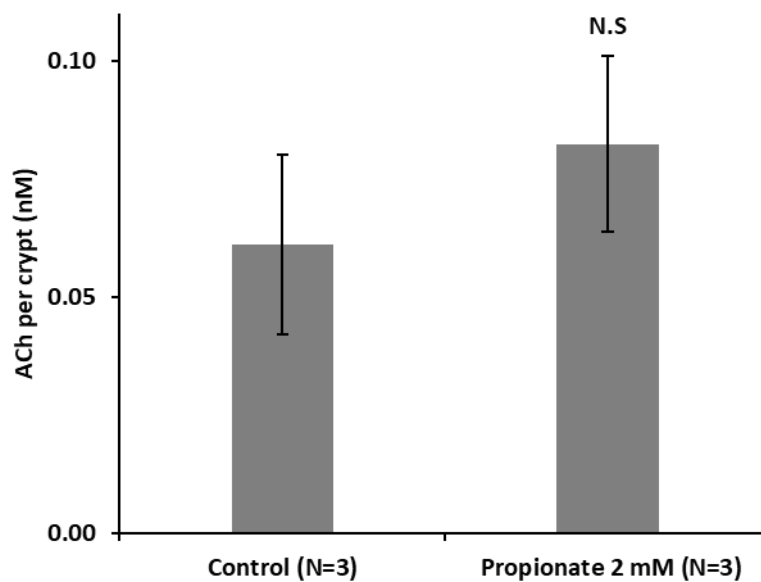
Figure 104 – Propionate Did Not Increase Acetylcholine Synthesis/Secretion.

Alterative quantification of non-neuronal acetylcholine from crypt-cultured media in the presence/absence of propionate (2 mM). Not significant (N.S). N=3.

5.4.3 Crypt-Culture Media Induces Ca^{2+}-Signals.

In the previous chapter (Chapter 4), CCh (10 µM) was shown to be capable of inducing intracellular Ca^{2+}-signals in crypts and organoids loaded with the Ca^{2+}-sensitive ratiometric fluorescent dye, Fura-2. Through a series of experiments, CCh was elucidated to activate muscarinic receptor type 3 (M3) and causing local Ca^{2+}-signals via endolysosomal TPCs followed by global Ca^{2+}-signals via endoplasmic reticular IP3Rs and RYRs. Thus, crypt-culture media was proposed to also be capable of inducing intracellular Ca^{2+}-signals in crypts loaded Fura-2. Indeed, preliminary experiments showed that crypt-culture media which was quantified to contain acetylcholine (90 nM) was capable of inducing intracellular Ca^{2+}-signals in crypts (Figure 105) and could be inhibited by atropine, a non-specific antagonist of muscarinic receptors (McLendon and Preuss 2021). Data contributed by Mr George Lines.
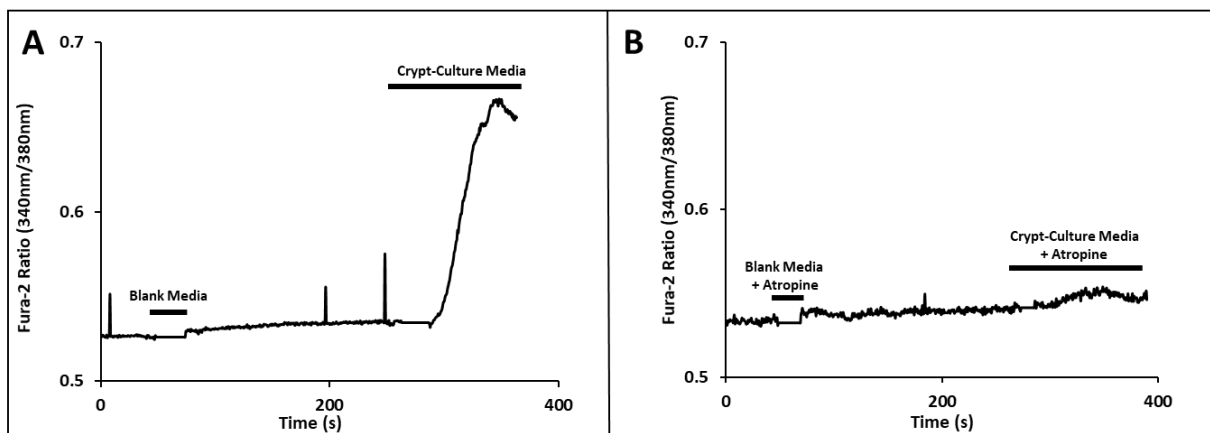
Figure 105 – Crypt-Culture Media Induces Ca^{2+}-Signals.

Exemplar trace of a crypt which was first stimulated by blank media followed by crypt-cultured media **(A)**, and with the presence of atropine **(B)**. N=1.

5.5 Discussion

In humans, non-neuronal acetylcholine has been quantified using UPLC-MS/MS in peripheral blood (Zhang, et al. 2016) and (Han, et al. 2017). In the context of the human GI, quantification of non-neuronal acetylcholine using mass spectrometry has not been done before. The closest to this is a study which used HPLC-MS/MS to quantify non-neuronal acetylcholine in mice (Takahashi, et al., 2014). Thus, this thesis set out to develop a novel method to quantify non-neuronal acetylcholine in human colonic crypts and organoids.

5.5.1 Sample Preparation and Extraction

The first step involved in sample preparation was the addition of rivastigmine (final concentration of 1 mM) into the culture media to inhibit the hydrolysis of acetylcholine by acetylcholinesterase (Willams, Nazarians and Gill 2003). In addition, rivastigmine is also capable of inhibiting butyrylcholinesterase (Kandiah, et al. 2017), which has a lower catalytic efficiency of hydrolysing acetylcholine, but contributes to acetylcholine homeostasis (Reale, et al. 2018). The next step of centrifugation was to separate culture media from insoluble components. Just prior to extracting the sample using WCX, the sample was filtered through a 10 µm cell strainer to remove residual (Matrigel and colonic tissue) which may interfere with the extraction and analysis.

One of the advantages of tandem mass spectrometry is that it is highly selectivity due to MRM using the instrument's triple quadrupole, which allows the bypass of time-consuming clean-up steps (Nie and Nie 2019). However, HILIC columns and the mass spectrometer are prone to contamination with components within culture media such as proteins, amino acids, and peptides. Contamination of the HILIC column results in the shift in analyte retention time and poor peak shape. Despite manufacture guidelines and customer service advice, contamination of the HILIC column was irreversible and expensive to replace. On the other hand, contamination of the mass spectrometer resulted in increased machine and background noise which affects the analysis and requires a specialist engineer to service. Hence, a sample preparation and extraction protocol was developed to remove as many contaminants as possible to preserve the HILIC column's lifespan and ensure the mass spectrometer's machine and background noise remained low.

The use of an internal standard – D4-acetylcholine – served as an inter-batch and intra-batch control. Being an isotopically labelled version of acetylcholine, D4-acetylcholine would be expected to have a similar extraction recovery, chromatographic retention time, and ionization response in the mass spectrometer's source. D4-acetylcholine (100 nM) was added to each extracted sample, calibration curve standard, and iQC. The internal standard peak area (IS Peak Area) showcases the variation of each extraction (Table 12), which can be negated by using ratio between the analyte peak area and the IS peak area, thereby serving as an inter-batch control. The D4-acetylcholine methanol stock solution (1 mg/ml) is kept at

negative 20ºC; each day a fresh batch was prepared in UPLC-grade water (100 nM). Large variation of the IS peak area from one day to another would indicate human or machine error had occurred at some point, thereby serving an intra-batch control.

As described, an early variant of the WCX extraction protocol (Figure 91) included a drying and reconstitution stage as recommended by the manufacturer. However, the drying process was slow and caused the analysis to be less reliable, hence that step was modified and removed. Other variables which were trialled during the method development phase included the composition of the elution solution (100% acetonitrile vs 80%), the concentration of formic acid in the elution solution (1-10%), the prospect of increasing sample load or reducing the elution solution, the necessity of removing HEPES buffer in culture media, and the UPLC-grade water used (Sigma-Aldrich vs VWR).

5.5.2 HILIC-MS/MS Method Development and Validation

The HILIC-MS/MS method was developed by configuring and optimising the HILIC column (Figure 92) and (Table 10), the Shimadzu LC-20 HPLC system (Chapter 5.2.2), and the API 4000 tandem mass spectrometer (Chapter 5.2.3). Next, the method was validated following guidelines from the (FDA 2018). After which, the method was applied to quantify non-neuronal acetylcholine from media cultured in human colonic crypts and organoids. Instrument and software training began in October 2016. By February 2019, the method had been developed, validated, and applied.

The developed method was validated to be specific and selective for acetylcholine, due to the instrument's triple quadrupole which enables MRM to determine the specific mass transition for the analytes of interest. Compared to the calibration curve prepared in aqueous solution (Figure 97), the linearity of the calibration curve prepared in media was less robust (Figure 98) and had to be selective (Table 14). The signal to noise ratio was low in aqueous spiked samples (Figure 96) and produced clear chromatogram peaks for acetylcholine and D4-acetylcholine. But once media standards were used instead, the signal to noise ratio worsened, the chromatogram peak shape suffered and the analyte peak area was reduced. In addition, the background noise gradually increased over time, indicating the API 4000 tandem mass spectrometer was gradually being contaminated by sample injections.

Batches of iQC standards were run during each extraction to ensure the accuracy of inter-batch and intra-batch analysis. When ten sets of iQCs standards were run (Table 13), the coefficient of variation for the lowest standard (6.3 nM) was 6%, meaning the method and analysis was reliable, consistent, and had an inter-batch lower limit of quantification that's less than 6.3 nM. However, the intra-batch records for iQC standards (Table 15) showed higher coefficients of variation at each point. The coefficient of variation for the iQC standards

closely resembled the coefficients of variation of the intra-batch records for the calibration curve standards (Table 14), from which the intra-batch lower limit of quantification determined to be around 11.5 nM. In order words, this method could accurately quantify non-neuronal acetylcholine in culture media down to 11.5 nM with a 15% coefficient of variation.

One concern about this method is internal bias, as the calibration standards, iQC standards, extraction and analysis were all carried out by one person. An ideal solution to that are external standards, which would be prepared, extracted, and analysed for each analytical set. However, there were no available sources of external standards for acetylcholine in cultured media during this thesis.

5.5.3 Differential ChAT Expression, Acetylcholine Quantification, and Ca^{2+}-signals

In both mucosa and crypts, ChAT labelling was observed higher within the lower half of the crypt compared to the upper half (Figure 100A-B). And in organoids, ChAT was non-existent (Figure 100C). This data supports the RNA gene transcriptomic data from earlier (Figure 29) which showed expression of ChAT RNA in mucosa and crypts, but no ChAT RNA in organoids. This reflects a shortcoming of the culture system, whereby it was unable to fully replicate the in-vivo environment support ChAT+ cells. Despite that setback, non-neuronal acetylcholine was successfully quantified from media which had been cultured overnight in crypts isolated from patients' mucosa samples (Table 16). Media which had been cultured overnight in organoids were also put through HILIC-MS/MS, and unsurprisingly they yielded no acetylcholine (data not shown). Of the samples quantified, one data point (8.6 nM) was considered under the lower limit of quantification. Due to this, its accuracy cannot be assured to be within a CV of 15% and hence was omitted. In addition, two data points were extrapolated since they were higher than the upper calibration curve standard (100 nM). Thus, future batches of calibration curve standards should have a higher upper limit to avoid extrapolation. Ideally, the upper iQC should be 20% higher than the maximum expected analyte quantification. Thus, future iQC batches should have an upper limit of 150 nM. One highlight from this dataset was the variability of quantified acetylcholine (8.6-124.2 nM), when even though during the isolation and plating stage, the density distribution of crypts within each well was ensured to be largely equal between samples. This may be due to the condition of the patient mucosa which the Williams group obtains tissue samples from. For example, a patient which has colon cancer may have different numbers of ChAT+ cells depending on the cancer stage and location. While these samples were obtained from distal sites of the surgery during right-hemicolectomy or anterior resection, it is not possible to determine whether these samples are truly 'normal when compared to a healthy individual. In addition to health status, other factors such as age and chemotherapy may influence the numbers of ChAT+ cells and would need to be considered in future attempts of quantifying non-neuronal acetylcholine.

In addition to quantifying non-neuronal acetylcholine, this thesis attempted to increase the amount of acetylcholine synthesized/secreted by crypts using propionate (2 mM). As described in the introduction, propionate is a short-chain fatty acids (SCFAs) metabolised by gut microbes from the catabolism of carbohydrates and starches which the human gut cannot digest (Hollister, Gao, & Versalovic, 2015). Propionate and other SCFAs have been shown to stimulate mucus secretion (Willemsen L. E., Koetsier, van Deventer, & van Tol, 2003) and regulate host immunity (Brown, et al., 2003). While propionate did increase the amount of acetylcholine quantified in the culture media (Figure 102) and per crypt (Figure 104), this difference was not significant. By contrast, the study (Bader, Klein and Diener 2014) which showed propionate stimulating acetylcholine release measured baseline acetylcholine release to be 1.8+/-0.4 (nmol/min), while propionate (2 mM) caused an increase in acetylcholine release of 15.8+/-4.3 (nmol/min). However, as described in the study's methodology, these experiments were conducted in mucosa samples. As the mucosa also contains myofibroblasts, blood vessels, nerves, and immune cells (Chapter 1.2), it is plausible that the acetylcholine they measure are secreted from non-epithelial cells. In addition, their observation was done using a short experiment where acetylcholine release was measured after several minutes of adding propionate. On the other hand, the quantification of acetylcholine in this thesis was done on media which had been cultured overnight. Furthermore, their HPLC samples were contained within buffered bathing solutions, which are far less likely to interfere with the extraction and HILIC-MS/MS method developed here. Indeed, the limit of detection of their system was 1 fmol. Finally, crypt-culture media was shown to be capable of inducing Ca^{2+}-signals in crypts loaded with Fura-2 and could be inhibited by atropine (Figure 105), which supports the hypothesis that cholinergic agonists (acetylcholine, carbachol) activate muscarinic receptors.

5.6 Conclusion

In conclusion, a standard operating protocol (SOP) for extracting, detecting, and quantifying non-neuronal acetylcholine from media which had been in culture in human colonic crypts was developed, and validated using FDA guidelines. Using this SOP, non-neuronal acetylcholine was quantified in crypt-cultured media. The concentration of acetylcholine quantified (90 nM) was found to be physiologically relevant, as it was capable of inducing Ca^{2+}-signals in crypts loaded with Fura-2. Now, the thesis moves on to investigate the consequences of mobilising intracellular Ca^{2+} stores on colonic epithelial physiology – namely mucus and fluid secretion, and proliferation.

6   Chapter 6 – Results Part 4: Physiological Consequences of Mobilising Intracellular Ca²⁺ Stores – Excitation-Mucus/Fluid Secretion and Proliferation

6.1 Introduction

As described in the introduction (Chapter 1.2), the monolayer intestinal epithelium is a semipermeable barrier separating the luminal contents of the intestines from the internal milieu (Figure 7), thereby protecting the host from threats originating or residing in the gut lumen. The secretion of mucus by goblet and DCS cells, and fluids by all epithelial cells, is an important means by which the intestinal epithelium prevents itself from coming into contact pathogens and unwanted substances. Among these, goblet cells are the most numerous; they comprise between 9-16% of the intestinal epithelium (Umar, 2011) and (Kim & Ho, 2010). On the other hand, Paneth cells (Sato, et al., 2011) and DCS cells (Sasaki, et al., 2016) intermingle with stem cells at the bottom of small intestinal and colonic crypts, respectively. Notably, DCS cells can be marked by MUC2 (Rothenberg, et al., 2012), implying these cells secrete mucus to flush away the luminal contents of the crypt and thereby protect the stem cell zone.

Intestinal epithelial mucous synthesis, processing, and secretion is a complex pathway (Chapter 1.2.1). Briefly, is an aqueous viscoelastic secretion whose composition varies depending on their underlying secretory epithelium, which affects its physicochemical properties such as pore size, viscoelasticity, pH, and ionic strength (Leal, Smyth, & Ghosh, 2018). The major structural component of mucus are mucin glycoproteins, of which seventeen genes have been identified in humans (NCBI, 2020) and twelve of which are present in the human GI tract. Mucins can be classified as transmembrane or gel-forming (Table 1.3). In both the small intestine and colon, MUC2 is the prominent gel-forming mucin secreted by goblet cells. Intestinal mucus secretion can be induced by a host of secretagogues. These include propionate, acetate, and butyrate (Willemsen L. E., Koetsier, van Deventer, & van Tol, 2003), bacterial infection activation of the NLRP6 inflammasome (Wlodarska, et al., 2014), reactive oxygen species (Patel, et al., 2013), ATP (Kreda, et al., 2010), and acetylcholine (Specian & Neutra, 1980).

Intestinal epithelial fluid secretion is driven by the movement of anions such as chloride ions across the lumen, accompanied by water through osmosis. In the colonic epithelium, chloride ion uptake is mediated by the Na⁺-K⁺-2Cl⁻ (NKCC1) co-transporter located on the basolateral membranes (Bachmann, et al. 2003). On the apical membrane of epithelial cells, cystic fibrosis transmembrane conductance regulator (CFTR) channels regulate the movement of chloride ions into the lumen (Greger 2000). Through the calcium-activated chloride channel regulator 1 (CLCA1), chloride ions are also involved in the production and processing of mucus by goblet cells of the colon (Nyström, Arike, Ehrencrona, Hansson, & Johansson, 2019). Intestinal fluid secretion can be induced by a range of secretagogues. These include 5-HT (Diwakarla,

Fothergill, Fakhry, Callaghan, & Furness, 2018), serotonin (Alcaino, et al., 2018), and acetylcholine (Reynolds, Parris, et al. 2007).

Mucus secretion, fluid secretion and proliferation of the intestinal epithelium are dependent on intracellular Ca^{2+}-signals (Chapter 1.4.3). Activation of the muscarinic acetylcholine receptor 3 (M3) by acetylcholine induces intracellular Ca^{2+}-signals modulates NKCC1 trafficking to the membrane, which regulates Cl^- uptake and subsequent fluid secretion (Reynolds, Parris, et al. 2007). A latter study showed this process is activated via muscarinic receptors and mediated Ca^{2+} release via IP3R (Yang, et al. 2018). CLCA1 plays an essential role in the production and processing of mucus within goblet cell. It also contributes to mucus homeostasis by converting the firm inner mucus layer to the loose outer mucus layer and is dependent on Ca^{2+}, as removing Ca^{2+} from the proteolysis assay buffer blocked the reaction (Nyström, et al., 2018). Mucus exocytosis relies heavily on SNARE proteins to regulate the fusion of mucus granules with the plasma membrane. Syntaxin is a SNARE protein which has been shown to be Ca^{2+}-dependent and serves as a critical sensor of stimulated mucin secretion (Pang, et al., 2006) and (Adler, Tuvim, & Dickey, 2013).

Besides secretion of mucus and fluid, the intestinal epithelium rapidly renews and replenishes itself, a process known as tissue homeostasis. This process is driven by intestinal stem cells (ISCs) which reside at the bottom of intestinal crypts (Chapter 1.3.1) and are well characterized by the marker Lgr5 (Barker, et al., 2007). ISCs are sensitive to physiological and pathological injuries, as well as ionizing radiation. However, the intestine is capable of regenerating ISCs from quiescent DNA label-retaining cells (Buczacki, et al., 2013) and/or from epithelial cell plasticity such as secretory progenitor cells (van Es, et al., 2012). ISCs of the small intestines and colon are supported by Paneth cells (Sato, et al., 2011) and DCS cells (Sasaki, et al., 2016), respectively. These cells and others maintain the stem cell zone by ensuring a high level of Wnt and Notch signalling, while keeping BMP and TGF levels low (Gehart and Clevers 2019).

Previous work by the Williams group showed that cholinergic stimulation of M3 mobilises Ca^{2+} stored within endolysosomal via TPCs, causes mucus secretion, and induces proliferation (Kam 2015); which can be inhibited by blocking TPCs but not IP3Rs (Pelaez-Llaneza 2019). This chapter aims to elaborate on those studies, by investigating whether the physiological consequences (mucus secretion, fluid secretion, and proliferation) of the mobilisation of Ca^{2+} stored within endolysosomes are affected by specific and non-specific pharmacological antagonists which were explored in the previous chapter. This chapter also attempts to visualize mucus secretion and compound exocytosis induced by cholinergic stimulation using the cell permeable dyes FM1-43, FM1-43X, and Cell Tracker™ Deep Red.

6.2 Results

Experiments investigating mucus secretion (Chapter 2.8), fluid secretion (Chapter 2.9) and proliferation (Chapter 2.10) were carried out in human colonic crypts and organoids. First, cholinergic activation of muscarinic receptor signalling was shown to induce mucus secretion, which was inhibited using selective pharmacological agents. This was carried out in crypts which were immunolabelled with MUC2, in the presence/absence of CCh and/or pharmacological agents. Next, fluorescence lipid dyes were used to visualize secretion and compound exocytosis of mucus granules upon cholinergic stimulation. This was carried out in crypts and organoids using live confocal imaging. In addition, cholinergic activation of muscarinic receptor signalling also induced fluid secretion and was also inhibited using selective pharmacological agents. This was carried out in organoids cultured over days in the presence/absence of CCh and/or pharmacological agents. Finally, cholinergic activation of muscarinic receptor signalling was shown to promote proliferation and could also be inhibited pharmacologically. This was carried out in crypts labelled with EdU in the presence/absence of CCh and/or Ned-19. Some of these data were contributed by Dr Nicolas Pelaez Llaneza, Dr Victoria Jones, and current PhD candidate Mr Sean Tattan.

6.2.1 CCh-Induced Mucus Secretion is Dependent on Ca^{2+} Released by TPCs and RYRs

Immunolabelling of MUC2 was done in whole human native colonic tissue (mucosa), cultured human colonic crypts (crypts), cultured human colonic organoids (organoids), and single cells. MUC2+ cells were present throughout the mucosa, crypts, and organoids (Figure 106A-C top), including within the stem cell zone at the base (Figure 106A-C bottom). Previous work by the Williams group showed that the percentage of MUC2+ cells are approximately 30% in all three tissue models and are expressed higher within the base of mucosa and crypts compared to the top (Pelaez-Llaneza 2019). In addition to those three, single cells were generated by degrading organoids enzymatically and mechanically, then plated as a heterogeneous cell population. MUC2 immunolabeling and confocal imaging was carried out on these single cells (Figure 106D) using the standard protocol (Chapter 2.5).

Next, mucus depletion assays were carried out following a developed protocol (Patel, et al., 2013) which had been used by the Williams group. First, the temporal characteristics of mucus secretion was determined. Crypts were stimulated with CCh (10 µM) for varying amounts of time (1, 5, 10, 15, 20, and 30 minutes) before fixing and immunolabelling them with MUC2 (Figure 107). Between 1 to 30 minutes (Figure 107A-F), MUC2 fluorescence gradually changed from being solely contained within the cells' cytoplasmic space to being present in the crypt lumen. Mucus secretion was observed to occur within 5 minutes, due to depleted MUC2-labelling on the apical pole of cells (Figure 107B). From 10 minutes onwards, goblet-shaped cells were observed to have less MUC2 within their apical region, which indicate mucus secretion (Figure 107C). After ten minutes, there were prominent quantities of MUC2-labelling within the lumen (Figure 107C-F).
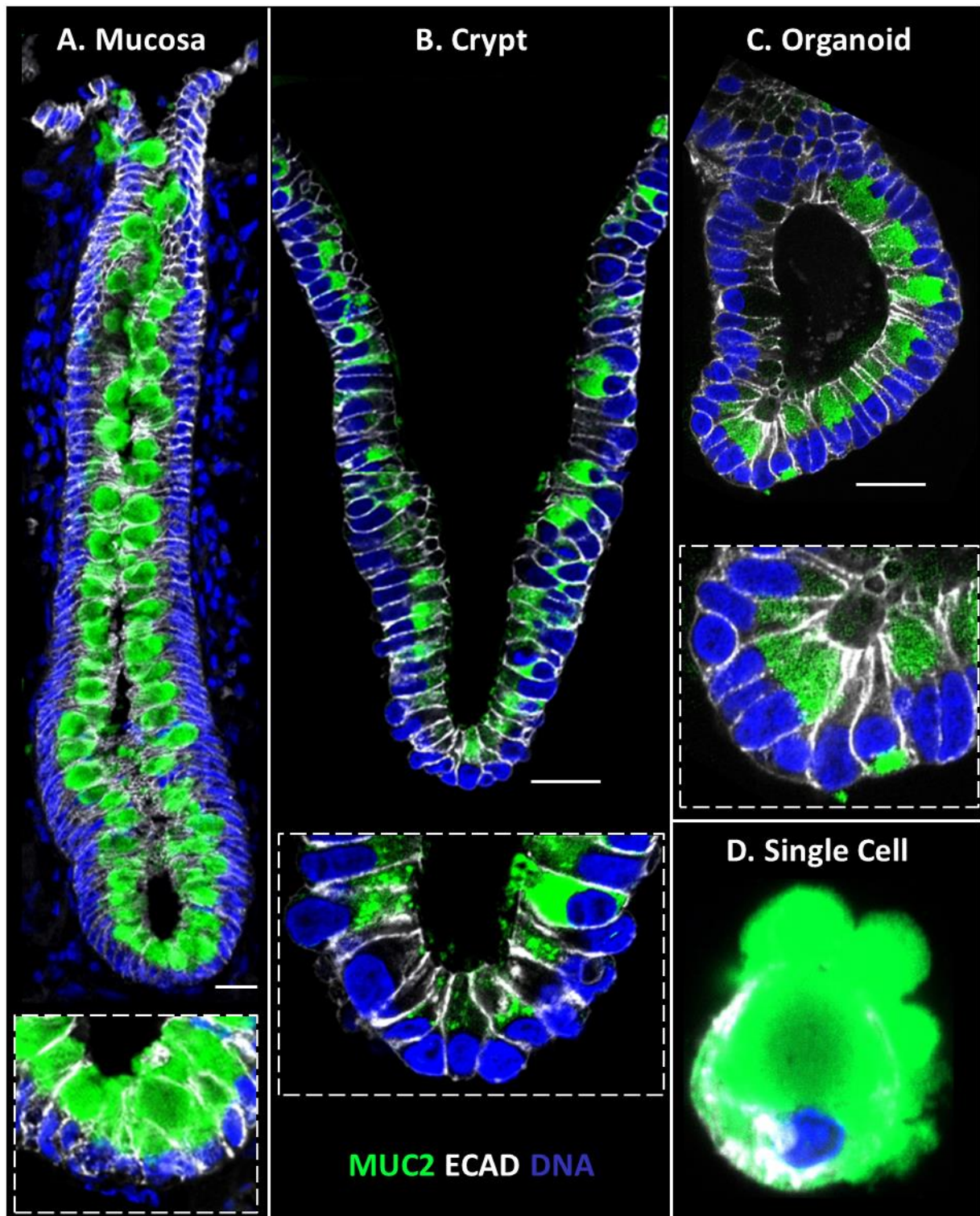
Figure 106 – Presence and Distribution of MUC2-positive Cells.

Representative confocal images of whole mucosa **(A)**, crypts **(B)**, organoids **(C)** and single cells **(D)** immunolabelled with E-Cadherin (ECAD) in white and MUC2 in green. Nuclei was stained with Sytox Blue (DNA). Zoom view provided for mucosa, crypts and organoids. Scale bar = 25 µm.

MUC2 ECAD DNA
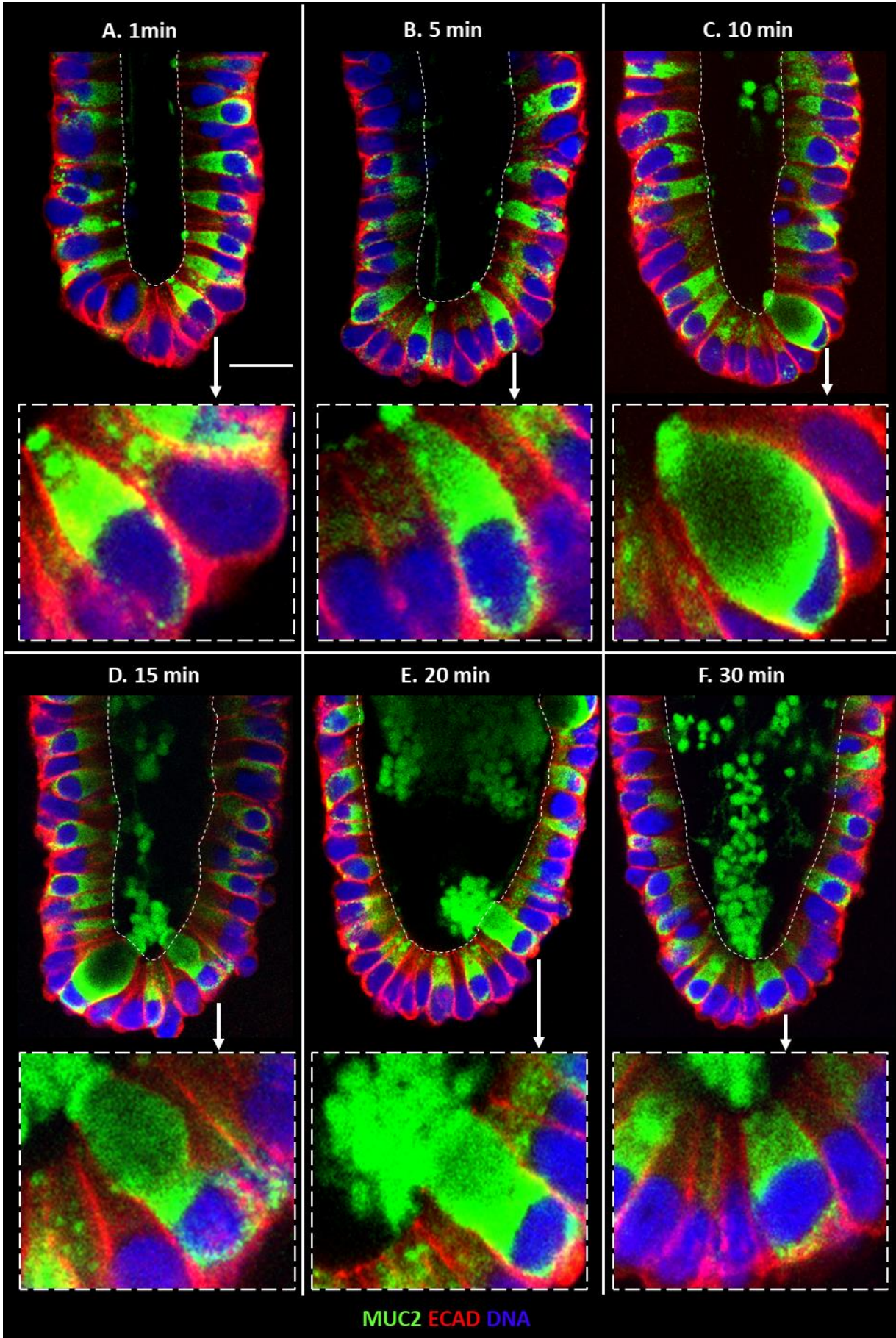
Figure 107 – Temporal Characteristics of CCh-Induced Mucus Secretion.

Representative confocal images of colonic crypts treated with CCh (10 μM) for 1 (A), 5 (B), 10 (C), 15 (D), 25 (E) and 30 (D) minutes before being fixed and immunolabelled with Muc2 (red) and Ecad (green) antibodies, and the nucleus stained with Sytox blue (blue). White dotted lines mark the apical membrane. Dotted white boxes contain the zoom-in view for single MUC2+ cells from each timepoint. Asterisks indicate presence of secreted luminal mucus. Scale bar 20 μm.

Having established the temporal characteristics of mucus secretion in crypts in response to cholinergic stimulation, a series of mucus depletion assays were carried out in conjunction with some of the pharmacological antagonists introduced in the previous chapter, with the goal of investigating whether CCh-induced mucus secretion was affected by pharmacological inhibition of intracellular Ca^{2+} release channels. Previous work by Dr Nicolas Pelaez Llaneza showed that compared to control (t=0 minutes), MUC2 fluorescence intensity was lowest after 5 minutes of CCh (10 μM) stimulation compared to longer CCh stimulation (Pelaez-Llaneza 2019). Hence, crypts were stimulated with CCh for 5 minutes before being fixed and immunolabelled with MUC2. Cytoplasmic MUC2 fluorescence intensity was measured following the described protocol (Figure 21).

Firstly, TPC-antagonists Ned-19 (250 μM) and tetrandrine (20 μM) were used to investigate whether TPC-inhibition affected CCh-induced mucus secretion. Crypts which were stimulated with CCh had 20% less MUC2 compared to control and was statistically significant, which was inhibited by Ned-19 (Figure 108). The presence of Ned-19 alone caused a 3% increase in MUC2 intensity and was not significant compared to control, while CCh and Ned-19 crypts had identical MUC2 intensity to control and was statistically significant compared to CCh alone. Likewise, CCh-induced mucus secretion was inhibited by tetrandrine in crypts (Figure 109). The presence of tetrandrine alone caused a 15% increase in MUC2 intensity and was not significant compared to control, while CCh and tetrandrine crypts had nearly identical MUC2 intensity to control and was statistically significant compared to CCh alone.

Next, IP3R-antagonists 2-APB (100 μM) and caffeine (10 mM) were used to investigate whether IP3R-inhibition affected CCh-induced mucus secretion. Crypts which were stimulated with CCh had 18% less MUC2 compared to control and was statistically significant, which was not inhibited by 2-APB (Figure 110). The presence of 2-APB alone caused a 3% decrease in MUC2 intensity and was not significant compared to control, but the combination of CCh and 2-APB had 16% less MUC2 intensity compared to control and was statistically significant. In the case of caffeine, organoids which were stimulated with CCh had 15% less MUC2 compared to control and was statistically significant, which was inhibited by caffeine (Figure 111). The presence of caffeine alone caused a 6% decrease in MUC2 intensity and was not significant compared to control, while crypts with CCh and caffeine had 2% more MUC2 intensity compared to control and was statistically significant compared to CCh alone.
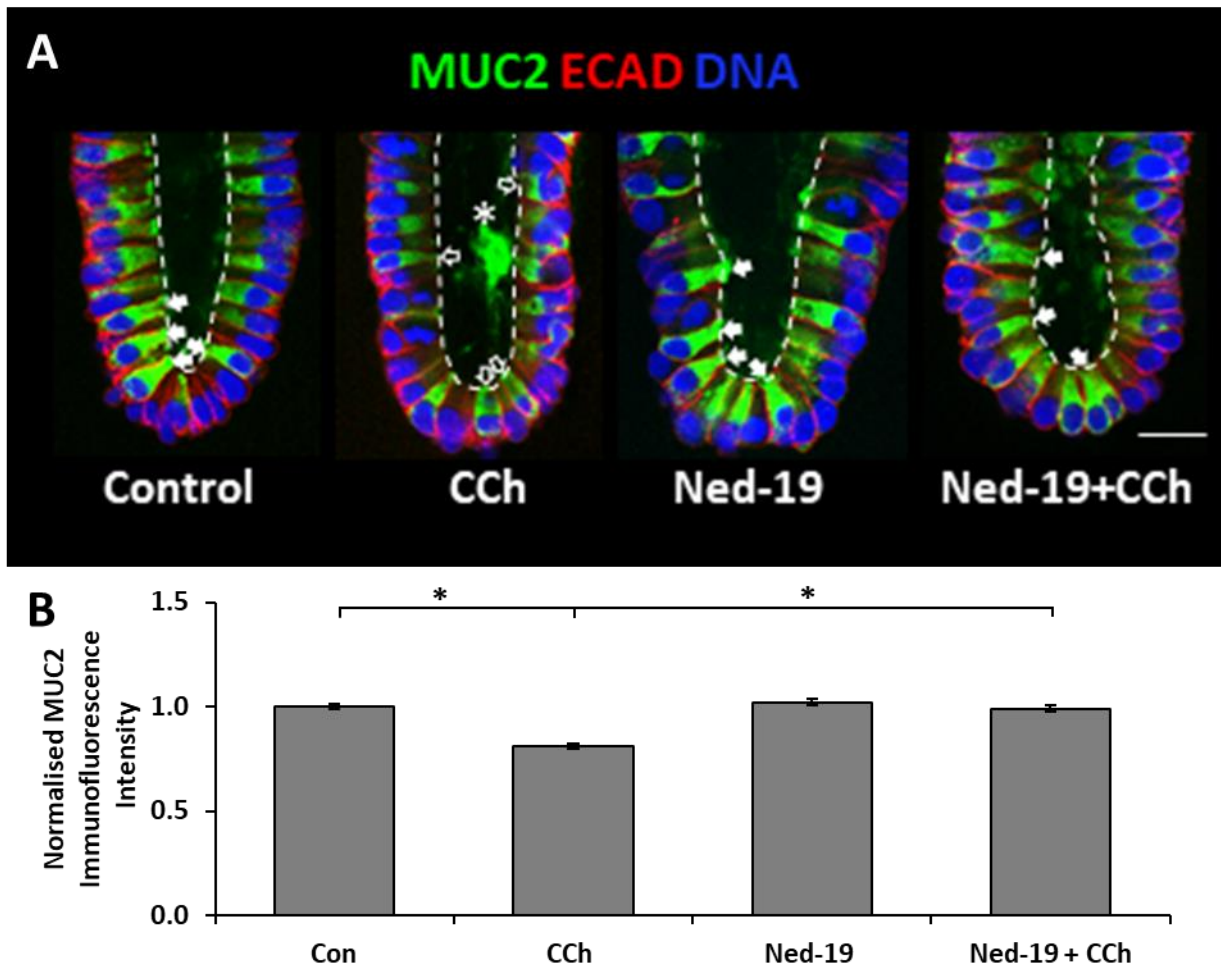
Figure 108 – Ned-19 Inhibits CCh-Induced Mucus Secretion in Crypts.

Representative confocal images colonic crypt base labelled with Muc2 (green) and Ecad (red), and nuclei (DNA) stained with Sytox Blue **(A)**. From left to right: crypt stimulated with culture media (Control), crypt stimulated with CCh (10 μM) within culture media (CCh), crypt incubated with Ned-19 (250 μM) followed by stimulation with culture media (Ned-19), and crypt incubated with Ned-19 followed by stimulation with CCh within culture media (Ned19+CCh). White arrows indicate crypts full of MUC2. Black arrows indicate crypts with depleted MUC2. Asterisks indicate presence of luminal MUC2 labelling. Scale bar 20 μm. Bar chart summarising the normalised MUC2 immunofluorescence intensity of crypts stimulated with culture media (Con), crypts stimulated with CCh within culture media (CCh), crypts incubated with Ned-19 followed by stimulation with culture media (Ned-19), and crypts incubated with Ned-19 followed by stimulation with CCh within culture media (Ned19+CCh) **(B)**. Data normalised to control and displayed as mean +/- SEM. $P > 0.05$ (*). N=3. For every "N", n≥5.
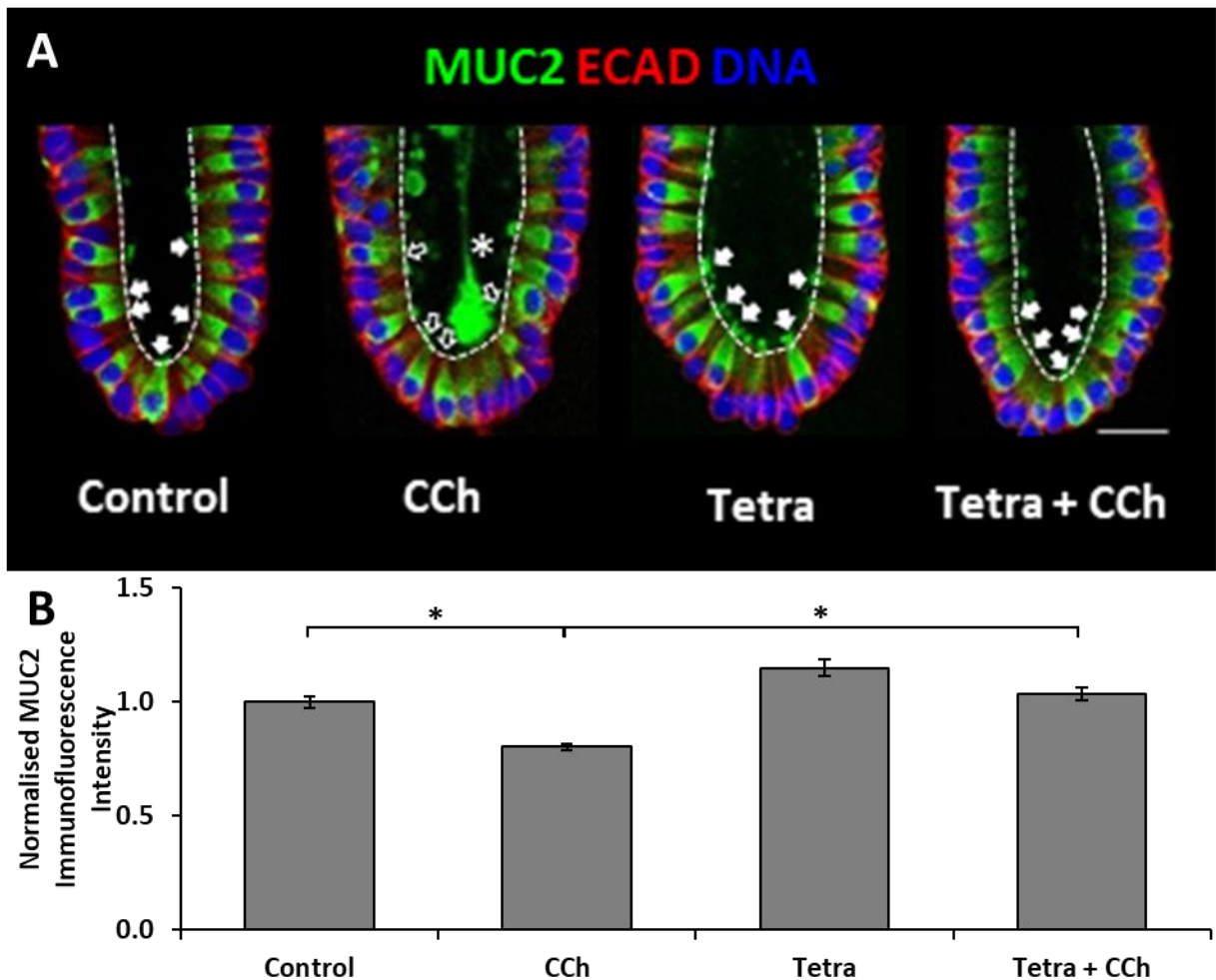
Figure 109 – Tetrandrine Inhibits CCh-Induced Mucus Secretion in Crypts.

Representative confocal images colonic crypt base labelled with Muc2 (green) and Ecad (red), and nuclei (DNA) stained with Sytox Blue **(A)**. From left to right: crypt stimulated with culture media (Control), crypt stimulated with CCh (10 µM) within culture media (CCh), crypt incubated with tetrandrine (20 µM) followed by stimulation with culture media (Tetra), and crypt incubated with tetrandrine followed by stimulation with CCh within culture media (Tetra+CCh). White arrows indicate crypts full of MUC2. Black arrows indicate crypts with depleted MUC2. Asterisks indicate presence of luminal MUC2 labelling. Scale bar 20 µm. Bar chart summarising the normalised MUC2 immunofluorescence intensity of crypts stimulated with culture media (Control), crypts stimulated with CCh within culture media (CCh), crypts incubated with tetrandrine followed by stimulation with culture media (Tetra), and crypts incubated with tetrandrine followed by stimulation with CCh within culture media (Tetra+CCh) **(B)**. Data normalised to control and displayed as mean +/- SEM. $P > 0.05$ (*). N=3. For every "N", n≥5.
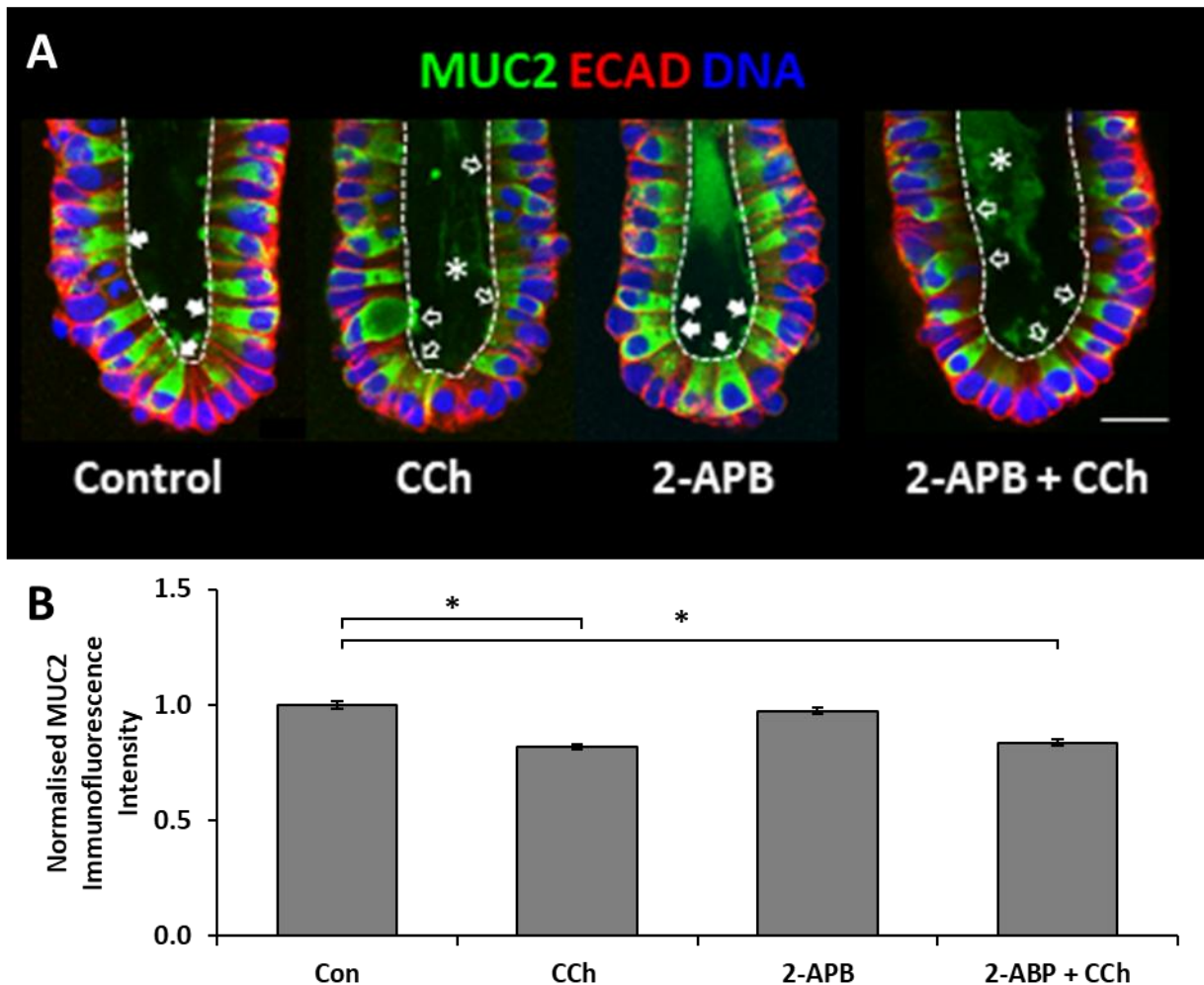
Figure 110 – 2-APB Does Not Inhibit CCh-Induced Mucus Secretion in Crypts.

Representative confocal images colonic crypt base labelled with Muc2 (green) and Ecad (red), and nuclei (DNA) stained with Sytox Blue **(A)**. From left to right: crypt stimulated with culture media (Control), crypt stimulated with CCh (10 µM) within culture media (CCh), crypt incubated with 2-APB (100 µM) followed by stimulation with culture media (2-APB), and crypt incubated with 2-APB followed by stimulation with CCh within culture media (2-APB+CCh). White arrows indicate crypts full of MUC2. Black arrows indicate crypts with depleted MUC2. Asterisks indicate presence of luminal MUC2 labelling. Scale bar 20 µm. Bar chart summarising the normalised MUC2 immunofluorescence intensity of crypts stimulated with culture media (Con), crypts stimulated with CCh within culture media (CCh), crypts incubated with 2-APB followed by stimulation with culture media (2-APB), and crypts incubated with 2-APB followed by stimulation with CCh within culture media (2-APB+CCh) **(B)**. Data normalised to control and displayed as mean +/- SEM. P>0.05 (*). N=3. For every "N", n≥5.
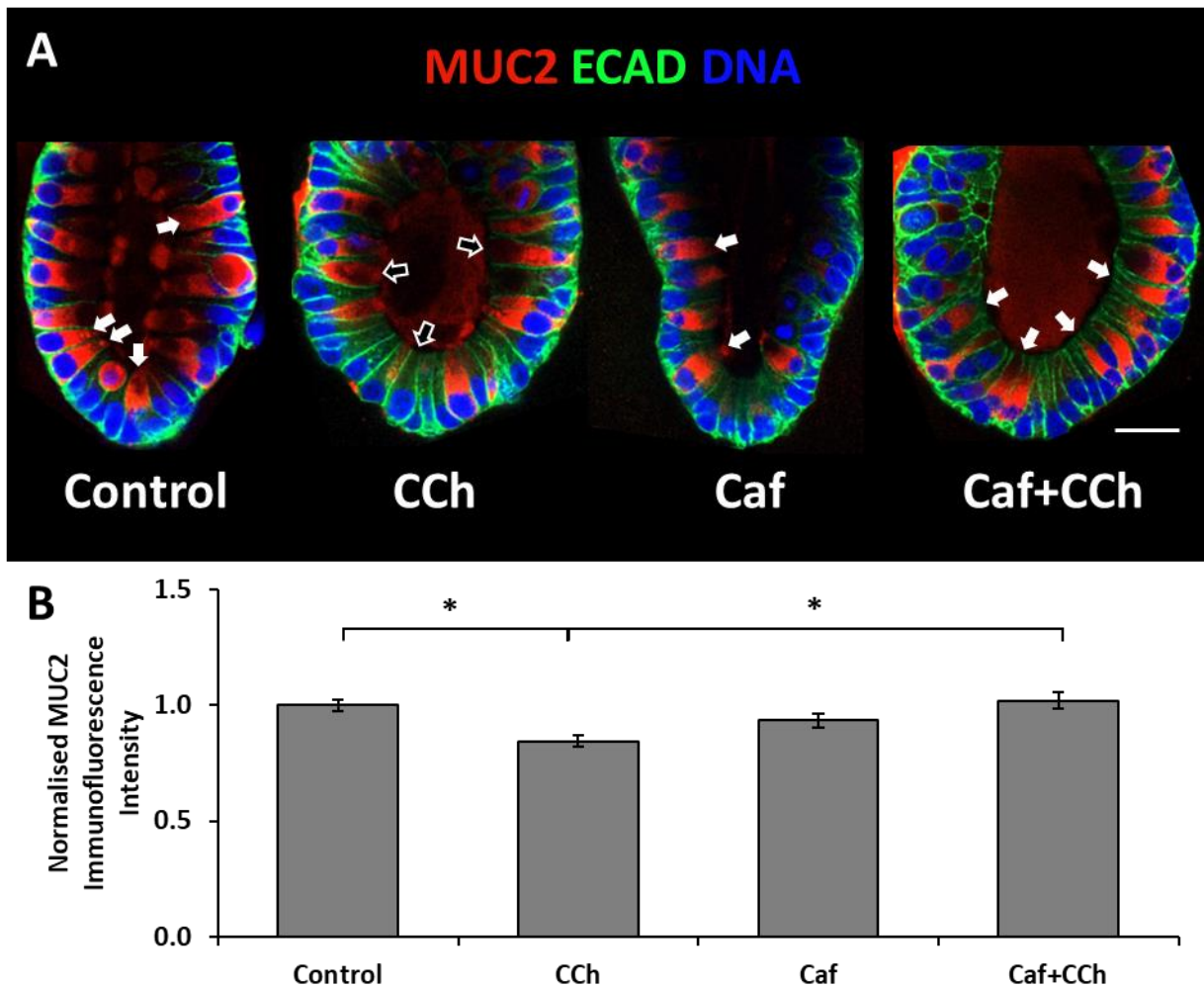
Figure 111 – Caffeine Inhibits CCh-Induced Mucus Secretion in Crypts.

Representative confocal images organoid base labelled with Muc2 (red) and Ecad (green), and nuclei (DNA) stained with Sytox Blue **(A)**. From left to right: organoid stimulated with culture media (Control), organoid stimulated with CCh (10 µM) within culture media (CCh), organoid incubated with caffeine (10 mM) followed by stimulation with culture media (Caf), and organoid incubated with caffeine followed by stimulation with CCh within culture media (Caf+CCh). White arrows indicate crypts full of MUC2. Black arrows indicate crypts with depleted MUC2. Scale bar 20 µm. Bar chart summarising the normalised MUC2 immunofluorescence intensity of crypts stimulated with culture media (Control), crypts stimulated with CCh within culture media (CCh), crypts incubated with caffeine followed by stimulation with culture media (Caf), and crypts incubated with caffeine followed by stimulation with CCh within culture media (Caf+CCh) **(B)**. Data normalised to control and displayed as mean +/- SEM. $P > 0.05$ (*). N=2. For every "N", n≥5.

Following this, RYR1/3-antagonist dantrolene (30 µM) and non-specific RYR-antagonist procaine (1 mM) were used to investigate whether RYR-inhibition affected CCh-induced mucus secretion. Crypts which were stimulated with CCh had 31% less MUC2 compared to control and was statistically significant, which was inhibited by dantrolene (Figure 112). The presence of dantrolene alone caused a 4% increase in MUC2 intensity and was not significant compared to control, which was identical to that of CCh and dantrolene crypts and who was statistically significant compared to CCh alone. Likewise, CCh-induced mucus secretion was inhibited by procaine in crypts (Figure 113). The presence of procaine alone caused a 2% decrease in MUC2 intensity and was not significant compared to control, but CCh and procaine crypts had 13% increased MUC2 intensity compared to control and was statistically significant to both CCh and control.

Lastly, crypts were stimulated with CPA (20 µM) to determine whether an increase in cytoplasmic $[Ca^{2+}]$ via emptying endoplasmic reticular stores (Figure 114A-B), and UTP (50 µM) to determine whether P2Y2-activated intracellular Ca^{2+}-signals (Figure 114C); were capable of inducing mucus secretion. While crypts which were stimulated with CCh had 19% less MUC2 compared to control and was statistically significant, crypts which were stimulated with CPA had 16% more MUC2 compared to control and was not statistically significant (Figure 114B). On the other hand, crypts which were stimulated with UTP had 22% less MUC2 compared to control and was statistically significant (Figure 114C).
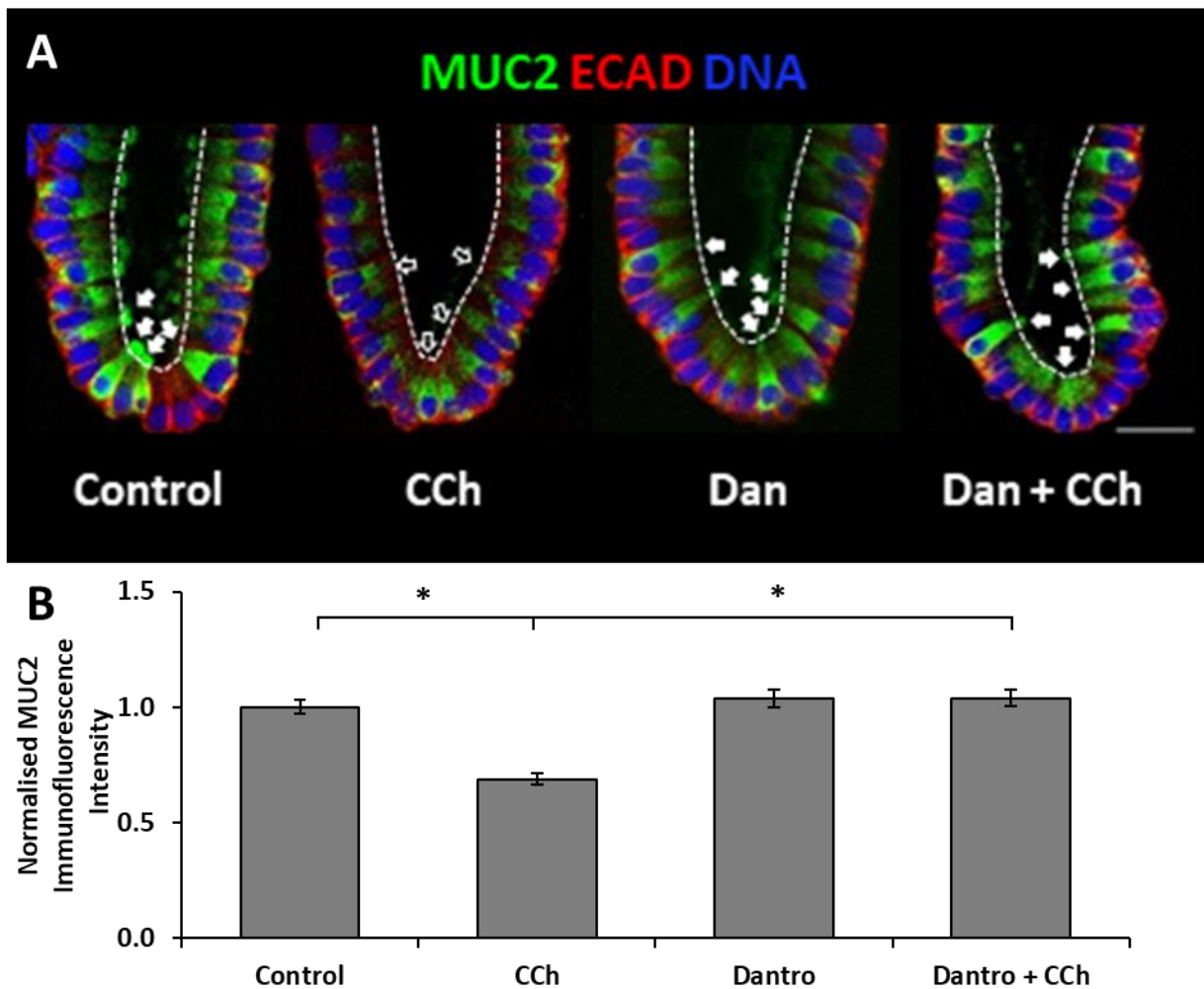
Figure 112 – Dantrolene Inhibits CCh-Induced Mucus Secretion in Crypts.

Representative confocal images colonic crypt base labelled with Muc2 (green) and Ecad (red), and nuclei (DNA) stained with Sytox Blue **(A)**. From left to right: crypt stimulated with culture media (Control), crypt stimulated with CCh (10 µM) within culture media (CCh), crypt incubated with dantrolene (30 µM) followed by stimulation with culture media (Dan), and crypt incubated with dantrolene followed by stimulation with CCh within culture media (Dan+CCh). White arrows indicate crypts full of MUC2. Black arrows indicate crypts with depleted MUC2. Asterisks indicate presence of luminal MUC2 labelling. Scale bar 20 µm. Bar chart summarising the normalised MUC2 immunofluorescence intensity of crypts stimulated with culture media (Control), crypts stimulated with CCh within culture media (CCh), crypts incubated with dantrolene followed by stimulation with culture media (Dan), and crypts incubated with dantrolene followed by stimulation with CCh within culture media (Dan+CCh) **(B)**. Data normalised to control and displayed as mean +/- SEM. P>0.05 (*). N=3. For every "N", n≥5.
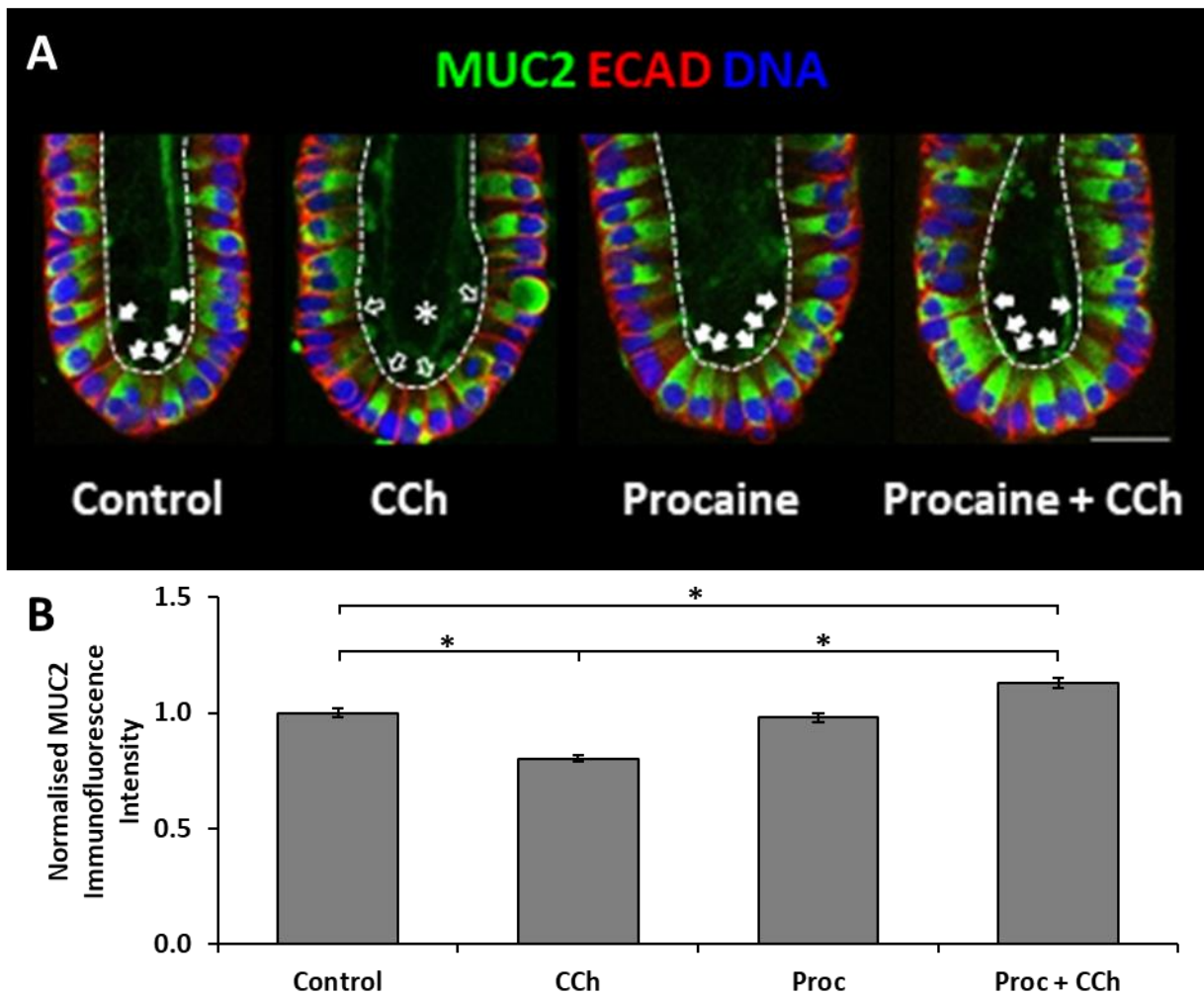
Figure 113 – Procaine Inhibits CCh-Induced Mucus Secretion in Crypts.

Representative confocal images colonic crypt base labelled with Muc2 (green) and Ecad (red), and nuclei (DNA) stained with Sytox Blue **(A)**. From left to right: crypt stimulated with culture media (Control), crypt stimulated with CCh (10 µM) within culture media (CCh), crypt incubated with procaine (1 mM) followed by stimulation with culture media (Procaine), and crypt incubated with procaine followed by stimulation with CCh within culture media (Procaine+CCh). White arrows indicate crypts full of MUC2. Black arrows indicate crypts with depleted MUC2. Asterisks indicate presence of luminal MUC2 labelling. Scale bar 20 µm. Bar chart summarising the normalised MUC2 immunofluorescence intensity of crypts stimulated with culture media (Control), crypts stimulated with CCh within culture media (CCh), crypts incubated with procaine followed by stimulation with culture media (Proc), and crypts incubated with procaine followed by stimulation with CCh within culture media (Proc+CCh) **(B)**. Data normalised to control and displayed as mean +/- SEM. $P>0.05$ (*). N=3. For every "N", n≥5.
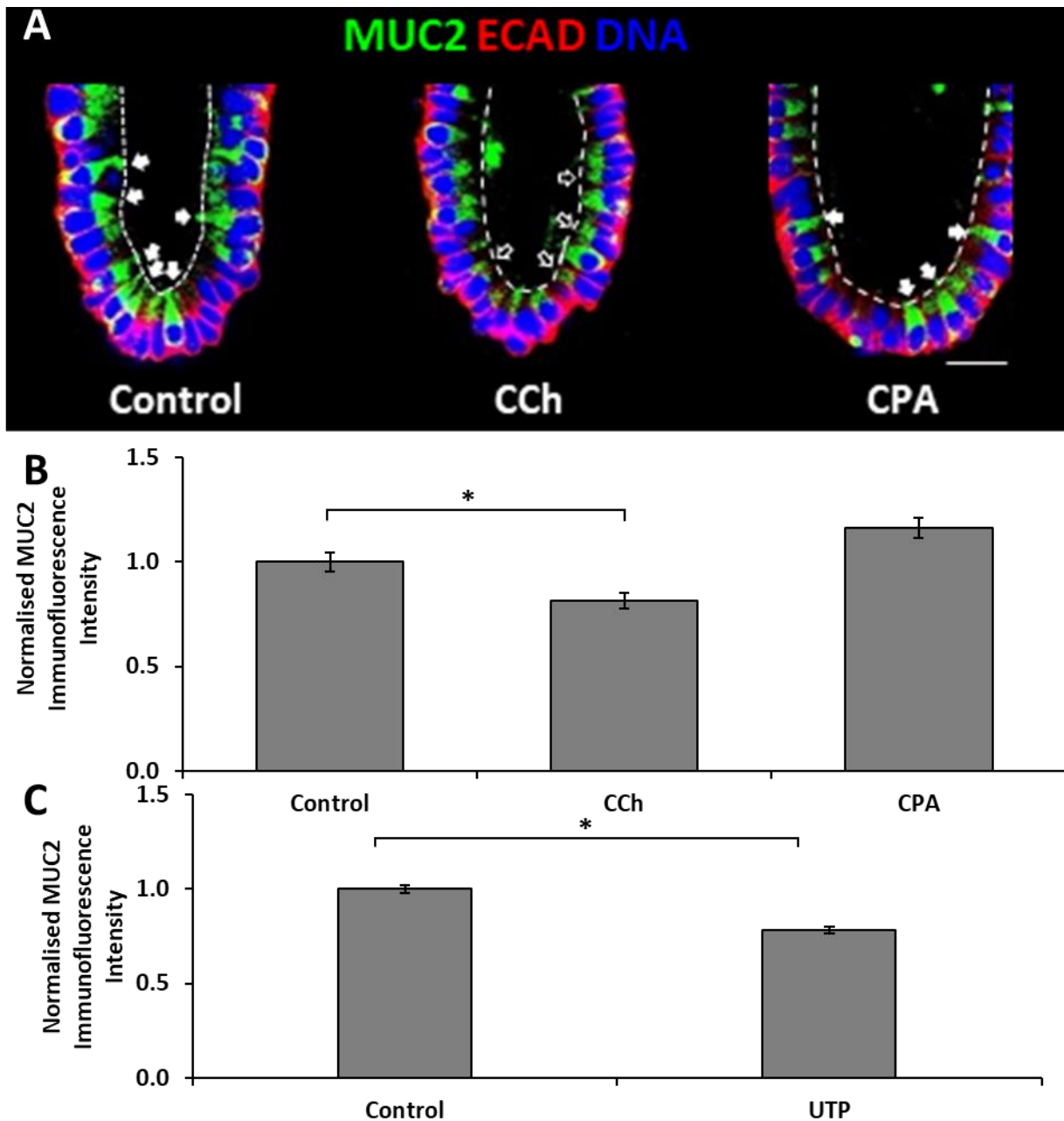
Figure 114 – CPA Does Not Induce Mucus Secretion in Crypts While UTP Does.

Representative confocal images colonic crypt base labelled with Muc2 (green) and Ecad (red), and nuclei (DNA) stained with Sytox Blue **(A)**. From left to right: crypt stimulated with culture media (Control), crypt stimulated with CCh (10 µM) within culture media (CCh), and crypt stimulated with CPA (20 µM) within culture media (CPA). White arrows indicate crypts full of MUC2. Black arrows indicate crypts with depleted MUC2. Asterisks indicate presence of luminal MUC2 labelling. Scale bar 20 µm. Bar chart summarising the normalised MUC2 immunofluorescence intensity of crypts stimulated with culture media (Control), crypts stimulated with CCh within culture media (CCh), and crypts stimulated with CPA within culture media (CPA) **(B)**. Data normalised to control and displayed as mean +/- SEM. N=3 for each condition. P>0.05 (*). Bar chart summarising the normalised MUC2 immunofluorescence intensity of crypts stimulated with culture media (Control) and crypts stimulated with UTP (50 µM) within culture media (UTP) **(C)**. Data normalised to control and displayed as mean +/- SEM. P>0.05 (*). N=3. For every "N", n≥5.

6.2.2 Live Visualisation of Mucus Granule Secretion and Compound Exocytosis

Mucus is stored within secretory vesicles/granules, which consist of a lipid bilayer which originate from the *trans* Golgi following mucin maturation (Bansil & Turner, 2018). Due to this, lipophilic dyes were used as an alternative means of visualizing mucus secretion. These dyes – FM1-43 and Deep Red – were expected to label the secretory granules' lipid bilayer and allow real-time (5-10 second interval) visualisation of mucus granule secretion, and compound exocytosis.

Previous work by Dr Nicolas Pelaez Llaneza showed that crypts which were loaded overnight with FM1-43 resulted in the plasma membrane being labelled, which was recorded using confocal microscopy using the 488 nm excitation laser and visualised in green pseudo-colour. Likewise, in this thesis, when crypts loaded with FM1-43 were stimulated with CCh (10 µM), 'bubbles' formed from the apical pole of cells (Figure 115). These 'bubbles' were lipid-bound membranes due to being labelled with FM1-43, and over the course of 30 minutes were visually ejected into the lumen and washed away from the crypt base. In contrast to control experiments (N=2) where CCh was absent from the stimulation solution, fewer 'bubbles' were observed forming from the crypt apical pole (Figure 116). Organoids (N=2) were also loaded with FM1-43 and stimulated with CCh (Figure 117), during which few 'bubbles' were observed. But in control experiments (N=2) where CCh was absent from the stimulation solution, no bubbles were observed forming from the apical or basal pole (Figure 118).

In every case, regardless of whether CCh was present in the stimulation solution or not, crypts and organoids were observed to 'swell'. As a result, crypts and organoids were typically on a different plane of focus; this was clearly observed between 0 to 30 minutes of (Figure 116). In addition, the thickness of the apical-basal membranes of crypts and organoids were observed to be reduced following CCh stimulation, which inspired another experiment which will be described later. Furthermore, real-time visualisation allowed the tracking of 'bubbles' formation and secretion (Figure 115) and (Figure 117). In addition, lipid debris within the lumen could also be tracked, which was most notable in (Figure 117). The presence of debris did not correlate with stimulation conditions, and typically moved away from the crypt/organoid base in response when stimulated by CCh/control.
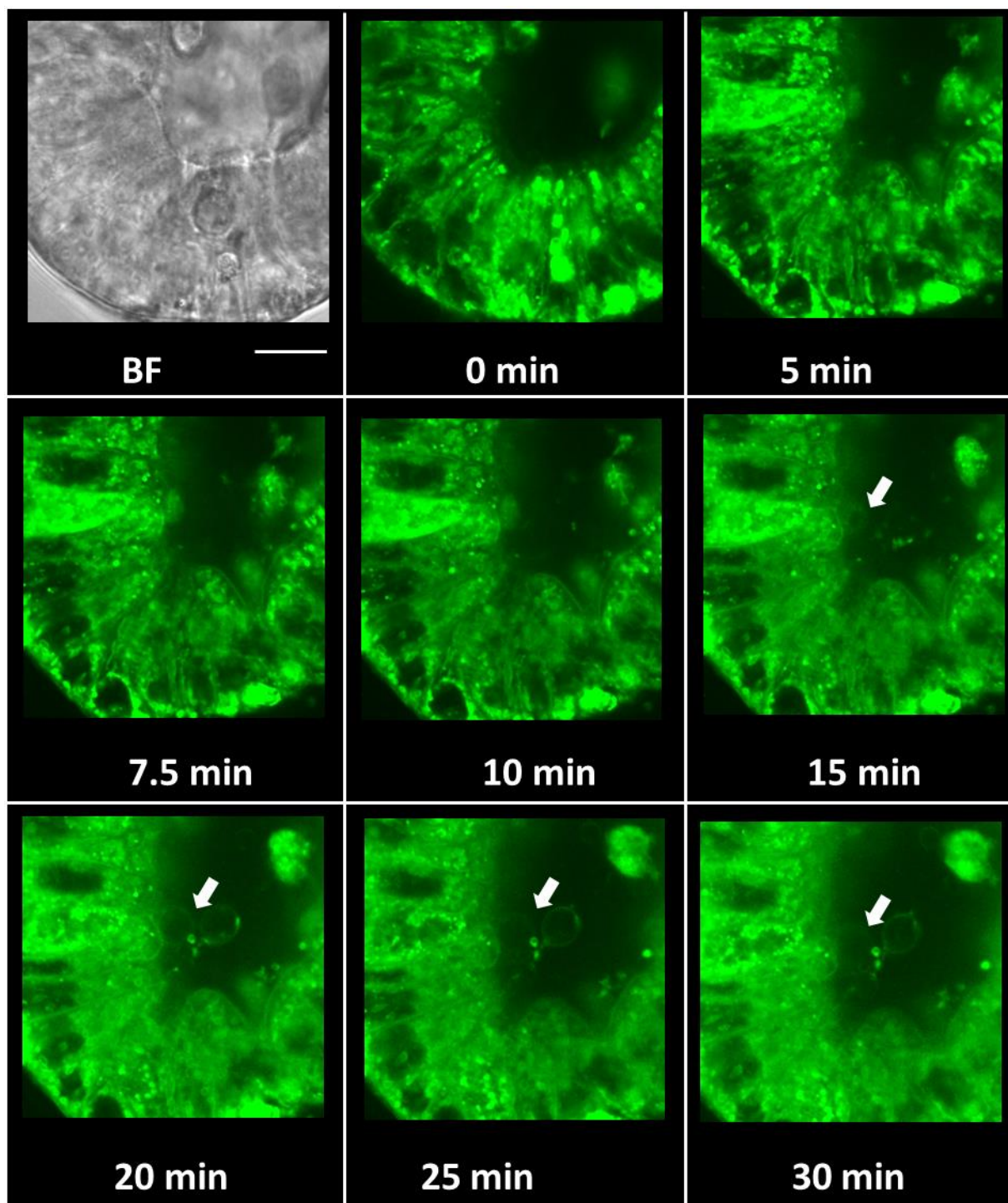
Figure 115 – CCh Induces Secretion and Compound Exocytosis in FM1-43 Labelled Crypt.

Representative confocal images of live microscopy time series of the base of crypts labelled with FM1-43 (green) upon stimulation with CCh (10 μM) up to 30 minutes. White arrow indicates a 'bubble'. Scale bar 25 μm. N≥1. For every "N", n≥3.
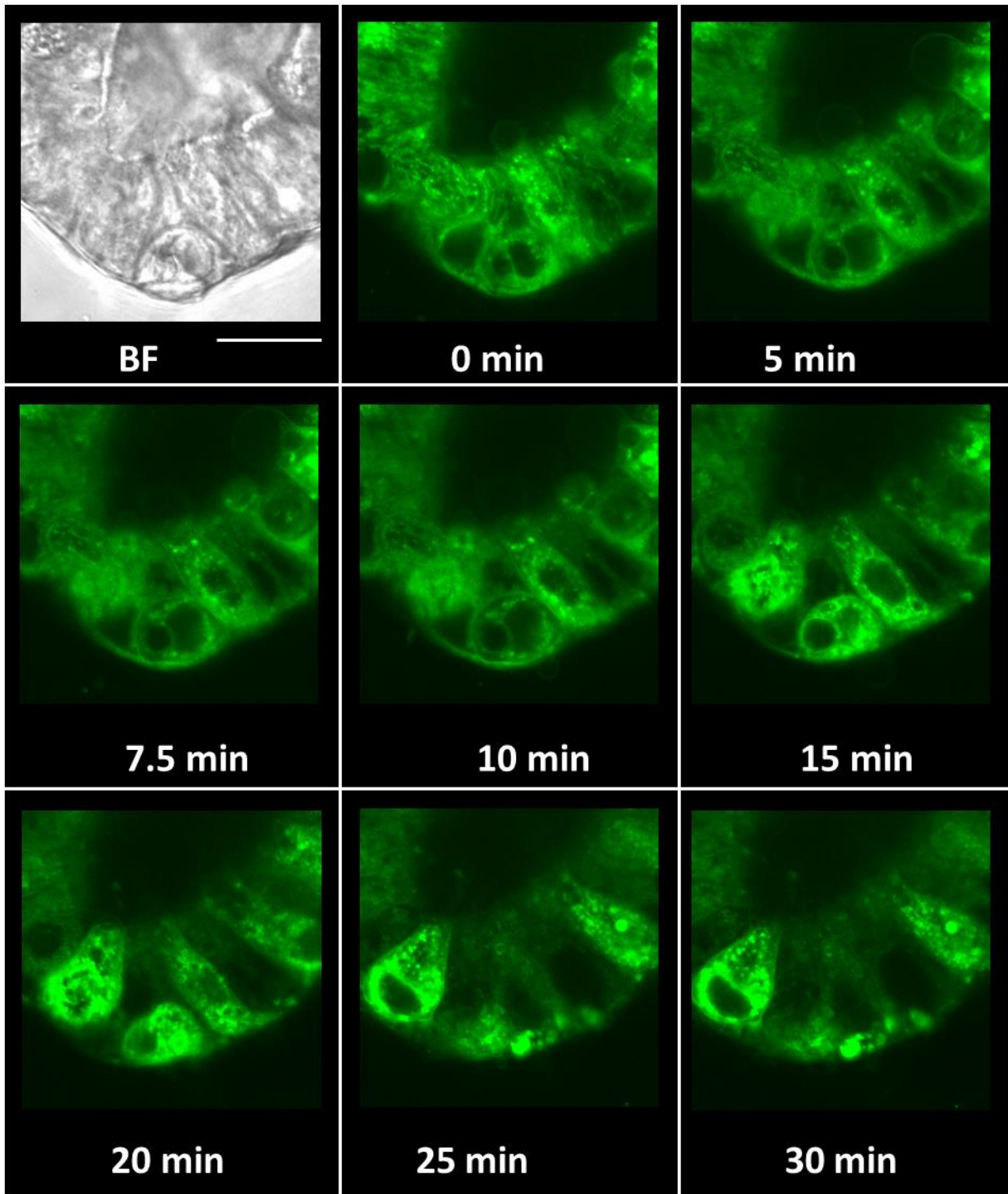
Figure 116 – Lack of Secretion and Compound Exocytosis in Control FM1-43 Labelled Crypt.

Representative confocal images of live microscopy time series of the base of crypts labelled with FM1-43 (green) upon stimulation with control up to 30 minutes. Brightfield (BF). Scale bar 25 μm. N≥1. For every "N", n≥3.
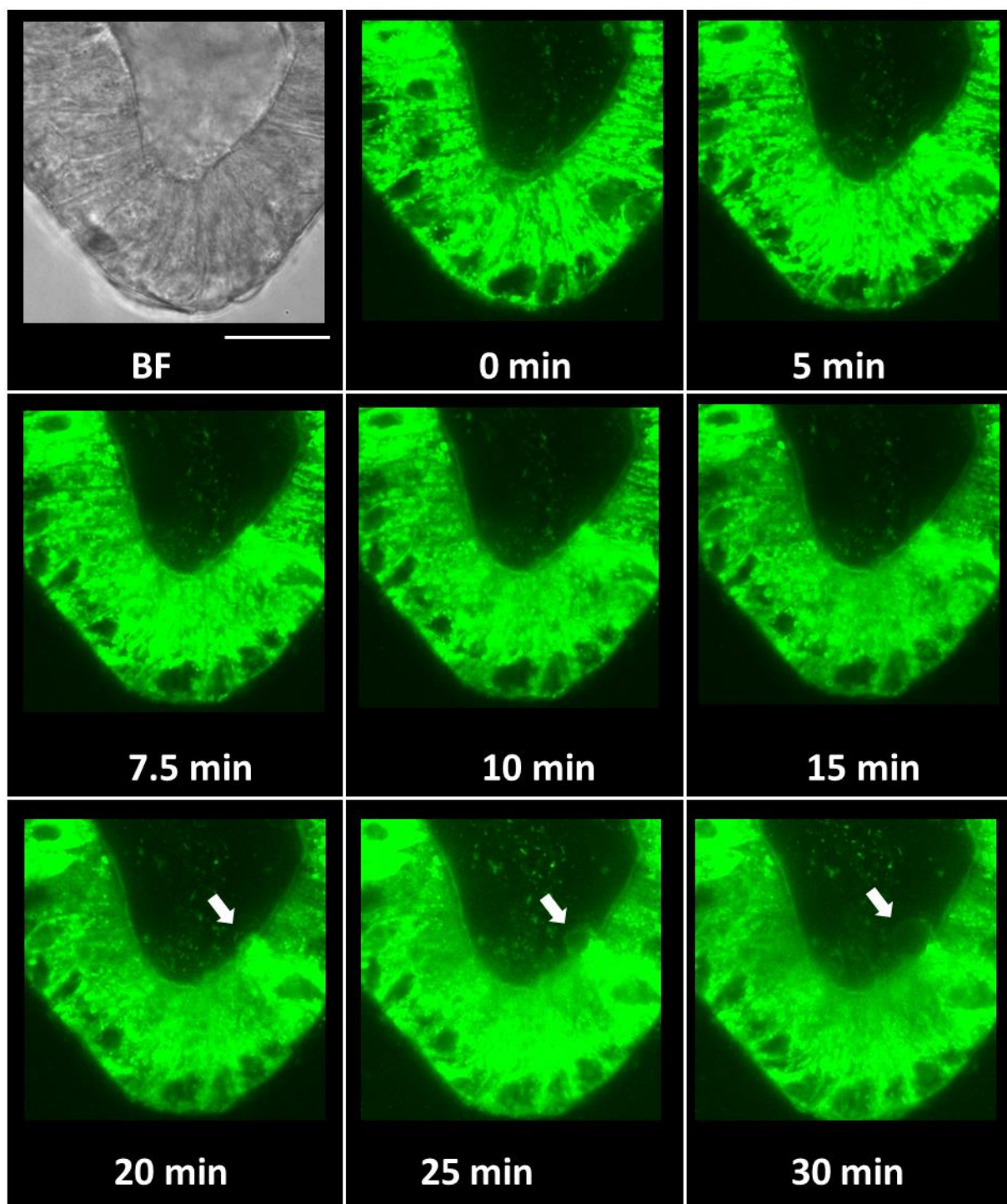
Figure 117 – CCh Induces Secretion and Compound Exocytosis in FM1-43 Labelled Organoid.

Representative confocal images of live microscopy time series of the base of organoids labelled with FM1-43 (green) upon stimulation with CCh (10 μM) up to 30 minutes. White arrow indicates a 'bubble'. Brightfield (BF). Scale bar 25 μm. N≥1. For every "N", n≥3.
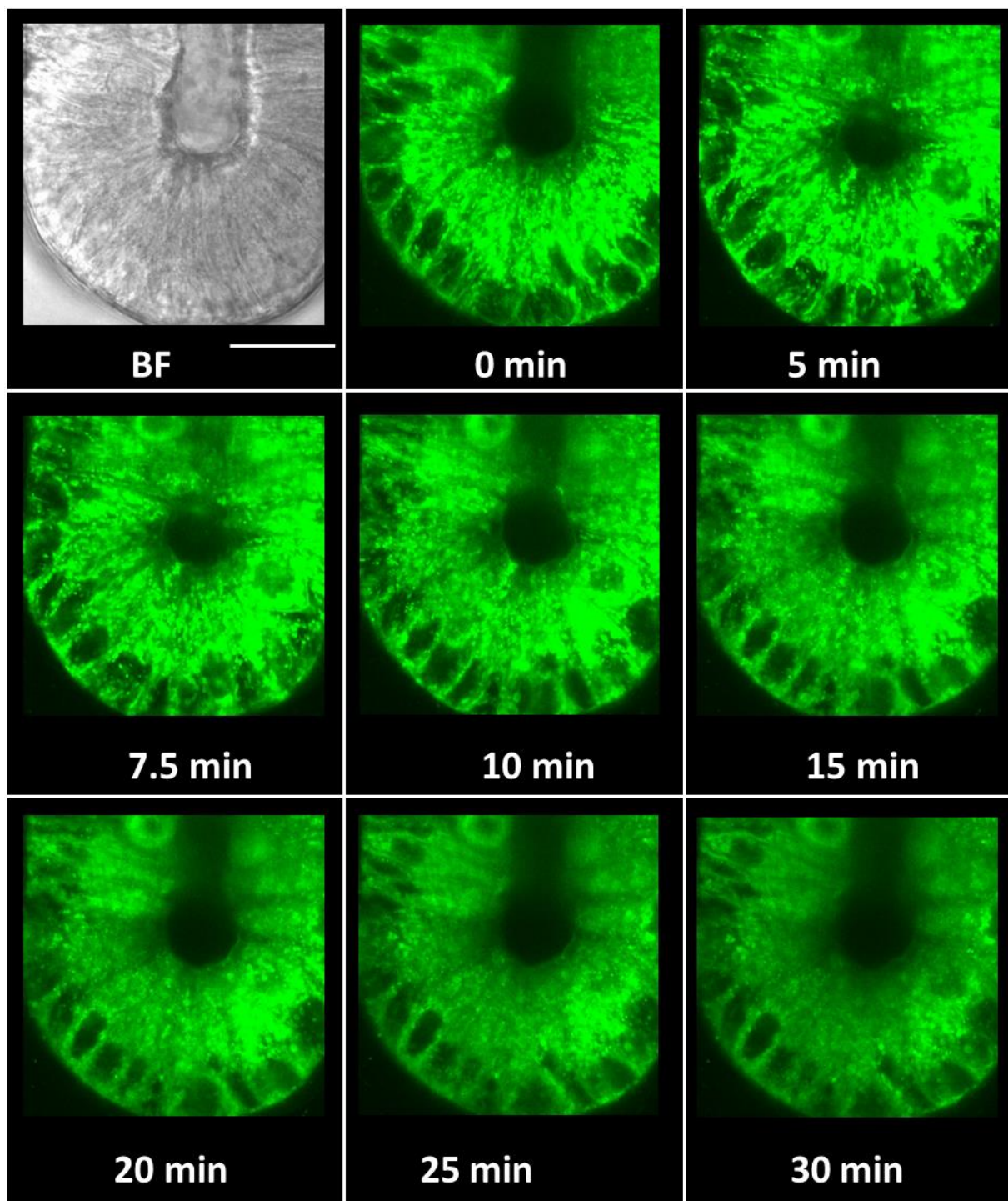
Figure 118 – Lack of Secretion and Compound Exocytosis in Control FM1-43 Labelled Organoid.

Representative confocal images of live microscopy time series of the base of organoids labelled with FM1-43 (green) upon stimulation with control up to 30 minutes. Brightfield (BF). Scale bar 25 µm. N≥1. For every "N", n≥3.

Another fluorescent lipid dye used to label the plasma membrane was FM1-43X. Compared to FM1-43, FM1-43X is designed to be retained following fixation. This was not possible for FM1-43; attempts to do so resulted in the dye being washed away (data not shown). While it could also be used for real-time visualization (5-10 second intervals), its purpose was to compliment the mucus assays, which were all conducted on crypts that were fixed prior to confocal microscopy imaging.

Similar to FM1-43, crypts (N=2) were cultured overnight with FM1-43X. Next, FM1-43X labelled crypts were imaged under confocal microscopy using the 488 nm excitation laser and visualised in green pseudo-colour. Then, crypts stimulated with CCh (Figure 119) or control (Figure 120) for 30 minutes before being fixed with PFA for 2 hours before being re-imaged using confocal microscopy using the same acquisition settings. Notably, more 'bubbles' were observed within crypts before CCh/control stimulation (Figure 119-20; middle column). However, crypts which were stimulated with CCh and fixed had more 'bubbles' subsequently (Figure 119; right-side column) compared to crypts which were stimulated with control and fixed (Figure 120; right-side column). This was also repeated in organoids (N=2), during which fewer 'bubbles' were observed from organoids stimulated with CCh (Figure 121). However, there were noticeable continuous fluorescent lines within the organoids' lumen just outside their apical membrane, which were suspected to be 'bubbles' which were secreted but remain trapped. In contrast, organoids which were stimulated with control had little to no 'bubbles' and continuous fluorescent lines were not observed within their lumen (Figure 122).

The final fluorescent lipid dye used to label the plasma membrane was Cell Tracker™ Deep Red. Similar to FM1-43, it could be used for real-time visualization (5-10 second intervals) and was non-toxic over long-term incubation. Crypts were cultured up to three days with Deep Red, resulting in their plasma membrane and intracellular granules being labelled which was recorded using confocal microscopy using the 647 nm excitation laser and visualised in far red pseudo-colour. When Deep Red crypts (N=3) were stimulated with CCh, 'bubbles' formed from the apical pole of cells (Figure 123), which over the course of 30 minutes were visually ejected into the lumen. In contrast to control experiments (N=3) where CCh was absent from the stimulation solution, no 'bubbles' were observed (Figure 124). Organoids (N=2) were also loaded with Deep Red and stimulated with CCh (Figure 125). When zoomed right into the crypt base to capture several cells, 'bubbles' were observed forming from the apical pole of cells and were visually ejected into the lumen over the course of 30 minutes. But in control experiments (N=2) where CCh was absent from the stimulation solution, no bubbles were observed forming from the apical or basal pole (Figure 126). Similar to FM1-43, crypts and organoids were observed to 'swell' when stimulated with CCh or control, often resulting the sample shifting onto a different plane of focus. Likewise, the thickness of the apical-basal membranes of crypts and organoids were also observed to be reduced following CCh stimulation.
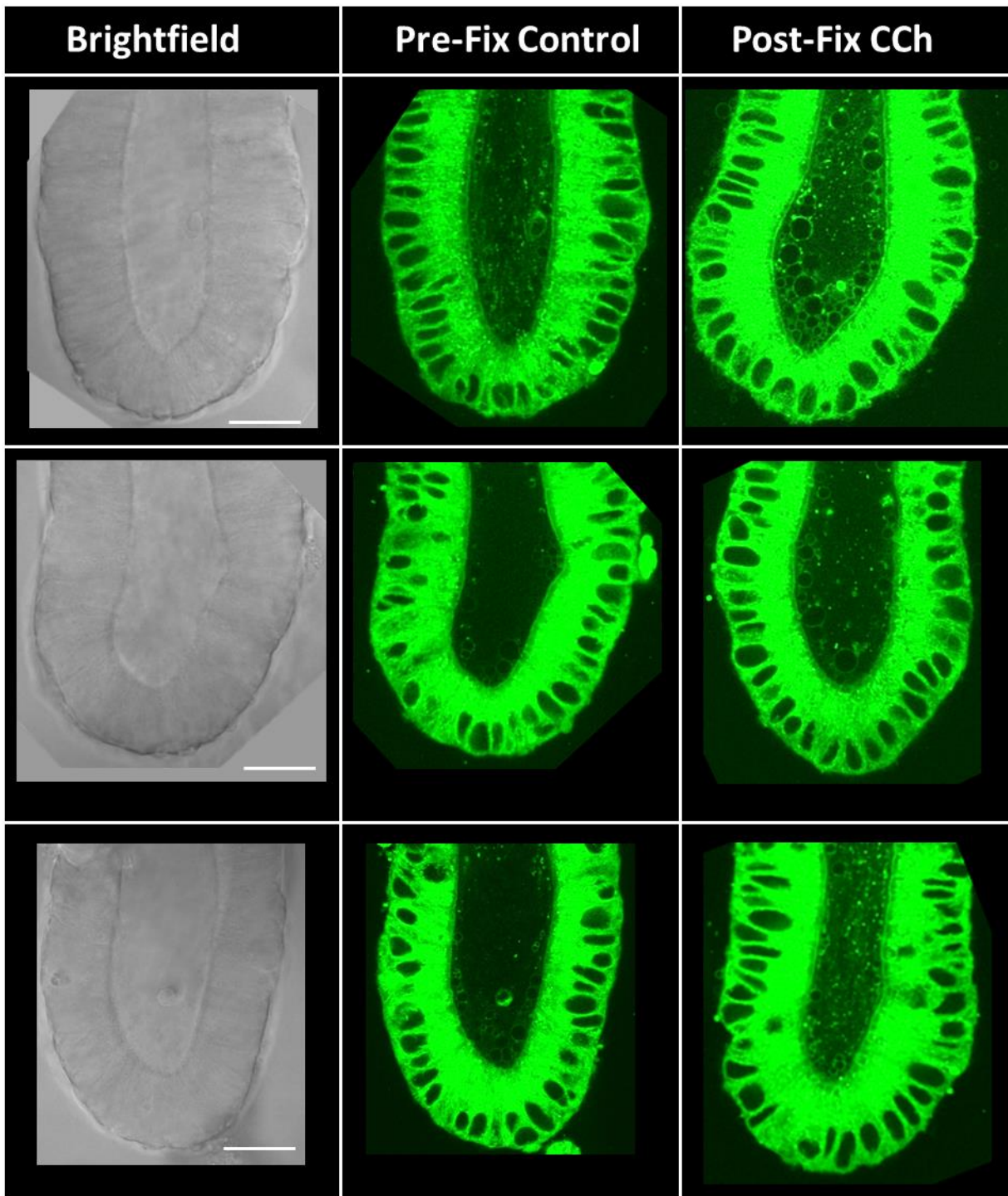
Figure 119 – CCh Induces Secretion and Compound Exocytosis in FM1-43X Labelled Crypt.

Representative confocal images of live microscopy time series of the base of three crypts labelled with FM1-43X (green). Left-side column, brightfield images. Middle column, FM1-43X labelling prior to stimulation with CCh (10 μM). Right-side column, FM1-43X labelling after 30 minutes CCh stimulation followed by PFA fixation. Scale bar 25 μm. N≥1. For every "N", n≥3.
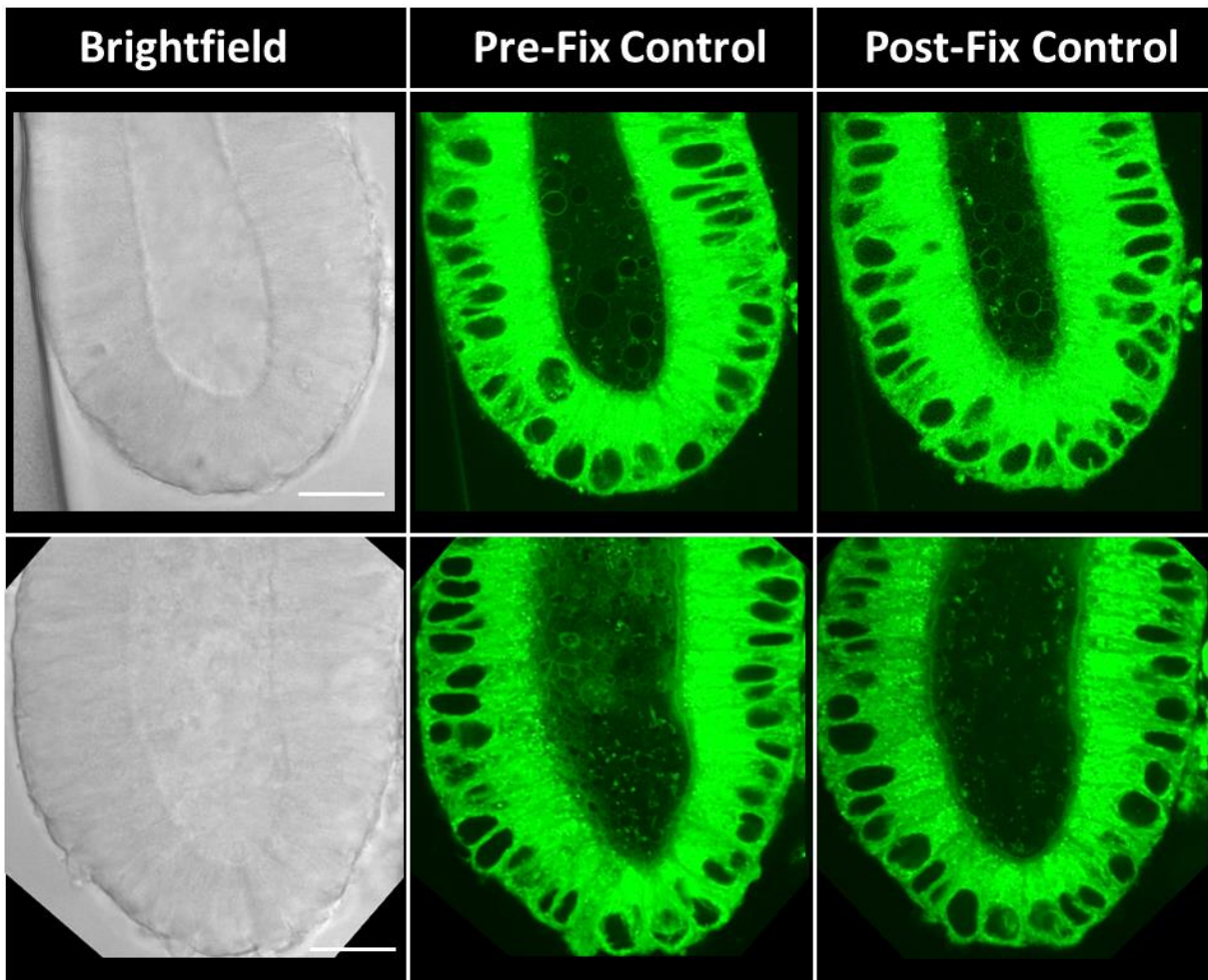
Figure 120 – Lack of Secretion and Compound Exocytosis in Control FM1-43X Labelled Crypt.

Representative confocal images of live microscopy time series of the base of two crypts labelled with FM1-43X (green). Left-side column, brightfield images. Middle column, FM1-43X labelling prior to stimulation with control. Right-side column, FM1-43X labelling after 30 minutes control stimulation followed by PFA fixation. Scale bar 25 µm. N≥1. For every "N", n≥3.
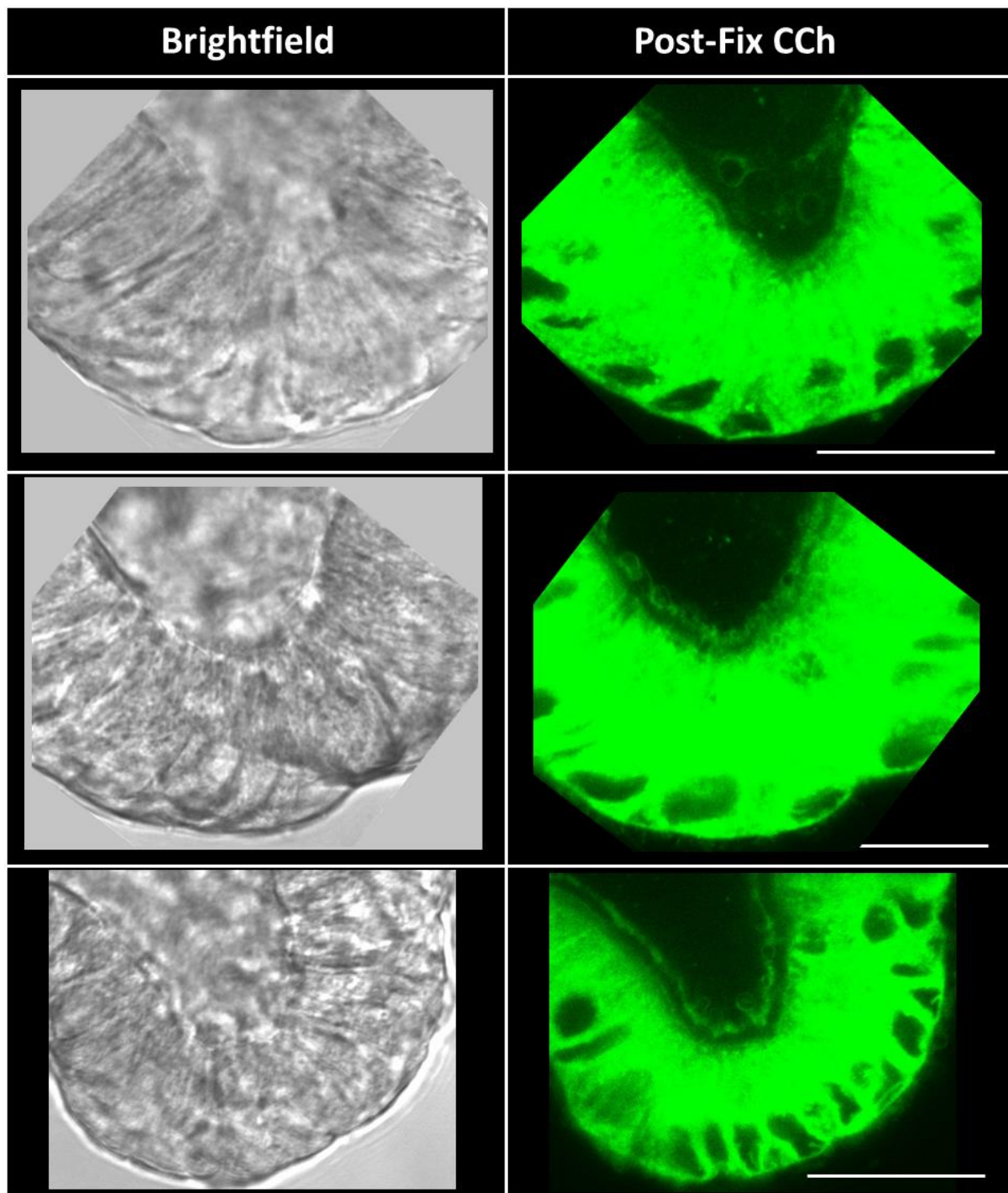
Figure 121 – CCh Induces Secretion and Compound Exocytosis in FM1-43X Labelled Organoid.

Representative confocal images of live microscopy time series of the base of three organoids labelled with FM1-43X (green). Left-side column, brightfield images. Middle column, FM1-43X labelling prior to stimulation with CCh (10 μM). Right-side column, FM1-43X labelling after 30 minutes CCh stimulation followed by PFA fixation. Scale bar 25 μm. N≥1. For every "N", n≥3.
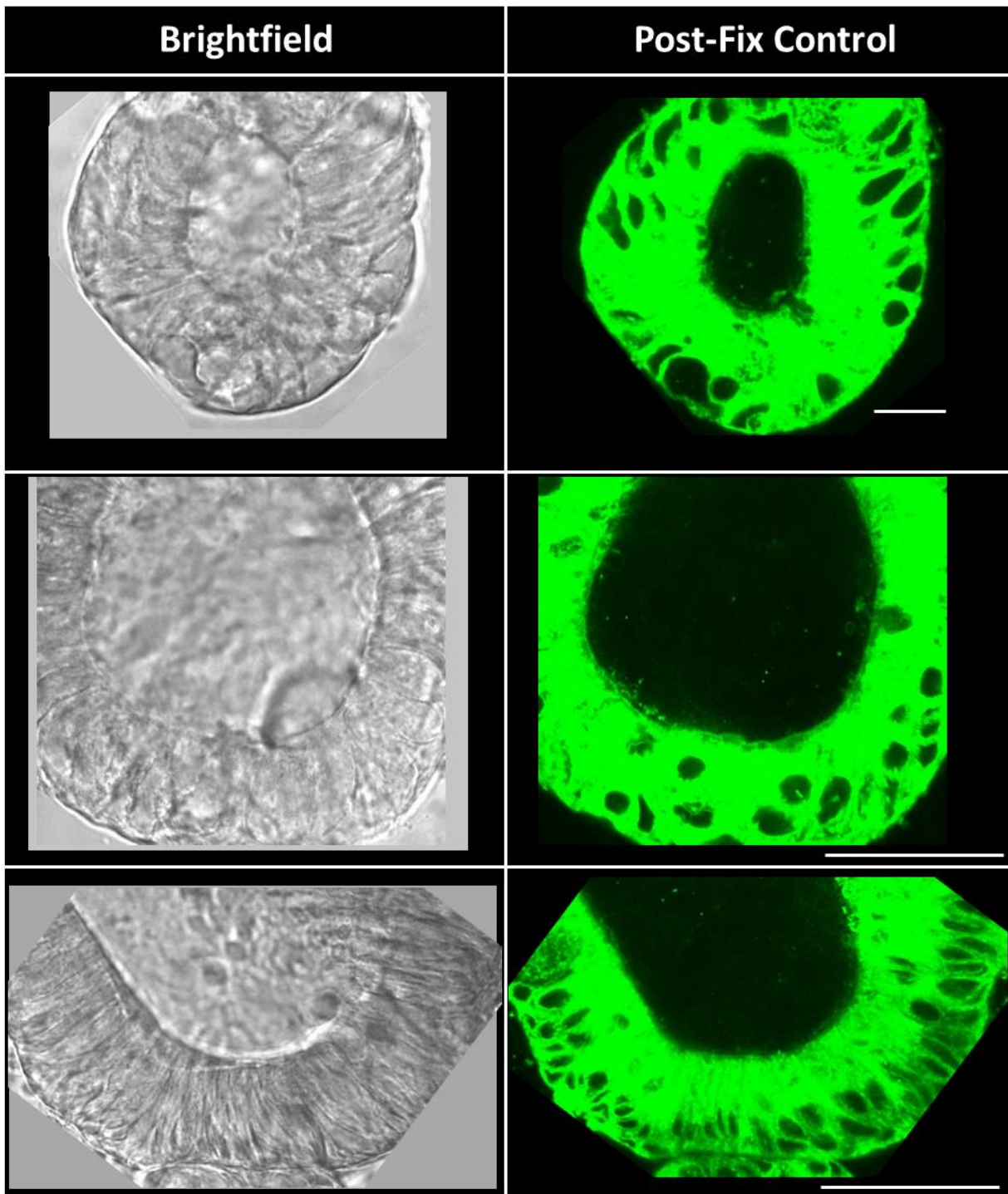
Figure 122 – Lack of Secretion & Compound Exocytosis in Control FM1-43X Labelled Organoid.

Representative confocal images of live microscopy time series of the base of three organoids labelled with FM1-43X (green). Left-side column, brightfield images. Middle column, FM1-43X labelling prior to stimulation with control. Right-side column, FM1-43X labelling after 30 minutes control stimulation followed by PFA fixation. Scale bar 25 µm. N≥1. For every "N", n≥3.
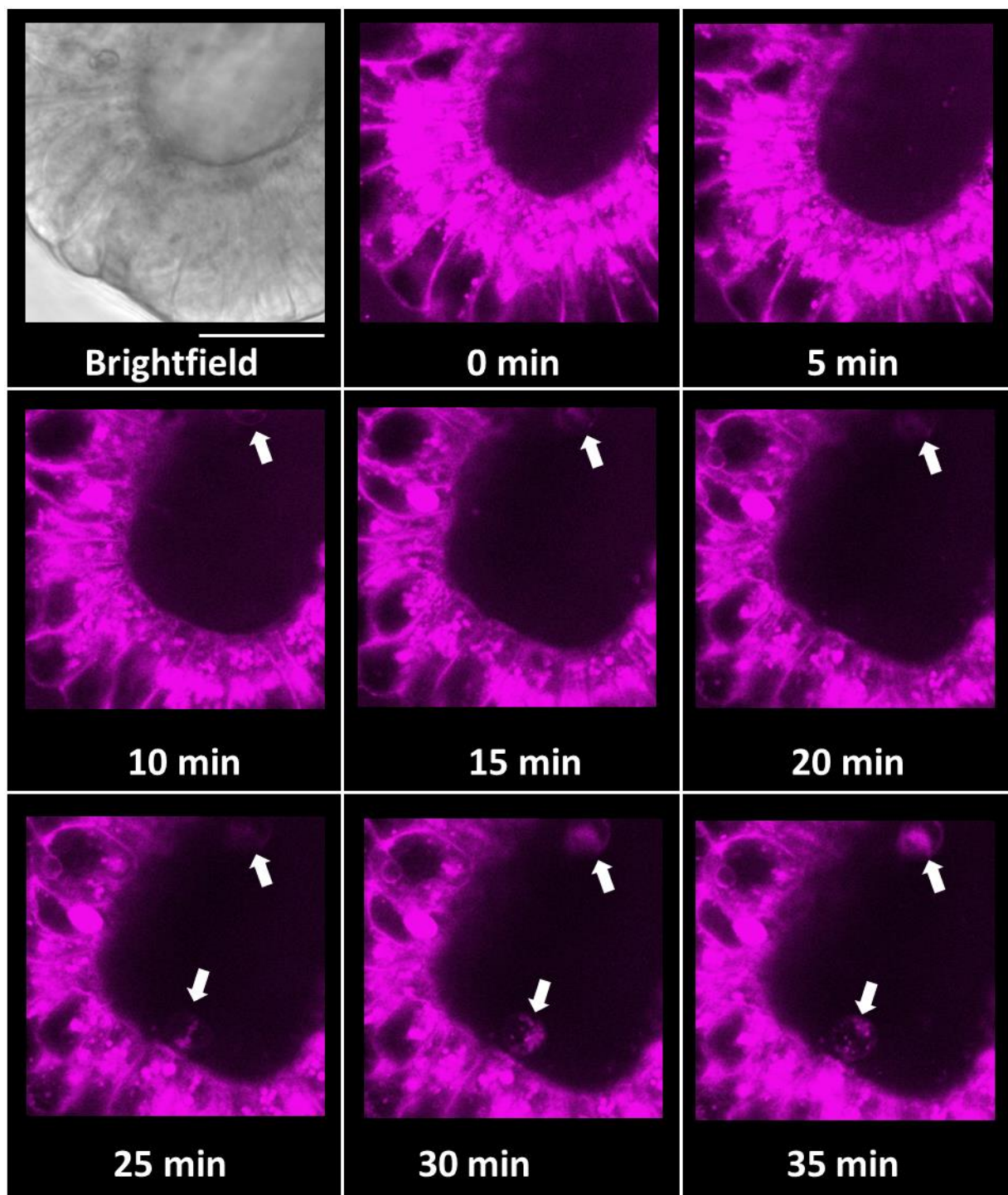
Figure 123 – Deep Red Labelling of CCh-Induced Secretion and Compound Exocytosis in Crypt.

Representative confocal images of live microscopy time series of the base of crypts labelled with Deep Red (Far Red) upon stimulation with CCh (10 µM) up to 35 minutes. White arrow indicates a 'bubble'. Brightfield (BF). Scale bar 25 µm. N≥1. For every "N", n≥3.
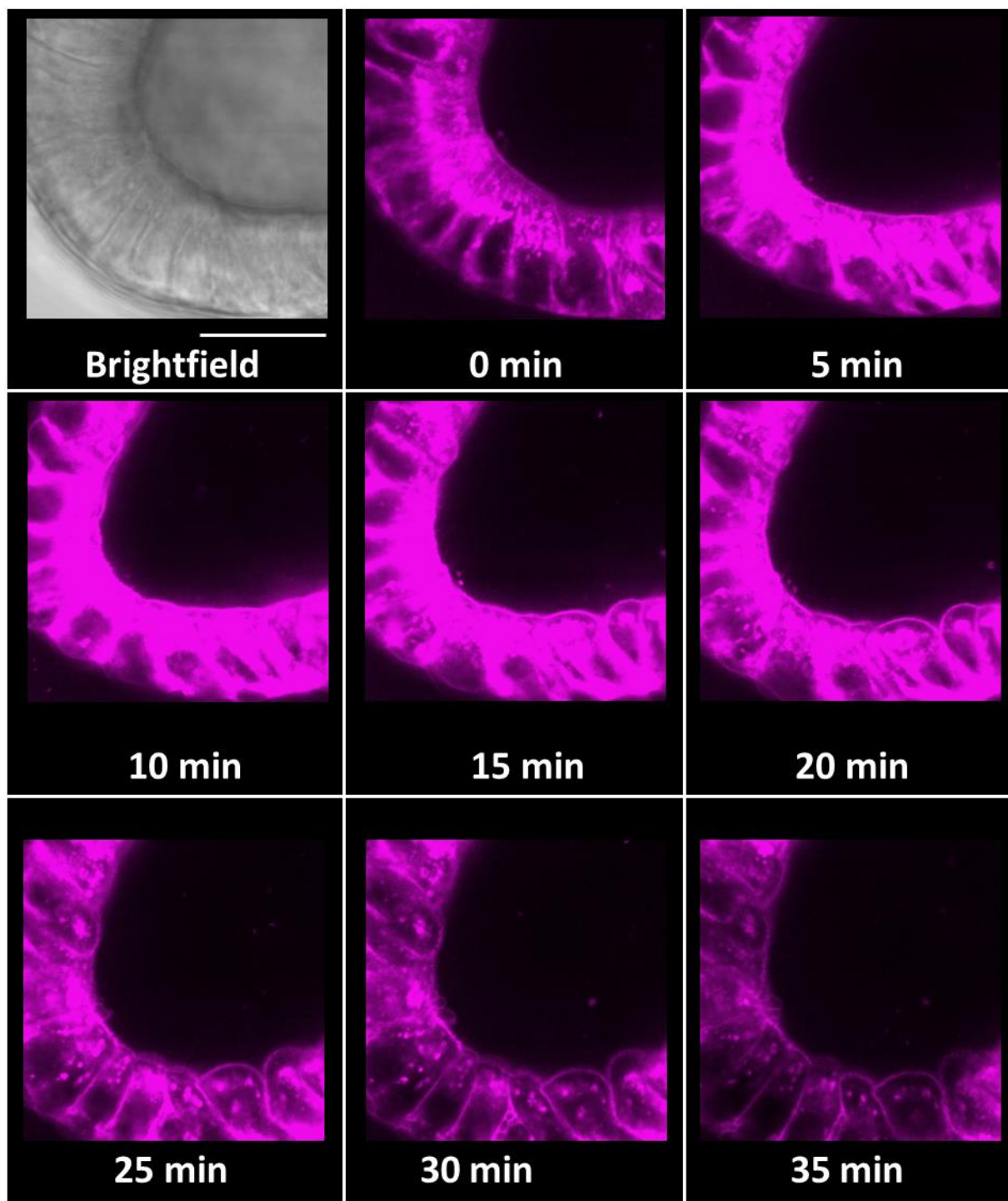
Figure 124 – Deep Red Labelling of Control Secretion and Compound Exocytosis in Crypt.

Representative confocal images of live microscopy time series of the base of crypts labelled with Deep Red (Far Red) upon stimulation with control up to 35 minutes. Brightfield (BF). Scale bar 25 μm. N≥1. For every "N", n≥3.
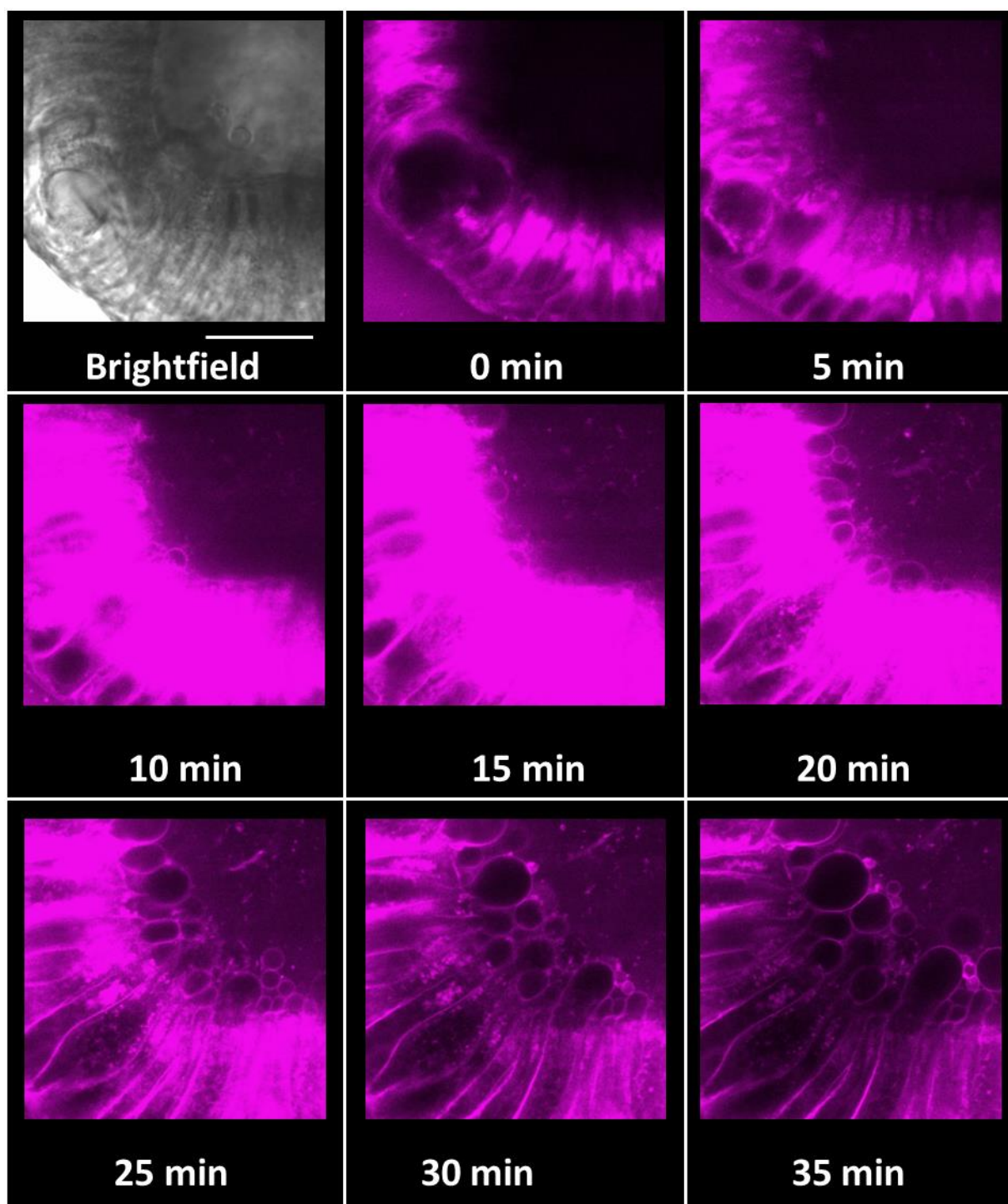
Figure 125 – Deep Red Labelling of CCh-Induced Secretion & Compound Exocytosis in Organoid.

Representative confocal images of live microscopy time series of the base of organoids labelled with Deep Red (Far Red) upon stimulation with CCh (10 µM) up to 35 minutes. Brightfield (BF). Scale bar 25 µm. N≥1. For every "N", n≥3.
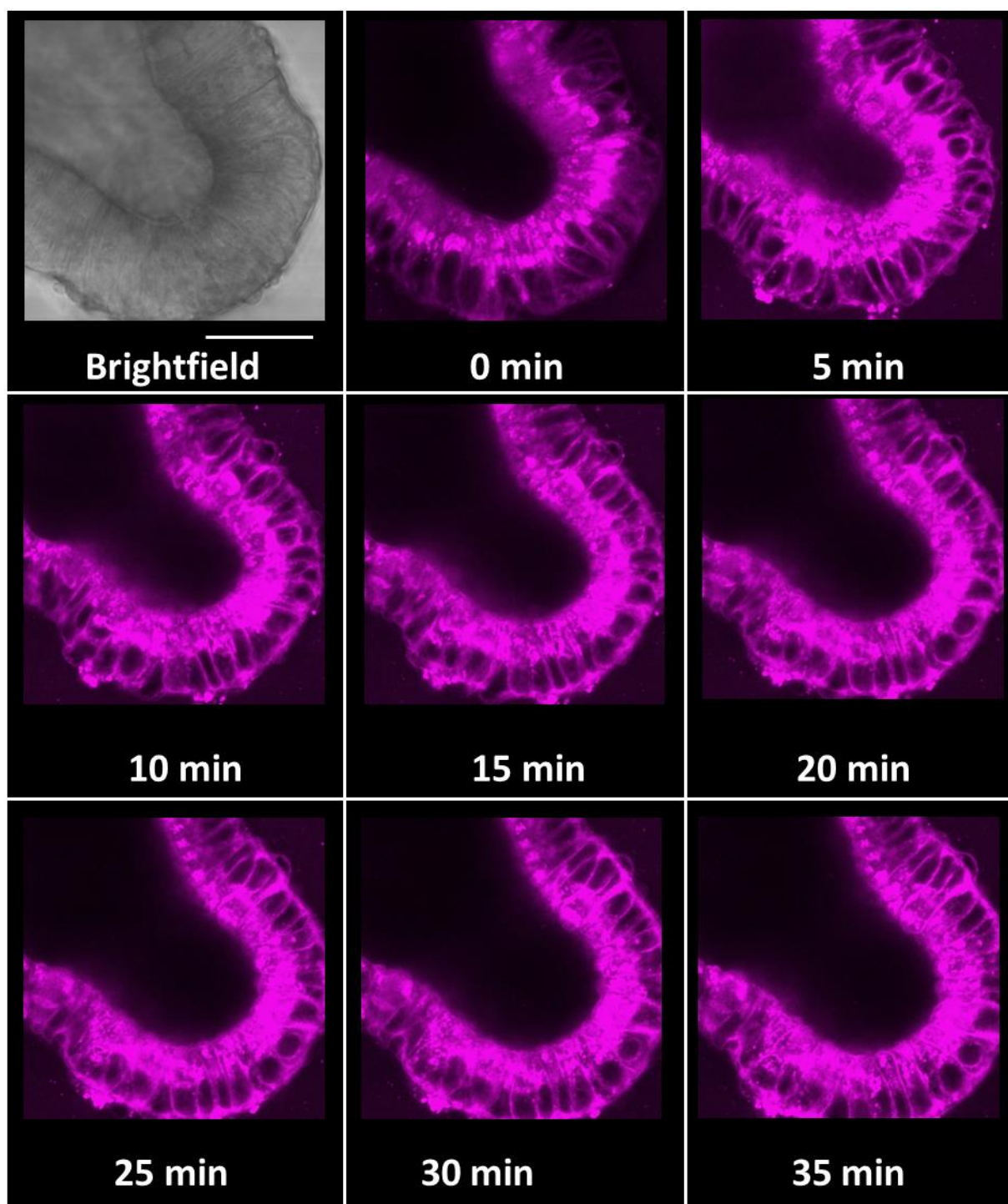
Figure 126 – Deep Red Labelling of Control Secretion and Compound Exocytosis in Organoid.

Representative confocal images of live microscopy time series of the base of organoids labelled with Deep Red (Far Red) upon stimulation with control up to 35 minutes. Brightfield (BF). Scale bar 25 μm. N≥1. For every "N", n≥3.

6.2.3. CCh-Induced Fluid Secretion is Dependent on Ca^{2+} Released by TPCs, IP3Rs and RYRs

The observed swelling of crypts and organoids in the previous results chapter indicate the secretion of fluid across the apical membrane and into the lumen, resulting in increased pressure within the luminal space and hence causing it to swell. Thus, a series of fluid secretion experiments were carried out to characterise the effects of pharmacological inhibition of CCh-induced fluid secretion. The goal of these experiments was to determine if fluid secretion was dependent on certain intracellular Ca^{2+} stores/channels. Pharmacological agents used in this series of experiments include TPC-antagonist Ned-19 (500 µM) and tetrandrine (20 µM), non-specific Ca^{2+} antagonist diltiazem (300 µM), IP3R1-antagonist 2-APB (100 µM), RYR1/3-antagonist dantrolene (50 µM), and non-specific RYR antagonist procaine (1 mM). These experiments were carried out in organoids which were stimulated with CCh for 2 hours, then imaged using the Nikon time lapse microscope. Fluid secretion was measured by comparing the cross-sectional area fold change of organoids at T=2h compared to T=0h.

In summary, the results were similar regardless of pharmacological antagonists. CCh induced fluid secretion in every experiment, resulting in 14-34% increase in cross-sectional area fold change and all of which were statistically significant compared to control (Figure 127-132). The presence of Ned-19 (Figure 127), tetrandrine (Figure 128), diltiazem (Figure 129), 2-APB (Figure 130), dantrolene (Figure 131), and procaine (Figure 132) alone caused a mild decrease (7%) or increase (10%) in cross-sectional area fold change, none of which were statistically significant compared to control. However, the presence of pharmacological antagonist and CCh resulted in cross-sectional area fold changes there were similar to pharmacological antagonists alone and were statistically not significant compared to control but were statistically significant compared to CCh in every case. Due to data corruption, high magnification time lapse images of organoids with/without 2-APB could not be generated (Figure 130).
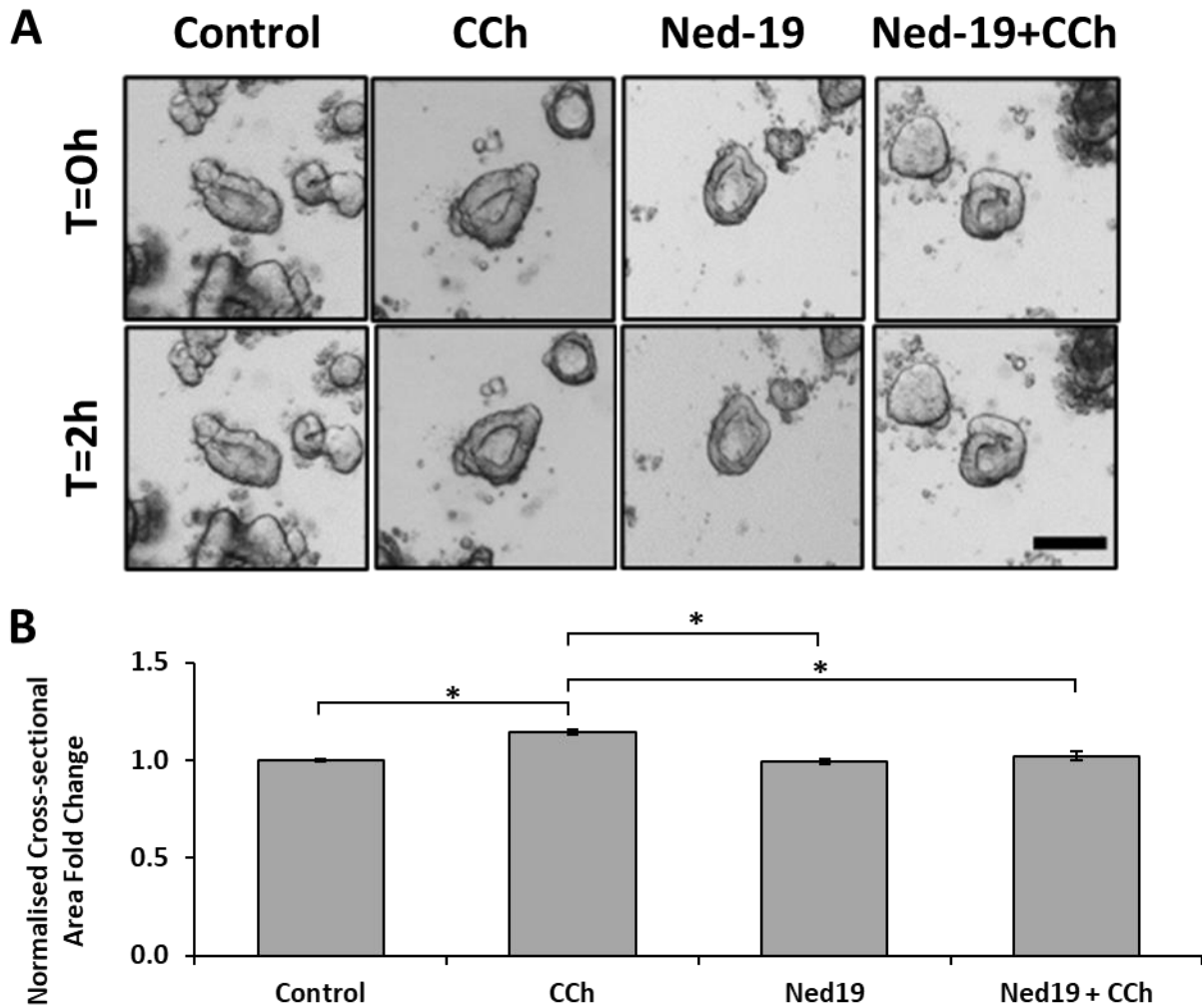
Figure 127 – Ned-19 Inhibits CCh-induced Organoid Swelling.

Representative high magnification time lapse images of organoids at T=0h and T=2h **(A)**. From left to right: organoids stimulated with culture media (Control), organoids stimulated with CCh (10 µM) within culture media (CCh), organoids incubated with Ned-19 (500 µM) followed by stimulation with culture media (Ned-19), and organoids incubated with Ned-19 followed by stimulation with CCh within culture media (Ned-19+CCh). Scale bar 20 µm. Bar chart summarising the normalised cross-sectional area fold change **(B)** of organoids stimulated with culture media (Control), organoids stimulated with CCh within culture media (CCh), organoids incubated with Ned-19 followed by stimulation with culture media (Ned-19), and organoids incubated with Ned-19 followed by stimulation with CCh within culture media (Ned-19+CCh). Data normalised to control and displayed as mean +/- SEM. $P>0.05$ (*). N=2. For every "N", n≥10.
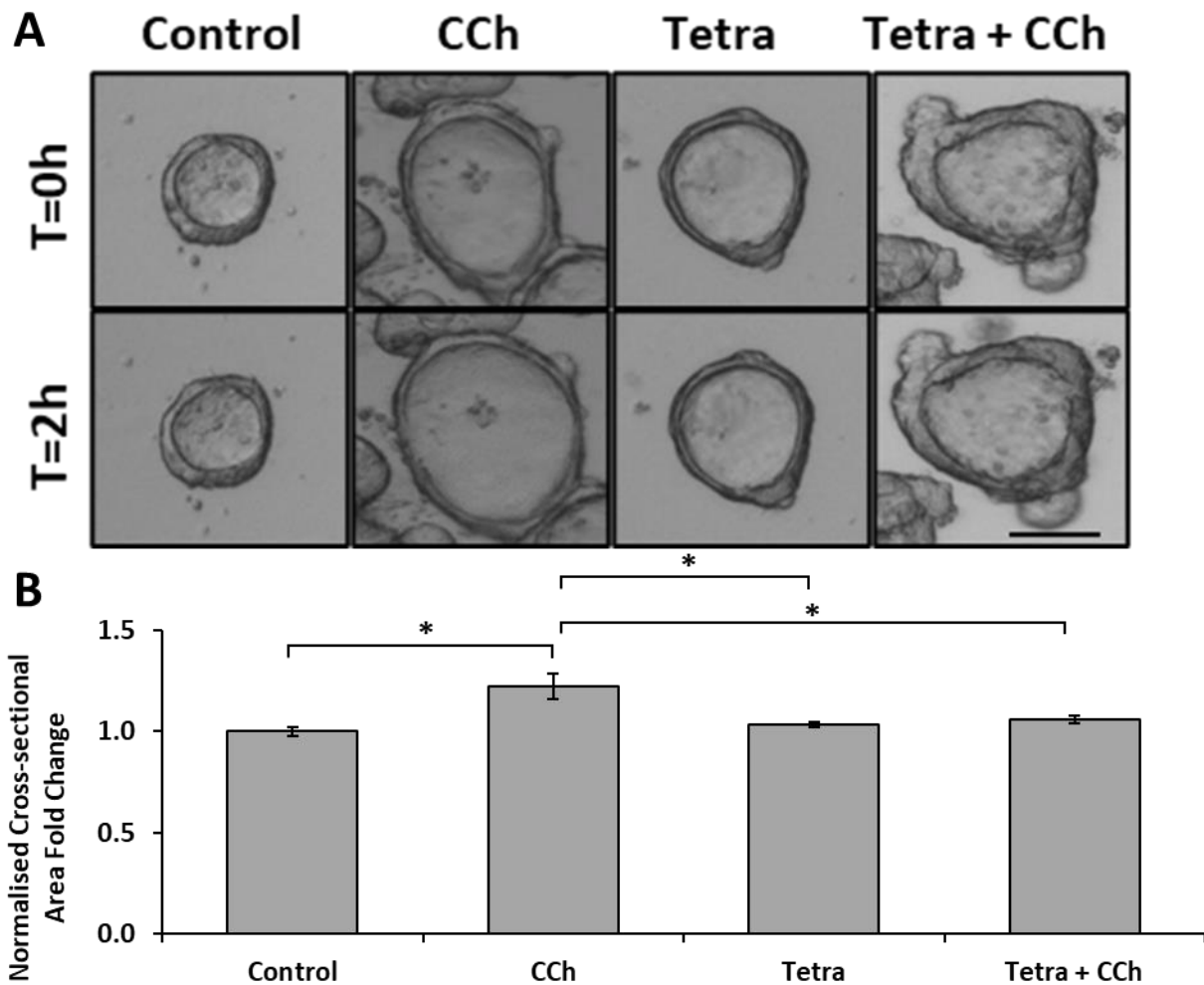
Figure 128 – Tetrandrine Inhibits CCh-induced Organoid Swelling.

Representative high magnification time lapse images of organoids at T=0h and T=2h **(A)**. From left to right: organoids stimulated with culture media (Control), organoids stimulated with CCh (10 µM) within culture media (CCh), organoids incubated with tetrandrine (20 µM) followed by stimulation with culture media (Tetra), and organoids incubated with tetrandrine followed by stimulation with CCh within culture media (Tetra+CCh). Scale bar 20 µm. Bar chart summarising the normalised cross-sectional area fold change **(B)** of organoids stimulated with culture media (Control), organoids stimulated with CCh within culture media (CCh), organoids incubated with tetrandrine followed by stimulation with culture media (Tetra), and organoids incubated with tetrandrine followed by stimulation with CCh within culture media (Tetra+CCh). Data normalised to control and displayed as mean +/- SEM. $P>0.05$ (*). N=2. For every "N", n≥10.
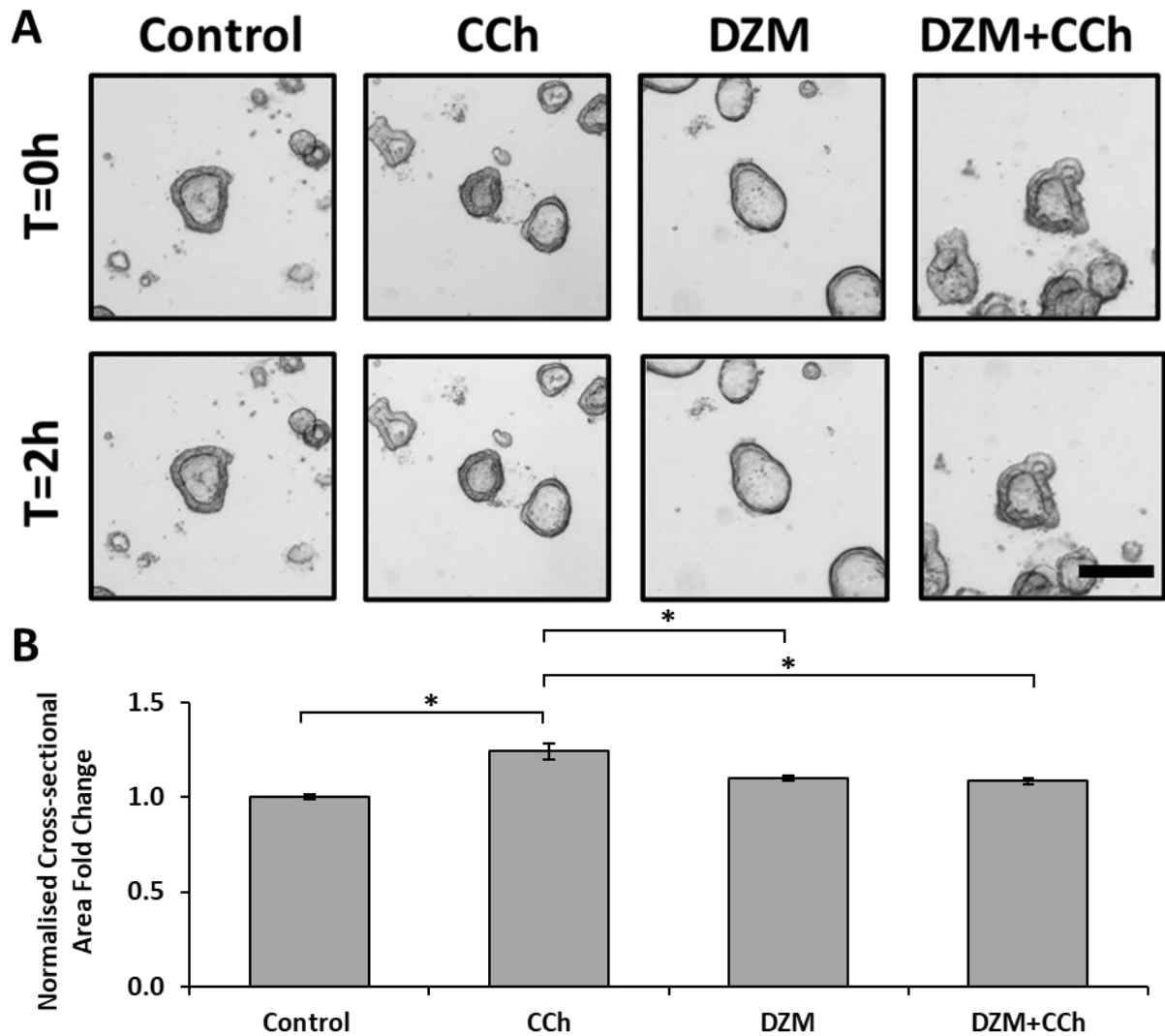
Figure 129 – Diltiazem Inhibits CCh-induced Organoid Swelling.

Representative high magnification time lapse images of organoids at T=0h and T=2h **(A)**. From left to right: organoids stimulated with culture media (Control), organoids stimulated with CCh (10 µM) within culture media (CCh), organoids incubated with diltiazem (300 µM) followed by stimulation with culture media (DZM), and organoids incubated with diltiazem followed by stimulation with CCh within culture media (DZM+CCh). Scale bar 20 µm. Bar chart summarising the normalised cross-sectional area fold change **(B)** of organoids stimulated with culture media (Control), organoids stimulated with CCh within culture media (CCh), organoids incubated with diltiazem followed by stimulation with culture media (DZM), and organoids incubated with diltiazem followed by stimulation with CCh within culture media (DZM+CCh). Data normalised to control and displayed as mean +/- SEM. P>0.05 (*). N=2. For every "N", n≥10.
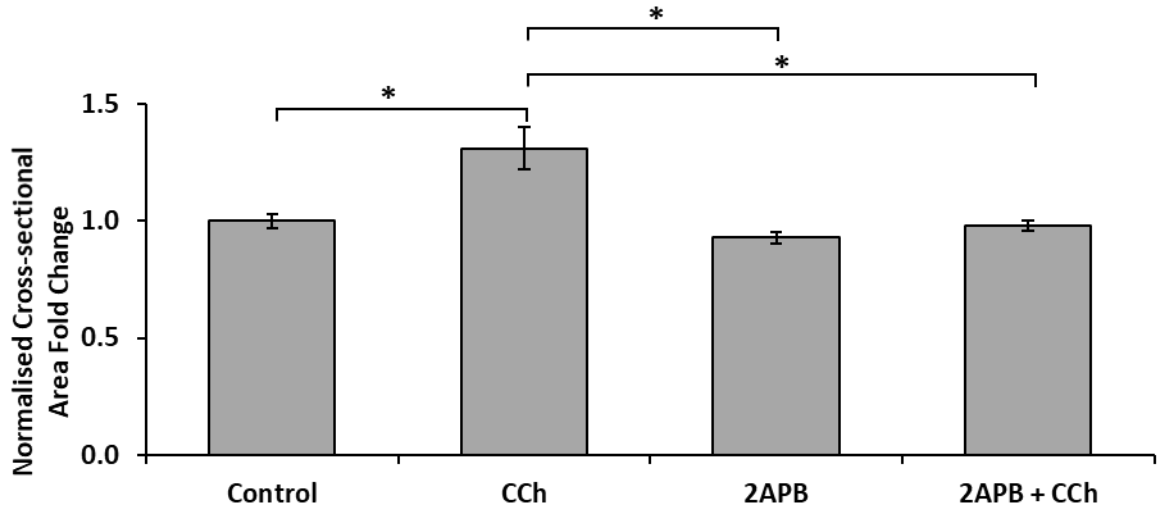
Figure 130 – 2-APB Inhibits CCh-induced Organoid Swelling.

Bar chart summarising the normalised cross-sectional area fold change **(A)** of organoids stimulated with culture media (Control), organoids stimulated with CCh (10 µM) within culture media (CCh), organoids incubated with 2-APB (100 µM) followed by stimulation with culture media (2APB), and organoids incubated with 2-APB followed by stimulation with CCh within culture media (2APB+CCh). Data normalised to control and displayed as mean +/- SEM. P>0.05 (*). N=2. For every "N", n≥10.
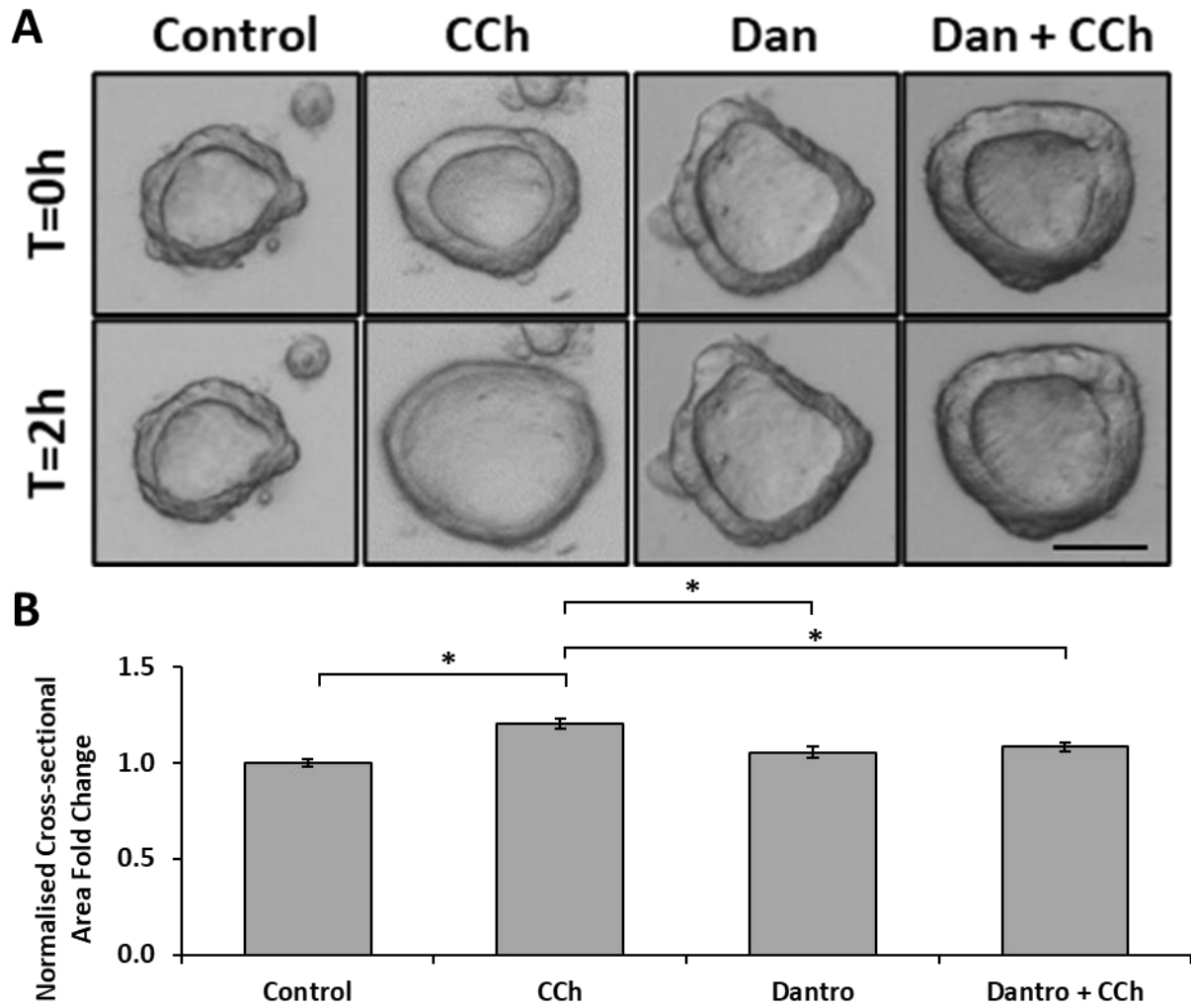
Figure 131 – Dantrolene Inhibits CCh-induced Organoid Swelling.

Representative high magnification time lapse images of organoids at T=0h and T=2h **(A)**. From left to right: organoids stimulated with culture media (Control), organoids stimulated with CCh (10 μM) within culture media (CCh), organoids incubated with dantrolene (50 μM) followed by stimulation with culture media (Dan), and organoids incubated with dantrolene followed by stimulation with CCh within culture media (Dan+CCh). Scale bar 20 μm. Bar chart summarising the normalised cross-sectional area fold change **(B)** of organoids stimulated with culture media (Control), organoids stimulated with CCh within culture media (CCh), organoids incubated with dantrolene followed by stimulation with culture media (Dantro), and organoids incubated with dantrolene followed by stimulation with CCh within culture media (Dantro+CCh). Data normalised to control and displayed as mean +/- SE. P>0.05 (*). N=2. For every "N", n≥10.
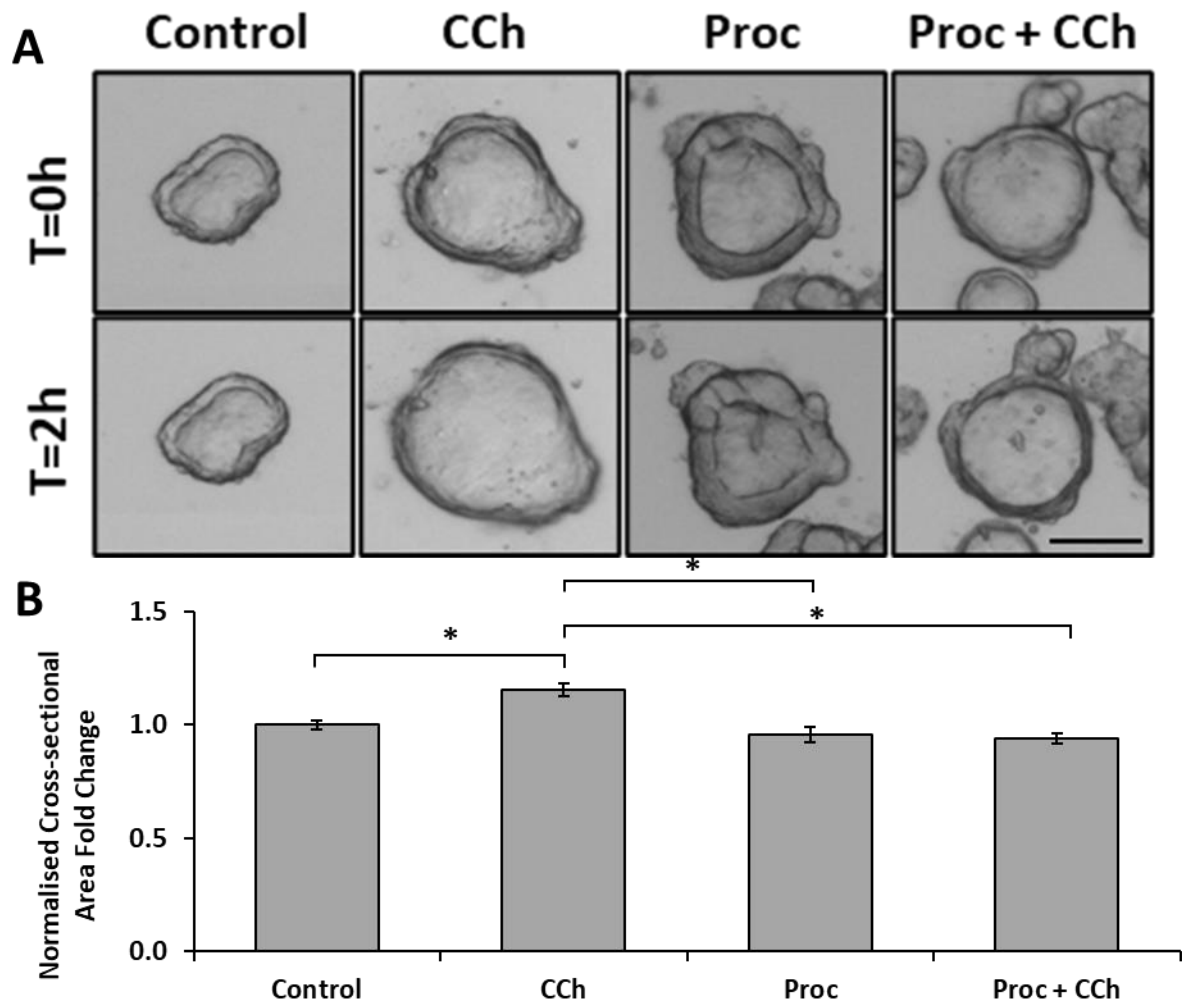
Figure 132 – Procaine Inhibits CCh-induced Organoid Swelling.

Representative high magnification time lapse images of organoids at T=0h and T=2h **(A)**. From left to right: organoids stimulated with culture media (Control), organoids stimulated with CCh (10 μM) within culture media (CCh), organoids incubated with procaine (1 mM) followed by stimulation with culture media (Proc), and organoids incubated with procaine followed by stimulation with CCh within culture media (Proc+CCh). Scale bar 20 μm. Bar chart summarising the normalised cross-sectional area fold change **(B)** of organoids stimulated with culture media (Control), organoids stimulated with CCh within culture media (CCh), organoids incubated with procaine followed by stimulation with culture media (Proc), and organoids incubated with procaine followed by stimulation with CCh within culture media (Proc+CCh). Data normalised to control and displayed as mean +/- SEM. P>0.05 (*). N=2. For every "N", n≥10.

6.2.4 CCh-Induced Proliferation is Dependent on Ca^{2+} Released by TPCs.

Finally, this thesis studied whether TPC-mediated release of Ca^{2+} is needed for inducing proliferation of colonic epithelial cells. To this end, a series of proliferation experiments were carried out in crypts using the EdU assay, whereby a fluorescent analogue of thymidine is inserted every time a cell replicates its DNA and undergoes mitosis. Crypts were incubated with EdU and stimulants for 2 days. During this period crypts were either stimulated with control, CCh (10 µM), Ned-19 (125 µM), or Ned-19+CCh (Figure 133). During analysis, crypts were separated into four regions: the first twenty nuclei counting from the very bottom of the crypt (Base), the next twenty nuclei above it (Supra Base), the subsequent twenty nuclei above it (Mid), and the remaining nuclei (Top). In control, the percentage of EdU+ cells across those four regions were 39.1%, 24.9%, 5.7%, and 0.5% respectively. By contrast, the percentage of EdU+ cells for crypts treated with CCh were increased across all four regions at 43.6%, 25.3%, 8.9% and 0.8%, respectively. Of these, the base and mid regions of CCh-treated crypts were statistically significant than their control counterpart. Next, the percentage of EdU+ cells for crypts treated with Ned-19 were greatly decreased across all four regions at 27.7%, 2.0%, 0.0% and 0.0%, respectively. All of which were statistically significant than their control counterpart. Likewise, the percentage of EdU+ cells for crypts treated with Ned-19+CCh were greatly decreased across all four regions at 22.4%, 0.8%, 0.0% and 0.0%, respectively. Again, all of these were statistically significant than their control counterpart.
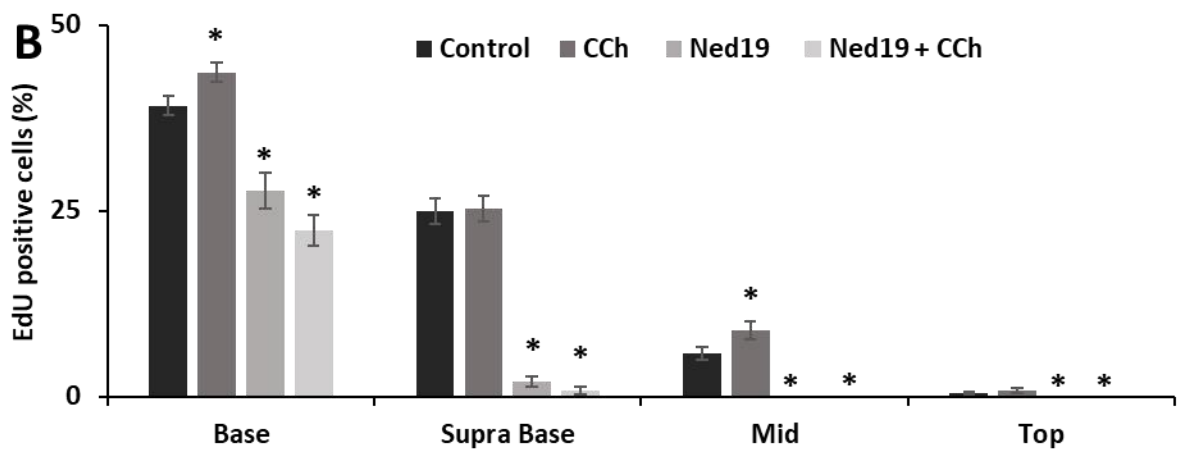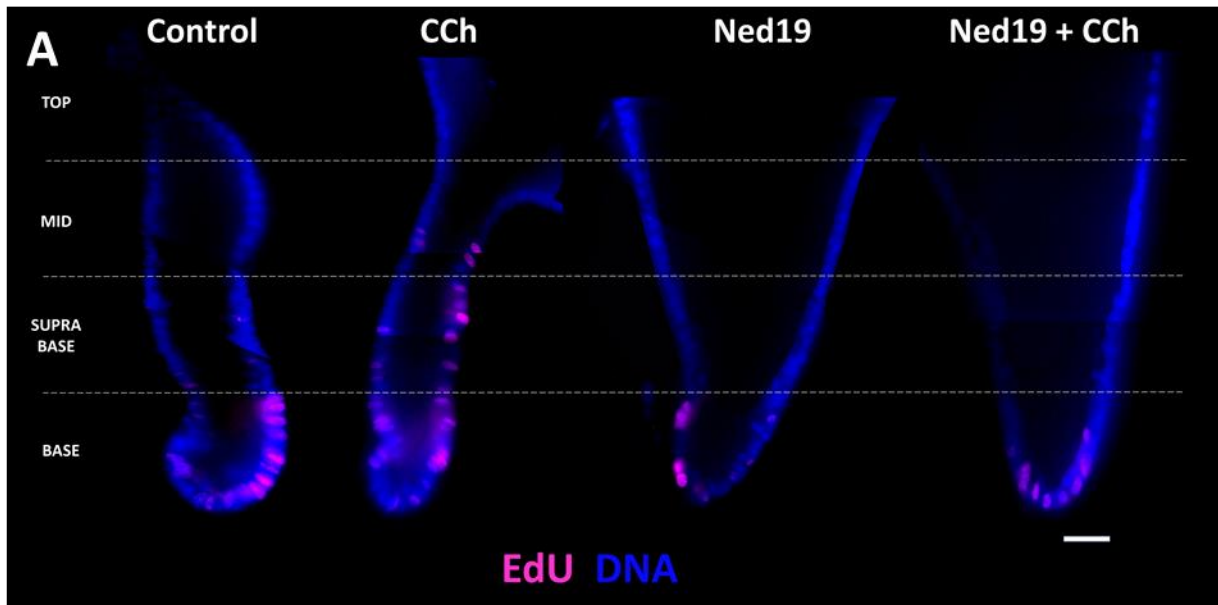
Figure 133 – Ned-19 Inhibits CCh-Induced Cell Proliferation.

Representative epifluorescence images **(A)** of whole crypts labelled with thymidine analogue (EdU) in pink and nuclei (DNA) stained with Hoechst in blue. Scale bar 25 µm. Bar chart summary of EdU cell percentage across the different crypt regions as compared to the total number of nuclei **(B)**. N=2. For every "N", n≥5.

6.3 Discussion

In this results chapter, the physiological consequences of pharmacologically inhibiting Ca^{2+} mobilisation from endolysosomes and endoplasmic reticulum were investigated in the human colonic epithelium. This body of work was built upon by previous work carried out by the Williams group, whereby stimulation of M3 by cholinergic agonists mobilised endolysosomal Ca^{2+} via TPCs to induce mucus secretion and proliferation (Kam 2015) and (Pelaez-Llaneza 2019). In a previous results chapter (Chapter 4), CCh was confirmed to activate M3 receptors and cause release of localised Ca^{2+}-signals via endolysosomal TPCs, which induced global Ca^{2+}-signals via endoplasmic reticular IP3Rs and RYRs. Thus, this chapter set out to investigate whether pharmacological inhibition of TPCs, IP3Rs and RYRs affected mucus secretion, fluid secretion, and proliferation.

6.3.1 CCh-Induced Mucus Secretion is Dependent on Ca^{2+} Released by TPCs and RYRs

In the first results chapter (Chapter 3.2), MUC2 labelling was shown to be present within the stem cell zone of isolated human colonic crypts (crypts), and cultured human colonic organoids (organoids). Specifically, MUC2 labelling was shown to be present within cells labelled with intracellular Ca^{2+}-signalling components such as TPC1 (Figure 38) and TPC2 (Figure 40), CD38 (Figure 42) and M1/3/5 (Figure 46-8). To complement those, MUC2 was shown to be expressed throughout whole mucosal crypts, cultured crypts, organoids, and in single cells (Figure 106). While one can propose these MUC2-cells to all belong to the goblet cell lineage, it would be misleading to claim all MUC2-labelled cells as goblet cells, for three reasons. First, the morphology of MUC2 labelled cells were not always goblet cell-shaped, especially those at the very bottom of mucosal crypts, cultured crypts, and organoids (Figure 106). Secondly, the proportion of goblet cells had been shown to range between 9% (Umar, 2011) to 16% (Kim & Ho, 2010) depending on the location. By contrast, the number of MUC2 labelled cells were consistently observed to be higher in this thesis. Indeed, previous work within the Williams lab quantified the number of MUC2-labelled cells and reported approximately 30% MUC2+ cells in mucosal crypts, cultured crypts, and organoids (Pelaez-Llaneza 2019). Thirdly, MUC2-labelling cells at the bottom of crypts which do not resemble goblet cells are likely deep crypt secretory cells, which have been shown to express MUC2 (Rothenberg, et al., 2012). Regardless of the identity of these slender MUC2-labelled cells, these are still mucus-secreting cells whose in-vivo physiological role is to secrete mucus constitutively to maintain the mucus barrier, or in response to extracellular signalling such as acetylcholine (Birchenough, Johansson, Gustafsson, Bergström, & Hansson, 2015).

Before carrying out pharmacological inhibition of mucus secretion induced by CCh (10 µM), the temporal characteristics of mucus secretion was first determined (Figure 107). Mucus secretion was observed to occur within 5 minutes, due to the observance of depleted MUC2-labelling on the apical pole of cells (Figure 107B). That said, even in the absence of stimulation, crypts are capable of secreting mucus at a slow rate (Neutra, Grand and Trier 1977). Previous work by the Williams lab showed that the change in normalized fluorescence intensity was

greatest after 5 minutes of CCh-stimulation (Pelaez-Llaneza 2019), after which normalized fluorescence intensity slowly returns closer to control which has been observed in another study (Gustafsson, et al. 2012). Thus, during the subsequent mucus depletion assays, crypts were stimulated with CCh for 5 minutes before being fixed and immunolabelled with MUC2.

In every mucus depletion assay (Figure 108-113), crypts which were stimulated CCh had reduced normalised MUC2 immunofluorescence intensity that was statistically significant compared to control. TPC-antagonist Ned-19 (250 µM) and tetrandrine (20 µM) were both shown to inhibit CCh-induced mucus secretion (Figure 108-9). IP3R1-antagonist 2-APB (100 µM) did not inhibit CCh-induced mucus secretion (Figure 110), but IP3R3-antagonist caffeine (10 mM) did (Figure 111). When crypts were incubated with Ned-19/tetrandrine/2-APB/caffeine only, the resulting normalised MUC2 immunofluorescence intensity was statistically not significant compared to control, indicating that baseline mucus secretion was not dependent on TPCs/IP3Rs. However, the combination of Ned-19/tetrandrine/caffeine with CCh was statistically not significant compared to control but was statistically significant compared to CCh alone, indicating that pharmacological inhibition of CCh-induced Ca^{2+}-release from endolysosomal TPCs and endoplasmic reticular IP3R3 blocked mucus secretion. On the flipside, the normalised MUC2 immunofluorescence intensity of 2-APB+CCh crypts were statistically significant compared to control but statistically not significant compared to CCh; indicating that pharmacological inhibition of CCh-induced Ca^{2+}-release from endoplasmic reticular IP3R1 was insufficient to block mucus secretion. Moving on to RYR1/3-antagonist dantrolene (30 µM) and non-specific RYR-antagonist procaine (1 mM), they were also found to inhibit CCh-induced mucus secretion (Figure 112-13). The normalised MUC2 immunofluorescence intensity of crypts which were incubated with dantrolene/procaine were statistically not significant compared to control, again indicating that baseline mucus secretion was not dependent on RYRs. However, the combination of dantrolene/procaine with CCh was statistically not significant compared to control but was statistically significant compared to CCh alone, indicating that pharmacological inhibition of CCh-induced Ca^{2+}-release from endoplasmic reticular RYRs blocked mucus secretion. One thing to note about these experiments was that, besides 2-APB, the presence of pharmacological antagonist alone resulted in higher MUC2 intensity, which may indicate blockage of baseline MUC2 secretion and resulting in MUC2 accumulation within the cytoplasm.

Taken together, these experiments indicate that mucus secretion are driven by intracellular Ca^{2+} second messengers. Specifically, it requires local Ca^{2+}-signals from endolysosomal TPCs and global Ca^{2+}-signals from endoplasmic reticular IP3R3 and RYR1/3. Further supporting that proposal was previous work by the Williams group (Pelaez-Llaneza 2019), which showed that CCh-induced MUC2 secretion was inhibited when intracellular Ca^{2+} was chelated using BAPTA-AM (66 µM). One missing experiment which should be done in the future to confirm that CCh-induced Ca^{2+} signals resulted from muscarinic receptor activation, is whether 4-DAMP inhibits CCh-induced mucus secretion.

Having shown that inhibition of TPCs and RYR1/3s blocked mucus secretion induced by CCh, it raises the question whether releasing endoplasmic reticular Ca^{2+} was capable of inducing mucus secretion. To investigate this, mucus depletion assays were carried out using the SERCA pump inhibitor, CPA (20 µM). Interestingly, CPA did not induce mucus secretion (Figure 114A-B). This would indicate that mucus secretion requires the initial release of Ca^{2+} stored within endolysosomes, which is supported by a previous study that showed intracellular Ca^{2+}-signals generated by M3-receptor activation is necessary for mucus secretion (Lindqvist, et al. 2002). Alternatively, since the Ca^{2+}-signal induced by CPA takes longer to reach the same amplitude as CCh, approximately 200s compared to 100s (Figure 86), it could be that more time would be needed to observe mucus secretion induced by CPA, which could be investigated in future studies.

Finally, UTP (50 µM) was shown to be capable of inducing mucus secretion (Figure 114C), which indicate purinergic signalling via P2Y2 playing a role in mucus secretion. Future studies should explore this by carrying out mucus depletion assays using purinergic secretagogues UTP/ATP, alongside P2Y2 receptor-antagonist AR-C118925XX and pharmacological antagonists used thus far, to elucidate the mechanism of purinergic-induced mucus secretion.

6.3.2 Live Visualisation of Mucus Granule Secretion and Compound Exocytosis
While mucus depletion assays enable the quantification of MUC2 secretion in response to CCh and the effects of pharmacological antagonists, this thesis was also interested in visualising the movement of mucus granules and its secretion into the lumen. To that end, fluorescent lipid dyes were used as a tool to record mucus exocytosis in real time.

FM1-43 was used to label the plasma membrane and other membrane-bound vesicles. In both crypts and organoids, goblet-shaped cells were particularly well-labelled with FM1-43 within their cytoplasm (Figure 115-8). Live confocal imaging of crypts (Figure 115) and organoids (Figure 117) loaded with FM1-43 which were stimulated with CCh resulted in the formation of 'bubbles' from the apical membranes, expanding into the lumen and eventually being exocytosed into the lumen. These 'bubbles' were likely the membranes of mucus granules that had fused with the plasma membrane which, upon being secreted into the lumen, results in its mucin contents expanding and leading to enlargement of the 'bubbles'. However, the presence of 'bubbles' was not exclusive to CCh-stimulation, as crypts (Figure 116) and organoids (Figure 118) treated with control were also observed to form 'bubbles', albeit less frequently. Interestingly, the formation of 'bubbles' usually took more than ten minutes to generate, which would imply that the secretion of mucus after 5 minutes of CCh-stimulation – which was visualized and quantified previously – occurs prior to 'bubbles' forming. One explanation is that short-term stimulation with CCh induced small amounts of mucus secretion, which in the long-term results mucus granule expansion into bubbles. Or, it

may that that long term stimulation with CCh results in compound exocytosis. Follow up studies should elucidate whether bubbles are indeed a result of compound exocytosis. It should also investigate whether mucus secretion is a multivesicular process; whereby upon CCh-stimulation, mature granules close to the apical membrane fuses with the plasma membrane and releases its contents into the lumen, while underlying mucus granules fuse with one another before being exocytosed from the apical membrane as a 'bubble'. More importantly, future studies should validate whether the contents of these 'bubbles' are mucins.

In addition to FM1-43, its fixable variant FM1-43X was also used to visualize mucus secretion. While it can also be used under live confocal imaging, its purpose was to determine if 'bubbles' remained after fixation. Interestingly, crypts which were loaded with FM1-43X and imaged live presented higher numbers of 'bubbles' prior to stimulation or fixation (Figure 119-20). Assuming these 'bubbles' indeed contain mucus, it would indicate baseline mucus secretion which can be visualized by FM1-43X. Noted, this was only achieved by enhancing the gain to the point of saturating the rest of the crypt. More importantly, when crypts were treated with CCh for 30 minutes and fixed with PFA, the resulting number of luminal 'bubbles' increased, complimenting the observations seen with FM1-43. When this was repeated in organoids (Figure 121-22), the amount of 'bubbles' resulting from CCh-stimulation was much lower. Instead, the presence of a continuous fluorescent green line within the organoids' lumen just outside their apical membrane was typically observed. These lines were suspected to be 'bubbles' which were secreted but remain trapped due to some organoids not having an opening like crypts to allow them to expand. Lastly, Cell Tracker^{TM} Deep Red was used to as an alternative fluorescent lipid dye. Similar to FM1-43, crypts (Figure 123) and organoids (Figure 125) which were loaded with Deep Red and stimulated with CCh formed 'bubbles' from their apical poles which were visually ejected into the lumen over the course of 30 minutes. And in control crypts (Figure 124) and organoids (Figure 126), fewer/no 'bubbles' were observed.

Taken together, FM1-43, FM1-43X and Deep Red were shown to be viable tools for studying mucus secretion. Being fixable, FM1-43X would be an alternative method of conducting the mucus depletion assays. On the other hand, FM1-43 Deep Red would be suitable for live recording of mucus secretion. Possible means of quantifying the data generated from these fluorescent images would be to measure the normalised fluorescence intensity or the amount of 'bubbles' formed. Future studies could investigate the effects of other secretagogues on crypts and organoids loaded with these fluorescent lipid dyes and determine the consequences of when in the presence of pharmacological antagonists. And, since UTP was shown to be capable of depleting mucus (Figure 114C), these fluorescent lipid dyes could be used to visualise purinergic-induced mucus granule secretion and compound exocytosis.

6.3.3 CCh-Induced Fluid Secretion is Dependent on Ca^{2+} Released by TPCs, IP3Rs and RYRs

While using fluorescent lipid dyes to visualize mucus secretion, an interesting observation was noted. Whether from control or CCh-stimulation, crypts and organoids were typically observed to swell and move over time. As a result, the apical and basal membrane of the entire crypt/organoid were usually thinner at the end of the experiment, alongside their lumen being wider. Due to this, fluid secretion was proposed to occur alongside mucus secretion, with the purpose of flushing the lumen of crypts/organoids and maintain mucus hydration. A range of secretagogues are capable of inducing fluid secretion in the human colonic epithelium including CCh, histamine, PGE-2 and adenosine (Halm and Halm 2000), 5-HT (Diwakarla, Fothergill, Fakhry, Callaghan, & Furness, 2018), and forskolin (de Winter-de Groot, et al. 2020). However, the observation of swelling in control condition indicated a non-secretagogues means of fluid secretion, which was postulated to be mechanosensitive Piezo channels on enterochromaffin cells (Alcaino, Farrugia, & Beyder, 2017) and (Alcaino, et al., 2018), which also induces Ca^{2+}-signals as demonstrated earlier (Figure 89). Other groups have investigated fluid secretion in gut organoids using cAMP (Fujii, et al. 2016) and PGE-2 (Schwank, et al. 2013). However, the relevance of intracellular Ca^{2+}-signals were not considered in those studies.

Using the same strategy with mucus depletion assays, fluid secretion was investigated in organoids in the form of organoid swelling assays. Organoid swelling assays were carried out using CCh for 2 hours, in the presence/absence of pharmacological antagonists, to determine if cholinergic stimulation enhanced organoid swelling and whether if it was Ca^{2+}-dependent. Pharmacological antagonists used in these assays included TPC-antagonists Ned-19 (500 µM) and tetrandrine (20 µM), non-specific TPC-antagonist diltiazem (300 µM), IP3R1-antagonist 2-APB (100 µM), RYR1/3-antagonist dantrolene (50 µM), and non-specific RYR antagonist procaine (1 mM). The cross-sectional area of the control increased by approximately 2% between T=0hrs to T=2hrs (data not shown), which may indicate baseline fluid secretion. Stimulating organoids with CCh (10 µM) induced a 14-34% increase in organoid cross-sectional area fold change compared to control (Figure 127-132), thereby showcasing CCh as fluid secretion secretagogue. The presence of pharmacological antagonists alone did not affect the organoid cross-sectional area fold change compared to control, and neither did antagonist plus CCh. However, both were statistically significant compared to CCh, which indicate that TPCs, IP3Rs and RYRs are required for fluid secretion. These compliment other studies which show Ca^{2+}-signalling being important for fluid secretion (Reynolds, Parris, et al. 2007) and (Yang, et al. 2018).

It was interesting to note that mucus secretion was unaffected by IP3R1 inhibition using 2-APB (Figure 110) while fluid secretion was not (Figure 130). The later had been explored by a study which showed fluid secretion being dependent on muscarinic-activated Ca^{2+} release from endoplasmic reticular IP3Rs (Ambudkar 2000). Future experiments should show that CCh-induced fluid secretion was inhibited by M1/3-antagonist 4-DAMP and Ca^{2+}-chelator

EGTA, in order to confirm CCh-induced fluid secretion occurs via muscarinic receptor activation and requires Ca^{2+}-signals. Besides those, in would be of interest to know if purinergic secretagogues ATP/UTP, piezo channel activator Yoda1, and SERCA-pump inhibitor CPA could also induce fluid secretion.

6.3.4 CCh-Induced Proliferation is Dependent on Ca^{2+} Released by TPCs.
While a recent study found acetylcholine and subsequent muscarinic receptor activation to downregulate proliferation (Takahashi, et al., 2014), many studies found neuronal and non-neuronal acetylcholine to promote colonic epithelial cell proliferation (Cheng, et al., 2008), (Hayakawa, et al., 2017) and (Pan, Zhang, Shao, & Huang, 2020). Previous work in the Williams lab (Pelaez-Llaneza 2019) showed that organoids incubated for 6 days with cholinergic agonist CCh (10-100 µM) or muscarinic agonist oxotremorine (1-10 µM) developed more buds compared to control, thus showing muscarinic receptor activation promotes proliferation in organoids.

To further these findings, an EdU proliferation assay was carried out to show that CCh induced proliferation in crypts and was dependent on release of endolysosomal Ca^{2+} via TPCs. To that end, crypts which were incubated with CCh for 2 days had markedly more EdU+ cells in every region (Figure 133), the greatest increase occurring at the base region where it increased by 4.5% (P<0.05), followed by the mid region (3.2%; P<0.05), the supra base region (0.4%; N.S) and the top region (0.3%; N.S). This was sensible, as stem cells within the crypt base were expected to be sensitive to acetylcholine stimulation. As the supra base represented cells within the transit amplifying zone and mid region represented cells that had passed the transit amplifying zone (Figure 8), both regions were expected to have significantly higher percentage of EdU+ cells, which was not the case (Figure 133). This could mean that acetylcholine promotes symmetrical stem cell division rather than asymmetrical (van der Flier and Clevers 2009) and also affects cell division within the transit amplification zone, which should be further investigated in future studies. The lack of increased EdU+ cells in the top region was not too surprising, as they represent cells that had already passed the transit amplification zone by the time crypts were stimulated with CCh and thus were not expected to proliferate.

The presence of Ned-19 (125 µM) was shown to inhibit the percentage of EdU+ cells induced by CCh in crypts (Figure 133). While the concentration used may seem to contradict the Fura-2 experiments, whereby Ned-19 (125 µM) was unable to inhibit CCh-induced Ca^{2+}-signals while high concentrations (500 µM) did (Figure 67), this was simply because high concentrations of Ned-19 (500 µM) was toxic to crypts, which was observed in crypts/organoids left in Ned-19 for prolonged periods. Hence, the proliferation assay used a lower concentration over a longer period (2 days) to demonstrate TPC-inhibition without causing toxicity, whereas for Fura-2 a high concentration over a shorter time (4 hours) was

required to block TPCs. Interestingly, Ned-19 and Ned-19+CCh both resulted in significantly decreased the percentage of EdU+ cells compared to control. This might indicate that baseline colonic epithelial proliferation relies heavily on Ca^{2+}-signals from endolysosomal TPCs, which when inhibited results in decreased proliferation and should be investigated in future studies. Future studies should consider using antagonists of M1/3 (4-DAMP), IP3Rs (2-APB), RYRs (dantrolene), and other non-specific antagonists (atropine, diltiazem, procaine, etc) to consider whether colonic epithelial proliferation relies on endoplasmic reticular stored Ca^{2+} too. Besides that, it would also be of interest to investigate whether purinergic secretagogues (ATP/UTP) could induce proliferation and determine their pharmacological inhibition profiles.

6.4 Conclusion

First, cholinergic agonist CCh was shown to induce mucus secretion, which was blocked by TPC, IP3R3 and RYR inhibition, but not IP3R1. This was carried out in crypts which were immunolabelled with MUC2, in the presence/absence of CCh and/or pharmacological agents. Next, fluorescence lipid dyes FM1-43, FM1-43X and Deep Red were shown to be able to visualize mucus secretion and compound exocytosis of mucus granules induced by CCh in crypts and organoids under live confocal microscopy, by the formation of 'bubbles' from their apical membranes. Next, CCh was shown to induce fluid secretion in organoids and could be blocked by TPC, IP3R and RYR inhibition. This was carried out in organoids in the presence/absence of CCh and/or pharmacological agents. Lastly, CCh was shown to induce colonic epithelial proliferation that was significantly higher at the crypt base and mid region and could be blocked by TPC inhibition. In the next and final chapter, this thesis compares the gene and protein expression of Ca^{2+} signalling toolkit components in human tumour colonic tissue, as well as the pharmacological profiles of these Ca^{2+} signalling toolkit components, against normal human colonic tissue (Chapter 3 & 4).

7 Chapter 7 – Results Part 5: Comparison of Muscarinic and Purinergic Signals in Relation to Colorectal Cancer

7.1 Introduction

Colorectal cancer (CRC) is a complex disease whose development and progression relies on several genetic and molecular alterations. There are many lifestyle risk factors associated with CRC, including tobacco, high alcohol consumption, high stress, high saturated fat or red meat, low dietary fibre, and low exercise (Lin 2009). Besides those, inflammatory bowel diseases such as ulcerative colitis and Crohn's disease have higher risk for developing CRC. This is a result of changes in cellular features of the epithelium due to continuous damage and repair leading to mutations, genomic instability, and atypical cellular development at multiple sites (Manne, et al. 2012). Finally, somatic mutations and inheritance of specific genes such as APC (Barker, et al., 2009), Bmpr1a, Smad4, and PTEN (He, et al., 2004) are associated with increased risk of CRC.

Ca^{2+} signalling has a complex role on the development and progression of colorectal cancer, which has been surmised in a recent review (Wang, et al. 2019). For example, increased expression of plasma membrane V-ATPase helps create a hypoxic microenvironment with an acidic extracellular pH, which correlated with invasiveness and metastatic potential (Sennoune, et al., 2004). When V-ATPase was downregulated in colon cancer cells, it inhibited tumour cell invasiveness and increases its sensitivity to chemotherapeutic agent 5-FU (Lozupone, et al., 2015). Remodelling of store-operated Ca^{2+} entry (SOCE) through the partial depletion of the endoplasmic reticular Ca^{2+} stores is characteristic of CRC. Receptors which enable depletion of the endoplasmic reticulum Ca^{2+} store include IP3Rs and RYRs. IP3R3 are associated with decreased 5-year survival chances and suggested it confers a survival advantage in CRC by inhibiting apoptosis (Shibao, et al., 2010), and a gene transcriptomic analysis study found IP3R3 being absent from normal cells but expressed in cancer cells (Pérez-Riesgo, et al., 2017). Another Ca^{2+} store whose depletion has been associated with CRC are endolysosomes, which release Ca^{2+} by several channels including VGCCs, TRPs and TPCs (Figure 17B). TPCs have also been studied extensively in the context of CRC (Alharbi & Parrington, 2019). NAADP-mediated TPC1 lysosomal Ca^{2+} release had been shown to trigger ERK and the PI3K/AKT signalling pathways to promote proliferation (Faris, et al., 2019), and in human breast cancer cell lines the expression of TPC1 transcripts is three to eight times higher than TPC2 transcripts (Brailoiu, et al., 2009).

On the GPCR level, changes in certain muscarinic receptors (M1-5) and metabotropic P2Y receptors have also been implicated in CRC (von Rosenvinge and Raufman 2011) and (Bellefeuille, Molle and Gendron 2019). M3 in particular is associated with CRC, with studies showing its activation by various agonists including CCh and bile acids promoting proliferation in human colon cancer cells (Frucht, et al. 1999), (Yang and Frucht 2000) and (Cheng, Chen,

et al. 2002). P2Y2 receptors have also been associated with CRC as an oncogene, with studies showing its expression being increased in human CRC compared to normal colonic tissue (Nylund, Hultman, Nordgren, & Delbro, 2007), which was also observed in mice (Hatanaka, et al. 2007) and (Künzli, et al. 2011).

Thus, this results chapter is interested in comparing patient-matched normal versus tumour colonic mucosa samples. First, transcriptomic analysis of Ca^{2+} signalling toolkit expression in tumour colonic mucosa samples was compared against normal colonic mucosa samples. Next, the protein expression of these Ca^{2+} signalling toolkit were confirmed in tumoroids using immunolabelling. Finally, Fura-2 experiments were carried out to determine the pharmacological profiles of tumour crypts and tumoroids in response to CCh and UTP, and compared against crypts and organoids.

7.2 Results

Transcriptomic analysis of Ca^{2+} signalling toolkit expression was performed on native human tumour colonic mucosa (tumour mucosa), isolated tumour crypts (tumour crypts), and cultured tumoroids (tumoroids), and compared against the transcriptomic analysis done in organoids (Chapter 3.2.1). Next, Ca^{2+} signalling toolkit components were labelled in tumour mucosa, tumour crypts, and tumoroids using immunolabelling and their localisation visualized using confocal imaging. Finally, a range of pharmacological agents were used to inhibit Ca^{2+}-signals induced by CCh/UTP; their normalized pharmacological profiles were compared against organoids (Chapter 4.2).

7.2.1 Comparative Transcriptomic Analysis of Ca^{2+} Signalling Toolkit Expression

RNA sequencing was used to compare the gene expression of Ca^{2+} signalling toolkit components in tumoroids. These components can be divided as intracellular Ca^{2+} release channels, muscarinic and purinergic GPCRs, and proteins related to production or packaging of endogenous ligands. Intracellular Ca^{2+} release channels refer to endoplasmic reticular IP3Rs and RYRs, and endolysosomal TPCs. In addition to those, CD38 which catalyses the synthesis of TPC ligand NAADP, was analysed. Purinergic GPCRs specifically refers to ATP-sensitive P2Y receptors. Endogenous ligands specifically refer to acetylcholine and ATP. Proteins related to the production acetylcholine are ChAT. Packaging of ATP is mediated by VNUT. In addition, proteins related to GLP1 production were also compared. These are proglucagon and neuroendocrine convertase 1; the latter processes the former to form GLP1.

Analysis of IP3R gene expression confirmed the presence of all three subtypes in every tumour colon tissue sample (Figure 134). The expression of IP3R1 and IP3R2 were higher in tumoroids compared to tumour crypts and tumour mucosa. The expression of IP3R3 were similar across each tumour colon tissue sample and were much higher compared to IP3R1 and IP3R2. Compared to normal colonic tissue samples, the gene expression of IP3R1 and IP3R2 were higher in every tumour colon tissue sample, with the greatest differences observed in tumoroids. On the flipside, IP3R3 expression in reduced in tumour colon tissue samples compared to normal colon tissue samples.

Analysis of RYR gene expression confirmed the presence of all three subtypes in almost every tumour colon tissue sample (Figure 135). The expression of RYR2 was most abundant of the three RYR subtypes. The expression of RYR1 and RYR2 were higher in tumoroids compared to tumour crypts and tumour mucosa. The expression of RYR3 was extremely low or non-detectable in every tumour colon tissue sample. Compared to normal colon tissue samples, the gene expression of RYR2 was higher in every tumour colon tissue sample, with the greatest differences observed in tumoroids. RYR1 hardly differed in tumour mucosa and tumour crypts but were much higher in tumoroids. While large differences were seen for RYR3, its significance is questionable due to low RPKM.

	Log 2 (Tumour Mucosa / Normal Mucosa)	Log 2 (Tumour Crypt / Normal Crypt)	Log 2 (Tumoroid / Organoid)
ITPR1	0.728	1.428	2.568
ITPR2	0.337	0.108	2.873
ITPR3	-0.039	-0.293	-0.727
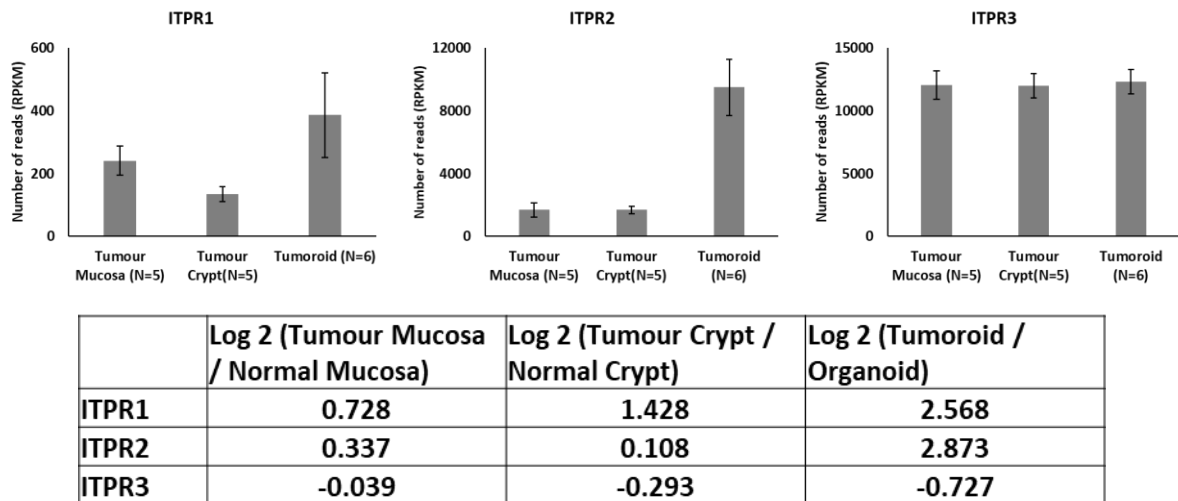
Figure 134 – Gene Expression of IP3Rs in Tumour versus Normal Colon Tissue Samples.

(Top) Bar chart representation of the gene expression for IP3R1 (ITPR1), IP3R2 (ITPR2) and IP3R3 (ITPR3) in native human tumour colonic mucosa, isolated tumour crypts, and cultured tumoroids. Data obtained from five or six human samples (N=5/6). Data is expressed as number of reads per kilo base per million mapped reads (RPKM). **(Bottom)** Table summarising the Log2 ratio of IP3R1-3 gene transcript expression in normal versus tumour colon tissue samples.

	Log 2 (Tumour Mucosa / Normal Mucosa)	Log 2 (Tumour Crypt / Normal Crypt)	Log 2 (Tumoroid / Organoid)
RYR1	-0.322	0.111	4.793
RYR2	5.970	7.894	7.547
RYR3	-1.573	N/A	1
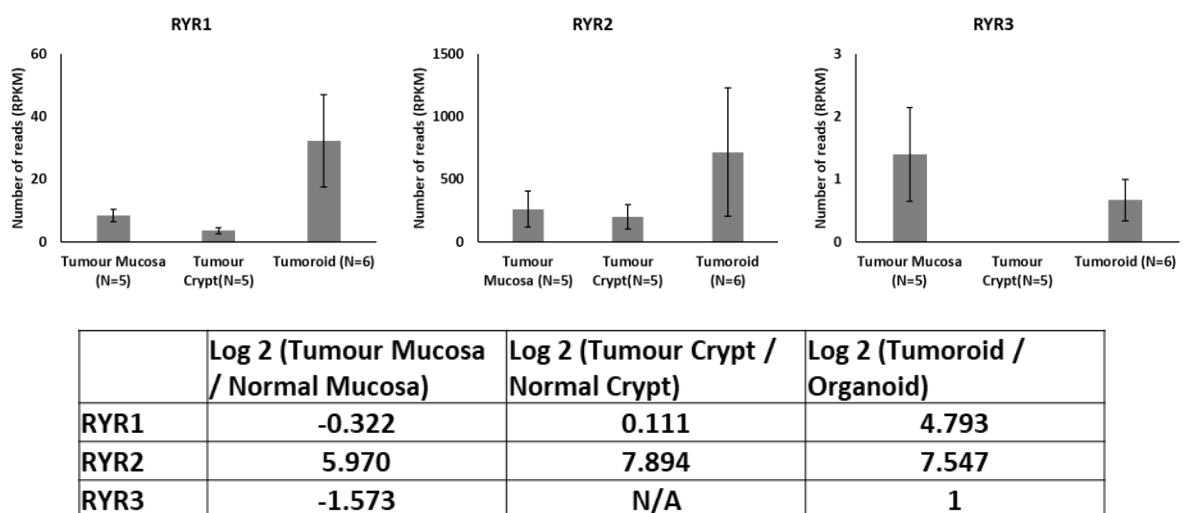
Figure 135 – Gene Expression of RYRs in Tumour versus Normal Colon Tissue Samples.

(Top) Bar chart representation of the gene expression for RYR1, RYR2 and RYR3 in native human tumour colonic mucosa, isolated tumour crypts, and cultured tumoroids. Data obtained from five or six human samples (N=5/6). Data is expressed as number of reads per kilo base per million mapped reads (RPKM). **(Bottom)** Table summarising the Log2 ratio of RYR1-3 gene transcript expression in normal versus tumour colon tissue samples.

Analysis of TPC gene expression confirmed the presence of both subtypes in every tumour colon tissue sample (Figure 136). The expression of TPC1 was higher than TPC2 in every tumour colon tissue sample. Compared to normal colon tissue samples, the gene expression of TPC1 and TPC2 in every tumour colon tissue sample did not increase or decrease by much.

Analysis of CD38 gene expression confirmed its presence in every tumour colon tissue sample (Figure 137). The expression of CD38 varied greatly tumoroids compared to tumour mucosa and tumour crypts, resulting in higher average number of reads but massive standard errors. Compared to organoids, the gene expression of CD38 in tumoroids was much higher. Compared to mucosa and crypts, the gene expression of CD38 varied little in tumour mucosa and tumour crypts.
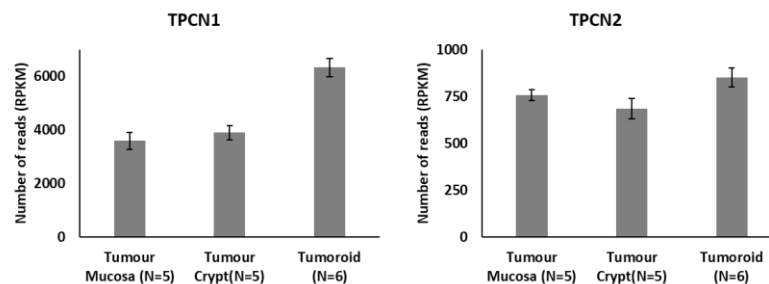
	Log 2 (Tumour Mucosa / Normal Mucosa)	Log 2 (Tumour Crypt / Normal Crypt)	Log 2 (Tumoroid / Organoid)
TPCN1	-0.027	-0.195	0.566
TPCN2	0.320	-0.078	-0.299

Figure 136 – Gene Expression of TPCs in Tumour versus Normal Colon Tissue Samples.

(Top) Bar chart representation of the gene expression for TPC1 (TPCN1) and TPC2 (TPCN2) in native human tumour colonic mucosa, isolated tumour crypts, and cultured tumoroids. Data obtained from five or six human samples (N=5/6). Data is expressed as number of reads per kilo base per million mapped reads (RPKM). **(Bottom)** Table summarising the Log2 ratio of TPC1-2 gene transcript expression in normal versus tumour colon tissue samples.
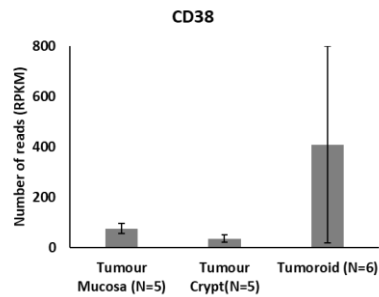
	Log 2 (Tumour Mucosa / Normal Mucosa)	Log 2 (Tumour Crypt / Normal Crypt)	Log 2 (Tumoroid / Organoid)
CD38	0.116	-0.389	3.803

Figure 137 – Gene Expression of CD38 in Tumour versus Normal Colon Tissue Samples.

(Top) Bar chart representation of the gene expression for CD38 in native human tumour colonic mucosa, isolated tumour crypts, and cultured tumoroids. Data obtained from five or six human samples (N=5/6). Data is expressed as number of reads per kilo base per million mapped reads (RPKM). **(Bottom)** Table summarising the Log2 ratio of CD38 gene transcript expression in normal versus tumour colon tissue samples.

Analysis of mAChR gene expression showed differential expression of M1-4 subtypes in every tumour colon tissue sample (Figure 138). Expression of M3, followed by M1, was much higher than M2 and M4 in every tumour colon tissue sample. Expression of M1-4 were roughly similar between every tumour colon tissue sample. M2 was not detected in tumoroids. Similar to normal colon tissue samples, the RNAseq for M5 was not done and thus cannot be analysed in this thesis. Compared to normal colon tissue samples, the gene expression of M1 was lower in every tumour colon tissue sample. M3 expression was higher in tumour mucosa and tumour crypts compared to normal mucosa and normal crypts, and hardly differed in tumoroids versus organoids. M2 and M4 expression varied between slight decrease to high increase, but their significance is questionable due to low RPKM.

Analysis of ATP-sensitive purinergic P2Y receptor showed gene expression differential expression in every tumour colon tissue sample (Figure 139). Expression of P2Y1/1/11 were much higher than P2Y13 in every tumour colon tissue sample. Expression of P2Y1/2/11 were roughly similar between every tumour colon tissue sample. As for P2Y13, it was expressed in tumour mucosa compared to tumour crypts, and absent in tumoroids. Compared to normal colon tissue samples, the gene expression of P2Y1 and P2Y2 was lower in every tumour colon tissue sample. P2Y11 expression varied, but hardly differed in tumour colon tissue samples versus normal colon tissue samples. P2Y13 expression varied between slight decrease to high increase, but their significance is questionable due to low RPKM.

Analysis of ChAT gene expression showed differential expression across every tumour colon tissue sample (Figure 140). Expression of ChAT was lower in tumour mucosa and non-existent in tumour crypts and tumoroids. Compared to normal colon tissue samples, the gene expression of ChAT in tumour mucosa was decreased compared to normal mucosa.

Analysis of VNUT gene expression confirmed its presence in every tumour colon tissue sample (Figure 141). Its expression was roughly similar between every tumour colon tissue sample. Compared to normal colon tissue samples, the gene expression of VNUT was increased in every tumour colon tissue sample, the highest being in tumour mucosa followed by tumour crypt
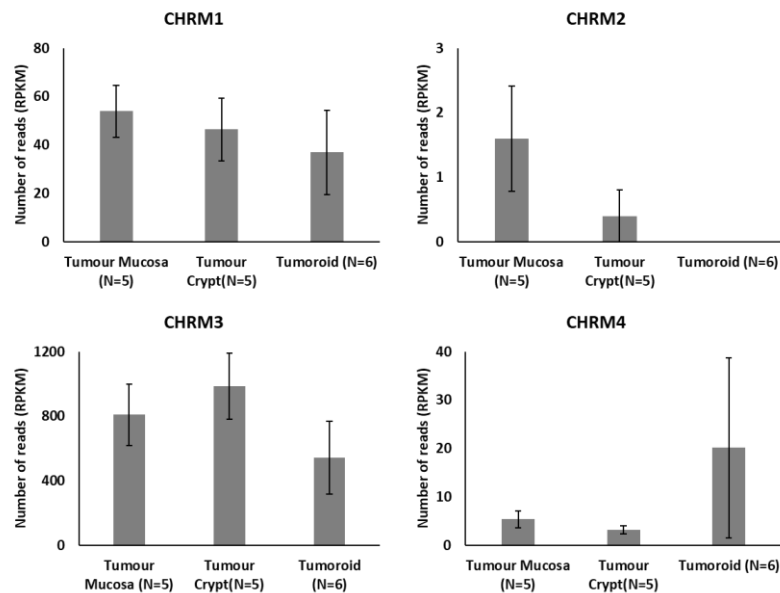
	Log 2 (Tumour Mucosa / Normal Mucosa)	Log 2 (Tumour Crypt / Normal Crypt)	Log 2 (Tumoroid / Organoid)
CHRM1	-0.737	-1.435	-0.628
CHRM2	-0.644	NA	NA
CHRM3	0.704	1.200	-0.054
CHRM4	0.160	-0.866	2.275

Figure 138 – Gene Expression of mAChRs in Tumour versus Normal Colon Tissue Samples.

(Top) Bar chart representation of the gene expression for M1 (CHRM1), M2 (CHRM2), M3 (CHRM3) and M4 (CHRM4) in native human tumour colonic mucosa, isolated tumour crypts, and cultured tumoroids. Data obtained from five or six human samples (N=5/6). Data is expressed as number of reads per kilo base per million mapped reads (RPKM). **(Bottom)** Table summarising the Log2 ratio of M1-4 gene transcript expression in normal versus tumour colon tissue samples.
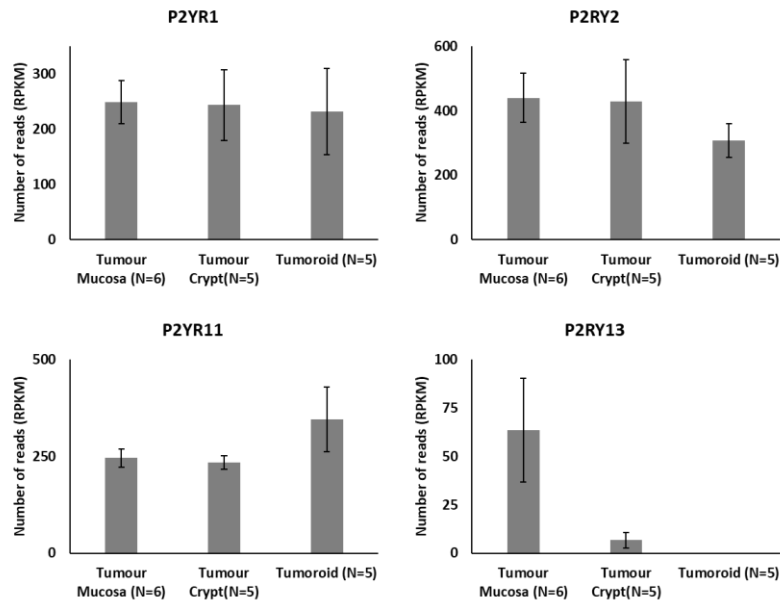
	Log 2 (Tumour Mucosa / Normal Mucosa)	Log 2 (Tumour Crypt / Normal Crypt)	Log 2 (Tumoroid / Organoid)
P2RY1	-1.497	-1.505	-1.956
P2RY2	-0.838	-0.712	-1.323
P2RY11	0.542	-0.250	0.747
P2RY13	0.129	1.350	NA

Figure 139 – Gene Expression of P2YRs in Tumour versus Normal Colon Tissue Samples.

(Top) Bar chart representation of the gene expression for P2Y1 (P2RY1), P2Y2 (P2RY2), P2Y11 (P2RY11) and P2Y13 (P2RY13) in native human tumour colonic mucosa, isolated tumour crypts, and cultured tumoroids. Data obtained from five or six human samples (N=5/6). Data is expressed as number of reads (RPKM). **(Bottom)** Table summarising the Log2 ratio of P2Y1/2/11/13 gene transcript expression in normal versus tumour colon tissue samples.
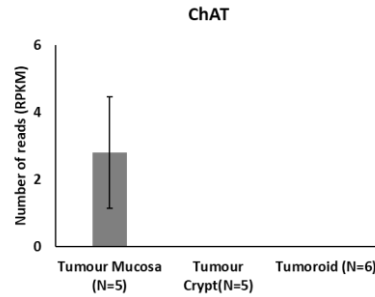
ChAT

	Log 2 (Tumour Mucosa / Normal Mucosa)	Log 2 (Tumour Crypt / Normal Crypt)	Log 2 (Tumoroid / Organoid)
CHAT	-2.339	NA	NA

Figure 140 – Gene Expression of ChAT in Tumour versus Normal Colon Tissue Samples.

(Top) Bar chart representation of the gene expression for ChAT in native human tumour colonic mucosa, isolated tumour crypts, and cultured tumoroids. Data obtained from five or six human samples (N=5/6). Data is expressed as number of reads per kilo base per million mapped reads (RPKM). **(Bottom)** Table summarising the Log2 ratio of ChAT gene transcript expression in normal versus tumour colon tissue samples.
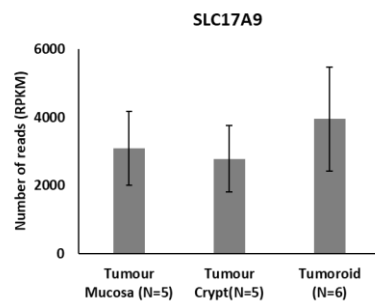
SLC17A9

	Log 2 (Tumour Mucosa / Normal Mucosa)	Log 2 (Tumour Crypt / Normal Crypt)	Log 2 (Tumoroid / Organoid)
SLC17A9	2.029	0.928	0.620

Figure 141 – Gene Expression of VNUT in Tumour versus Normal Colon Tissue Samples.

(Top) Bar chart representation of the gene expression for VNUT (SLC17A9) in native human tumour colonic mucosa, isolated tumour crypts, and cultured tumoroids. Data obtained from five or six human samples (N=5/6). Data is expressed as number of reads per kilo base per million mapped reads (RPKM). **(Bottom)** Table summarising the Log2 ratio of VNUT gene transcript expression in normal versus tumour colon tissue samples.

Lastly, analysis of the gene expression for proglucagon and neuroendocrine convertase 1 showed differential expression across every tumour colon tissue sample (Figure 142). For both, their gene expression was higher in tumour mucosa compared to tumour crypts and much lower in tumoroids. Compared to normal colon tissue samples, the gene expression of proglucagon was highly decreased in every tumour colon tissue sample. As for neuroendocrine convertase 1, its gene expression was increased in tumour mucosa and tumour crypts compared to normal mucosa and normal crypts, but decreased in tumoroids compared to organoids.

	Log 2 (Tumour Mucosa / Normal Mucosa)	Log 2 (Tumour Crypt / Normal Crypt)	Log 2 (Tumoroid / Organoid)
GCG	-2.532	-4.151	-7.863
PCSK1	1.742	1.556	-2.478
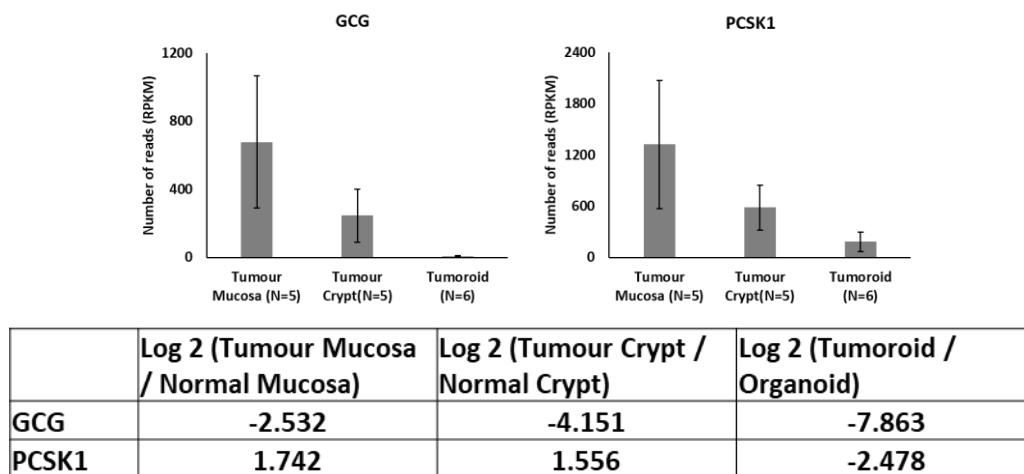
Figure 142 – Gene Expression of GCG & PCSK1 in Tumour versus Normal Colon Tissue Samples.

(Top) Bar chart representation of the gene expression for proglucagon (GCG) and neuroendocrine convertase 1 (PCSK1) in native human tumour colonic mucosa, isolated tumour crypts, and cultured tumoroids. Data obtained from five or six human samples (N=5/6). Data is expressed as number of reads per kilo base per million mapped reads (RPKM). **(Bottom)** Table summarising the Log2 ratio of GCG and PCSK1 gene transcript expression in normal versus tumour colon tissue samples.

7.2.2 Immunofluorescent Localisation of Ca²⁺-Signalling Toolkit in Tumoroids

Transcriptomic analysis using RNA sequencing confirmed the presence of Ca²⁺ signalling toolkit RNA within tumour mucosa, tumour crypts and tumoroids. Thus, the next question was whether protein expression of these Ca²⁺ signalling toolkit were present. Immunolabelling and confocal imaging were used to visualize and characterize the localisation of intracellular Ca²⁺ release channels at the base of tumoroids. Intracellular Ca²⁺ release channels refer specifically to endoplasmic reticular IP3R1-3 and RYR1-3, endolysosomal TPC1-2, with the complementary addition of CD38. In addition, the localisation of Ca²⁺ coupled muscarinic and purinergic GPCRs were visualized using immunolabelling and confocal imaging. This referred specifically to G$_q$-coupled M1, M3, M5. P2Y2 immunolabelling in tumoroids were not done in time. Finally, immunolabelling and confocal imaging were used to visualize and characterize the localisation of ChAT in tumoroids. Contributors to this data include Dr Victoria Jones, Dr Nicolas Pelaez Llaneza and Ms Jordan Champion.

All three IP3R subtypes were found to be present in tumoroids (Figure 143). IP3R1 expression seemed to be ubiquitous except for the nuclear space (Figure 143A), which was vaguely similar IP3R1 labelling in organoids (Figure 32C). IP3R2 expression was prominent along the basal membrane (Figure 143B), which was similarly observed in organoids (Figure 32B). IP3R3 expression appears to be present in the entire tumoroid including the nuclear space (Figure 143C), which somewhat resembled organoids where the labelling was also restricted to the apical pole and along the basal membranes (Figure 33C).

All three RYR subtypes were also found to be present in tumoroids (Figure 144). RYR1 expression was prominent in the apical pole of cells, with strong labelling in the cytoplasm, apical membranes, and basolateral membranes (Figure 144A). This resembled RYR1 labelling in mucosa and crypts, but not organoids (Figure 34). RYR2 expression was similarly prominent in the apical pole of cells, especially along the apical and basolateral membranes (Figure 144B), which was quite different compared to RYR2 labelling in organoids and crypts (Figure 35B-C) where its labelling was predominantly basal. RYR3 expression appears to be prominent on the basal pole of the cell (Figure 144C), with labelling along the basal membrane and some basolateral membranes. This was similar to RYR3 labelling in crypts and organoids (Figure 36).

Endolysosomal TPC1 and TPC2 were both shown to be present in tumoroids (Figure 145A-B). TPC1 expression was limited to the nuclear space and apical membranes of some cells (Figure 145A), which was very similar to TPC1 labelling crypts and organoids (Figure 37B-C). TPC2 expression was prominent in the cytoplasmic space, apical membranes, and basolateral membranes of cells (Figure 145B), which is vaguely similar to TPC1 labelling mucosa (Figure 39A). In addition, CD38 was shown to be expressed in the nucleus of every tumoroid cell (Figure 145C), which was identical to CD38 labelling in crypts and organoids (Figure 41). G$_q$-

coupled muscarinic acetylcholine receptors M1-3 were shown to be present in tumoroids (Figure 146). For all three receptor subtypes, their expression was limited to the basal membranes, which was similar to their labelling in organoids (Figure 43C/44C/45C). Lastly, ChAT was shown to be absent in tumoroids (Figure 147), which matched the labelling of ChAT in organoids (Figure 51C).
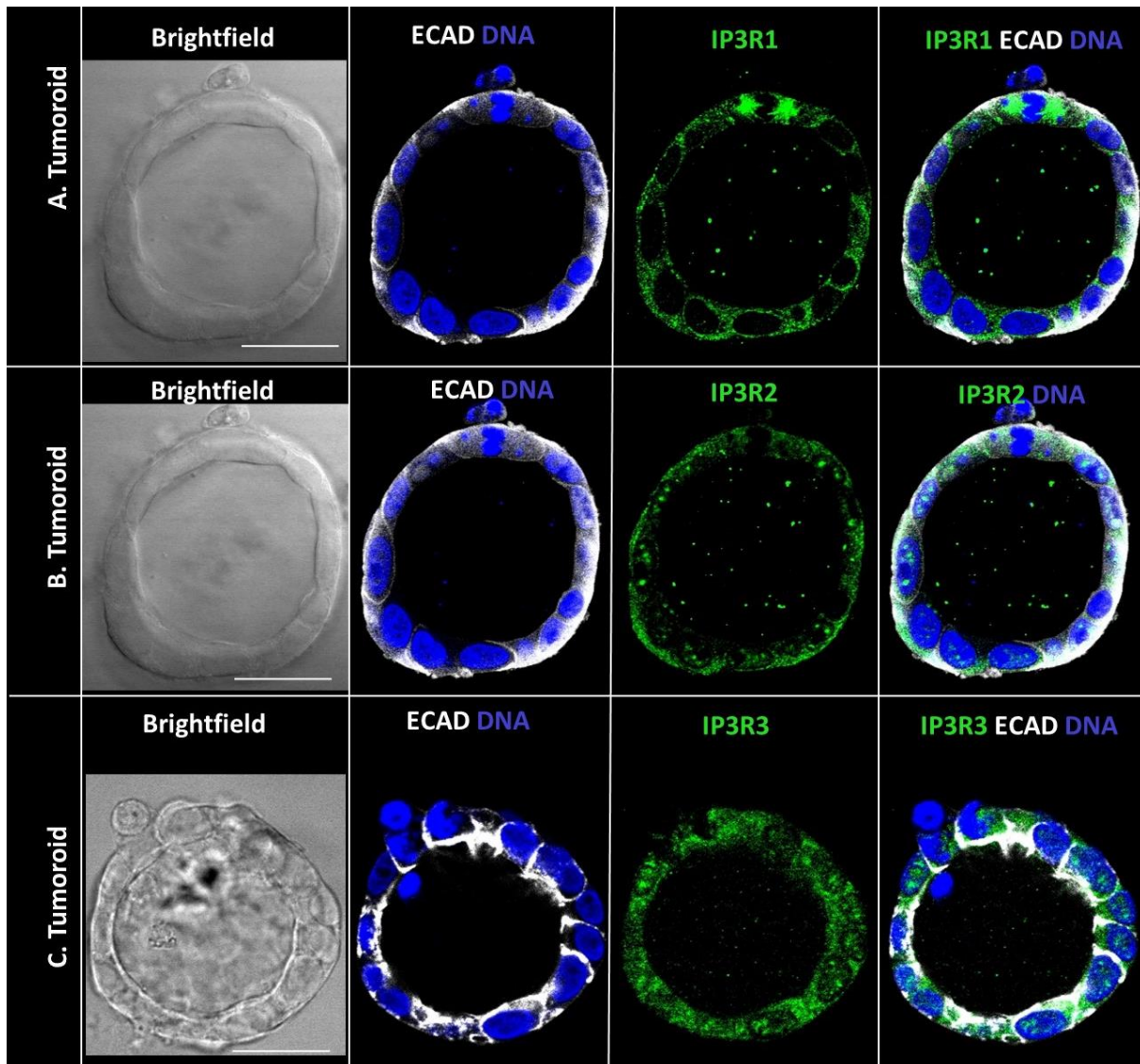
Figure 143 – Immunolabelling of IP3R1-3 in Tumoroids.

Representative confocal images of tumoroids immunolabelled with E-Cadherin (ECAD) in white and IP3R1 **(A)** or IP3R2 **(B)** or IP3R3 **(C)** in green. Nuclei was stained with Sytox Blue (DNA). Brightfield depicted on the left. Scale bar = 25 µm.
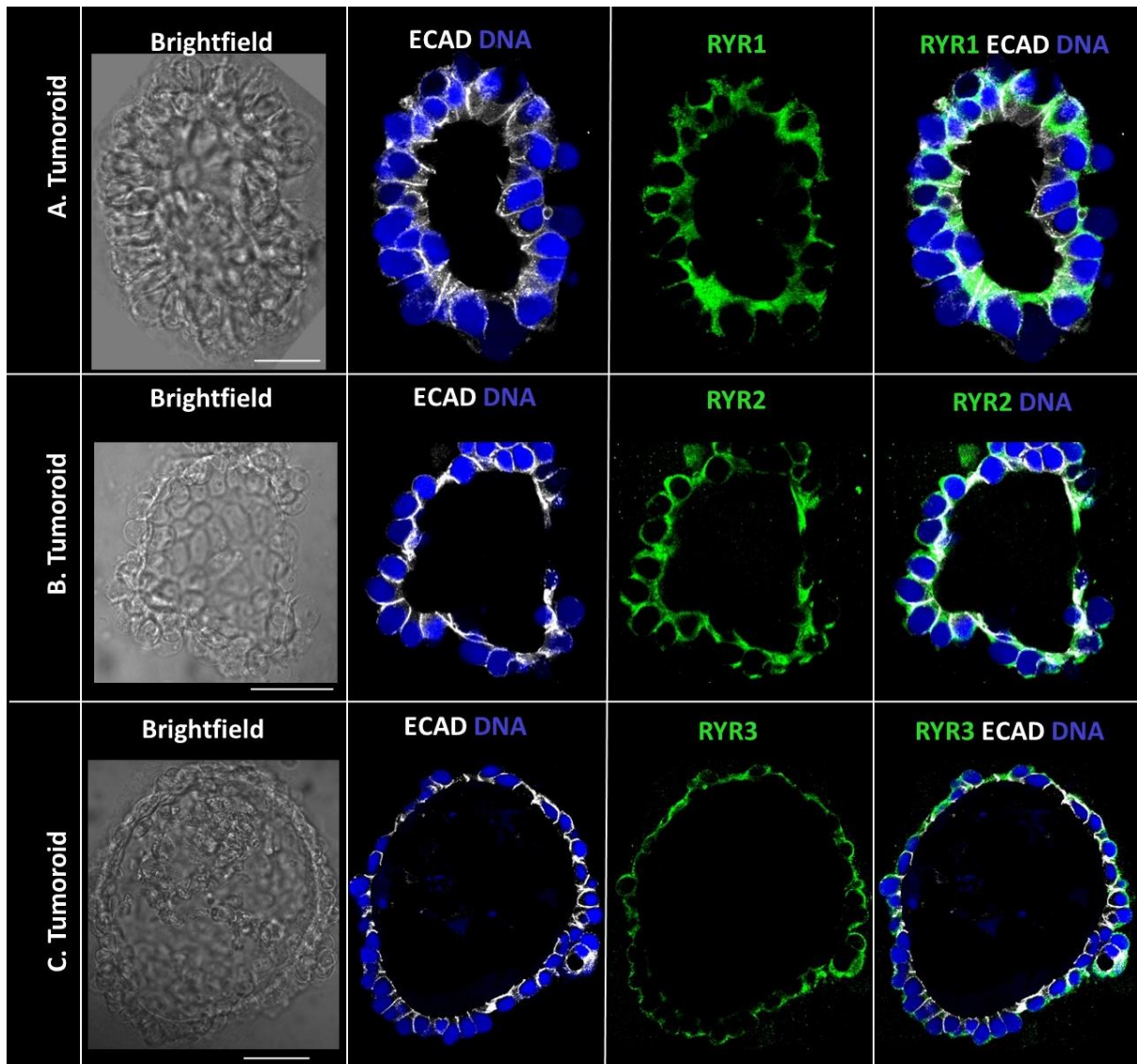
Figure 144 – Immunolabelling of RYR1-3 in Tumoroids.

Representative confocal images of tumoroids immunolabelled with E-Cadherin (ECAD) in white and RYR1 **(A)** or RYR2 **(B)** or RYR3 **(C)** in green. Nuclei was stained with Sytox Blue (DNA). Brightfield depicted on the left. Scale bar = 25 µm.
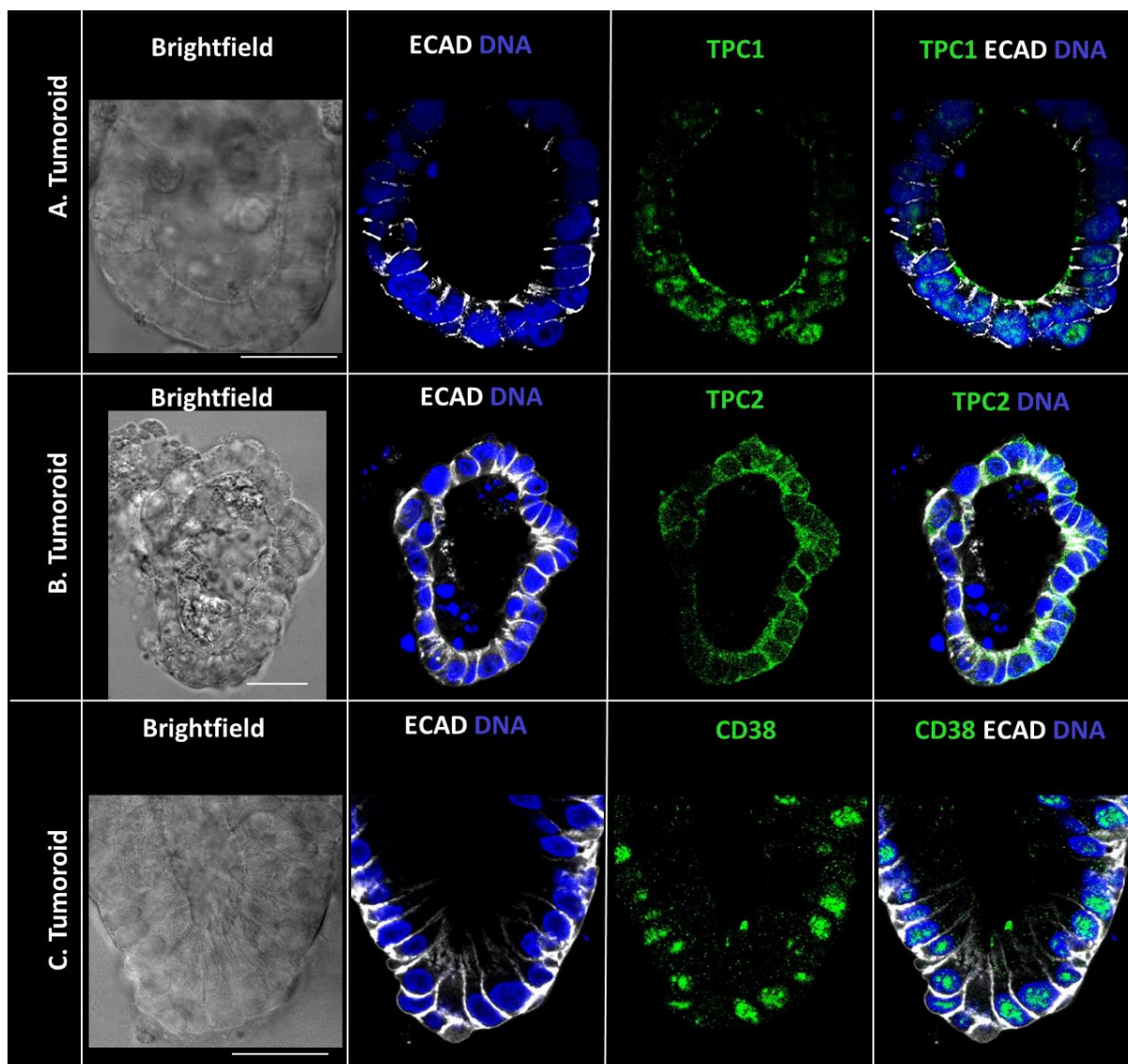
Figure 145 – Immunolabelling of TPC1-2 and CD38 in Tumoroids.

Representative confocal images of tumoroids immunolabelled with E-Cadherin (ECAD) in white and TPC1 **(A)** or TPC2 **(B)** or CD38 **(C)** in green. Nuclei was stained with Sytox Blue (DNA). Brightfield depicted on the left. Scale bar = 25 μm.
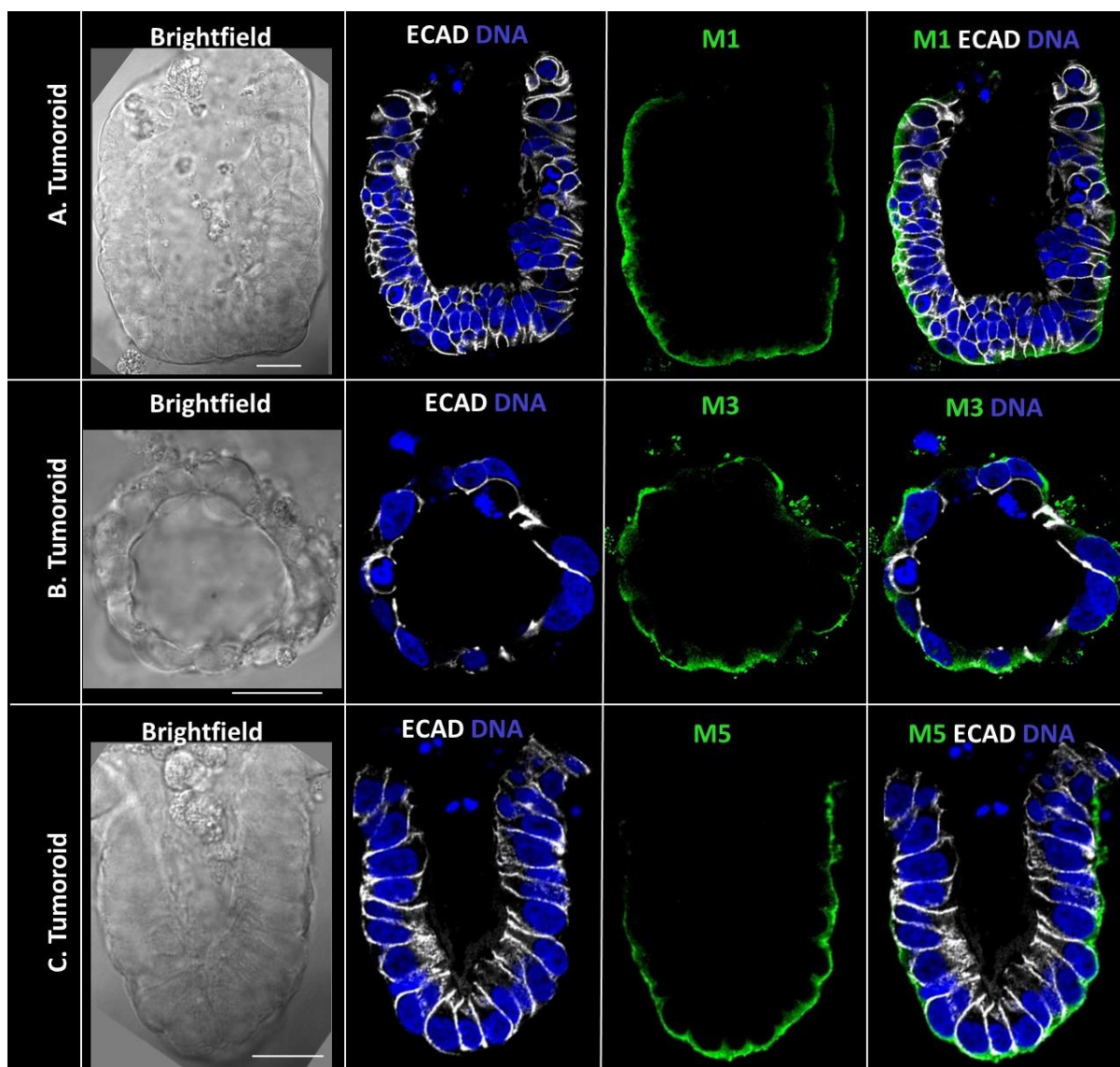
Figure 146 – Immunolabelling of M1/3/5 in Tumoroids.

Representative confocal images of tumoroids immunolabelled with E-Cadherin (ECAD) in white and M1 **(A)** or M3 **(B)** or M5 **(C)** in green. Nuclei was stained with Sytox Blue (DNA). Brightfield depicted on the left. Scale bar = 25 μm.
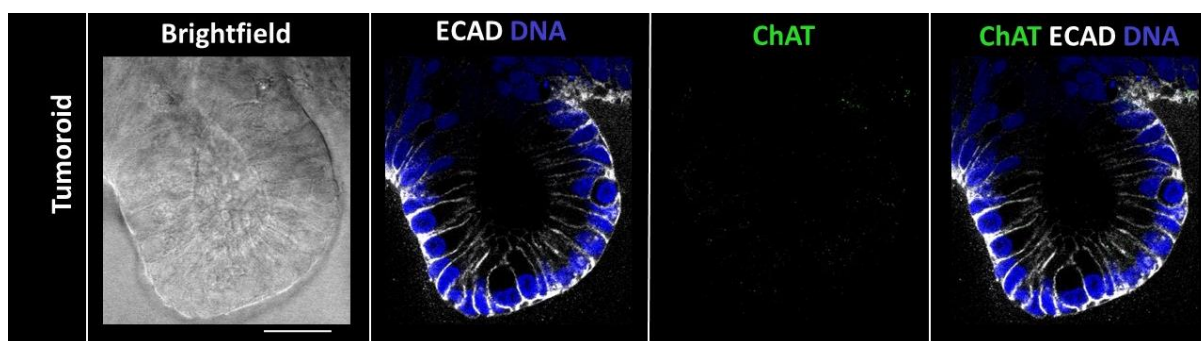
Figure 147 – Immunolabelling Expression of ChAT in Tumoroids.

Representative confocal images of tumoroids immunolabelled with E-Cadherin (ECAD) in white and ChAT in green. Nuclei stained with Sytox Blue (DNA). Brightfield depicted on left. Scale bar = 25 μm.

7.2.3 Comparative Pharmacological Profiles of Tumour Crypts & Tumoroids

Fura-2 Ca^{2+} experiments were carried out in crypts which had been isolated tumour mucosa (tumour crypts) and organoids which were generated from tumour crypts (tumoroids). Tumour crypts and tumoroids which had been grown for 24-72 hours were loaded with Fura-2-AM (5 µM) for 2 hours in HBS at room temperature (see Chapter 2.5). Certain antagonists which require incubation in culture media at 37°C (Table 9) were done prior to Fura-2 loading. "N" denotes the number of patients whose tumoroids were used to generate data. Each patient sample would further be tested at least three times (n=/>3). "N.S." denotes the data is not statistically significant (P>0.05). "*" denotes the data is statistically significant (P<0.05).

TPC-antagonists Ned-19 (Figure 148) and tetrandrine (Figure 149) were first used to evaluate CCh and UTP-induced Ca^{2+} signals in tumoroids. High concentrations of Ned-19 (500 µM) inhibited CCh-induced Ca^{2+} signals by 81% in tumour crypts (Figure 148A) and 89% in tumoroids (Figure 148B), which were very similar to the pharmacological profile of Ned-19 (500 µM) in crypts (79%) and organoids (81%) (Figure 148E). In tumour crypts, a lower concentration of Ned-19 (250 µM) reduced CCh-induced Ca^{2+} signals by 46% (Figure 148A). It was substantially lower compared to Ned-19 (250 µM) in crypts, which instead increased CCh-induced Ca^{2+} signals by 21% (Figure 148E). As for UTP-induced Ca^{2+} signals in tumour crypts (Figure 148C) and tumoroids (Figure 148D), it was not inhibited by Ned-19 (250-500 µM), similar to in crypts and organoids (Figure 148F). Tetrandrine (20 µM) inhibited CCh-induced Ca^{2+} signals by 95% in tumoroids (Figure 149A), more compared to organoids which was only inhibited by 84% using the same concentration (Figure 149C). As for UTP-induced Ca^{2+} signals in tumoroids (Figure 149B), tetrandrine (20 µM) reduced UTP-induced Ca^{2+} signals by 43%, substantially lower compared to in organoids which instead increased UTP-induced Ca^{2+} signals by 42% (Figure 149D).

Next, IP3R1-antagonist 2-APB was used to evaluate CCh and UTP-induced Ca^{2+} signals in tumoroids (Figure 150). In tumour crypts, 2-APB (100 µM) reduced CCh-induced Ca^{2+} signals by 66% and was nearly statistically significant (Figure 150A), compared to in crypts which was only reduced by 21% (Figure 150E). In tumoroids, CCh-induced Ca^{2+} signals were slightly increased (13-30%) in the presence of 2-APB (50-100 µM) (Figure 150B), the reverse of which was observed in organoids where it inhibited CCh-induced Ca^{2+} signals by 3-28% instead (Figure 150E). As for UTP-induced Ca^{2+} signals, in tumour crypts it was inhibited by 2-APB (100 µM) by 72% (Figure 150C), which was very similar in crypts which inhibited UTP-induced Ca^{2+} signals by 76% using the same 2-APB concentration (Figure 150F). In tumoroids, 2-APB (50 µM) inhibited UTP-induced Ca^{2+} signals 67%, while 2-APB (100 µM) reduced it by 39% and was not statistically significant. Compared to in organoids, 2-APB (50 µM) performed very similarly with a 63% inhibition, while 2-APB (100 µM) performed quite differently with a 65% inhibition.
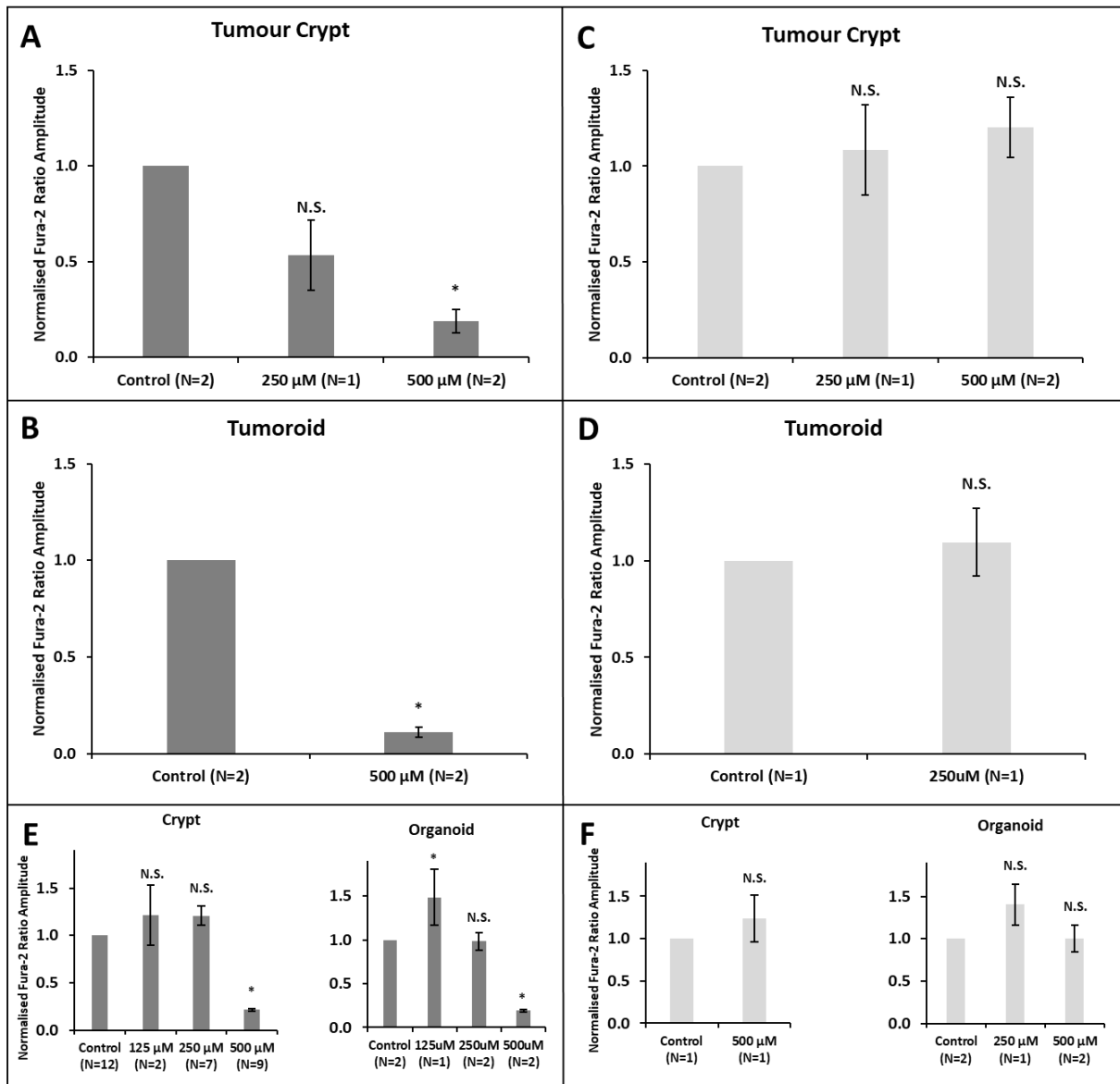
Figure 148 – Ned-19 Inhibits CCh but not UTP-induced Ca^{2+} Signals in Tumoroids.

Bar charts summarising the normalized Fura-2 ratio amplitude comparing CCh-induced Ca^{2+} signals with various concentrations of Ned-19 in tumour crypts **(A)** and tumoroids **(B)** against control, UTP-induced Ca^{2+} signals with various concentrations of Ned-19 in tumour crypts **(C)** and tumoroids **(D)** against control, and the pharmacological profile of Ned-19 in crypts and organoids stimulated with CCh **(E)** and UTP **(F)**. Data normalised to control and displayed as mean +/- SEM. Not significant (N.S). P>0.05 (*). N≥1. For every "N", n≥3.
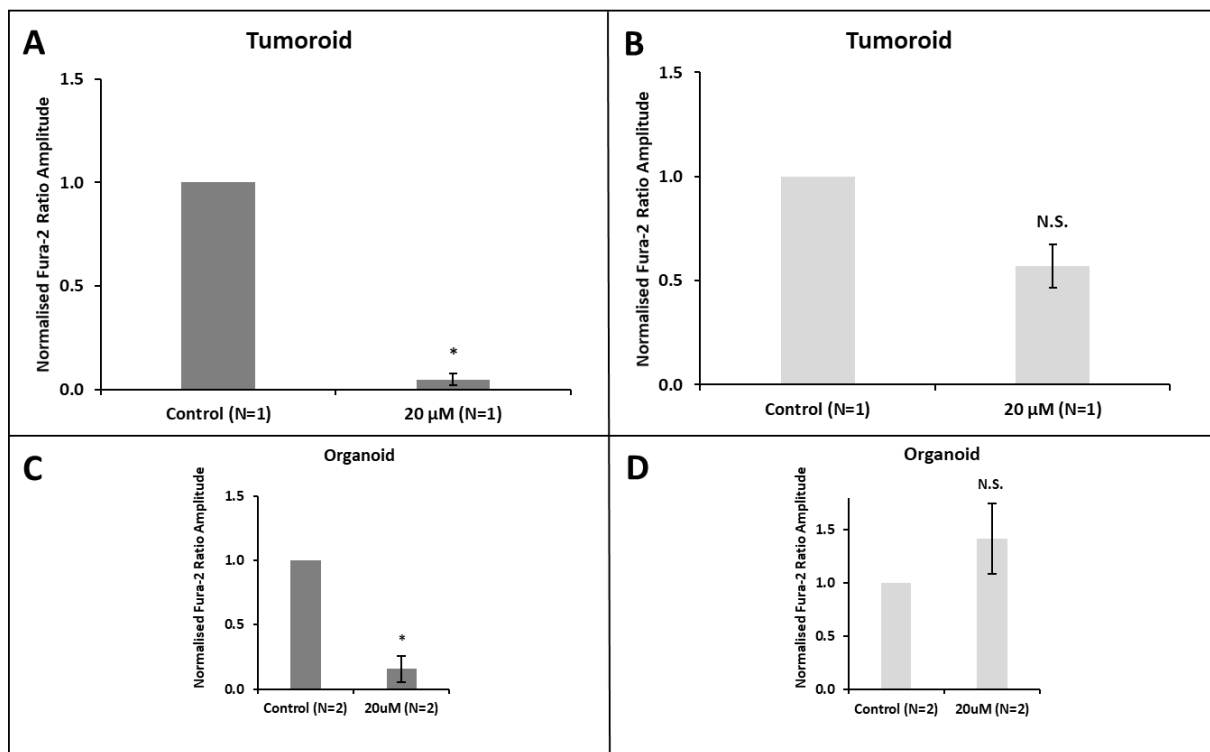
Figure 149 – Tetrandrine Inhibits CCh but not UTP-induced Ca^{2+} Signals in Tumoroids.

Bar charts summarising the normalized Fura-2 ratio amplitude comparing CCh-induced Ca^{2+} signals with tetrandrine in tumoroids **(A)** against control, UTP-induced Ca^{2+} signals with tetrandrine in tumoroids **(B)** against control, and the pharmacological profile of tetrandrine in organoids stimulated with CCh **(C)** and UTP **(D)**. Data normalised to control and displayed as mean +/- SEM. Not significant (N.S.). P>0.05 (*). N≥1. For every "N", n≥3.
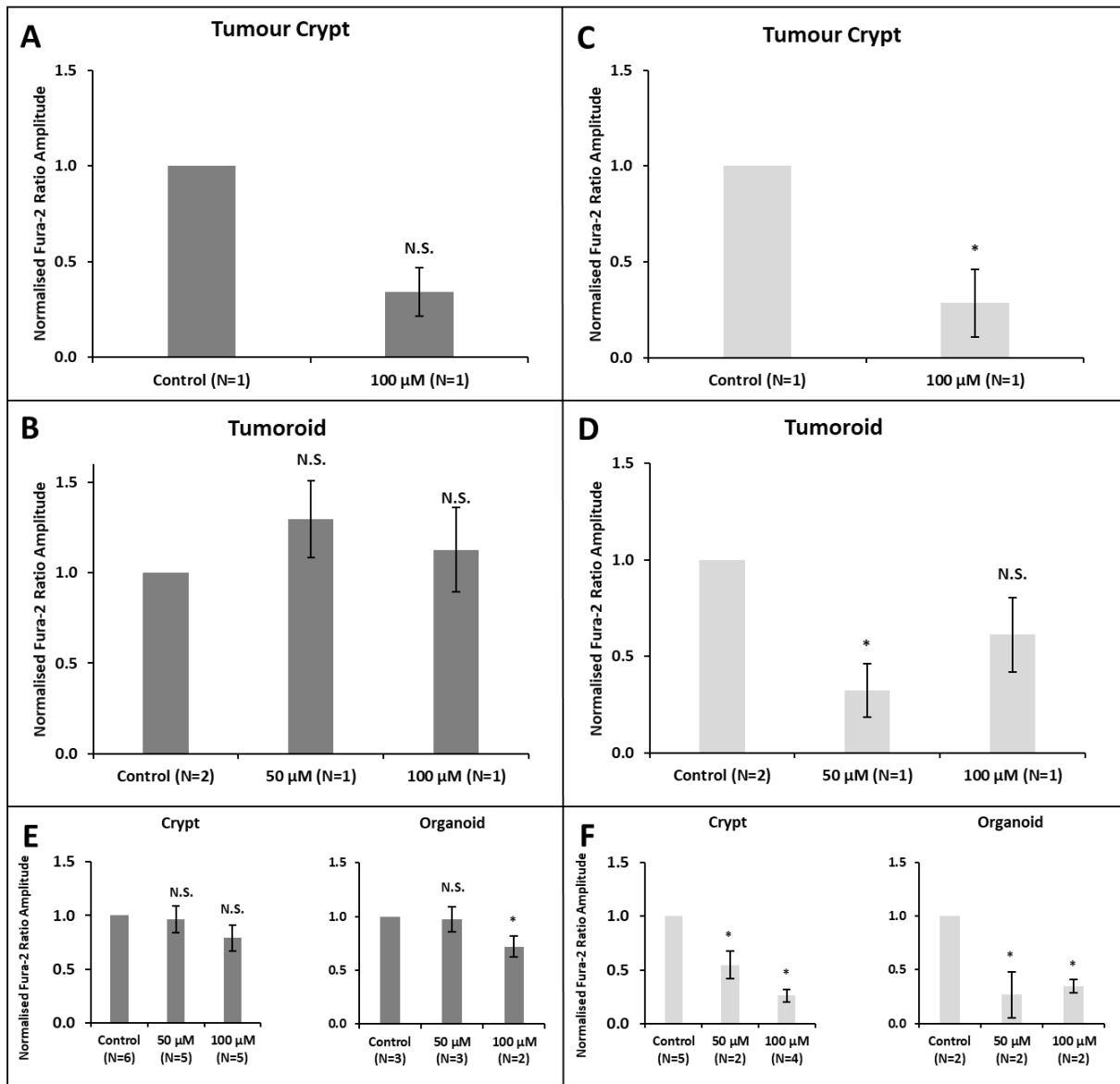
Figure 150 – 2-APB Inhibits UTP but not CCh-induced Ca^{2+} Signals in Tumoroids.

Bar charts summarising the normalized Fura-2 ratio amplitude comparing CCh-induced Ca^{2+} signals with various concentrations of 2-APB in tumour crypts **(A)** and tumoroids **(B)** against control, UTP-induced Ca^{2+} signals with various concentrations of 2-APB in tumour crypts **(C)** and tumoroids **(D)** against control, and the pharmacological profile of 2-APB in crypts and organoids stimulated with CCh **(E)** and UTP **(F)**. Data normalised to control and displayed as mean +/- SEM. Not significant (N.S). P>0.05 (*). N≥1. For every "N", n≥3.

Following this, muscarinic and purinergic Ca^{2+} signals were evaluated using 'slow channel blocking agents' verapamil and diltiazem, and non-specific Ca^{2+} antagonists TMB8. Verapamil (50 µM) inhibited CCh-induced Ca^{2+} signals by 99% in tumoroids (Figure 151A), much more compared to organoids which was only inhibited by 75% using the same concentration (Figure 151C). As for UTP-induced Ca^{2+} signals in tumoroids (Figure 151B), verapamil (50 µM) reduced UTP-induced Ca^{2+} signals by 35%, the reverse of which was observed in organoids where it increased UTP-induced Ca^{2+} signals by 20% instead (Figure 151D). Moving on to diltiazem (250-500 µM), it inhibited CCh-induced Ca^{2+} signals by 79-87% in tumoroids (Figure 152A), which was similar in organoids but varied more (65-94%) by comparison (Figure 152C). UTP-induced Ca^{2+} signals were not inhibited by diltiazem (250-500 µM) (Figure 152B), which was similar to what was observed in organoids (Figure 152D). The pharmacology profile of TMB8 in tumoroids closely resembled organoids (Figure 153). CCh-induced Ca^{2+} signals were inhibited by TMB8 (50-100 µM) in tumoroids (87-100%) and organoids (95%) (Figure 153A&C); UTP-induced Ca^{2+} signals increased by TMB8 (50-100 µM) in tumoroids (5-56%) and organoids (2-30%) but no statistical significance (Figure 153B&D).

Finally, muscarinic and purinergic Ca^{2+} signals were evaluated using non-specific RYR-antagonist procaine (Figure 154) and RYR1/3-antagonist dantrolene (Figure 155). Procaine (1 mM) inhibited CCh-induced Ca^{2+} signals by 87% in tumoroids (Figure 154A), much greater compared to the 47% inhibition observed in organoids under the same procaine concentration (Figure 154C). As for UTP-induced Ca^{2+} signals, it was not inhibited by procaine (1 mM) in both tumoroids (Figure 154B) and organoids (Figure 154D). Lastly, the pharmacology profile of dantrolene (50 µM) in tumoroids closely resembled organoids, albeit with greater potency (Figure 155). In tumoroids, dantrolene (50 µM) inhibited CCh-induced Ca^{2+} signals by 100% (Figure 155A) and UTP-induced Ca^{2+} signals by 78% (Figure 155B), much greater than in organoids where it inhibited CCh-induced Ca^{2+} signals by 78% (Figure 155C) and UTP-induced Ca^{2+} signals by 36% (Figure 155D).

From these experiments, the Ca^{2+}-signal induced by CCh and UTP – measured by the change in Fura-2 ratio amplitude – were compared between normal crypts versus tumour crypts and in organoids versus tumoroids (Figure 156). The change in of Fura-2 ratio amplitude induced by CCh was 0.38 and 0.37 in normal crypts and tumour crypts, respectively, and was not statistically significant (Figure 156A). And, the change in of Fura-2 ratio amplitude induced by UTP was 0.40 and 0.37 in normal crypts and tumour crypts, respectively, and was also not statistically significant. However, the change in of Fura-2 ratio amplitude induced by CCh was 0.36 and 0.25 in organoids and tumoroids, respectively, and was statistically significant (Figure 156B). And likewise, the change in of Fura-2 ratio amplitude induced by UTP was 0.22 and 0.43 in organoids and tumoroids, respectively, and was also statistically significant.
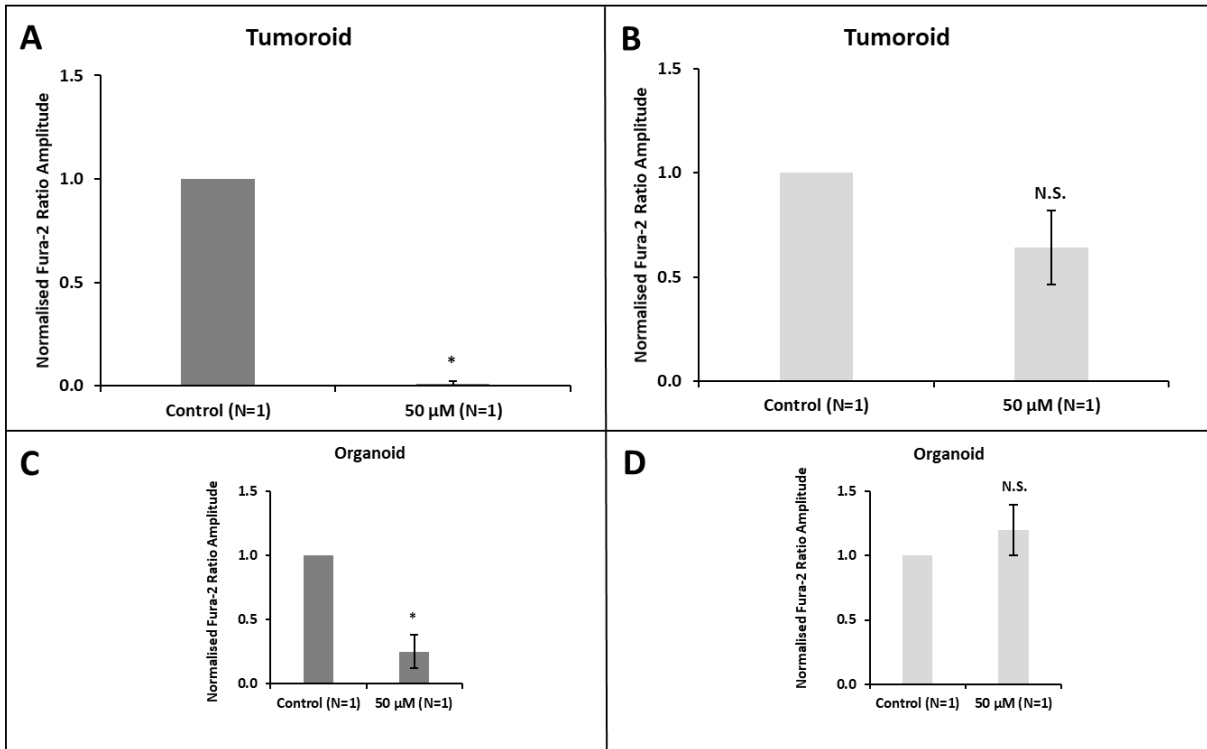
Figure 151 – Verapamil Inhibits CCh but not UTP-induced Ca²⁺ Signals in Tumoroids.

Bar charts summarising the normalized Fura-2 ratio amplitude comparing CCh-induced Ca²⁺ signals with verapamil in tumoroids **(A)** against control, UTP-induced Ca²⁺ signals with verapamil in tumoroids **(B)** against control, and the pharmacological profile of verapamil in organoids stimulated with CCh **(C)** and UTP **(D)**. Data normalised to control and displayed as mean +/- SEM. Not significant (N.S). P>0.05 (*). N≥1. For every "N", n≥3.
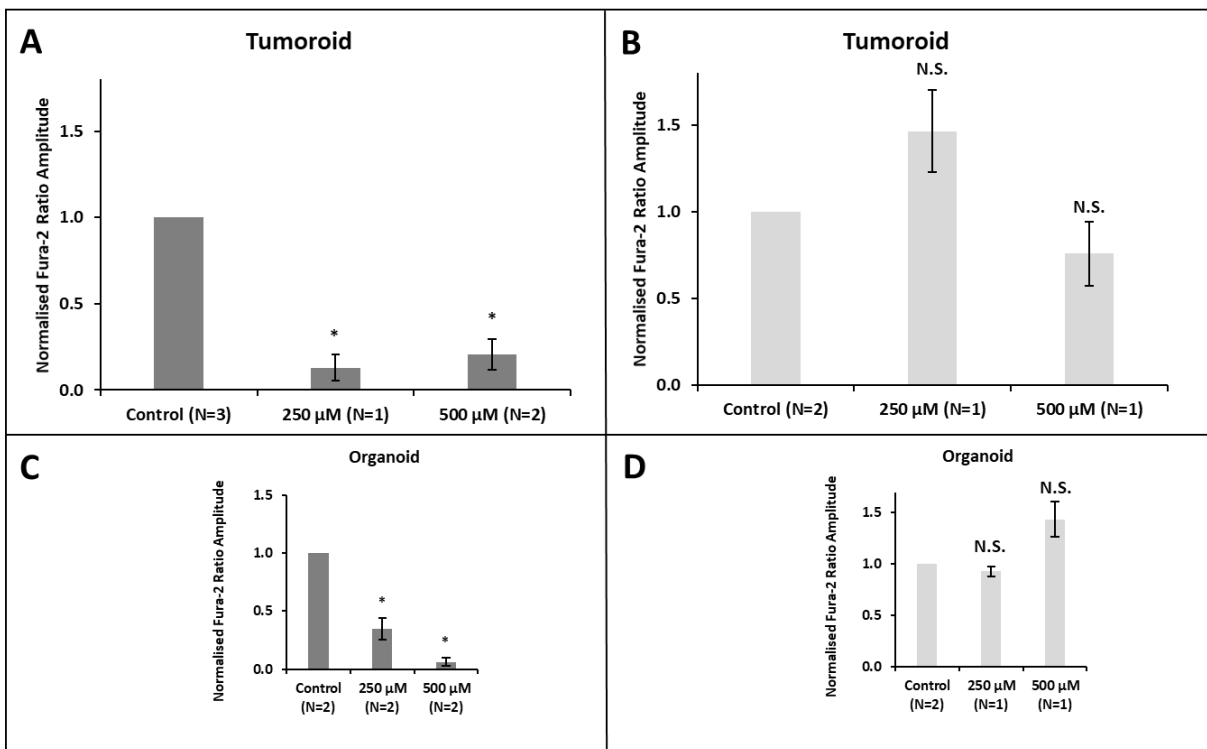
Figure 152 – Diltiazem Inhibits CCh but not UTP-induced Ca²⁺ Signals in Tumoroids.

Bar charts summarising the normalized Fura-2 ratio amplitude comparing CCh-induced Ca²⁺ signals with various concentrations of diltiazem in tumoroids **(A)** against control, UTP-induced Ca²⁺ signals with various concentrations of diltiazem in tumoroids **(B)** against control, and the pharmacological profile of various concentrations of diltiazem in organoids stimulated with CCh **(C)** and UTP **(D)**. Data normalised to control and displayed as mean +/- SEM. Not significant (N.S). P>0.05 (*). N≥1. For every "N", n≥3.
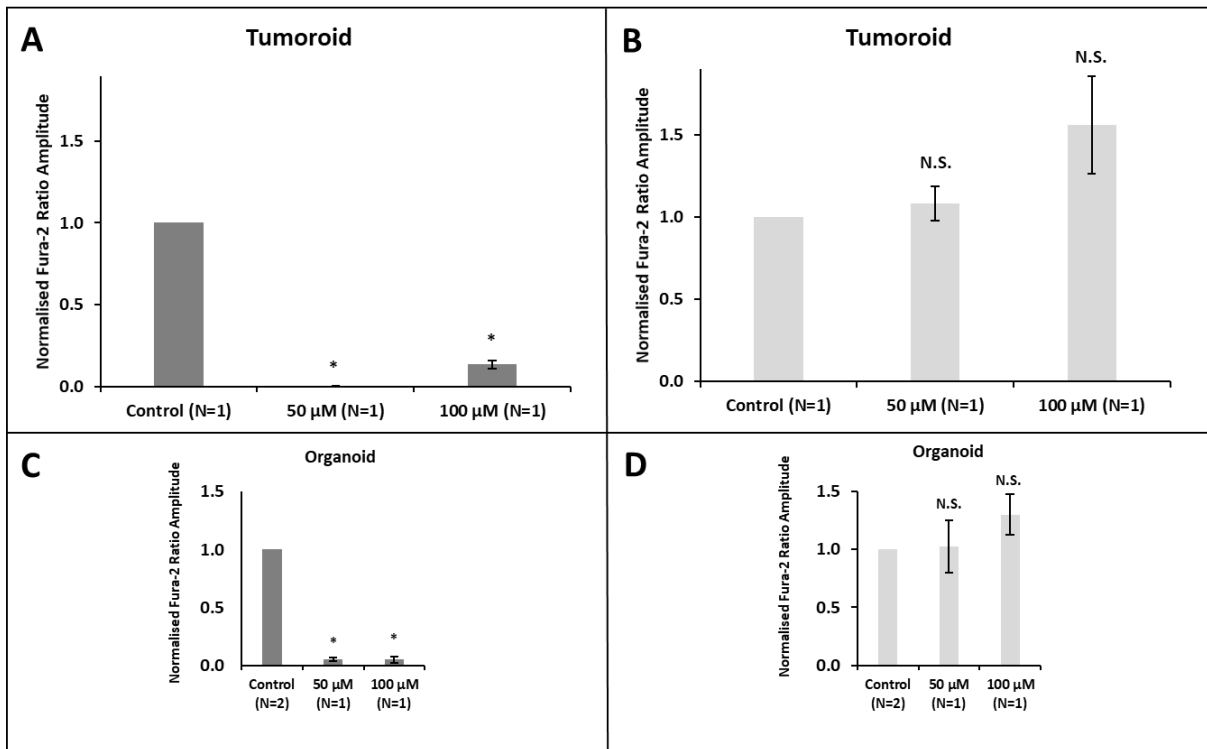
Figure 153 – TMB8 Inhibits CCh but not UTP-induced Ca²⁺ Signals in Tumoroids.

Bar charts summarising the normalized Fura-2 ratio amplitude comparing CCh-induced Ca²⁺ signals with various concentrations of TMB8 in tumoroids **(A)** against control, UTP-induced Ca²⁺ signals with various concentrations of TMB8 in tumoroids **(B)** against control, and the pharmacological profile of various concentrations of TMB8 in organoids stimulated with CCh **(C)** and UTP **(D)**. Data normalised to control and displayed as mean +/- SEM. Not significant (N.S). P>0.05 (*). N≥1. For every "N", n≥3.
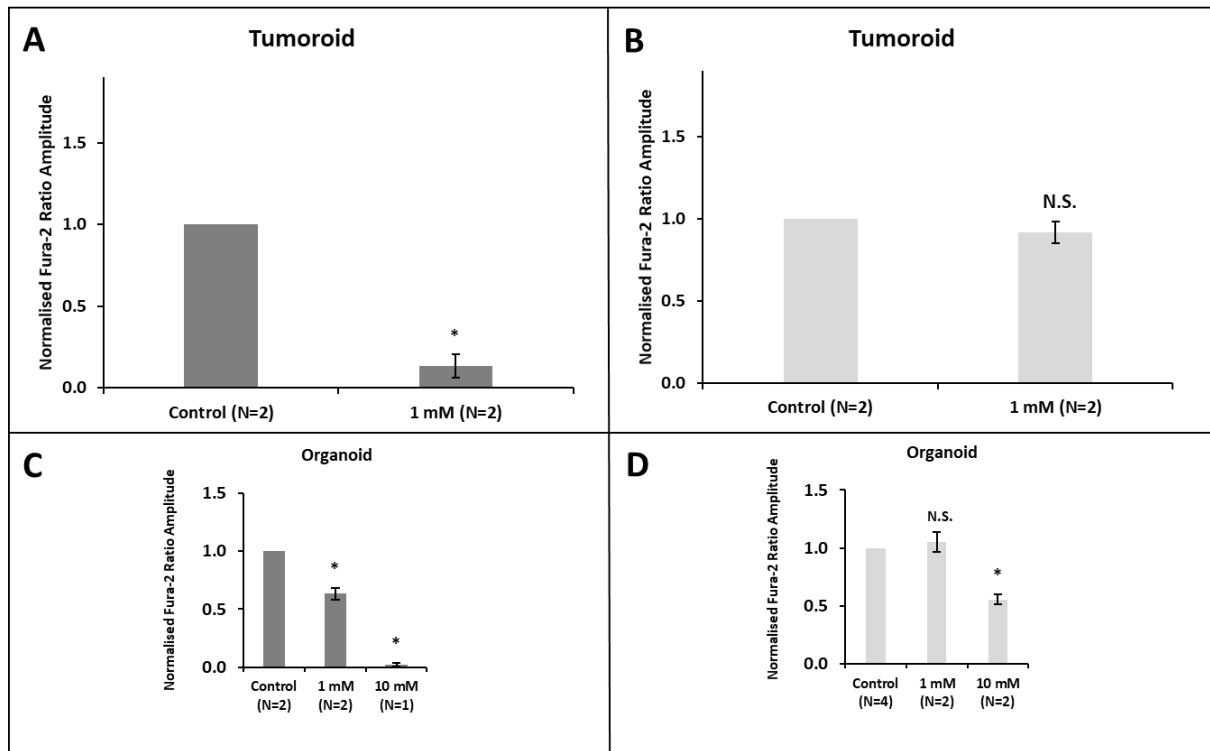
Figure 154 – Low Dosage of Procaine Inhibits CCh-induced Ca^{2+} Signals in Tumoroids.

Bar charts summarising the normalized Fura-2 ratio amplitude comparing CCh-induced Ca^{2+} signals with procaine in tumoroids **(A)** against control, UTP-induced Ca^{2+} signals with procaine in tumoroids **(B)** against control, and the pharmacological profile of various concentrations of procaine in organoids stimulated with CCh **(C)** and UTP **(D)**. Data normalised to control and displayed as mean +/- SEM. Not significant (N.S). P>0.05 (*). N≥1. For every "N", n≥3.
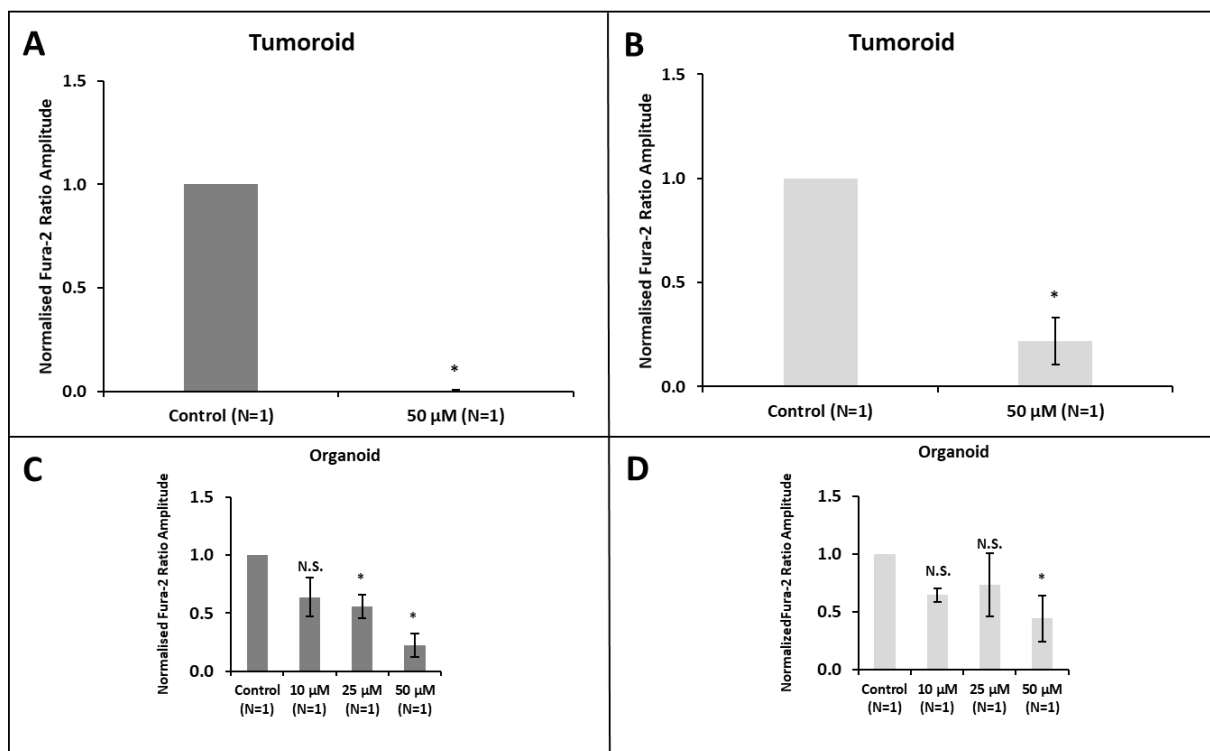
Figure 155 – Dantrolene Inhibits both CCh and UTP-induced Ca²⁺ Signals in Tumoroids.

Bar charts summarising the normalized Fura-2 ratio amplitude comparing CCh-induced Ca²⁺ signals with dantrolene in tumoroids **(A)** against control, UTP-induced Ca²⁺ signals with dantrolene in tumoroids **(B)** against control, and the pharmacological profile of various concentrations of dantrolene in organoids stimulated with CCh **(C)** and UTP **(D)**. Data normalised to control and displayed as mean +/- SEM. Not significant (N.S). P>0.05 (*). N≥1. For every "N", n≥3.
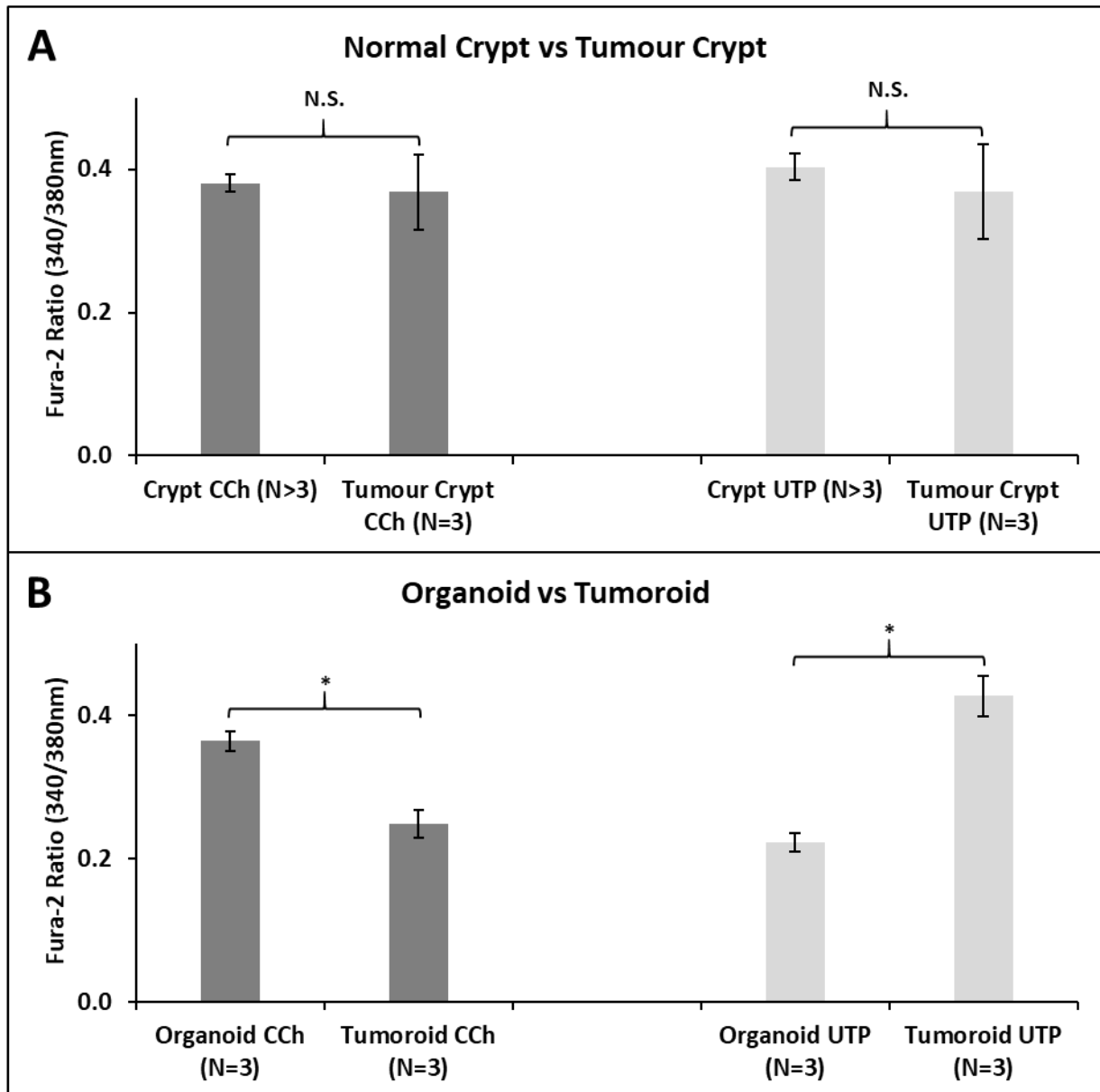
Figure 156 – Organoids are More Sensitive to CCh, Tumoroids are More Sensitive to UTP.

Bar charts summarising the Fura-2 ratio amplitude comparing CCh-induced Ca²⁺ signals and UTP-induced Ca²⁺ signals in normal versus tumour crypts **(A)**, and in organoids versus tumoroids **(B)**. N≥3. For every "N", n≥3.

7.3 Discussion

In this final results chapter, the gene transcriptomic analysis and pharmacology profile of tumour colon tissue samples were compared against normal colon tissue samples. Transcriptomic analysis of tumour colon tissue samples was carried out using RNA sequencing to demonstrate the gene expression of intracellular Ca^{2+} release channels, muscarinic and purinergic GPCRs, and proteins related to production or packaging of endogenous acetylcholine and ATP. These results were compared against the transcriptomic analysis of normal colon tissue samples using the Log2 fold change. Next, the protein expression of Ca^{2+} signalling toolkit components were confirmed in tumoroids using immunolabelling. Finally, Fura-2 experiments were conducted to determine the pharmacological profile of inhibiting CCh and UTP-induced Ca^{2+}-signals in tumour crypts and tumoroids. These results were directly compared against the normal colon tissue samples.

7.3.1 Differential RNA Expression in Tumour vs Normal Colon Tissue Samples

In both tumour (Figure 134) and normal colon tissue samples (Figure 23), IP3R3 was the most prominent IP3R subtype. These data go against another transcriptomic analysis study which found IP3R3 to be absent from normal colon cells but expressed in cancer colon cells (Pérez-Riesgo, et al., 2017). However, that study was conducted using immortalized cell lines (NCM460 and HT29), while in this thesis transcriptomic analysis was conducted on native normal and tumour mucosa, crypts which were isolated and cultured from mucosa, and organoids/tumoroids which developed from crypts after long-term culture. The samples in this thesis would be morphologically, genetically, and functionally be more similar to the *in vivo* scenario, meaning the transcriptomic analysis data generated from these models would be more relevant and reflective of the *in vivo* environment compared to cell lines.

While IP3R1 and IP3R2 were higher in tumour compared to normal colon tissue samples, IP3R3 was decreased (Figure 134). This would contradict a study which showed that IP3R3 was associated with decreased 5-year survival chances (Shibao, et al., 2010) and thus would be expected to be increased in tumoroids. But again, that study observed that using the Caco-2 cell line and may not reflect the *in vivo* environment. That said, the human colonic tissue samples used in this thesis were obtained patients who had undergone right-hemicolectomy or anterior resection at the Norfolk and Norwich University Hospital. These patients would be on medication or had undergone chemo/radiotherapy, meaning the status of their normal and tumour colon tissue samples may not be similar compared to a person who did not receive medical treatment. In addition, this transcriptomic analysis was conducted on five or six patient-matched tumour and normal colon tissue samples. This small population sample would not be reflective of all CRC variations, of which there are several dozen common genetic variants which affect a range of biological pathways (Zhang, et al. 2014).

Of the RYR subtypes, RYR2 was most abundant in tumour colon tissue sample (Figure 135) and was much higher compared to normal colon tissue samples. This finding is complementary to a study which found several genes including RYR2 were frequently mutated in colon carcinoma (Wolff, et al. 2018). In a study using breast cancer cell lines, RYR2 gene expression was upregulated by over 40 times and propose it was involved in epithelial-mesenchymal transition via an EGF-induced Ca^{2+}-signalling pathway (Davis, et al. 2013). Overall, this implies RYR2 being involved in CRC development, likely via releasing stored endoplasmic reticular Ca^{2+}.

In both tumour (Figure 136) and normal colon tissue samples (Figure 25), TPC1 expression was higher than TPC2. And between tumour and normal, TPC1 and TPC2 gene expression did not differ by much. More interestingly, CD38 was expressed much higher in tumoroids (Figure 137) versus organoids (Figure 36), while in tumour/normal mucosa and crypts CD38 expression varied little. This was due to higher average expression of CD38 in tumoroids, however it varied greatly between patient resulting in a large standard error. One study tested the presence of full-sized and alternative forms of CD38 mRNA in tumour colon tissue samples and in cell line (Perenkov, et al. 2012). They found CD38 to be present in some cell lines and absent in others and found CD38 to be expressed in tumour tissue in the first stage of CRC, which decreased in second, third and fourth stages. Taken together these results indicate CD38, which catalyses the production of TPC-agonist NAADP, may be involved in early CRC development but is subsequently lost during later disease stages.

In both tumour (Figure 138) and normal colon tissue samples (Figure 27), M3 expression was highest among the four subtypes analysed. And, M3 expression was higher in tumour mucosa and tumour crypts compared to normal mucosa and normal crypts, and hardly differed in tumoroids versus organoids. This finding is complimentary to a host of studies which show M3 to be associated with CRC by promoting cancer cell proliferation through a complex signal transduction pathway involving EGFR (Frucht, et al. 1999), (Yang and Frucht 2000) and (Cheng, Chen, et al. 2002), which when inhibited in murine models attenuates intestinal neoplasia (von Rosenvinge and Raufman 2011) and has been proposed to be a target for CRC therapy (Felton, Hu and Raufman 2019).

Moving onto ATP-sensitive purinergic P2Y receptors, P2Y1/2 were higher than P2Y11/13 in both tumour (Figure 139) and normal colon tissue samples (Figure 28). P2Y1 and P2Y2 gene expression levels were similar across and between normal colon tissue samples. That said, when tumour and normal colon tissue samples compared, P2Y1 and P2Y2 expression was reduced in tumour colon tissue samples. These conflict with one study which found P2Y1 to be highly expressed in human epithelial carcinoma cell lines (Coutinho-Silva, et al., 2005). However, that same study found high concentrations of ATP to be pro-apoptotic and caused an increase in cytoplasmic $[Ca^{2+}]$, while lower concentrations of ATP stimulated proliferation.

By that reasoning, it may be that reduction of P2Y1 *in vivo* promotes proliferation due to fewer P2Y1 receptor-activated signal transduction. Another conflicting study found P2Y2 to be overexpressed in human colon cancer cell lines to regulate cell growth (Nylund, Hultman, Nordgren, & Delbro, 2007) and in patient breast cancer specimens to regulate metastasis (Kim, et al. 2020).

ChAT expression was lower in tumour mucosa (Figure 140) compared to normal mucosa (Figure 29) and non-existent in tumour crypts and tumoroids. This was unexpected, as studies have proposed colon cancer cells to be capable of autologous acetylcholine secretion to stimulate proliferation (Cheng, et al., 2008); or promoted innervation and tuft cell expansion, resulting in increased neuronal and non-neuronal acetylcholine secretion which induces cholinergic signalling to activate Wnt signals (Hayakawa, et al., 2017).

On the flipside, gene expression for VNUT (SLC17A9) was increased in every tumour colon tissue sample (Figure 141) compared to normal (Figure 30). Lastly, gene expression for proglucagon (GCG) were drastically lower in every tumour colon tissue sample (Figure 144) compared to normal (Figure 31), but conversely had increased neuroendocrine convertase 1 (PCSK1) gene expression in tumour mucosa/crypts than normal mucosa/crypts, and reduced in tumoroids than organoids. Taken together, these data indicate that tumour colon tissue secrete more ATP and may or may not be more capable of synthesizing GLP1 compared to normal colon tissue sample.

7.3.2 Tumoroids Express the Ca^{2+}-Signalling Toolkit Components

To compliment the transcriptomic analyses, immunolabelling was done in tumoroids to visualize the Ca^{2+} signalling toolkit components. For the most part, the labelling pattern for most Ca^{2+} signalling toolkit components were similar in tumoroids compared to organoids. The biggest exception to that were RYRs, where RYR1 and RYR2 were prominent along the apical pole including the cytoplasm and apical membrane (Figure 144), while in organoids (Figure 34-5) their labelling was predominantly on the basal pole. This would suggest that the expression and localisation of RYR1-2 are altered in tumoroids.

7.3.3 Tumoroids are More Sensitive to TPC and RYR Inhibition

CCh-induced Ca^{2+} signals were more sensitive to TPC-inhibition using Ned-19 (250-500 µM) and tetrandrine (20 µM) in tumour colon tissues (Figure 148-9). In the presence of Ned-19 (500 µM), CCh-induced Ca^{2+} signals were slightly lower in tumour crypts and tumoroids compared to crypts and organoids (Figure 148A, B, E). However, CCh-induced Ca^{2+} signals were reduced by half in the presence of Ned-19 (250 µM) in tumour crypts while in crypts it increased by a quarter (Figure 148B & E). Likewise, CCh-induced Ca^{2+} signals were inhibited by 95% in the presence of tetrandrine (20 µM) in tumoroids while in organoids that inhibition

was 84% (Figure 149A & C). This was interesting, as the RNAseq analysis showed similar M3, similar TPC1-2 and higher CD38 in tumoroids compared to organoids (Chapter 7.3.1), which would suggest TPC-inhibition being consequentially similar or less effective in tumoroids compared to organoids. Explanations for this could be that protein misfolding or modifications or turnover may be enhanced in tumoroids compared to organoids (Chen, et al. 2017) and (Ly, et al. 2018), leading to increased sensitivity to TPC-inhibition. Whether that is the case, would be an interesting study for the future. As for UTP- induced Ca^{2+} signals, the pharmacological profile of Ned-19 (250-500 µM) were almost identical in tumour crypts and tumoroids versus crypts and organoids (Figure C, D, F). However, tetrandrine (20 µM) reduced UTP-induced Ca^{2+} signals by nearly half in tumoroids, while in organoids it increased UTP-induced Ca^{2+} signals by nearly half. As this was conducted in only one patient's tumoroid line (N=1), it would be appropriate to repeat this on another patient tumoroid line before drawing any conclusions.

The pharmacological profile of IP3R1- antagonist 2-APB (50-100 µM) in human tumour colon tissues were mostly similar to normal human colon tissues (Figure 150). The only exception was 2-APB (100 µM) reducing CCh-induced Ca^{2+} signals by three times as much in tumour crypts compared to normal crypts (Figure 150A & E). However, given this data was generated from only one patient's tumoroid line (N=1), it would be appropriate to repeat this on another patient tumoroid line before drawing any conclusions. Likewise, the pharmacological profiles of 'slow channel blocking agents' verapamil (50 µM) and diltiazem (250-500 µM), and non-specific Ca^{2+} antagonists TMB8 (50-100 µM) in tumoroids were mostly similar to organoids (Figure 151-3). That said, tumoroid CCh and UTP-induced Ca^{2+} signals were more susceptive to verapamil compared to organoids (Figure 151), which again could be due to protein misfolding or modifications or turnover being enhanced in tumoroids compared to organoids, leading to increased sensitivity to pharmacological inhibition. Finally, similar to tetrandrine and 2-APB, most of these data were generated from one patient tumoroid line (N=1) and should ideally be repeated.

With that said, CCh and UTP-induced Ca^{2+} signals were more sensitive to RYR inhibition. Non-specific RYR antagonist procaine (1 mM) inhibited CCh-induced Ca^{2+} signals in tumoroids by 87% compared to 37% in organoids (Figure 154A & C). Likewise, RYR1/3- antagonist dantrolene (50 µM) inhibited CCh-induced Ca^{2+} signals in tumoroids by 100% compared to 78% in organoids, and also inhibited UTP-induced Ca^{2+} signals in tumoroids by 78% compared to 56% in organoids (Figure 155). This is complimented by the enhanced RYR1 and RYR2 gene expression (Figure 135) and prominent apical labelling of RYR1 and RYR2 (Figure 144A-B) in tumoroids compared to organoids (Figure 34-5), which could suggest tumour colon tissues altering the gene and protein expression of RYR1 and RYR2 to promote aberrant Ca^{2+}-signalling.

Lastly, changes in Fura-2 ratio amplitude induced by CCh (10 μM) and UTP (50 μM) were compared between normal crypts versus tumour crypts, and in organoids versus tumoroids. The Fura-2 ratio amplitude induced by CCh and UTP were similar to crypts and tumour crypts (Figure 156A). However, in organoids and tumoroids the Fura-2 ratio amplitude induced by CCh and UTP were remarkably different (Figure 156B); tumoroids were 31% less responsive to CCh and 95% more responsive to UTP. This data clearly shows tumoroids having an altered Ca^{2+}-signalling characteristics compared to organoids, likely due to increasing RYR1 gene expression and possibly due to changes in RYR2 expression. This data also indicates that tumour crypts, which were isolated from tumour mucosa, may not a reliable model for investigating colon cancer. This is because there is no guarantee that every crypt isolated from tumour mucosa are tumour crypts; in practice it is likely that a mixture of tumour crypts and normal crypts are isolated from tumour mucosa. On the other hand, tumoroids were generated by culturing crypts isolated from tumour mucosa in Wnt-free media. As a result, only cells that have APC mutations which result in constitutive Wnt activation can survive and develop into tumoroids.

7.4 Conclusion

In this final results chapter, the gene transcriptomic analysis and pharmacology profile of tumour colon tissue samples were compared against normal colon tissue samples. The gene expression of IP3R1&2, RYR1&2 and M3 were consistently higher in tumour colon tissue samples. Pharmacologically, tumour colon tissue samples were more sensitive to TPC and RYR inhibition. Lastly, the status of Ca^{2+}-signals in tumoroids is remarkably different compared to organoids; tumoroids were more sensitive to UTP-induced purinergic signalling and less sensitive to CCh-induced muscarinic signalling.

8 Chapter 8 – Overall Discussion and Future Work

During this thesis, several important discoveries were found which furthered our understanding of the mechanisms regulating human colonic epithelial physiology. First, Ca^{2+} signalling toolkit components were identified in three human colonic tissue samples (mucosa, crypts, and organoids) at the gene and protein level using RNA transcriptomic analysis and immunolabelling (Chapter 3). The involvement of these Ca^{2+} signalling toolkit components were evaluated by stimulating Fura-2-loaded crypts and organoids with muscarinic receptor agonist CCh (10 µM) and purinergic receptor agonist UTP (50 µM), in conjunction with a host of pharmacological antagonists and agonists (Chapter 4), to elucidate the muscarinic and purinergic-induced Ca^{2+}-signalling pathway. A HILIC-MS/MS method was then developed and validated to quantify non-neuronal acetylcholine in media which had been cultured in human colonic crypts and organoids (Chapter 5). Next, CCh was shown to induce fluid and mucus secretion, as well as promote proliferation, and were differentially affected by inhibition of certain Ca^{2+} signalling toolkit components (Chapter 6). Finally, the Ca^{2+} signalling toolkit components and pharmacological profiles of human colonic tumours were compared against normal human colonic tissues (Chapter 7).

8.1 Organoids as Model Systems for Studying the Human Colonic Epithelium

In the past two decades, 3D culture systems have increasingly been used as a model to study cells/tissues in the in vivo environment. Compared to 2D culture systems, 3D culture systems incorporate extracellular matrixes which exist for nearly all cells, thereby creating an environment that is comparable to the *in vivo* architecture. The growth of cells in these 3D culture systems gave rise to tissue-like structures which resemble miniature organs, hence their name organoids (Simian and Bissell 2017). Due to this, organoids developed using 3D culture systems are more reliable than monolayer cells grown in 2D culture systems in terms of studying growth conditions, proliferation, gene and protein expression, and drug discovery or pharmacology (Edmondson, et al. 2014). For the human colonic epithelium, the Clevers group were the pioneers who developed organoids from colon, adenoma, and adenocarcinoma (Sato, Stange, et al. 2011). Since then, numerous research labs including the Williams group (Pelaez-Llaneza 2019) have used organoids to study the human colonic epithelium.

The intestinal epithelium consists of a monolayer of polarised epithelial columnar cells which have rapid renewal time of 3-5 days (Barker 2014). In the large intestine, the epithelial monolayer is organized in tube-like glands termed "crypts of Lieberkühn", or simply crypts (Figure 2C). At the base of these intestinal crypts, multipotent intestinal stem cells (ISCs) divide asymmetrically and give rise to mature epithelial cell types including goblet cells, enterocytes, enteroendocrine cells, and tuft cells (Gehart and Clevers 2019). The organisation of crypts – tube-like with stem cells at the base – serves to protect ISCs in a protective niche, away from chemical and microbial hazards contained in the lumen. The culture system developed by the Williams lab enables the propagation of organoids/tumoroids indefinitely

and without losing their phenotypic or pharmacological or physiological signatures. During the course of this thesis, five patient-matched organoids/tumoroids lines were generated and preserved in cryofreeze. Following a short recovery period, organoids/tumoroids were not damaged by the freeze-thaw process and were used for transcriptomic analyses, Fura-2 Ca^{2+} experiments, and physiological functional studies (Chapter 3-7). As a result, within the Williams group organoids/tumoroids are readily available and patient-matched organoid/tumoroid lines can be studied over long term.

In this thesis, organoids were shown to be suitable models of studying human colonic epithelial biology. Organoids were generated from human colonic crypts that were isolated from normal colonic mucosa and cultured for long-term (months to years) with periodic passaging and reseeding. Over the course of several days after reseeding, organoids grew larger and developed crypt-like 'buds' with noticeable lumens (Figure 157A). This indicated organoids developing into functional crypt-like structures, with buds representing the longitudinal crypt axis and lumens representing cellular apical-basal polarity. Transcriptomic analysis between mucosa, crypts and organoids showed comparable levels of most Ca^{2+} signalling toolkit components within the three tissue models (Chapter 3.2.1). This supports an earlier study which showed organoids being genetically stable over long-term culture (Sato, van Es, et al. 2011). Cases where gene expression in mucosa were higher compared to crypts and organoids, like IP3R3 (Figure 23), would likely be due to non-epithelial sources of RNA such as neurons and immune cells within the lamina propria basement membrane. In cases where gene expression was lower in mucosa compared to crypts and organoids, like IP3R3 (Figure 23) and TPC2 (Figure 25), it would indicate changes in gene expression within crypts and organoids that were cultured in Matrigel compared to mucosa. These changes in gene expression are probably caused either due to lack of downregulation mechanisms present in mucosa, or upregulation caused by Matrigel – a reconstituted basement membrane preparation extracted from mouse sarcoma that is biologically active (Kleinman and Martin 2005). As a result, one cannot rule out differences in gene regulation in organoids and crypts cultured in Matrigel compared to crypts in *in vivo*. One means to resolve that issue is to develop a matrix whose physicochemical properties are identical to in vivo, which is currently being developed by other members of the Williams group.

The next step of demonstrating organoids to be ideal models of studying colonic epithelial biology was to show they possess similar protein expression and cellular composition, and that they were pharmacologically and physiologically comparable to crypts. The first two were achieved by comparing the immunolabelling of Ca^{2+} signalling toolkit components and markers of epithelial cells in mucosa, crypts, and organoids (Chapter 3.2.3). In summary, organoids which had been cultured for long-term had similar protein localisation and cellular identities as freshly isolated crypts and mucosa. Co-labelling of Ca^{2+} signalling toolkit components with markers of epithelial cells also gives clues as to the physiological roles of certain Ca^{2+} signalling components. For example, co-labelling of TPC1 – but not TPC2 – and

MUC2 indicate TPC1 playing a role in mucus secretion via Ca^{2+}-signals originating from endolysosomes, which had been described but not fully elucidated (Perez-Vilar, Olsen, et al. 2005), (Ambort, et al., 2012) and (Kam 2015). Pharmacologically, organoids and crypts that were loaded with Fura-2 performed almost identically in response to stimulation or inhibition (Chapter 5), which shows that the biological activities of organoids are functionally equivalent to crypts. Likewise, crypts and organoids which were loaded with fluorescent lipid dyes (FM1-43, FM1-43X, and Deep Red) showed comparable mucus granule secretion and compound exocytosis (Chapter 7), which demonstrates organoids having functionally similar cellular fluid-secretion machineries as crypts. In addition, previous work by the Williams group showed organoids being a comparable model for studying mucus secretion by comparing the expression of epithelial cell markers in mucosal crypts and cultured crypts and organoids (Pelaez-Llaneza 2019).

On the other hand, tumoroids were generated from long-term culture of human tumour colonic crypts that were isolated from tumour colonic mucosa. While tumoroids also grew larger over time, their ability to form 'buds' were poor, in fact typically forming spheroids with thinner apical-basal membranes and less defined tissue cohesion (Figure 157B). This had been observed by other groups (Kashfi, et al. 2018) and is likely due to tumoroids having genetic mutations, leading to dysregulation of essential molecular and cellular signalling pathways required to maintain normal growth and function (van de Wetering, et al. 2015). This was supported by comparisons of the transcriptomic analysis of Ca^{2+} signalling toolkit components between tumour and normal colon tissue samples supports that statement (Chapter 7) – tumour colon tissue samples expressed more RNA for IP3R1, IP3R2, RYR2, CD38, and VNUT; and less RNA for IP3R3, M1, and P2Y2R. This again may give clues as to as to the physiological roles of certain Ca^{2+} signalling components which are favoured by tumoroids.
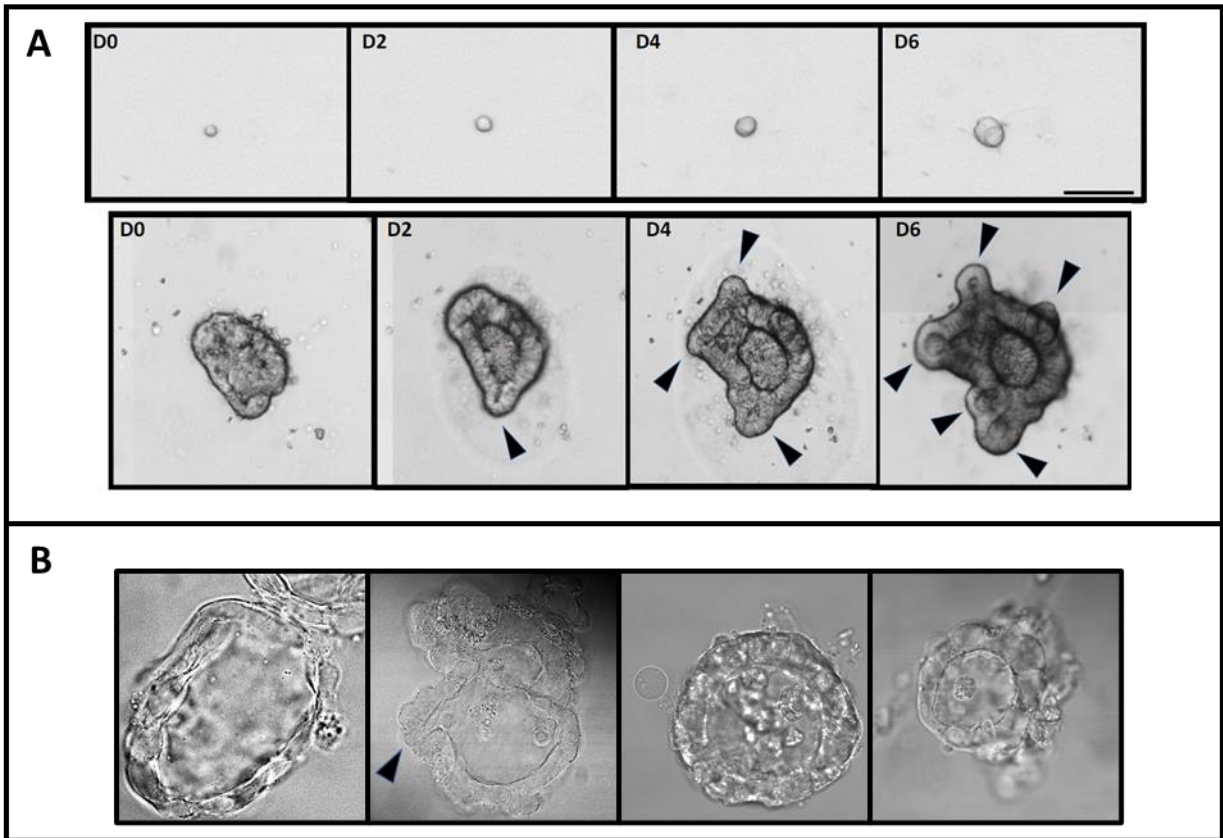
Figure 157 – Growth of Cultured Colonic Organoids and Single Cells, Versus Tumoroids.

Colonic single cells (N=1) grow over days (A top) and develop into budding organoids after successive passaging and reseeding (A bottom). By comparison, tumoroids (N=4) often fail to form buds and grow into spheroids. Arrows indicate buds. Scale bar 150 μm.

The ability of the Williams group to culture patient-matched organoids/tumoroids lines which can be kept indefinitely in cryofreeze raises the possibility of developing personalized medicine (Figure 158). For example, colonic organoids and tumoroids grown from patient-matched tissue samples could be treated with different chemotherapy drugs to determine the most suitable chemotherapy regime for them. Alternatively, once more patient-matched lines have been sequenced, tumoroids which have certain mutations can be subjected to targeted treatments with the goal of promoting death of tumour cells while ensuring the survivability of patient-match organoids. Currently, the Williams group is working to genetically manipulate or engineer organoids/tumoroids using CRISPR/Cas and SiRNA. Applications of these techniques include selectively target candidate genes in organoids in order to study changes in Ca^{2+}-signals and investigate the physiological consequences of silencing selected genes.

However, the long-term genetic stability of the lab's organoids and tumoroids will need to be considered. Since these organoids and tumoroids are *ex-vivo* culture systems that are bathed in media to promote growth and are passaged every three or four days, it is highly likely that these organoids and tumoroids will acquire genetic mutations over time. One way to monitor the genetic stability of organoids and tumoroids cultured in the long-term, would be to put them and their native frozen counterparts through RNAseq to compare their RNA gene expression. And in the event where the RNA gene expression of organoids and tumoroids cultured in the long-term culture is significantly different compared to their frozen counterparts, a sensible solution would be to generate fresh organoid and tumoroid lines that have been frozen.

In addition to crypts, organoids and tumoroids, another potential model which the Williams lab could develop to study human colonic epithelium biology would be using single cells. These single cells could be segregated using fluorescence-activated cells sorting (FACS) into mature colonic epithelial cells such as stem cells, goblet cells, EECs, Tuft cells, etc. The use of single cells was explored briefly in this thesis, whereby single goblet-cells were immunolabelled using MUC2 (Figure 106). One strategy of using single populations of colonic epithelial cells would be to identify genes that are up/downregulated in those populations, which may indicate specific receptors and their associated pathways which these mature epithelial cell types rely on.

A Healthy/Tumour Colonic Crypt (2-4 days) → Organoid/Tumoroid (Indefinite) → Patient-Matched Biobank (Indefinite)

B 1. Gene Expression Comparisons

	Log 2 (Tumour Mucosa / Normal Mucosa)	Log 2 (Tumour Crypt / Normal Crypt)	Log 2 (Tumoroid / Organoid)
ITPR1	0.728	1.428	2.568
ITPR2	0.337	0.108	2.873
ITPR3	-0.039	-0.293	-0.727

2. Ca²⁺ Signal Comparisons

3. Acetylcholine Secretion Comparisons

4. Physiological Comparisons

Future I. Genetic Manipulation

Future II. Drug Screening & Personalized Medicine

Figure 158 – Current & Future Applications of Patient-Matched Organoid/Tumoroid Culture.

Patient-matched organoid and tumoroid lines (which can be cultured indefinitely) have been developed from human colonic crypts (which can be kept in culture for 2-4 days) and can be used to generate a colon tissue biobank **(A)**. Currently, organoids and tumoroids can be used for comparative gene expression studies **(B1)**, Ca^{2+} experiments **(B2)**, non-neuronal acetylcholine secretions **(B3)**, and proliferation experiments **(B4)**. Future applications include genetic manipulation **(BI)** and drug screening for the purpose of personalized medicine **(BII)**.

8.2 Ca²⁺ as a Signal Integrator in the Colonic Epithelium

The colonic epithelium is susceptive to a host of different signals which regulate each epithelial cell and overall maintain tissue homeostasis. In order to process these diverse signals, epithelial cells use second messengers to coordinate various signal transduction pathways to achieve the correct physiological outcome. In this thesis, Ca²⁺ is proposed to be the second messenger used by colonic epithelial cells to coordinate several signal transduction pathways which, when altered, subverts physiological processes into driving pathological outcomes (Bootman and Bultynck 2020). Ca²⁺ signals have been studied extensively in the context of muscle (Cho, et al. 2017) and neuronal (Brini, Calì, et al. 2014) cell biology. By comparison, Ca²⁺ only became a topic of interest in colonic epithelial biology in recent years, such as cell-cell connection (McClintock, et al. 2020), secretion of mucus (Ambort, et al., 2012) and fluid (Yang, et al. 2018), regulating ISC proliferation and differentiation (Deng, Gerencser and Jasper 2016), and its role in colonic diseases.

During resting conditions, intracellular [Ca²⁺] is low and is maintained by an assortment of buffers, channels, pumps, and transporters (Figure 17). These are the Ca²⁺ signalling toolkit components, whose presence and distribution patterns varies depending on the cell type. This thesis focuses on Ca²⁺ signalling toolkit components of the muscarinic and purinergic signalling pathways. These include muscarinic (M1-5) and metabotropic purinergic (P2Y) GPCR receptors, endoplasmic reticular IP3Rs and RYRs, endolysosomal TPCs, CD38 which catalyses TPC-ligand NAADP, ChAT which catalyses acetylcholine, VNUT which is involved in storing and releasing vesicular ATP, and GCG/PCSK1 which are involved in GLP1 synthesis. Besides these, previous work in the Williams group analysed the gene expression of cellular Ca²⁺ ATPases such as SERCA, PMCA, and SPCA (Pelaez-Llaneza 2019). The reason why muscarinic and metabotropic purinergic receptors were focused on in this thesis were due to the role of secretagogues acetylcholine and ATP in modulating colonic epithelial physiology by inducing intracellular Ca²⁺-signals. In the case of acetylcholine, this thesis was interested in autocrine cholinergic signalling, whereby epithelial ChAT+ tuft cells synthesizes and secretes acetylcholine in an autocrine manner to stimulate locally or adjacent G_q-coupled M1/3/5 receptors and thereby affect a host of colonic epithelial physiology (Chapter 1.4.4). As for ATP, it has been shown to be an important extracellular signalling molecule which affects colonic epithelial biology in health and disease through its activation of G_q-coupled P2Y1/2/11/13 (Chapter 1.4.5). Similar to acetylcholine's autocrine signalling dynamic, intestinal L-type enteroendocrine cells have been shown to be capable of secreting ATP alongside gut peptide hormones GLP1 and PYY (Lu, et al. 2019), the former triggering P2Y2 receptors in neighbouring enterocytes and afferent neuronal P2X2/3 receptors to synergize with the functions of elevated gut peptide hormones.

Gene and protein expression of these Ca²⁺ signalling toolkit components in human colonic tissue samples were confirmed using RNAseq and immunolabelling (Chapter 4). The first notable finding was the ten/hundred-fold higher gene expression of IP3R3 compared to

IP3R1/2 in human colonic native mucosa, cultured crypts, and organoids (Figure 23), which might indicate IP3R3 playing an important role in colonic epithelial biology. That notion was supported by differential IP3R subtype immunolabelling patterns (Figure 32-33); nonspecific for IP3R1, prominently basal for IP3R2, and prominently apical for IP3R3. Another interesting finding was that while RYR1-3 gene expression was much lower or non-existent (Figure 24), immunolabelling confirmed they were present (Figure 34-36). This shows that one cannot rely solely on transcriptomic analysis to draw conclusions regarding protein expression as it does not account for rate of protein synthesis and turnover. The only component which was consistently absent at both gene (Figure 29) and protein (Figure 51) level was ChAT in organoids. This was an unfortunate setback which highlight the culture system to be unable to support ChAT+ tuft cells in long-culture, which will need to be focused on in future studies; in order to properly study the role of autocrine cholinergic signalling in the human colonic epithelium. Even so, ChAT labelling was prominent in mucosa crypts; low ChAT labelling in goblet cells (Figure 52), strong co-labelling with tuft cells (Figure 53), and some co-labelling with enteroendocrine cells (Figure 54). This was exciting, as other studies have only shown ChAT to be expressed/secreted by tuft cells (Ualiyeva, et al., 2020), (Hollenhorst, et al., 2020), and (Pan, Zhang, Shao, & Huang, 2020).

Having determined the gene and protein expression of these Ca^{2+} signalling toolkit components, Fura-2 experiments were carried out (Chapter 5) to characterise the spatio-temporal characteristics of CCh-induced muscarinic and UTP-induced purinergic Ca^{2+} signalling, as well as elucidate the muscarinic and purinergic Ca^{2+}-signalling pathways. CCh-induced Ca^{2+} signals consistently initiated at the apical pole of cells within the very base of crypts, spreads to the basal pole and propagates up the crypt axis (Figure 57) and (Figure 58A). This implicates TPC1 and/or IP3R3 to be the origin of CCh-induced Ca^{2+}-signals, as immunolabelling experiments showed that they are expressed apically (Figure 38) and (Figure 33). On the other hand, UTP-induced Ca^{2+} signals typically initiated higher up the crypt axis on either apical or basal poles and propagates to adjacent cells (Figure 62 A-B). This implicates IP3Rs and RYRs in general, as immunolabelling experiments showed that they are expressed apically and basally (Figure 32-6). Future studies should investigate the means by which the global wave of Ca^{2+} propagation occurs. There are currently two proposals regarding this propagating wave of Ca^{2+} signal following agonist stimulation: Ca^{2+} is crossing into neighbouring cells via gap junctions to induce CICR, or most cells are capable of responding to agonist stimulation albeit at different capacities due to differential Ca^{2+} signalling toolkit component expression. The first proposal was investigated in this thesis using carbenoxolone (Figure 73), however the data using this drug is not definitive since it is not specific for gap junctions. One way of investigating the second proposal would be to observe the effects of CCh/UTP stimulation in single cells to determine if specific cells are susceptive to muscarinic and/or purinergic receptor activation.

Alternatively, using the LSM910 confocal microscopy, live-imaging experiments that was conducted by other members of the Williams group showed that slender cells – which are likely intestinal stem cells – to be the origin of CCh-induced Ca^{2+}-signals (Figure 159A). In those experiments, they showed that stimulating Fluo-4 loaded crypts with CCh (10 µM) resulted in Ca^{2+} signals initiating from the apical pole (Figure 159B left) of slender cells at the base of crypts and spreading to the basal pole (Figure 159B right). This should be replicated using ATP/UTP to determine the cellular origins of purinergic receptor activation.
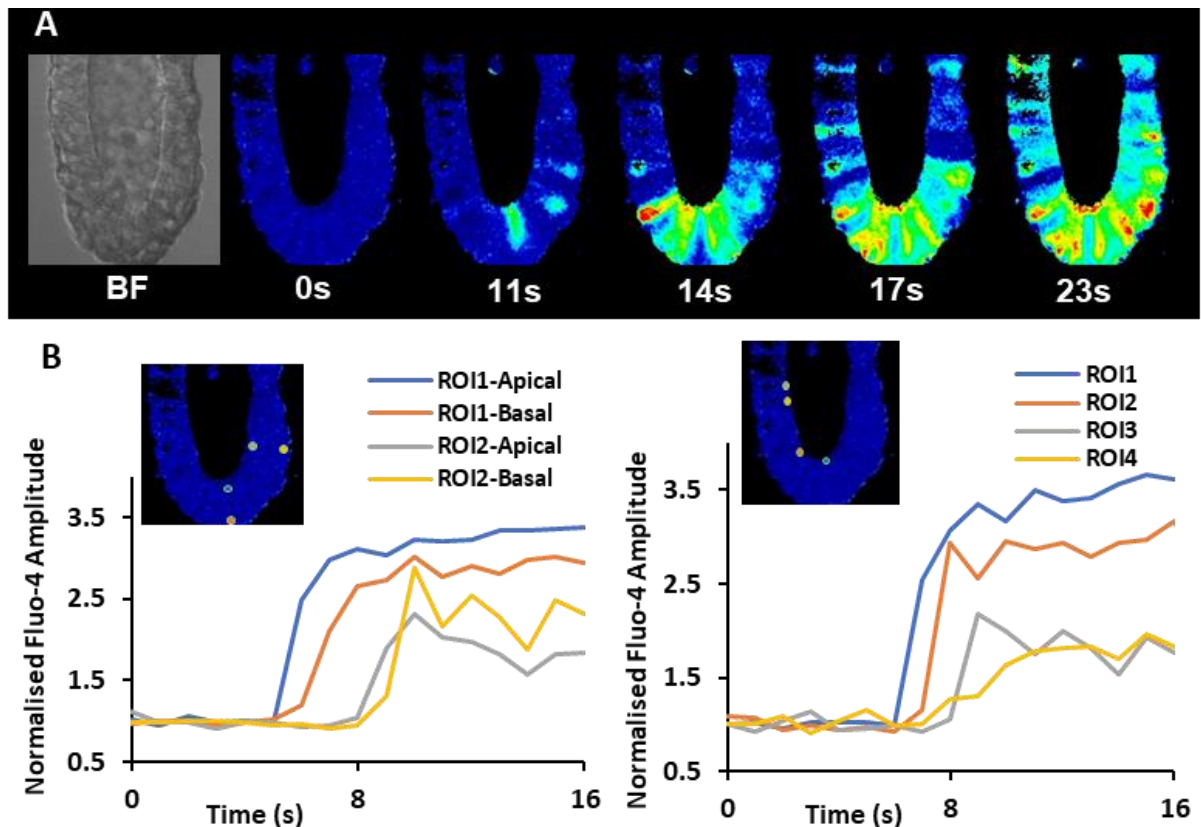
Figure 159 – Intestinal Stem Cells are the Origin of CCh-Induced Ca^{2+} Signals

Representative series of epi-fluorescent live images of a crypt loaded with Fluo-4 (5 µM) being stimulated with CCh (10 µM) over time in seconds (s) **(A)**. Line graphs illustrating the polarity **(B left)** and topology **(B right)** increase in normalized Fluo-4 fluorescence amplitude induced by CCh (10 µM) over time (s). ROI – region of interest.

The consistent initiation of apical Ca^{2+}-signals induced by CCh initially seemed peculiar, as G_q-coupled muscarinic receptors (M1/3/5) were consistently shown to be expressed on the basal pole (Chapter 3.2.3). That said, apical Ca^{2+} spikes have been characterised in highly polarised epithelial pancreatic acinar cells (Petersen and Tepikin 2008) and are due to sophisticated and complex Ca^{2+} signalling mechanisms between the endoplasmic reticulum and endolysosomes. Likewise, it is plausible that colonic epithelial cells express their Ca^{2+} signalling toolkit components in specific locations, given the observation of differential IP3Rs, RYRs and TPC immunolabelling patterns.

Using highly specific pharmacological antagonists 4-DAMP (100 nM) and AR-C118925XX (5 μM), CCh was shown to activate M3 receptors (Figure 60) while UTP was shown to activate P2Y2 receptors (Figure 65), respectively. Both muscarinic and purinergic-induced Ca^{2+} signals were shown to originate from organellar Ca^{2+} stores, as the Ca^{2+} signal was not significantly reduced when extracellular Ca^{2+} was chelated using EGTA (1 mM) (Figure 59) and (Figure 64). That said, there was a 6-20% decrease compared to control, which reflects the gradual leakage of intracellular Ca^{2+}. Subsequent experiments using an array of pharmacological agonists and specific/non-specific antagonists (Table 9) elucidated the intracellular Ca^{2+}-signalling pathway induced by muscarinic and purinergic receptor activation. In short, muscarinic receptor activation (M3 receptors) initiates local Ca^{2+}-signals via endolysosomal TPC1/2 which triggers endoplasmic reticular Ca^{2+}-release via IP3R3, while purinergic receptor activation (P2Y2 receptors) initiates Ca^{2+}-signals from endoplasmic reticular IP3R1-3; at this point they converge on RYR1/3 to cause global Ca^{2+}-signals which propagates as a wave through the cell. A schematic diagram representing the proposed signalling pathway is presented (Figure 160).

CD38 was proposed to be the link between basal muscarinic receptor activation and TPC Ca^{2+}-release, as it synthesizes NAADP which is a known ligand of TPCs (Ruas, Rietdorf, et al. 2010). To that end, CD38 was shown to be present at the gene (Figure 26) and protein (Figure 41-2) level. However, the exact mechanism by which muscarinic receptor activation leads to NAADP catalysis by CD38 remains unclear and should be investigated in future studies. It is also unclear whether CD38 catalyses NAADP on the apical pole of cells (Figure 41-2), possibly within acidic endosomes which provides CD38 the low pH required for catalyse NAADP (Figure 22). Recent TPC1-2 immunolabelling that was visualized on the LSM910 confocal microscope provided clearer TPC1-2 labelling (Figure 161). Once again, TPC1 labelling was concentrated on the apical membrane (Figure 161A-B), while TPC2 labelling was prominent on the basal side (Figure 161C-D). In addition, two Rab proteins (Rab 5 & 11) were co-immunolabelled with TPC1-2. Rab proteins are members of the Ras superfamily of small G proteins, many of which are involved in endocytic trafficking (Wandinger-Ness and Zerial 2014). Rab5 in particular is involved in the maturation of early endosomes into late endosomes via the *trans*-Golgi (Nagano, et al. 2019), and Rab11 regulates the exocytosis of recycling vesicles at the plasma membrane (Takahashi, et al. 2012) and are localised on early endosomes (Kobayashi and

Fukuda 2013). Due to TPC1 co-labelling with Rab11, it indicates TPC1 labelling early endosomes and are involved in exocytosis of mucus granules. These will need to be replicated in mucosa and crypts in future studies.

Tentative experiments using tricyclic anti-depressants (TCA) chlorpromazine and nortriptyline were shown to induce Ca^{2+}-release via TPCs (Figure 80 & 87). Future work should expand on the pharmacological profiles of these TCAs compared to CCh. In addition to muscarinic and purinergic receptor activation, other means of generating intracellular Ca^{2+}-signals – mechanosensitive PIEZO1 channels (Figure 89) and mucolipin TRP channels TRPML1 (Figure 89) – were explored due to their importance GI function during health and disease (Alcaino, et al., 2018) and (Santoni, Santoni, Maggi, Marinelli, & Morelli, 2020). The significance of intracellular Ca^{2+}-signals generated by these means would also be of interest in the future. Lastly, in this thesis only the intracellular Ca^{2+}-signals induced by P2Y2 receptor activation was investigated, as P2Y2 receptors are sensitive to ATP/UTP and is specifically inhibited by AR-C118925XX (5 µM). The contribution and relevance of other ATP-sensitive, G_q-coupled P2Y1/11 receptors should be explored in future studies.

Agonists:
- CCh (mAChR3)
- ATP (P2Y1/2/11R)
- UTP (P2Y2R)
- Yoda1 (Piezo1)
- ML-SA1 (TRPML1)
- Chlorpromazine (TPCs)
- Nortriptyline (TPCs)

GPCR-inhibitors:
- 4-DAMP (M3)
- AR-C118925XX (P2Y2R)

Other inhibitors:
- CPA (SERCA pump)
- BAF A1 (H^+-ATPase)
- Chloroquine (acidic stores)
- GsMTx4 (Piezo1)

Specific TPC-inhibitors:
- Ned-19 (TPCs)
- Tetrandrine (TPCs)

Non-specific TPC-inhibitors:
- Diltiazem (TPCs, L-type Ca^{2+} channel)
- Verapamil (TPCs, L-type Ca^{2+} channel)
- Nifedipine (TPCs, VGCC)

IP3R-inhibitors:
- 2-APB (IP3R1)
- Caffeine (IP3R3)

Non-specific IP3R-inhibitors:
- Xestospongin-C (Ca^{2+}-ATPase)

RYR-inhibitors:
- Dantrolene (RYR1/3)
- Flecainide (RYR2)
- Ryanodine (open state)

Non-specific RYR-inhibitors:
- Tetracaine (RYR1, Na^{2+} channels)
- Procaine (RYRs, nAChRs)

Other Non-specific inhibitors:
- Carbenoxolone (GJ, VGCC, GPCRs)
- TMB8 (IP3Rs, nAChRs, mAChRs)
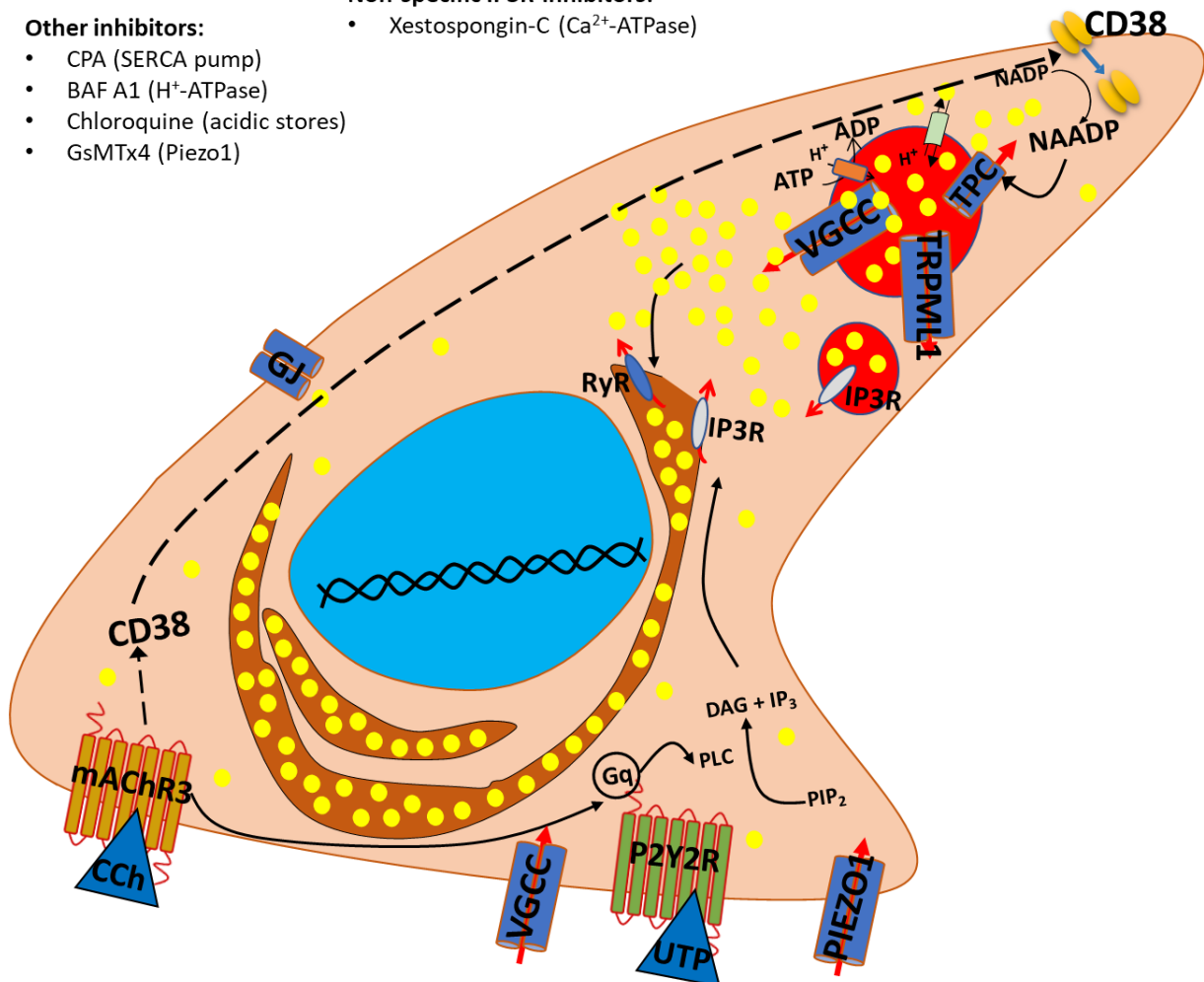
Figure 160 – Proposed Ca^{2+}-Signalling Pathways in Colonic Epithelial Cells in the Stem Cell Zone.

Summary diagram depicting the involvement of most Ca^{2+}-signalling toolkit components in muscarinic, purinergic, mechanosensitive, and mucolipin TRP intracellular Ca^{2+}-signals. Agonists and antagonists listed above.
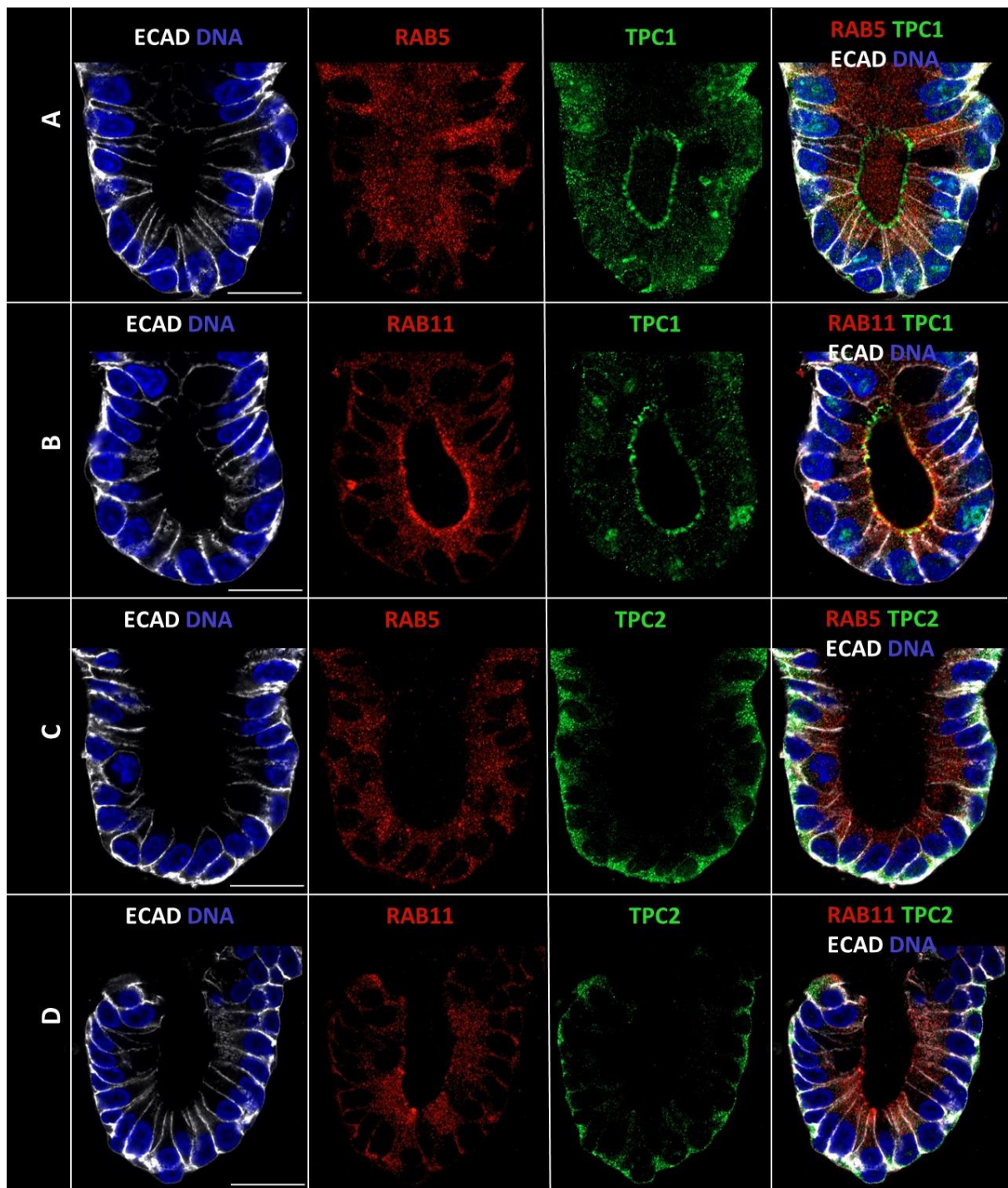
Figure 161 – Immunolabelling of TPC1/2 with Rab5/11 in Organoids.

Representative confocal images of TPC1 **(A-B)** and TPC2 **(C-D)** immunolabelled in organoids with E-Cadherin (ECAD) in white, TPC1/2 in green, and co-labelled with Rab5 **(A & C)** or Rab11 **(B & D)** in red. Nuclei was stained with Sytox Blue (DNA). Scale bar = 25 µm.

8.3 Sources of Non-Neuronal Acetylcholine

Acetylcholine is an important molecule that is involved in many aspects of colonic epithelial biology. Numerous studies have shown chemosensory cells – such as tuft cells of the colonic epithelium – expressing ChAT and secreting acetylcholine to modulate various physiological roles (Deckmann, et al., 2014), (Pan, Zhang, Shao, & Huang, 2020), (Ualiyeva, et al., 2020).

In this thesis, ChAT immunolabelling was consistently found in mucosa and crypts (Figure 51). It strongly co-labels with tuft cells (Figure 53) and CHGA enteroendocrine cells (Figure 54). Tuft cells are specialised chemosensory cells (0.5% of the intestinal epithelium) which can sample the lumen and trigger a variety of immune responses (Gerbe & Jay, 2016). Enteroendocrine cells are secretory cells (1% of the intestinal epithelium) who possesses receptors for sweet, savoury, and bitter (Rozengurt & Sternini, 2007), and secretes a range of hormones with a diverse range of functions. One study in mouse showed that disruption of muscarinic signals promoted tuft cell expansion who adopted an enteroendocrine phenotype which contributed to acetylcholine synthesis and induced proliferation (Middelhoff, et al., 2020). One of the proposed functions for CHAT+ tuft and enteroendocrine cells secreting acetylcholine is to stimulate mucus and/or fluid secretion to flush the crypt lumen, thereby keeping pathogens and toxins away from the stem cell zone. Another proposal is that sustained acetylcholine secretion by CHAT+ epithelial cells may induce intestinal stem cells to proliferate, which in normal conditions promote tissue regeneration and restore epithelial barrier integrity, while under aberrant conditions promote excessive cell division and tumorigenesis. During Fura-2 Ca^{2+} experiments, CCh (10 μM) was used to activate G_q-coupled muscarinic receptors. This is due to CCh being a pharmacological analogue of acetylcholine that is resistant to acetylcholinesterase hydrolysis (Streichert and Sargent 1992). At this point, the thesis was interested in quantifying the amount of non-neuronal acetylcholine and determine if the concentration was biologically active.

Due to scent amount of literature for quantifying acetylcholine and variability between their methodology, a large proportion of time and effort was devoted to developing an effective HILIC-MS/MS standard operating protocol (SOP) at the BCRE, for the purpose of quantifying non-neuronal acetylcholine in media cultured in human colonic tissue. After a year of method development (Chapter 5.2) and validation (Chapter 5.3), an operating HILIC-MS/MS SOP was ready. Using this SOP (Chapter 5.4), an average of 70 nM of acetylcholine was quantified from media that been cultured in colonic crypts isolated from ten patients (N=10) (Table 16). Media that had been cultured in organoids yielded no quantifiable amount of acetylcholine, which supports the absence of ChAT gene and protein expression in organoids (Chapter 3). This concentration of acetylcholine was shown to be biologically relevant, as it was capable of capable of inducing Ca^{2+}-signals in crypts loaded with Fura-2 and could be inhibited by atropine (Figure 105). This thesis then attempted to induce greater synthesis and secretion of acetylcholine using propionate (2 mM), a SCFA. While propionate did increase the amount of acetylcholine quantified in the culture media (Figure 102) and per crypt (Figure 104), this

difference was not significant. Longer propionate incubation may be the solution, however the culture system currently does not favour ChAT cells after long-term culture. Besides propionate, crypts were once incubated with quinine – a bitter tastant – due to studies showing bitter substances promoting acetylcholine biosynthesis and secretion (Deckmann, et al., 2014) and (Saunders, Christensen, Finger, & Tizzano, 2014). No differences were found (data not shown). Future studies should first optimise the culture conditions to ensure ChAT cells are retained in organoids after long-term. After that, experiments can be designed to promote or inhibit ChAT expression in tuft or enteroendocrine cells, after which the developed HILIC-MS/MS SOP can be used to compare changes in secreted acetylcholine concentrations. Finally, the means by which the colonic epithelium acquires choline or secretes acetylcholine is currently unknown, since CHT1 and vAChT are absent in tuft cells (Schütz, et al., 2019). Elucidating this would be a matter of interest for future studies (Figure 162).
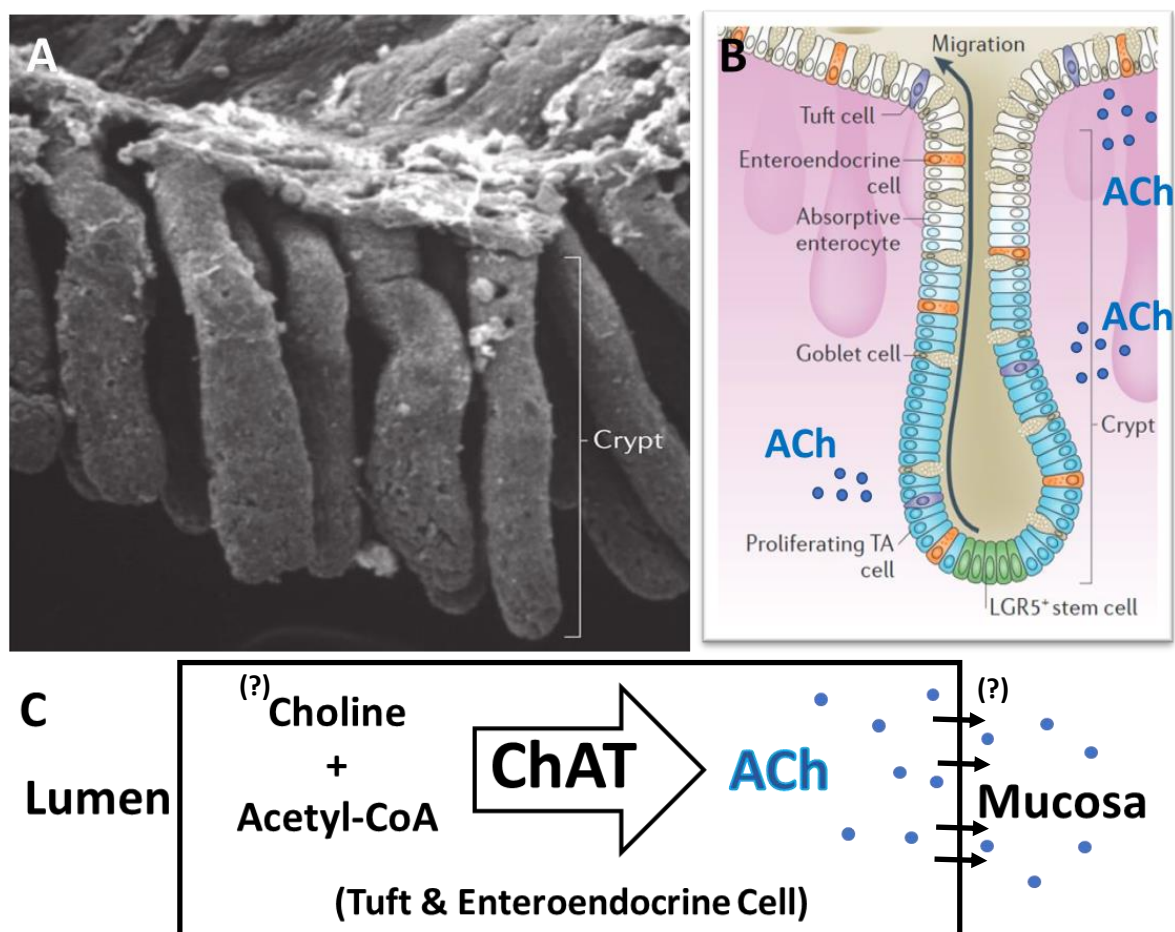
Figure 162 – Proposed Sources of Non-Neuronal Acetylcholine.

Scanning electron micrographs of mouse colonic epithelium illustrating colonic crypts **(A)**, adapted from (McCartney, Gleeson, & Brayden, 2016). Typical organisation of epithelial cells within a colonic crypt **(B)**, adapted from (Barker, 2013). Proposed biosynthesis and secretion of non-neuronal acetylcholine by tuft and enteroendocrine cells **(C)**, including unknown (?) mechanisms of acquiring choline and secreting acetylcholine.

8.4 Physiological Consequences of Mobilising Intracellular Ca^{2+}

Having characterised the Ca^{2+}-signalling toolkit components in the human colonic epithelium (Chapter 3), elucidated the muscarinic and purinergic Ca^{2+}-signalling pathways (Chapter 4), and determined the relevance of non-neuronal acetylcholine as a muscarinic receptor agonist (Chapter 5), this thesis then investigated the physiological consequences of mobilizing intracellular Ca^{2+} in the context of mucus and fluid secretion, followed by proliferation.

8.4.1 Mucus Secretion

The colonic epithelial barrier physically and chemically inhibits the infiltration of pathogens and toxins (Chelakkot, Ghim, & Ryu, 2018). Two means by which it performs that function is secreting mucus and fluid into basal luminal space. The colon has two mucus layers, a stratified adherent inner mucus layer and a loosely adhesive outer mucus layer (Figure 5). Under homeostatic conditions, the colonic epithelium secretes mucus and fluid at a baseline level to maintain the mucus layers' composition and physicochemical properties such as: pore size, viscoelasticity, pH, and ionic strength (Leal, Smyth, & Ghosh, 2018). This not only serves to maintain sterility of the epithelial layer, it also protects the stem cell niche from harmful pathogens or toxins. However, mucus secretion can also occur via compound exocytosis in response to mucus barrier compromise (Pickett & Edwardson, 2006), whereby mucus granules undergo vesicle-to-vesicle fusion before fusing with the plasma membrane and releasing their contents *en masse*. Two colonic epithelial cell types which this thesis propose are responsible for mucus secretion are goblet cells and deep crypt secretory (DCS) cells. Both goblet cells and DCS cells are known to express MUC2 (Rothenberg, et al., 2012). One physical difference between goblet cells and DCS cells was their morphology (Figure 52B); goblet cells are goblet-shaped, while DCS cells are slender-shaped. Interestingly, these slender MUC2-labelled DCS cells co-labelled with TPC1 (Figure 38B), which raises the possibility that they respond to cholinergic muscarinic receptor activation by secreting mucus. The mucus depletion assays (Chapter 6.2.1) confirmed that mucus secretion induced by cholinergic muscarinic receptor activation (CCh 10 µM) was driven by intracellular Ca^{2+} signalling. Specifically, release of localised Ca^{2+}-signals from endolysosomal TPCs – followed by global Ca^{2+}-signals from endoplasmic reticular IP3R3 and RYRs – were required for mucus secretion (Figure 108-14). However, mucus secretion induced by cholinergic muscarinic receptor activation requires the initial localised Ca^{2+}-signals from endolysosomal stores, as raising the cytoplasmic [Ca^{2+}] by emptying the endoplasmic reticular stores using CPA (20 µM) was unable to evoke mucus secretion (Figure 114A-B). Purinergic receptor activation using UTP (50 µM) was also demonstrated to induce mucus secretion (Figure 114C) and should be expanded upon in future studies. Future studies should also explore whether generating intracellular Ca^{2+}-signals by other means (Piezo, TCAs) also induces mucus secretion, and whether mucus secretion was affected by other antagonist used in this thesis (Table 8).

Future studies should aim to characterise DCS cells to better understand their roles in maintaining the stem cell zone. One marker which this thesis propose labels DCS cells is

WFDC2, a bioactive molecule that has been described to maintain sterility of the inner mucus layer by inhibiting serine and cysteine proteases (Chhikara, et al., 2012) and (Parikh, et al., 2019), thereby preventing premature conversion of the inner mucus layer to the outer layer. WFDC2 has also been shown to be a selective bactericide (O'Sullivan, Gilmer, & Medina, 2015). In this thesis, WFDC2 consistently co-labels with slender MUC2+ cells at the base of crypts (Figure 52A) and are also expressed in organoids (data not shown). This supports the thesis's theory of the existence of two colonic epithelial cell types (goblet cells and DCS cells) whose overlapping roles are to secrete mucus. Based on the labelling patterns, goblet cells (goblet-shaped, MUC2+) are expressed throughout the crypt, while DCS cells (slender-shaped, MUC2+, WFDC2+) are expressed within the stem cell zone in close proximity to ISCs. Both these cells secrete mucus to maintain epithelial barrier integrity; DCS cells in particular protects the stem cell zone. Whether they are directly activated by cholinergic/purinergic stimulation or rely on second messengers from neighbouring cells via gap junctions, remains unknown and should be investigated in future studies. The use of single cells (Figure 106) demonstrated the potential of using single goblet/DCS cells to investigate whether excitation-induced mucus secretion relies on neighbouring epithelial cells (possibly via gap junctions) or not. Future work could also investigate the regulatory mechanisms of WFDC2, and the consequences of impaired synthesis/secretion of this bioactive molecule.

While pharmacological inhibition of TPCs/IP3Rs/RYRs provided insights as to the Ca^{2+}-signalling pathway required for mucus secretion, the mechanisms between intracellular Ca^{2+} signals and mucus secretion were not explored in this thesis. Even so, conjectures can be made using other studies. Both baseline and compound mucus secretions are regulated by SNARE proteins, which form SNARE complexes to regulate fusion and exocytosis (Südhof & Rothman, 2009). Syt2 has been shown to be Ca^{2+}-dependent and serves as a critical sensor of stimulated mucin secretion (Adler, Tuvim, & Dickey, 2013). Another protein, KChiP3, is a RYR-dependent Ca^{2+}-binder that is expressed on mucus granules and prevents mucus exocytosis during low intracellular Ca^{2+} oscillations (Cantero-Recasens, et al. 2018). During increased Ca^{2+} oscillations or KChiP3 depletion, mucin hypersecretion was observed. Conversely, overexpressing KChiP3 resulted in reduced Ca^{2+}-sensing and inhibited baseline secretion. Future studies should investigate whether the proposed mechanism indeed occurs in colonic tissues (Figure 163). The use of lipophilic fluorescent dyes (FM1-43, FM1-43X and Deep Red) allowed the visualisation of compound exocytosis in the form of 'bubbles' which formed from the apical membranes of crypts and organoids following CCh-stimulation (Chapter 6.2.2). FM1-43 and Deep Red allowed live visualisation of 'bubbles' being secreted into the lumen and expanding before being flushed away. The synthesis, packaging, and release of mucins is pH and Ca^{2+}-dependent (Ambort, et al., 2012); low pH and high [Ca^{2+}] are needed for mucins to be packed within secretory granules. Upon release, mucin unfolds and expands up to 1,000-fold in volume (Round, et al., 2012). The observation of these 'bubbles' raises the possibility that they contain tightly packed mucus which, upon secretion into the lumen, is exposed to conditions which results in unfolding and expansion. Whether this is the case of not, would be a matter of great interest in future studies.
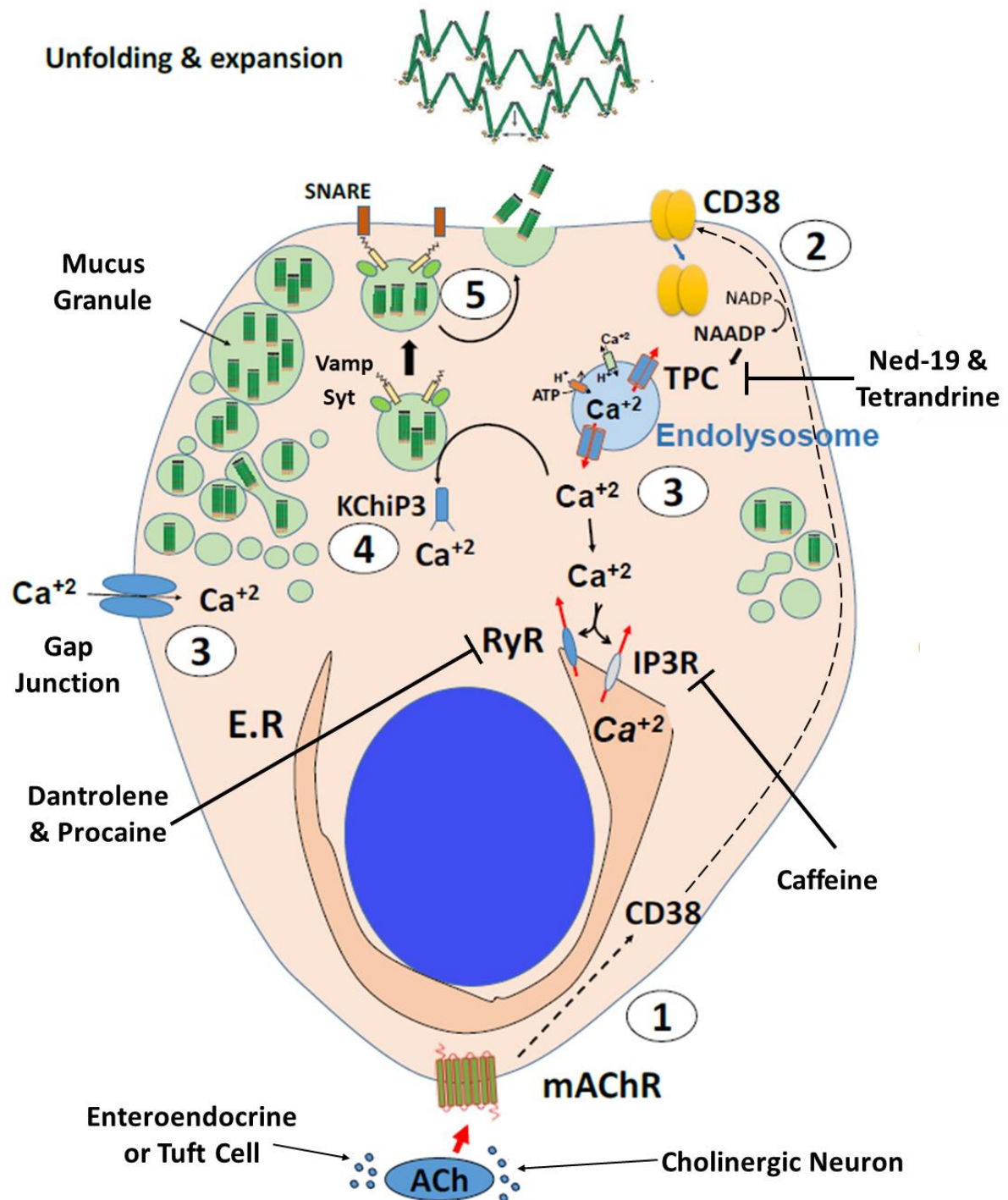
Figure 163 – Proposed Mechanism of Cholinergic-Induced Mucus Secretion.

Neuronal (cholinergic neurons) and non-neuronal (enteroendocrine and tuft cells) acetylcholine binds with muscarinic receptors and activates a signalling pathway that results in NAADP production mediated by CD38 **(1)**. NAADP activates TPCs and induces the release of endolysosomal Ca^{2+} **(2)**. This local Ca^{2+} signal induces CICR from endoplasmic reticular IP3Rs and RYRs **(3)**. Elevated levels of intracellular Ca^{2+} are sensed by KChiP3 **(4)**, which allows mucus membrane SNARE proteins (Syt and Vamp) to form SNARE complexes on the plasma membrane which results in membrane fusion and the release of mucus into the lumen **(5)** where it unfolds and expands. Figure adapted from (Pelaez-Llaneza 2019)

8.4.2 Fluid Secretion

Besides mucus secretion, fluid secretion was also investigated following the mobilization of intracellular Ca^{2+}. During experiments involving crypts and organoids loaded with FM1-43 or Deep Red, CCh-stimulation consistently caused luminal swelling and shrinkage of apical-basal membrane thickness, which indicated fluid secretion accompanying mucus secretion. The secretion of fluids by the intestinal epithelium serves to flush the lumen of pathogens/toxins, and hydrates mucus to allow proper unfolding and expansion. Epithelial fluid secretion is regulated by the secretions of anions (e.g. Cl^-, HCO_3^-) into the lumen, which establishes a negative electrical driving force for trans-epithelial Na^+ secretion via paracellular pathways and generating the osmotic driving force for water flow (Frizzell & Hanrahan, 2012). In the colonic epithelium, uptake of Na^+, K^+ and Cl^- is mediated by NKCC1 co-transporter located on the basolateral membranes (Bachmann, et al. 2003). On the apical membrane, CFTR channels regulate the movement of Cl^- and HCO_3^- into the lumen (Greger 2000), which drives the movement of water by osmosis. Previous work by the Williams group have shown NKCC1 to be regulated by intracellular Ca^{2+} (Reynolds, Parris, et al. 2007), confirmed the presence of NKCC1 and CFTR in colonic goblet cells and conducted preliminary studies showing that muscarinic-coupled Ca^{2+} signals are capable of inducing secretion of fluid into the lumen (Pelaez-Llaneza 2019). This thesis expanded on those works by considering which Ca^{2+}-signalling toolkit components were essential to fluid secretion (Chapter 6.2.3).

Using colonic organoids, CCh-induced muscarinic receptor activation was shown to increase in organoid cross-sectional area fold change compared to control (Figure 127-32), which was proposed to be fluid secretion in combination with mucus secretion/expansion. Inhibiting TPCs using Ned-19 (500 µM) and tetrandrine (20 µM), IP3R1 using 2-APB (100 µM), RYR1/3 using dantrolene (50 µM), and non-specific RYR antagonist procaine (1 mM); abolished the increase in organoid cross-sectional area fold change. This could indicate fluid secretion via NKCC1 and CFTR being dependent on overall increase in cytoplasmic $[Ca^{2+}]$, rather than a specific pathway. Whether this is true or not should be explored in future studies. Another question would be whether the entire colonic epithelium or only specific cell-types are capable of fluid secretion; this could be investigated using single cells. Future studies should also explore whether generating intracellular Ca^{2+}-signals by other means (Piezo, TCAs, CPA) also induces fluid secretion. Mechanosensory-induced Ca^{2+}-signals would be of particular interest, as organoids which were treated with control also swelled – albeit much less (2%) compared to CCh-induced (14-34%). It would be of interest to know whether this was due to mechanosensory stimulation or merely baseline secretion. Finally, fluid secretion can also be explored when exposed to other antagonists used in this thesis (Table 8).

8.4.3. Cell Proliferation

The third physiological consequences of mobilizing intracellular Ca^{2+} that was explored in this thesis, was cell proliferation. In 2016, Deng and colleagues identified Ca^{2+} signals as a central regulator of ISC activity in *Drosophila* (Deng, Gerencser and Jasper 2016), whereby activation of certain GPCRs by dietary L-Glu recruited Gaq and resulted in changes in ISC cytosolic Ca^{2+} oscillations which promoted ISC proliferation. When they knocked down STIM/SERCA/PMCA or over-expressed STIM-Orai/IP3R, they observed sustained elevation of cytosolic $[Ca^{2+}]$ and increased ISC proliferation rates. They then showed that calcineurin (CaN) promoted the nuclear translocation of CREB regulated transcription co-activator (CRTC) to induce ISC proliferation; silencing a regulatory subunit of CaN significantly abrogated ISC proliferation, while constitutive activation of CRTC was sufficient to induce ISC proliferation independently of GPCR-activation or G-protein recruitment or intracellular Ca^2 signals. They also explored ISC Ca^{2+} oscillations under other mitogenic conditions such as bacterial infection, Notch signal knockdown, and DNA damage. In every case, changes in ISC Ca^{2+} oscillations were observed which led to increased ISC proliferation, and when proliferation subsided these Ca^{2+} oscillations returned to basal states.

The findings of that paper were applied to the human colonic epithelium in this thesis. In the case of humans, many studies have shown activation of muscarinic receptors (Lundgren, Jodal, Jansson, Ryberg, & Svensson, 2011), (Muise, Gandotra, Tackett, Bamdad, & Cowles, 2017) and (Greig, Armenia, & Cowles, 2020). One of the ligands of muscarinic receptors is acetylcholine, which activates Wnt signals and promote epithelial stem cell proliferation (Hayakawa, et al., 2017). In this thesis, CCh was shown to induce proliferation of colonic epithelial cells within the stem cell zone, was attenuated when TPCs were inhibited using Ned-19 (125 µM) (Figure 133). Subsequent gene regulation as a result of CCh-induced Ca^{2+}-signals were not explored in this thesis, but has been explored by other members of the Williams group (Pelaez-Llaneza 2019), whereby they identified two transcription factors – YAP1 and NFATc3 – to translocated to the nucleus following elevated cytoplasmic Ca^{2+}-levels induced by muscarinic receptor activation. Both YAP1 and NFATc3 are known to activate cell proliferation in the GI tract (Deng, Gerencser and Jasper 2016). The exact mechanisms by which YAP1 and NFATc3 activates cell proliferation will need to be investigated in future studies. That said, they are likely mediated by CaN and/or calmodulin, two highly sensitive Ca^{2+}-sensing proteins (Figure 164). Calmodulin is known to mediates a variety of cellular signalling processes including gene expression (Zhang, et al., 2013). CaN is a serine/threonine phosphatase which is activated by increased intracellular $[Ca^{2+}]$ to phosphorylate a range of substrates, one of which is NFAT (Park, Yoo, Kim, & Kim, 2020) and is associated with metastatic capacity in colon cancer (Tripathi, et al., 2015). Besides that, future studies should also investigate whether purinergic receptor activation promotes colonic epithelial proliferation, due to studies which indicated ATP-sensitive P2Y receptors (P2Y1/2/4) being overexpressed in carcinoma (Coutinho-Silva, et al., 2005), (Nylund, Hultman, Nordgren, & Delbro, 2007), and (Kim, et al. 2020).
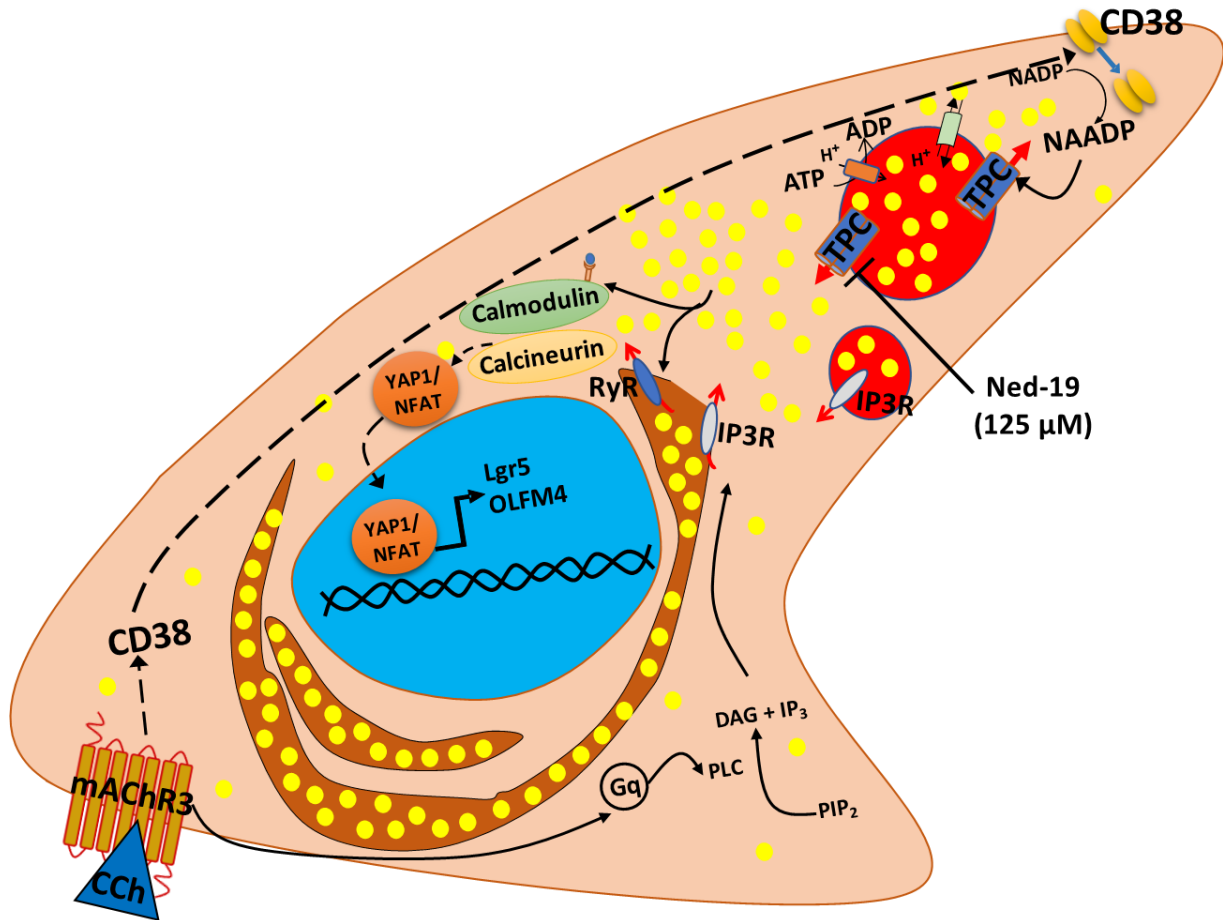
Figure 164 – Proposed Mechanism of Cholinergic-Induced Intestinal Stem Cell Proliferation.

Acetylcholine activates muscarinic receptors (M3) on the basal membrane, which initiates an intracellular signalling pathway resulting in the activation of CD38 and the generation NAADP. NAADP induces Ca^{2+}-release from endolysosomes via TPCs, which causes CICR via endoplasmic reticular IP3Rs and RYRs. The resulting increase in cytosolic $[Ca^{2+}]$ activates Ca^{2+}-sensors (calmodulin and/or calcineurin), which interacts with transcription factors (NFATc3 and YAP1) possibly by dephosphorylation. As a result, these transcription factors translocates to the nucleus and promote expression of proliferation genes (Lgr5, OLFM4, etc.)

8.4.4 Secretion of Gut Hormones and ATP

One other colonic epithelial physiological function that was briefly touched upon in this thesis but not explored in detail, was the secretion of gut hormones – such as GLP1 – by enteroendocrine cells. Enteroendocrine cells account for approximately 1% of the intestinal epithelium and whose main role is secreting hormones (Worthington, Reimann, & Gribble, 2017). The effects of these secreted hormones are diverse: appetite control, stimulate or inhibit gastric acid release, induction of nutrient transporters and digestive enzymes, stimulate or inhibit intestinal motility, triggering emesis and nausea, and release of other hormones (insulin, growth hormones). Among the numerous types of enteroendocrine cells, enterochromaffin cells and L-cells are more prominent in the lower GI tract (Gunawardene, Corfe, & Staton, 2011).

In thesis, the gene expression of proglucagon and neuroendocrine convertase 1 – which are related to GLP1 production – was confirmed in human colonic tissue samples, and enteroendocrine cells were visualised using CHGA and GLP1 (Chapter 3). CHGA is a marker of enterochromaffin cells (Modlin, Kidd, Pfragner, Eick, & Champaneria, 2006) while GLP1 marks L-cells and is a gut hormone with a broad range effects (Gribble and Reimann 2019) including insulin secretion (Jones, et al. 2018). The actions of GLP1 has been proposed to be mediated through activation of GLP1R, a GPCR located on vagal afferent nerve terminals (Dockray 2013) which associates with $G_{\alpha s}$ to generate cAMP (Girada, et al. 2017). A recent paper identified ATP to be co-secreted with gut hormones GLP1 and PYY (Lu, et al. 2019), which activated P2Y2 receptors on afferent neurons and neighbouring enterocytes. They also determined ATP was loaded into secretory vesicles via vesicular nucleotide transporter (VNUT) and proposed its role was to synergise with the actions of secreted gut hormones. Likewise, gene expression of VNUT was confirmed in human colonic tissue samples (Figure 30). Studies have shown that the exocytosis of secretory vesicles containing ATP is Ca^{2+}-dependent (Ho, et al. 2015) and (Xiong, et al. 2018), although the mechanisms by which Ca^{2+}-signals promotes ATP vesicle exocytosis remains uncertain. One study highlighted intracellular Ca^{2+} to be necessary (Murana, et al. 2017). Another paper which studied ATP release via connexin channels showed that ATP activated P2Y receptors, generated IP3 and induced endoplasmic reticular Ca^{2+} release via IP3R, which promoted further ATP release and induced paracrine signalling in neighbouring epithelial cells (Ceriani, Pozzan and Mammano 2016).

Considering these papers, it is possible that the intracellular Ca^{2+} signalling toolkit components explored in this thesis could also regulate the secretion of ATP and/or gut hormone by enteroendocrine cells and should be explored in the future. If ATP and/or gut hormone is indeed regulated by intracellular Ca^{2+} signals, it adds another cellular process which Ca^{2+} can regulate to mediate different physiological functions.

8.5 Implications for Colorectal Cancer

Colorectal cancer (CRC) is a major burden on global health. It is the fourth most-common cancer and the third most-common cause of cancer-related mortality in the world (Figure 3) (Rawla, Sunkara, & Barsouk, 2019) and (Cancer Research UK, 2020). CRC is a complex disease whose development and progression relies on several genetic and molecular alterations (Chapter 7.1) (Kuipers, et al. 2016). CRC initiates from colonic epithelial cells progressively accumulating genetic and epigenetic alterations that activate oncogenes and inactivate tumour suppressor genes, leading to the loss of genomic and/or epigenomic stability and the development of early neoplastic lesions (Grady and Carethers 2008) and (Colussi, et al. 2013). This further accelerates the accumulations of mutations and epigenetic alterations in tumour suppressor genes and oncogenes, which drives the transformation of colon cells into highly proliferative cells that are aggressively malignant. Ca^{2+} signalling has a complex role on the development and progression of CRC (Wang, et al. 2019). In this thesis, the gene expression of muscarinic and purinergic Ca^{2+}-signalling toolkit components in tumour versus normal colonic tissue was compared in order to identify whether these pathways are altered in tumour human tissue to favour tumorigenesis. Protein expression was also compared and found to be expressed similar between tumour and normal colonic tissue

8.5.1 Altered Ca^{2+} Signalling Toolkit Gene Expression and Pharmacology in CRC

On the GPCR level, changes in certain muscarinic receptors (M1-5) and metabotropic P2Y receptors have been implicated in CRC (von Rosenvinge and Raufman 2011) and (Bellefeuille, Molle and Gendron 2019). M3 in particular is associated with CRC, with studies showing its activation by various agonists including CCh and bile acids promoting proliferation in human colon cancer cells (Frucht, et al. 1999), (Yang and Frucht 2000) and (Cheng, Chen, et al. 2002). In this thesis, M3 gene expression was higher in tumour mucosa and tumour crypts compared to normal mucosa and normal crypts (Figure 138), which compliments those studies. P2Y1 and P2Y2 receptors have also been associated with CRC as an oncogene, with studies showing their expression being increased in human CRC compared to normal colonic tissue (Coutinho-Silva, et al., 2005) and (Nylund, Hultman, Nordgren, & Delbro, 2007). The opposite was observed in this thesis; P2Y1 and P2Y2 expression was reduced in tumour colon tissue samples compared to normal colon tissue samples (Figure 139). This implicates the involvement of M3 in the development and progression of CRC.

Acetylcholine is a ligand for muscarinic receptors. Studies have shown aberrant acetylcholine secretion by neuronal and non-neuronal sources altering intracellular Ca^{2+} signalling and promoting CRC (Cheng, et al., 2008), (Beckmann and Lips 2013) and (Hayakawa, et al., 2017). In the colonic epithelium, Tuft cells are known to synthesize and secrete acetylcholine (Pan, Zhang, Shao, & Huang, 2020) which this thesis has confirmed by the visualisation of ChAT co-labelling with Tuft cell markers (Figure 53). Due to this, this thesis hypothesized that aberrant acetylcholine release would lead to dysregulated Ca^{2+}-signalling which leads to enhanced expression of proliferative genes. Unfortunately, ChAT expression was lower in tumour

mucosa compared to normal mucosa and non-existent in tumour crypts and tumoroids (Figure 140). This may be due to patients undergoing chemo/radiotherapy prior to surgery, or due to culture conditions not favouring Tuft cell differentiation. On the flipside, gene expression for VNUT – which is involved in the loading of ATP into secretory vesicles – was consistently increased in tumour colon tissue sample compared to normal (Figure 141). A recent study showed that endogenous release of ATP promoted growth and invasion of breast cancer via purinergic receptor activation (Kim, et al. 2020). They also showed highly metastatic cells releasing more ATP and exhibiting greater P2Y2 receptor activity compared to lowly metastatic cells. ATP has also been shown to induce acetylcholine secretion in olfactory epithelial cells (Fu, Ogura, Luo, & Lin, 2018). Thus, tumour colon tissue may secrete ATP – as well as acetylcholine – to promote tumorigenesis via dysregulated Ca^{2+}-signalling and possibly by inducing acetylcholine secretion from Tuft cells.

Remodelling of store-operated Ca^{2+} entry (SOCE) through the partial depletion of the endoplasmic reticular Ca^{2+} stores is another characteristic of CRC. Receptors which enable depletion of the endoplasmic reticulum Ca^{2+} store include IP3Rs and RYRs. IP3R3 in particular are associated with decreased 5-year survival chances, possibly by conferring a survival advantage in CRC by inhibiting apoptosis (Shibao, et al., 2010). A gene transcriptomic analysis study also found IP3R3 to be absent from normal cells but expressed in cancer cells (Pérez-Riesgo, et al., 2017). In this thesis, IP3R3 was shown to be present in both tumour (Figure 134) and normal colon tissue samples (Figure 23). Rather than increased, its expression was decreased in tumour compared to normal colon tissue samples, while the opposite – increased gene expression – was shown for IP3R1 and IP3R2. As for RYRs, a study showed that mutations in the RYR2 gene was common in colon carcinoma (Wolff, et al. 2018) and another study found RYR2 gene expression to be upregulated by over 40 times (Davis, et al. 2013). In this thesis, RYR2 was consistently higher in every tumour colon tissue sample compared to normal. Taken together, IP3R1, IP3R2 and RYR2 may be involved in the development and progression CRC.

Another Ca^{2+} store whose depletion has been associated with CRC are endolysosomes, which release Ca^{2+} by several channels including TPCS (Figure 17B). TPCs have also been studied extensively in the context of CRC (Alharbi & Parrington, 2019). NAADP-mediated TPC1 lysosomal Ca^{2+} release had been shown to trigger ERK and the PI3K/AKT signalling pathways to promote proliferation (Faris, et al., 2019), and in human breast cancer cell lines the expression of TPC1 transcripts is three to eight times higher than TPC2 transcripts (Brailoiu, et al., 2009). In this thesis, the gene expression of TPC1 and TPC2 did not differ by much between tumour and normal colon tissue samples (Figure 136). This would imply TPCs not being involved in the development and progression CRC.

8.5.2 Altered Ca^{2+} Signalling Pharmacology in CRC

Having characterised the differences in Ca^{2+} signalling toolkit gene expression between tumour and normal colonic tissues, Fura-2 Ca^{2+} experiments were carried out to determine whether the pharmacology of tumour colonic tissues was different compared to normal colonic tissues. Tumour colon tissues that were stimulated with CCh were more sensitive to TPC-inhibition using Ned-19 (250-500 µM) and tetrandrine (20 µM) (Figure 148-9) and RYR inhibition using procaine (1 mM) and dantrolene (50 µM) (Figure 154-55). The increased sensitivity of tumour colonic tissues to TPC-inhibition (despite similar TPC gene expression) was an interesting finding and should be investigated in future studies. One explanation could be TPC protein misfolding or modifications or turnover being enhanced in tumoroids compared to organoids, making them more sensitive to pharmacological inhibition (Chen, et al. 2017) and (Ly, et al. 2018). The increased sensitivity of tumour colonic tissues to RYR-inhibition (in conjunction with increased gene expression of RYR2) would suggest RYRs being essential for generating intracellular Ca^{2+} signals within cancer cells.

In addition to changes in pharmacology sensitivity, changes in Fura-2 ratio amplitude induced by CCh (10 µM) and UTP (50 µM) between tumour and normal colonic tissues gave insights into their Ca^{2+}-signalling status. While CCh and UTP-induced Fura-2 ratio amplitude increase were similar between normal crypts and tumour crypts (Figure 156A), they were significantly different between organoids and tumoroids (Figure 156B). Compared to organoids, tumoroids were consistently more sensitive to UTP (50 µM) and less sensitive to CCh (10 µM). The physiological relevance of these changes in sensitivity against muscarinic/purinergic receptor stimulation will need to be investigated in future studies in the form of mucus/fluid secretion (Figure 163). Since chronic inflammation such as IBD is a major risk for CRC (Axelrad, Lichtiger and Yajnik 2016), one would expect baseline and agonist-induced mucus and fluid secretion to be reduced in tumour colonic tissues.

One paradigm is that the cellular origin of most CRCs are ISCs or ISC-like cells which reside within the stem cell zone at the base of crypts (Barker, et al., 2009) and (Zeki, Graham and Wright 2011). In that paradigm, these cells acquire mutations in oncogenes and tumour suppressor genes which leads to the formation of cancer stem cells that initiates and maintains tumorigenesis. With that in mind, future studies should investigate whether mobilising intracellular Ca^{2+} from tumour colonic stem cells increases proliferation at a higher rate compared to normal colonic stem cells (Figure 164).

8.6 Concluding Remarks

This thesis first identified the gene and protein expression of muscarinic and purinergic calcium signalling components in human colonic mucosa, crypts, and organoids. Next, it focused on investigating the spatial-temporal status of muscarinic and purinergic Ca^{2+} signals in them human colonic epithelium. A novel HILIC-MS/MS SOP of quantifying low-nanomolar concentrations (11.5 nM) of acetylcholine within cultured media was then developed during this thesis, which in the future may prove useful in comparing the difference in secreted non-neuronal acetylcholine by normal versus tumour colonic tissues. This thesis then explored the physiological role of Ca^{2+} signalling induced by muscarinic receptor activation in maintaining gut tissue homeostasis in the form of mucus/fluid secretion and proliferation. Finally, this thesis investigated the status of Ca^{2+} signalling in CRC, by comparing the Ca^{2+}-signalling toolkit gene expression and pharmacological profiles of tumour versus normal human colonic epithelial tissues.

9   Chapter 9 – References

Bibliography

Ackerman, Dorothy L, Kelly M Craft, Ryan S Doster, Weitkamp Jörn-Hendrik, David M Aronoff, Jennifer A Gaddy, and Steven D Townsend. 2018. "Antimicrobial and Antibiofilm Activity of Human Milk Oligosaccharides against Streptococcus agalactiae, Staphylococcus aureus, and Acinetobacter baumannii." *ACS Infectious Diseases* 4 (3): 315-24. doi:10.1021/acsinfecdis.7b00183.

Acosta, Andres, Michael Camilleri, Andrea Shin, Maria I Vazquez-Roque, Johanna Iturrino, Duane Burton, Jessica O'Neill, Deborah Eckert, and Alan R Zinsmeister. 2014. "Quantitative gastrointestinal and psychological traits associated with obesity and response to weight-loss therapy." *Gastroenterology* 148 (3): 537-46. doi:10.1053/j.gastro.2014.11.020.

Adler, Kenneth B, Michael J Tuvim, and Burton F Dickey. 2013. "Regulated Mucin Secretion from Airway Epithelial Cells." *Frontiers in Endocrinology* 4: 129. doi:10.3389/fendo.2013.00129.

Ahmad, R, R Chaturvedi, D Olivares-Villagómez, T Habib, M Asim, P Shivesh, D B Polk, et al. 2014. "Targeted colonic claudin-2 expression renders resistance to epithelial injury, induces immune suppression, and protects from colitis." *Mucosal Immunology* 7 (6): 1340-53. doi:10.1038/mi.2014.21.

Aihara, Takeshi, Yusuke Nakamura, Makoto M Taketo, Minoru Matsui, and Susumu Okabe. 2005. "Cholinergically stimulated gastric acid secretion is mediated by M(3) and M(5) but not M(1) muscarinic acetylcholine receptors in mice." *American Journal of Physiology-Gastrointestinal and Liver Physiology* 288 (6): G1199-207. doi:10.1152/ajpgi.00514.2004.

Albers, R Wayne, and George J Siegel. 1999. "ATP-Dependent Ca2+ Pumps." In *Basic Neurochemistry: Molecular, Cellular and Medical Aspects. 6th edition.*, by G J Siegel, B W Agranoff, R W Albers and et al. American Society for Neurochemistry. https://www.ncbi.nlm.nih.gov/books/NBK27906/.

Albrecht, Tobias, Yongxin Zhao, Trang Hai Nguyen, Robert E Campbell, and James D Johnson. 2015. "Fluorescent biosensors illuminate calcium levels within defined beta-cell endosome subpopulations." *Cell Calcium* 57 (4): 263-74. doi:10.1016/j.ceca.2015.01.008.

Alcaino, C, G Farrugia, and A Beyder. 2017. "Mechanosensitive Piezo Channels in the Gastrointestinal Tract." *Current Topics in Membranes* 79: 219-44. doi:10.1016/bs.ctm.2016.11.003.

Alcaino, Constanza, Kaitlyn R Knutson, Anthony J Treichel, Gulcan Yildiz, Peter R Strege, David R Linden, Joyce H Li, et al. 2018. "A population of gut epithelial enterochromaffin cells is mechanosensitive and requires Piezo2 to convert force into serotonin release." *PNAS* 115 (32): E7632-41. doi:10.1073/pnas.1804938115.

Alexander, J S, Vijay C Ganta, P A Jordan, and Marlys H Wittec. 2010. "Gastrointestinal Lymphatics in Health and Disease." *Pathophysiology* 17 (4): 315-35. doi:10.1016/j.pathophys.2009.09.003.

Aley, Parvinder K, Anna M Mikolajczyk, Barbara Munz, Grant C Churchill, Antony Galione, and Felicitas Berger. 2010. "Nicotinic acid adenine dinucleotide phosphate regulates skeletal muscle differentiation via action at two-pore channels." *PNAS* 107 (46): 19927-32. doi:10.1073/pnas.1007381107.

Alharbi, Abeer F, and John Parrington. 2019. "Endolysosomal Ca2+ Signaling in Cancer: The Role of TPC2, From Tumorigenesis to Metastasis." *Frontiers in Cell and Developmental Biology* 7: 302. doi:10.3389/fcell.2019.00302.

Allen, Adrian, and Gunnar Flemström. 2005. "Gastroduodenal mucus bicarbonate barrier: protection against acid and pepsin." *American Journal of Physiology- Cell Physiology* 288 (1): 1-19. doi:10.1152/ajpcell.00102.2004.

Altmann, G G. 1983. "Morphological observations on mucus-secreting nongoblet cells in the deep crypts of the rat ascending colon." *The American Journal of Anatomy* 167 (1): 95-117. doi:10.1002/aja.1001670109.

Amato, Antonella, Sara Baldassano, and Flavia Mulè. 2016. "GLP2: an underestimated signal for improving glycaemic control and insulin sensitivity." *Journal of Endocrinology* 229 (2): 57-66. doi:10.1530/JOE-16-0035.

Ambort, Daniel, Malin EV Johansson, Jenny K Gustafsson, Harriet E Nilsson, Anna Ermund, Bengt R Johansson, Philip JB Koeck, Hans Hebert, and Gunnar C Hansson. 2012. "Calcium and pH-dependent packing and release of the gel-forming MUC2 mucin." *PNAS* 109 (15): 5645-50. doi:10.1073/pnas.1120269109.

Ambudkar, I S. 2000. "Regulation of calcium in salivary gland secretion." *Critical Reviews in Oral Biology & Medicine* 11 (1): 4-25. doi:10.1177/10454411000110010301.

American Cancer Society. 2020. *American Cancer Society.* 29 Jun. https://www.cancer.org/cancer/colon-rectal-cancer/detection-diagnosis-staging/survival-rates.html.

Andrews, Caroline, Mairi H McLean, and Scott K Durum. 2018. "Cytokine Tuning of Intestinal Epithelial Function." *Frontiers in Immunology* 9: 1270. doi:10.3389/fimmu.2018.01270.

Antoni, Lena , Sabine Nuding, Jan Wehkamp, and Eduard F Stange. 2014. "Maintenance of Intestinal Homeostasis by mucosal barriers." *World Journal of Gastroenterology* 20 (5): 1165-79. doi:10.3748/wjg.v20.i5.1165.

Arndt, Lilli, Jan Castonguay, Elisabeth Arlt, Dorke Meyer, Sami Hassan, Heike Borth, Susanna Zierler, et al. 2014. "NAADP and the two-pore channel protein 1 participate in the acrosome reaction in mammalian spermatozoa." *Molecular Biology of the Cell* 25 (6): 948-64. doi:10.1091/mbc.E13-09-0523.

Arnold, Melina, Mónica S Sierra, Mathieu Laversanne, Isabelle Soerjomataram, Ahmedin Jemal, and Freddie Bray. 2016. "Global Patterns and Trends in Colorectal Cancer Incidence and Mortality." *Gut* 66: 683-91. doi:10.1136/gutjnl-2015-310912.

Asfaha, Samuel, Yoku Hayakawa, Ashlesha Muley, Sarah Stokes, Trevor A Graham, Russell Ericksen, Christoph B Westphalen, et al. 2016. "Krt19(+)/Lgr5(−) cells are radioresistant cancer initiating stem cells in the colon and intestine." *Cell Stem Cell* 16 (6): 627-38. doi:10.1016/j.stem.2015.04.013.

Asker, Noomi, Magnus AB Axelsson, Sven-Olof Olofsson, and Gunnar C Hansson. 1998. "Dimerization of the Human MUC2 Mucin in the Endoplasmic Reticulum Is Followed by a N-Glycosylation-dependent Transfer of the Mono- and Dimers to the Golgi Apparatus." *Biological Chemistry*

(journal) - Wikipediaen.wikipedia.org › wiki › Biological_Chemistry_(journal) 273 (30): 18857-63. doi:10.1074/jbc.273.30.18857.

Atarashi, Koji, Takeshi Tanoue, Tatsuichiro Shima, Akemi Imaoka, Tomomi Kuwahara, Yoshika Momose, Genhong Cheng, et al. 2014. "Induction of Colonic Regulatory T Cells by Indigenous Clostridium Species." *Science* 331 (6015): 337-41. doi:10.1126/science.1198469.

Atuma, C, V Strugala, A Allen, and L Holm. 2001. "The adherent gastrointestinal mucus gel layer: Thickness and physical state in vivo." *American Journal of Physiology-Gastrointestinal and Liver Physiology* 280 (5): 922-9. doi:10.1152/ajpgi.2001.280.5.G922.

Aung, Cho, Sarah Roberts-Thomson, and Gregory Monteith. 2007. "Role of plasma membrane calcium ATPase (PMCA) in colon cancer." *AACR Centennial Conference: Translational Cancer Medicine.* Singapore: American Association for Cancer Research. https://clincancerres.aacrjournals.org/content/13/22_Supplement/A35.

Axelrad, Jordan E, Simon Lichtiger, and Vijay Yajnik. 2016. "Inflammatory bowel disease and cancer: The role of inflammation, immunosuppression, and cancer treatment." *World Journal of Gastroenterology* 22 (20): 4794-801. doi:10.3748/wjg.v22.i20.4794.

Azzouz, LL, and S Sharma. 2020. "Physiology, Large Intestine." *NCBI.* 27 July. https://www.ncbi.nlm.nih.gov/books/NBK507857/#_ncbi_dlg_citbx_NBK507857.

Bachmann, O, K Wüchner, H Rossmann, J Leipziger, B Osikowska, W H Colledge, R Ratcliff, M J Evans, M Gregor, and U Seidler. 2003. "Expression and regulation of the Na+-K+-2Cl– cotransporter NKCC1 in the Normal and CFTR-deficient murine colon." *The Journal of Physiology* 549 (Pt2): 525-36. doi:10.1113/jphysiol.2002.030205.

Bader, Sandra, Jochen Klein, and Martin Diener. 2014. "Choline acetyltransferase and organic cation transporters are responsible for synthesis and propionate-induced release of acetylcholine in colon epithelium." *The European Journal of Pharmacology* 733: 23-33. doi:10.1016/j.ejphar.2014.03.036.

Bae, Chilman, Frederick Sachs, and Philip A Gottlieb. 2011. "The mechanosensitive ion channel Piezo1 is inhibited by the peptide GsMTx4." *Biochemistry* 50 (29): 6295-300. doi:10.1021/bi200770q.

Bagur, Rafaela, and György Hajnóczky. 2018. "Intracellular Ca2+ sensing: role in calcium homeostasis and signaling." *Molecular Cell* 66 (6): 780-8. doi:10.1016/j.molcel.2017.05.028.

Bain, Calum C, and Anika Schridde. 2018. "Origin, Differentiation, and Function of Intestinal Macrophages." *Frontiers in Immunology* 9 (2733). doi:10.3389/fimmu.2018.02733.

Bajnath, R B, K Dekker, A B Vaandrager, H R de Jonge, and J A Groot. 1992. "Biphasic increase of apical Cl- conductance by muscarinic stimulation of HT-29cl.19A human colon carcinoma cell line: evidence for activation of different Cl- conductances by carbachol and forskolin." *The Journal of Membrane Biology* 127 (2): 81-94. doi:10.1007/BF00233281.

Bansil, Rama, and Bradley S Turner. 2018. "The biology of mucus: Composition, synthesis and organization." *Advanced Drug Delivery* 124: 3-15. doi:10.1016/j.addr.2017.09.023.

Barbara, Giovanni. 2006. "Mucosal Barrier Defects in Irritable Bowel Syndrome. Who Left the Door Open?" *The American Journal of Gastroenterology* 101 (6): 1295-8. doi:10.1111/j.1572-0241.2006.00667.x.

Barker, Nick. 2013. "Adult intestinal stem cells: critical drivers of epithelial homeostasis and regeneration." *Nature Reviews Molecular Cell Biology* 15: 19-33. doi:10.1038/nrm3721.

Barker, Nick. 2014. "Adult Intestinal Stem Cells: Critical Drivers of Epithelial Homeostasis and Regeneration." *Nature Reviews Molecular Cell Biology* 15: 19-33. doi:10.1038/nrm3721.

Barker, Nick, Johan H van Es, Jeroen Kuipers, Pekka Kujala, Maaike van den Born, Miranda Cozijnsen, Andrea Haegebarth, et al. 2007. "Identification of stem cells in small intestine and colon by marker gene Lgr5." *Nature* 449 (7165): 1003-7. doi:10.1038/nature06196.

Barker, Nick, Marc van de Wetering, and Hans Clevers. 2008. "The intestinal stem cell." *Genes & Development* 22 (14): 1856-64. doi:10.1101/gad.1674008.

Barker, Nick, Rachel A Ridgway, Johan H van Es, Marc van de Wetering, Harry Begthel, Maaike van den Born, Esther Danenberg, Alan R Clarke, Owen J Sansom, and Hans Clevers. 2009. "Crypt stem cells as the cells-of-origin of intestinal cancer." *Nature* 457 (7229): 608-11. doi:10.1038/nature07602.

Barry, Evan R, Teppei Morikawa, Brian L Butler, Kriti Shrestha, Rosemarie de la Rosa, Kelley S Yan, Charles S Fuchs, et al. 2013. "Restriction of intestinal stem cell expansion and the regenerative response by YAP." *Nature* 493 (7430): 106-10. doi:10.1038/nature11693.

Basak, Onur, Joep Beumer, Kay Wiebrands, Hiroshi Seno, Alexander van Oudenaarden, and Hans Clevers. 2017. "Induced Quiescence of Lgr5+ Stem Cells in Intestinal Organoids Enables Differentiation of Hormone-Producing Enteroendocrine Cells." *Cell Stem Cell* 20 (2): 177-90. doi:10.1016/j.stem.2016.11.001.

Bastide, Pauline, Charbel Darido, Julie Pannequin, Ralf Kist, Sylvie Robine, Christiane Marty-Double, Frédéric Bibeau, et al. 2007. "Sox9 regulates cell proliferation and is required for Paneth cell differentiation in the intestinal epithelium." *Journal of Cell Biology* 178 (4): 635-48. doi:10.1083/jcb.200704152.

Batlle, Eduard, Jeffrey T Henderson, Harry Beghtel, Maaike MW van den Born, Elena Sancho, Gerwin Huls, Jan Meeldijk, et al. 2002. "Beta-catenin and TCF mediate cell positioning in the intestinal epithelium by controlling the expression of EphB/ephrinB." *Cell* 111 (2): 251-63. doi:10.1016/s0092-8674(02)01015-2.

Beck, Andreas, Robin Zur Nieden, Hans-Peter Schneider, and Joachim W Deitmer. 2004. "Calcium release from intracellular stores in rodent astrocytes and neurons in situ." *Cell Calcium* 35 (1): 47-58. doi:10.1016/s0143-4160(03)00171-4.

Beckmann, Janet, and Katrin Susanne Lips. 2013. "The non-neuronal cholinergic system in health and disease." *Pharmacology* 92 (5-6): 286-302. doi:10.1159/000355835.

Behrens, Juliane, Petra Kameritsch, and Stefan Wallne. 2010. "The carboxyl tail of Cx43 augments p38 mediated cell migration in a gap junction-independent manner." *European Journal of Cell Biology* 89 (11): 828-38. doi:10.1016/j.ejcb.2010.06.003.

Bellefeuille, Steve Dagenais, Caroline M Molle, and Fernand-Pierre Gendron. 2019. "Reviewing the role of P2Y receptors in specific gastrointestinal cancers." *Purinergic Signalling* 15 (4): 451-63. doi:10.1007/s11302-019-09678-x.

Bencherif, M, C M Eisenhour, R J Prince, P M Lippiello, and R J Lukas. 1995. "The "calcium antagonist" TMB-8 [3,4,5-trimethoxybenzoic acid 8-(diethylamino)octyl ester] is a potent, non-competitive, functional antagonist at diverse nicotinic acetylcholine receptor subtypes." *Journal of Pharmacology and Experimental Therapeutics* 275 (3): 1418-26. https://pubmed.ncbi.nlm.nih.gov/8531111/.

Benias, Petros C, Rebecca G Wells, Bridget Sackey-Aboagye, Heather Klavan, Jason Reidy, Darren Buonocore, Markus Miranda, et al. 2018. "Structure and Distribution of an Unrecognized Interstitium in Human Tissues." *Scientific Reports* 8 (1). doi:10.1038/s41598-018-23062-6.

Bennett, Kaila M, Erinn A Parnell, Candice Sanscartier, Sophia Parks, Gang Chen, Meera G Nair, and David D Lo. 2016. "Induction of Colonic M Cells during Intestinal Inflammation." *The American Journal of Pathology* 186 (5): 1166-79. doi:10.1016/j.ajpath.2015.12.015.

Bennett, Kaila M, Sharon L Walker, and David D Lo. 2014. "Epithelial microvilli establish an electrostatic barrier to microbial adhesion." *Infection and Immunity* 82 (7): 2860-71. doi:10.1128/IAI.01681-14.

Berridge, M J. 1993. "Inositol trisphosphate and calcium signalling." *Nature* 361 (6410): 315-25. doi:10.1038/361315a0.

Berridge, Michael J. 2004. "Calcium signal transduction and cellular control mechanisms." *Biochimica et Biophysica Acta* 1742 (1-3): 3-7. doi:10.1016/j.bbamcr.2004.08.012.

Bettess, Michael D, Nicole Dubois, Mark J Murphy, Christelle Dubey, Catherine Roger, Sylvie Robine, and Andreas Trumpp. 2005. "c-Myc Is Required for the Formation of Intestinal Crypts but Dispensable for Homeostasis of the Adult Intestinal Epithelium." *Molecular and Cellular Biology* 25 (17): 7868-78. doi:10.1128/MCB.25.17.7868-7878.2005.

Beumer, Joep, Jens Puschhof, Julia Bauzá-Martinez, Adriana Martínez-Silgado, Rasa Elmentaite, Kylie R James, Alexander Ross, et al. 2020. "High-Resolution mRNA and Secretome Atlas of Human Enteroendocrine Cells." *Cell* 181 (6): 1291-306. doi:10.1016/j.cell.2020.04.036.

Beyaz, Semir, Miyeko D Mana, Jatin Roper, Dmitriy Kedrin, Assieh Saadatpour, Sue-Jean Hong , Khristian E Bauer-Rowe, et al. 2016. "High-fat diet enhances stemness and tumorigenicity of intestinal progenitors." *Nature* 531 (7592): 53-8. doi:10.1038/nature17173.

Bhat, Ajaz A, Srijayaprakash Uppada, Iman W Achkar, Sheema Hashem, Santosh K Yadav, Muralitharan Shanmugakonar, Hamda A Al-Naemi, Mohammad Haris, and Shahab Uddin. 2019. "Tight Junction Proteins and Signaling Pathways in Cancer and Inflammation: A Functional Crosstalk." *Frontiers in Physiology* 9 (1942). doi:10.3389/fphys.2018.01942.

Bilate, Angelina M, and Juan J Lafaille. 2012. "Induced CD4+Foxp3+ regulatory T cells in immune tolerance." *Annual Review of Immunology* 30: 733-58. doi:10.1146/annurev-immunol-020711-075043.

Birchenough, G MH, M EV Johansson, J K Gustafsson, J H Bergström, and G C Hansson. 2015. "New developments in goblet cell mucus secretion and function." *Mucosal Immunology* 8 (4): 712-9. doi:10.1038/mi.2015.32.

Bishop, M R, B V Sastry, and W B Stavinoha. 1977. "Identification of acetylcholine and propionylcholine in bull spermatozoa by integrated pyrolysis, gas chromatography and mass spectrometry." *Biochimica et Biophysica Acta* 500 (2): 440-4. doi:10.1016/0304-4165(77)90036-8.

Bizzozero, G. 1893. "Third communication on the tubular glands of the gastrointestinal canal and the relation of their epithelium to the surface epithelium of the mucous membrane." *Microscopic anatomy archive* 42: 82-152. https://link.springer.com/article/10.1007%2FBF02975307.

Bjerknes, M, and H Cheng. 1981. "The stem-cell zone of the small intestinal epithelium. I. Evidence from Paneth cells in the adult mouse." *American Journal of Anatomy* 160 (51): 51-63. doi:10.1002/aja.1001600105.

Bjerknes, Matthew, and Hazel Cheng. 1999. "Clonal analysis of mouse intestinal epithelial progenitors." *Gastroenterology* 116 (1): 7-14. doi:10.1016/s0016-5085(99)70222-2.

Bobek, L A, H Tsai, A R Biesbrock, and M J Levine. 1993. "Molecular cloning, sequence, and specificity of expression of the gene encoding the low molecular weight human salivary mucin (MUC7)." *Biochemical Journal* 268 (27): 20563-9. https://pubmed.ncbi.nlm.nih.gov/7690757/.

Bode, Lars. 2012. "Human milk oligosaccharides: every baby needs a sugar mama." *Glycobiology* 22 (9): 1147-62. doi:10.1093/glycob/cws074.

Boittin, François-Xavier, Florian Alonso, Loïc Le Gal, Florent Allagnat, Jean-Louis Bény, and Jacques-Antoine Haefliger. 2013. "Connexins and M3 muscarinic receptors contribute to heterogeneous Ca(2+) signaling in mouse aortic endothelium." *Cellular Physiology & Biochemistry* 31 (1): 166-78. doi:10.1159/000343358.

Bootman, Martin D, and Geert Bultynck. 2020. "Fundamentals of Cellular Calcium Signaling: A Primer." *Cold Spring Harbor Perspectives in Biology* 12 (1): a038802. doi:10.1101/cshperspect.a038802.

Bornstein, J C. 2008. "Purinergic Mechanisms in the Control of Gastrointestinal Motility." *Purinergic Signalling* 4 (3): 197-212. doi:10.1007/s11302-007-9081-z.

Borradori, Luca, and Arnoud Sonnenberg. 1999. "Structure and Function of Hemidesmosomes: More Than Simple Adhesion Complexes." *Journal of Investigative Dermatology* 112 (4): 411-8. doi:10.1046/j.1523-1747.1999.00546.x.

Botello-Smith, Wesley M, Wenjuan Jiang, Han Zhang, Alper D Ozkan, Yi-Chun Lin, Christine N Pham, Jérôme J Lacroix, and Yun Luo. 2019. "A mechanism for the activation of the mechanosensitive Piezo1 channel by the small molecule Yoda1." *Nature Communications* 10 (1): 4503. doi:10.1038/s41467-019-12501-1.

Brailoiu, Eugen, Dev Churamani, Xinjiang Cai, Michael G Schrlau, G Cristina Brailoiu, Xin Gao, Robert Hooper, et al. 2009. "Essential requirement for two-pore channel 1 in NAADP-mediated calcium signaling." *Journal of Cell Biology* 201-9. doi:10.1083/jcb.200904073.

Brandman, Onn, Jen Liou, Wei Sun Park, and Tobias Meyer. 2007. "STIM2 is a feedback regulator that stabilizes basal cytosolic and endoplasmic reticulum Ca2+ levels." *Cell* 131 (7): 1327-39. doi:10.1016/j.cell.2007.11.039.

Braun, Kristin M, and Fiona M Watt. 2004. "Epidermal Label-Retaining Cells: Background and Recent Applications." *Journal of Investigative Dermatology Symposium Proceedings* 9 (3): 196-201. doi:10.1111/j.1087-0024.2004.09313.x.

Brini, Marisa, and Ernesto Carafoli. 2009. "Calcium pumps in health and disease." *Physiological Reviews* 89 (4): 1341-78. doi:10.1152/physrev.00032.2008.

Brini, Marisa, Tito Calì, Denis Ottolini, and Ernesto Carafoli. 2014. "Neuronal calcium signaling: function and dysfunction." *Cellular and Molecular Life Sciences* 71 (15): 2787-814. doi:10.1007/s00018-013-1550-7.

Brodskiy, Pavel A, and Jeremiah J Zartman. 2018. "Calcium as a Signal Integrator in Developing Epithelial Tissues." *Physical Biology* 15 (5). doi:10.1088/1478-3975/aabb18.

Brown, Andrew J, Susan M Goldsworthy, Ashley A Barnes, Michelle M Eilert, Lili Tcheang, Dion Daniels, Alison I Muir, et al. 2003. "The Orphan G protein-coupled receptors GPR41 and GPR43 are activated by propionate and other short chain carboxylic acids." *Journal of Biological Chemistry* 278 (13): 11312-9. doi:10.1074/jbc.M211609200.

Browning, Kirsteen N, and Alberto R Travagli. 2014. "Central Nervous System Control of Gastrointestinal Motility and Secretion and Modulation of Gastrointestinal Functions." *Comprehensive Physiology* 4 (4): 1339-68. doi:10.1002/cphy.c130055.

Brownlee, Iain A, John Knight, Peter W Dettmar, and Jeffrey P Pearson. 2007. "Action of reactive oxygen species on colonic mucus secretions." *Free Radical Biology and Medicine* 43 (5): 800-8. doi:10.1016/j.freeradbiomed.2007.05.023.

Brügger, Michael David, Tomas Valenta, Hassan Fazilaty, George Hausmann, and Konrad Basler . 2020. "Distinct populations of crypt-associated fibroblasts act as signaling hubs to control colon homeostasis." *PLos Biology* 18 (12). doi:10.1371/journal.pbio.3001032.

Buchon, Nicolas, Nichole A Broderick, Mickael Poidevin, Sylvain Pradervand, and Bruno Lemaitre. 2009. "Drosophila Intestinal Response to Bacterial Infection: Activation of Host Defense and Stem Cell Proliferation." *Cell Host & Microbe* 5 (2): 200-11. doi:10.1016/j.chom.2009.01.003.

Buczacki, Simon JA, Heather Ireland Zecchini, Anna M Nicholson, Roslin Russell, Louis Vermeulen, Richard Kemp, and Douglas J Winton . 2013. "Intestinal label-retaining cells are secretory precursors expressing Lgr5." *Nature* 495: 65-9. doi:10.1038/nature11965.

Buffa, R, C Capella, P Fontana, L Usellini, and E Solcia. 1978. "Types of endocrine cells in the human colon and rectum." *Cell and Tissue Research* 192 (2): 227-40. doi:10.1007/BF00220741.

Bukauskas, F F, and R Weingart. 1993. "Multiple conductance states of newly formed single gap junction channels between insect cells." *Pflügers Archiv* 423 (1-2): 152-4. doi:10.1007/BF00374973.

Burdick, M D, A Harris, C J Reid, T Iwamura, and M A Hollingsworth. 1997. "Oligosaccharides expressed on MUC1 produced by pancreatic and colon tumor cell lines." *The Journal of Biological Chemistry* 272 (39): 24198-202. doi:10.1074/jbc.272.39.24198.

Burnstock, Geoffrey. 2011. "P2X receptors in the gut." *Wiley Online Library.* Oct. doi:10.1002/wmts.16.

Burnstock, Geoffrey. 2014. "Purinergic Signalling in the Gastrointestinal Tract and Related Organs in Health and Disease." *Purinergic Signalling* 10 (1): 33-50. doi:10.1007/s11302-013-9397-9.

Buzzi, Natalia, Ricardo Boland, and Ana Russo de Boland. 2010. "Signal transduction pathways associated with ATP-induced proliferation of colon adenocarcinoma cells." *Biochimica et Biophysica Acta* 1800 (9): 946-55. doi:10.1016/j.bbagen.2010.05.009.

Cai, Jie, Evangelia Pardali, Gonzalo Sánchez-Duffhues, and Peter ten Dijke. 2012. "BMP signaling in vascular diseases." *FEBS Letters* 586 (14): 1993-2002. doi:10.1016/j.febslet.2012.04.030.

Cai, Jing, Nailing Zhang, Yonggang Zheng, Roeland F de Wilde, Anirban Maitra, and Duojia Pan. 2010. "The Hippo signaling pathway restricts the oncogenic potential of an intestinal regeneration program." *Genes & Development* 24 (21): 2383-8. doi:10.1101/gad.1978810.

Calcraft, Peter J, Margarida Ruas, Zui Pan, Xiaotong Cheng, Abdelilah Arredouani, Xuemei Hao, Jisen Tang, et al. 2009. "NAADP mobilizes calcium from acidic organelles through two-pore channels." *Nature* 459 (7246): 596-600. doi:10.1038/nature08030.

Cancer Research UK. 2020. *Bowel cancer incidence statistics.* https://www.cancerresearchuk.org/health-professional/cancer-statistics/statistics-by-cancer-type/bowel-cancer/incidence#heading-Two.

Cang, Chunlei, Biruk Bekele, and Dejian Ren. 2014. "The voltage-gated sodium channel TPC1 confers endolysosomal excitability." *Nature Chemical Biology* 10 (6): 463-9. doi:10.1038/nchembio.1522.

Cantero-Recasens, Gerard, Cristian M Butnaru, Miguel A Valverde, José R Naranjo, Nathalie Brouwers, and Vivek Malhotra. 2018. "KChIP3 coupled to Ca 2+ oscillations exerts a tonic brake on baseline mucin release in the colon." *Elife* 7: e39729. doi:10.7554/eLife.39729.

Cardoso-Silva, Danielle, Deborah Delbue, Alice Itzlinger, Renée Moerkens, Sebo Withoff, Federica Branchi, and Michael Schumann. 2019. "Intestinal Barrier Function in Gluten-Related Disorders." *Nutrients* 11 (10): 2325. doi:10.3390/nu11102325.

Carlson, Taylor L, Hasan Yildiz, Zaineb Dar, Jaclyn Y Lock, and Rebecca L Carrier. 2018. "Lipids alter microbial transport through intestinal mucus." *PLoS One* 13 (12). doi:10.1371/journal.pone.0209151.

Cash, Heather L, Cecilia V Whitham, Cassie L Behrendt, and Lora V Hooper. 2009. "Symbiotic Bacteria Direct Expression of an Intestinal Bactericidal Lectin." *Science* 313 (5790): 1126-30. doi:10.1126/science.1127119.

Catterall, William A. 2011. "Voltage-Gated Calcium Channels." *Cold Spring Harbor Perspectives in Biology* 3 (8). doi:10.1101/cshperspect.a003947.

Celli, Jonathan P, Bradley S Turner, Nezam H Afdhal, Randy H Ewoldt, Gareth H McKinley, Rama Bansil, and Shyamsunder Erramilli. 2007. "Rheology of gastric mucin exhibits a pH-dependent sol-gel transition." *Biomacromolecules* 8 (5): 1580-6. doi:10.1021/bm0609691.

Center, Melissa M, Ahmedin Jemal, and Elizabeth Ward. 2009. "International Trends in Colorectal Cancer Incidence Rates." *Cancer Epidemiology, Biomarkers & Prevention* 18 (6): 1688-94. doi:10.1158/1055-9965.

Ceriani, Federico, Tullio Pozzan, and Fabio Mammano. 2016. "Critical role of ATP-induced ATP release for Ca2+ signaling in nonsensory cell networks of the developing cochlea." *PNAS* 113 (46): E7194-201. doi:10.1073/pnas.1616061113.

Charlesworth, P, I Jacobson, G Pocock, and C D Richards. 1992. "The mechanism by which procaine inhibits catecholamine secretion from bovine chromaffin cells." *The British Journal of Pharmacology* 106 (4): 802-12. doi:10.1111/j.1476-5381.1992.tb14416.x.

Chaudhari, Nirupa, and Stephen D Roper. 2010. "The cell biology of taste." *Journal of Cell Biology* 190 (3): 285-96. doi:10.1083/jcb.201003144.

Chelakkot, Chaithanya, Jaewang Ghim, and Sung Ho Ryu. 2018. "Mechanisms regulating intestinal barrier integrity and its pathological implications." *Experimental and Molecular Medicine* 50 (103). doi:10.1038/s12276-018-0126-x.

Chen, Hui, Dong Zhang, Jiang Hua Ren, and Sheng Ping Chao. 2013. "Effects of L-type Calcium Channel Antagonists Verapamil and Diltiazem on fKv1.4ΔN Currents in Xenopus oocytes." *Iranian Journal of Pharmaceutical Research* 12 (4): 855-66. https://www.ncbi.nlm.nih.gov/pmc/articles/PMC3920693/.

Chen, Liang, Michael D Brewer, Lili Guo, Ruoxing Wang, Peng Jiang, and Xiaolu Yang. 2017. "Enhanced degradation of misfolded proteins promotes tumorigenesis." *Cell Reports* 18 (13): 3143-54. doi:10.1016/j.celrep.2017.03.010.

Chen, Wei, Ping An, Xiao-Jing Quan, Jun Zhang, Zhong-Yin Zhou, Li-Ping Zou, and He-Sheng Luo. 2017. "Ca2+/calmodulin-dependent protein kinase II regulates colon cancer proliferation and migration via ERK1/2 and p38 pathways." *World Journal of Gastroenterology* 23 (33): 6111-8. doi:10.3748/wjg.v23.i33.6111.

Chen, Xi, Zehong Yang, Huiling Hu, Wentao Duan, Aiping Wang, Yanbin Dong, Weihang Gao, et al. 2019. "Differentiation and Proliferation of Intestinal Stem Cells and its Underlying Regulated Mechanisms during Weaning." *Current Protein & Peptide Science* 20 (7): 690-5. doi:10.2174/1389203720666190125101834.

Cheng, H, and C P Leblond. 1974. "Origin, differentiation and renewal of the four main epithelial cell types in the mouse small intestine. V. Unitarian Theory of the origin of the four epithelial cell types." *American Journal of Anatomy* 141 (4): 537-61. doi:10.1002/aja.1001410407.

Cheng, Kunrong, Roxana Samimi, Guofeng Xie, Jasleen Shant, Cinthia Drachenberg, Mark Wade, Richard J Davis, George Nomikos, and Jean-Pierre Raufman. 2008. "Acetylcholine release by human colon cancer cells mediates autocrine stimulation of cell proliferation." *The American Journal of Physiology-Gastrointestinal and Liver Physiology* 295 (3): G591-7. doi:10.1152/ajpgi.00055.2008.

Cheng, Kunrong, Ying Chen, Piotr Zimniak, Jean-Pierre Raufman, Yinghua Xiao, and Harold Frucht. 2002. "Functional interaction of lithocholic acid conjugates with M3 muscarinic receptors on a human colon cancer cell line." *Biochimica et Biophysica Acta* 1588 (1): 48-55. doi:10.1016/s0925-4439(02)00115-1.

Chhikara, Nirmal, Mayank Saraswat, Anil Kumar Tomar, Sharmistha Dey, Sarman Singh, and Savita Yadav. 2012. "Human epididymis protein-4 (HE-4): a novel cross-class protease inhibitor." *PLos One* 7 (11). doi:10.1371/journal.pone.0047672.

Cho, Chung-Hyun, Jin Seok Woo, Claudio F Perez, and Eun Hui Lee. 2017. "A focus on extracellular Ca 2+ entry into skeletal muscle." *Experimental & Molecular Medicine* 49 (9): e378. doi:10.1038/emm.2017.208.

Choudhury, Barun K, Xuan-Zheng Shi, and Sushil K Sarna. 2009. "Gene plasticity in colonic circular smooth muscle cells underlies motility dysfunction in a model of postinfective IBS." *American Journal of Physiology-Gastrointestinal and Liver Physiology* 296 (3): 632-42. doi:10.1152/ajpgi.90673.2008.

Christensen, Kenneth A, Jesse T Myers, and Joel A Swanson. 2002. "pH-dependent regulation of lysosomal calcium in macrophages." *Journal of Cell Science* 115 (3): 599-607. https://pubmed.ncbi.nlm.nih.gov/11861766/.

Christofi, Fievos L, Jacqueline Wunderlich, Jun Ge Yu, Y-Z Wang, Jianjing Xue, Jorge Guzman, Najma Javed, and Helen Cooke. 2004. "Mechanically evoked reflex electrogenic chloride secretion in rat distal colon is triggered by endogenous nucleotides acting at P2Y1, P2Y2, and P2Y4 receptors." *Journal of Comparative Neurology* 469 (1): 16-36. doi:10.1002/cne.10961.

Clarke, Gerard, Roman M Stilling, Paul J Kennedy, Catherine Stanton, John F Cryan, and Timothy G Dinan. 2014. "Minireview: Gut Microbiota: The Neglected Endocrine Organ." *Molecular Endocrinology* 28 (8): 1221-38. doi:10.1210/me.2014-1108.

Clevers, Hans C, and Charles L Bevins. 2013. "Paneth cells: maestros of the small intestinal crypts." *Annual Review of Physiology* 75: 289-311. doi:10.1146/annurev-physiol-030212-183744.

Clevers, Hans. 2013. "The Intestinal Crypt, A Prototype Stem Cell Compartment." *Cell* 154 (2): 274-84. doi:10.1016/j.cell.2013.07.004.

Clevers, Hans. 2006. "Wnt/beta-catenin signaling in development and disease." *Cell* 127 (3): 469-80. doi:10.1016/j.cell.2006.10.018.

Clevers, Hans, and Roel Nusse. 2012. "Wnt/β-catenin signaling and disease." *Cell* 149 (6): 1192-205. doi:10.1016/j.cell.2012.05.012.

Collado, Maria Carmen, Samuli Rautava, Juhani Aakko, Erika Isolauri, and Seppo Salminen. 2016. "Human gut colonisation may be initiated in utero by distinct microbial communities in the placenta and amniotic fluid." *Scientific Reports* 6 (23129). doi:10.1038/srep23129.

Colussi, Dora, Giovanni Brandi, Franco Bazzoli, and Luigi Ricciardiello. 2013. "Molecular pathways involved in colorectal cancer: implications for disease behavior and prevention." *International Journal of Molecular Sciences* 14 (8): 16365-85. doi:10.3390/ijms140816365.

Coste, Bertrand, Jayanti Mathur, Manuela Schmidt, Taryn J Earley, Sanjeev Ranade, Matt J Petrus, Adrienne E Dubin, and Ardem Patapoutian. 2010. "Piezo1 and Piezo2 are essential components of distinct mechanically activated cation channels." *Science* 330 (6000): 55-60. doi:10.1126/science.1193270.

Cotter, Kristina, Laura Stransky, Christina McGuire, and Michael Forgac. 2015. "Recent Insights into the Structure, Regulation, and Function of the V-ATPases." *Trends in Biochemical Sciences* 40 (10): 611-22. doi:0.1016/j.tibs.2015.08.005.

Coutinho-Silva, Robson, Lynn Stahl, Kwok-Kuen Cheung, Nathalia Enes de Campos, Carolina de Oliveira Souza, David M Ojcius, and Geoffrey Burnstock. 2005. "P2X and P2Y purinergic

receptors on human intestinal epithelial carcinoma cells: effects of extracellular nucleotides on apoptosis and cell proliferation." *American Journal of Physiology-Gastrointestinal and Liver Physiology* 288 (5): G1024-35. doi:10.1152/ajpgi.00211.2004.

Creamer, Trevor P. 2020. "Calcineurin." *Cell Communication and Signaling* 18 (1): 137. doi:10.1186/s12964-020-00636-4.

Creeth, J M. 1978. "Constituents of mucus and their separation." *British Medical Bulletin* 34 (1): 17-24. doi:10.1093/oxfordjournals.bmb.a071454.

Cunningham, Kellie E, Elizabeth A Novak, Garret Vincent, Vei Shaun Siow, Brian D Griffith, Sarangarajan Ranganathan, Matthew R Rosengart, Jon D Piganelli, and Kevin P Mollen. 2019. "Calcium/calmodulin–dependent protein kinase IV (CaMKIV) activation contributes to the pathogenesis of experimental colitis via inhibition of intestinal epithelial cell proliferation." *The FASEB Journal* 33 (1): 1330-46. doi:10.1096/fj.201800535R.

Curtis, Tim M, and C Norman Scholfield. 2001. "Nifedipine blocks Ca2+ store refilling through a pathway not involving L-type Ca2+ channels in rabbit arteriolar smooth muscle." *The Journal of Physiology* 532 (Pt3): 609-23. doi:10.1111/j.1469-7793.2001.0609e.x.

Darby, Matthew, Corinna Schnoeller, Alykhan Vira, Fiona Jane Culley, Saeeda Bobat, Erin Logan, Frank Kirstein, et al. 2015. "The M3 muscarinic receptor is required for optimal adaptive immunity to helminth and bacterial infection." *PLOS Pathogens* 11 (1): e1004636. doi:10.1371/journal.ppat.1004636.

Das, Srustidhar, Prabin D Majhi, Mona H Al-Mugotir, Satyanarayana Rachagani, Paul Sorgen, and Surinder K Batra. 2015. "Membrane proximal ectodomain cleavage of MUC16 occurs in the acidifying Golgi/post-Golgi compartments." *Scientific Reports* 5 (9759). doi:10.1038/srep09759.

Daulagala, Amanda C, Mary Catherine Bridges, and Antonis Kourtidis. 2019. "E-cadherin Beyond Structure: A Signaling Hub in Colon Homeostasis and Disease." *International Journal of Molecular Sciences* 20 (11). doi:10.3390/ijms20112756.

Davis, C William, and Burton F Dickey. 2008. "Regulated airway goblet cell mucin secretion." *Annual Review of Physiology* 70: 487-512. doi:10.1146/annurev.physiol.70.113006.100638.

Davis, Felicity M, Michelle T Parsonage, Peter J Cabot, Marie-Odile Parat, Erik W Thompson, Sarah J Roberts-Thomson, and Gregory R Monteith. 2013. "Assessment of gene expression of intracellular calcium channels, pumps and exchangers with epidermal growth factor-induced epithelial-mesenchymal transition in a breast cancer cell line." *Cancer Cell International* 13 (1): 76. doi:10.1186/1475-2867-13-76.

Davis, Stephanie E, and Elizabeth P Bauer. 2012. "L-type voltage-gated calcium channels in the basolateral amygdala are necessary for fear extinction." *Journal of Neuroscience* 32 (39): 13582-6. doi:10.1523/JNEUROSCI.0809-12.2012.

De Arcangelis, Adèle, Hussein Hamade, Fabien Alpy, Sylvain Normand, Emilie Bruyère, Olivier Lefebvre, Agnès Méchine-Neuville, et al. 2017. "Hemidesmosome integrity protects the colon against colitis and colorectal cancer." *Gut* 66 (10): 1748-60. doi:10.1136/gutjnl-2015-310847.

de Lau, Wim, Pekka Kujala, Kerstin Schneeberger, Sabine Middendorp, Vivian SW Li, Nick Barker, Anton Martens, et al. 2012. "Peyer's patch M cells derived from Lgr5(+) stem cells require SpiB and are induced by RankL in cultured "miniguts"." *Molecular and Cellular Biology* 32 (18): 3639-47. doi:10.1128/MCB.00434-12.

de Lau, Wim, Weng Chuan Peng, Piet Gros, and Hans Clevers. 2014. "The R-spondin/Lgr5/Rnf43 module: regulator of Wnt signal strength." *Genes & Development* 28 (4): 305-16. doi:10.1101/gad.235473.113.

De Schepper, Sebastiaan, Simon Verheijden, Javier Aguilera-Lizarraga, Maria Francesca Viola, Werend Boesmans, Nathalie Stakenborg, Iryna Voytyuk, et al. 2018. "Self-maintaining gut macrophages are essential for intestinal homeostasis." *Cell* 175 (2): 400-15. doi:10.1016/j.cell.2018.07.048.

de Winter-de Groot, K M, G Berkers, R EP Marck-van der Wilt, R van der Meer, A Vonk, J F Dekkers, M Geerdink, et al. 2020. "Forskolin-induced swelling of intestinal organoids correlates with disease severity in adults with cystic fibrosis and homozygous F508del mutations." *The Journal of Cystic Fibrosis* 19 (4): 614-19. doi:10.1016/j.jcf.2019.10.022.

Deal, E Jr C, A D Cherniack, and L B Eberlin. 1984. "Effects of verapamil on histamine-and carbachol-induced contraction of pulmonary tissues in vitro." *Chest* 86 (5): 762-6. doi:10.1378/chest.86.5.762.

Deckmann, Klaus, Katharina Filipski, Gabriela Krasteva-Christ, Martin Fronius, Mike Althaus, Amir Rafiq, Tamara Papadakis, et al. 2014. "Bitter triggers acetylcholine release from polymodal urethral chemosensory cells and bladder reflexes." *PNAS* 111 (22): 8287-92. doi:10.1073/pnas.1402436111.

Degirmenci, Bahar, Tomas Valenta, Slavica Dimitrieva, George Hausmann, and Konrad Basler. 2018. "GLI1-expressing mesenchymal cells form the essential Wnt-secreting niche for colon stem cells." *Nature* 558: 449-53. doi:10.1038/s41586-018-0190-3.

del Rocío Campos-Contreras, Anaí, Mauricio Díaz-Muñoz, and Francisco G Vázquez-Cuevas. 2020. "Purinergic Signaling in the Hallmarks of Cancer." *Cells* 9 (7): 1612. doi:10.3390/cells9071612.

Deng, Hansong, Akos A Gerencser, and Heinrich Jasper. 2016. "Signal Integration by Ca2+ Regulates Intestinal Stem Cell Activity." *Nature* 528 (7581): 212-7. doi:10.1038/nature16170.

Derendorf, Hartmut. 2020. "Excessive lysosomal ion-trapping of hydroxychloroquine and azithromycin." *The International Journal of Antimicrobial Agents* 55 (6): 106007. doi:10.1016/j.ijantimicag.2020.106007.

Derler, Isabella, Isaac Jardin, and Christoph Romanin. 2016. "Molecular mechanisms of STIM/Orai communication." *American Journal of Physiology-Cell Physiology* 310 (8): 643-62. doi:10.1152/ajpcell.00007.2016.

Desai, Mahesh S, Anna M Seekatz, Nicole M Koropatkin, Nobuhiko Kamada, Christina A Hickey, Mathis Wolter, Nicholas A Pudlo, et al. 2016. "A Dietary Fiber-Deprived Gut Microbiota Degrades the Colonic Mucus Barrier and Enhances Pathogen Susceptibility." *Cell* 167 (5): 1339-53. doi:10.1016/j.cell.2016.10.043.

Dharmani, Poonam, Vikas Srivastava, Vanessa Kissoon-Singh, and Kris Chadee. 2009. "Role of intestinal mucins in innate host defense mechanisms against pathogens." *Journal of Innate Immunity* 1 (2): 123-35. doi:10.1159/000163037.

Dhawan, Shobhit, Cathy Cailotto, Lucien F Harthoorn, and Wouter J de Jonge. 2012. "Cholinergic Signalling in Gut Immunity." *Life Sciences* 91 (21-22): 1038-42. doi:10.1016/j.lfs.2012.04.042.

Di Virgilio, Francesco, Jean-Marie Boeynaems, and Simon C Robson. 2009. "Extracellular nucleotides as negative modulators of immunity." *Current Opinion in Pharmacology* 9 (4): 507-13. doi:10.1016/j.coph.2009.06.021.

Diwakarla, Shanti, Linda J Fothergill, Josiane Fakhry, Brid Callaghan, and John B Furness. 2018. "Heterogeneity of enterochromaffin cells within the gastrointestinal tract." *Neurogastroenterology & Motility* 29 (6). doi:10.1111/nmo.13101.

Dockray, Graham J. 2013. "Enteroendocrine cell signalling via the vagus nerve." *Current Opinion in Pharmacology* 13 (6): 954-8. doi:10.1016/j.coph.2013.09.007.

Dong, Xiao, Eric James Smoll, Kwang Hyun Ko, Jonathan Lee, Jimmy Yip Chow, Ho Dong Kim, Paul A Insel, and Hui Dong. 2009. "P2Y receptors mediate Ca2+ signaling in duodenocytes and contribute to duodenal mucosal bicarbonate secretion." *American Journal of Physiology-Gastrointestinal and Liver Physiology* 296 (2): G424-32. doi:10.1152/ajpgi.90314.2008.

Drugbank. 2005. *Chloroquine.* Jun. https://go.drugbank.com/drugs/DB00608.

—. 2005. *Procaine.* Jun. https://go.drugbank.com/drugs/DB00721.

Dunel-Erb, S, C Chevalier, P Laurent, A Bach, F Decrock, and Y Le Maho. 2001. "Restoration of the jejunal mucosa in rats refed after prolonged fasting." *Biochemistry and Physiology Part A: Molecular & Integrative Physiology* 129 (4): 933-47. doi:10.1016/s1095-6433(01)00360-9.

Dunn, Jacob, and Michael H Grider. 2020. "Physiology, Adenosine Triphosphate." In *Physiology, Adenosine Triphosphate*. StatPearls. https://www.ncbi.nlm.nih.gov/books/NBK553175/.

Durand, Aurélie, Bridgitte Donahue, Grégory Peignon, Franck Letourneur, Nicolas Cagnard, Christian Slomianny, Christine Perret, Noah F Shroyer, and Béatrice Romagnolo. 2012. "Functional intestinal stem cells after Paneth cell ablation induced by the loss of transcription factor Math1 (Atoh1)." *Proceedings of the National Academy of Sciences* 109 (23): 8965-70. doi:10.1073/pnas.1201652109.

Echevarría, Wihelma, M Fatima Leite, Mateus T Guerra, Warren R Zipfel, and Michael H Nathanson. 2003. "Regulation of calcium signals in the nucleus by a nucleoplasmic reticulum." *Nature Cell Biology* 5 (5): 440-6. doi:10.1038/ncb980.

Eckburg, Paul B, Elisabeth M Bik, Charles N Bernstein, Elizabeth Purdom, Les Dethlefsen, Michael Sargent, Steven R Gill, Karen E Nelson, and David A Relman. 2006. "Diversity of the Human Intestinal Microbial Flora." *Science* 308 (5728): 1635-8. doi:10.1126/science.1110591.

Edmondson, Rasheena, Jessica Jenkins Broglie, Audrey F Adcock, and Liju Yang. 2014. "Three-Dimensional Cell Culture Systems and Their Applications in Drug Discovery and Cell-Based Biosensors." *ASSAY and Drug Development Technologies* 12 (4): 207-18. doi:10.1089/adt.2014.573.

Ehrlich, B E, E Kaftan, S Bezprozvannaya, and I Bezprozvanny. 1994. "The pharmacology of intracellular Ca(2+)-release channels." *Trends in Pharmacological Sciences* 15 (5): 145-9. doi:10.1016/0165-6147(94)90074-4.

Eisenberg, Eli, and Erez Y Levanon. 2013. "Human housekeeping genes, revisited." *Trends in Genetics* 29 (10): 569-74. doi:10.1016/j.tig.2013.05.010.

Elphick, D A, and Y R Mahida. 2005. "Paneth cells: their role in innate immunity and inflammatory disease." *Gut* 54 (12): 1802-9. doi:10.1136/gut.2005.068601.

El-Sabban, Marwan E, Agnel J Sfeir, Myriam H Daher, Nada Y Kalaany, Rola A Bassam, and Rabih S Talhouk. 2003. "ECM-induced gap junctional communication enhances mammary epithelial cell differentiation." *Journal of Cell Science* 116: 3531-41. doi:10.1242/jcs.00656.

El-Sabban, Marwan E, Lina F Abi-Mosleh, and Rabih S Talhouk . 2003. "Developmental Regulation of Gap Junctions and Their Role in Mammary Epithelial Cell Differentiation." Oct: 463-73. doi:10.1023/B:JOMG.0000017432.04930.76.

Elsing, C, C Hübner, B A Fitscher, A Kassner, and W Stremmel. 1997. "Muscarinic acetylcholine receptor stimulation of biliary epithelial cells and its effect on bile secretion in the isolated perfused liver [corrected]." *Hepatology* 25 (4): 804-13. doi:10.1002/hep.510250404.

Esterházy, Daria, Jakob Loschko, Mariya London, Veronica Jove, Thiago Y Oliveira, and Daniel Mucida. 2016. "Classical dendritic cells are required for dietary antigen–mediated induction of peripheral Treg cells and tolerance." *Nature Immunology* 17: 545-55. doi:10.1038/ni.3408.

Evans, Elizabeth L, Kevin Cuthbertson, Naima Endesh, Baptiste Rode, Nicola M Blythe, Adam J Hyman, Sally J Hall, et al. 2018. "Yoda1 analogue (Dooku1) which antagonizes Yoda1-evoked activation of Piezo1 and aortic relaxation." *The British Journal of Pharmacology* 175 (10): 1744-59. doi:10.1111/bph.14188.

Fabiato, A. 1983. "Calcium-induced release of calcium from the cardiac sarcoplasmic reticulum." *American Journal of Physiology* 245 (1): C1-14. doi:10.1152/ajpcell.1983.245.1.C1.

Faris, Pawan, Giorgia Pellavio, Federica Ferulli, Francesca Di Nezza, Mudhir Shekha, Dmitry Lim, Marcello Maestri, et al. 2019. "Nicotinic Acid Adenine Dinucleotide Phosphate (NAADP) Induces Intracellular Ca 2+ Release through the Two-Pore Channel TPC1 in Metastatic Colorectal Cancer Cells." *Cancers* 11 (4): 542. doi:10.3390/cancers11040542.

Faris, Pawan, Mudhir Shekha, Daniela Montagna, Germano Guerra, and Francesco Moccia. 2019. "Endolysosomal Ca2+ Signalling and Cancer Hallmarks: Two-Pore Channels on the Move, TRPML1 Lags Behind!" *Cancers (Basel)* 11 (1): 27. doi:10.3390/cancers11010027.

Favia, Annarita, Marianna Desideri, Guido Gambara, Alessio D'Alessio, Margarida Ruas, Bianca Esposito, Donatella Del Bufalo, et al. 2014. "VEGF-induced neoangiogenesis is mediated by NAADP and two-pore channel-2-dependent Ca2+ signaling." *PNAS* 111 (44): E4706-15. doi:10.1073/pnas.1406029111.

FDA. 2018. "Bioanalytical Method Validation Guidance for Industry." *FDA.* May. https://www.fda.gov/regulatory-information/search-fda-guidance-documents/bioanalytical-method-validation-guidance-industry.

Felton, Jessica, Shien Hu, and Jean-Pierre Raufman. 2019. "Targeting M3 Muscarinic Receptors for Colon Cancer Therapy." *Current Molecular Pharmacology* 11 (3): 184-90. doi:10.2174/1874467211666180119115828.

Fernández-Sánchez, María Elena, Sandrine Barbier, Joanne Whitehead, Gaëlle Béalle, Aude Michel, Heldmuth Latorre-Ossa, Colette Rey, et al. 2015. "Mechanical induction of the tumorigenic β-catenin pathway by tumour growth pressure." *Nature* 523 (7558): 92-5. doi:10.1038/nature14329.

Feske, Stefan, Yousang Gwack, Murali Prakriya, Sonal Srikanth, Sven-Holger Puppel, Bogdan Tanasa, Patrick G Hogan, Richard S Lewis, Mark Daly, and Anjana Rao. 2006. "A mutation in Orai1 causes immune deficiency by abrogating CRAC channel function." *Nature* 441 (7090): 179-85. doi:10.1038/nature04702.

Filippini, Antonio, Antonella D'Amore, Fioretta Palombi, and Armando Carpaneto. 2020. "Could the Inhibition of Endo-Lysosomal Two-Pore Channels (TPCs) by the Natural Flavonoid Naringenin Represent an Option to Fight SARS-CoV-2 Infection?" *Frontiers in Microbiology* 11: 11970. doi:10.3389/fmicb.2020.00970.

Forgac, Michael. 2007. "Vacuolar ATPases: rotary proton pumps in physiology and pathophysiology." *Nature Reviews Molecular Cell Biology* 8 (11): 917-29. doi:10.1038/nrm2272.

Forsythe, Sean M, Paul C Kogut, John F McConville, Yiping Fu, Joel A McCauley, Andrew J Halayko, Hong Wei Liu, et al. 2002. "Structure and transcription of the human m3 muscarinic receptor gene." *American Journal of Respiratory Cell and Molecular Biology* 26 (3): 298-305. doi:10.1165/ajrcmb.26.3.4564.

Fox, R I. 1993. "Mechanism of action of hydroxychloroquine as an antirheumatic drug." *Seminars in Arthritis and Rheumatism* 23 (2 Suppl 1): 82-91. doi:10.1016/s0049-0172(10)80012-5.

France, Marion M, and Jerrold R Turner. 2017. "The mucosal barrier at a glance." *Journal of Cell Science* 130 (2): 307-14. doi:10.1242/jcs.193482.

Frey, A, K T Giannasca, R Weltzin, P J Giannasca, H Reggio, W I Lencer, and M R Neutra. 1996. "Role of the glycocalyx in regulating access of microparticles to apical plasma membranes of intestinal epithelial cells: implications for microbial attachment and oral vaccine targeting." *Journal of Experimental Medicine* 184 (3): 1045-59. doi:10.1084/jem.184.3.1045.

Frizzell, Raymond A, and John W Hanrahan. 2012. "Physiology of Epithelial Chloride and Fluid Secretion." *Cold Spring Harbor Perspectives in Medicine* 2 (6): a009563. doi:10.1101/cshperspect.a009563.

Frucht, H, R T Jensen, D Dexter, W L Yang, and Y Xiao. 1999. "Human colon cancer cell proliferation mediated by the M3 muscarinic cholinergic receptor." *Clinical Cancer Research* 5 (9): 2532-9. https://pubmed.ncbi.nlm.nih.gov/10499630/.

Fu, Ziying, Tatsuya Ogura, Wangmei Luo, and Weihong Lin. 2018. "ATP and Odor Mixture Activate TRPM5-Expressing Microvillous Cells and Potentially Induce Acetylcholine Release to Enhance Supporting Cell Endocytosis in Mouse Main Olfactory Epithelium." *Frontiers in Cellular Neuroscience* 12 (71). doi:10.3389/fncel.2018.00071.

Fujii, Satoru, Kohei Suzuki, Ami Kawamoto, Fumiaki Ishibashi, Toru Nakata, Tatsuro Murano, Go Ito, et al. 2016. "PGE 2 is a direct and robust mediator of anion/fluid secretion by human intestinal epithelial cells." *Scientific Reports* 6: 36795. doi:10.1038/srep36795.

Fukuda, Shinji, Hidehiro Toh, Koji Hase, Kenshiro Oshima, Yumiko Nakanishi, Kazutoshi Yoshimura, Toru Tobe, et al. 2011. "Bifidobacteria can protect from enteropathogenic infection through production of acetate." *Nature* 469 (7331): 543-7. doi:10.1038/nature09646.

Furness, John B, Leni R Rivera, Hyun-Jung Cho, David M Bravo, and Brid Callaghan. 2013. "The gut as a sensory organ." *Nature Reviews Gastroenterology & Hepatology* 10: 729-40. doi:10.1038/nrgastro.2013.180.

Furusawa, Yukihiro, Yuuki Obata, Shinji Fukuda, Takaho A Endo, Gaku Nakato, Daisuke Takahashi, Yumiko Nakanishi, et al. 2013. "Commensal microbe-derived butyrate induces the differentiation of colonic regulatory T cells." *Nature* 504 (7480): 446-50. doi:10.1038/nature12721.

Gabriel, Iwona, Anita Olejek, Krystyna Stencel-Gabriel, and Wielgoś Miroslaw. 2018. "The influence of maternal vaginal flora on the intestinal colonization in newborns and 3-month-old infants." *The Journal of Maternal-Fetal & Neonatal Medicine* 31 (11): 1448-53. doi:10.1080/14767058.2017.1319352.

Gajda, Angela M, and Judith Storch. 2014. "Enterocyte Fatty Acid Binding Proteins (FABPs): Different Functions of Liver- and Intestinal- FABPs in the Intestine." *Prostaglandins, Leukotrienes & Essential Fatty Acids* 93: 9-16. doi:10.1016/j.plefa.2014.10.001.

Gammaitoni, Arnold R, Henry T Goitz, Stephanie Marsh, Thomas B Marriott, and Bradley S Galer. 2013. "Heated lidocaine/tetracaine patch for treatment of patellar tendinopathy pain." *Journal of Pain Research* 6: 565-70. doi:10.2147/JPR.S46239.

Gao, Xinyan, Yuxue Zhao, Yangshuai Su, Kun Liu, Xiaochun Yu, Changxiang Cui, Zhaokun Yang, Hong Shi, Xianghong Jing, and Bing Zhu. 2016. "β1/2 or M2/3 Receptors Are Required for Different Gastrointestinal Motility Responses Induced by Acupuncture at Heterotopic or Homotopic Acupoints." *PLoS One* 11 (12): e0168200. doi:10.1371/journal.pone.0168200.

Garland, C, R B Shekelle, E Barrett-Connor, M H Criqui, A H Rossof, and O Paul. 1985. "Dietary vitamin D and calcium and risk of colorectal cancer: a 19-year prospective study in men." *Lancet* 1 (8424): 307-9. doi:10.1016/s0140-6736(85)91082-7.

Garrity, Abigail G, Wuyang Wang, Crystal Md Collier, Sara A Levey, Qiong Gao, and Haoxing Xu. 2016. "The endoplasmic reticulum, not the pH gradient, drives calcium refilling of lysosomes." *eLife* 5: e15887. doi:10.7554/eLife.15887.

Garrod, David, and Martyn Chidgey. 2008. "Desmosome structure, composition and function." *Biochimica et Biophysica Acta - Biomembranes* 1778 (3): 572-87. doi:10.1016/j.bbamem.2007.07.014.

Gassler, Nikolaus. 2017. "Paneth cells in intestinal physiology and pathophysiology." *World Journal of Gastrointestinal Pathophysiology* 8 (4): 150-60. doi:10.4291/wjgp.v8.i4.150.

GBD 2017 Inflammatory Bowel Disease Collaborators. 2019. "The Global, Regional, and National Burden of Inflammatory Bowel Disease in 195 Countries and Rerritories, 1990–2017: a

Systematic Analysis for the Global Burden of Disease Study 2017." *The Lancet Gastroenterology and Hepatology* 5 (1): 17-30. doi:10.1016/S2468-1253(19)30333-4.

Gehart, Helmuth , and Hans Clevers. 2018. "Tales from the crypt: new insights into intestinal stem cells." *Nature Reviews Gastroenterology & Hepatology* 16: 19-34. doi:10.1038/s41575-018-0081-y.

Gehart, Helmuth, and Hans Clevers. 2019. "Tales From the Crypt: New Insights Into Intestinal Stem Cells." *Nature Reviews Gastroenterology & Hepatology* 16: 19-34. doi:10.1038/s41575-018-0081-y.

Genander, Maria, Michael M Halford, Nan-Jie Xu, Malin Eriksson, Zuoren Yu, Zhaozhu Qiu, Anna Martling, et al. 2010. "Dissociation of EphB2 signaling pathways mediating progenitor cell proliferation and tumor suppression." *Cell* 139 (4): 679-92. doi:10.1016/j.cell.2009.08.048.

Gerbe, François, and Philippe Jay. 2016. "Intestinal tuft cells: epithelial sentinels linking luminal cues to the immune system." *Mucosal Immunology* 9 (6): 1353-9. doi:10.1038/mi.2016.68.

Gerbe, François, Bénédicte Brulin, Leila Makrini, Catherine Legraverend, and Philippe Jay. 2009. "DCAMKL-1 Expression Identifies Tuft Cells Rather Than Stem Cells in the Adult Mouse Intestinal Epithelium." *Gastroenterology* 137 (6): 2179-80. doi:10.1053/j.gastro.2009.06.072.

Gerbe, François, Catherine Legraverend, and Philippe Jay. 2012. "The intestinal epithelium tuft cells: specification and function." *Cellular and Molecular Life Sciences* 69 (17): 2907-17. doi:10.1007/s00018-012-0984-7.

Gerbe, François, Emmanuelle Sidot, Danielle J Smyth, Makoto Ohmoto, Ichiro Matsumoto, Valérie Dardalhon, Pierre Cesses, et al. 2016. "Intestinal epithelial tuft cells initiate type 2 mucosal immunity to helminth parasites." *Nature* 529 (7585): 226-30. doi:10.1038/nature16527.

Gerling, Marco, Nikè VJA Büller, Leonard M Kirn, Simon Joost, Oliver Frings, Benjamin Englert, Åsa Bergström, et al. 2016. "Stromal Hedgehog signalling is downregulated in colon cancer and its restoration restrains tumour growth." *Nature Communications* 7: 12321. doi:10.1038/ncomms12321.

Ghanem, Esam, Bernard Robaye, Teresinha Leal, Jens Leipziger, Willy Van Driessche, Renaud Beauwens, and Jean-Marie Boeynaems. 2005. "The role of epithelial P2Y2 and P2Y4 receptors in the regulation of intestinal chloride secretion." *British Journal of Pharmacology* 146 (3): 354-9. doi:10.1038/sj.bjp.0706353.

Giaroni, C, G E Knight, H-Z Ruan, R Glass, M Bardini, S Lecchini, G Frigo, and G Burnstock. 2002. "P2 receptors in the murine gastrointestinal tract." *Neuropharmacology* 43 (8): 1313-23. doi:10.1016/s0028-3908(02)00294-0.

Gillis, J M, and Ph Gailly. 1994. "Measurements of [Ca2+]i with the Diffusible Fura-2 AM: Can Some Potential Piffalls be Evaluated?" *Biophysical Journal* 67: 476-7.

Girada, Shravan Babu, Ramya S Kuna, Shilpak Bele, Zhimeng Zhu, N R Chakravarthi, Richard D DiMarchi, and Prasenjit Mitra. 2017. "Gαs regulates Glucagon-Like Peptide 1 Receptor-mediated cyclic AMP generation at Rab5 endosomal compartment." *Molecular Metabolism* 6 (10): 1173-85. doi:10.1016/j.molmet.2017.08.002.

Goodenough, Daniel A, and David L Paul. 2009. "Gap Junctions." *Cold Spring Harbor Perspectives in Biology* 1 (1): a002576. doi:10.1101/cshperspect.a002576.

Görlach, Agnes, Katharina Bertram, Sona Hudecova, and Olga Krizanova. 2015. "Calcium and ROS: A mutual interplay." *Redox Biology* 6: 260-71. doi:10.1016/j.redox.2015.08.010.

Goto, Yoshiyuki. 2019. "Epithelial Cells as a Transmitter of Signals From Commensal Bacteria and Host Immune Cells." *Frontiers in Immunology* 10 (2057). doi:10.3389/fimmu.2019.02057.

Grady, William M, and John M Carethers. 2008. "Genomic and epigenetic instability in colorectal cancer pathogenesis." *Gastroenterology* 135 (4): 1079-99. doi:10.1053/j.gastro.2008.07.076.

Greenwood, Jeffrey M, and Michael Dragunow. 2010. "M3 muscarinic receptors promote cell survival through activation of the extracellular regulated kinase (ERK1/2) pathway." *European Journal of Pharmacology* 640 (1-3): 38-45. doi:10.1016/j.ejphar.2010.05.013.

Greger, R. 2000. "Role of CFTR in the colon." *The Annual Review of Physiology* 62: 467-91. doi:10.1146/annurev.physiol.62.1.467.

Gregorieff, Alex, Yu Liu, Mohammad R Inanlou, Yuliya Khomchuk, and Jeffrey L Wrana. 2015. "Yap-dependent reprogramming of Lgr5(+) stem cells drives intestinal regeneration and cancer." *Nature* 526 (7575): 715-8. doi:10.1038/nature15382.

Greig, Chasen J, Sarah J Armenia, and Robert A Cowles. 2020. "The M1 muscarinic acetylcholine receptor in the crypt stem cell compartment mediates intestinal mucosal growth." *Experimental Biology and Medicine* 245 (14): 1194-9. doi:10.1177/1535370220938375.

Gribble, Fiona M, and Frank Reimann. 2019. "Function and mechanisms of enteroendocrine cells and gut hormones in metabolism." *Nature Reviews Endocrinology* 15 (4): 226-37. doi:10.1038/s41574-019-0168-8.

Groussard, C, I Morel, M Chevanne, M Monnier, J Cillard, and A Delamarche. 2000. "Free radical scavenging and antioxidant effects of lactate ion: an in vitro study." *The Journal of Applied Physiology* 89 (1): 169-75. doi:10.1152/jappl.2000.89.1.169.

Gruber, A D, R C Elble, H L Ji, K D Schreur, C M Fuller, and B U Pauli. 1998. "Genomic cloning, molecular characterization, and functional analysis of human CLCA1, the first human member of the family of Ca2+-activated Cl- channel proteins." *Genomics* 54 (2): 200-14. doi:10.1006/geno.1998.5562.

Guilmeau, S, I Niot, J P Laigneau, H Devaud, V Petit, N Brousse, R Bouvier, et al. 2007. "Decreased expression of Intestinal I- and L-FABP levels in rare human genetic lipid malabsorption syndromes." *Histochemistry and Cell Biology* 128 (2): 115-23. doi:10.1007/s00418-007-0302-x.

Gunaratne, Gihan S, Yang Yang, Fang Li, Timothy F Walseth, and Jonathan S Marchant. 2018. "NAADP-dependent Ca 2+ signaling regulates Middle East respiratory syndrome-coronavirus pseudovirus translocation through the endolysosomal system." *Cell Calcium* 75: 30-41. doi:10.1016/j.ceca.2018.08.003.

Gunawardene, Ashok R, Bernard M Corfe, and Carolyn A Staton. 2011. "Classification and functions of enteroendocrine cells of the lower gastrointestinal tract." *International Journal of Experimental Pathology* 92 (4): 219-31. doi:10.1111/j.1365-2613.2011.00767.x.

Günzel, Dorothee, and Alan SL Yu. 2013. "Claudins and the modulation of tight junction permeability." *Physiological Reviews* 93 (2): 525-69. doi:10.1152/physrev.00019.2012.

Gustafsson, J K, A Ermund, M EV Johansson, A Schütte, G C Hansson, and H Sjövall. 2012. "An ex vivo method for studying mucus formation, properties, and thickness in human colonic biopsies and mouse small and large intestinal explants." *The American Journal of Physiology-Gastrointestinal and Liver Physiology* 302 (4): G430-8. doi:10.1152/ajpgi.00405.2011.

Györke, S, V Lukyanenko, and I Györke. 1997. "Dual effects of tetracaine on spontaneous calcium release in rat ventricular myocytes." *The Journal of Physiology* 500 (Pt2): 297-309. doi:10.1113/jphysiol.1997.sp022021.

Haber, Adam L, Moshe Biton, Noga Rogel, Rebecca H Herbst, Karthik Shekhar, Christopher Smillie, Grace Burgin, et al. 2018. "A single-cell survey of the small intestinal epithelium." *Nature* 551 (7680): 333-39. doi:10.1038/nature24489.

Haberberger, Rainer, Gerhard Schultheiss, and Martin Diener. 2006. "Epithelial muscarinic M1 receptors contribute to carbachol-induced ion secretion in mouse colon." *European Journal of Pharmacology* 530 (3): 229-33. doi:10.1016/j.ejphar.2005.11.055.

Halm, D R, and S T Halm. 2000. "Secretagogue response of goblet cells and columnar cells in human colonic crypts." *The American Journal of Physiology-Cell Physiology* 278 (1): C212-33. doi:10.1152/ajpcell.2000.278.1.C212.

Han, Bin, Chao Zhang, Shoufeng Liu, Yiping Xia, Hao Sun, Zhongying Gong, Alain R Simard, Qiang Liu, and Junwei Hao. 2017. "Non-neuronal cholinergic activity is potentiated in myasthenia gravis." *BMC Neurology* 17 (1): 28. doi:10.1186/s12883-016-0772-3.

Haramis, Anna-Pavlina G, Harry Begthel, Maaike van den Born, Johan van Es, Suzanne Jonkheer, G JA Offerhaus, and Hans Clevers. 2004. "De novo crypt formation and juvenile polyposis on BMP inhibition in mouse intestine." *Science* 303 (5664): 1684-6. doi:10.1126/science.1093587.

Hardcastle, J, P T Hardcastle, and J M Noble. 1984. "The involvement of calcium in the intestinal response to secretagogues in the rat." *The Journal of Physiology* 355: 465-78. doi:10.1113/jphysiol.1984.sp015432.

Harris, Tony JC, and Ulrich Tepass. 2010. "Adherens junctions: from molecules to morphogenesis." *Nature Reviews Molecular Cell Biology* 11 (7): 502-14. doi:10.1038/nrm2927.

Hartmann, V, and H Magnussen. 1985. "Effect of diltiazem on histamine- and carbachol-induced bronchospasm in normal and asthmatic subjects." *Chest* 87 (2): 174-9. doi:10.1378/chest.87.2.174.

Hasnain, Sumaira Z, Huaqing Wang, Jean-Eric Ghia, Nihal Haq, Yikang Deng, Anna Velcich, Richard K Grencis, David J Thornton, and Waliul I Khan. 2010. "Mucin gene deficiency in mice impairs host resistance to an enteric parasitic infection." *Gastroenterology* 138 (5): 1763-71. doi:10.1053/j.gastro.2010.01.045.

Hatanaka, Hisashi, Shuji Takada, Young Lim Choi, Shin-ichiro Fujiwara, Manabu Soda, Munehiro Enomoto, Kentaro Kurashina, et al. 2007. "Transforming activity of purinergic receptor P2Y, G-protein coupled, 2 revealed by retroviral expression screening." *Biochemical and Biophysical Research Communications* 356 (3): 723-6. doi:10.1016/j.bbrc.2007.03.048.

Hauso, Ø, B I Gustafsson, and H L Waldum. 2007. "Long slender cytoplasmic extensions: a common feature of neuroendocrine cells?" *Journal of Neuroendocrinology* 19 (9): 739-42. doi:10.1111/j.1365-2826.2007.01578.x.

Hayakawa, Yoku, Kosuke Sakitani, Mitsuru Konishi, Samuel Asfaha, Ryota Niikura, Hiroyuki Tomita, Bernhard W Renz, et al. 2017. "Nerve Growth Factor Promotes Gastric Tumorigenesis through Aberrant Cholinergic Signaling." *Cancer Cell* 31 (1): 21-34. doi:10.1016/j.ccell.2016.11.005.

He, Tianzhen, De Yang, Xiao-Qing Li, Mengmeng Jiang, Md Sahidul Islam, Shaokui Chen, Yibo Chen, et al. 2020. "Inhibition of two-pore channels in antigen-presenting cells promotes the expansion of TNFR2-expressing CD4 + Foxp3 + regulatory T cells." *Science Advances* 6 (40): eaba6584. doi:10.1126/sciadv.aba6584.

He, Xi C, Jiwang Zhang, Wei-Gang Tong, Ossama Tawfik, Jason Ross, David H Scoville, Qiang Tian, et al. 2004. "BMP signaling inhibits intestinal stem cell self-renewal through suppression of Wnt-beta-catenin signaling." *Nature Genetics* 36 (10): 1117-21. doi:10.1038/ng1430.

Henry, P D. 1980. "Comparative pharmacology of calcium antagonists: nifedipine, verapamil and diltiazem." *American Journal of Cardiology* 46 (6): 1047-58. doi:10.1016/0002-9149(80)90366-5.

Herath, Madushani, Suzanne Hosie, Joel C Bornstein, Ashley E Franks, and Elisa L Hill-Yardin. 2020. "The Role of the Gastrointestinal Mucus System in Intestinal Homeostasis: Implications for Neurological Disorders." *Frontiers in Cellular and Infection Microbiology* 10: 248. doi:10.3389/fcimb.2020.00248.

Hershberg, R M, and L F Mayer. 2000. "Antigen processing and presentation by intestinal epithelial cells - polarity and complexity." *Immunology Today* 21 (3): 123-8. doi:10.1016/s0167-5699(99)01575-3.

Hershberg, R M, P E Framson, D H Cho, L Y Lee, S Kovats, J Beitz, J S Blum, and G T Nepom. 1997. "Intestinal epithelial cells use two distinct pathways for HLA class II antigen processing." *Journal of Clinical Investigation* 100 (1): 204-15. doi:10.1172/JCI119514.

Hidalgo, Cecilia, Gina Sánchez, Genaro Barrientos, and Paula Aracena-Parks. 2006. "A transverse tubule NADPH oxidase activity stimulates calcium release from isolated triads via ryanodine receptor type 1 S -glutathionylation." *Journal of Biological Chemistry* 281 (36): 26473-82. doi:10.1074/jbc.M600451200.

Hilkens, J, F Buijs, and M Ligtenberg. 1989. "Complexity of MAM-6, an epithelial sialomucin associated with carcinomas." *Cancer Research* 49 (4): 786-93. https://pubmed.ncbi.nlm.nih.gov/2643463/.

Hill, David B, Robert F Long, William J Kissner, Eyad Atieh,, Ian C Garbarine, Matthew R Markovetz, Nicholas C Fontana, et al. 2018. "Pathological mucus and impaired mucus clearance in cystic fibrosis patients result from increased concentration, not altered pH." *European Respiratory Journal* 52 (6). doi:10.1183/13993003.01297-2018.

Hill, M J. 1997. "Intestinal flora and endogenous vitamin synthesis." *European Journal of Cancer Prevention* 6 (Suppl 1): 43-5. doi:10.1097/00008469-199703001-00009.

Hilliard, Fredrick A, Derek S Steele, Derek Laver, Zhaokang Yang, Sylvain J Le Marchand, Nagesh Chopra, David W Piston, Sabine Huke, and Björn C Knollmann. 2010. "Flecainide inhibits arrhythmogenic Ca2+ waves by open state block of ryanodine receptor Ca2+ release channels and reduction of Ca2+ spark mass." *The Journal of Molecular and Cellular Cardiology* 48 (2): 293-301. doi:10.1016/j.yjmcc.2009.10.005.

Hillman, Ethan T, Hang Lu, Tianming Yao, and Cindy H Nakatsu. 2017. "Microbial Ecology along the Gastrointestinal Tract." *Microbes and Environments* 32 (4): 300-13. doi:10.1264/jsme2.ME17017.

Hirota, C L, and B M McKay. 2006. "Cholinergic Regulation of Epithelial Ion Transport in the Mammalian Intestine." *British Journal of Clinical Pharmacology* 149 (5): 463-79. doi:10.1038/sj.bjp.0706889.

Hirota, Christina L, and Derek M McKay. 2006. "M3 muscarinic receptor-deficient mice retain bethanechol-mediated intestinal ion transport and are more sensitive to colitis." *Canadian Journal of Physiology and Pharmacology* 84 (11): 1153-61. doi:10.1139/y06-068.

Hirota, S, K Isozaki, Y Moriyama, K Hashimoto, T Nishida, S Ishiguro, K Kawano, et al. 1998. "Gain-of-function mutations of c-kit in human gastrointestinal stromal tumors." *Science* 279 (5350): 577-80. doi:10.1126/science.279.5350.577.

Ho, S B, A M Roberton, L L Shekels, C T Lyftogt, G A Niehans, and N W Toribara. 1995. "Expression cloning of gastric mucin complementary DNA and localization of mucin gene expression." *Gastroenterology* 109 (3): 735-47. doi:10.1016/0016-5085(95)90380-1.

Ho, Tracy, Andrew I Jobling, Ursula Greferath, Trinette Chuang, Archana Ramesh, Erica L Fletcher, and Kirstan A Vessey. 2015. "Vesicular expression and release of ATP from dopaminergic neurons of the mouse retina and midbrain." *Frontiers in Cellular Neuroscience* 9: 389. doi:10.3389/fncel.2015.00389.

Hollenhorst, Monika I, Innokentij Jurastow, Rajender Nandigama, Silke Appenzeller, Lei Li, Jörg Vogel, Stephanie Wiederhold, et al. 2020. "Tracheal brush cells release acetylcholine in response to bitter tastants for paracrine and autocrine signaling." *The FASEB Journa* 34 (1): 316-32. doi:10.1096/fj.201901314RR.

Hollister, Emily B, Chunxu Gao, and James Versalovic. 2015. "Compositional and Functional Features of the Gastrointestinal Microbiome and Their Effects on Human Health." *Gastroenterology* 146 (6): 1449-58. doi:10.1053/j.gastro.2014.01.052.

Hoover, Ben, Valentina Baena, Melanie M Kaelberer, Feven Getaneh, Skarleth Chinchilla, and Diego V Bohórquez. 2017. "The intestinal tuft cell nanostructure in 3D." *Scientific Reports* 7 (1): 1652. doi:10.1038/s41598-017-01520-x.

Hoth, M, and R Penner. 1993. "Calcium release-activated calcium current in rat mast cells." *Journal of Physiology* 465: 359-86. doi:10.1113/jphysiol.1993.sp019681.

Hou, Qihang, Lulu Ye, Lulu Huang, and Qinghua Yu. 2017. "The Research Progress on Intestinal Stem Cells and Its Relationship with Intestinal Microbiota." *Frontiers in Immunology* 8 (599): 1-9. doi:10.3389/fimmu.2017.00599.

Hou, Xiaowei, Leanne Pedi, Melinda M Diver, and Stephen B Long. 2012. "Crystal structure of the calcium release-activated calcium channel Orai." *Science* 338 (6112): 1308-13. doi:10.1126/science.1228757.

Hounnou, G, C Destrieux, J Desmé, P Bertrand, and S Velut. 2001. "Anatomical study of the length of the human intestine." *Surgical and Radiologic Anatomy* 24: 290-4. doi:10.1007/s00276-002-0057-y.

Howitt, Michael R, Sydney Lavoie, Monia Michaud, Arthur M Blum, Sara V Tran, Joel V Weinstock, Carey Ann Gallini, et al. 2016. "Tuft Cells, Taste-Chemosensory Cells, Orchestrate Parasite Type 2 Immunity in the Gut." *Science* 351 (6279): 1329-33. doi:10.1126/science.aaf1648.

Hu, Zhan-Dong, Jun Yan, Kai-Yue Cao, Zhi-Qi Yin, Wei-Wei Xin, and Ming-Fang Zhang. 2019. "MCOLN1 Promotes Proliferation and Predicts Poor Survival of Patients with Pancreatic Ductal Adenocarcinoma." *Disease Markers* 2019: 9436047. doi:10.1155/2019/9436047.

Huang, Lei, Dongshu Chen, Derek Liu, Li Yin, Surender Kharbanda, and Donald Kufe. 2005. "MUC1 oncoprotein blocks glycogen synthase kinase 3beta-mediated phosphorylation and degradation of beta-catenin." *Cancer Research* 65 (22): 10413-22. doi:10.1158/0008-5472.CAN-05-2474.

Huang, Xin, Tony E Godfrey, William E Gooding, Kenneth Jr S McCarty, and Susanne M Gollin. 2006. "Comprehensive genome and transcriptome analysis of the 11q13 amplicon in human oral cancer and synteny to the 7F5 amplicon in murine oral carcinoma." *Genes Chromosomes and Cancer* 45 (11): 1058-69. doi:10.1002/gcc.20371.

Huels , David J, Rachel A Ridgway, Sorina Radulescu, Marc Leushacke, Andrew D Campbell, Sujata Biswas, Simon Leedham, et al. 2015. "E-cadherin can limit the transforming properties of activating β-catenin mutations." *The EMBO Journal* 34 (18): 2321-33. doi:10.15252/embj.201591739.

Jadhav, Unmesh, Madhurima Saxena, Nicholas K O'Neill, Assieh Saadatpour, Guo-Cheng Yuan, Zachary Herbert, Kazutaka Murata, and Ramesh A Shivdasani. 2018. "Dynamic reorganization of chromatin accessibility signatures during dedifferentiation of secretory precursors into Lgr5+ intestinal stem cells." *Cell Stem Cell* 21 (1): 65-75. doi:10.1016/j.stem.2017.05.001.

Jaimovich, Enrique, César Mattei, José Luis Liberona, Cesar Cardenas, Manuel Estrada, Julien Barbier, Cécile Debitus, Dominique Laurent, and Jordi Molgó. 2005. "Xestospongin B, a competitive inhibitor of IP3-mediated Ca2+ signalling in cultured rat myotubes, isolated myonuclei, and neuroblastoma (NG108-15) cells." *FEBS Letters* 579 (10): 2051-7. doi:10.1016/j.febslet.2005.02.053.

Jang, Myoung Ho, Mi-Na Kweon, Koichi Iwatani, Masafumi Yamamoto, Kazutaka Terahara, Chihiro Sasakawa, Toshihiko Suzuki, et al. 2004. "Intestinal villous M cells: an antigen entry site in the mucosal epithelium." *PNAS* 101 (16): 6110-5. doi:10.1073/pnas.0400969101.

Jensen, Pia Hønnerup, Simon Mysling, Peter Højrup, and Ole Nørregaard Jensen. 2013. "Glycopeptide enrichment for MALDI-TOF mass spectrometry analysis by hydrophilic interaction liquid chromatography solid phase extraction (HILIC SPE)." *Methods in Molecular Biology* 951: 131-44. doi:10.1007/978-1-62703-146-2_10.

Jeong, Danielle, Daniela Lozano Casasbuenas, Archana Gengatharan, Kyshona Edwards, Armen Saghatelyan, David R Kaplan, Freda D Miller, and Scott A Yuzwa. 2020. "LRIG1-Mediated Inhibition of EGF Receptor Signaling Regulates Neural Precursor Cell Proliferation in the Neocortex." *Cell Reports* 33 (2): 108257. doi:10.1016/j.celrep.2020.108257.

Jha, Archana, Malini Ahuja, Sandip Patel, Eugen Brailoiu, and Shmuel Muallem. 2014. "Convergent regulation of the lysosomal two-pore channel-2 by Mg^{2+}, NAADP, $PI(3,5)P_2$ and multiple protein kinases." *The EMBO Journal* 33 (5): 501-11. doi:10.1002/embj.201387035.

Jiang, Dawei, Bailong Xiao, Dongmei Yang, Ruiwu Wang, Philip Choi, Lin Zhang, Heping Cheng, and S RW Chen. 2004. "RyR2 mutations linked to ventricular tachycardia and sudden death reduce the threshold for store-overload-induced Ca2+ release (SOICR)." *PNAS* 101 (35): 13062-7. doi:10.1073/pnas.0402388101.

Jiménez, Esther, Leonides Fernández, María L Marín, Juan M Odriozola, Carmen Nueno-Palop, Arjan Narbad, Mónica Olivares, Jordi Xaus, and Juan M Rodríguez. 2005. "Isolation of Commensal Bacteria from Umbilical Cord Blood of Healthy Neonates Born by Cesarean Section." *Current Microbiology* 51: 270-4. doi:10.1007/s00284-005-0020-3.

Jin, Xuhui, Yuxuan Zhang, Abeer Alharbi, Ali Hanbashi, Ali Alhoshani, and John Parrington. 2020. "Targeting Two-Pore Channels: Current Progress and Future Challenges." *Trends in Pharmacological Sciences* 41 (8): 582-94. doi:10.1016/j.tips.2020.06.002.

Johansson, Barbro B. 2007. "Regeneration and plasticity in the brain and spinal cord." *Journal of Cerebral Blood Flow & Metabolism* 27 (8): 1417-30. doi:10.1038/sj.jcbfm.9600486.

Johansson, Malin E V, Mia Phillipson, Joel Petersson, Anna Velcich, Lena Holm, and Gunnar C Hansson. 2008. "The inner of the two Muc2 mucin-dependent mucus layers in colon is devoid of bacteria." *PNAS* 105 (39): 15064-9. doi:10.1073/pnas.0803124105.

Johansson, Malin EV. 2012. "Fast renewal of the distal colonic mucus layers by the surface goblet cells as measured by in vivo labeling of mucin glycoproteins." *PLoS One* 7 (7): e41009. doi:10.1371/journal.pone.0041009.

Johansson, Malin EV, Henrik Sjövall, and Gunnar C Hansson. 2013. "The gastrointestinal mucus system in health and disease." *Nature Reviews Gastroenterology & Hepatology* 10 (6): 352-61. doi:10.1038/nrgastro.2013.35.

Johnson, Darryl, Barry Boyes, and Ron Orlando. 2013. "The Use of Ammonium Formate as a Mobile-Phase Modifier for LC-MS/MS Analysis of Tryptic Digests." *Journal of Biomolecular Techniques* 24 (4): 187-97. doi:10.7171/jbt.13-2404-005.

Jones, Ben, Stephen R Bloom, Teresa Buenaventura, Alejandra Tomas, and Guy A Rutter. 2018. "Control of insulin secretion by GLP-1." *Peptides* 100: 75-84. doi:10.1016/j.peptides.2017.12.013.

Joo, Min Cheol, Yong Sung Kim, Eul Sik Choi, Jung Taek Oh, Hyun Joon Park, and Moon Young Lee. 2011. "Changes in the Muscarinic Receptors on the Colonic Smooth Muscles of Rats with Spinal Cord Injury." *Annals of Rehabilitation Medicine* 35 (5): 589-98. doi:10.5535/arm.2011.35.5.589.

Jositsch, Gitte, Tamara Papadakis, Rainer V Haberberger, Miriam Wolff, Jürgen Wess, and Wolfgang Kummer. 2009. "Suitability of muscarinic acetylcholine receptor antibodies for

immunohistochemistry evaluated on tissue sections of receptor gene-deficient mice."
Naunyn-Schmiedeberg's Archives of Pharmacology 379 (4): 389-95. doi:10.1007/s00210-008-0365-9.

Jung, Jewon, Kwang-Jin Cho, Ali K Naji, Kristen N Clemons, Ching On Wong, Mariana Villanueva, Steven Gregory, et al. 2019. "HRAS-driven cancer cells are vulnerable to TRPML1 inhibition." *EMBO Reports* 20 (4): e46685. doi:10.15252/embr.201846685.

Jung, Peter, Christian Sommer, Francisco M Barriga, Simon J Buczacki, Xavier Hernando-Momblona, Marta Sevillano, Miquel Duran-Frigola, et al. 2015. "Isolation of Human Colon Stem Cells Using Surface Expression of PTK7." *Stem Cell Reports* 5 (6): 979-87. doi:10.1016/j.stemcr.2015.10.003.

Kachintorn, U, M Vajanaphanich, A E Traynor-Kaplan, K Dharmsathaphorn, and K E Barrett. 1993. "Activation by calcium alone of chloride secretion in T84 epithelial cells." *British Journal of Pharmacology* 109 (2): 510-7. doi:10.1111/j.1476-5381.1993.tb13599.x.

Kahwati, Leila C, Rachel Palmieri Weber, Huiling Pan, Margaret Gourlay, Erin LeBlanc, Manny Coker-Schwimmer, and Meera Viswanathan. 2018. "Vitamin D, Calcium, or Combined Supplementation for the Primary Prevention of Fractures in Community-Dwelling Adults: Evidence Report and Systematic Review for the US Preventive Services Task Force." *The Journal of the American Medical Association* 319 (15): 1600-12. doi:10.1001/jama.2017.21640.

Kam, Christy Siu Kei. 2015. *MECHANISM AND ROLE OF CALCIUM IN EXCITATION-MUCUS SECRETION COUPLING IN HUMAN COLONIC EPITHELIUM.* Norwich: University of East Anglia.

Kandiah, Nagaendran, Ming-Chyi Pai, Vorapun Senanarong, Irene Looi, Encarnita Ampil, Kyung Won Park, Ananda Krishna Karanam, and Stephen Christopher. 2017. "Rivastigmine: the advantages of dual inhibition of acetylcholinesterase and butyrylcholinesterase and its role in subcortical vascular dementia and Parkinson's disease dementia." *Clinical Interventions in Aging* 12: 697-707. doi:10.2147/CIA.S129145.

Kang, Sang Soo, Kyung-Seok Han, Bo Mi Ku, Yeon Kyung Lee, Jinpyo Hong, Hye Young Shin, Antoine G Almonte, et al. 2010. "Caffeine-mediated inhibition of calcium release channel inositol 1,4,5-trisphosphate receptor subtype 3 blocks glioblastoma invasion and extends survival." *Cancer Research* 70 (3): 1173-83. doi:10.1158/0008-5472.CAN-09-2886.

Karra, Efthimia, Keval Chandarana, and Rachel L Batterham. 2009. "The role of peptide YY in appetite regulation and obesity." *Journal of Physiology* 587: 19-25. doi:10.1113/jphysiol.2008.164269.

Kashfi, Seyed MH, Sheema Almozyan, Nicholas Jinks, Bon-Kyoung Koo, and Abdolrahman S Nateri. 2018. "Morphological alterations of cultured human colorectal matched tumour and healthy organoids." *Oncotarget* 9 (12): 10572-84. doi:10.18632/oncotarget.24279.

Kaske, Silke, Gabriele Krasteva, Peter König, Wolfgang Kummer, Thomas Hofmann, Thomas Gudermann, and Vladimir Chubanov. 2007. "TRPM5, a taste-signaling transient receptor potential ion-channel, is a ubiquitous signaling component in chemosensory cells." *BMC Neuroscience* 8 (49). doi:10.1186/1471-2202-8-49.

Kawashima, K, H Oohata, K Fujimoto, and T Suzuki. 1987. "Plasma concentration of acetylcholine in young women." *Neuroscience Letters* 80 (3): 339-42. doi:10.1016/0304-3940(87)90478-2.

Kay, Sophie K, Heather A Harrington, Sarah Shepherd, Keith Brennan, Trevor Dale, James M Osborne, David J Gavaghan, and Helen M Byrne. 2017. "The role of the Hes1 crosstalk hub in Notch-Wnt interactions of the intestinal crypt." *PLOS Computational Biology* 13 (2). doi:10.1371/journal.pcbi.1005400.

Kayahara, Takahisa, Mitsutaka Sawada, Shigeo Takaishi, Hirokazu Fukui, Hiroshi Seno, Hiroaki Fukuzawa, Katsumasa Suzuki, et al. 2003. "Candidate markers for stem and early progenitor cells, Musashi-1 and Hes1, are expressed in crypt base columnar cells of mouse small intestine." *FEBS Letters* 535 (1-3): 131-5. doi:10.1016/s0014-5793(02)03896-6.

Keely, Stephen J. 2011. "Epithelial acetylcholine – a new paradigm for cholinergic regulation of intestinal fluid and electrolyte transport." *The Journal of Physiology* 589 (Pt4): 771-2. doi:10.1113/jphysiol.2010.204263.

Khan, K, R Hardy, A Haq, O Ogunbiyi, D Morton, and M Chidgey. 2006. "Desmocollin switching in colorectal cancer." *British Journal of Cancer* 95 (10): 1367-70. doi:10.1038/sj.bjc.6603453.

Khan, Nabab, Peter W Halcrow, Koffi L Lakpa, Zahra Afghah, Nicole M Miller, Steven F Dowdy, Jonathan D Geiger, and Xuesong Chen. 2020. "Two-pore channels regulate Tat endolysosome escape and Tat-mediated HIV-1 LTR transactivation." *The FASEB Journa* 34 (3): 4147-62. doi:10.1096/fj.201902534R.

Khananshvili, Daniel. 2014. "Sodium-calcium exchangers (NCX): molecular hallmarks underlying the tissue-specific and systemic functions." *Pflügers Archiv* 466 (1): 43-60. doi:10.1007/s00424-013-1405-y.

Khananshvili, Daniel. 2013. "The SLC8 gene family of sodium-calcium exchangers (NCX) - structure, function, and regulation in health and disease." *Molecular Aspects of Medicine* 34 (2-3): 220-35. doi:10.1016/j.mam.2012.07.003.

Khatri, I A, C Ho, R D Specian, and J F Forstner. 2001. "Characteristics of rodent intestinal mucin Muc3 and alterations in a mouse model of human cystic fibrosis." *American Journal of Physiology-Gastrointestinal and Liver Physiology* 280 (6): G1321-30. doi:10.1152/ajpgi.2001.280.6.G1321.

Kidder, G 3rd W. 1973. "Effects of the ATP analog 5'-adenylyl methylenediphosphonate on acid secretion in frog gastric mucosa." *Biochimica et Biophysica Acta* 298 (3): 732-42. doi:10.1016/0005-2736(73)90090-4.

Kilpatrick, Bethan S, Emily R Eden, Anthony H Schapira, Clare E Futter, and Sandip Patel. 2013. "Direct mobilisation of lysosomal Ca2+ triggers complex Ca2+ signals." *Journal of Cell Science* 126 (Pt1): 60-6. doi:10.1242/jcs.118836.

Kim , Ki-Wook, Alexandra Vallon-Eberhard, Ehud Zigmond, Julia Farache, Elias Shezen, Guy Shakhar, Andreas Ludwig, Sergio A Lira, and Steffen Jung. 2011. "In vivo structure/function and expression analysis of the CX3C chemokine fractalkine." *Blood* 118 (22): 156-67. doi:10.1182/blood-2011-04-348946.

Kim, Chang-Kyung, Vincent W Yang, and Agnieszka B Bialkowska. 2017. "The Role of Intestinal Stem Cells in Epithelial Regeneration Following Radiation-Induced Gut Injury." *Current Stem Cell Reports* 3 (4): 320-332. doi:10.1007/s40778-017-0103-7.

Kim, Dong Chul, Hana Jin, Jong Sil Lee, Euna Son, Gyeong Won Lee, and Hye Jung Kim . 2020. "P2Y2 R has a significant correlation with Notch-4 in patients with breast cancer." *Oncology Letters* 20 (1): 647-54. doi:10.3892/ol.2020.11630.

Kim, Hyun Jin, Abigail A Soyombo, Sandra Tjon-Kon-Sang, Insuk So, and Shmuel Muallem. 2009. "The Ca(2+) channel TRPML3 regulates membrane trafficking and autophagy." *Traffic* 10 (8): 1157-67. doi:10.1111/j.1600-0854.2009.00924.x.

Kim, Myunghoo, Carolina Galan, Andrea A Hill, Wan-Jung Wu, Hannah Fehlner-Peach, Hyo Won Song, Deborah Schady, et al. 2019. "Critical role for the microbiota in CX3CR1+ intestinal mononuclear phagocyte regulation of intestinal T cell responses." *Immunity* 49 (1): 151-63. doi:10.1016/j.immuni.2018.05.009.

Kim, Tae-Hee, Silvia Escudero, and Ramesh A Shivdasani. 2012. "Intact function of Lgr5 receptor-expressing intestinal stem cells in the absence of Paneth cells." *Proceedings of the National Academy of Sciences* 109 (10): 3932-7. doi:10.1073/pnas.1113890109.

Kim, Young S, and Samuel B Ho. 2010. "Intestinal goblet cells and mucins in health and disease: recent insights and progress." *Current Gastroenterology Reports* 12 (5): 319-30. doi:10.1007/s11894-010-0131-2.

Kimura, Tomohiko, Atsushi Obata, Masashi Shimoda, Ikki Shimizu, Gabriela da Silva Xavier, Seizo Okauchi, Hidenori Hirukawa, et al. 2018. "Down-regulation of vascular GLP-1 receptor expression in human subjects with obesity." *Scientific Reports* 8: 10644. doi:10.1038/s41598-018-28849-1.

Kintzer, Alexander F, and Robert M Stroud. 2018. "On the structure and mechanism of two-pore channels." *The FEBS Journal* 285 (2): 233-243. doi:10.1111/febs.14154.

Klein, Sabine, Barbara Seidler, Anna Kettenberger, Andrei Sibaev, Michael Rohn, Robert Feil, Hans-Dieter Allescher, et al. 2013. "Interstitial cells of Cajal integrate excitatory and inhibitory neurotransmission with intestinal slow-wave activity." *Nature Communications* 4. doi:10.1038/ncomms2626.

Kleinman, Hynda K, and George R Martin. 2005. "Matrigel: basement membrane matrix with biological activity." *Seminars in Cancer Biology* 15 (5): 378-86. doi:10.1016/j.semcancer.2005.05.004.

Knight, P A, J K Brown, and A D Pemberton. 2008. "Innate immune response mechanisms in the intestinal epithelium: potential roles for mast cells and goblet cells in the expulsion of adult Trichinella spiralis." *Parasitology* 135 (6): 655-70. doi:10.1017/S0031182008004319.

Kobayashi, Hotaka, and Mitsunori Fukuda. 2013. "Arf6, Rab11 and transferrin receptor define distinct populations of recycling endosomes." *Communcative & Integrative Biology* 6 (5): e25036. doi:10.4161/cib.25036.

Kolterud, Asa, Ann S Grosse, William J Zacharias, Katherine D Walton, Katherine E Kretovich, Blair B Madison, Meghna Waghray, et al. 2009. "Paracrine Hedgehog signaling in stomach and

intestine: new roles for hedgehog in gastrointestinal patterning." *Gastroenterology* 137 (2): 618-28. doi:10.1053/j.gastro.2009.05.002.

Konishi, Mitsuru, Yoku Hayakawa, and Kazuhiko Koike. 2019. "Role of Muscarinic Acetylcholine Signaling in Gastrointestinal Cancers." *Biomedicines* 7 (3). doi:10.3390/biomedicines7030058.

Koo, Bon-Kyoung, Maureen Spit, Ingrid Jordens, Teck Y Low, Daniel E Stange, Marc van de Wetering, Johan H van Es, et al. 2012. "Tumour suppressor RNF43 is a stem-cell E3 ligase that induces endocytosis of Wnt receptors." *Nature* 488 (7413): 665-9. doi:10.1038/nature11308.

Korinek, V, N Barker, P J Morin, D van Wichen, R de Weger, K W Kinzler, B Vogelstein, and H Clevers. 1997. "Constitutive transcriptional activation by a beta-catenin-Tcf complex in APC-/- colon carcinoma." *Science* 275 (5307): 1784-7. doi:10.1126/science.275.5307.1784.

Kosinski, Cynthia, Daniel E Stange, Chuanrui Xu, Annie Sy Chan, Coral Ho, Siu Tsan Yuen, Randy C Mifflin, et al. 2010. "Indian hedgehog regulates intestinal stem cell fate through epithelial-mesenchymal interactions during development." *Gastroenterology* 139 (3): 893-903. doi:10.1053/j.gastro.2010.06.014.

Kosinski, Cynthia, Vivian SW Li, Annie SY Chan, Ji Zhang, Coral Ho, Wai Yin Tsui, Tsun Leung Chan, et al. 2007. "Gene expression patterns of human colon tops and basal crypts and BMP antagonists as intestinal stem cell niche factors." *PNAS* 104 (39): 15418-23. doi:10.1073/pnas.0707210104.

Kreda, Silvia M, Lucia Seminario-Vidal, Catharina A van Heusden, Wanda O'Neal, Lisa Jones, Richard C Boucher, and Eduardo R Lazarowski. 2010. "Receptor-promoted exocytosis of airway epithelial mucin granules containing a spectrum of adenine nucleotides." *Journal of Physiology* 588 (Pt12): 2255-67. doi:10.1113/jphysiol.2009.186643.

Kruse, Andrew C, Brian K Kobilka, Dinesh Gautam, Patrick M Sexton, Arthur Christopoulos, and Jürgen Wess. 2014. "Muscarinic acetylcholine receptors: novel opportunities for drug development." *Nature Reviews Drug Discovery* 13: 549-60. doi:10.1038/nrd4295.

Krutetskaia, Z I, O E Lebedev, N I Krutetskaia, and T V Petrova. 1997. "Organic and inorganic blockers of potential-dependent Ca2+ channels inhibit store-dependent entry of Ca2+ into rat peritoneal macrophages." *Tsitologiia* 39 (12): 1131-41. https://pubmed.ncbi.nlm.nih.gov/9505352/.

Kuipers, Ernst J, William M Grady, David Lieberman, Thomas Seufferlein, Joseph J Sung, Petra G Boelens, Cornelis JH van de Velde, and Toshiaki Watanabe. 2016. "COLORECTAL CANCER." *Nature Reviews Disease Primers* 1: 15065. doi:10.1038/nrdp.2015.65.

Kummer, Wolfgang, and Gabriela Krasteva-Christ. 2014. "Non-neuronal cholinergic airway epithelium biology." *Current Opinion in Pharmacology* 16: 43-9. doi:10.1016/j.coph.2014.03.001.

Künzli, Beat M, Maria-Isabell Bernlochner, Stephan Rath, Samuel Käser, Eva Csizmadia, Keiichi Enjyoji, Peter Cowan, et al. 2011. "Impact of CD39 and purinergic signalling on the growth and metastasis of colorectal cancer." *Purinergic Signalling* 7 (2): 232-41. doi:10.1007/s11302-011-9228-9.

Lagostena, Laura, Margherita Festa, Michael Pusch, and Armando Carpaneto. 2017. "The human two-pore channel 1 is modulated by cytosolic and luminal calcium." *Scientific Reports* 7: 43900. doi:10.1038/srep43900.

Lamprecht, G, and U Seidler. 2006. "The emerging role of PDZ adapter proteins for regulation of intestinal ion transport." *American Journal of Physiology-Gastrointestinal and Liver Physiology* 291 (5): G766-77. doi:10.1152/ajpgi.00135.2006.

Leal, Jasmim, Hugh DC Smyth, and Debadyuti Ghosh. 2018. "Physicochemical properties of mucus and their impact on transmucosal drug delivery." *International Journal of Pharmaceutics* 532 (1): 555-72. doi:10.1016/j.ijpharm.2017.09.018.

Leblond, C P, and C E Stevens. 1948. "The constant renewal of the intestinal epithelium in the albino rat." *The Anatomical Record:* 100 (3): 357-77. doi:10.1002/ar.1091000306.

Lei, Weiwei, Wenwen Ren, Makoto Ohmoto, Joseph Jr F Urban, Ichiro Matsumoto, Robert F Margolskee, and Peihua Jiang. 2018. "Activation of intestinal tuft cell-expressed Sucnr1 triggers type 2 immunity in the mouse small intestine." *PNAS* 115 (21): 5552-7. doi:10.1073/pnas.1720758115.

Leipziger, J, J Thomas, P Rubini-Illes, R Nitschke, and R Greger. 1996. "8-(N,N-diethylamino)octyl 3,4,5-trimethoxybenzoate (TMB-8) acts as a muscarinic receptor antagonist in the epithelial cell line HT29." *Naunyn-Schmiedeberg's Archives of Pharmacology* 353 (3): 295-301. doi:10.1007/BF00168631.

Levitin, Fiana, Omer Stern, Mordechai Weiss, Chava Gil-Henn, Ravit Ziv, Zofnat Prokocimer, Nechama I Smorodinsky, Daniel B Rubinstein, and Daniel H Wreschner. 2005. "The MUC1 SEA module is a self-cleaving domain." *Journal of Biological Chemistry* 280 (39): 33374-86. doi:10.1074/jbc.M506047200.

Li, Hui Joyce, Archana Kapoor, Maryann Giel-Moloney, Guido Rindi, and Andrew B Leiter. 2012. "Notch signaling differentially regulates the cell fate of early endocrine precursor cells and their maturing descendants in the mouse pancreas and intestine." *Developmental Biology* 371 (2): 156-69. doi:10.1016/j.ydbio.2012.08.023.

Li, Linheng, and Hans Clevers. 2014. "Coexistence of Quiescent and Active Adult Stem Cells in Mammals." *Science* 327 (5965): 542-5. doi:10.1126/science.1180794.

Li, Mufeng, Shai D Silberberg, and Kenton J Swartz. 2013. "Subtype-specific control of P2X receptor channel signaling by ATP and Mg2+." *PNAS* 110 (36): 3455-63. doi:10.1073/pnas.1308088110.

Liang, Shaonan, Xue-Kun Guo, Jiayao Ou, Rongyao Huang, Qing Xue, Bin Zhang, Yeonseok Chung, et al. 2019. "Nutrient Sensing by the Intestinal Epithelium Orchestrates Mucosal Antimicrobial Defense via Translational Control of Hes1." *Cell Host & Microbe* 25 (5): 706-8. doi:10.1016/j.chom.2019.03.012.

Lidell, Martin E, and Gunnar C Hansson. 2006. "Cleavage in the GDPH sequence of the C-terminal cysteine-rich part of the human MUC5AC mucin." *The Biochemical Journal* 399 (1): 121-9. doi:10.1042/BJ20060443.

Lin, Otto S. 2009. "Acquired risk factors for colorectal cancer." *Methods in Molecular Biology* 472: 361-72. doi:10.1007/978-1-60327-492-0_16.

Lindén, Sara K, Yong H Sheng, Alison L Every, Kim M Miles, Emma C Skoog, Timothy HJ Florin, Philip Sutton, and Michael A McGuckin. 2009. "MUC1 limits Helicobacter pylori infection both by steric hindrance and by acting as a releasable decoy." *PLOS Pathogens* 5 (10). doi:10.1371/journal.ppat.1000617.

Lindqvist, S M, P Sharp, I T Johnson, Y Satoh, and M R Williams. 1998. "Acetylcholine-induced calcium signaling along the rat colonic crypt axis." *Gastroenterology* 115 (5): 1131-43. doi:10.1016/s0016-5085(98)70084-8.

Lindqvist, Susanne, James Hernon, Paul Sharp, Neil Johns, Sarah Addison, Mark Watson, Richard Tighe, et al. 2002. "The colon-selective spasmolytic otilonium bromide inhibits muscarinic M(3) receptor-coupled calcium signals in isolated human colonic crypts." *The British Journal of Pharmacology* 137 (7): 1134-42. doi:10.1038/sj.bjp.0704942.

Lin-Moshier, Yaping, Timothy F Walseth, Dev Churamani, Sean M Davidson, James T Slama, Robert Hooper, Eugen Brailoiu, Sandip Patel, and Jonathan S Marchant. 2012. "Photoaffinity labeling of nicotinic acid adenine dinucleotide phosphate (NAADP) targets in mammalian cells." *Journal of Biological Chemistry* 287 (4): 2296-307. doi:10.1074/jbc.M111.305813.

Liou, Jen, Man Lyang Kim, Won Do Heo, Joshua T Jones, Jason W Myers, James Jr E Ferrell, and Tobias Meyer. 2005. "STIM is a Ca2+ sensor essential for Ca2+-store-depletion-triggered Ca2+ influx." *Current Biology* 15 (13): 1235-41. doi:10.1016/j.cub.2005.05.055.

Lipkin, M, and H Newmark. 1985. "Effect of added dietary calcium on colonic epithelial-cell proliferation in subjects at high risk for familial colonic cancer." *The New England Journal of Medicine* 313 (22): 1381-4. doi:10.1056/NEJM198511283132203.

Liu, Cong-Lin, and Guo-Ping Shi. 2019. "Calcium-activated chloride channel regulator 1 (CLCA1): More than a regulator of chloride transport and mucus production." *World Allergy Organization* 12 (11): 100077. doi:10.1016/j.waojou.2019.100077.

Liu, Yang, Mingpeng Jin, Yaya Wang, Jianjun Zhu, Rui Tan, Jing Zhao, Xiaoying Ji, et al. 2020. "MCU-induced mitochondrial calcium uptake promotes mitochondrial biogenesis and colorectal cancer growth." *Signal Transduction and Targeted Therapy* 5: 59. doi:10.1038/s41392-020-0155-5.

López-Sanjurjo, Cristina I, Stephen C Tovey, David L Prole, and Colin W Taylor. 2013. "Lysosomes shape Ins(1,4,5)P3-evoked Ca2+ signals by selectively sequestering Ca2+ released from the endoplasmic reticulum." *Journal of Cell Science* 126 (Pt1): 289-300. doi:10.1242/jcs.116103.

Lozupone, F, M Borghi, F Marzoli, T Azzarito, P Matarrese, E Iessi, G Venturi, et al. 2015. "TM9SF4 is a novel V-ATPase-interacting protein that modulates tumor pH alterations associated with drug resistance and invasiveness of colon cancer cells." *Oncogene* 34 (40): 5163-74. doi:10.1038/onc.2014.437.

Lu, Van B, Juraj Rievaj, Elisabeth A O'Flaherty, Christopher A Smith, Ramona Pais, Luke A PattisoN, Gwen Tolhurst, et al. 2019. "Adenosine Triphosphate is Co-Secreted With Glucagon-Like Peptide-1 to Modulate Intestinal Enterocytes and Afferent Neurons." *Nature Communications* 10 (1029). doi:10.1038/s41467-019-09045-9.

Lundgren, Ove, Mats Jodal, Madeleine Jansson, Anders T Ryberg, and Lennart Svensson. 2011. "Intestinal Epithelial Stem/Progenitor Cells Are Controlled by Mucosal Afferent Nerves." *PLoS One* 6 (2): e16295. doi:10.1371/journal.pone.0016295.

Ly, Tony, Aki Endo, Alejandro Brenes, Marek Gierlinski, Vackar Afzal, Andrea Pawellek, and Angus I Lamond. 2018. "Proteome-wide analysis of protein abundance and turnover remodelling during oncogenic transformation of human breast epithelial cells." *Wellcome Open Research* 3: 51. doi:10.12688/wellcomeopenres.14392.1.

Ma, Hongdi, Wanyin Tao, and Shu Zhu. 2019. "T lymphocytes in the intestinal mucosa: defense and tolerance." *Cellular & Molecular Immunology* 16: 216-24. doi:10.1038/s41423-019-0208-2.

Mabbott, N A, D S Donaldson, H Ohno, I R Williams, and A Mahajan. 2013. "Microfold (M) cells: important immunosurveillance posts in the intestinal epithelium." *Mucosal Immunology* 6 (4): 666-77. doi:10.1038/mi.2013.30.

Macao, Bertil, Denny GA Johansson, Gunnar C Hansson, and Torleif Härd. 2006. "Autoproteolysis coupled to protein folding in the SEA domain of the membrane-bound MUC1 mucin." *Nature Structural and Molecular Biology* 13 (1): 71-6. doi:10.1038/nsmb1035.

Maekawa, Hiromitsu, Yuichi Oike, Shigeru Kanda, Yasuhiro Ito, Yoshihiro Yamada, Hiroki Kurihara, Ryozo Nagai, and Toshio Suda. 2003. "Ephrin-B2 induces migration of endothelial cells through the phosphatidylinositol-3 kinase pathway and promotes angiogenesis in adult vasculature." *Arteriosclerosis, Thrombosis, and Vascular Biology* 23 (11): 2008-14. doi:10.1161/01.ATV.0000096655.56262.56.

Mah, Amanda T, Kelley S Yan, and Calvin J Kuo. 2016. "Wnt pathway regulation of intestinal stem cells." *Journal of Physiology* 594 (17): 4837-47. doi:10.1113/JP271754.

Mahida, Y R, and R N Cunliffe. 2004. "Defensins and mucosal protection." *Novartis Foundation Symposia* 262 (discussion 77-84, 211-8.): 71-7. doi:10.1002/0470090480.ch6.

Maj, Jerzy G, François Paris, Adriana Haimovitz-Friedman, Ennapadam Venkatraman, Richard Kolesnick, and Zvi Fuks. 2003. "Microvascular function regulates intestinal crypt response to radiation." *Cancer Research* 63 (15): 4338-41. https://pubmed.ncbi.nlm.nih.gov/12907601/.

Maklad, Ahmed, Anjana Sharma, and Iman Azimi. 2019. "Calcium Signaling in Brain Cancers: Roles and Therapeutic Targeting." *Cancers* 11 (2): 145. doi:10.3390/cancers11020145.

Manjarrez-Marmolejo, Joaquín, and Javier Franco-Pérez. 2016. "Gap Junction Blockers: An Overview of their Effects on Induced Seizures in Animal Models." *Current Neuropharmacology* 14 (7): 759-71. doi:10.2174/1570159X14666160603115942.

Mann, Elizabeth R, David Bernardo, Nicholas R English, Jon Landy, Hafid O Al-Hassi, Simon TC Peake, Ripple Man, et al. 2015. "Compartment-specific immunity in the human gut: properties and functions of dendritic cells in the colon versus the ileum." *Gut* 65: 256-70. doi:10.1136/gutjnl-2014-307916.

Manne, Upender, Chandrakumar Shanmugam, Venkat R Katkoori, Harvey L Bumpers, and William E Grizzlea. 2012. "Development and progression of colorectal neoplasia." *Cancer Biomarkers* 9 (1-6): 235-65. doi:10.3233/CBM-2011-0160.

Mao, Junhao, Byeong-Moo Kim, Mihir Rajurkar, Ramesh A Shivdasani, and Andrew P McMahon. 2010. "Hedgehog signaling controls mesenchymal growth in the developing mammalian digestive tract." *Development* 137 (10): 1721-9. doi:10.1242/dev.044586.

Marchant, J, N Callamaras, and I Parker. 1999. "Initiation of IP(3)-mediated Ca(2+) waves in Xenopus oocytes." *The EMBO Journal* 18 (19): 5285-99. doi:10.1093/emboj/18.19.5285.

Marchi, Saverio, and Paolo Pinton. 2014. "The mitochondrial calcium uniporter complex: molecular components, structure and physiopathological implications." *Journal Overview The Journal of Physiology* 592 (Pt5): 829-39. doi:10.1113/jphysiol.2013.268235.

Marcobal, Angela, Mariana Barboza, John W Froehlich, David E Block, J Bruce German, Carlito B Lebrilla, and David A Mills. 2010. "Consumption of Human Milk Oligosaccharides by Gut-related Microbes." *Journal of Agricultural and Food Chemistry* 58 (9): 5334-40. doi:10.1021/jf9044205.

Marshman, Emma, Catherine Booth, and Christopher S Potten. 2002. "The intestinal epithelial stem cell." *BioEssays* 24 (1): 91-8. doi:10.1002/bies.10028.

Matos, J E, B Robaye, J M Boeynaems, R Beauwens, and J Leipziger. 2005. "K+ secretion activated by luminal P2Y2 and P2Y4 receptors in mouse colon." *The Journal of Physiology* 564 (Pt1): 269-79. doi:10.1113/jphysiol.2004.080002.

Matsumoto, T, T Nakane, and S Chiba. 1997. "UTP induces vascular responses in the isolated and perfused canine epicardial coronary artery via UTP-preferring P2Y receptors." *The British Journal of Pharmacology* 122 (8): 1625-32. doi:10.1038/sj.bjp.0701559.

Mauvezin , Caroline, and Thomas P Neufeld. 2015. "Bafilomycin A1 disrupts autophagic flux by inhibiting both V-ATPase-dependent acidification and Ca-P60A/SERCA-dependent autophagosome-lysosome fusion." *Autophagy* 11 (8): 1437-8. doi:10.1080/15548627.2015.1066957.

May, Randal, Sripathi M Sureban, Nguyet Hoang, Terrence E Riehl, Stan A Lightfoot, Rama Ramanujam, James H Wyche, Shrikant Anant, and Courtney W Houchen. 2009. "Doublecortin and CaM kinase-like-1 and leucine-rich-repeat-containing G-protein-coupled receptor mark quiescent and cycling intestinal stem cells, respectively." *Stem Cells* 27 (10): 2571-9. doi:10.1002/stem.193.

Mayo Clinic. 2018. *Colon polyps.* 28 Aug. https://www.mayoclinic.org/diseases-conditions/colon-polyps/symptoms-causes/syc-20352875.

Mazzini, Elisa, Lucia Massimiliano, Giuseppe Penna, and Maria Rescigno. 2014. "Oral tolerance can be established via gap junction transfer of fed antigens from CX3CR1(+) Macrophages to CD103(+) dendritic cells." *Immunity* 40 (2): 248-61. doi:10.1016/j.immuni.2013.12.012.

McAuley, Julie L, Sara K Linden, Chin Wen Png, Rebecca M King, Helen L Pennington, Sandra J Gendler, Timothy H Florin, Geoff R Hill, Victoria Korolik, and Michael A McGuckin. 2007. "MUC1 cell surface mucin is a critical element of the mucosal barrier to infection." *Journal of Clinical Investigation* 117 (8): 2313-24. doi:10.1172/JCI26705.

McCartney, Fiona, John P Gleeson, and David J Brayden. 2016. "Safety concerns over the use of intestinal permeation enhancers: A mini-review." *Tissue Barriers* 4 (2). doi:10.1080/21688370.2016.1176822.

McCauley, Heather A, Andrea L Matthis, Jacob R Enriquez, Jonah T Nichol, J Guillermo Sanchez, William J Stone, Nambirajan Sundaram, et al. 2020. "Enteroendocrine Cells Couple Nutrient Sensing to Nutrient Absorption by Regulating Ion Transport." *Nature Communications* 11 (4791). doi:10.1038/s41467-020-18536-z.

McClintock, Shannon D, Durga Attili, Michael K Dame, Aliah Richter, Sabrina S Silvestri, Maliha M Berner, Margaret S Bohm, et al. 2020. "Differentiation of human colon tissue in culture: Effects of calcium on trans-epithelial electrical resistance and tissue cohesive properties." *PLoS One* 15 (3): e222058. doi:10.1371/journal.pone.0222058.

McLean, Leon P, Allen Smith, Lumei Cheung, Joseph Jr F Urban,, Rex Sun, Viktoriya Grinchuk, Neemesh Desai, Aiping Zhao, Jean-Pierre Raufman, and Terez Shea-Donohue. 2016. "Type 3 muscarinic receptors contribute to intestinal mucosal homeostasis and clearance of Nippostrongylus brasiliensis through induction of TH2 cytokines." *American Journal of Physiology-Gastrointestinal and Liver Physiology* 311 (1): G130-41. doi:10.1152/ajpgi.00461.2014.

McLendon, Kevin, and Charles V Preuss. 2021. "Atropine." In *StatPearls* . StatPearls Publishing LLC. https://pubmed.ncbi.nlm.nih.gov/29262018/.

Meador, W E, A R Means, and F A Quiocho. 1992. "Target enzyme recognition by calmodulin: 2.4 A structure of a calmodulin-peptide complex." *Science* 257 (5074): 1251-5. doi:10.1126/science.1519061.

Medema, Jan Paul, and Louis Vermeulen. 2011. "Microenvironmental regulation of stem cells in intestinal homeostasis and cancer." *Nature* 474: 318-26. doi:10.1038/nature10212.

Meissner, G. 1986. "Ryanodine activation and inhibition of the Ca2+ release channel of sarcoplasmic reticulum." *Journal of Biological Chemistry* 261 (14): 6300-6. https://pubmed.ncbi.nlm.nih.gov/2422165/.

Melchionda, Manuela, Jon K Pittman, Roberto Mayor, and Sandip Patel. 2016. "Ca2+/H+ exchange by acidic organelles regulates cell migration in vivo." *Journal of Cell Biology* 212 (7): 803-13. doi:10.1083/jcb.201510019.

Meng, Zhipeng, Toshiro Moroishi, and Kun-Liang Guan. 2016. "Mechanisms of Hippo pathway regulation." *Genes & Development* 30 (1): 1-17. doi:10.1101/gad.274027.115.

Merlin, D, C Augeron, X Y Tien, X Guo, C L Laboisse, and U Hopfer. 1994. "ATP-stimulated electrolyte and mucin secretion in the human intestinal goblet cell line HT29-Cl.16E." *The Journal of Membrane Biology* 137 (2): 137-49. doi:10.1007/BF00233483.

Merritt, A J, C S Potten, C J Kemp, J A Hickman, A Balmain, D P Lane, and P A Hall. 1994. "The role of p53 in spontaneous and radiation-induced apoptosis in the gastrointestinal tract of normal and p53-deficient mice." *Cancer Research* 54 (3): 614-7. https://pubmed.ncbi.nlm.nih.gov/8306319/.

Meşe, Gülistan, Gabriele Richard, and Thomas W White. 2007. "Gap Junctions: Basic Structure and Function." *Journal of Investigative Dermatology* 127 (11): 2516-24. doi:10.1038/sj.jid.5700770.

Middelhoff, Moritz, Henrik Nienhüser, Giovanni Valenti, H Carlo Maurer, Yoku Hayakawa, Ryota Takahashi, Woosook Kim, et al. 2020. "Prox1-positive cells monitor and sustain the murine

intestinal epithelial cholinergic niche." *Nature Communications* 11 (1): 111. doi:10.1038/s41467-019-13850-7.

Mirzaie, Ali Zare, Hakimeh Khakpour, Masoud Mireskandari, Nasrin Shayanfar, and Ladan Fatahi. 2016. "Investigating The Frequency of Serrated Polyps/Adenomas and Their Subtypes in Colonic Polyp Samples." *Medical Archives* 70 (3): 198-202. doi:10.5455/medarh.2016.70.198-202.

Mishra, Jyotsna, Bong Sook Jhun, Stephen Hurst, Jin O-Uchi, György Csordás, and Shey-Shing Sheu. 2017. "The Mitochondrial Ca2+ Uniporter: Structure, Function and Pharmacology." *Handbook of Experimental Pharmacology* 240: 129-56. doi:10.1007/164_2017_1.

Missiaen, L, G Callewaert, H De Smedt, and J B Parys. 2001. "2-Aminoethoxydiphenyl borate affects the inositol 1,4,5-trisphosphate receptor, the intracellular Ca2+ pump and the non-specific Ca2+ leak from the non-mitochondrial Ca2+ stores in permeabilized A7r5 cells." *Cell Calcium* 29 (2): 111-6. doi:10.1054/ceca.2000.0163.

Mitchelson, F, and A Ziegler. 1984. "The effect of gallamine, gallopamil and nifedipine on responses to acetylcholine and carbachol in the taenia of the guinea-pig caecum." *British Journal of Pharmacology* 83 (1): 145-55. doi:10.1111/j.1476-5381.1984.tb10129.x.

Modlin, Irvin M, Mark Kidd, Roswitha Pfragner, Geeta N Eick, and Manish C Champaneria. 2006. "The functional characterization of normal and neoplastic human enterochromaffin cells." *Journal of Clinical Endocrinology & Metabolism* 91 (6): 2340-8. doi:10.1210/jc.2006-0110.

Montgomery, Robert K, Diana L Carlone, Camilla A Richmond, Loredana Farilla, Mariette EG Kranendonk, Daniel E Henderson, Nana Yaa Baffour-Awuah, et al. 2011. "Mouse telomerase reverse transcriptase (mTert) expression marks slowly cycling intestinal stem cells." *PNAS* 108 (1): 179-84. doi:10.1073/pnas.1013004108.

Morgan, Anthony J, Frances M Platt, Emyr Lloyd-Evans, and Antony Galione. 2011. "Molecular mechanisms of endolysosomal Ca2+ signalling in health and disease." *Biochemical Journal* 439 (3): 349-74. doi:10.1042/BJ20110949.

Morgan, Anthony J, Lianne C Davis, Siegfried KTY Wagner, Alexander M Lewis, John Parrington, Grant C Churchill, and Antony Galione. 2013. "Bidirectional Ca²⁺ signaling occurs between the endoplasmic reticulum and acidic organelles." *Journal of Cell Biology* 200 (6): 789-805. doi:10.1083/jcb.201204078.

Mori, M, H Hosomi, T Nishizaki, K Kawahara, and Y Okada. 1997. "Calcium release from intracellular stores evoked by extracellular ATP in a Xenopus renal epithelial cell line." *Journal of Physiology* 502 (Pt2): 365-73. doi:10.1111/j.1469-7793.1997.365bk.x.

Mori-Akiyama, Yuko, Maaike van den Born, Johan H van Es, Stanley R Hamilton, Henry P Adams, Jiexin Zhang, Hans Clevers, and Benoit de Crombrugghe. 2007. "SOX9 is required for the differentiation of paneth cells in the intestinal epithelium." *Gastroenterology* 133 (2): 539-46. doi:10.1053/j.gastro.2007.05.020.

Moriyama, Yoshinori, Miki Hiasa, Shohei Sakamoto, Hiroshi Omote, and Masatoshi Nomura. 2017. "Vesicular nucleotide transporter (VNUT): appearance of an actress on the stage of purinergic signaling." *Purinergic Signalling* 13 (3): 387-404. doi:10.1007/s11302-017-9568-1.

Moroni, Mirko, M Rocio Servin-Vences, Raluca Fleischer, Oscar Sánchez-Carranza, and Gary R Lewin. 2018. "Voltage gating of mechanosensitive PIEZO channels." *Nature Communications* 9 (1): 1096. doi:10.1038/s41467-018-03502-7.

Mueller, Noel T, Elizabeth Bakacs, Joan Combel, Zoya Grigoryan, and Maria G Dominguez-Bello. 2014. "The infant microbiome development: mom matters." *Trends in Molecular Medicine* 21 (2): 109-17. doi:10.1016/j.molmed.2014.12.002.

Muise, Eleanor D, Neeru Gandotra, John J Tackett, Michaela C Bamdad, and Robert A Cowles. 2017. "Distribution of muscarinic acetylcholine receptor subtypes in the murine small intestine." *Life Sciences* 169: 6-10. doi:10.1016/j.lfs.2016.10.030.

Muller, Paul Andrew, Balázs Koscsó, Gaurav Manohar Rajani, Korey Stevanovic, Marie-Luise Berres, Daigo Hashimoto, Arthur Mortha, et al. 2014. "Crosstalk between muscularis macrophages and enteric neurons regulates gastrointestinal motility." *Cell* 158 (2): 300-13. doi:10.1016/j.cell.2014.04.050.

Müller, T D, B Finan, S R Bloom, D D'Alessio, D J Drucker, P R Flatt, A Fritsche, et al. 2019. "Glucagon-like peptide 1 (GLP-1)." *Molecular Metabolism* 30: 72-130. doi:10.1016/j.molmet.2019.09.010.

Muncan, Vanesa, Owen J Sansom, Leon Tertoolen, Toby J Phesse, Harry Begthel, Elena Sancho, Alicia M Cole, et al. 2006. "Rapid loss of intestinal crypts upon conditional deletion of the Wnt/Tcf-4 target gene c-Myc." *Molecular and Cellular Biology* 26 (22): 8418-26. doi:10.1128/MCB.00821-06.

Muñoz, Javier, Daniel E Stange, Arnout G Schepers, Marc van de Wetering, Bon-Kyoung Koo, Shalev Itzkovitz, Richard Volckmann, et al. 2012. "The Lgr5 intestinal stem cell signature: robust expression of proposed quiescent '+4' cell markers." *The EMBO Journal* 31 (14): 3079-91. doi:10.1038/emboj.2012.166.

Muoboghare, Markie O, Robert M Drummond, and Charles Kennedy. 2019. "Characterisation of P2Y 2 receptors in human vascular endothelial cells using AR-C118925XX, a competitive and selective P2Y 2 antagonist." *The British Journal of Pharmacology* 176 (16): 2894-904. doi:10.1111/bph.14715.

Murakami, Tomohiko, Johan Ockinger, Jiujiu Yu, Vanessa Byles, Aisleen McColl, Aldebaran M Hofer, and Tiffany Horng. 2012. "Critical role for calcium mobilization in activation of the NLRP3 inflammasome." *PNAS* 109 (28): 11282-87. doi:10.1073/pnas.1117765109.

Murana, E, F Pagani, B Basilico, M Sundukova, L Batti, S Di Angelantonio, B Cortese, et al. 2017. "ATP release during cell swelling activates a Ca2+-dependent Cl– current by autocrine mechanism in mouse hippocampal microglia." *Scientific Reports* 7 (1): 4184. doi:10.1038/s41598-017-04452-8.

Murrell-Lagnado, Ruth D. 2018. "A role for P2X4 receptors in lysosome function." *Journal of General Physiology* 150 (2): 185-7. doi:10.1085/jgp.201711963.

Musrap, Natasha, Alessandra Tuccitto, George S Karagiannis, Punit Saraon, Ihor Batruch, and Eleftherios P Diamandis. 2015. "Comparative Proteomics of Ovarian Cancer Aggregate Formation Reveals an Increased Expression of Calcium-activated Chloride Channel Regulator

1 (CLCA1)." *Journal of Biological Chemistry* 290 (28): 17218-27. doi:10.1074/jbc.M115.639773.

Nadjsombati, Marija S, John W McGinty, Miranda R Lyons-Cohen, James B Jaffe, Lucian DiPeso, Christoph Schneider, Corey N Miller, et al. 2018. "Detection of Succinate by Intestinal Tuft Cells Triggers a Type 2 Innate Immune Circuit." *immunity* 49 (1): 33-41. doi:10.1016/j.immuni.2018.06.016.

Nagano, Makoto, Junko Y Toshima, Daria Elisabeth Siekhaus, and Jiro Toshima. 2019. "Rab5-mediated endosome formation is regulated at the trans-Golgi network." *Communications Biology* 2: 419. doi:10.1038/s42003-019-0670-5.

Nagatake, Takahiro, Harumi Fujita, Nagahiro Minato, and Yoko Hamazaki . 2014. "Enteroendocrine Cells Are Specifically Marked by Cell Surface Expression of Claudin-4 in Mouse Small Intestine." *PLos One* 9 (3). doi:10.1371/journal.pone.0090638.

Nair, N, E W Newell, C Vollmers, S R Quake, J M Morton, M M Davis, X S He, and H B Greenberg. 2016. "High-dimensional immune profiling of total and rotavirus VP6-specific intestinal and circulating B cells by mass cytometry." *Mucosal Immunology* 9 (1): 68-82. doi:10.1038/mi.2015.36.

National High Magnetic Field Laboratory. 2015. *Tandem Mass Spectrometry (MS/MS).* Sept. https://nationalmaglab.org/user-facilities/icr/techniques/tandem-ms.

National Library of Medicine. 2004. *Carbachol.* Accessed Feb 2021. doi:https://pubchem.ncbi.nlm.nih.gov/compound/Carbachol.

NCBI. 2020. Dec. Accessed Dec 2020. https://www.ncbi.nlm.nih.gov/gene.

Neshatian, Leila, Peter R Strege, Poong-Lyul Rhee, Robert E Kraichely, Amelia Mazzone, Cheryl E Bernard, Robert R Cima, et al. 2015. "Ranolazine inhibits voltage-gated mechanosensitive sodium channels in human colon circular smooth muscle cells." *The American Journal of Physiology-Gastrointestinal and Liver Physiology* 309 (6): G506-12. doi:10.1152/ajpgi.00051.2015.

Neu, Josef, and Jona Rushing. 2011. "Cesarean versus Vaginal Delivery: Long term infant outcomes and the Hygiene Hypothesis." *Clinics in Perinatology* 38 (2): 321-31. doi:10.1016/j.clp.2011.03.008.

Neurath, Markus F. 2014. "Cytokines in inflammatory bowel disease." *Nature Reviews Immunology* 14 (5): 329-42. doi:10.1038/nri3661.

Neutra, M R, R J Grand, and J S Trier. 1977. "Glycoprotein synthesis, transport, and secretion by epithelial cells of human rectal mucosa: normal and cystic fibrosis." *Laboratory Investigation* 36 (5): 535-46. https://pubmed.ncbi.nlm.nih.gov/865081/.

Nevo, Shir, Noam Kadouri, and Jakub Abramson. 2019. "Tuft cells: From the mucosa to the thymus." *Immunology Letters* 210: 1-9. doi:10.1016/j.imlet.2019.02.003.

Newton, Alexandra C, Martin D Bootman, and John D Scott. 2016. "Second Messengers." *Cold Spring Harbor Perspectives in Biology* 8 (8). doi:10.1101/cshperspect.a005926.

Nezami, Behtash Ghazi, and Shanthi Srinivasan. 2013. "Enteric Nervous System in the Small Intestine: Pathophysiology and Clinical Implications." *Current Gastroenterology Reports* 12 (5): 358-65. doi:10.1007/s11894-010-0129-9.

Nie, Qixing, and Shaoping Nie. 2019. "High-performance liquid chromatography for food quality evaluation." Chap. 13, 267-99. Woodhead Publishing Series in Food Science, Technology and Nutrition. doi:10.1016/B978-0-12-814217-2.00013-5.

Niess, Jan Hendrik, Stephan Brand, Xiubin Gu, Limor Landsman, Steffen Jung, Beth A McCormick, Jatin M Vyas, et al. 2005. "CX3CR1-mediated dendritic cell access to the intestinal lumen and bacterial clearance." *Science* 307: 254-8. doi:10.1126/science.1102901.

Nievers, Mirjam G, Roel QJ Schaapveld, and Arnoud Sonnenberg. 1999. "Biology and function of hemidesmosomes." *Matrix Biology* 18 (1): 5-17. doi:10.1016/s0945-053x(98)00003-1.

Nishi, Tsuyoshi, and Michael Forgac. 2002. "The vacuolar (H+)-ATPases--nature's most versatile proton pumps." *Nature Reviews Molecular Cell Biology* 3 (2): 94-103. doi:10.1038/nrm729.

Notomi, Takuya, Miyuki Kuno, Akiko Hiyama, Tadashige Nozaki, Kiyoshi Ohura, Yoichi Ezura, and Masaki Noda. 2017. "Role of lysosomal channel protein TPC2 in osteoclast differentiation and bone remodeling under normal and low-magnesium conditions." *Journal of Biological Chemistry* 292 (51): 20998-1010. doi:10.1074/jbc.M117.780072.

Nusse, Roel, and Hans Clevers. 2017. "Wnt/β-Catenin Signaling, Disease, and Emerging Therapeutic Modalities." *Cell* 169 (6): 985-99. doi:10.1016/j.cell.2017.05.016.

Nusse, Ysbrand M, Adam K Savage, Pauline Marangoni, Axel KM Rosendahl-Huber, Tyler A Landman, Frederic J de Sauvage, Richard M Locksley, and Ophir D Klein. 2018. "Parasitic helminthes induce fetal-like reversion in the intestinal stem cell niche." *Nature* 559 (7712): 109-113. doi:10.1038/s41586-018-0257-1.

Nylund, G, L Hultman, S Nordgren, and D S Delbro. 2007. "P2Y2- and P2Y4 purinergic receptors are over-expressed in human colon cancer." *Autonomic & Autacoid Pharmacology* 27 (2): 79-84. doi:10.1111/j.1474-8673.2007.00389.x.

Nyström, Elisabeth EL, George MH Birchenough, Sjoerd van der Post, Liisa Arike, Achim D Gruber, Gunnar C Hansson, and Malin EV Johansson. 2018. "Calcium-activated Chloride Channel Regulator 1 (CLCA1) Controls Mucus Expansion in Colon by Proteolytic Activity." *EBioMedicine* 33: 134-43. doi:10.1016/j.ebiom.2018.05.031.

Nyström, Elisabeth EL, Liisa Arike, Erik Ehrencrona, Gunnar C Hansson, and Malin EV Johansson. 2019. "Calcium-activated chloride channel regulator 1 (CLCA1) forms non-covalent oligomers in colonic mucus and has mucin 2–processing properties." *Journal of Biological Chemistry* 294 (45): 17075-89. doi:10.1074/jbc.RA119.009940.

Ogunbayo, Oluseye A, Jingxian Duan, Jian Xiong, Qiaochu Wang, Xinghua Feng, Jianjie Ma, Michael X Zhu, and A Mark Evans. 2018. "mTORC1 controls lysosomal Ca 2+ release through the two-pore channel TPC2." *Science Signaling* 11 (525): eaao5775. doi:10.1126/scisignal.aao5775.

Ogunbayo, Oluseye A, Yingmin Zhu, Bing Shen, Ejaife Agbani, Jie Li, Jianjie Ma, Michael X Zhu, and A Mark Evans. 2015. "Organelle-specific subunit interactions of the vertebrate two-pore channel family." *Journal of Biological Chemistry* 290 (2): 1086-95. doi:10.1074/jbc.M114.610493.

Oka, Tatsuya, Koichi Sato, Masatoshi Hori, Hiroshi Ozaki, and Hideaki Karaki. 2004. "Xestospongin C, a novel blocker of IP3 receptor, attenuates the increase in cytosolic calcium level and degranulation that is induced by antigen in RBL-2H3 mast cells." *British Journal of Pharmacology* 92 (2): 1252-6. doi:10.1152/jn.00148.2004.

Okumura, Ryu, and Kiyoshi Takeda. 2018. "Maintenance of intestinal homeostasis by mucosal barriers." *Inflammation and Regeneration* 38 (5). doi:10.1186/s41232-018-0063-z.

O'Leary, A D, and E C Sweeney. 1986. "Lymphoglandular complexes of the colon: structure and distribution." *Histopathology* 10 (3): 267-83. doi:10.1111/j.1365-2559.1986.tb02481.x.

Ostasiewicz, Beata, Paweł Ostasiewicz, Kamila Duś-Szachniewicz, Katarzyna Ostasiewicz, and Piotr Ziółkowski. 2016. "Quantitative analysis of gene expression in fixed colorectal carcinoma samples as a method for biomarker validation." *Molecular Medicine Reports* 13 (6): 5084-92. doi:10.3892/mmr.2016.5200.

O'Sullivan, Shane, John F Gilmer, and Carlos Medina. 2015. "Matrix metalloproteinases in inflammatory bowel disease: an update." *Mediators of Inflammation* 2015. doi:10.1155/2015/964131.

Ota, S, K Yoshiura, M Takahashi, Y Hata, O Kohmoto, T Kawabe, T Shimada, et al. 1994. "P2 purinergic receptor regulation of mucus glycoprotein secretion by rabbit gastric mucous cells in a primary culture." *Gastroenterology* 106 (6): 1485-92. doi:10.1016/0016-5085(94)90401-4.

O'Toole, Timothy J, and Sandeep Sharma. 2020. "Physiology, Somatostatin." In *StatPearls*. StatPearls Publishing. https://www.ncbi.nlm.nih.gov/books/NBK538327/.

Pafumi, Irene, Margherita Festa, Francesca Papacci, Laura Lagostena, Cristina Giunta, Vijay Gutla, Laura Cornara, et al. 2017. "Naringenin Impairs Two-Pore Channel 2 Activity And Inhibits VEGF-Induced Angiogenesis." *Scientific Reports* 7 (1): 5121. doi:10.1038/s41598-017-04974-1.

Palade, P, R D Mitchell, and S Fleischer. 1983. "Spontaneous calcium release from sarcoplasmic reticulum. General description and effects of calcium." *Journal of Biological Chemistry* 258 (13): 8098-107. https://pubmed.ncbi.nlm.nih.gov/6863278/.

Palm, Noah W, Marcel R de Zoete, Thomas W Cullen, Natasha A Barry, Jonathan Stefanowski, Liming Hao, Patrick H Degnan, et al. 2014. "Immunoglobulin A coating identifies colitogenic bacteria in inflammatory bowel disease." *Cell* 158 (5): 1000-10. doi:10.1016/j.cell.2014.08.006.

Pamarthy, Sahithi, Arpita Kulshrestha, Gajendra K Katara, and Kenneth D Beaman. 2018. "The curious case of vacuolar ATPase: regulation of signaling pathways." *Molecular Cancer* 17 (1): 41. doi:10.1186/s12943-018-0811-3.

Pan, Jun, Leyi Zhang, Xuan Shao, and Jian Huang. 2020. "Acetylcholine From Tuft Cells: The Updated Insights Beyond Its Immune and Chemosensory Functions." *Frontiers in Cell and Developmental Biology* 8 (606). doi:10.3389/fcell.2020.00606.

Paneth, Josef. 1887. "About the secreting cells of the epithelium of the small intestine." *Microscopic anatomy archive* 31 (113). https://link.springer.com/article/10.1007/BF02955706.

Pang, Zhiping P, Ernestina Melicoff, Daniel Padgett, Yun Liu, Andrew F Teich, Burton F Dickey, Weichun Lin, Roberto Adachi, and Thomas C Südhof. 2006. "Synaptotagmin-2 is essential for survival and contributes to Ca2+ triggering of neurotransmitter release in central and neuromuscular synapses." *Journal of Neuroscience* 26 (52): 13493-504. doi:10.1523/JNEUROSCI.3519-06.2006.

Parikh, Kaushal, Agne Antanaviciute, David Fawkner-Corbett, Marta Jagielowicz, Anna Aulicino, Christoffer Lagerholm, Simon Davis, et al. 2019. "Colonic epithelial cell diversity in health and inflammatory bowel disease." *Nature* 567 (7746): 49-55. doi:10.1038/s41586-019-0992-y.

Park, Eun Taek, Hee Kyung Oh, James R Gum Jr, Suzanne C Crawley, Sanjay Kakar, Juan Engel, Ching Ching Leow, Wei-Qiang Gao, and Young S Kim. 2006. "HATH1 expression in mucinous cancers of the colorectum and related lesions." *Clinical Cancer Research* 12 (18): 5403-10. doi:10.1158/1078-0432.CCR-06-0573.

Park, Yune-Jung, Seung-Ah Yoo, Mingyo Kim, and Wan-Uk Kim. 2020. "The Role of Calcium-Calcineurin-NFAT Signaling Pathway in Health and Autoimmune Diseases." *Frontiers in Immunology* 11: 195. doi:10.3389/fimmu.2020.00195.

Parris, A, and M Williams. 2015. "A human colonic culture system to study regulation of stem cell-driven tissue renewal and physiological function." *Methods in Molecular Biology* 1212: 141-61. doi:10.1007/7651_2015_197.

Patel, Khushbu K, Hiroyuki Miyoshi, Wandy L Beatty, Richard D Head, Nicole P Malvin, Ken Cadwell, Jun-Lin Guan, et al. 2013. "Autophagy proteins control goblet cell function by potentiating reactive oxygen species production." *The EMBO Journal* 32 (24): 3130-44. doi:10.1038/emboj.2013.233.

Patel, Sandip, and Bethan S Kilpatrick. 2018. "Two-pore channels and disease." *Biochimica et Biophysica Acta* 1865 (11PartB): 1678-86. doi:10.1016/j.bbamcr.2018.05.004.

Paudel, Sudip, Regan Sindelar, and Margaret Saha. 2018. "Calcium Signaling in Vertebrate Development and Its Role in Disease." *International Journal of Molecular Sciences* 19 (11): 3390. doi:10.3390/ijms19113390.

Pelaez-Llaneza, Nicolas. 2019. *Deciphering cryptic calcium signals in the human colonic epithelium.* Norwich: University of East Anglia.

Pelaseyed, Thaher, and Gunnar C Hansson. 2011. "CFTR anion channel modulates expression of human transmembrane mucin MUC3 through the PDZ protein GOPC." *Journal of Cell Science* 124 (18): 3074-83. doi:10.1242/jcs.076943.

Pelaseyed, Thaher, Jenny K Gustafsson, Ida J Gustafsson, Anna Ermund, and Gunnar C Hansson. 2013. "Carbachol-induced MUC17 endocytosis is concomitant with NHE3 internalization and CFTR membrane recruitment in enterocytes." *American Journal of Physiology-Cell Physiology* 305 (4): C457-67. doi:10.1152/ajpcell.00141.2013.

Pelaseyed, Thaher, Michael Zäch, Asa C Petersson, Frida Svensson, Denny GA Johansson, and Gunnar C Hansson. 2013. "Unfolding dynamics of the mucin SEA domain probed by force spectroscopy suggest that it acts as a cell-protective device." *The FEBS Journal* 280 (6): 1491-501. doi:10.1111/febs.12144.

Percy, W H, J M Warren, and J T Brunz. 1999. "Characteristics of the muscularis mucosae in the acid-secreting region of the rabbit stomach." *American Journal of Physiology* 276 (5): G1213-20. doi:10.1152/ajpgi.1999.276.5.G1213.

Perenkov, A D, D V Novikov, N A Sakharnov, A V Aliasova, O V Utkin, A Iu Baryshnikov, and V V Novikov. 2012. "Heterogeneous expression of CD38 gene in tumor tissue in patients with colorectal cancer." *Molecular Biology* 46 (5): 786-91. https://pubmed.ncbi.nlm.nih.gov/23156678/.

Perez-Muñoz, Maria Elisa , Marie-Claire Arrieta, Amanda E Ramer-Tait, and Jens Walter. 2017. "A critical assessment of the "sterile womb" and "in utero colonization" hypotheses: implications for research on the pioneer infant microbiome." *Microbiome* 5 (1). doi:10.1186/s40168-017-0268-4.

Pérez-Riesgo, Enrique, Lucía G Gutiérrez, Daniel Ubierna, Alberto Acedo, Mary P Moyer, Lucía Núñez, and Carlos Villalobos. 2017. "Transcriptomic Analysis of Calcium Remodeling in Colorectal Cancer." *International Journal of Molecular Sciences* 18 (5): 922. doi:10.3390/ijms18050922.

Perez-Vilar, J, and R L Hill. 1999. "The structure and assembly of secreted mucins." *Biological Chemistry* 274 (45): 31751-4. doi:10.1074/jbc.274.45.31751.

Perez-Vilar, Juan. 2007. "Mucin Granule Intraluminal Organization." *The American Journal of Respiratory Cell and Molecular Biology* 36 (2): 183-90. doi:10.1165/rcmb.2006-0291TR.

Perez-Vilar, Juan, John C Olsen, Michael Chua, and Richard C Boucher. 2005. "pH-dependent intraluminal organization of mucin granules in live human mucous/goblet cells." *The Journal of Biological Chemistry* 280 (17): 16868-81. doi:10.1074/jbc.M413289200.

Petersen, Ole H, and Alexei V Tepikin. 2008. "Polarized calcium signaling in exocrine gland cells." *Annual Review of Physiology* 70: 273-99. doi:10.1146/annurev.physiol.70.113006.100618.

Philipson, Kenneth D, and Debora A Nicoll. 2000. "Sodium-Calcium Exchange: A Molecular Perspective." *Annual Review of Physiology* 62: 111-33. doi:10.1146/annurev.physiol.62.1.111.

Phillips, Melissa J, and Gia K Voeltz. 2016. "Structure and function of ER membrane contact sites with other organelles." *Nature Reviews Molecular Cell Biology* 17 (2): 69-82. doi:10.1038/nrm.2015.8.

Pickard, Joseph M, and Alexander V Chervonsk. 2015. "Intestinal fucose as a mediator of host-microbe symbiosis." *The Journal of Immunology* 194 (12): 5588-93. doi:10.4049/jimmunol.1500395.

Pickett, James A, and J Michael Edwardson. 2006. "Compound exocytosis: mechanisms and functional significance." *Traffic* 7 (2): 109-16. doi:10.1111/j.1600-0854.2005.00372.x.

Platt, Manu O, Arian J Roman, Alan Wells, Douglas A Lauffenburger, and Linda G Griffith. 2011. "Sustained epidermal growth factor receptor levels and activation by tethered ligand binding enhances osteogenic differentiation of multi-potent marrow stromal cells." *Journal of Cellular Physiology* 221 (2): 306-317. doi:10.1002/jcp.21854.

Plesch, Eva, Cheng-Chang Chen, Elisabeth Butz, Anna Scotto Rosato, Einar K Krogsaeter, Hua Yinan, Karin Bartel, et al. 2018. "Selective agonist of TRPML2 reveals direct role in chemokine release from innate immune cells." *eLife* 7: e39720. doi:10.7554/eLife.39720.

Ponce-Balbuena, Daniela, Aldo A Rodríguez-Menchaca, Angélica López-Izquierdo, Tania Ferrer, Harley T Kurata, Colin G Nichols, and José A Sánchez-Chapula. 2012. "Molecular Mechanisms of Chloroquine Inhibition of Heterologously Expressed Kir6.2/SUR2A Channels." *Molecular Pharmacology* 82 (5): 803-13. doi:10.1124/mol.112.079152.

Potten, C S, R Gandara, Y R Mahida, M Loeffler, and N A Wright. 2009. "The stem cells of small intestinal crypts: where are they?" *Cell Proliferation* 42 (6): 731-50. doi:10.1111/j.1365-2184.2009.00642.x.

Potten, Christopher S. 1977. "Extreme sensitivity of some intestinal crypt cells to X and γ irradiation." *Nature* 269: 518-21. doi:10.1038/269518a0.

Potten, Christopher S, Catherine Booth, Gregory L Tudor, Dawn Booth, Gerard Brady, Patricia Hurley, Gary Ashton, Robert Clarke, Shin-ichi Sakakibara, and Hideyuki Okano. 2003. "Identification of a putative intestinal stem cell and early lineage marker; musashi-1." *Differentiation* 71 (1): 28-41. doi:10.1046/j.1432-0436.2003.700603.x.

Potten, Christopher S, William J Hume, Peter Reid, and John Cairns. 1978. "The segregation of DNA in epithelial stem cells." *Cell* 15 (3): 899-906. doi:10.1016/0092-8674(78)90274-x.

Poutrain, Pierre, Christian Mazars, Martine Thiersault, Marc Rideau, and Olivier Pichon. 2009. "Two distinct intracellular Ca2+-release components act in opposite ways in the regulation of the auxin-dependent MIA biosynthesis in Catharanthus roseus cells." *Journal of Experimental Botany* 60 (4): 1387-98. doi:10.1093/jxb/erp017.

Powell, Anne E, Yang Wang, Yina Li, Emily J Poulin, Anna L Means, Mary K Washington, James N Higginbotham, et al. 2012. "The pan-ErbB negative regulator Lrig1 is an intestinal stem cell marker that functions as a tumor suppressor." *Cell* 149 (1): 146-58. doi:10.1016/j.cell.2012.02.042.

Prins, Daniel, and Marek Michalak. 2011. "Organellar Calcium Buffers." *Cold Spring Harbor Perspectives in Biology* 3 (3): a004069. doi:10.1101/cshperspect.a004069.

Prole, David L, and Colin W Taylor. 2019. "Structure and Function of IP 3 Receptors." *Cold Spring Harbor Perspectives in Biology* 11 (4). doi:10.1101/cshperspect.a035063.

Puchałowicz, Kamila, Maciej Tarnowski, Irena Baranowska-Bosiacka, Dariusz Chlubek, and Violetta Dziedziejko. 2014. "P2X and P2Y Receptors—Role in the Pathophysiology of the Nervous System." *International Journal of Molecular Sciences* 15 (12): 23672-704. doi:10.3390/ijms151223672.

Qi, Zhen, Yehua Li, Bing Zhao, Chi Xu, Yuan Liu, Haonan Li, Bingjie Zhang, et al. 2017. "BMP restricts stemness of intestinal Lgr5 + stem cells by directly suppressing their signature genes." *Nature Communications* 8: 13824. doi:10.1038/ncomms13824.

Quigley, Eamonn M. M. 2013. "Gut Bacteria in Health and Disease." *Journal of Gastroenterology and Hepatology* 9 (9): 560-9. doi:PMC3983973.

Qumseya, Bashar J, Susan Coe, and Michael B Wallace. 2012. "The Effect of Polyp Location and Patient Gender on the Presence of Dysplasia in Colonic Polyps." *Clinical and Translational Gastroenterology* 3 (7): e20. doi:10.1038/ctg.2012.14.

Rahman, Taufiq, Xinjiang Cai, Cristina G Brailoiu, Mary E Abood, Eugen Brailoiu, and Sandip Patel. 2015. "Two-pore channels provide insight into the evolution of voltage-gated Ca2+ and Na+ channels." *Science Signaling* 7 (352): ra109. doi:10.1126/scisignal.2005450.

Ramos, Isabela, Adrian Reich, and Gary M Wessel. 2014. "Two-pore channels function in calcium regulation in sea star oocytes and embryos." *Development* 141 (23): 4598-4609. doi:10.1242/dev.113563.

Rao, J N, and J Y Wang. 2016. *Regulation of Gastrointestinal Mucosal Growth.* Vol. 8. San Rafael (CA): Morgan & Claypool Life Sciences. doi:10.4199/C00145ED2V01Y201610ISP068.

Rao, Meenakshi, and Michael D Gershon. 2016. "The Bowel and Beyond: The Enteric Nervous System in Neurological Disorders." *Nature Reviews Gastroenterology & Hepatology* 13: 517-28. doi:10.1038/nrgastro.2016.107.

Raufman, Jean-Pierre, Jasleen Shant, Guofeng Xie, Kunrong Cheng, Xue-Min Gao, Brian Shiu, Nirish Shah, et al. 2011. "Muscarinic receptor subtype-3 gene ablation and scopolamine butylbromide treatment attenuate small intestinal neoplasia in Apcmin/+ mice." *Carcinogenesis* 32 (9): 1396-402. doi:10.1093/carcin/bgr118.

Rawla, Prashanth , Tagore Sunkara, and Adam Barsouk. 2019. "Epidemiology of Colorectal Cancer: Incidence, Mortality, Survival, and Risk Factors." *Przegląd Gastroenterologiczny* 14 (2): 89-103. doi:10.5114/pg.2018.81072.

Reale, Marcella, Erica Costantini, Marta Di Nicola, Chiara D'Angelo, Sara Franchi, Marco D'Aurora, Maria Di Bari, et al. 2018. "Butyrylcholinesterase and Acetylcholinesterase polymorphisms in Multiple Sclerosis patients: implication in peripheral inflammation." *Scientific Reports* 8 (1): 1319. doi:10.1038/s41598-018-19701-7.

Reynolds, A, A Parris, L A Evans, S Lindqvist, P Sharp, M Lewis, R Tinghe, and M R Williams. 2007. "Dynamic and differential regulation of NKCC1 by calcium and cAMP in the native human colonic epithelium." *The Journal of Physiology* 15 (582 (Pt 2)): 507-24. doi:10.1113/jphysiol.2007.129718.

Reynolds, A, N Wharton, A Parris, E Mitchell, A Sobolewski, C Kam, L Bigwood, et al. 2014. "Canonical Wnt signals combined with suppressed TGFβ/BMP pathways promote renewal of the native human colonic epithelium." *Gut* 63 (4): 610-21. doi:10.1136/gutjnl-2012-304067.

Ricciotti, Emanuela, and Garret A FitzGerald. 2012. "Prostaglandins and Inflammation." *Arteriosclerosis, Thrombosis, and Vascular Biology* 31 (5): 986-1000. doi:10.1161/ATVBAHA.110.207449.

Richmond, Camilla A, Manasvi S Shah, Diana L Carlone, and David T Breault. 2017. "An Enduring Role for Quiescent Stem Cells." *Developmental Dynamics* 245 (7): 718-26. doi:10.1002/dvdy.24416.

Richmond, Camilla A, Manasvi S Shah, Luke T Deary, Danny C Trotier, Horatio Thomas, Dana M Ambruzs, Lijie Jiang, et al. 2015. "Dormant Intestinal Stem Cells Are Regulated by PTEN and Nutritional Status." *Cell Reports* 13 (11): 2403-11. doi:10.1016/j.celrep.2015.11.035.

Rodríguez-Colman, Maria J, Matthias Schewe, Maaike Meerlo, Edwin Stigter, Johan Gerrits, Mia Pras-Raves, Andrea Sacchetti, et al. 2017. "Interplay between metabolic identities in the intestinal crypt supports stem cell function." *Nature* 543 (7645): 424-7. doi:10.1038/nature21673.

Roe, M W, J J Lemasters, and B Herman. 1990. "Assessment of Fura-2 for measurements of cytosolic free calcium." *Cell Calcium* 11 (2-3): 63-73. doi:10.1016/0143-4160(90)90060-8.

Romac, Joelle M-J, Rafiq A Shahid, Sandip M Swain, Steven R Vigna, and Rodger A Liddle. 2018. "Piezo1 is a mechanically activated ion channel and mediates pressure induced pancreatitis." *Nature Communications* 9: 1715. doi:10.1038/s41467-018-04194-9.

Roman, R M, and J G Fitz. 1999. "Emerging Roles of Purinergic Signaling in Gastrointestinal Epithelial Secretion and Hepatobiliary Function." *Gastroenterology* 116 (4): 964-79. doi:10.1016/s0016-5085(99)70081-8.

Rooney, T A, E J Sass, and A P Thomas. 1990. "Agonist-induced cytosolic calcium oscillations originate from a specific locus in single hepatocytes." *Journal of Biological Chemistry* 265 (18): 10792-6. https://pubmed.ncbi.nlm.nih.gov/2113061/.

Rosato, A Scotto, S Montefusco, C Soldati, S Di Paola, A Capuozzo, J Monfregola, E Polishchuk, et al. 2019. "TRPML1 links lysosomal calcium to autophagosome biogenesis through the activation of the CaMKKβ/VPS34 pathway." *Nature Communications* 10 (1): 5630. doi:10.1038/s41467-019-13572-w.

Rosen, Daniel, Alexander M Lewis, Akiko Mizote, Justyn M Thomas, Parvinder K Aley, Sridhar R Vasudevan, Raman Parkesh, et al. 2009. "Analogues of the Nicotinic Acid Adenine Dinucleotide Phosphate (NAADP) Antagonist Ned-19 Indicate Two Binding Sites on the NAADP Receptor*." *The Journal of Biological Chemistry* 284 (50): 34930-4. doi:10.1074/jbc.M109.016519.

Roth, Sabrina, Patrick Franken, Andrea Sacchetti, Andreas Kremer, Kurt Anderson, Owen Sansom, and Riccardo Fodde. 2012. "Paneth Cells in Intestinal Homeostasis and Tissue Injury." *PLoS One* 7 (6): e38965. doi:10.1371/journal.pone.0038965.

Rothenberg, Michael E, Ysbrand Nusse, Tomer Kalisky, John J Lee, Piero Dalerba, Ferenc Scheeren, Neethan Lobo, et al. 2012. "Identification of a cKit(+) colonic crypt base secretory cell that supports Lgr5(+) stem cells in mice." *Gastroenterology* 142 (5): 1195-205. doi:10.1053/j.gastro.2012.02.006.

Round, Andrew N, Neil M Rigby, Angela Garcia de la Torre, Adam Macierzanka, E N Mills, and Alan R Mackie. 2012. "Lamellar structures of MUC2-rich mucin: a potential role in governing the barrier and lubricating functions of intestinal mucus." *Biomacromolecules* 13 (10): 3253-61. doi:10.1021/bm301024x.

Round, June L, and Sarkis K Mazmanian. 2010. "Inducible Foxp3+ regulatory T-cell development by a commensal bacterium of the intestinal microbiota." *PNAS* 107 (27): 12204-9. doi:10.1073/pnas.0909122107.

Rozengurt, Enrique, and Catia Sternini. 2007. "Taste receptor signaling in the mammalian gut." *Current Opinion in Pharmacology* 7 (6): 557-62. doi:10.1016/j.coph.2007.10.002.

Ruas, Margarida, Kai-Ting Chuang, Lianne C Davis, Areej Al-Douri, Patricia W Tynan, Ruth Tunn, Lydia Teboul, Antony Galione, and John Parrington. 2014. "TPC1 has two variant isoforms, and

their removal has different effects on endo-lysosomal functions compared to loss of TPC2." *Molecular and Cellular Biology* 34 (21): 3981-92. doi:10.1128/MCB.00113-14.

Ruas, Margarida, Katja Rietdorf, Abdelilah Arredouani, Lianne C Davis, Emyr Lloyd-Evans, Heidi Koegel, Timothy M Funnell, et al. 2010. "Purified TPC isoforms form NAADP receptors with distinct roles for Ca(2+) signaling and endolysosomal trafficking." *Current Biology* 20 (8): 703-9. doi:10.1016/j.cub.2010.02.049.

Rubinfeld, B, I Albert, E Porfiri, C Fiol, S Munemitsu, and P Polakis. 1996. "Binding of GSK3beta to the APC-beta-catenin complex and regulation of complex assembly." *Science* 1023-6. doi:10.1126/science.272.5264.1023.

Rybalchenko, Volodymyr, Malini Ahuja, Jessica Coblentz, Dev Churamani, Sandip Patel, Krill Kiselyov, and Shmuel Muallem. 2012. "Membrane potential regulates nicotinic acid adenine dinucleotide phosphate (NAADP) dependence of the pH- and Ca2+-sensitive organellar two-pore channel TPC1." *Journal of Biological Chemistry* 287 (24): 20407-16. doi:10.1074/jbc.M112.359612.

Sakurai, Yasuteru, Andrey A Kolokoltsov, Cheng-Chang Chen, Michael W Tidwell, William E Bauta, Norbert Klugbauer, Christian Grimm, Christian Wahl-Schott, Martin Biel, and Robert A Davey. 2016. "Two pore channels control Ebolavirus host cell entry and are drug targets for disease treatment." *Science* 347 (6225): 995-8. doi:10.1126/science.1258758.

Saleem, Huma, Stephen C Tovey, Tedeusz F Molinski, and Colin W Taylor. 2014. "Interactions of antagonists with subtypes of inositol 1,4,5-trisphosphate (IP3) receptor." *The British Journal of Pharmacology* 171 (13): 3298-312. doi:10.1111/bph.12685.

Samadi, Nazanin, Martina Klems, and Eva Untersmayr. 2018. "The Role of Gastrointestinal Permeability in Food Allergy." *American College of Allergy, Asthma & Immunology* 121: 168-73. doi:10.1016/j.anai.2018.05.010.

Samanta, Amrita, Taylor ET Hughes, and Vera Y Moiseenkova-Bell. 2018. "Transient Receptor Potential (TRP) Channels." *SUBCELLULAR BIOCHEMISTRY* 87: 141-65. doi:10.1007/978-981-10-7757-9_6.

Sancho, Rocio, Catherine A Cremona, and Axel Behrens. 2015. "Stem cell and progenitor fate in the mammalian intestine: Notch and lateral inhibition in homeostasis and disease." *EMBO Reports* 16 (5): 571-81. doi:10.15252/embr.201540188.

Sanders, Kenton M, Sang Don Koh, Seungil Ro, and Sean M Ward. 2012. "Regulation of gastrointestinal motility—insights from smooth muscle biology." *Nature Reviews Gastroenterology & Hepatology* 9 (11): 633-45. doi:10.1038/nrgastro.2012.168.

Sangiorgi, Eugenio, and Mario R Capecchi. 2008. "Bmi1 is expressed in vivo in intestinal stem cells." *Nature Genetics* 40 (7): 915-20. doi:0.1038/ng.165.

Santoni, Giorgio, Matteo Santoni, Federica Maggi, Oliviero Marinelli, and Maria Beatrice Morelli. 2020. "Emerging Role of Mucolipins TRPML Channels in Cancer." *Frontiers in Oncology* 10: 659. doi:10.3389/fonc.2020.00659.

Saqui-Salces, Milena, Theresa M Keeley, Ann S Grosse, Xiaotan T Qiao, Mohamad El-Zaatari, Deborah L Gumucio, Linda C Samuelson, and Juanita L Merchant. 2013. "Gastric Tuft Cells Express

DCLK1, and Increase in Hyperplasia." *Histochemistry and Cell Biology* 136 (2): 191-204. doi:10.1007/s00418-011-0831-1.

Sasaki, Nobuo, Norman Sachs, Kay Wiebrands, Saskia IJ Ellenbroek, Arianna Fumagalli, Anna Lyubimova, Harry Begthel, et al. 2016. "Reg4+ deep crypt secretory cells function as epithelial niche for Lgr5+ stem cells in colon." *PNAS* 113 (37): 5399-407. doi:10.1073/pnas.1607327113.

Sato, T, D E Stange, M Ferrante, R G Vries, J H Van Es, S Van den Brink, W J Van Houdt, et al. 2011. "Long-term expansion of epithelial organoids from human colon, adenoma, adenocarcinoma, and Barrett's epithelium." *Gastroenterology* 141 (5): 1762-72. doi:10.1053/j.gastro.2011.07.050.

Sato, Toshiro, Johan H van Es, Hugo J Snippert, Daniel E Stange, Robert G Vries, Maaike van den Born, Nick Barker, Noah F Shroyer, Marc van de Wetering, and Hans Clevers. 2011. "Paneth cells constitute the niche for Lgr5 stem cells in intestinal crypts." *Nature* 469 (7330): 415-8. doi:10.1038/nature09637.

Satoh, H, and N Sperelakis. 1995. "Modulation of L-type Ca2+ current by isoprenaline, carbachol and phorbol ester in cultured rat aortic vascular smooth muscle (A7r5) cells." *General Pharmacology* 26 (2): 369-79. doi:10.1016/0306-3623(94)00193-q.

Saunders, Cecil J, Michael Christensen, Thomas E Finger, and Marco Tizzano. 2014. "Cholinergic neurotransmission links solitary chemosensory cells to nasal inflammation." *PNAS* 111 (16): 6075-80. doi:10.1073/pnas.1402251111.

Schmitt, Mark, Matthias Schewe, Andrea Sacchetti, Danny Feijtel, Wesley S van de Geer, Miriam Teeuwssen, Hein F Sleddens, et al. 2018. "Paneth Cells Respond to Inflammation and Contribute to Tissue Regeneration by Acquiring Stem-like Features through SCF/c-Kit Signaling." *Cell Reports* 24 (9): 2312-2328. doi:10.1016/j.celrep.2018.07.085.

Schneider, Christoph, Claire E O'Leary, Jakob von Moltke, Hong-Erh Liang, Qi Yan Ang, Peter J Turnbaugh, Sridhar Radhakrishnan, Michael Pellizzon, Averil Ma, and Richard M Locksley. 2018. "A Metabolite-Triggered Tuft Cell-ILC2 Circuit Drives Small Intestinal Remodeling." *Cell* 174 (2): 271-84. doi:10.1016/j.cell.2018.05.014.

Schneider, Michael, Valéa Schumacher, Timo Lischke, Karsten Lücke, Catherine Meyer-Schwesinger, Joachim Velden, Friedrich Koch-Nolte, and Hans-Willi Mittrücker. 2015. "CD38 Is Expressed on Inflammatory Cells of the Intestine and Promotes Intestinal Inflammation." *PLoS One* 10 (5): e126007. doi:10.1371/journal.pone.0126007.

Schuijers, Jurian, Laurens G van der Flier, Johan van Es, and Hans Clevers. 2014. "Robust cre-mediated recombination in small intestinal stem cells utilizing the olfm4 locus." *Stem Cell Reports* 3 (2): 234-41. doi:10.1016/j.stemcr.2014.05.018.

Schulz, Olga, Elin Jaensson, Emma K Persson, Xiaosun Liu, Tim Worbs, William W Agace, and Oliver Pabst. 2009. "Intestinal CD103+, but not CX3CR1+, antigen sampling cells migrate in lymph and serve classical dendritic cell functions." *Journal of Experimental Medicine* 206 (13): 3101-14. doi:10.1084/jem.20091925.

Schütz, Burkhard, Anna-Lena Ruppert, Oliver Strobel, Michael Lazarus, Yoshihiro Urade, Markus W Büchler, and Eberhard Weihe. 2019. "Distribution pattern and molecular signature of

cholinergic tuft cells in human gastro-intestinal and pancreatic-biliary tract." *Scientific Reports* 9 (1): 17466. doi:10.1038/s41598-019-53997-3.

Schütz, Burkhard, Innokentij Jurastow, Sandra Bader, Cornelia Ringer, Jakob von Engelhardt, Vladimir Chubanov, Thomas Gudermann, et al. 2015. "Chemical coding and chemosensory properties of cholinergic brush cells in the mouse gastrointestinal and biliary tract." *Frontiers in Physiology* 6: 87. doi:10.3389/fphys.2015.00087.

Schwaller, Beat. 2010. "Cytosolic Ca2+ Buffers." *Cold Spring Harbor Perspectives in Biology* 2 (11): a004051. doi:10.1101/cshperspect.a004051.

Schwank, Gerald, Bon-Kyoung Koo, Valentina Sasselli, Johanna F Dekkers, Inha Heo, Turan Demircan, Nobuo Sasaki, et al. 2013. "Functional repair of CFTR by CRISPR/Cas9 in intestinal stem cell organoids of cystic fibrosis patients." *Cell Stem Cell* 13 (6): 653-8. doi:10.1016/j.stem.2013.11.002.

Sei, Y, K L Gallagher, and J W Daly. 2001. "Multiple effects of caffeine on Ca2+ release and influx in human B lymphocytes." *Cell Calcium* 29 (3): 146-60. doi:10.1054/ceca.2000.0175.

Sei, Yoshitatsu, Jianying Feng, Carson C Chow, and Stephen A Wank. 2019. "Asymmetric cell division-dominant neutral drift model for normal intestinal stem cell homeostasis." *American Journal of Physiology-Gastrointestinal and Liver Physiology* 316 (1): 64-74. doi:10.1152/ajpgi.00242.2018.

Sennoune, Souad R, Karina Bakunts, Gloria M Martínez, Jenny L Chua-Tuan, Yamina Kebir, Mohamed N Attaya, and Raul Martínez-Zaguilán. 2004. "Vacuolar H+-ATPase in human breast cancer cells with distinct metastatic potential: distribution and functional activity." *American Journal of Physiology-Cell Physiology* 286 (6): C1443-52. doi:10.1152/ajpcell.00407.2003.

Shaalan, Abeer Kamal, Guy Carpenter, and Gordon Proctor. 2017. "Measurement of intracellular calcium of submandibular glands using a high throughput plate reader." *Journal of Biological Methods* 4 (3): e74. doi:10.14440/jbm.2017.180.

Shapiro, Lawrence, and William I Weis. 2009. "Structure and biochemistry of cadherins and catenins." *Cold Spring Harbor Perspectives in Biology* 1 (3): a003053. doi:10.1101/cshperspect.a003053.

Shibao, Kazunori, Michael J Fiedler, Jun Nagata, Noritaka Minagawa, Keiji Hirata, Yoshifumi Nakayama, Yasuko Iwakiri, Michael H Nathanson, and Koji Yamaguchi. 2010. "The type III inositol 1,4,5-trisphosphate receptor is associated with aggressiveness of colorectal carcinoma." *Cell Calcium* 48 (6): 315-23. doi:10.1016/j.ceca.2010.09.005.

Shirazi, T, R J Longman, A P Corfield, and C S Probert. 2000. "Mucins and inflammatory bowel disease." *Postgraduate Medical Journal* 76 (898): 473-8. doi:10.1136/pmj.76.898.473.

Shroyer, Noah F, Deeann Wallis, Koen JT Venken, Hugo J Bellen, and Huda Y Zoghbi. 2005. "Gfi1 functions downstream of Math1 to control intestinal secretory cell subtype allocation and differentiation." *Genes & Development* 19 (20): 2412-7. doi:10.1101/gad.1353905.

Siefjediers, Anne, Martin Hardt, Gundula Prinz, and Martin Diener. 2007. "Characterization of inositol 1,4,5-trisphosphate (IP3) receptor subtypes at rat colonic epithelium." *Cell Calcium* 41 (4): 303-15. doi:10.1016/j.ceca.2006.07.009.

Sigalas, Charalambos, Maria Belen Mayo-Martin, David E Jane, and Rebecca Sitsapesan. 2009. "Ca2+-Calmodulin Increases RyR2 Open Probability yet Reduces Ryanoid Association with RyR2." *Biophysical Journal* 97 (7): 1907-16. doi:10.1016/j.bpj.2009.07.027.

Simian, Marina, and Mina J Bissell. 2017. "Organoids: A historical perspective of thinking in three dimensions." *Journal of Cell Biology* 216 (1): 31-40. doi:10.1083/jcb.201610056.

SinoBiological. 2020. *Epidermal Growth Factor (EGF) Signaling Transduction.* https://www.sinobiological.com/research/signal-transduction/egf.

Skelding, Kathryn A, and John AP Rostas. 2012. "The role of molecular regulation and targeting in regulating calcium/calmodulin stimulated protein kinases." *Advancesin Experimental Medicine and Biology* 740: 703-30. doi:10.1007/978-94-007-2888-2_31.

Skelding, Kathryn Anne, and John AP Rostas. 2019. "Regulation of Multifunctional Calcium/Calmodulin Stimulated Protein Kinases by Molecular Targeting." *Advances in Experimental Medicine and Biology* 1131: 649-79. doi:10.1007/978-3-030-12457-1_26.

Slack, Emma , Maria L Balmer, and Andrew J Macpherson. 2014. "B cells as a critical node in the microbiota-host immune system network." *Immunological Reviews* 260 (1): 50-66. doi:10.1111/imr.12179.

Smorodinsky, N, M Weiss, M L Hartmann, A Baruch, E Harness, M Yaakobovitz, I Keydar, and D H Wreschner. 1996. "Detection of a secreted MUC1/SEC protein by MUC1 isoform specific monoclonal antibodies." *Biochemical and Biophysical Research Communications* 228 (1): 115-21. doi:10.1006/bbrc.1996.1625.

Smyth, Jeremy T, Wayne I DeHaven, Gary S Bird, and James Jr W Putney, Jr. 2008. "Calcium Store-Dependent and Independent Reversal of STIM1 Localization and Function." *Journal of Cell Science* 121 (Pt6): 762-72. doi:10.1242/jcs.023903.

Snary, David, Adrian Allen, and Roger H Pain. 1971. "The Structure of Pig Gastric Mucus Conformational Transitions Induced by Salt." *European Journal of Biochemistry* 24 (1): 183-9. doi:10.1111/j.1432-1033.1971.tb19669.x.

Snippert, Hugo J, Arnout G Schepers, Johan H van Es, Benjamin D Simons, and Hans Clevers. 2014. "Biased competition between Lgr5 intestinal stem cells driven by oncogenic mutation induces clonal expansion." *EMBO Reports* 15 (1): 62-9. doi:10.1002/embr.201337799.

Soboloff, Jonathan, Brad S Rothberg, Muniswamy Madesh, and Donald L Gill. 2012. "STIM proteins: dynamic calcium signal transducers." *Nature Reviews Molecular Cell Biology* 13 (9): 549-65. doi:10.1038/nrm3414.

Soler, F, F Plenge-Tellechea, I Fortea, and F Fernandez-Belda. 1998. "Cyclopiazonic acid effect on Ca2+-dependent conformational states of the sarcoplasmic reticulum ATPase. Implication for the enzyme turnover." *Biochemistry* 37 (12): 4266-74. doi:10.1021/bi971455c.

Solovyova, N, P Fernyhough, G Glazner, and A Verkhratsky. 2002. "Xestospongin C empties the ER calcium store but does not inhibit InsP3-induced Ca2+ release in cultured dorsal root ganglia neurones." *Cell Calcium* 32 (1): 49-52. doi:10.1016/s0143-4160(02)00094-5.

Sommer, Felix, and Fredrik Bäckhed. 2013. "The gut microbiota — masters of host development and physiology." *Nature Reviews Microbiology* 11: 227-38. doi:10.1038/nrmicro2974.

Soto, Pedro, Jin Zhang, and Kermit L Carraway. 2006. "Enzymatic cleavage as a processing step in the maturation of Muc4/sialomucin complex." *The Journal of Cellular Biochemistry* 97 (6): 1267-74. doi:10.1002/jcb.20718.

Spagnol, Gaelle, Andrew J Trease, Li Zheng, Mirtha Gutierrez, Ishika Basu, Cleofes Sarmiento, Gabriella Moore, Matthew Cervantes, and Paul L Sorgen. 2018. "Connexin43 Carboxyl-Terminal Domain Directly Interacts with β-Catenin." *International Journal of Molecular Sciences* 19 (6). doi:10.3390/ijms19061562.

Specian, R D, and M R Neutra. 1980. "Mechanism of rapid mucus secretion in goblet cells stimulated by acetylcholine." *Journal of Cell Biology* 85 (3): 626-40. doi:10.1083/jcb.85.3.626.

Spencer, J, and L M Sollid . 2016. "The human intestinal B-cell response." *Mucosal Immunology* 9: 1113-24. doi:10.1038/mi.2016.59.

Stagg, A J, A L Hart, S C Knight, and M A Kamm. 2003. "The dendritic cell: its role in intestinal inflammation and relationship with gut bacteria." *Gut* 52 (10): 1522-9. doi:10.1136/gut.52.10.1522.

Stagg, Andrew J. 2018. "Intestinal Dendritic Cells in Health and Gut Inflammation." *Frontiers in Immunology* 9 (2883). doi:10.3389/fimmu.2018.02883.

Stange, Daniel E, Bon-Kyoung Koo, Meritxell Huch, Greg Sibbel, Onur Basak, Anna Lyubimova, Pekka Kujala, et al. 2013. "Differentiated Troy+ chief cells act as reserve stem cells to generate all lineages of the stomach epithelium." *Cell* 155 (2): 357-68. doi:10.1016/j.cell.2013.09.008.

Stanger, BenZ, Radhika Datar, L Charles Murtaugh, and Douglas A Melton. 2005. "Direct regulation of intestinal fate by Notch." *PNAS* 102 (35): 12433-8. doi:10.1073/pnas.0505690102.

Stathopulos, Peter B, Le Zheng, Guang-Yao Li, Michael J Plevin, and Mitsuhiko Ikura. 2008. "Structural and mechanistic insights into STIM1-mediated initiation of store-operated calcium entry." *Cell* 135 (1): 110-22. doi:10.1016/j.cell.2008.08.006.

Steen, Mareike, Tanja Kirchberger, and Andreas H Guse. 2007. "NAADP mobilizes calcium from the endoplasmic reticular Ca(2+) store in T-lymphocytes." *Journal of Biological Chemistry* 282 (26): 18864-71. doi:10.1074/jbc.M610925200.

Stevens, C E, and C P Leblond. 1947. "Rate of renewal of the cells of the intestinal epithelium in the rat." *The Anatomical Record* 97 (3): 373. https://pubmed.ncbi.nlm.nih.gov/20341868/.

Storch, Judith, and Betina Corsico. 2008. "The Emerging Functions and Mechanisms of Mammalian Fatty Acid–Binding Proteins." *Annual Review of Nutrition* 28: 73-95. doi:10.1146/annurev.nutr.27.061406.093710.

Strehler, E E, and D A Zacharias. 2001. "Role of alternative splicing in generating isoform diversity among plasma membrane calcium pumps." *Physiological Reviews* 81 (1): 21-50. doi:10.1152/physrev.2001.81.1.21.

Strehler, Emanuel E, Ariel J Caride, Adelaida G Filoteo, Yuning Xiong, John T Penniston, and Agnes Enyedi. 2007. "Plasma membrane Ca2+ ATPases as dynamic regulators of cellular calcium handling." *Annals of the New York Academy of Sciences* 1099: 226-36. doi:10.1196/annals.1387.023.

Streichert, L C, and P B Sargent. 1992. "The role of acetylcholinesterase in denervation supersensitivity in the frog cardiac ganglion." *The Journal of Physiology* 445: 249-60. doi:10.1113/jphysiol.1992.sp018922.

Stzepourginski, Igor, Giulia Nigro, Jean-Marie Jacob, Sophie Dulauroy, Philippe J Sansonetti, Gérard Eberl, and Lucie Peduto. 2017. "CD34+ mesenchymal cells are a major component of the intestinal stem cells niche at homeostasis and after injury." *PNAS* 114 (4): 506-13. doi:10.1073/pnas.1620059114.

Südhof, Thomas C. 2012. "Calcium Control of Neurotransmitter Release." *Cold Spring Harbor Perspectives in Biology* 4 (1): a011353. doi:10.1101/cshperspect.a011353.

Südhof, Thomas C, and James E Rothman. 2009. "Membrane fusion: grappling with SNARE and SM proteinsThomas C Südhof." *Science* 323 (5913): 474-7. doi:10.1126/science.1161748.

Sui, Guiping, Chris H Fry, Bruce Montgomery, Max Roberts, Rui Wu, and Changhao Wu. 2014. "Purinergic and muscarinic modulation of ATP release from the urothelium and its paracrine actions." *The American Journal of Physiology-Renal Physiology* 306 (3): F286-98. doi:10.1152/ajprenal.00291.2013.

Sun, Wei, and Jianbo Yue. 2018. "TPC2 mediates autophagy progression and extracellular vesicle secretion in cancer cells." *Experimental Cell Research* 370 (2): 478-89. doi:10.1016/j.yexcr.2018.07.013.

Suurväli, Jaanus, Pierre Boudinot, Jean Kanellopoulos, and Sirje Rüütel Boudinot. 2017. "P2X4: A fast and sensitive purinergic receptor." *Biomedical Journal* 40 (5): 245-56. doi:10.1016/j.bj.2017.06.010.

Svanborg, C, G Aniansson, J Mestecky, and H Sabharwal. 1991. "Anti-adhesive molecules in human milk." *Advances in Experimental Medicine and Biology* 310: 167-71. doi:10.1007/978-1-4615-3838-7_20.

Syngai, Gareth Gordon, and Giasuddin Ahmed. 2019. "Lysozyme: A Natural Antimicrobial Enzyme of Interest in Food Applications." In *Enzymes in Food Biotechnology*, 169-79. Academic Press. doi:10.1016/B978-0-12-813280-7.00011-6.

Takahashi, Senye, Keiji Kubo, Satoshi Waguri, Atsuko Yabashi, Hye-Won Shin, Yohei Katoh, and Kazuhisa Nakayama. 2012. "Rab11 regulates exocytosis of recycling vesicles at the plasma membrane." *Journal of Cell Science* 125 (Pt17): 4049-57. doi:10.1242/jcs.102913.

Takahashi, Toshio, Akira Shiraishi, and Jun Murata. 2018. "The Coordinated Activities of nAChR and Wnt Signaling Regulate Intestinal Stem Cell Function in Mice." *International Journal of Molecular Sciences* 19 (3): 738. doi:10.3390/ijms19030738.

Takahashi, Toshio, Hiroe Ohnishi, Yuki Sugiura, Kurara Honda, Makoto Suematsu, Takashi Kawasaki, Tomonori Deguchi, et al. 2014. "Non-neuronal acetylcholine as an endogenous regulator of proliferation and differentiation of Lgr5-positive stem cells in mice." *The FEBS Journal* 281 (20): 4672-90. doi:10.1111/febs.12974.

Takeda, Norifumi, Rajan Jain, Matthew R LeBoeuf, Qiaohong Wang, Min Min Lu, and Jonathan A Epstein. 2011. "Interconversion between intestinal stem cell populations in distinct niches." *Science* 334 (6061): 1420-4. doi:10.1126/science.1213214.

Takeichi, Masatoshi. 2014. "Dynamic contacts: rearranging adherens junctions to drive epithelial remodelling." *Nature Reviews Molecular Cell Biology* 15 (6): 397-410. doi:10.1038/nrm3802.

Takemoto-Kimura, Sayaka, Kanzo Suzuki, Shin-Ichiro Horigane, Satoshi Kamijo, Masatoshi Inoue, Masayuki Sakamoto, Hajime Fujii, and Haruhiko Bito. 2017. "Calmodulin kinases: essential regulators in health and disease." *Journal of Neurochemistry* 141 (6): 808-18. doi:10.1111/jnc.14020.

Takeuchi, Koji, Takuya Endoh, Shusaku Hayashi, and Takeshi Aihara. 2016. "Activation of Muscarinic Acetylcholine Receptor Subtype 4 Is Essential for Cholinergic Stimulation of Gastric Acid Secretion: Relation to D Cell/Somatostatin." *Frontiers in Pharmacology* 7: 278. doi:10.3389/fphar.2016.00278.

Tammela, Tuomas, Francisco J Sanchez-Rivera, Naniye Malli Cetinbas, Katherine Wu, Nikhil S Joshi, Katja Helenius, Yoona Park, et al. 2017. "A Wnt-producing niche drives proliferative potential and progression in lung adenocarcinoma." *Nature* 545 (7654): 355-9. doi:10.1038/nature22334.

Tarlow, Branden D, Carl Pelz, Willscott E Naugler, Leslie Wakefield, Elizabeth M Wilson, Milton J Finegold, and Markus Grompe. 2014. "Bipotential adult liver progenitors are derived from chronically injured mature hepatocytes." *Cell Stem Cell* 15 (5): 605-8. doi:10.1016/j.stem.2014.09.008.

Taylor, Amanda L, Lisa M Schwiebert, Jeffrey J Smith, Chris King, Julie R Jones, Eric J Sorscher, and Erik M Schwiebert. 1999. "Epithelial P2X purinergic receptor channel expression and function." *Journal of Clinical Investigation* 104 (7): 875-84. doi:10.1172/JCI7270.

Tedeschi, Valentina, Tiziana Petrozziello, and Agnese Secondo. 2019. "Calcium Dyshomeostasis and Lysosomal Ca2+ Dysfunction in Amyotrophic Lateral Sclerosis." *Cells* 8 (10): 1216. doi:10.3390/cells8101216.

Tedeschi, Valentina, Tiziana Petrozziello, Maria José Sisalli, Francesca Boscia, Lorella M T Canzoniero, and Agnese Secondo. 2019. "The activation of Mucolipin TRP channel 1 (TRPML1) protects motor neurons from L-BMAA neurotoxicity by promoting autophagic clearance." *Scientific Reports* 9 (1): 10743. doi:10.1038/s41598-019-46708-5.

Tetteh, Paul W, Onur Basak, Henner F Farin, Kay Wiebrands, Kai Kretzschmar, Harry Begthel, Maaike van den Born, et al. 2016. "Replacement of Lost Lgr5-Positive Stem Cells through Plasticity of Their Enterocyte-Lineage Daughters." *Cell Stem Cell* 18 (2): 203-13. doi:10.1016/j.stem.2016.01.001.

Thaiss, Christoph A, Maayan Levy, Inna Grosheva, Danping Zheng, Eliran Soffer, Eran Blacher, Sofia Braverman, et al. 2018. "Hyperglycemia Drives Intestinal Barrier Dysfunction and Risk for Enteric Infection." *Science* 359 (6382): 1376-83. doi:10.1126/science.aar3318.

The BMJ. 2020. "Hydroxychloroquine for covid-19: the end of the line?" *The BMJ.* Jun. https://www.bmj.com/content/369/bmj.m2378.

Thillaiappan, Nagendra Babu, Alap P Chavda, Stephen C Tovey, David L Prole, and Colin W Taylor. 2017. "Ca 2+ signals initiate at immobile IP 3 receptors adjacent to ER-plasma membrane junctions." *Nature Communications* 8 (1): 1505. doi:10.1038/s41467-017-01644-8.

Tian, Ai-Ling, Qi Wu, Peng Liu, Liwei Zhao, Isabelle Martins, Oliver Kepp, Marion Leduc, and Guido Kroemer. 2021. "Lysosomotropic agents including azithromycin, chloroquine and hydroxychloroquine activate the integrated stress response." *Cell Death & Disease* 12 (1): 6. doi:10.1038/s41419-020-03324-w.

Tian, Hua, Brian Biehs, Søren Warming, Kevin G Leong, Linda Rangell, Ophir D Klein, and Frederic J de Sauvage. 2011. "A reserve stem cell population in small intestine renders Lgr5-positive cells dispensable." *Nature* 478 (7368): 255-9. doi:10.1038/nature10408.

Tinkum, Kelsey L, Kristina M Stemler, Lynn S White, Andrew J Loza, Sabrina Jeter-Jones, Basia M Michalski, Catherine Kuzmicki, et al. 2015. "Fasting protects mice from lethal DNA damage by promoting small intestinal epithelial stem cell survival." *PNAS* 112 (51): 7148-54. doi:10.1073/pnas.1509249112.

Tripathi, Manish K, Natasha G Deane, Jing Zhu, Hanbing An, Shinji Mima, Xiaojing Wang, Sekhar Padmanabhan, et al. 2015. "NFAT transcriptional activity is associated with metastatic capacity in colon cancer." *Cancer Research* 74 (23): 6947-57. doi:10.1158/0008-5472.CAN-14-1592.

Tuddenham, Susan, and Cynthia L Sears. 2016. "The Intestinal Microbiome and Health." *Current Opinion in Infectious Diseases* 28 (5): 464-70. doi:10.1097/QCO.0000000000000196.

Ualiyeva, Saltanat, Nils Hallen, Yoshihide Kanaoka, Carola Ledderose, Ichiro Matsumoto, Wolfgang G Junger, and Nora A Barrett. 2020. "Airway brush cells generate cysteinyl leukotrienes through the ATP sensor P2Y2." *Science Immunology* 5 (43). doi:10.1126/sciimmunol.aax7224.

Umar, Shahid. 2011. "Intestinal Stem Cells." *Current Gastroenterology Reports* 12 (5): 340-8. doi:10.1007/s11894-010-0130-3.

US National Library of Medicine. 2003. "Upper Gastrointestinal Tract." *US National Library of Medicine.* 9 7. https://meshb.nlm.nih.gov/record/ui?name=Upper%20Gastrointestinal%20Tract.

Vais, Horia, Kevin Foskett, and Don-On Daniel Mak. 2010. "Unitary Ca2+ current through recombinant type 3 InsP3 receptor channels under physiological ionic conditions." *Journal of General Physiology* 136 (6): 687-700. doi:10.1085/jgp.201010513.

Vaishnava, Shipra, Miwako Yamamoto, Kari M Severson, Kelly A Ruhn, Xiaofei Yu, Omry Koren, Ruth Ley, Edward K Wakeland, and Lora V Hooper. 2012. "The antibacterial lectin RegIIIγ promotes the spatial segregation of microbiota and host in the intestine." *Science* 334 (6053): 255-8. doi:10.1126/science.1209791.

van Amerongen, Renée, and Roel Nusse. 2009. "Towards an integrated view of Wnt signaling in development." *Development* 136 (19): 3205-14. doi:10.1242/dev.033910.

Van Baelen, Kurt, Leonard Dode, Jo Vanoevelen, Geert Callewaert, Humbert De Smedt, Ludwig Missiaen, Jan B Parys, Luc Raeymaekers, and Frank Wuytack. 2004. "The Ca2+/Mn2+ pumps in the Golgi apparatus." *Biochimica et Biophysica Acta* 1742 (1-3): 103-12. doi:10.1016/j.bbamcr.2004.08.018.

van de Wetering, Marc, Hayley E Francies, Joshua M Francis, Gergana Bounova, Francesco Iorio, Apollo Pronk, Winan van Houdt, et al. 2015. "Prospective derivation of a living organoid biobank of colorectal cancer patients." *Cell* 161 (4): 933-45. doi:10.1016/j.cell.2015.03.053.

van der Flier, Laurens G, and Hans Clevers. 2009. "Stem Cells, Self-Renewal, and Differentiation in the Intestinal Epithelium." *Annual Review of Physiology* 71: 241-60. doi:10.1146/annurev.physiol.010908.163145.

van der Flier, Laurens G, Andrea Haegebarth, Daniel E Stange, Marc van de Wetering, and Hans Clevers. 2009. "OLFM4 is a robust marker for stem cells in human intestine and marks a subset of colorectal cancer cells." *Gastroenterology* 137 (1): 15-7. doi:10.1053/j.gastro.2009.05.035.

Van der Sluis, Maria , Barbara AE De Koning, Adrianus CJM De Bruijn, Anna Velcich, Jules PP Meijerink, Johannes B Van Goudoever, Hans A Büller, et al. 2006. "Muc2-deficient mice spontaneously develop colitis, indicating that MUC2 is critical for colonic protection." *Gastroenterology* 131 (1): 117-29. doi:10.1053/j.gastro.2006.04.020.

van Dop, Willemijn A, Anja Uhmann, Mark Wijgerde, Esther Sleddens-Linkels, Jarom Heijmans, G Johan Offerhaus, Marius A van den Bergh Weerman, et al. 2009. "Depletion of the colonic epithelial precursor cell compartment upon conditional activation of the hedgehog pathway." *Gastroenterology* 136 (7): 2195-2203. doi:10.1053/j.gastro.2009.02.068.

van Es, Johan H, Marielle E van Gijn, Orbicia Riccio, Maaike van den Born, Marc Vooijs, Harry Begthel, Miranda Cozijnsen, et al. 2010. "Notch/gamma-secretase inhibition turns proliferative cells in intestinal crypts and adenomas into goblet cells." *Current Gastroenterology Reports* 12 (5): 319-30. doi:10.1007/s11894-010-0131-2.

van Es, Johan H, Toshiro Sato, Marc van de Wetering, Anna Lyubimova, Annie N Yee Nee, Alex Gregorieff, Nobuo Sasaki, et al. 2012. "Dll1+ secretory progenitor cells revert to stem cells upon crypt damage." *Nature Cell Biology* 14 (10): 1099-104. doi:10.1038/ncb2581.

Van Landeghem, Laurianne, Julien Chevalier, Maxime M Mahé, Thilo Wedel, Petri Urvil, Pascal Derkinderen, Tor Savidge, and Michel Neunlist. 2011. "Enteric glia promote intestinal mucosal healing via activation of focal adhesion kinase and release of proEGF." *The American Journal of Physiology-Gastrointestinal and Liver Physiology* 300 (6): 976-87. doi:10.1152/ajpgi.00427.2010.

Van Petegem, Filip. 2012. "Ryanodine Receptors: Structure and Function." *Journal of Biological Chemistry* 287 (38): 31624-32. doi:10.1074/jbc.R112.349068.

van Putten, Jos PM, and Karin Strijbis. 2017. "Transmembrane Mucins: Signaling Receptors at the Intersection of Inflammation and Cancer." *Journal of Innate Immunity* 9 (3): 281-99. doi:10.1159/000453594.

Vandecaetsbeek, Ilse, Peter Vangheluwe, Luc Raeymaekers, Frank Wuytack, and Jo Vanoevelen. 2011. "The Ca2+ Pumps of the Endoplasmic Reticulum and Golgi Apparatus." *Cold Spring Harbor Perspectives in Biology* 3 (5). doi:10.1101/cshperspect.a004184.

VanDussen, Kelli L, and Linda C Samuelson. 2010. "Mouse atonal homolog 1 directs intestinal progenitors to secretory cell rather than absorptive cell fate." *Developmental Biology* 346 (2): 215-23. doi:10.1016/j.ydbio.2010.07.026.

Vanoevelen, Jo, Leonard Dode, Kurt Van Baelen, Rebecca J Fairclough, Ludwig Missiaen, Luc Raeymaekers, and Frank Wuytack. 2005. "The secretory pathway Ca2+/Mn2+-ATPase 2 is a Golgi-localized pump with high affinity for Ca2+ ions." *Journal of Biological Chemistry* 280 (24): 22800-8. doi:10.1074/jbc.M501026200.

Vecchia, C La. 1992. "Cancers associated with high-fat diets." *Journal of the National Cancer Institute* (12): 79-85. https://pubmed.ncbi.nlm.nih.gov/1616815/.

Verdugo, P, M Aitken, L Langley, and M J Villalon. 1987. "Molecular mechanism of product storage and release in mucin secretion. II. The role of extracellular Ca++." *Biorheology* 24 (6): 625-33. doi:10.3233/bir-1987-24615.

Verma, V, C Carter, S Keable, D Bennett, and P Thorn. 1996. "Identification and function of type-2 and type-3 ryanodine receptors in gut epithelial cells." *Biochemical Journal* 319 (Pt2): 449-54. doi:10.1042/bj3190449.

Vermeulen, Louis, Felipe De Sousa E Melo, Maartje van der Heijden, Kate Cameron, Joan H de Jong, Tijana Borovski, Jurriaan B Tuynman, et al. 2010. "Wnt activity defines colon cancer stem cells and is regulated by the microenvironment." *Nature Cell Biology* 12 (5): 468-76. doi:10.1038/ncb2048.

Vessey, John P, Melanie R Lalonde, Hossein A Mizan, Nicole C Welch, Melanie EM Kelly, and Steven Barnes. 2004. "Carbenoxolone inhibition of voltage-gated Ca channels and synaptic transmission in the retina." *The Journal of Neurophysiology* 92 (2): 1252-6. doi:10.1152/jn.00148.2004.

Volkers, Linda, Yasmine Mechioukhi, and Bertrand Coste. 2015. "Piezo channels: from structure to function." *Pflügers Archiv* 467 (1): 95-9. doi:10.1007/s00424-014-1578-z.

von Rosenvinge, Erik C, and Jean-Pierre Raufman. 2011. "Muscarinic Receptor Signaling in Colon Cancer." *Cancers* 3 (1): 971-81. doi:10.3390/cancers3010971.

Walseth, Timothy F, Yaping Lin-Moshier, Pooja Jain, Margarida Ruas, John Parrington, Antony Galione, Jonathan S Marchant, and James T Slama. 2012. "Photoaffinity labeling of high affinity nicotinic acid adenine dinucleotide phosphate (NAADP)-binding proteins in sea urchin egg." *Journal of Biological Chemistry* 287 (4): 2308-15. doi:10.1074/jbc.M111.306563.

Walsh, Kathleen T, and Anne E Zemper. 2019. "The Enteric Nervous System for Epithelial Researchers: Basic Anatomy, Techniques, and Interactions With the Epithelium." *Cellular and Molecular Gastroenterology and Hepatology* 8 (3): 369-78. doi:10.1016/j.jcmgh.2019.05.003.

Wandinger-Ness, Angela, and Marino Zerial. 2014. "Rab proteins and the compartmentalization of the endosomal system." *Cold Spring Harbor Perspectives in Biology* 6 (11): a022616. doi:10.1101/cshperspect.a022616.

Wang, Honghe, Erik P Lillehoj, and K Chul Kim. 2003. "Identification of four sites of stimulated tyrosine phosphorylation in the MUC1 cytoplasmic tail." *Biochemical and Biophysical Research Communications* 310 (2): 341-6. doi:10.1016/j.bbrc.2003.09.030.

Wang, Wei, Suyun Yu, Shuai Huang, Rui Deng, Yushi Ding, Yuanyuan Wu, Xiaoman Li, et al. 2019. "A Complex Role for Calcium Signaling in Colorectal Cancer Development and Progression." *Molecular Cancer Research* 17 (11): 2145-53. doi:10.1158/1541-7786.MCR-19-0429.

Wang, Wuyang, Xiaoli Zhang, Qiong Gao, and Haoxing Xu. 2014. "TRPML1: an ion channel in the lysosome." *Handbook of Experimental Pharmacology* 222: 631-45. doi:10.1007/978-3-642-54215-2_24.

Wang, Xiang, Xiaoli Zhang, Xian-Ping Dong, Mohammad Samie, Xinran Li, Xiping Cheng, Andrew Goschka, et al. 2012. "TPC proteins are phosphoinositide- activated sodium-selective ion channels in endosomes and lysosomes." *Cell* 151 (2): 372-83. doi:10.1016/j.cell.2012.08.036.

Wang, Xi-Tao, Yasushi Nagaba, Heide S Cross, Fritz Wrba, Lin Zhang, and Sandra E Guggino. 2000. "The mRNA of L-Type Calcium Channel Elevated in Colon Cancer." *The American Journal of Pathology* 157 (5): 1549-62. doi:10.1016/S0002-9440(10)64792-X.

Wang, Y, E J Poulin, and R J Coffey. 2013. "LRIG1 is a triple threat: ERBB negative regulator, intestinal stem cell marker and tumour suppressor." *British Journal of Cancer* 108 (9): 1765-70. doi:10.1038/bjc.2013.138.

Webb, Sarah E, Jeffrey J Kelu, and Andrew L Miller. 2020. "Role of Two-Pore Channels in Embryonic Development and Cellular Differentiation." *Cold Spring Harbor Perspectives in Biology* 12 (1): a035170. doi:10.1101/cshperspect.a035170.

Wessler, I, C J Kirkpatrick, and K Racké. 1998. "Non-neuronal acetylcholine, a locally acting molecule, widely distributed in biological systems: expression and function in humans." *Pharmacology & Therapeutics* 77 (1): 59-79. doi:10.1016/s0163-7258(97)00085-5.

Wessler, I, E Roth, C Deutsch, P Brockerhoff, F Bittinger, C J Kirkpatrick, and H Kilbinger. 2001. "Release of non-neuronal acetylcholine from the isolated human placenta is mediated by organic cation transporters." *British Journal of Pharmacology* 134 (5): 951-6. doi:10.1038/sj.bjp.0704335.

Wickström, C, J R Davies, G V Eriksen, E C Veerman, and I Carlstedt. 1998. "MUC5B is a major gel-forming, oligomeric mucin from human salivary gland, respiratory tract and endocervix: identification of glycoforms and C-terminal cleavage." *Biochemical Journal* 15 (334): 685-93. doi:10.1042/bj3340685.

Wilkens, Stephan, Zhenyu Zhang, and Yesha Zheng. 2005. "A structural model of the vacuolar ATPase from transmission electron microscopy." *Micron* 36 (2): 109-26. doi:10.1016/j.micron.2004.10.002.

Wilkerson, Paul M, and Jorge S Reis-Filho. 2013. "The 11q13-q14 amplicon: clinicopathological correlations and potential drivers." *Genes, Chromosomes and Cancer* 52 (4): 333-55. doi:10.1002/gcc.22037.

Willams, G R, A Nazarians, and M A Gill. 2003. "A review of rivastigmine: a reversible cholinesterase inhibitor." *Clinical Therapeutics* 25 (6): 1634-53. https://www.ncbi.nlm.nih.gov/pubmed/12860489.

Willemsen, L EM, M A Koetsier, S JH van Deventer, and E AF van Tol. 2003. "Short Chain Fatty Acids Stimulate Epithelial Mucin 2 Expression Through Differential Effects on Prostaglandin E1 and E2 Production by Intestinal Myofibroblasts." *Gut* 52 (10): 1442-47. doi:10.1136/gut.52.10.1442.

Winton, D J, M A Blount, and B A Ponder. 1988. "A clonal marker induced by mutation in mouse intestinal epithelium." *Nature* 333 (6172): 463-6. doi:10.1038/333463a0.

Wlodarska, Marta, Christoph A Thaiss, Roni Nowarski, Eran Elinav, B Brett Finlay, and Richard A Flavell. 2014. "NLRP6 Inflammasome Orchestrates the Colonic Host-Microbial Interface by Regulating Goblet Cell Mucus Secretion." *Cell* 156 (5): 1045-59. doi:10.1016/j.cell.2014.01.026.

Wolff, Roger K, Michael D Hoffman, Erica C Wolff, Jennifer S Herrick, Lori C Sakoda, Wade S Samowitz, and Martha L Slattery. 2018. "Mutation analysis of adenomas and carcinomas of the colon: Early and late drivers." *Genes Chromosomes and Cancer* 57 (7): 366-76. doi:10.1002/gcc.22539.

Wong, Andrea KC, Paola Capitanio, Valentina Lissandron, Mario Bortolozzi, Tullio Pozzan, and Paola Pizzo. 2013. "Heterogeneity of Ca2+ handling among and within Golgi compartments." *Journal of Molecular Cell Biology* 5 (4): 266-76. doi:10.1093/jmcb/mjt024.

Wong, Vivian WY, Daniel E Stange, Mahalia E Page, Simon Buczacki, Agnieszka Wabik, Satoshi Itami, Marc van de Wetering, et al. 2012. "Lrig1 controls intestinal stem-cell homeostasis by negative regulation of ErbB signalling." *Nature Cell Biology* 14 (4): 401-8. doi:10.1038/ncb2464.

World Cancer Research Fund. 2020. *Bowel cancer.* https://www.wcrf-uk.org/uk/preventing-cancer/cancer-types/bowel-cancer.

—. 2018. "Other dietary exposures and the risk of cancer." *World Cancer Research Fund.* https://www.wcrf.org/sites/default/files/Other-dietary-exposures.pdf.

World Health Organization. 2020. *CANCER TODAY.* Accessed 1 1, 2021. https://gco.iarc.fr/today/home.

Worthington, J J, F Reimann, and F M Gribble. 2017. "Enteroendocrine cells-sensory sentinels of the intestinal environment and orchestrators of mucosal immunity." *Nature* 11: 3-20. doi:10.1038/mi.2017.73.

Wu, Yi-Fan, Ping Zhao, Xi Luo, Jin-Chao Xu, Lu Xue, Qi Zhou, Mingrui Xiong, et al. 2017. "Chloroquine inhibits Ca2+ permeable ion channels-mediated Ca2+ signaling in primary B lymphocytes." *Cell & Bioscience* 7 (28). doi:10.1186/s13578-017-0155-5.

Wu, Zhengming, and Kun-Liang Guan. 2021. "Hippo Signaling in Embryogenesis and Development." *Trends in Biochemical Sciences* 46 (1): 51-63. doi:10.1016/j.tibs.2020.08.008.

Xie, Jianlin , and Steven H Itzkowitz. 2008. "Cancer in Inflammatory Bowel Disease." *World Journal of Gastroenterology* 14 (3): 378-89. doi:10.3748/wjg.14.378.

Xiong, Yingfei, Suhua Sun, Sasa Teng, Mu Jin, and Zhuan Zhou. 2018. "Ca2+-Dependent and Ca2+-Independent ATP Release in Astrocytes." *Frontiers in Cellular Neuroscience* 11: 224. doi:10.3389/fnmol.2018.00224.

Xu, L, R Jones, and G Meissner. 1993. "Effects of local anesthetics on single channel behavior of skeletal muscle calcium release channel." *Journal of General Physiology* 101 (2): 207-33. doi:10.1085/jgp.101.2.207.

Xu, Mengnan, Shekoufeh Almasi, Yiming Yang, Chi Yan, Andra Mihaela Sterea, Alia KR Syeda, Bing Shen, et al. 2019. "The lysosomal TRPML1 channel regulates triple negative breast cancer

development by promoting mTORC1 and purinergic signaling pathways." *Cell Calcium* 79: 80-8. doi:10.1016/j.ceca.2019.02.010.

Yajima, Takaji, Ryo Inoue, Megumi Matsumoto, and Masako Yajima. 2011. "Non-neuronal release of ACh plays a key role in secretory response to luminal propionate in rat colon." *Journal of Physiology* 589 (Pt4): 953-62. doi:10.1113/jphysiol.2010.199976.

Yan, Kelley S, Olivier Gevaert, Grace XY Zheng, Benedict Anchang, Christopher S Probert, Kathryn A Larkin, Paige S Davies, et al. 2017. "Intestinal Enteroendocrine Lineage Cells Possess Homeostatic and Injury-Inducible Stem Cell Activity." *Cell Stem Cell* 21 (1): 78-90. doi:10.1016/j.stem.2017.06.014.

Yang, Bo, Lin Cao, Jiaen Liu, Yanjie Xu, Gillian Milne, Wanhei Chan, Steven D Heys, Colin D McCaig, and Jin Pu. 2015. "Low expression of chloride channel accessory 1 predicts a poor prognosis in colorectal cancer." *Cancer* 121 (10): 1570-80. doi:10.1002/cncr.29235.

Yang, Junsheng, Zhuangzhuang Zhao, Mingxue Gu, Xinghua Feng, and Haoxing Xu. 2018. "Release and uptake mechanisms of vesicular Ca2+ stores." *Protein & Cell* 10: 8-19. doi:10.1007/s13238-018-0523-x.

Yang, W L, and H Frucht. 2000. "Cholinergic receptor up-regulates COX-2 expression and prostaglandin E(2) production in colon cancer cells." *Carcinogenesis* 21 (10): 1789-93. doi:10.1093/carcin/21.10.1789.

Yang, Xin, Guorong Wen, Biguang Tuo, Fenglian Zhang, Hanxing Wan, Jialin He, Shiming Yang, and Hui Dong. 2018. "Molecular Mechanisms of Calcium Signaling in the Modulation of Small Intestinal Ion Transports and Bicarbonate Secretion." *Oncotarget* 9 (3): 3727-40. doi:10.18632/oncotarget.23197.

Yilmaz, Ömer H, Pekka Katajisto, Dudley W Lamming, Yetis Gültekin, Khristian E Bauer-Rowe, Shomit Sengupta, Kivanc Birsoy, et al. 2012. "mTORC1 in the Paneth cell niche couples intestinal stem-cell function to calorie intake." *Nature* 486 (7404): 490-5. doi:10.1038/nature11163.

Zacharias, William J, Xing Li, Blair B Madison, Katherine Kretovich, John Y Kao, Juanita L Merchant, and Deborah L Gumucio. 2010. "Hedgehog is an anti-inflammatory epithelial signal for the intestinal lamina propria." *Gastroenterology* 138 (7): 2368-77. doi:10.1053/j.gastro.2010.02.057.

Zahradníková, A, and P Palade. 1993. "Procaine effects on single sarcoplasmic reticulum Ca2+ release channels." *Biophysical Journal* 64 (4): 991-1003. doi:10.1016/S0006-3495(93)81465-6.

Zeissig, S, N Bürgel, D Günzel, J Richter, J Mankertz, U Wahnschaffe, A J Kroesen, M Zeitz, M Fromm, and J D Schulzke. 2007. "Changes in expression and distribution of claudin 2, 5 and 8 lead to discontinuous tight junctions and barrier dysfunction in active Crohn's disease." *Gut* 56 (1): 61-72. doi:10.1136/gut.2006.094375.

Zeki, Sebastian S, Trevor A Graham, and Nicholas A Wright. 2011. "Stem cells and their implications for colorectal cancer." *Nature Reviews Gastroenterology & Hepatology* 8 (2): 90-100. doi:10.1038/nrgastro.2010.211.

Zhang, Chao, Yiping Xia, Wei Jiang, Chunyang Wang, Bin Han, and Junwei Hao. 2016. "Determination of non-neuronal acetylcholine in human peripheral blood mononuclear cells by use of

hydrophilic interaction ultra-performance liquid chromatography–tandem mass spectrometry." *Journal of Chromatography B. Analytical Technologies in the Biomedical and Life Sciences* 1022: 265-73. doi:10.1016/j.jchromb.2016.04.024.

Zhang, Jiachang, Wen Li Liu, Delia C Tang, Ling Chen, Min Wang, Svetlana D Pack, Zhengping Zhuang, and Griffin P Rodgers. 2002. "Identification and characterization of a novel member of olfactomedin-related protein family, hGC-1, expressed during myeloid lineage development." *Gene* 283 (1-2): 83-93. doi:10.1016/s0378-1119(01)00763-6.

Zhang, Kejin, Jesse Civan, Sushmita Mukherjee, Fenil Patel, and Hushan Yang. 2014. "Genetic variations in colorectal cancer risk and clinical outcome." *World Journal of Gastroenterology* 20 (15): 4167-77. doi:10.3748/wjg.v20.i15.4167.

Zhang, Miao, Cameron Abrams, Liping Wang, Anthony Gizzi, Liping He, Ruihe Lin, Yuan Chen, Patrick J Loll, John M Pascal, and Ji-fang Zhang. 2013. "Structural basis for calmodulin as a dynamic calcium sensor." *Structure* 20 (5): 911-23. doi:10.1016/j.str.2012.03.019.

Zhang, Shenyuan L, Ying Yu, Jack Roos, J Ashot Kozak, Thomas J Deerinck, Mark H Ellisman, Kenneth A Stauderman, and Michael D Cahalan. 2005. "STIM1 is a Ca2+ sensor that activates CRAC channels and migrates from the Ca2+ store to the plasma membrane." *Nature* 437 (7060): 902-5. doi:10.1038/nature04147.

Zhang, Xiaoli, Wei Chen, Ping Li, Raul Calvo, Noel Southall, Xin Hu, Melanie Bryant-Genevier, et al. 2019. "Agonist-specific voltage-dependent gating of lysosomal two-pore Na+ channels." *eLife* 8: e51423. doi:10.7554/eLife.51423.

Zhang, Y W, I Morita, M Ikeda, K W Ma, and S Murota. 2001. "Connexin43 suppresses proliferation of osteosarcoma U2OS cells through post-transcriptional regulation of p27." *Oncogene* 20 (31): 4138-49. doi:10.1038/sj.onc.1204563.

Zhang, Zhe-Hao, Ying-Ying Lu, and Jianbo Yue. 2013. "Two pore channel 2 differentially modulates neural differentiation of mouse embryonic stem cells." *PLoS One* 8 (6): e66077. doi:10.1371/journal.pone.0066077.

Zhao, F, P Li, S R Chen, C F Louis, and B R Fruen. 2001. "Dantrolene inhibition of ryanodine receptor Ca2+ release channels. Molecular mechanism and isoform selectivity." *The Journal of Biological Chemistry* 276 (17): 13810-6. doi:10.1074/jbc.M006104200.

Zhao, Yongjuan, Richard Graeff, and Hon Cheung Lee. 2012. "Roles of cADPR and NAADP in pancreatic cells." *Acta Biochimica et Biophysica Sinica* 44 (9): 719-29. doi:10.1093/abbs/gms044.

Zheng, Le, Peter B Stathopulos, Rainer Schindl, Guang-Yao Li, Christoph Romanin, and Mitsuhiko Ikura. 2011. "Auto-inhibitory role of the EF-SAM domain of STIM proteins in store-operated calcium entry." *PNAS* 108 (4): 1337-42. doi:10.1073/pnas.1015125108.

Zhong, Xi Zoë, Yiming Yang, Xue Sun, and Xian-Ping Dong. 2017. "Methods for monitoring Ca 2+ and ion channels in the lysosome." *Cell Calcium* 64: 20-8. doi:10.1016/j.ceca.2016.12.001.

Zhou, Dawang, Yongyou Zhang, Hongtan Wu, Evan Barry, Yi Yin, Earl Lawrence, Dawn Dawson, et al. 2011. "Mst1 and Mst2 protein kinases restrain intestinal stem cell proliferation and colonic tumorigenesis by inhibition of Yes-associated protein (Yap) overabundance." *PNAS* 108 (49): 1312-20. doi:10.1073/pnas.1110428108.

Zitvogel, Laurence , Sophie Vi, Sophie Viaud, Marie Vétizou, Romain Daillère, Miriam Merad, and Guido Kroemer. 2015. "Cancer and the Gut Microbiota: An Unexpected Link." *Science Translational Medicine* 7 (271). doi:10.1126/scitranslmed.3010473.